eNergetics 2018

Proceedings of the 4th Virtual International Conference on Science, Technology and Management in Energy

Editors: Janjić, A., Stajić, Z.

Publishers: Research and Development Center "ALFATEC", Niš, Serbia
Complex System Research Center, Niš, Serbia

Serbia, Niš, October 25-26, 2018

eNergetics 2018

4th Virtual International Conference on Science, Technology and Management in Energy

Proceedings

Editors: Janjić, A., Stajić, Z.

Publishers: Research and Development Center
"ALFATEC", Niš, Serbia;
Complex System Research Centre, Niš, Serbia

Serbia, Niš, October 25-26, 2018

Proceedings of **4th Virtual International Conference on Science, Technology and Management in Energy**

Serbia, Niš, October 25-26, 2018

Editors: Prof. Dr. Aleksandar Janjić and Prof. Dr. Zoran Stajić

Technical Editor: Dr. Lazar Z. Velimirović

Published by: Research and Development Center "ALFATEC", Niš, Serbia, and Complex System Research Centre, Niš, Serbia

Printed by: Blue Copy, Niš, Serbia

Number of copies printed: 100

The publishing year: 2018

Printing of this edition has been financially supported by Serbian Ministry of Education, Science and Technological Development

ISBN 978-86-80616-03-2

CIP - Каталогизација у публикацији - Народна библиотека Србије, Београд

620.9(082)(0.034.2)

VIRTUAL International Conference on Science Technology and Management in Energy (4 ; 2018 ; Niš)
Energetics 2018 [Elektronski izvor] : proceedings / 4th Virtual International Conference on Science Technology and Management in Energy, Niš, October 25-26, 2018 ; editors Janjić A.[Aleksandar], Stajić Z.[Zoran]. - Niš : Research and Development Centar "Alfatec" : Complex System Research Centre, 2018 (Niš : Blue Copy). - 1 elektronski optički disk (DVD) ; 12 cm

Sistemski zahtevi: Nisu navedeni. - Nasl. sa naslovne strane dokumenta. - Tiraž 100. - Bibliografija uz svaki rad.

ISBN 978-86-80616-03-2 (RDCA)

a) Енергетика - Зборници
COBISS.SR-ID 271975436

4th Virtual International Conference on Science, Technology and Management in Energy

Organizer:

- **Research and Development Center "ALFATEC"**

Co-organizers:

- **Mathematical Institute of the Serbian Academy of Sciences and Arts**
- **Faculty of Technical Sciences, UKLO University St. Climent Ohridski**
- **Complex System Research Centre**
- **Academy of Sciences and Arts of the Republika Srpska**
- **Faculty of Mining and Geology, University of Belgrade**

Supported by:

- **Serbian Ministry of Education, Science and Technological Development**

Program Committee

Chair:

Prof. Dr. Aleksandar Janjić, Faculty of Electronic Engineering, Serbia

Members:

Prof. Dr. Zoran Stajić, Faculty of Electronic Engineering, Serbia

Prof. Dr. Gorazd Stumberger, Faculty of Electrical Engineering and Computer Science, Slovenia

Prof. Dr. Detelin Markov, Faculty of Power Engineering and Power Machines, Bulgaria

Prof. Dr. Marko Serafimov, Faculty of Mechanical Engineering, Macedonia

Prof. Dr. Mileta Janjić, Faculty of Mechanical Engineering, Montenegro

Prof. Dr. Miomir Stanković, Faculty of Occupational Safety, Serbia

Prof. Dr. Enver Agić, Public Enterprise Electric Utility of Bosnia and Herzegovina, Bosnia and Herzegovina

Prof. Dr. Niko Majdandžić, Faculty of Mechanical Engineering, Croatia

Prof. Dr. Serkan Abbasoglu, Cyprus International University, Turkey

Dr. Lazar Velimirović, Mathematical Institute of the Serbian Academy of Sciences and Arts, Serbia

Prof. Dr. Bojan Srđević, Faculty of Agriculture, Serbia

Prof. Dr. Jovica Milanović, School of Electrical and Electronic Engineering, UK

Prof. Dr. Abdelhak Djoudi, National Polytechnic School, Algeria

Prof. Dr. Suzana Savić, Faculty of Occupational Safety, Serbia

Prof. Dr. Zdravko Milovanović, Faculty of Mechanical Engineering, Bosnia and Herzegovina

Prof. Dr. Miloš Jelić, Research and Development Center Alfatec, Serbia

Prof. Dr. Zoran Markov, Faculty of Mechanical Engineering, Macedonia

Prof. Dr. Krsto Miljanović, Agromediterranean Faculty, Bosnia and Herzegovina

Prof. Dr. Krum Todorov, Faculty of Power Engineering and Power Machines, Bulgaria

Prof. Dr. Zoran Jovanović, Faculty of Electronic Engineering, Serbia

Prof. Dr. Dragoljub Mirjanić, Academy of Sciences and Arts of Republic of Srpska, Bosnia and Herzegovina

Prof. Dr. Tomislav Pavlović, Faculty of Sciences and Mathematics, Serbia

Prof. Dr. Božidar Popović, Faculty of Electrical Engineering, Bosnia and Herzegovina

Prof. Dr. Zoran Gligorić, Faculty of Mining and Geology, Serbia

Prof. Dr. Ljubiša Papić, Faculty Faculty of Technical Sciences Cacak, Serbia

Prof. Dr. Goran Janaćković, Faculty of Occupational Safety, Serbia

Dr. Wassila Issaadi, Faculty of Technology, University of Bejaia, Algeria

Prof. Dr. Roddy Lollchund, University of Mauritius, Republic of Mauritius

Organizing Committee

Chair:

Dr. Lazar Velimirović, Mathematical Institute of the Serbian Academy of Sciences and Arts, Serbia

Members:

Prof. Dr. Miomir Stanković, Faculty of Occupational Safety, Serbia

Prof. Dr. Zoran Stajić, Faculty of Electronic Engineering, Serbia

Dr. Petar Vranić, Mathematical Institute of the Serbian Academy of Science and Arts, Serbia

M.Sc. Ljubiša Stajić, Research and Development Center "ALFATEC", Serbia

M.Sc. Radmila Janković, Mathematical Institute of the Serbian Academy of Science and Arts, Serbia

M.Sc. Jelena Velimirović, Mathematical Institute of the Serbian Academy of Sciences and Arts, Serbia

M.Sc. Biserka Mijucić, Research and Development Center "ALFATEC", Serbia

Table of Contents

Crude Oil Prices Effect on Enhanced Oil Recovery Projects

Vesna Karović Maričić

University of Belgrade-Faculty of mining and geology, Belgrade, Serbia,
vesna.karovic@rgf.bg.ac.rs

Abstract— **Enhanced or tertiary oil recovery methods (EOR) contribute significantly in increasing oil recovery factor up to 60%. Additional oil recovery values depend on the type of the applied EOR method (thermal methods that include steam injection, in situ combustion; chemical methods such as polymer, alkaline or surfactant injection and injection of hydrocarbon, carbon dioxide or other gaseous fluids). Implementation of complex EOR methods involves high capital and operational costs, longer period of investment`s payback period and more risk and uncertainty in comparison to the use of conventional primary and secondary recovery methods of oil reservoirs.**
In general, oil prices have the largest impact on the EOR projects' economic viability.
Crude oil price decline since June 2014 had large impact at the world energy market, as well as at the application of oil exploitation methods and their commercial viability. In this paper are presented considerations of oil price impact on the oil production by EOR methods.

Keywords - oil production, enhanced oil recovery, crude oil price

I. INTRODUCTION

Tertiary recovery phase of an oil reservoir implies application of an enhanced oil recovery methods (EOR methods). These methods aim to mobilize the residual oil trapped in porous medium in existing producing oil fields. It is estimated that approximately 2/3 of the oil originally in place worldwide is still unrecoverable by conventional production methods, i.e. by natural depletion and waterflooding during primary and secondary oil recovery process [1, 2, 3]. EOR processes include application of: thermal methods (steam injection and in situ combustion), chemical methods (injection of polymers, alkaline or surfactants), injection of gases (hydrocarbon gases, carbon dioxide or other gaseous fluids in miscible or immiscible conditions) and other methods such as microbial, acoustic, electromagnetic that have for now small application.

Enhanced oil recovery techniques are not the new ones. They are developed and applied since 1970s with up and downs in number of EOR implemented projects that is directly related to the fluctuation of an oil price at the world market.

The most used EOR methods for decades were thermal ones i.e. steam injection, but lately the injection of CO_2 is becoming dominant method since it is considered also as an option for CO_2 geological storage and thus contributes to the CO_2 emission mitigation.

World oil production by application of EOR methods is at the about same level for years. It is about 3,5% of an overall world oil production [4,5]. So, the question that arise out of previous facts is: why EOR methods that contribute in increasing oil recovery factor up to 60% with production of million tones daily have relatively small application. The answer involves several reasons: implementation of EOR is complex process and it involves high capital and operational costs, longer period of investment payback period and more risk and uncertainty in comparison to the use of conventional primary and secondary recovery methods of oil reservoirs [6].

II. APPLICATION OF EOR METHODS RELATED TO OIL PRICE

In general, oil prices have the largest impact on the EOR projects' economic viability. So, the most of the EOR projects were implemented in the 1980s, when a sudden rise in oil price has happened. Since 1986 when oil price decreased

ISBN: 978-86-80616-03-2

significantly, the number of implemented EOR projects had a moderate continuous declining trend with significant fall from 1994 when oil price was less than 20$/bbl [7]. Following increase in the EOR methods` use, primarily of implemented CO_2-EOR projects, was in the second half of the 1st decade in this century until 2014. From 2014 to date, the number of new EOR projects has significantly dropped; moreover, it has been practically ceased, since oil price decrease has been present in 2014-2018 period. Figure 1 shows the number of implemented EOR projects by applied methods in the world for 2004, 2010, 2012 and 2014 (last available data) [8, 9, 10].

Figure 2 presents the oil price trend during the 2000-2018 period [11]. The fluctuation of oil price is present in different extent. First largest oil price fall was in this century was in 2008 due to global economic crisis. After that, in June 2014 crude oil price has crashed from its peak of 115$ to the lowest price of 30$ in February 2016, and in 2018 has begun to slowly raise up.

By analyzing time relationship between number of implemented EOR projects and oil price, it could be noticed that is characterized with time delay. Reasons are that implementation of EOR projects is time lasting process that involves several phases: first phase of selecting an appropriate EOR method by multicriteria analysis, laboratory testing and numerical modeling; second phase of pilot test application and third phase of implementation at the whole field if pilot test results are positive. So, it takes 6-10 years for achieving additional production by EOR methods application [2, 6, 12].

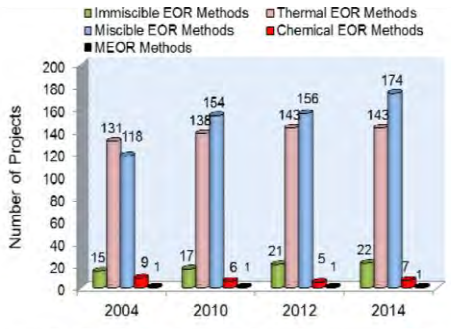

Figure 1. Number of implemented EOR projects by applied methods

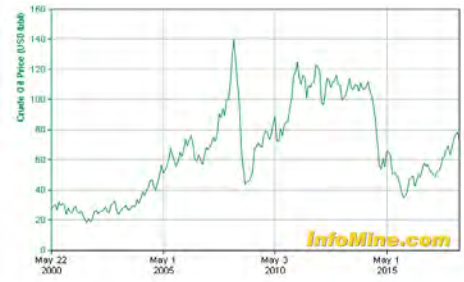

Figure 2. Crude oil price trend during the 2000-2018 period

It is well known that that the oil price depends on financial factors such as demand and supply, exchange rate of US dollar, inflation, status of global, regional or big countries` economy, as well as on the geopolitical factors and oil market speculations.

There are many different opinions on what of mentioned factors prevails in determining the oil price volatility at the world market, but the common one is that oil market recently became significantly more complex with many present uncertainties. For that reason, it is very difficult to make relevant long-term prediction of oil price trend.

Related to that issue, worldwide energy studies and reports use different scenario approach in analysis of future trends in oil production and demand. Thus, in the World Energy Outlook for 2014 (last available data) are considered three different scenarios by assumptions on deployment and future development of government energy and the environment policies: New Policies Scenario, Current Policies Scenario and the 450 Scenario. Central scenario in these projections is The New Policies Scenario that gives projection on the basis of adopted policies and regulations in 2014 on energy and environmental issues such as renewable energy, energy efficiency, programs and plans for carbon dioxide emission mitigation, etc. [13].

The New Policy Scenario of world oil production by 2040 estimated by International Energy Agency (EIA) is presented in Figure 3 [13]. According to that forecast, about 5 million barrels per day will be produced in 2040 by EOR methods, that indicates an increase of EOR share in future world oil production in comparison to today's 3 million.

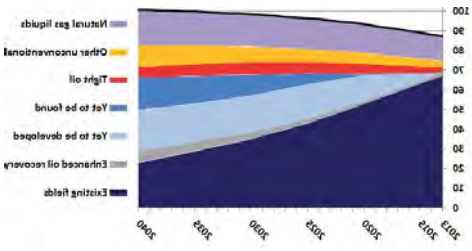

Figure 3. New Policies Scenario- Crude oil world production by 2040 (10^6 bbl/day)

Even with the low oil price, development of new technologies and techniques in the area of geophysics, drilling, reservoir and production engineering, as well as in reservoir modeling is improving cost efficiency and reducing risks in implementation of EOR projects. Importance in further developing EOR projects lies in the facts that the current production from most known oil fields has declining trend with large amounts of remaining oil reserves whose recovery could be increased and field production period extended only by application of these methods. EOR processes are less controversial compared to hydraulic fracking applied for production from unconventional resources (oil shale) and increase of their application is one of the main long-term strategies of major world oil companies such as: British Petroleum, Chevron Corporation, Cenovus Energy Inc., Canadian Natural Resources Limited, China National Petroleum Corporation, etc. [14].

III. The Brief Description of EOR Projects` Economics

Application of EOR technique involves high capital and operational expenditures, delayed revenue with high sensitivity to discount rates since more time is needed for production increase in comparison to conventional production methods. Capital and operational costs of EOR methods can be classified as process independent and process dependent costs [15]. Process independent costs are same as the costs of oil production in primary and secondary recovery phase such as: well drilling, well completion, workover costs, process maintenance costs, accompanying operational costs, surface equipment and infrastructure. Process dependent costs are related to the specifics of applied EOR methods and primarily involve: cost of injected fluids, costs of injection wells and costs of injection plants. The cost of injected fluid (chemicals, CO_2, hydrocarbon gases, nitrogen, etc.,) has a largest impact besides oil price on project economic viability. OPEX are the highest costs and account for 60 to 80% of the overall project costs depending on the type of applied EOR method [16]. The analysis of crude oil price, capital and operational costs of EOR projects′ application, where cost of injected fluid has a highest share, points out that the minimum oil price for commercially viable project is about 60-80 US $/barrel [17]. The production costs of CO_2 and other EOR methods related to the costs of other oil resources is given in Figure 4 [18].

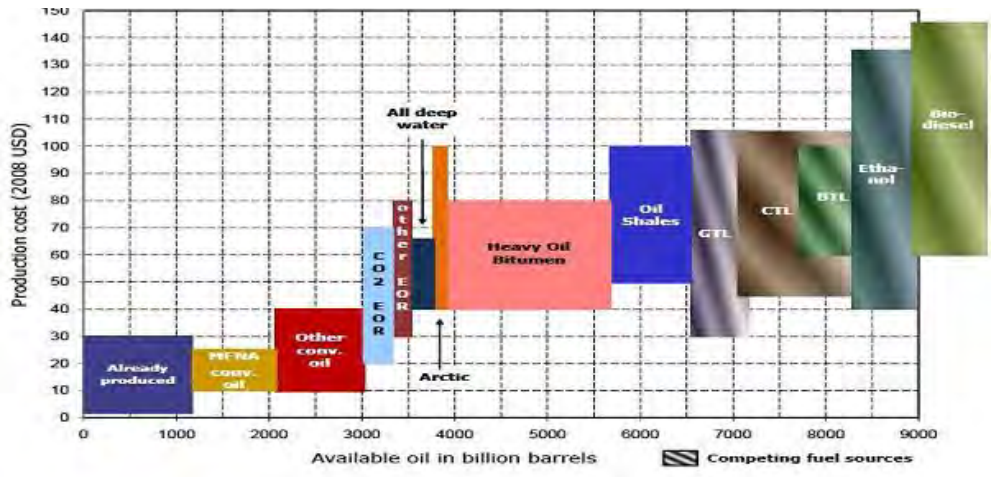

Figure 4. Production costs of oil resources

A. Thermal methods

Thermal methods have the greatest application of all EOR methods, primarily method of steam injection with share of about 60%. They are applied for increasing recovery of heavy oil reservoirs, extra heavy oil reservoirs and oil sands. Their main mechanism for producing additional oil is reduction of oil viscosity.

Depending on the way of generating heat in the oil reservoir, thermal methods are classified into: steam injection (cyclic and continuous injection-steam flooding) and in-situ combustion.

In the first group of methods, the conversion of water into the steam is carried out in surface steam generators, and after that stem is injected by injection well into the productive reservoir layer. In situ combustion, heat is produced in the reservoir due to combustion of certain part of oil in the productive layer. Oil combustion occurs by its spontaneous or induced ignition in the presence of injected air or air/water mixture. In Figures 5 and 6 are presented schemes of steam flooding and in situ combustion with zones that are formed in layer during these processes [19, 20].

Thermal methods are the least expensive EOR methods where highest share in operational costs are energy costs for steam generation. Cyclic steam injection involves three operating cycles: steam injection period, period of well shut-in and period of reproduction. This process is characterized by greater increase in oil production, lower capital costs, and lower operating pressures compared to the continuous steam injection. It produces 20-40% of additional oil recovery, with the ratio of injected steam and produced oil of 3-5, which means that for production of 1m^3 of oil it is required to inject 3-5 m^3 of steam [21, 22]. The steam oil ratio (SOR) is parameter that shows efficiency and cost-effectiveness of oil production during steam injection. Approximately one third of the additional produced oil is used to generate needed amount of steam [23]. So, it is considered that the steam injection project is cost-effective at SOR values up to 8 [24].

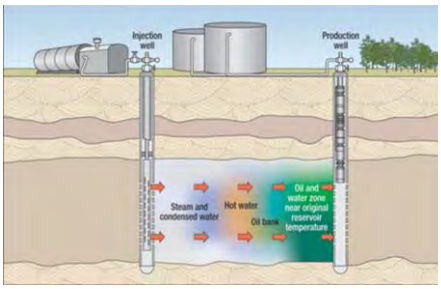

Figure 5. Steam flooding process

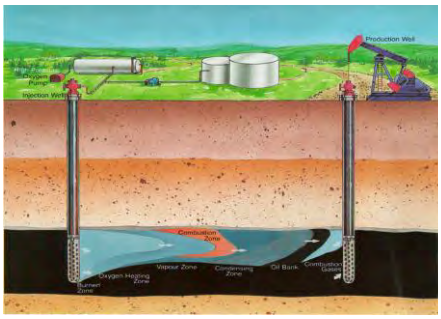

Figure 6. In situ combustion process

Steam flooding can increase oil recovery up to 60%, while recently most used „Steam assisted gravity drainage“ technique of steam injection for heavy oil production from oil sands, primarily in Canada and Venezuela, can achieve recovery up to 80% [5, 16].

In situ combustion applied projects have shown significant contribution to the increase of heavy oil recovery, but they are not applied so much in comparison to the steam injection. Main reasons are high risk of project failure mainly due to difficulties of process control and monitoring.

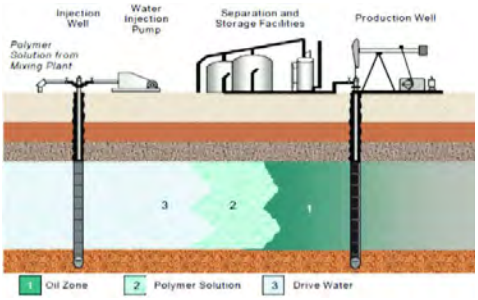

Figure 6. Polymer flooding

B. *Chemical methods*

Chemical methods include injection of polymers, alkaline or surfactants added to water for increasing production of light and medium residual oil in mature and waterflooded fields. Additional oil production mechanisms are: increase of oil microscopic displacement by reduction of interphase tension between oil and reservoir rock or wettability alternation and improving macroscopic oil displacement by controlling oil /injected fluid mobility ratio. The most applied chemical EOR process is polymer flooding (Figure 7) [25]. Chemical EOR is receiving lately more attention primarily due to increasing cost effectiveness and improving performance such as: development of stable surfactants at high temperatures, less expensive surfactants of low concentration which effectively reduce the value of interphase tension, and due to increasing use of combined chemicals such as alkaline-surfactant-polymer (ASP) [6]. For chemical processes, OPEX depend on type and quantity of injected chemicals where polymers are less expensive comparing to alkaline or surfactants, on type and capacity of surface chemical injection and treating facilities and additional costs if drilling of new injection wells is needed after waterflooding.

C. *Gas injection methods*

Gas injection methods involve injection of hydrocarbon gases, carbon dioxide, nitrogen and flue gases in light oil reservoirs for producing residual oil by lowering oil viscosity in miscible conditions, increase or maintain reservoir pressure, oil swelling, vaporization of oil and reduction of interfacial tension.

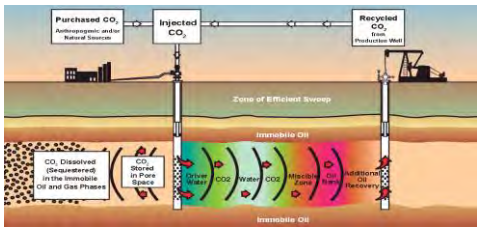

Figure 7. CO_2 injection“water alternate gas” method

The most applied are CO_2 injection processes that differ by the used CO_2 injection technique. The most successful one is the „water alternate gas“(WAG) method that involves the injection of slugs of water alternately with certain amount of CO_2 (Figure 8) [26].

Recent growing interest in CO_2-EOR method lies in the facts that this method represents one of the main new technological solutions for CO_2 emission mitigation by storing certain amount of used CO_2 in deep geological formations[27]. About 30-40% percent of injected CO_2 is recycled while the rest of injected CO_2 is stored in reservoir [28].

Major investments in CO_2 injection project represents purchase of CO_2 and costs of facilities for separating CO_2 from produced oil and compression for reinjection into the reservoir. The cost of CO_2 depends on the type of source type, source location related to the oil reservoir, and on availability of pipeline infrastructure. In the USA, which is the greatest oil producer by CO_2 injection (6% of its total oil production in last two decades) 20% of used CO_2 is anthropogenic in origin i.e., from industrial sources, such as natural gas processing plants, hydrocarbon conversion facilities [29]. CO_2 costs that include purchase price and recycle costs are estimated as 25% to 50% of the total cost per barrel of oil produced. Specifics of CO_2 injection projects in USA it is that their number has continuous increasing trend with significant additional production independently of oil price volatility. That is explained by their relatively lower costs due to presence of many natural cheap CO_2 sources and pipelines for CO_2 transportation to the oil field.

IV. CONCLUSION

The potential of EOR method application for oil recovery increase has been recognized for many years, but their use is still disproportionate to the contribution, i.e. significant additional production, due to an unstable economic factors-oil prices and a more complex process of oil reservoir recovery by using these methods in comparison to the production by conventional methods. Since oil prices have the largest impact on the EOR projects’ economic viability it is obvious that in the period of high oil price, the most of EOR processes have been developed and applied, and contrary, in the period of low oil price the number of new EOR processes has decreased. The certain exceptions are CO_2 injection projects. Oil price drop is slowing down investments in EOR production for the reason that these projects require high operational costs where largest share has a cost of injected fluid. On the other side, it should be considered that

EOR projects brings additional oil production in period of 6-10 years, so in the period of low price their development should not be ceased, but put on delay. Importance in further developing EOR projects lies in the facts that the current production from most known oil fields has declining trend with large amounts of remaining oil reserves whose recovery could be increased and field production period extended only by application of these methods.

Development of the new EOR oil production techniques, as well as further development of seismics, reservoir simulation models, application of horizontal, multilateral wells and hydraulic fracturing methods will enable more cost effective implementation of the EOR methods in the future period.

ACKNOWLEDGMENT

This article is the result of the project financed by the Ministry of Education and Science of Republic of Serbia (Project No. 33001). We thank the ministry for the support.

REFERENCES

[1] L. W. Lake and M.P. Walsh, „Enhanced oil recovery (EOR)", Technical report, Department of Petroleum and Geosystems Engineering, University of Texas at Austin, Austin, TX, 2008.

[2] P. Bonder (2010). EOR-the time is now: Its contribution of world energy supply, Society of petroleum engineers. Available at: https://www.spe.org/dl/?redirected_from=/dl/%202010.php

[3] American petroleum institute, Oil production statistics. Available at: https://www.api.org/

[4] S. Kokal, and A. Al Kaabi, „Enhanced oil recovery: chalanges and opportunities. World Petroleum Council: Official Publication.Global energy solution, 2010, pp.64-69

[5] E. Manirique, C. Thomas, R. Ravikiran et al., "EOR: Current Status and Opportunities," SPE paper 130113, presented at the IOR Symposium, Tulsa, OK, 2010, April 26-28.

[6] V. Karovic Maricic, D. Danilovic, and B. Lekovic, „Factors influencing successful implementation of enhanced oil recovery projects" , Undergroung mining engineering, 25, 2014, pp 41-50.

[7] J.J. Taber, F.D.Martin and R.S Seright, „EOR screening criteria revisited-part 2: Application nd impact of oil prices", SPERE, August 1997, pp.199-205.

[8] G. Moritis, "2010 Worldwide EOR Survey," OGJ, vol.108, No. 14, 2010, pp. 42–44.

[9] L., Koottungal, "2012 Worldwide EOR Survey," OGJ, vol. 110, No. 4, 2012, pp. 57–69

[10] L., Koottungal, "2014 Worldwide EOR Survey," OGJ, , vol. 112, No. 5, 2014, pp.79–91

[11] Infomine. (2018). Crude Oil Prices and Crude Oil Price Charts. Available at http://www.infomine.com/investment/metal-prices/crude-oil/

[12] Schlumberger. (2014).Seizing the EOR opportunity. Available at: http://www.slb.com

[13] International Energy Agency (2017). World Energy Outlook 2014. Available at: https://www.iea.org/publications/freepublications/publication/WEO2014.pdf

[14] Visiongain (2014).The 25 Leading Companies in Enhanced Oil Recovery (EOR). Available at: https://www.visiongain.com

[15] National Petroleum Council (1984). Enhanced oil recovery. Available at: https://www.npc.org/reports/rd1984-Enhanced_Oil_Recovery.pdf

[16] V. Alvarado, and E.Manrique, "Enhanced oil recovery: An update review", Energies, 2010, 3(9), pp. 1529-1575

[17] International Energy Agency. (2016). Data and publications. Available at: https://webstore.iea.org/world-energy-investmentI

[18] International Energy Agency (2010). Resources to Reserve – Production Cost Curve, Available at: www.iea.org.

[19] M. James, R. Wing, and Wood Group ESP Inc. (2018). Steam Flooding, Available at: http://www.upstreampumping.com/article/production/high-temperature-electric-submersible-pumps-effective-oil-sands-production

[20] A. Turta. (2018). In-Situ Combustion. Available at: http://www.insitucombustion.ca/

[21] I. Sandrea, and R Sandrea, „Global oil reserves—1: Recovery factors leave vast target for EOR technologies," Oil and Gas Journal 105(41), 2007, pp. 44-47

[22] National Petroleum Council, „Heavy oil, extra-heavy oil and bitumen unconventional oil", NPC Global Oil and Gas Study, 2007.

[23] A. Satter, and G. Thakur, „Integrated petroleum reservoir management", PennWell books, Tulsa, 1994.

[24] C.Chu, „State-of-the-Art Review of Steamflood Field Projects", J. Pet Technol 37 (10), 1985, pp. 1887-1902.

[25] N. El-Hoshoudy, M.Y. Elkady, and S. A. Mahmoud, "Hydrophobic Polymers Flooding", Chapter In book: Application and Characterization of Surfactants, 2017, DOI: 10.5772/intechopen.69645

[26] ARI. and Melzer Consulting, „Optimization of CO2 storage in CO2 enhanced oil recovery projects", Department of Energy and Climate Change, 2010.

[27] L. Tomić, V. Karović Maričić, D. Danilović and M. Crnogorac, „Criteria for CO2 storage in geological formations" , Undergroung mining engineering 32 (2018), pp 61-74

[28] S.Holloway, et al., „Carbon dioxide transport, injection and geological storage", IPCC Guidelines for National Greenhouse Gas Inventories, vol.2, Energy. 5.2., 2006.

[29] V. Kuuskraa et al, „ CO2 Utilization from "Next Generation" CO2 Enhanced Oil Recovery Technology", Energy Procedia 37 ,2013, pp. 6854 – 6866

Low Cost Cup Electronic Anemometer

Elson Avallone[1], Paulo César Mioralli[1], Pablo Sampaio Gomes Natividade[1], Paulo Henrique Palota[1], José Ferreira da Costa[1]

[1]Federal Instituteof Education,Scienceand Technology of Sao Paulo, Catanduva-SP, Brazil, elson.avallone@ifsp.edu.br; mioralli@ifsp.edu.br; pablo.sgn@ifsp.edu.br; palota@ifsp.edu.br; joseferreira@ifsp.edu.br

Abstract—**In all studies involving wind speed, such as meteorology, wind turbines and agriculture, require accurate speed information for decision making. There are several types of anemometers, with medium and high costs, such as Cup, hot wire and Pitot tubes, and the hot wire is more sensitive and expensive than others.The device developed in this work is the Cup anemometer, to be easy to build. The great advantage of this device is the low cost, with an approximate value of US$ 50.00, using simple materials and easy to find in commercial stores. The Reed Switch sensor is also another advantage as it does not require a sophisticated programming, as well as the open platform Arduino. The use of aerodynamic drag coefficients and the presented calculations resulted in values very close to a commercial anemometer with a good coefficient of determination (R^2). The present sensor was developed as part of the project of a meteorological station to monitor the micro-climate of the city of Catanduva-SP, Brazil.**

Keywords- Anemometer, low cost, air speed, Arduino.

Nomenclature

cd_1	Frontal Cup drag coefficient	Dimensionless
cd_2	Rear Cup drag coefficient	Dimensionless
f	Pulse per revolution (Arduino)	$[hz]$
K	Anemometer Factor	Dimensionless
r	Anemometer radius	$[m]$
V	Air speed	$[m/s]$
ω	Angular speed	$[rad/s]$

I. INTRODUCTION

There is a wide variety of anemometers and the most common are Cup anemometers. They consist of Cups attached to stems that are fixed to a central axis. Other anemometers, such as hot wire that measure the temperature change of a wire heated electrically by the passage of wind; Pitot probes use the Bernoulli Principle and the propeller anemometers have a front propeller to determine wind speed.

The first anemometer, applying scientific principles, was developed by [1]. In the meteorology studies, the anemometer is an important instrument in the atmospheric analyzes [2 - 3], where the authors used the equations of angular motion and frequency to determine the rotation of the instrument.. In the work developed by [4], the authors discuss a study involving ultrasound transducers to measure wind speed at an approximate cost of US$ 150.00. The researchers [5] studied the influence of lattice towers on the Cup anemometers, analyzing the best distance of less turbulence between the tower and the anemometer. To develop a rotational anemometer of conical Cups, [6] used an electronic blocks system, requiring calibration to validate the results. Another application of the anemometer is in the estimation and measurement of the efficiency of wind turbines [7]. The most common use of Cup anemometers is in meteorology and agriculture, to optimize agricultural practices with more precise decision-making. The use of this equipment in Brazilian agriculture is limited by its high cost [8]. Instead of using a first degree function in anemometer calibration, [9] uses two harmonic constants, which represent the influence of Cup geometry. Also [10] refers to the use of anemometers in wind energy and uses the front

and rear drag coefficients and the radius of rotation to determine the instrument constant.

The device chosen for this work is the Cup anemometer because it is simple and uses only a reed-switch sensor to measure the rotation of the device.

II. Materials and Methods

To build the anemometer were used three 70 mm aluminum confectionery Cups, three 3 mm diameter stems, a center bearing for fixing the stems with screws, a central axis to support the assembly, a neodymium magnet and a reed switch sensor, as shows the Fig. 1.

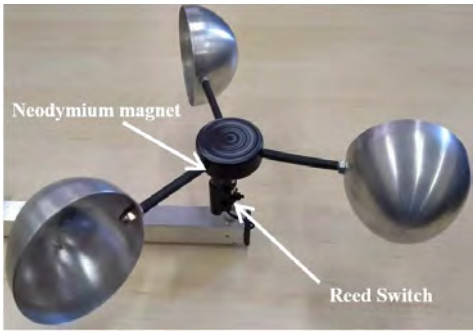

Figure 1.Anemometer mounted.

The neodymium magnet was coupled in the lower region of the central bearing of the anemometer as shown in Fig. 1.

Figure 2 shows the top view of the anemometer with the stems, the central bearing and the Cups.

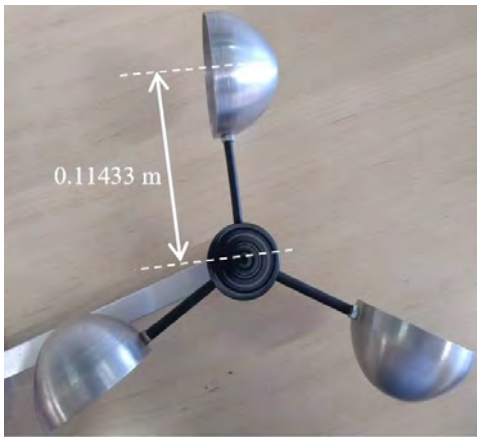

Figure 2. Top view of the anemometer.

The spacing between the magnet and the reed-switch sensor [11] is 3 millimeters and when these two components are crossed, the sensor "S1" closes the circuit (Fig. 3), counting one pulse at each full revolution. The pulse register is counted and controlled by the Arduino software [12], which was previously loaded into the processor memory. The 10 $k\Omega$ resistor adjusts the logic signal.

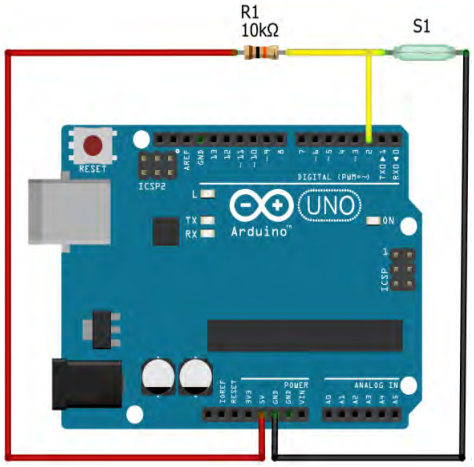

Figure 3. Eletronic circuit.

To calculate the air speed, [13] suggest the calculation procedure described in (1), (2) and (3), where k_d is a relationship between the frontal and reardrag coefficients are $c_{d1} = 1.42$ drag $c_{d2} = 0.3$, respectively and extracted from [14]. The anemometer factor (K) is defined by the aerodynamic characteristics of the Cups, extracted from (1) or a relationship between air speed (V), anemometer radius $r = 0.11433\ m$ and angular speed (ω) defined in (4).

By (5) is determined air speed in $[m/s]$. The index (f) represents the pulses per each revolution measured at reed switch sensor.

$$k_d = \sqrt{\frac{c_{d1}}{c_{d2}}}, \quad (1)$$

$$K = \frac{V}{r \cdot \omega} = \frac{k_d + 1}{k_d - 1}, \quad (2)$$

$$V = K.\omega.r, \quad (3)$$

$$\omega = 2.\pi.f \quad (4)$$

$$V = 2.27.f \quad (5)$$

The same calculation procedure was used by [15] and [16].

A. *Programming the Arduino platform*

A small part of the Arduino programming is shown in Fig. 4, where air speed is calculated from constant 2.27 shown in (5) and (f) are the pulses measured by the reed-switch sensor.

```
    }
    Pulse = 1000.0*countPulse/(millis()-timeold);
    if (pulse==0){
      AirSpeed=0;
    }
      else if (pin==2){
        AirSpeed = 2.27 * f;
      }
}
```

Figure 4. Part of Arduino programming.

III. Results and Discussions

The calibration procedure of the Cup anemometer for instrument certification was carried at IPMet-UNESP Bauru/Brazil from 08:00 to 19:00, with a measurement interval of 1 minute. The reference instrument was a propeller anemometer [17], generating a linear function and coefficient of determination (R^2), which were included in the graphic of Fig. 5. With the anemometer air speed V_{Cup} is inserted into calibration equation, thus obtaining the calibrated airspeed (V_{Real}).

The comparison between the two instruments is presented in Fig. 6, with small acceptable variations in the range of 4.5 and 7.3 m/s.

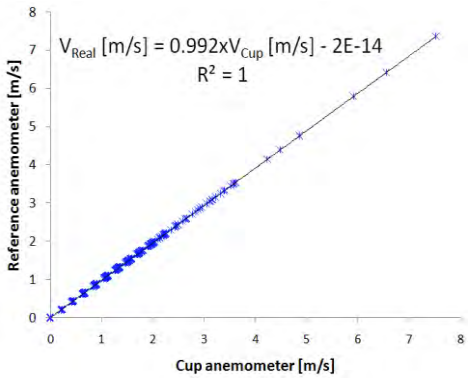

Figure 5. Calibration curve.

IV. Conclusion

The Cup anemometer presented excellent agreement with the reference sensor. It is a great choice for use not only for small farmers, but also for evaluation of wind turbines and especially for meteorological stations.

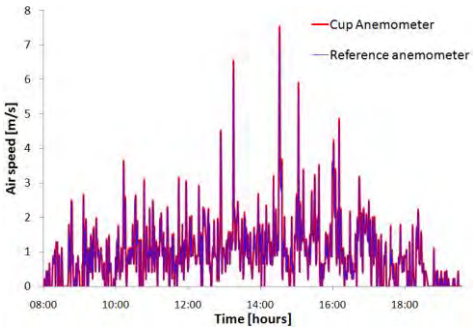

Figure 6. Air speed comparison curves.

The great attraction of this instrument is its low cost, with a value of US$ 50.00, even considering the value of the machiningtime, because its components are very simple.

Acknowledgment

To the Federal Institute of Education, Science and Technology of Sao Paulo, Catanduva-SP, Brazil for the support and incentive. To the Meteorological Research Institute IPMet-UNESP-Bauru/Brazil for scientific support.

References

[1] T. R. Robinson, "On a New Anemometer", *Proceedings of the Royal Irish Academy (1836-1869)*, vol. 4, p. 566–572, 1847.

[2] T. Ali, S. Nayeem, M. O. Faruk, M. Shidujaman, e S. M. Ferdous, "Design & implementation of a linear IC based low cost anemometer for wind speed measurement", *International Conference on Informatics, Electronics & Vision*, Dhaka, Bangladesch, 2012, p. 99–102.

[3] C. D. diCenzo, B. Szabados, e N. K. Sinha, "Digital Measurement of Angular Velocity for Instrumentation and Control", *Transactions on Industrial Electronics and Control Instrumentation*, vol. 23, nº 1, fev-1976.

[4] M. P. del Valle, J. A. U. Castelan, Y. Matsumoto, e R. C. Mateos, "Low Cost Ultrasonic Anemometer", in *2007 4th International Conference on Electrical and Electronics Engineering*, 2007, p. 213–216.

[5] R. N. Ferrugia e T. Sant, "Modelling wind speeds for Cup anemometers mounted on opposite sides of a lattice tower: A case study", *Journal of Wind Engineering and Industrial Aerodynamics*, vol. 115, p. 173–183, abr-2013.

[6] J. T. Fasinmirin, P. G. Oguntunde, K. O. Ladipo, e L. Dalbianco, “Development and calibration of a self-recording Cup anemometer for wind speed measurement”, *African Journal of Environmental Science and Technology*, vol. 5, nº 3, 2011.

[7] A. Accetta, M. Pucci, G. Cirrincione, e M. Cirrincione, “On-line wind speed estimation in IM wind generation systems by using adaptive direct and inverse modelling of the wind turbine”, in *2016 IEEE Energy Conversion Congress and Exposition (ECCE)*, 2016, p. 1–8.

[8] C. A. Sampaio, M. N. Ullmann, e M. Camargo, “Desenvolvimento e avaliacao de anemometro de copos de facil construcao e operacao.”, *Revista de Ciencias Agroveterinarias*, vol. 4, nº 1, p. 11–16, 2005.

[9] S. Pindado, J. Cubas, e F. Sorribes-Palmer, “On the harmonic analysis of Cup anemometer rotation speed: A principle to monitor performance and maintenance status of rotating meteorological sensors”, *Measurement*, vol. 73, p. 401–418, set. 2015.

[10] S. Pindado, J. Perez-Alvarez, e S. Sanches, “On Cup anemometer rotor aerodynamics”, *Sensors*, vol. 14, p. 6198–6217, 2012.

[11] Super Ultraminiature, “Reed switch”. 2012.

[12] Arduino, “Arduino”, *Arduino*, 2018. [Online]. https://www.arduino.cc/.

[13] S. Pindado, J. Cubas, e F. Sorribes-Palmer, “The Cup Anemometer, a Fundamental MeteorologicalInstrument for the Wind Energy Industry. Research at the IDR/UPM Institute”, *Sensors*, vol. 14, p. 21418–21452, 2014.

[14] B. R. Munson, D. F. Young, T. H. Okiishi, e W. W. Huebsch, *Fundamentals of fluid mechanics*, 6º ed, vol. 1, 1 vols. U.S.A.: Wiley, 2009.

[15] R. E. Predolin, “Desenvolvimento de um sistema de aquisição de dados usando plataforma aberta”, Master’s thesis, Universidade Estadual Paulista “Júlio de Mesquita Filho” - UNESP/FEB, Brazil, 2017.

[16] E. Avallone, “Estudo de um coletor solar, tipo tubo evacuado modificado, utilizando um concentrador cilíndrico parabólico (CPC)”, PhD Thesis, Universidade Estadual Paulista “Júlio de Mesquita Filho” - UNESP/FEB, Brazil, 2017.

[17] S. I. Campbell, “SP-LITE Silicon Pyranometer - Instruction manual”. Campbell, Scientific Inc - Utah - USA, 2004.

Analysis of Multiple Injection Impact on Fuel Supply Parameters

Mikhail G. Shatrov[1], Leonid N. Golubkov[2], Andrey Y. Dunin[3], Pavel V. Dushkin[4]

Moscow Automobile and Road Construction State Technical University (MADI), Moscow, Russia,
[1]dvs@madi.ru,[2]dvsgolubkov@yandex.ru,[3]a.u.dunin@yandex.ru,[4]levvap@gmail.com

Abstract—**Fuel injection causes considerable oscillations of fuel pressure at the injector inlet. One of the reasons is hydraulic impact originating when closing the injector nozzle needle. Evidently, these oscillations influence the fuel supply process in case of multiple injections: the previous injections would influence on the following ones. The influence of the interval between the impulses of a double injection on the injection rate value of the second portion was investigated. The superposition of waves in case of multiple injection may result both in amplification and damping of oscillations process. It is shown that with multiple injection, the controllability of fuel supply deteriorates, therefore, either a special design study of the fuel system for multiple injection or the introduction of additional electronic correction of control pulses by the diesel control system is required. On the other hand, it is shown how multiple injection can produce a stepwise injection characteristic, which can serve as a means of reducing nitrogen oxides and noise. Applied research and experimental developments are carried out with financial support of the state represented by the Ministry of Education and Science of the Russian Federation under the Agreement № 14.580.21.0002 of 27.07.2015, the Unique Identifier PNIER: RFMEFI58015X0002.**

Keywords- diesel engine, common rail fuel injection system, common rail injector, multiple injections, pressure oscillations

I. INTRODUCTION

The further tightening of ecological standards specifying the content of toxic emissions in the exhaust gases of diesel engines [1, 2, 3] jointly with the need to improve fuel efficiency creates prerequisites for perfection of the CR fuel systems of diesel engines. The fields of this perfection are:

- raising injection pressure up to 300 MPa [4, 5];

- control of fuel distribution by the combustion chamber zones [6];

- ensuring the required shape of the front edge of the injection rate [7, 8].

One of specific features of Common Rail fuel systems for diesel engines is the opportunity of flexible multiple injection. *Multiple (intermittent)* injection is understood to be several fuel injections during one working cycle of a diesel engine. Each individual fuel injection included into the multiple injection is called a *portion*. In the present work, a double injection is realized which consists, correspondingly, of two portions.

Practicability of multiple fuel injection is stipulated by the need to comply with the strict modern toxic and noise level standards. Though it complicates the working process of fuel injection system mainly due to wave processes in the fuel line (p_{in}, Fig. 1). The previous works carried out in MADI [9, 10, 11] and by foreign researchers [12] demonstrated that fuel injection causes considerable pressure oscillations in fuel lines which depend on: pressure, quantity of fuel injected, geometric parameters of the fuel line, injector design and physical propertied of fuel.

The paper shows the results of investigations of specific features of the Common Rail fuel system working process in case of multiple injections carried out in MADI.

ISBN: 978-86-80616-03-2

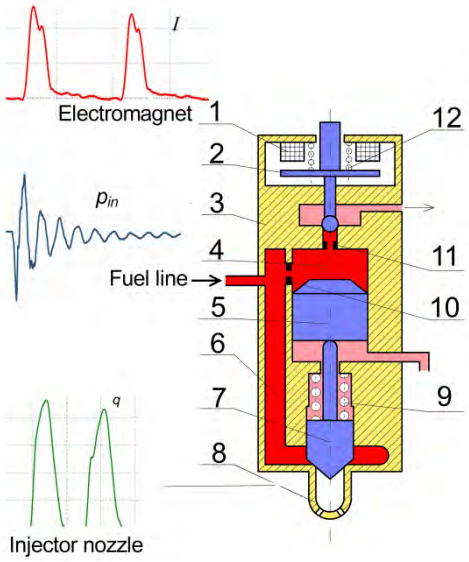

Figure 1. Schematic of the injector investigated: 1 – electromagnet; 2 – control valve; 3 – injector body; 4 – control chamber; 5 – multiplier piston; 6 – injector internal volume; 7 – injector needle valve; 8 – nozzle; 9 – needle valve spring; 10 – inlet jet; 11 – outlet jet; 12 – control valve spring.

II. Research of Fuel System Working Process in Case of Multiple Injection

The tests were carried out on a test-stand which was described in details in paper [13]. The test-stand was developed in MADI and was used for testing Common Rail fuel systems. It enables to attain the pressure in the common rail up to 350 MPa, is equipped with test-stand measuring system and control system also developed in MADI.

A *Bosch* company electro-hydraulic (Common Rail) fuel injector was used for the research with an electro-hydraulic control valve manufactured for *N*1 category vehicles. The injector nozzle has 7 holes with diameter d_c=0.12 mm.

Schematic of the injector is shown in Fig. 1. The injector is connected to the common rail by the fuel line having length l=650 mm and internal diameter d=2.2 mm. The work was carried out using diesel fuel at a steady fuel pressure in the common rail at the level p_{cr}=180 MPa.

The following values and designations are used in Fig. 1…5: I – current passing through the electromagnet of the control valve, p_{in} – pressure in the fuel line at the inlet to the injector, p_{av} – averaged value of p_{in}, q – injection rate (velocity of fuel flow through the fuel injector nozzle holes), Q – injection integral characteristic (the quantity of fuel injected during the control time interval), Q_{inj} – fuel mass injected, p_{cr} – pressure in the common rail, τ_{imp_1}, τ_{imp_2} – durations of the first and second control impulses of multiple injection, $\Delta\tau$ – interval between the control impulses of multiple injection.

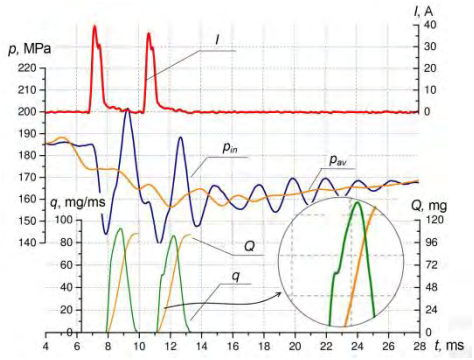

Figure 2. Basic characteristics of fuel injection process (p_{cr}=180 MPa, τ_{imp_1}=τ_{imp_2}=0.7 ms, $\Delta\tau$=3 ms).

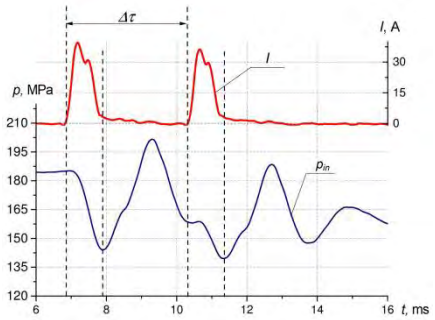

Figure 3. Basic characteristics of fuel injection process, enlarged scale (p_{cr}=180 MPa, τ_{imp_1}=τ_{imp_2}=0.7 ms, $\Delta\tau$=4.5 ms).

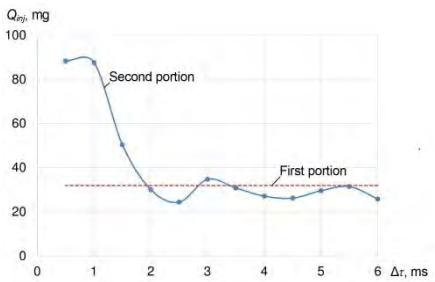

Figure 4. The value of fuel mass injected in case of changing the interval between the injections $\Delta\tau$ (p_{cr}=180 MPa, τ_{imp_1}=τ_{imp_2}=0.15 ms).

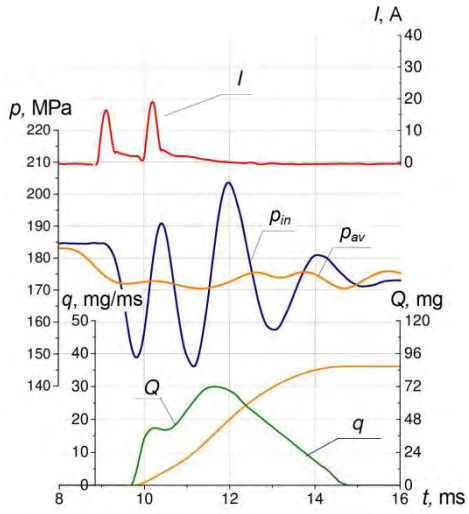

Figure 5. Basic characteristics of the fuel injection process (p_{cr}=180 MPa, $\tau_{imp\_1}=\tau_{imp\_2}$=0.15 ms, $\Delta\tau$=1 ms).

Supply of the first fuel portion causes oscillations in the fuel line. In Fig. 2, the maximal peak-to-peak amplitude (p_{in}) is 62 MPa, and pressure decrease in the common rail that can be indirectly estimated by the value of p_{av} is 25 MPa.

The reason of the emerging oscillation processes is an abrupt stop (hydroshock) of the fuel moving in the fuel line and injector which takes place when the injector nozzle needle valve is closed.

The actual injection pressure is reflected most accurately by the pressure in the sack volume (pressure under the needle valve 7 in Fig. 1) which is closely associated with pressure at the injector inlet (p_{in}). On the basis of data shown in Fig. 2 and Fig. 3, one can note that fuel supply is practically effected at considerably lower pressure than in the common rail. This negative effect will be higher when the speed of fuel flow through the nozzle holes (q) increases, therefore, for engines having high fuel mass injected, the internal diameter of the fuel line should be increased and additional common rail should be incorporated in the injector body.

At the present injection mode ($\tau_{imp\_1}=\tau_{imp\_2}$=0.7 ms, $\Delta\tau$=3 ms), both the fuel portions are practically equal. It can be seen from the injection rate (q) and integral injection characteristic (Q). The difference between them is within the limit of accuracy of the measurement method of these parameters.

An important phenomenon in the working process of the fuel system in case of multiple injection is the origination of the step (boot-shape) front edge of the second portion injection rate (Fig. 3). The issues of forming the stepped injection rate and the influence of the control impulse shape on the injection rate are reviewed separately in more details in the works performed in MADI and MGTU named after Bauman [7, 8, 14].

As demonstrated in papers [9, 10, 11], depending on operation conditions and design factors, the influence of the wave propagation may have a more considerable impact on the fuel injection process resulting in changing by several times the value of the second portion of the fuel injected just due to the variation of the $\Delta\tau$ value (Fig. 3).

The interesting fact is that when the control impulses come close to each other, the value of the second portion can increase considerably (Fig.4).

The reason of this phenomenon is illustrated in Fig. 5. When two short impulses with interval $\Delta\tau$=1 ms are supplied, the injector nozzle does not have enough time to close between the first and the second portions of multiple injection which results in the growth of fuel injection duration. This clearly follows from the growth of the injection rate q which takes a stepped shape.

Forming the stepped shape of the injection rate is advantageous for the diesel engine working process enabling to get lower severity of the diesel engine working process and hence - lower emissions of nitrogen oxide NO_x and noise.

It is seen from data presented in Fig. 3 that the wave process attenuates pretty fast and does not have any considerable influence on the injection process in the next working cycle. Though in a multicylinder high-speed diesel engine, the influence of injections on each other in different cylinders is possible.

Data in Fig. 3...5 was indicated for two control impulses having equal duration. It was found experimentally that the influence of a small primary injection on a large main injection is also significant. For example, at the operating conditions p_{cr}=50 MPa, τ_{imp_1}=0.15 ms (corresponds to fuel mass injected Q_{inj_1}=2.4 mg), the magnitude of the second portion (τ_{imp_2}=0.70 ms) varies within the range

Q_{inj_2}=30…39 mg only due to variation of the interval Δτ (Fig. 3). And when the second impulse approaches the value Δτ<1, the injection rate takes the stepped shape when the fuel mass injected grows to Q_{inj}=76 mg.

From analysis of the results obtained, it follows that multiple injection of fuel portions is not always equivalent to two individual injections separated from each other by the time of the working cycle duration of the diesel engine. For this reason, in case of multiple injection, to calculate the quantity of fuel supplied to the cylinder of the diesel engine, one should know not only the flow characteristic of the injector but also take into account the effects described above.

In this connection, during the process of diesel engine control system development, one should carry out tests on stands for fuel equipment investigation whose results, for example, may be used as a basis for the algorithm ensuring correction of the control impulses duration. The aim of this correction may be ensuring the desired fuel mass injected which is formed by multiple injection. Or a special design study of the fuel system is required, for example, integration of a volume for damping the hydroshock inside the injector [15].

As there are many factors which influence the process investigated, conduction of an experiment enabling to derive an empirical formula for the correction algorithm is a hard task which may be simplified thanks to mathematical modeling. Today, various complex mathematical models of the fuel systems are being developed and sophisticated [16, 17, 18] enabling to carry out the primary calibration of the algorithms of diesel engine control system (for example, a PID-controller of pressure in the common rail) and carry out calculation experiments on computer.

III. CONCLUSION

1. In case of multiple injection, the Common Rail fuel system working process becomes more complicated, controllability of the fuel supply system decreases. One should take into account this information when developing diesel engine control system, selecting a fuel system for the engine and its development.

2. To improve controllability, one should carry out a special design study of the fuel system, for example, create an additional volume in the injector for damping the hydroshock.

3. It is reasonable to implement electronic correction for compensation of the influence of variation of the internal between the control impulses on the fuel mass injected.

4. Multiple injection may be an instrument for forming the stepped shape of the injection rate which may be used as a method for sophistication of the diesel engine working process.

ACKNOWLEDGMENT

Applied research and experimental developments are carried out with financial support of the state represented by the Ministry of Education and Science of the Russian Federation under the Agreement № 14.580.21.0002 of 27.07.2015, the Unique Identifier PNIER: RFMEFI58015X0002.

REFERENCES

[1] M. G. Shatrov, V. V. Sinyavski, A. U. Dunin, I. G. Shishlov, A. V. Vakulenko, “Method of conversion of high- and middle-speed diesel engines into gas diesel engines”, Facta universitatis. Series: Mechanical Engineering, vol. 15, № 3, 2017, pp. 383–395.

[2] V. V. Sinyavski, I. V. Alekseev, I. Ye. Ivanov, S. N. Bogdanov, Yu. V. Trofimenko, “Physical Simulation of High- and Medium-Speed Engines Powered by Natural Gas”, Pollution Research, vol. 36 (3), 2017, pp. 684–690.

[3] M. G. Shatrov, V. V. Sinyavski, A. Yu. Dunin, I. G. Shishlov, A. V. Vakulenko, A. L. Yakovenko, “Using simulation for development of the systems of automobile gas diesel engine and its operation control”, International Journal of Engineering and Technology, No 7 (2.28), 2018, pp. 288–295.

[4] M. G. Shatrov, L. N. Golubkov, A. U. Dunin, A. L. Yakovenko, P. V. Dushkin, “Influence of high injection pressure on fuel injection performances and diesel engine working process”, Thermal Science, volume 19, issue 6, 2015, pp. 2245–2253.

[5] M. G. Shatrov, L. N. Golubkov, A. U. Dunin, A. L. Yakovenko, P. V. Dushkin, “Research of the impact of injection pressure 2000 bar and more on diesel engine parameters”, International Journal of Applied Engineering Research, volume 10, number 20, 2015, pp. 41098–41102.

[6] M. G. Shatrov, V. I. Malchuk, A. U. Dunin, A. L. Yakovenko, “The influence of location of input edges of injection holes on hydraulic characteristics of injector of the diesel fuel system”, International Journal of Applied Engineering Research, volume 11, number 20, 2016, pp. 10267–10273.

[7] M. G. Shatrov, L. N. Golubkov, A. U. Dunin, P. V. Dushkin, A. L. Yakovenko, “A method of control of injection rate shape by acting upon electromagnetic control valve of common rail injector”, International journal of mechanical engineering and technology (IJMET), volume 8, issue 11, November 2017, 2017, pp. 676–690.

[8] M. G. Shatrov, L. N. Golubkov, A. U. Dunin, P. V. Dushkin, A. L. Yakovenko, “The new generation of common rail fuel injection system for Russian locomotive diesel engines”, Pollution Research, vol. 36 (3), 2017, pp. 678–684.

[9] M. G. Shatrov, L. N. Golubkov, A. U. Dunin, A. L. Yakovenko, P. V. Dushkin, “Experimental research of hydrodynamic effects in common rail fuel system in case of multiple injection”, International Journal of Applied Engineering Research ISSN 0973-4562, volume 11, number 10, 2016, pp. 6949–6953.

[10] P. V. Dushkin, “Increasing efficiency of Commoin Rail fuel system with injection pressure up to 300 MPa”, PhD thesis, Moscow Automobile and Road Construction State Technical University (MADI), Moscow, 2017.

[11] M. G. Shatrov, L. N. Golubkov, A. U. Dunin, P. V. Dushkin, A. L Yakovenko, “Experimental research of hydrodynamic effects in Common Rail fuel systems in case of multiple injection”, AAI Journal (Journal of Automotive Engineers), No 2 (97), 2016, pp. 15–17.

[12] 1. A. E. Catania, A. Ferrari, M. Manno, E. Spessa, “Experimental investigation of dynamics effects on multiple-injection Common Rail system performance”, Journal of engineering for gas turbines and power, vol. 130, 2008, pp. 328061–3280613.

[13] A. U. Dunin, P. V. Dushkin, “Results of testing of Common Rail fuel systems with injection pressure up to 300 MPa”, Vestnik MGTU im. Baumana, issue 1 (106), 2016, pp. 80–88.

[14] L. V. Grekhov, U. E. Dragan, A. A. Denisov, E. E. Starkov, “Injection rate shaping with possibilities of general design Common Rail system”, Research journal of pharmaceutical, biological and chemical sciences, vol. 6(3), 2015, pp. 1890–1902.

[15] D. Schöppe, S. Zülch, M. Hardy, D. Geurts, R. W. Jorach, N. Baker, “Delphi Common Rail system with Direct Acting Injector”, MTZ Worldwide, vol. 69, 2008, pp. 32–38.

[16] A. G. Kuznecov, “Dynamic model of combined diesel engine”, Izvestiya vysshih uchebnyh zavedenij, Mashinostroenie, Moscow, No 11, 2011, pp. 39–43.

[17] S. N. Krivcov, “Mathematical description of the process of forming fuel pressure in Common Rail fuel supply systems of vehicles with diesel engines”, AAI Journal (Journal of Automotive Engineers), No 3 (98), 2016, pp. 38–41.

[18] L. N. Golubkov, P. V. Duskin, “Mathematical model of electro-hydraulic injector with integrated common rail and modified control valve”, Vestnik MADI, Moscow, MADI, issue 3 (42), 2015, pp. 11–18.

Calculation of Losses in the Distribution Grid Based on Big Data

Lazar Sladojević[1], Aleksandar Janjić[1], Marko Ćirković[1]

[1] Faculty of Electronic Engineering, Niš, Serbia, E-mail: lazar.sladojevic@elfak.rs

Abstract — **This paper represents an approach for calculation of losses in a distribution power grid from data which are normally collected by the grid operator. The proposed approach utilizes the least squares optimization method in order to calculate the coefficients needed for estimation of losses. The amount of data used in calculations is very large due to the fact that electrical energy injected in distribution grid is measured every fifteen minutes. Therefore, this approach is classified as the big data analysis. The used data set is available in the Serbian distribution grid operator's report for the year 2017. Obtained results are fairly accurate and can be used for losses classification as well as future losses estimation.**

Keywords – grid losses, least squares optimization, big data

I. INTRODUCTION

Big data analysis is rapidly becoming one of the most important tools in many aspects of engineering. Data are collected everywhere, and their numbers and collection rates are increasing each day. Therefore, various methods for processing of this data have been developed in recent years. These methods are efficient not only for extracting valuable information from a mass of data and their visualization, but also for developing predictive models for various applications.

Increasingly high amount of data can also be observed in a field of electrical power engineering. Electrical power grid is being modernized faster than ever, with large number of smart sensors being installed in many points of the grid. These sensors collect information about various electrical variables which are important for normal grid operation. These data are used everywhere, from the power generation side management to the demand side management. A good overview of many different applications of big data in electrical energy management and most common methods for data processing can be found in [1].

One of the most important usage of big data is prediction of solar and wind power generation based on collected weather data. Weather has a major impact on production from renewable sources, and therefore it is very important to observe the relationship between the two.

Another, very interesting application of big data is detection of different consumption profiles based on measurements of different variables. Example would be [2], where the authors have used hourly electricity consumption readings and external temperature measurements to compute consumption profiles for residential customers.

Electrical faults in power grid can present a big problem, especially when the fault occurs on a geographically distant part of a network. Fault detection, identification and location [3] can also be obtained from the data collected in various measurement points in the grid.

Another big problem for electrical energy suppliers is energy theft. Theft of electrical energy can in some places reach astonishingly high values. Therefore, an approach for estimating the amount of stolen electrical energy based on smart meter data and least squares method for data processing has been developed and proposed in [4]. This topic is closely related to this paper, since the energy theft is observed as a non-technical loss which is also evaluated here.

II. PROBLEM DESCRIPTION

In this paper, an approach for estimation of losses in distribution grid based on big data analysis is proposed. These losses comprise of two components, namely technical losses (TL) and non-technical losses (NTL). The proposed approach is based on analysis of losses data

collected in year 2017. This data will be used to estimate parameters of a predictive model for future losses estimation.

A. Physical interpretation

Technical losses can be split into two terms. The first term represents the constant losses. These mainly represent the losses in magnetic cores of distribution transformers, but other factors, such as losses due to corona, constantly operating measurement equipment, leakage currents and losses in dielectrics also contribute.

The other term is variable losses. They appear mainly in conductors but a small part of these losses can also be observed in other current carrying parts, such as switch contact resistances and busbars. These losses are proportional to the square of the current or, equivalently, to the square of active power.

Non-technical or commercial losses appear due to infrequent or bad reading of measurement equipment and electrical power thefts. Therefore, these losses are proportional to the active power.

In distribution power grid of Serbia, electrical energy received from the transmission grid is measured every fifteen minutes throughout whole year. On the other hand, energy supplied to end users is measured once every month. Total losses represent the difference between total energy received from the transmission grid and total energy supplied to end users during one month. These data are collected and can be used for future losses estimation and losses classification. One method that allows this kind of estimation is described in the following section.

B. Mathematical Model

There are several ways to model the losses in the distribution grid, but they all need information about energy obtained from the transmission grid and distributed sources and energy delivered to end users. The model chosen here represents the losses in the following polynomial form [5,6]:

$$\Delta W_{c,j} = \sum_{i} \left(a + b_j \cdot P_i + c \cdot P_i^2 \right) \cdot \Delta t_i \qquad (1)$$

where $\Delta W_{c,j}$ are the calculated (estimated) total losses for month j, i is the index of fifteen-minute interval Δt_i in month j, P_i is an average input power for the that interval, a represents the amount of constant losses, b_j is the coefficient associated with the commercial losses and is proportional to input power P_i in month j, and finally c is the variable losses coefficient, proportional to the square of power. Coefficients a and c are considered constant throughout the whole year, while the coefficient b varies by month. This assumption will be addressed in the following chapter.

On the other hand, measured losses, denoted as $\Delta W_{m,j}$ are already available as a difference between measured input and measured output energy.

For calculation of coefficients a, b and c, least squares method was used, which means that the sum of squared differences between the calculated and measured values of losses was minimized. Total number of variables is 14 (one for constant losses – coefficient a, twelve for commercial losses for each month – coefficients b_j and one for variable losses – coefficient c). Objective function for minimization can now be written as:

$$\min F(a,b,c) = \sum_{j=1}^{12} \left(\Delta W_{c,j} - \Delta W_{m,j} \right)^2 = \\ = \sum_{j=1}^{12} \left(\sum_{i} \left(a + b_j \cdot P_i + c \cdot P_i^2 \right) \cdot \Delta t_i - \Delta W_{m,j} \right)^2 . \qquad (2)$$

Coefficient values are constrained to a certain range: for coefficient a: $a_{min} \le a \le a_{max}$, for coefficients b_j: $b_{min} \le b_j \le b_{max}$ and for coefficient c: $c_{min} \le c \le c_{max}$. Constraints for coefficients a, b_j and c have to be properly selected, based on their physical interpretation explained in the following chapter.

C. Restrictions of the Proposed Method

Proposed method has one drawback, it uses the monthly readings of energy consumption. This means that the value of measured losses is prone to errors due to bad or untimely readings. For example, in some rural areas, electricity consumption is read only every three months. This leads to slight under readings for certain months and slight over readings for others and, consecutively, to miscalculation of the b_j parameters.

Better results would be obtained if the consumption was read with higher frequency, preferably the same as the input readings. This would require large number of smart meters

installed at every point in the grid, which is not yet realized in practice. However, smart meters are being installed every day and, in the future, more reliable and accurate data will be available for analysis.

III. Mathematical Model Solving Method

For solving of non-linear programming problem given with (2), standard mathematical methods were used, in this case the interior point algorithm. Input parameters are the fifteen-minute readings of electrical energy injected from the transmission grid and distributed sources into distribution grid and the monthly measured values of losses in the distribution system. Output consists of the values of coefficients a, b and c.

For easy programing and formulation of problem, an open source optimization platform Yalmip [7] was used. Yalmip's syntax allows easy and intuitive definition of variables, objective function, constraints and other options. Yalmip was used with one of Matlab's integrated solvers for performing computations. It can select solver for a problem automatically, based on its structure, but also permits users to select the solver they think it fits best. This allows all kinds of problems to be defined in the same way, unlike the case of using each solver individually, where user would have to define the problem in a form specific to that particular solver.

The solver used for calculation of coefficients is Matlab's *fmincon* nonlinear programming solver. This solver utilizes several different algorithms for objective function minimization, but the one used here was the so-called interior point algorithm [8].

Variables involved in calculations are already denoted a, b_j and c, with $j = 1...12$. Objective function is given with (2).

Constraints are chosen based on real data, and the realistic values of coefficients. The total nominal iron core losses power of all transformers in the distribution system of Serbia is approximately 32 MW. Therefore, the parameter a constriction adopted is $30 \leq a \leq 40$. Commercial losses always exist, but they do not exceed 10 % in Serbian distribution grid. Thus, adopted constraints for parameters b_j are $0.01 \leq b_j \leq 0.1$. Unlike the previous parameters whose extreme values are relatively easy to estimate, parameter c cannot be constrained in such a straight-forward manner. Since it is multiplied by a square of power, its value is undoubtedly very small. Based on author's previous experience, adopted constriction for this parameter is $0.00002 \leq c \leq 0.00006$. Since the grid topology and number of transformers remains very much the same throughout the whole year, it makes sense to keep coefficients a and c constant. On the other hand, coefficient b is affected by many external factors and therefore it is considered variable.

IV. Numerical Results

Obtained results are presented in table I and Fig. 1. Table I contains the real values of coefficients, while the values of coefficients b_j and c in Fig. 1 are scaled. The scaling is used only to make all values visible on a chart. After the scaling, coefficients b_j are shown in percent, while the coefficient c is now dimensionally equal to W^{-1}. Fig. 2 represents the comparison between calculated and measured values of losses. These losses are measured in MWh.

It can be observed from Fig. 2 that the computations were done successfully. Calculated and measured losses are equal which means that the coefficients are well estimated. Statistically speaking, it can be said that the input data, defined in the previous chapter are the training data for the model (1). From Fig. 2 it is obvious that the model fits the training data well. Now these coefficients can be used for future estimation of losses.

TABLE I. Calculated values for coefficients

Month	Coefficient a	Coefficient b	Coefficient c
January	32.739	0.091499	0.000020609
February	32.739	0.072052	0.000020609
March	32.739	0.061105	0.000020609
April	32.739	0.039002	0.000020609
May	32.739	0.057862	0.000020609
June	32.739	0.013125	0.000020609
July	32.739	0.019671	0.000020609
August	32.739	0.014427	0.000020609
September	32.739	0.018085	0.000020609
October	32.739	0.043728	0.000020609
November	32.739	0.051645	0.000020609
December	32.739	0.065777	0.000020609

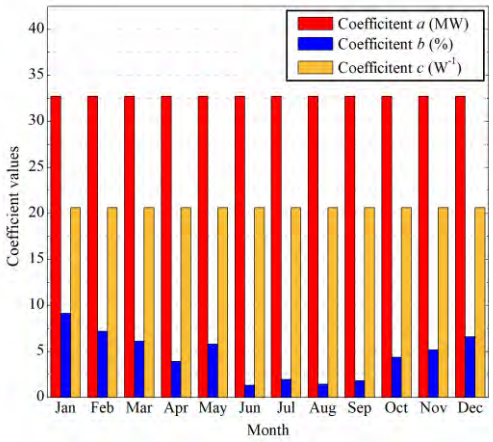

Figure 1. Scaled values of the calculated coefficients

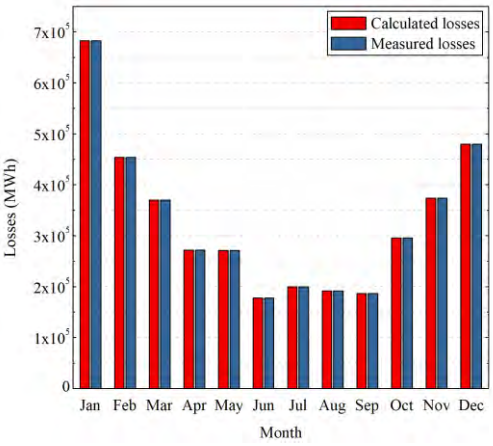

Figure 2. Comparison between calculated and measured losses

V. CONCLUSIONS

In this paper, a new approach for calculation of losses in the electrical distribution grid was presented. There are two general classes of losses: technical and non-technical losses. Both types are unavoidable, but it is important to know how each type affects the total amount of losses, i.e. they have to be classified. This is done by analyzing the data available from the distribution grid operator. The data contain the distribution grid input energy measurement for every fifteen-minute time interval and the monthly measurements of energy delivered to end users. Difference between these two are the real total losses for a certain month. On the other hand, a polynomial equation is introduced to calculate that same losses based on the grid input power. Coefficients for this equation are computed using the least squares method, by minimizing the squared differences between the calculated and real losses. These coefficient values are constrained based on their physical interpretation and authors experience. Results show that the minimization was successful and that the losses can clearly be classified this way. Additionally, calculated coefficients can be used for future estimation of losses. However, this whole concept can be improved. Future research will be focused on clustering the coefficients by seasons and processing the data for the previous few years. This could allow the researchers to observe some specific trends and focus on minimizing each kind of losses individually.

ACKNOWLEDGMENT

This research is partly supported by project grant III44006 financed by the Ministry of education, science and technology development of the Republic of Serbia.

REFERENCES

[1] K. Zhou, C. Fu and S. Yang, “Big data driven smart energy management: From big data to big insights”, Renewable and Sustainable Energy Reviews 56, 2016, 215–225.

[2] O. Ardakanian, N. Koochakzadeh, R. P. Singh, L. Golab, and S.Keshav, “Computing Electricity Consumption Profiles from Household Smart Meter Data,” in EDBT Workshop on Energy Data Management, 2014, pp. 140–147.

[3] H. Jiang, J. Zhang, W. Gao, and Z. Wu, “Fault detection, identification, and location in smart grid based on data-driven computational methods,” IEEE Transaction on Smart Grid, vol. 5, no. 6, 2015, pp. 2947–2956.

[4] D. N. Nikovski, Z. Wang, A. Esenther, H. Sun, K. Sugiura, T. Muso,and K. Tsuru, “Smart meter data analysis for power theft detection”, in Proc. Int. Workshop Machine Learning and Data Mining in Pattern Recognition, ser. LNCS, vol. 7988. Springer, 2013, pp. 379–389.

[5] M. Järvinen, “Developing network loss forecasting for Distribution System Operator”, Master of Science Thesis, Tampere University of Technology, 2013

[6] https://www.ofgem.gov.uk/ofgem-publications/43519/sohn-overview-losses-final-internet-version.pdf

[7] J. Löfberg, “YALMIP: A Toolbox for Modeling and Optimization in MATLAB”, In Proceedings of the CACSD Conference, Taipei, Taiwan, 2–4 September 2004

[8] Waltz, R. A., J. L. Morales, J. Nocedal, and D. Orban, “An interior algorithm for nonlinear optimization that combines line search and trust region steps,” Mathematical Programming, Vol 107, No. 3, pp. 391–408, 2006

Wind Farm Multiobjective Optimization using Nested Extremum Seeking Controls

Turaj Ashuri[1], Reza Hamidi[2], Subjanjan Bista[3]

[1]Department of Mechanical Engineering, Arkansas Tech University, Russellville, AR 72802, USA, tashuri@atu.ecu
[2]Department of Electrical Engineering, Arkansas Tech University, Russellville, AR 72802, USA, reza.j.hamidi@gmail.com
[3]Department of Mecanical Engineering, Arkansas Tech University, Russellville, AR 72802, USA, sbista@atu.edu

Abstract— **Wind farm optimization has been the focus of research in recent years. Most of the control algorithms available to maximize the energy capture or reduce structural loads are model-based. A Model-based controller is designed for wind turbines in ideal condition of operation. In real world, the actual wind power is a function of factors such as wind shear, temperature and surface roughness of the blade. This reduces the effectiveness of a model-based controller. Extremum seeking controls is a real-time, model-free optimization algorithm that can adapt to the changes in the design and environment. Previous studies have shown the e effectiveness of the algorithm to only maximize the energy capture, without considering the increase of structural loads. This paper presents a novel multiobjective nested extremum seeking controls algorithm to maximize the energy production and minimize the structural loads. The results show 30% reduction of the damage equivalent loads of the main shaft, and 25% reduction of the tower while increasing 1% power output of a wind farm compared to a baseline controller.**

Keywords - Wind Farm Power Maximization, Wind Farm Load Reduction, Extremum Seeking Controls, Multiobjective Optimization

I. INTRODUCTION

In 2015, the US coal-fired power plants experienced a reduction of 12.9 GW in power generation. At the same time, wind energy power generation demonstrated an increase of 9.8 GW in capacity[1]. This energy shift is a response to the adverse effects of climate change that pushes the energy sector transition into renewable energies with a great emphasis on wind energy. Although wind energy power generation seems promising, its cost is in general higher than that of conventional energy resources [1-3]. Several efforts have been made to reduce the cost such as improving blade design, new manufacturing techniques, upscaling wind turbines, power maximization, and better operation and maintenance strategies [4-11].

Wind power maximization is an effective strategy to reduce operational cost. Typically, this optimization takes place at either individual wind turbine level or wind farm level. However, maximizing the energy output of individual wind turbines [12-14] does not guarantee the maximum energy output of the entire wind farm [15]. This sub-optimality is because the wake of the upstream turbines reduces the power production of the downstream turbines, leading to under performance, as well as altering the structural loads.

Among the early studies to perform wind farm power optimization, Marden et al. [16] proposed a game theoretic optimization algorithm for an array of three wind turbines.

[1] US energy information administration, http://www.eia.gov/todayinenergy/detail.cfm?id=20292, Retrieved September 29, 2018

ISBN: 978-86-80616-03-2

Gebraad and Wingerden [17] proposed a quasi-Newton maximum power point tracking (MPPT) algorithm to optimize the power output of a three turbine array. Creaby et al. [18] proposed a multivariable optimization algorithm based on power output of the turbine as the input to the controller. Hawkins et al. [19] proposed optimizing the energy capture of wind turbines using a Lyaponov-based extremum seeking controls (ESC). Yang et al. [20] optimized the power output of a cascaded wind turbine array along the prevailing wind direction using a nested extremum seeking controls (NESC).

An alternative approach to reduce the design cost and extending the wind turbine life is the mitigation of structural loads as presented by limited studies in the literature. Soleimanzadeh and Wisniewski [21] presented a control algorithm to optimize the structural loads on a turbine using a distributed feedforward scheme. Kristalny and Madjidian [22] proposed a decentralized feedforward scheme to optimize the loads. Spudic et al. [23] proposed a hierarchical wind power and load optimization with disturbance compensation. Van Dijk et al. [24] developed a technique to optimize the power output and loads of a wind farm using yaw-misalignment and a gradient-based optimizer.

These studies mainly focus on either maximizing the power output or reducing the structural loads, and we still lack studies aiming at concurrent optimization of power output and structural loads. This paper investigates the concurrent multiobjective optimization of wind farm power output and structural loads based on the extension of earlier works in this area [25-27]. A novel NESC is developed to maximize the energy output with penalties on structural loads. Tower bending moment and shaft torsional moment are used to investigate the changes in structural loads. An array of 3 wind turbines is used to model the wind farm and the dynamic wake effect among them.

The reminder of the paper is structured as follows. First, the methodology to study the wind farm multiobjective optimization is presented. This includes the simulation platform to model the wind farm and its wake, the development of the NESC algorithm, and the multiobjective optimization formulation for the power output and structural loads. Next, the results are demonstrated and discussed. Finally, the conclusion is presented.

II. METHODOLOGY

To study wind farm optimization, we developed a Matlab Simulink model as explained by Yang et al. [20]. The model is constructed using SimWindFarm (SWF) computational platform [28]. This model is dynamically generated using a MATLAB script, based on input parameters such as mean wind speed, turbulence intensity and the location of the wind turbines within the wind farm. As Fig. 1 shows, the model is used to evaluate three different controllers including a baseline controller for power optimization of individual wind turbines, the NESC for power optimization of the wind farm, and the NESC for multiobjective power output and structural loads optimization of the wind farm.

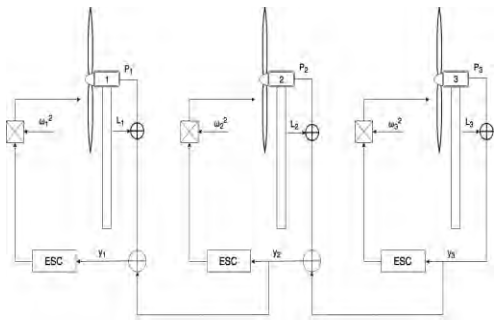

Figure 1. Cascaded NESC implementation

A. Simulation Platform

As explained earlier, the simulation platform to develop the NESC is SWF. SWF is a powerful toolbox that provides an environment to develop new control algorithms. It consists of a turbine model and functionality for wake simulation. Based on the inputs such as mean wind speed, turbulence intensity, the number of turbines and their locations, a windfield is generated that enables dynamic modeling of the wind farm.

To simplify the approach, we use a constant mean wind speed and direction, fixed yaw, and a 2D windfield at hub height. The 5 MW NREL wind turbine model incorporated in the platform allows extraction of two moments to represent the structural loads [29]. These moments are the shaft torsion and tower bending. The shaft moment can be measured from the drive train model. It is modeled as a

third-order system of two rotating shafts connected through a generator. The tower deflection is modeled as a second-order spring-damper system from which the tower moment can be measured. Wind turbine and wind farm generated electricity are direct output of the model for use in our optimization algorithm.

B. Controller

The performance of our multiobjective controller that incorporates both power and load optimization is justified by comparing it against the baseline controller of the NREL 5 MW turbine as explained next.

1) Baseline Control

The default strategy of the baseline contoller is divided into the below rated region and the above rated region. Below the rated region, a lookup table is used to find the generator power reference using the generator speed as input. In the region above the rated, the generator power reference is constant at its rated power and the rotor speed is controlled by varying the blade pitch using a gain scheduled PI controller.

2) ESC for power optimization

The ESC strategy as shown in Fig. 2 employs a gradient based search technique to find the desired optimal point. A dither signal, ($f_{dither} = asin(\omega t)$), is added to the input of the plant, u, as a sinusoidal probing signal, ($u_d = u + f_{dither}$), to excite the system. The output of the plant, ($y = l(u_d)$), is fed back as the input signal to the controller. A high-pass filter is used to remove the DC term while retaining the harmonics. A demodulation signal, ($f_{dem} = sin(\omega t)$), converts the first harmonic that is proportional to the gradient to a DC component. The higher order terms are then removed using a low-pass filter while retaining the DC component. An integrator is used to eliminate any steady state error present to reach zero gradient under the condition of plant's stability.

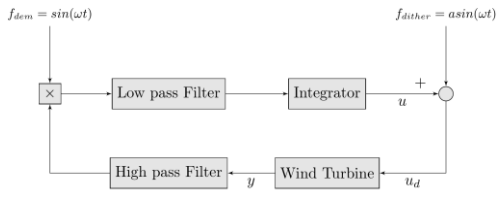

Figure 2. Block diagram of the ESC for a single wind turbine.

In real world operation, there is fluctuation in various factors such as wind speed that causes fluctuation in the power out. Therefore, the input (or objective function y) of the controller changes rapidly according to the turbulent fluctuation in the simulated wind speed. In the case of steady wind, the input to the ESC can be used directly to perform power optimization since there is no fluctuation resulting in the divergence of the algorithm. However, in the case of unsteady wind, this input can-not be used directly. This is because the fluctuations in the power due to the wind speed causes the controller to diverge from the optimal value. In this case, the input to the controller is conditioned to maintain the convergence and stability of the algorithm.

The dependency of the power output to the fluctuating wind speed can be mitigated by using the Array Power Coefficient (APC) instead of the aerodynamic power as the objective function. This is based on a similar approach by Corten et al. [30] and implemented by Yang et al. [20]. APC is defined as the ratio of the sum of aerodynamic power of the turbine i and all the n turbines in its wake to the estimated power. This can be represented as,

$$K_p^i = \frac{P^i + \sum_{n=1}^{j} P_a^n}{\frac{1}{2}\rho A U^3} \qquad (1)$$

Where, K_p^i is the APC of the i^{th} turbine where, P_a^j is the aerodynamic power of the most downwind turbine in the wake of turbine i, is air density, A is rotor area, and U is wind speed.

This equation can be extended with respect to actual time, t, to account for the delay in the traveling wake, T. The estimated power is calculated using the measured wind speed in front of the upwind turbine i and for the following j number of turbines in its wake. Therefore, the travel delay, Ti, is applied to the wind speed of the upwind turbines. That is,

$$K_p^i(t) = \frac{P^i(t-T_i) + \sum_{n=1}^{j} P_a^n(t-T_i)}{\frac{1}{2}\rho A U(t-T_i)^3} \qquad (2)$$

Any residual fluctuations in the APC signal due to the changes in wind speed appear as high frequencies in the signal that can be removed using a simple low-pass filter. Using a moving average filter, the trend of the APC signal can be captured. This modified signal is used as the

input to optimize the power output of the wind farm.

3) Multiobjective NESC for power and loads optimization

To simultaneously optimize the power and loads, the objective function is modified to incorporate a NESC with load feedback as a penalty function. This penalty function can be incorporated in either an additive penalty or a multiplicative penalty [31].

The additive penalty can be formulated by simply adding the penalizing term to the objective function of the ESC. The new objective function thus becomes,

$$K_{+}^{i}(t) = Kp^{i}(t) - K_{load}^{i}(t - T_i) \qquad (3)$$

Where $K_{+}^{i}(t)$ is the load coefficient of the i^{th} turbine, and:

$$K_{load}^{i}(t) = \left(\frac{U_0}{w_3}\right) \times \left[\left(\frac{w_1^i M_{tower}^i (t - T_i)}{M_{tower}^*}\right) - \left(\frac{w_2^i M_{shaft}^i (t - T_i)}{M_{shaft}^*}\right)\right] \qquad (3)$$

Where $K^{i}_{load}(t)$ is the load feedback of the i^{th} turbine, M^{*}_{tower} and M^{*}_{shaft} are the peak tower and shaft moments at rated wind speed, respectively, ω_1 and ω_1 are the moment weight factors to allow a trade off between the power and loads optimization in this multiobjective formulation, U_0 is the mean wind speed that is used together with ω_3 to have the same dimensions for loads and power.

Usually, the tower moments are in the order of 10^6 to 10^7, and the shaft moments are in the order of 10^5 to 10^6. To normalize this difference in the feedback, we divided the measured value by a factor to convert it to a similar order to that of the APC.

At the rated power speed of the 5 MW wind turbine, we find that the tower moment in our simulation is 9 x 107 Nm, and the shaft moment is 4.5 x 106 Nm. These terms normalize the two moments that have different orders of magnitude.

Optimization using an additive penalty is more tedious as we would have to manually alter the ω_3 to make sure that the objective function lies within certain limits. Exceeding these limits will require implementing gain scheduling strategy in the NESC for different wind speeds.

In the case of the multiplicative penalty function, this limitation can be mitigated since the input can be made to lie within 0 and 1 range. This allows us to design a more robust controller that can accommodate changes in wind speeds and loads. Also, since the shaft moment is directly proportional to the power output, it is not fed back to the controller. The objective function is thus formulated as:

$$K_{\times}^{i}(t) = K_{p}^{1}(t) \times \left[1 - K_{load}^{i}(t)\right] \qquad (5)$$

Where $K^{i}_{\times}(t)$ is the multiplicative penalty function, and $K^{i}_{Load}(t)$ can be represented as:

$$K_{load}^{i}(t) = \left(\frac{w_i \times M_{tower}^{i}(t - T_i)}{M_{tower}^{*}}\right) + \left(\frac{w_i \times M_{shaft}^{i}(t - T_i)}{M_{shaft}^{*}}\right) \qquad (6)$$

Combining (2) and (6), we get:

$$K_{\times}^{i}(t) = \left(\frac{P^{i}(t - T_i) + \sum_{n=1}^{j} P_a^n (t - T_i)}{\frac{1}{2}\rho A U (t - T_i)^3}\right) \times \left[1 - \left(\frac{w_i \times M_{tower}^{i}(t - T_i)}{M_{tower}^{*}}\right) + \left(\frac{w_i \times M_{shaft}^{i}(t - T_i)}{M_{shaft}^{*}}\right)\right] \qquad (7)$$

In (7) we vary a part of the power as a function of the tower moments, thus enabling optimization of the power and the loads simultaneously.

III. RESULTS

The ESC algorithm in general may derate the power of the first turbine to increase power output of the entire wind farm. This results in lower tower moments than compared to that of the baseline controller. While the wind farm power output shows an increase, the shaft moments experience a slight increase. This fact shows the importance of the correct implementation of the load reduction technique in the multiobjective optimization formulation. Therefore, both the additive and multiplicative techniques are studied to find the best trade off between the loads and power.

Fig. 3 is an illustrative example to see the impact of the ESC on different wind turbines in the farm to tune the torque gain for different objective functions. The simulation is performed at a steady wind speed of 8 m/s. More detailed simulation results for both the

additive and multiplicative objective functions follows next.

A. *Turbulent wind using additive penalty*

The results from Fig. 4 and 5 show that the additive penalty lowers the damage equivalent load of all the turbines on both the shaft and the tower while the mean shaft moments show an increase in comparison to an individual ESC.

The controller does however give more importance to the loads rather than the power output as seen in Fig. 6. This is one of the drawbacks of using this controller. As mentioned earlier, in Eq. 4, the output of the load term, (K^{i}_{load}), is susceptible to large variations and spikes in the load due to sudden change in wind speed that can affect the controller output.

B. *Turbulent wind using multiplicative penalty*

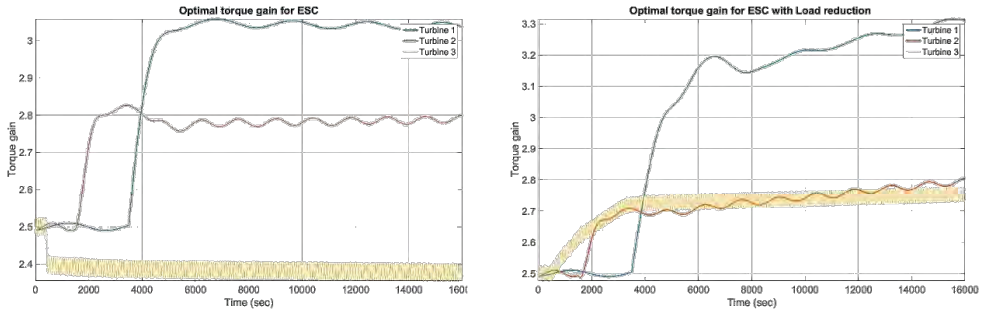

(a) ESC without load feedback (b) ESC with load feedback.

Figure 3. Optimal torque gain tuning at a steady wind speed of 8m/s for 16000 seconds. This is to maximize the power output of the entire wind farm using different objective functions.

Multiplicative penalty based NESC load reduction strategy uses the load coefficient to scale the value of the APC. The only concern is to maintain the value of the load coefficient to be less than 1. By doing so, we can maintain the value of the input signal to be a positive number that is in a similar order of magnitude to that of the NESC without the load optimization enabled. This makes it easier to find the input parameters of the NESC such as the dither and demodulation frequency and the integrator gain.

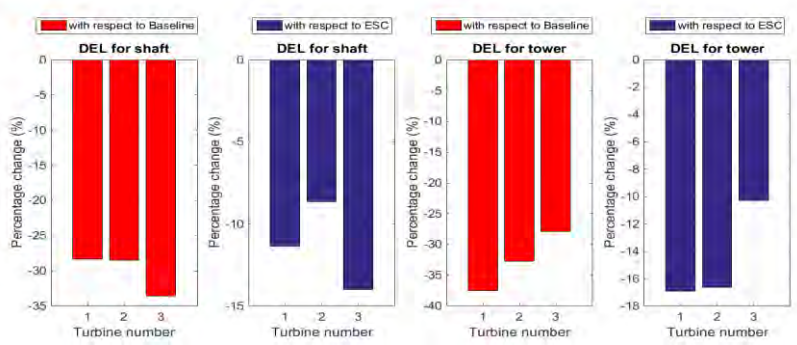

Figure 4. Percentage change of damage equivalent loads for the shaft and the tower with respect to the baseline controller and the ESC using additive penalty based ESC load feedback.

This is reflected in the results as seen in Fig. 7 and 8. The damage equivalent loads (though greater than that of the NESC without the load optimization) still are lower than the baseline

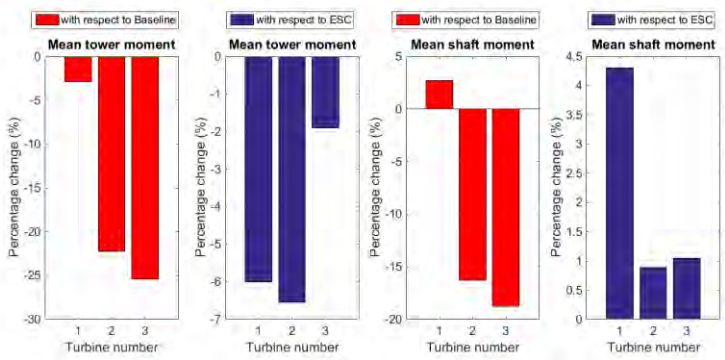

Figure 5. Percentage change of mean value of moments for the shaft and the tower with respect to the baseline controller and the ESC using additive penalty based ESC load feedback.

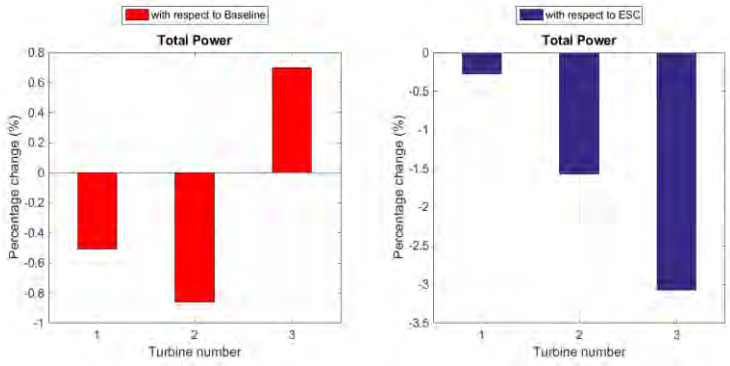

Figure 6. Percentage change of total power with respect to the baseline controller and the ESC using additive penalty based ESC load feedback.

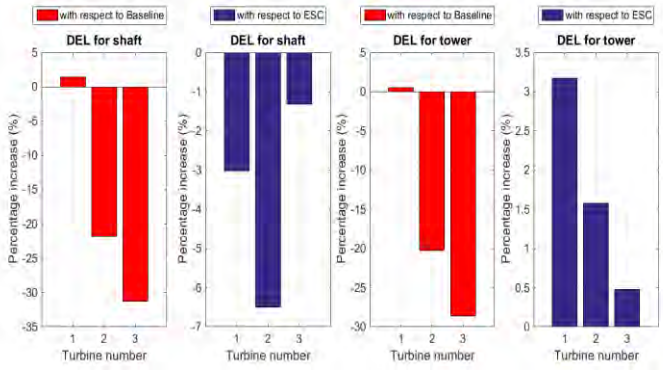

Figure 7. Percentage change of damage equivalent loads for the shaft and the tower with respect to the baseline controller and the multiplicative ESC.

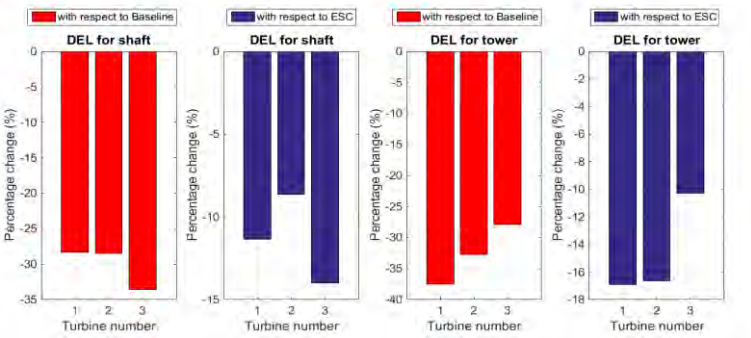

Figure 8. Percentage change of mean value of moments for the shaft and the tower with respect to the baseline controller and the multiplicative ESC.

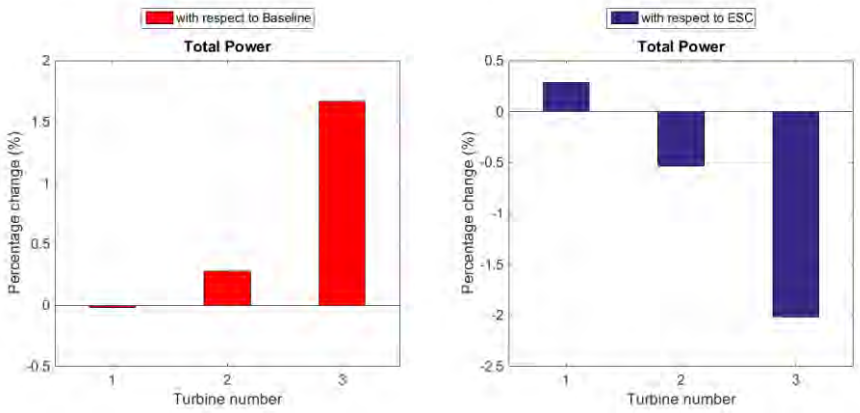

Figure 9. Percentage change of damage equivalent loads for the shaft and the tower with respect to the baseline controller and the multiplicative ESC.

It can also be seen in Fig. 9 that the power generated by the multiplicative penalty based NESC power and load optimization strategy (though lower than the ESC without load reduction) is still higher than that of the baseline controller.

It is worth to mention that the results obtained in this research can be changed to any desired level of loads or power output optimization. This can be achieved by playing with the weight factors ω_1 and ω_2.

Therefore, it is possible to either have a single objective structural loads optimization only, a single object power output optimization only or a multiobjective power output and loads optimization. Thus, the results presented in this research are only indicative of how the algorithm could be implemented, and in general any other combination of loads and power output optimization is possible.

IV. CONCLUSION

Based on the results, we can observe that the utilization of NESC to maximize the power output increases the structural loads as an adverse effect. Formulating the problem as a multiobjective optimization study by introducing of the loads as a penalty function decreases the intensity of the loads while still increasing the power output. Although, in the multiobjective case the power output is on average lower than only optimizing for power using NESC, it comes up to 30%

decrease in the loads experienced by the turbine.

Further, we compared the performance of two different types of load feedback and found that the multiplicative penalty based load feedback is simpler to incorporate and is capable of maintaining a balance between the baseline controller and the NESC.

REFERENCES

[1] A.Verbruggen, M.Fischedick, W.Moomaw, T.Weir, A.Nada, L.J.Nilsson, J.Nyboer, and J.Sathaye, "Renewable energy costs, potentials, barriers: Conceptual issues," Energy Policy, vol. 38, no. 2, 2010, pp. 850-861.

[2] T. Ashuri, M.B.Zaaijer, J.R.Martins, and J.Zhang, "Multidisciplinary design optimization of large wind turbines – technical, economic, and design challenges," Energy conversion and Management, vol. 123, 2016, pp.56-70.

[3] P.Menanteau, D.Finon, and M.L.Lamy, "Prices versus quantities: choosing policies for promoting the development of renewable energy,", Energy policy, vol. 31, no.8, 2013, pp.799-812.

[4] P.Söderholm, and G.Klaassen, "Wind power in Europe: A Simultaneous innovation-diffusion model," Environmental and resource economics, vol. 36, no.2, 2007, pp.163-190.

[5] T. Ashuri, J.R.Martins, M.B.Zaaijer, G.A.Kuik, and G.JW. Bussel, "Aeroservoelastic design definition of a 20 mw common research wind turbine model," Wind Energy, vol. 19, no.11, 2016, pp. 2071-2087.

[6] W. Xudong, W.Z.Shen, W.J.Zhu, J.N.Sorensen, and C.Jin, "Shape optimization of wind turbine blades," Wind Energy, vol. 12, no.8, 2009, pp. 781-803.

[7] G.Sieros, P.Chaviaropoulos, J.D.Sorensen, B.H.Bulder, and P.Jamieson, "Upscaling wind turbines: theoretical and practical aspects and their impact on the cost of energy," Wind Energy, vol. 15, no.1, 2012, pp.3-17.

[8] P.C.Capponi, T.Ashuri, G.J.W. van Bussel, and B.Kallesøe, "A non-linear upscaling approach for wind turbines blades based on stresses", European Wind Energy Conference and Exhibition, Brussels, Belgium, 2011, pp.1-8.

[9] A.Kusiak, and Z.Song, "Design of wind farm layout for maximum wind energy capture," Renewable Energy, vol. 35, no.3, 2010, pp.685-694.

[10] Z.Chen, J.M.Guerrero, and F.Blaabjerg, "A review of the state of the art of power electronics for wind turbines," IEEE Transactions on Power Electronics, vol. 24, no.8, 2009, pp.1859-1875.

[11] T.Ashuri, Beyond classical upscaling: integrated aeroservoelastic design and optimization of large offshore wind turbines. Delft University of Technology, the Netherlands, 2012.

[12] K.Z. Ostergaard, P.Brath, and J.Stoustrup, "Gain-scheduled linear quadratic control of wind turbines operating at high wind speed", IEEE International Conference on Control Applications, 2007, pp.276-281.

[13] M.Soliman, O.P.Malik, D.T.Westwick, "Multiple model predictive control for wind turbines with doubly fed induction generators," IEEE Transactions on Sustainable Energy, vol. 2, no.3, 2011, pp.215-225.

[14] T.Bakka, H.R.Karimi, and S. Christiansen, "Linear parameter-varying modeling and control of an offshore wind turbine with constrained information," Control Theory & Applications, vol. 8, no.1, 2014, pp.22-29.

[15] M.Steinbuch, W.W. De Boer, O.H.Bosgra, S.A.W.M.Peters, and J.Ploeg, "Optimal control of wind power plants,", Journal of Wind Engineering and Industrial Aerodynamics, vol. 27, no. 1-3, 1988, pp. 237-246.

[16] J.R.Marden, S.D.Ruben, and L.Y.Pao, "A model-free approach to wind farm control using game theoretic methods," IEEE Transactions on Control Systems Technology, vol. 21, no.4, 2013, pp.1207-1214.

[17] P.M.O. Gebraad, & J.W. Van Wingerden, "Maximum powerpoint tracking control for wind farms," Wind Energy, vol. 18, no.13, 2015, pp.429-447.

[18] J.Creaby, Y.Li, and J.Seem, "Maximizing wind turbine energy capture using multivariable extremum seeking control," Wind Engineering, vol. 33, no.4, 2009, pp.361-387.

[19] T. Hawkings, W.N.White, G.Hu, and F.D.Sahneh, "Region ii wind power capture maximization using robust control and estimation with alternating gradient search", IEEE American Control Conference, 2011, pp.2695-2700.

[20] Z.Yang, Y.Li, and J.E.Seem, "Maximizing wind firm energy capture via nested-loop extremum seeking control", ASME Dynamic Systems and Control Conference, 2013, pp. V003T49A005-V003T49A005.

[21] M.Soleimanzadeh, and R.Wisniewski, "Controller design for a wind farm, considering both power and load aspects," Mechatronics, vol. 21, no.4, 2011, pp.720-727.

[22] M.Kristalny, and D.Madjidian, "Decentralized feedforward control of wind farms: prospects and open problems," 50th IEEE Conference on Decision and Control and European Control Conference, 2011, pp.3464-3469.

[23] V.Spudic, M.Jelavic, M.Baotic, and N.Peric, "Hierarchical wind farm control for power/load optimization", The Science of Making Torque from Wind (Torque2010), 2010.

[24] M.T.van Dijk, J.W. van Wingerden, T.Ashuri, and Y.Li, "Wind farm multiobjective wake redirection for optimizing power production and loads," Energy, vol. 121, 2017, pp.561-569.

[25] T.Ashuri, M.Rotea, Y.Xiao, Y.Li, and C.V.Ponnurangam, "Wind turbine performance decline and its mitigation via extremum seeking controls", AIAA Science and Technology Forum and Exposition (SciTech), Wind Energy Symposium, San Diego, California, 2016, pp.1-11.

[26] T.Ashuri, E.V.Mayen, and R.Hamidi, "A new statistical approach to enchance the performance of model-free optimal controls algorithms", 2018 Multidisciplinary Analysis and Optimization Conference, pp. 3421, 2018.

[27] M.T. van Dijk, J.W. van Wingerden, T.Ashuri, Y.Li, and M.A.Rotea, "Yaw-misalignment and its impact on wind turbine loads and wind farm power output," Journal of Physics: Conference Series, vol. 753, 2016, pp.062013.

[28] J.D.Grunnet, M.Soltani, T.Knudsen, M.Kragelund, and T.Bak, "Aeolus toolbox for dynamics wind farm model, simulation and control", European Wind Energy Conference and Exhibition, 2010, pp. 3119-3129.

[29] J.Jonkman, S.Butterfield, W.Musial, and G.Scott, Definition of a 5-mw reference wind turbine for offshore system development. Technical Report No. NREL/TP-500-38060, National Renewable Energy Laboratory, Golden, CO, 2009.

[30] G.P.Corten, P.Schaak, and E.T.G. Bot, "More power and less loads in wind farms: 'Heat and flux'", European Wind Energy Conference and Exhibition, London, UK, 2004, pp.1-10.

[31] O.Yeniay, "Penalty function methods for constrained optimization with genetic algorithms," Mathematical and Computational Applications, vol. 10, no.1, 2005, pp.45-56.

Application of Multi-criteria Decision-making Methods in Energy Research - a Review

Petar Vranić[1], Ivana Veličkovska[2]

[1,2]Mathematical Institute SASA, Belgrade, Serbia, petarvvv@gmail.com; ivana.v.93@gmail.com

Abstract — **Multi-criteria decision making (MCDM) has been widely employed in different research domains that typically involve complex decision-making problems. Energy planning is one of the most challenging contemporary development domain. Building on previous studies, the objective of this paper is to review some characteristics of recent application of MCDM in energy research. 132 articles from the Scopus database, for period 2017-2018 were analyzed in respect to ten criteria. Besides the rising trend in application of MCDM it is shown that 1) the most used method is AHP, 2) the traditional form dominates, 3) MCDM are primarily used in evaluation studies, focusing on combined energy sources or solar energy, 4) hybrid approaches are employed more than individual methods, 5) most of the MCDM methods are applied in its original form, 6) the most researched spatial level is national, 7) top-ranked journal is Energy, and 8) most articles come from China.**

Keywords – multi-criteria decision making, energy research, review

I. INTRODUCTION

Ever-growing energy demand along with rising of digital society, climate change and diversification of energy sources brought about a number of new criteria that must be considered in the planning and design of energy systems. This adds complexity to decision analysis. Therefore, MCDM techniques became increasingly used in energy planning processes. In recent years, several authors conducted comprehensive reviews of the application of the MCDM approach in different areas of energy research [1] [2] [3]. In the following text, we briefly reflect on approaches used and key findings as a background of our study.

In their article *A review of multi-criteria decision making (MCDM) towards sustainable renewable energy development* authors analyzed the application of MCDM in energy research [1]. The article offers a detailed overview of selected MCDM methods. They analyzed following methods: Weighted Sum Method, Weighted Product method, AHP, MAUT, Goal Programming, TOPSIS, STEP, PROMETHEE, ELECTRE, and VIKOR focusing on their application in research on renewable energy sources (RES). The authors clustered mentioned methods into three main groups: Value measurement models, Goal, aspiration and reference level models and Outranking models. Each of the methods was analyzed with respect to the following criteria: area of application (e.g. optimization, energy planning, etc.), methodological steps, strength and weakness (e.g. computation complexity, sensitivity), software developed for calculation, objective (purpose of application), key performance indicators, study-type, energy scheme and geographical region. The study reveals significant diversity in terms of research problems, criteria used for evaluation and area of application. Moreover, they identified 24 softwares developed for MCDM. As they argue, no particular method can be ranked as the best or the worst. They highlighted the potential of using hybrid methods for overcoming the individual deficiencies of each method.

Another similar study *A review of multi-criteria decision-making applications to solve energy management problems: Two decades from 1995 to 2015*, focused among others on

energy, environmental, green, waste, land, management renewable and sustainable energies, economic energy and energy efficiency aspects. Among thirteen identified key application areas top two are environmental assessment and energy management [3]. They overview the distribution of published articles according to key application field and analysed each article in terms of the method applied, number of criteria used, research purpose, gap and contribution, solution and modeling, and achieved results. In line with suggestions from [1] their analysis shows that hybrid approaches have been used more extensively than other approaches. They are followed by AHP and TOPSIS method. In terms of the leading journal, the first rank was the journal *Renewable and Sustainable Energy Reviews,* followed by *Journal of Cleaner Production, Journal of Energy Policy* and *Journal of Operational Research*. In regard to geographical distribution, the most notable contribution was from Turkey. When it comes to trends, the authors argued that in different areas of energy management the use of MCDM techniques will increase.

In their article *A systematic review and meta-Analysis of SWARA and WASPAS methods: Theory and applications with recent fuzzy developments*, Mardani et al., (2017) reviewed methodologies and applications with recent fuzzy developments of two novel MCDM utility determining approaches 1) Step-wise Weight Assessment Ratio Analysis (SWARA) and 2) the Weighted Aggregated Sum Product Assessment (WASPAS) [2]. They analyzed the distribution of articles according to MCDM utility determining techniques considering WASPAS with fuzzy theory sets, interval type-2 fuzzy sets, single-valued neutrosophic set, with grey number and WASPAS based on interval-valued intuitionistic fuzzy numbers. This review is not particularly related to the application of MCDM in energy research, however, it does include energy aspects in some parts. For instance, looking at the application field review shows that construction management and manufacturing and operation management are ranked as first and second with significantly larger share comparing with sustainable and renewable energy which is in fourth place.

II. METHODOLOGY

Building on previous research, the objective of this paper is to review some characteristics of the recent application of MCDM in energy research. For the search of relevant literature, Elsevier Scopus database is considered. The time span was limited to articles published in the period 2017-2018. Search was performed using the following terms: *Energy* and *MCDM*. All articles that contained defined terms were considered for the first part of the analysis. In order to filter selected articles, each was analyzed by the authors. The articles that include the use of MCDM in a domain of practical or theoretical application in energy research were considered for further analysis. Articles that were marginally related to defined scope, or clearly irrelevant, were omitted from the analysis. Finally, 132 articles were selected for detail review according to criteria shown in Table I.

TABLE I. CRITERIA FOR ANALYSIS

MCDM approach	AHP MAUT TOPSIS ELECTRE	PROMETHEE VIKOR ANP WASPAS OTHER
MCDM methods	Traditional or crisp MCDM	Fuzzy and grey numbers MCDM
Research objective	Allocation Selection Optimization	Evaluation Planning Other
Type of energy according to a source	Solar Wind Hydro	Biogas Geothermal Nuclear Combined
Method applied	Individual	Hybrid
Innovation	Application Upgrade Development	
Calculation	Software used	
Spatial level	Reginal National County	City / municipality Local
Distribution of articles according to academic journals		
Distribution of articles according to study location		

III. FINDINGS

This paper considers period of only one and a half years, so any conclusion regarding the publishing trend should be seen as highly tentative. Nevertheless, out of 132 articles, 50.8% was published in 2017 while only during the first half of 2018 already 49.2% was published. Accordingly, and taking into account publication trend related to MCDM techniques in energy management field presented in [3], it is reasonable to expect that the number of articles published until the end of 2018 will exceed the

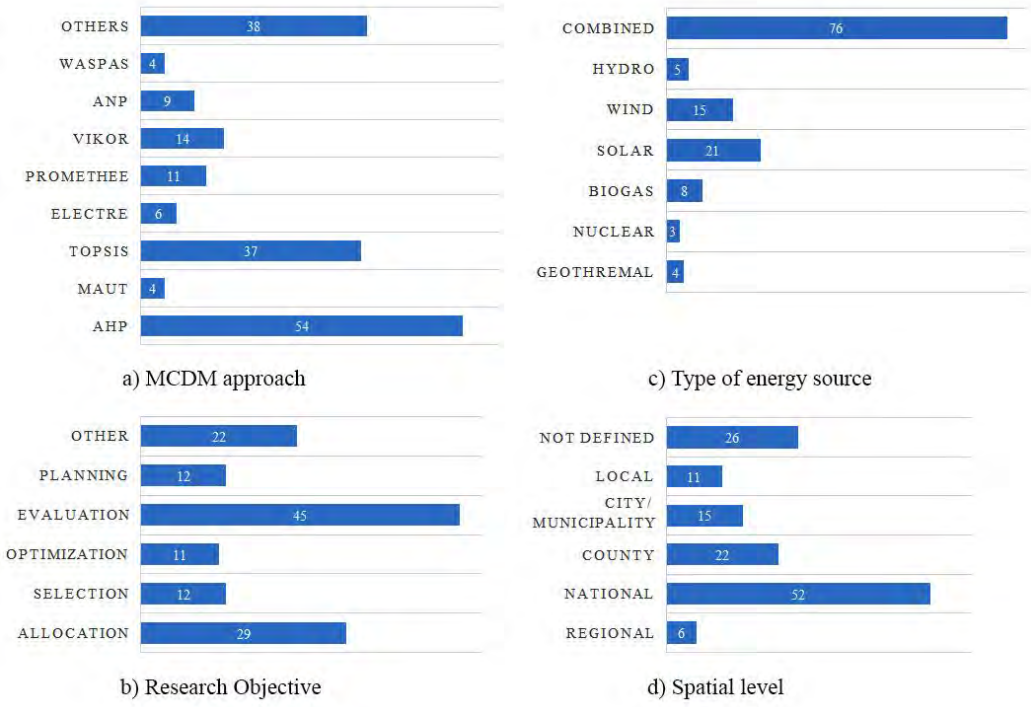

Figure 1. Findings a) MCDM approach, b) Research Objective, c) Type of energy source, d) Spatial level

number from 2017, and thus, confirm the rising trend.

MCDM approach. Although all the MCDM methods are present in energy research, AHP and TOPSIS contribute more than 50% of all analyzed articles (Figure 1a). In most of the analyzed articles, AHP was used for allocation or evaluation studies (e.g. port suitability assessment for developments in the offshore wind industry, development of fuzzy multi-criteria spatial decision support system for solar farm location planning, prioritization of smart grid technologies for the electricity infrastructure, etc.). On the other hand, TOPSIS was primarily employed for evaluation studies. Some examples include studies like the evaluation of RES using an integrated MCDM approach with linguistic interval fuzzy preference relations, or stakeholder-driven multi-attribute analysis for energy project selection under uncertainty. The second cluster includes VIKOR, PROMETHEE, and ANP with a cumulative share of 19.2%, while the least used methods are ELECTRE, MAUT and WASPAS (8%). A considerable number of articles (21.5%) employed methods other than commonly used one.

TABLE II. DISTRIBUTION OF ARTICLES BASED ON MCDM METHOD

MCDC approach	Crisp	Fuzzy
AHP	38	16
OTHER	23	15
TOPSIS	23	14
VIKOR	10	4
PROMETHEE	8	3
ANP	2	7
ELECTRE	3	3
MAUT	4	0
WASPAS	3	1

MCDM methods. In this paper, for the analysis of the distribution of articles based on MCDM methods, articles were classified into two groups: 1) articles that use MCDM in its traditional form (crisp form) and 2) articles that apply fuzzy sets and gray numbers. Results show the significantly broader application of MCDM in its crisp form (67.4%), while fuzzy approaches

(including gray numbers) contribute with 32.6%. The ratio is also reflected when looking at each method individually, except in case of ANP where five out of seven articles implemented a fuzzy approach and ELECTRE with the equal use of both approaches. The distribution of articles in this regard is shown in Table II.

Research objective. When it comes to the purpose of use, it appears that 34.4% of articles used MCDM methods for evaluation purposes i.e. the evaluation of the suitability of energy sources, technologies or so (Figure 1b). Some examples include sustainability ranking of energy storage technologies under uncertainties, risk evaluation of electric vehicle charging infrastructure public-private partnership projects using fuzzy TOPSIS, or integrated assessment of energy supply system of an energy-efficient house. Allocation studies contribute with 22.1%. They mostly relate to the selection of the appropriate sites for power plants (e.g. fuzzy score technique for the optimal location of wind turbines installations, fuzzy spatial decision tool for ranking suitable sites for allocation of bioenergy plants based on crop residue, etc.). They are followed by application of MCDM in researches related to planning, selection and optimization of energy systems (e.g. a multi-segment fuzzy goal programming approach for optimization of energy portfolios under uncertainty, identifying barriers to offshore wind power development using the grey DEMATEL approach, etc.). 16.8% belongs to researches with other than mentioned five objectives.

Type of energy according to a source. Looking at the distribution of articles according to energy sources results show that MCDM are used in research across all energy sources. Nevertheless, it appears that MCDM methods were used more in researches of solar and wind energy than other energy sources. Articles from this group cumulatively contribute 27.3% to a total number of the analyzed articles (Figure 1c). Some examples include application of intuitionistic fuzzy multi-criteria framework for large-scale rooftop PV project portfolio selection [4], or heuristic multi-objective multi-criteria demand response planning in a system with high penetration of wind power generators [5]. They are followed by research on biogas energy (6.1%), hydro energy (3.8%) and geothermal energy (3%). On the other hand, articles that applied MCDM methods for the exploration of challenges, evaluation, planning, optimization, etc., of combined energy source or deals with electrical, thermal or energy for transportation purposes, jointly contribute with 57.6% (e.g. investigation of the optimal location design of a hybrid wind-solar plant, evaluation of renewable power sources using a fuzzy MCDM based on cumulative prospect theory, application of extended TODIM-PROMETHEE method for waste-to-energy plant site selection, etc.).

Method applied. Similar to the type of energy sources, there is a slight prevalence of articles where hybrid MCDM methods (combination of two or more methods) are applied. Individual application counts for 43.9%, while hybrid methods have a share of 56.1%. We identified a considerable number different combinations. For instance, Wu et al., (2018) combine fuzzy ANP-VIKOR for site selection decision framework for large commercial rooftop PV system [6]. Asakereh et al., (2017) use GIS and Fuzzy-AHP method for the evaluation of the solar farms' location [7], while B et al., evaluate the performance of distributed and centralized biomass technologies integrating Entropy Weighting Method and PROMETHEE [8]. All identified combinations are shown in Table III.

TABLE III. HYBRID METHODS

FG-MCDM	TOPSIS, COPRAS, SAW
GIS-AHP	ANP
PFWG, PFNP VIKOR, PFS MABAC	TOPSIS, NLFP
CAB	Fuzzy, TOPSIS, AHP, LINMAP
ANP, DEMATEL	TIFN, AHP, PROMETHEE II
AHP	Fuzzy AHP, DEA
MAUT, RE3ASON	DEMATEL
AHP, LCA	Extended TOPSIS, LP
AHP, TOPSIS, LINMAP, Bellman-Zadeh fuzzy	Fuzzy TOPSIS
FUZZY, DEMATEL	GRASS, GIS
Fuzzy ANP, FGRA	Fuzzy AHP, GIS
TOPSIS, Linear programing graphical method	SAW
Stochastic programming	Fuzzy Score Method, Goal programming, SSAL-SAL
Optimization, LCA	Fuzzy AHP, ANFIS
TOPSIS, HFS, VIKOR	Fuzzy AHP, Fuzzy Goal programming
ELECTRE-based fuzzy MCGDM	PROMETHEE
IFAHP, CBD, IFTOPSIS	Interval TOPSIS, Fuzzy Best-Worst method
Entropy Weighting Method, VIKOR	TODIM, TIFN
AHP, ELECTRE III, optimization	AHP, Integrated Value Model for Sustainable Assessment
MS-FGP	WASPAS, TOPSIS, ARAS
LCA, AHP, COPRAS	AHP, TOPSIS

TIFN, Fuzzy ANP, Fuzzy VIKOR, Fuzzy TOPSIS, PROMETHEE II, ELECTRE III	VIKOR, IVHFS-DEMATEL
IT2HFE	AHP, VIKOR, Group Decision Making
IAHP, IFCODAS	MAUT, Mean-Variance Portfolio
FANP	Fuzzy AHP, Cumulative belief degree model (CBD)
Grey TOPSIS, MOGLP	Cloud weighted arithmetic averaging operator
Heuristic Multi-Objective MCDM	FAHP-TOPSIS, FAHP-VIKOR FAHP-ELECTRE,
TIFN, TODIM, PROMETHEE II	AHP, TOPSIS, PROMETHEE, MAUT
PROMETHEE, GIS	ANP, TOPSIS, DEMATEL, Linguistic Interval Fuzzy preference relations
MCDM, Goal Programming	FANP, FAHP, TOPSIS
TIFN	AHP, Particle Swarm Optimization
AHP, ELECTRE III, WSM, MAP-PAC, DEA	AHP, IOWA, DSM, Interval Linear programming, Bi-level Programming Method
AHP, TOPSIS, LCA	DEA
AHP, Range Based MAMCA, Monte Carlo	Multi-Criteria Analysis and Optimization, Multi attributes value theory
AHP, TOPSIS	Fuzzy TOPSIS
OWA, TODIM	Fuzzy TOPSIS, Fuzzy VIKOR
TOPSIS, Linear programing method	Fuzzy TOPSIS
Fuzzy Set Theory, AHP	AHP, Genetic Algorithm Optimization
AHP, CFD	WASPAS
MCDM method based on the Savage criterion	WASPAS, TOPSIS, ARAS, MADM
TOPSIS	DEMATEL
ASPID (Analysis and Synthesis of Parameters under Information Deficiency)	Fuzzy AHP, Fuzzy VIKOR, Entropy Method
Hierarchical Monte-Carlo multi-criteria assessment:, MCDA, social choice, and fallback bargaining	VIKOR, TOPSIS, PROMETHEE
HPFS, TOPSIS	TOPSIS, Grey Cumulative Prospect theory
AHP, MAUT, DEMATEL, ELECTRE, PROMETHEE, Borda ranking method	Fuzzy Logic, Fuzzy DEMATEL
Multi Criteria Analysis	Bayesian network
Best Worst Method	GIS, MCDA, DEMATEL, ANP, MABAC, VIKOR, TOPSIS, COPRAS
PROMETHEE, ANP, HFLTS	AHP, VIKOR, TOPSIS, GIS, OWA, OCRA
Interval number improved entropy weighting method	Fuzzy Vague Set Theory
	Hierarchical decision model

Innovation. Application of already developed MCDM significantly dominates with 80.2%. Only 11.5% of all selected articles offer an upgrade of existing methods. For instance Sun et al. suggest an innovative TOPSIS approach based on hesitant fuzzy correlation coefficient and its application in energy policy selection [6]. Mohsen and Fereshteh purpose extension of VIKOR method based on entropy measure for the failure model risk assessment in a geothermal power plant [7]. Articles that propose a novel MCDM in order to solve a particular energy issue contribute 8.4%. In their research, for example, Zhang et al., develop a new hybrid decision framework for prioritizing funding allocation in the energy sector [8].

Calculation. There is a number of softwares specialized for supporting MCDM calculation (e.g. 1000Minds, Decision Explorer, etc.). In their study Kumara et al., identified 23 commonly used for MCDM problems [1]. In analyzed articles, only 20% explicitly refer to particular software, while as much as 80% did not define it. Some of the listed examples include MATLAB, Super Decisions, Risk PALISADE, etc.

Spatial level. As shown in Figure 1d, a number of articles used MCDM in attempt to address energy issues (39.4%). At this level, MCDM are primarily used for prioritizing energy policy or strategy, and selecting, evaluating and allocating RES. The county, city/municipality, and local level have a joint share of 36.4%. A 19.7% relates to MCDM that does not have explicitly defined the spatial dimension. This cluster focuses on aspects such as the development of novel methods, comparison and evaluation of technologies, and the like, and doesn't necessarily deals with a particular territory.

TABLE IV. DISTRIBUTION OF ARTICLES ACCORDING TO ACADEMIC JOURNALS

Journal name	**Number of articles**	**%**
Energy	29	22.0
Journal of Cleaner Production	18	13.6
Renewable Energy	16	12.1
Applied Energy	8	6.1
Applied Thermal Engineering	2	1.5
Sustainable Cities and Society	6	4.5
Energy and Buildings	5	3.8
Solar energy	4	3.0

Applied Soft Computing	4	3.0
Sustainable Energy Technologies and Assessments	3	2.3
Energy Procedia	3	2.3
European Journal of Operational Research	2	1.5
Energy Strategy Reviews	2	1.5
International Journal of Hydrogen energy	2	1.5
Computers & Industrial Engineering	2	1.5
Geothermics	2	1.5
Procedia Engineering	2	1.5
Information Sciences	1	0.8
Journal of Air Transport Management	1	0.8
Energy Policy	1	0.8
Measurement	1	0.8
Journal of Building Engineering	1	0.8
Building and Environment	1	0.8
Technological Forecasting & Social Change	1	0.8
Applied Computing and Informatics	1	0.8
Sustainable Energy, Grids and Networks	1	0.8
Archives of Civil and Mechanical Engineering	1	0.8
Applied Geography	1	0.8
Future Generation Computer Systems	1	0.8
Applied Mathematical Modelling	1	0.8
Socio-Economic Planning Sciences	1	0.8
Research in Transportation Economics	1	0.8
Safety Science	1	0.8
Biomass and Bioenergy	1	0.8
Journal of Natural Gas Science and Engineering	1	0.8
Energy Economics	1	0.8
Transportation Research Part D	1	0.8
Ocean Engineering	1	0.8
Nuclear Engineering and Technology	1	0.8
Total	**132**	**100.0**

Distribution of articles according to academic journals. Based on the distribution of articles according to the journal, there is an apparent diversity of disciplines that deal with energy issues in the context of MCDM. During the analysis, articles from 40 refereed academic journals were identified (Table IV). Out of 132 articles, 53.8% are published in four journals as shown in Table 4, where all of them are from the field of energy research and with impact factor 4.9 and above, which confirms their academic influence. In this regard, the first four ranks among academic journals were *Energy, Journal of Cleaner Production, Renewable Energy,* and *Applied Energy*. Comparing with the findings of Mardani et al., [3], bearing in mind that review was restricted to application of MCDM for energy management issues, *Journal of Cleaner Production* appears to be the second ranked in both cases, while *Energy, Renewable Energy,* and *Applied Energy* are ranked as 9th, 10th, and 16th, respectively. In addition, as much as 20 out of 40 journals are from the research field other than energy (e.g. *Journal of Building Engineering, Sustainable Cities and Society, Safety Science*).

Distribution of articles according to study location. Geographical distribution of articles based on study location considers 39 countries, from all continents (Table 5.). However, only four countries nearly contribute 50% to all selected articles. The absolute leader in the application of MCDM in energy research for the observed period is China with 34 articles i.e. 25.8%. China is followed by Iran (12.9%), Turkey (7%) and India 4.5%. The remaining 35 countries jointly contribute with 46.2%. In reference [3] in regard to papers based on authors, China and Turkey have second and first ranks, while Iran and India have fifth and twelfth ranks.

TABLE V. DISTRIBUTION OF ARTICLES ACCORDING TO ACADEMIC JOURNALS

TABLE VI.

Country	Number of articles	%
China	34	25.8
Iran	17	12.9
Turkey	7	5.3
India	6	4.5
USA	5	3.8
Germany	5	3.8
Lithuania	4	3.0
Australia	3	2.3
Italy	3	2.3
France	3	2.3
Saudi Arabia	2	1.5
Korea	2	1.5
Great Britain	2	1.5

Nigeria	2	1.5
Portugal	2	1.5
Singapore	2	1.5
Serbia	2	1.5
Spain	2	1.5
Taiwan	2	1.5
Tanzania	1	0.8
Sri Lanka	1	0.8
Algeria	1	0.8
Canada	1	0.8
Chile	1	0.8
Colombia	1	0.8
Ecuador	1	0.8
Egypt	1	0.8
Ethiopia	1	0.8
Ireland	1	0.8
Jordan	1	0.8
Latvia	1	0.8
Lebanon	1	0.8
Malaysia	1	0.8
Mexico	1	0.8
Morocco	1	0.8
Nepal	1	0.8
Netherlands	1	0.8
Pakistan	1	0.8
Poland	1	0.8
Not defined	7	5.3
Total	**132**	**100.0**

IV. CONCLUDING REMARKS

This paper review some characteristics of the recent application of MCDM in energy research. It analyse 132 articles from forty academic journals for period 2017-2018. In line with previous research results confirms the rising trend in application of MCDM in energy research. Furthermore, the AHP is identified as the most used method, and it appears that the traditional form dominates over the fuzzy approaches. The evaluation of energy sources is recognized as the primary purpose of MCDM application. Significant number of studies focuses on combined energy sources or solar energy. Moreover, hybrid approaches are employed more than individual methods, and most of the MCDM methods are applied in its original form. The most researched spatial level is national while the top-ranked journal is *Energy*. China is first ranked when it comes to geographical distribution of articles.

This paper considers the period of only thirty-six months, which can be seen as one of the limitations of this approach. Besides, it focuses on articles published in English and analyze them in relation to eleven criteria. Therefore, deepening the structure of analysis, expanding the time-span and language choices can improve further reviews in this field.

ACKNOWLEDGMENT

This work is supported by the Ministry of Education, Science and Technological Development of the Republic of Serbia through Mathematical Institute of Serbian Academy of Sciences and Arts (Project III 044006).

REFERENCES

[1] A. Kumara, B. Sahb, A. R. Singhc, Y. Denga, X. He, P. Kumar / R. Bansald, „A review of multi criteria decision making (MCDM) towards sustainable,“ *Renewable and Sustainable Energy Reviews,* br. 69, p. 596–609, 2017.

[2] A. Mardani, M. Nilashib, N. Zakuan, N. Loganathan, S. Soheilirad, M. Z. Mat Saman / O. Ibrahim, „A systematic review and meta-Analysis of SWARA and WASPAS methods: Theory and applications with recent fuzzy developments,“ *Applied Soft Computing,* br. 57, pp. 265-292, 2017.

[3] A. Mardania, E. K. Zavadskas, Z. Khalifah, N. Zakuan, A. Jusoh, K. Md Nora / M. Khoshnoudic, „A review of multi-criteria decision-making applications to solve energy management problems: Two decades from 1995 to 2015,“ *Renewable and Sustainable Energy Reviews,* br. 71, p. 216–256, 2017.

[4] Y. Wu, C. Xu, Y. Ke / X. Sun, „An intuitionistic fuzzy multi-criteria framework for large-scale rooftop PV project portfolio selection: Case study in Zhejiang, China,“ *Energy,* t. 143, pp. 295-309, 2018.

[5] N. Hajibandeh, M. Shafie-khah, G. . J. Osório, J. Aghaei / J. P. Catalão, „A heuristic multi-objective multi-criteria demand response planning in a system with high penetration of wind power generators,“ *Applied Energy,* t. 212, pp. 721-732, 2018.

[6] Y. Wu, B. Zhang, C. Xu / L. Li, „Site selection decision framework using fuzzy ANP-VIKOR for large commercial rooftop PV system based on sustainability perspective,“ *Sustainable Cities and Society,* t. 40, pp. 454-470, 2018.

[7] A. Asakereh, M. Soleymani / M. J. Sheikhdavoodi, „A GIS-based Fuzzy-AHP method for the evaluation of solar farms locations: Case study in Khuzestan province, Iran,“ *Solar energy,* t. 155, pp. 342-353, 2017.

[8] W. Zhang, C. Wang, L. Zhang, Y. Xu, Y. Cui, Z. Lu / D. G. Street, „Evaluation of the performance of distributed and centralized biomass technologies in

rural China,“ *Renewable Energy,* t. 125, pp. 445-455, 2018.

[9] G. Sun, X. Guan, X. Yi / Z. Zhou, „An innovative TOPSIS approach based on hesitant fuzzy correlation coefficient and its applications,“ *Applied Soft Computing,* t. 68, pp. 249-267, 2018.

[10] O. Mohsen / N. Fereshteh, „An extended VIKOR method based on entropy measure for the failure model risk assessment - A case study of the geothermal power plant,“ *Safety Science,* t. 92, pp. 160-172, 2017.

[11] M. Alipour, S. Alighaleh, R. Hafezi / M. Omranievardi, „A new hybrid decision framework for prioritizing funding allocation to Iran's energy sector,“ *Energy,* t. 121, pp. 388-402, 2017.

Contribution of Renewable Energy Sources to Overall National Energy Security Policy

Žarko Vranjanac[1], Goran Janaćković[1], Dejan Vasović[1], Stevan Mušicki[2]

[1]University of Niš, Faculty of occupational safety in Niš, Niš, Serbia; [2]Ministry of Defense, Secondary Military School, Belgrade, Serbia; janackovic.goran@gmail.com

Abstract - **Energy is necessary for the functioning of every society. Although the development implies increasing energy efficiency, due to the increase in the number of inhabitants, introduction of various new technologies and development of automated industry, there is significant increase in energy needs. The lack of energy is therefore a threat to the security of every country. The use of renewable energy sources increases country energy independence. In this paper, the importance of application of renewable energy sources in Serbia in the context of its energy security policy has been considered.**

Keywords – renewable energy sources, energy security, energy policy, biofuels, Serbia

I. INTRODUCTION

Energy security of every country is important element of economic and political stability. When energy security is considered, the current position of country is analyzed, to assess dependencies on other countries in the field of energy production, and available energy production capacities and resources that one country has at its disposal [1].

Energy security means energy availability in sufficient quantity, at acceptable prices, with stable delivery, with physically secured energy facilities and critical infrastructure (oil pipelines, gas pipelines, electrical network) [2]. A critical energy infrastructure is of primary importance for delivering energy to final consumers (households, public companies and industry).

The problem of energy security is becoming more and more important, as world energy resources are limited, and their demand is growing with an increase in the number of inhabitants. Although new technologies are mostly energy-efficient, their introduction also increases energy consumption. Another significant problem is geographically uneven distribution of resource reserves and their consumption, as well as political character of relationships in the energy market.

II. ENERGY SECURITY ASSESSMENT – RISK DIMENSIONS AND APPLIED MODELS

Energy security and strength of a state are today most reflected in the quantity of oil, gas and water. However, in order to analyze energy security in more detail, it is necessary to introduce assessment models.

There are various aspects of risk considerations from the point of view of energy security. These aspects are usually grouped into four dimensions: political, economic, technical-energetic, and social. The characteristics of these dimensions are shown in Table I.

Although technical characteristics of energy systems, production methods, and available resources are the basis for social acceptability, political factors are of particular importance today. They affect implementation and realization of large transmission systems (oil pipelines, gas pipelines), availability of appropriate type of energy from a certain area, costs and final prices of delivered energy.

In order to obtain an adequate assessment of energy security, it is necessary to consider all previously mentioned dimensions. Table II provides an overview of various representative models for considering energy security [2,3,4].

ISBN: 978-86-80616-03-2

TABLE I. DIFFERENT ENERGY RISK DIMENSIONS

Dimensions	Description
Political	Effects of political, organizational or institutional factors that are local, external or international (institutional and organizational quality, rule of law, international influences and pressures, political instability)
Economical	Level of economic development, economic sustainability, industry characteristics, energy prices, trade properties, energy intensity
Technical-energetic	Available resources and energetic potential, location of available resources, market concentration, competitiveness of local producers, import dependence
Social	Social factors can initiate disturbance (problems in the labor market, inadequate salaries, inequality)

Most of presented models can be used for comparison of energy security of different countries, except US Energy security risk index.

TABLE II. REPRESENTATIVE MODELS OF ENERGY SECURITY AND THEIR MAIN PROPERTIES [2,3,4]

Model	Description
4 A's	Energy security is described by four aspects: availability (physical-geological), accessibility (technological-political), affordability (societal-environmental), acceptability (financial-organizational)
MOSES	Model of short-term energy security describing domestic and external risks and resilience
US Energy security risk index	37 indicators combined into 4 sub-indexes describing technological, environmental, economic, and geo-political security
EAPI	Global energy architecture performance index is score based on environmental sustainability, energy access/security, and economic growth/development
International energy security risk index	29 metric classified into 7 groups (global fuel, fuel import, energy expenditure, price and market volatility, energy use intensity, electric power sector, transportation, environmental effects) are used for energy security assessment

As shown in presented models, system approach is applied when considering energy security. The energy system is treated as an open system which is under influence of the environment, and which, when functioning, has certain performance. Identified risks are potential adverse events which can lead to decrease in energy system performance, and they are classified into groups, as shown in Table I. Higher risks lead to major potential problems in energy system, its functioning or the delivery of energy to end-users.

III. NATIONAL ENERGY SECURITY POLICY

National energy security policy defines set of laws, strategic documents, regulatory instruments, rules, and operative activities leading to achieving energy security for all country citizens. It defines organizational structure, roles and obligation schemes of all actors which enable the energy to be available to all final consumers, and to achieve sustainable growth. The elements of national energy security are presented in Table III.

TABLE III. ELEMENTS OF NATIONAL ENERGY SECURITY

Element	Description
Objectives	Definition of basics of energy security policy in the context of national security, rational use of resources and end users satisfaction; definition of stakeholders and their obligations
Strategies	Strategic frameworks for energy development, environmental impact assessment, definition of energy balances
Laws	Laws on energy and efficient use of energy
Action plans	Action plans for renewable sources, energy management systems and energy efficiency
Rulebooks	Determination of rules of behavior and function, minimal criteria for efficient functioning, system control and operation methods

Elements of national energy security are hierarchically organized, from basic goals and laws, to action plans and rules of working activities, from national level, to producers and end users of services. Such a complex system requires coordination of activities and collaboration of actors at different hierarchical levels to enable efficient functioning.

In order to increase energy security, it is necessary to make energy system more resistant to external influences (energy independence), increase diversification and decentralization, effectively use available resources and supplies, and to include diversification of energy sources. Therefore, especially significant sources of energy are renewable energy sources.

IV. SERBIA - NATIONAL ENERGY SECURITY AND USE OF RENEWABLE ENERGY SOURCES

Table IV presents basic energy indicators for Serbia during the period 2010-2017, where FE presents final energy, PE is primary energy [1,2]. The trend of increasing energy consumption can be evident as well as the stable percentage of households in consumption in the observed period.

TABLE IV. ENERGY INDICATORS FOR SERBIA [1,2]

	2010	**2011**	**2012**	**2013**	**2014**	**2015**	**2016**	**2017**
Transformation efficiency (FE/PE)	0.54	0.57	0.586	0.549	0.575	0.546	0.542	0.547
PE consumption (kg en/capita)	2048	2255	2017	2093	1853	2055	2129	2139
Electricity consumption (kWh/capita)	3802	3895	3774	3778	3634	3761	3752	3807
Household electricity consump. (%)	53	52	53	53	53	52	51	51

The following table presents the elements of Serbian national energy security policy [5,6,7,8]. Heavy dependence on imports of oil and gas caused the need to define specific national energy security policy. The main elements of the national energy security policy concerning energy sector development, energy security and use of renewable energy sources are presented in the following table.

TABLE V. MAIN ELEMENTS OF SERBIAN NATIONAL ENERGY SECURITY POLICY [5,6,7,8]

Element	**Corresponding document(s)**
Strategies	Energy Sector Development Strategy of the Republic of Serbia for the period by 2025 with projections by 2030 (Official Gazette of the Republic of Serbia, 101/2015)
	Strategic assessment of the impact of the Energy Development Strategy of the Republic of Serbia until 2025 with projections until 2030 on the environment
Laws	*Energy Law* (Official gazette of Republic of Serbia, 145/2014)
	Law on Efficient Use of Energy (Official Gazette of the Republic of Serbia, 25/2013)
Action plans	*National Action Plan for the use of Renewable Energy Sources* (NAPOIE) (Official Gazette of the Republic of Serbia, 53/2013)

A. Renewable energy sources in Serbia

The Action Plan of the Republic of Serbia for renewable energy sources in respect to obligations undertaken under the Energy Community Treaty defines activities to reach the target of 27% renewable energy sources in final energy consumption in 2020. According to the Directive 2006/32/EC of the European Parliament and the Council on the effective use of final energy, and previously presented energy indicators, Serbia has to achieve improvements in energy production and consumption. Until 2020 Serbia has to decrease final energy consumption for 10%, and increase the use of renewable energy sources other than hydropower potentials for 7% and biofuels in the transportation sector for 10%.

Biofuels are solid, liquid or gaseous fuels produced from biomass. Total quantity of available biomass in Serbia is approximately 12.5 million tons [8,9]. Implementation of the use of bio power plants in Serbia depends on regulations for development of bio-power plants, energy potential for biofuels, and positive environmental aspects.

The process of obtaining biodiesel is shown in Figure 1, and it consists of the following phases [10]: mixing the alcohol and the catalyst; transesterification reaction; separation; washing biodiesel; removal of alcohol; neutralization and glycerol removal; and determining the quality of the product. Most commonly, as raw material different types of vegetable oils (rapeseed, sunflower, soybean, palm, etc.) or their combinations can be used.

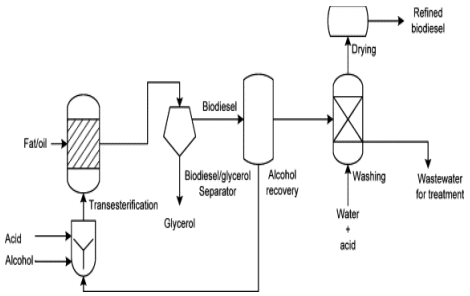

Figure 1. General scheme of the process of biodiesel production [10].

Main benefits of production and use of biofuels are waste reduction, pollution reduction, decreased dependence from imported fuels, and increased energy security [11]. The introduction of biofuels can significantly

improve the energy efficiency of transport and reduce its impact on air pollution.

B. *Serbian energy security*

Serbian energy security is described by the following models: EAPI, International energy security risk index, and Energy trilemma index. Overall scores and ranks, as well as scores and ranks for individual groups of indicators are presented in Table VI.

TABLE VI. SERBIAN ENERGY SECURITY ACCORDING TO REPRESENTATIVE MODELS

Model	Energy security
EAPI	Overall 2017 score: 0.59 (70/127) Economic growth and development: 0.50 Environmental sustainability: 0.54 Energy access and security: 0.73
International energy security risk index	Energy Security Risk Score 2016: 1,333 Risk Scores Relative to OECD Average Average Annual Difference 2006-16 48%
Energy trilemma index	Overall 2016 rank (balance): 73 (BBC) Energy security: 61 (B) Energy equity: 73 (B) Environmental sustainability: 89 (C)

According to all presented models, Serbia as developing country is in the middle of all analyzed countries in relation to energy security. Overall EAPI score of 0.59 puts Serbia into 70th place, while as the main problems economic growth and development indicators and sustainability are identified. Energy access and security received much higher grade (0.73).

International energy security risk index for Serbia in 2016 is 1,333. The risk is increased compared to 2015, and average annual difference of risk score compared relatively to OECD average for previous 10 years is just 48%, which means that the energy security risks for Serbia are approximately two times higher than in representative OECD countries.

However, overall rank in 2016 for Serbia according to energy trilemma index is 73, with BBC balance. Energy security and equity are at average level, but the main problem, according to this index, is environmental sustainability dimension.

V. CONCLUSION

The contribution of renewable energy sources to energy security is reflected in the reduction of import dependence, local character of energy sources, and reduction of pollution and preservation of non-renewable energy sources. Local character leads to diversification and decentralization of energy sources, as well as improvement of life in local communities by increasing the number of available jobs.

Based on applied energy security analysis methods, Serbia is a country with moderate risk. By increasing the use of available renewable energy sources and by increasing energy efficiency, this risk can be significantly reduced.

ACKNOWLEDGMENT

The research is part of projects III44006 and III42006, under the auspices of the Ministry of Education, Science and Technological Development, Republic of Serbia.

REFERENCES

[1] *Energy balance of the Republic of Serbia for 2017*, Official Gazette of the Republic of Serbia, No.110/2016.

[2] G. Janaćković, D. Vasović, J. Malenović Nikolić, Assessment of Energy Security based on Energy Indicators – a Serbian example, eNergetics 2016, September 22-23, 2016, pp. 47-53.

[3] *Global Energy Architecture Performance Index (EAPI) Report 2017*, World Economic Forum, Geneva, Switzerland.

[4] *International index of energy security risk: assessing risk in a global energy market – 2018 edition*, US Chamber of commerce, Washington, US.

[5] *Energy Law*, Official gazette of Republic of Serbia, No. 145/2014, December 2014.

[6] *Law on Efficient Use of Energy*, Official Gazette of the Republic of Serbia, No. 25/2013.

[7] *Energy Sector Development Strategy of the Republic of Serbia for the period by 2025 with projections by 2030*, Official Gazette of the Republic of Serbia, No. 101/2015.

[8] *National Action Plan for the use of Renewable Energy Sources* (NAPOIE), Official Gazette of the Republic of Serbia, No. 53/2013.

[9] M. Carić, D. Soleša, *Biomass as a renewable energy source and technology for the production of biogas*, Privredna akademija, Novi Sad, 2013.

[10] A. Demirbas, Biodiesel a realistic fuel alternative for diesel engines, Springer-Verlag London, 2008, pp. 24-103.

[11] R. Astbury, A review of the properties and hazards of some alternative fuels, Process safety and environmental protection, 2008, pp. 5-17.

Potential of Climate Change Mitigation Associated with the Utilization of Solar Thermal Energy in the Ice Cream Industry

Daniel de Paula Diniz[1], Monica Carvalho[2], Thiago Freire Melquiades[3], Luiz Moreira Coelho Junior[4]

Center of Alternative and Renewable Energy, Federal University of Paraíba, Brazil,
[1]danieldiniz@cear.ufpb.br, [2]monica@cear.ufpb.br,
[3]thiago.melquiades@cear.ufpb.br,[4]luiz@cear.ufpb.br

Abstract — **The negative environmental impact associated with the generation of thermal energy in the Brazilian industrial sector has become an increasing concern due to its contribution to global warming. The implementation of solar thermal energy, through flat collectors, has been studied to minimize negative environmental impacts. This can reduce atmospheric emissions associated with the installation and generation of thermal energy for use in industrial processes. The pasteurization process of ice cream was analysed herein, using the Life Cycle Assessment (LCA) methodology. SimaPro software v.8.5.0.0 was utilized, with the EcoInvent database. The environmental impact assessment method chosen was IPCC 2013 GWP 100y, which expresses the environmental impact in terms of kg CO_2-eq (carbon footprint). An ice cream factory located in João Pessoa (Northeast Brazil) was selected to represent the case study: the existing system (LPG burner) was compared with a solar thermal energy system. The carbon footprint of the existing system was 2172 kg CO_2-eq/year while the impact of the solar system (flat collectors) was only 117.9 kg CO_2-eq/year, demonstrating a reduction of 2054 kg CO_2- eq/year (-95%). These results highlight the introduction of solar thermal energy as an environmentally viable alternative.**

Keywords- Sustainability, Life Cycle Assessment, Carbon Footprint, Thermal Solar Energy, Pasteurization

I. INTRODUCTION

Concerns about excessive global warming due to anthropogenic activities have significantly increased interest in energy transition [1]. The carbon dioxide (CO_2) emissions generated by the combustion of fossil fuels are the main contributors to the global warming effect [2-4], and after analysis of various options and strategies, the progressive decarbonization of the global energy supply is crucial [1].

Energy decarbonization targets the use of low-carbon fuels or energy vectors to diversify the energy utility matrix, reduce dependence on fossil fuels, and mitigate climate change [5-7]. Energy decarbonization may include replacing fossil fuels with renewable energy.

In Brazil, environmental benefits were achieved as a consequence of the introduction of renewable energy generation (e.g., photovoltaic solar energy) in the Brazilian electricity mix [8]. According to [8], photovoltaic solar energy, despite being in full growth and providing consequent reductions in carbon emissions, is still inexpressive in the Brazilian energy matrix.

The use of solar thermal energy in industrial processes in Brazil still very timid compared to other countries in the world [9-11]. According to [12], the main sectors of the industry that require process heat are the food and beverage industry, especially dairy, processed meats and breweries. The favorable conditions are justified

ISBN: 978-86-80616-03-2

by the several production processes of the food industries that require high energy consumption and long execution time (e.g., cooking, bleaching, pasteurization and cleaning).

According to the Technical Office of Economic Studies of Banco do Nordeste, 28.7% of the industries installed in the Brazilian Northeast are food and beverage industries [13]. The large number of companies, approximately 23,000, and the high incidence of solar radiation in the region are a motivation to further investigate the introduction of solar technologies in this industrial sector. According to [10], the use of solar water heating in Brazilian industries is possible and represents an alternative that can contribute to the reduction of costs and energy consumption in 30% to 40% of low-temperature heating processes, especially in the food, beverage, textile and chemical sectors.

Another reason for the adoption of energy alternatives by the industry sector is the decrease in production costs, besides the concern of companies in making clear to the consumers that it is involved in sustainable causes and that sustainability is very important [14, 15]. The "six R's of sustainability" (Recycle, Rethink, Refuse, Reuse, Repair and Reduce) are steps for the planning of a new product or to improve one that already exists [16], and are directly related to the concept of Life Cycle Assessment (LCA).

In terms of sustainability, LCA is one of the most modern methodologies of strategic environmental management, as it provides important information to decision making. The LCA study has a holistic view on the chain of a product or service, indicating its environmental impacts from the extraction of the raw material to the post-consumption [17-18].

According to [19], global warming and the reduction of greenhouse gases (GHG) emissions are environmental priorities, and society is already beginning to demand products and processes with lower emissions [14-15]. Some countries already have carbon pricing mechanisms and Brazil has been studying the best economic approach to GHG emissions [20].

Recognizing the importance of climate change in the current global scenario, this work aims to estimate the potential of climate change mitigation associated with the use of solar thermal energy in the ice cream industries of the state of Paraíba, Northeast of Brazil. The LCA methodology is applied to the pasteurization process of an ice cream factory.

II. METODOLOGY

A. Number of industries in Paraiba

The Annual Report of the Brazilian Ministry of Labor Information [21] was consulted to obtain data on the number of ice cream industries in the Paraíba state (Northeast Brazil).

B. Life Cycle Assessment

LCA is a methodology for the quantification of environmental impacts throughout the life cycle of an activity, product or process, being internationally standardized by the International Organization for Standardization in its ISO 14040 [22] and 14044 [23] standards. In Brazil, these standards have been translated by the Brazilian Association of Technical Standards [24, 25].

LCA has four interrelated stages [22-23]: i) definition of the object and scope, where the boundaries of the analysis are defined; ii) inventory, which is a quantified survey of data regarding all inputs (materials, energy and resources) and outputs (products, by-products, emissions); iii) identification and evaluation in terms of potential impacts to the environment that can be associated with the data collected in the inventory, and finally iv) interpretation of results.

Software SimaPro [26] version 8.5.0.0 was utilized to develop the LCA, with EcoInvent database [27]. The environmental impact assessment method chosen was the IPCC 2013 GWP 100y [28], using the conversion factors published by the Intergovernmental Panel on Climate Change to convert GHG emissions into kilograms of carbon dioxide equivalent (kg CO_2-eq), also known as carbon footprint [19].

This case study focuses on a company manufacturing ice creams and other frozen novelties located in João Pessoa, Paraíba, Northeast Brazil. The process to be studied is pasteurization.

Pasteurization is a relatively mild heat treatment in which the food is heated below 100 °C for a specific period of time. In low-acid foods (e.g., milk) pasteurization is used to minimize possible health problems associated with pathogenic microorganisms and prolong

the shelf life for several days. In acidic foods (bottled juice) it is used to prolong the shelf life for several months by the destruction of deteriorating microorganisms (yeasts or molds) and/or enzymatic inactivation. In both types of foods, minimal changes in sensory characteristics or nutritional value occur [29].

In the case of ice cream, pasteurization will cause the destruction of pathogenic microorganisms thus increasing the shelf life of the product, and the binomial time/temperature can be as follows: 65 °C for 30 min; 71 °C for 10 min or 80 °C for 15 sec [29].

The current situation of the company, which uses Liquefied Petroleum Gas (LPG) in its pasteurization process, will be compared to an optimistic scenario in which the company uses solar thermal energy. Herein the processes studied included the manufacturing of each system (with corresponding lifetimes) and the consumption of energy resources necessary for the pasteurization process, per year.

C. *LPG Pasteurization*

The existing atmospheric burner consumes 6.41 kg/h of LPG. The useful volume of water for its operation is 185 liters, with annual losses considered null since it is a closed system. The pasteurization process occurs during 34 hours per month. Table I shows the material and energy flows associated with the existing LPG system.

TABLE I. -MATERIAL AND ENERGY COMPOSITION OF THE CURRENT LPG SYSTEM.

Process	Material/Energy composition
Atmospheric burner	5 kg tin-coated stainless steel, 10 kg fiberglass, 160 kg hot-rolled stainless steel
LPG combustion	71.522,68 MJ/kg LPG

The average efficiency of the burner was considered to be 75% [30]. After the end of its lifetime, the recyclable components of the equipment were recycled and the remainder was landfilled.

D. *Pasteurization with solar thermal energy*

For the optimistic scenario, solar collectors are used to convert the radiant energy to thermal energy, with a thermal reservoir that accumulates the hot water [31]. Table II shows the processes selected to compose the pasteurization process with solar collectors.

In the manufacturing process of the flat solar collectors, it was considered that the black copper coating was manufactured in the USA. After the lifetime (10 years), steel and iron were recycled, along with other recyclable materials. The remaining components of the equipment were landfilled.

TABLE II. MATERIAL COMPOSITION OF THE SOLAR COLLECTOR SYSTEM.

Process	Material
Hot water tank	47.04 kg aluminum, 33.84 kg copper, 109.32 kg solar glass, 49.68 kg stainless steel, 29.16 kg rock wool, 8.88 kg rubber
Flat solar collectors (12 m^2), installation and connections	19.98 kg glass wool, 2 kg PVC, 220 kg low-alloy hot-rolled steel, 40 kg stainless steel

III. RESULTS AND DISCUSSION

After the processes specified in Tables I and II were implemented in software Simapro [26] using the Ecoinvent database [27]. The IPCC 2013 GWP 100y [28] method was selected and the results are presented in Tables 3 and 4.

TABLE III -CARBON FOOTPRINT ASSOCIATED WITH THE LPG BURNER AND ITS OPERATION

Process	Annual Carbon Footprint
Atmospheric burner	86.0 kg CO_2-eq/year
Recycling Landfill	-34.3 kg CO_2-eq/year 0,3 kg CO_2-eq/year
LPG Combustion	2120 kg CO_2-eq/year
Total	2172 kg CO_2-eq/year

There is a considerable difference in the annual carbon footprint associated with the two systems: the use of solar thermal energy for the pasteurization process has approximately 95% less GHG emissions, resulting in avoided emissions of 2054 kg CO_2-eq/year.

TABLE IV. CARBON FOOTPRINT ASSOCIATED WITH THE SOLAR COLLECTOR SYSTEM.

Process	Annual Carbon Footprint
Hot Water Tank	85.8 kg CO_2-eq/year
Flat Plate Collectors	187 kg CO_2-eq/year
Recycling + Landfill	-161.2 kg CO_2-eq/year 6.3 kg CO_2-eq/year
Total	117.9 kg CO_2-eq/year

Figures 1 and 2 show the processes responsible for the higher shares of annual carbon footprints per system.

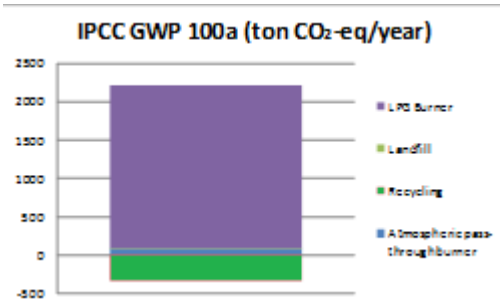

Figure 1. Composition of the annual carbon footprint for the LPG system.

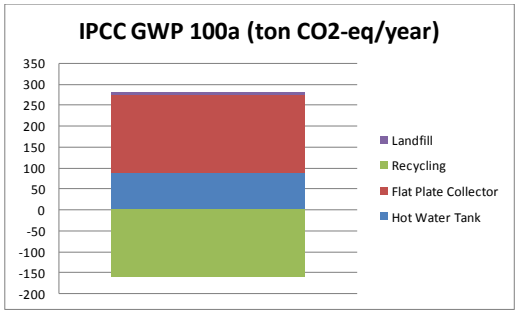

Figure 2.Composition of the annual carbon footprint for the flat collector system.

Considering the most recent data available, in Paraíba there are 58 industries manufacturing ice cream and frozen novelties, with 368 employees in total. 56.41% of the companies present between 1 and 4 employees, 17.95% between 5 and 9 employees, and 10.26% between 10 and 19 employees [21]. According to Resolution 267 of the Brazilian National Agency of Sanitary Surveillance [32], pasteurization is necessary for popsicles as well as for ice creams, and therefore the results herein obtained can be extrapolated. The avoided emissions of -2054 kg CO_2-eq/year can mean -119,132 kg CO_2-eq/year when considering only the pasteurization process in the manufacture of ice creams and frozen novelties in Paraíba.

An important feature of GHG emissions is that they have a global scope, i.e. the gases mix in the atmosphere regardless of political boundaries. Thus, the carbon market allows a country to acquire emission reductions generated in another country [33]. According to the Ministry of the Environment [33], there are clear environmental advantages in the carbon market, as well as the expansion of income and employment generation.

The carbon market can therefore be an important source of resources and incentive to invest in the introduction of renewable energy in industrial processes, without compromising the environmental quality of the environment. At the last auction of the sale of emission certificates on the São Paulo stock exchange in 2012, it was traded at € 3.30/tCO_2 [34].

The utilization of solar thermal energy in the food industry is not new: a solar collector was demonstrated with a cooling engine making ice cream at the Universal Exhibition in Paris, in 1878 [35]. However, environmental concerns and more stringent legal constraints have put renewable energy in the spotlight. [36] believes that solar energy should be given a chance even if the costs are currently not favorable; as oil reserves are depleted, oil prices should increase and thus solar systems could provide real economic benefits.

As shown herein, the Brazilian Northeast has great potential to utilize solar thermal energy to provide hot water to the food industry (at least at low temperatures). The Paraíba analysis, if extended to the remainder of the Northeast, is likely to conclude that flat collectors could provide sufficient thermal energy to meet the demands and requirements

of a considerable number of food industrial facilities.

IV. CONCLUSIONS

This article has developed a Life Cycle Assessment (LCA) for a thermal process (pasteurization) carried out in an ice cream industry located in João Pessoa - PB, focusing on greenhouse gas emissions (carbon footprint).The environmental impact associated with the pasteurization process was expressed in kg CO_2-eq/year.

A case study demonstrated the relevance of LCA when comparing the existing system for pasteurization, based on the burning of LPG, with a system based on solar thermal energy.

The carbon footprint associated with the existing system was ,172 kg CO_2-eq/year, while that of the solar thermal system was only 117.9 kg CO_2-eq/year. An approximately 95% reduction in GHG emissions was observed, resulting in -2054 kg CO_2-eq/year.

Future work by the authors include LCA of other thermal processes (cooking, bleaching and cleaning) within the different branches of the Brazilian food industry.

ACKNOWLEDGMENTS

The authors wish to thank the Brazilian National Council for Scientific and Technological Development (*Conselho Nacional de Desenvolvimento Científico e Tecnológico*, CNPq) for the productivity grant (303199/2015-6).

REFERENCES

[1] Smil, V. (2016). Examining energy transitions: a dozen insights based on performance. Energy Research & Social Science, No.22, pp.194-197.

[2] Houghton, J. T., Ding, Y. D. J. G., Griggs, D. J., Noguer, M., van der Linden, P. J., Dai, X., ... & Johnson, C. A. (2001). Climate change 2001: the scientific basis. The Press Syndicate of the University of Cambridge.

[3] Intergovernmental Panel on Climate Change – IPCC. (2007). Mitigation of climate change. Summary for Policymakers, Vol. 10.

[4] IPCC. (2015). Climate change 2014: mitigation of climate change (Vol. 3). Cambridge University Press.

[5] Smil, V. (2015). Proof of facts. Oil, Vol.8, No.30, pp.35-37.

[6] Smil, V. (2015). Energy transitions, renewables and rational energy use: A reality check. Organisation for Economic Cooperation and Development. The OECD Observer, No. 36.

[7] Kahn, S. (2016). Paths of the offer and demand of energy throughout the 21st century. Boletim de Conjuntura, No.10, pp. 8-10.

[8] Carvalho, M., & Delgado, D. (2017). Potential of photovoltaic solar energy to reduce the carbon footprint of the Brazilian electricity matrix. LALCA-Revista Latino Americana em Avaliação do Ciclo de Vida, Vol.1 No.1, pp. 64-85.

[9] Mesquita, L. (2013). Opportunities for solar thermal energy in industrial applications. Ambiente energia online. Available at: <https://www.ambienteenergia.com.br/index.php/2013/05/oportunidades-para-energia-solar-termica-em-aplicacoes-industriais/22797>. Access 26 june 2018. 2018.

[10] Carreira Junior, E., Sacomano, J. B., & Mollo Neto, M. (2014). Solar Thermal Energy: Water Heating Innovation For Industrial Processes. Revista Brasileira de Engenharia de Biossistemas, Vol 8 No. 3, pp. 209-219.

[11] Barbosa, R. R., Carvalho, M. (2018) Design of a solar heating water system for industrial applications Engevista (UFF), v. 20, n. 2. 10.22409/engevista.v20i2.1093. [In Portuguese].

[12] Kalogirou, S. A. (2016) Solar Energy Engineering – Processes and Systems. Rio de Janeiro: Elsevier.

[13] Damasceno, W. S. (2014) Reporto n macroeconomy, industry and services. Banco do Nordeste, Fortaleza. n. 6. Ano VIII.

[14] Carvalho, M., Freire, R. S., & Brito, A. M. V. G. (2016). Promotion of sustainability by quantifying and reducing the carbon footprint: new practices for organizations. In Energy, Transportation and Global Warming. Springer, Cham. (pp. 61-72)

[15] Freire, R. et al. (2016) Perspectives on the Implementation of Climate Change Public Policies in Brazil. In: Energy, Transportation and Global Warming. Springer, Cham. pp. 13-20.

[16] Brazilian Institute of Information on Science and Technology – IBICT (2014). Sustainable development and Life Cycle Assessment. CNI, Brasília.

[17] Guinée, J.B. (ed) (2001) Life Cycle Assessment: An operational guide to the ISO Standards; LCA in Perspective; Guide; Operational Annex to Guide. Centre for Environmental Science, Leiden University, The Netherlands.

[18] Guinée, J.B. (2002) Handbook on life cycle assessment: operational guide to the ISO standards. Kluwer Academic Publishers, Boston.

[19] Weidema, B. P., Thrane, M., Christensen, P., Schmidt, J., & Løkke, S. (2008). Carbon footprint. Journal of industrial Ecology, Vol.12 No.1, pp.3-6.

[20] Nicolletti, M., & Lefévre, G. B. (2016). Carbon pricing in Brazil: perspectives and lernings from a cap-and-trade simulation. In: Climate change: the challenge of the century. Cadernos Adenauer 2/2016. Available at http://www.kas.de/wf/doc/20323-1442-5-30.pdf Available 26 june 2018.

[21] Brazilian Ministry of Work and Employment. (2014) Annual report on Social Information. Available at: < http://trabalho.gov.br/rais/ > Access 29 june 2018. [In Portuguese].

[22] ISO 14040. (2006) Environmental management - Life cycle assessment - Principles and framework. International Organization for Standardization (ISO), Genebra.

[23] ISO 14044. (2006) Environmental management - Life cycle assessment - Requirements and guidelines. International Organization for Standardization (ISO), Genebra.

[24] ABNT – Brazilian Association of Technical Standards (2014) NBR ISO 14040/2014 – Environmental management – Life cycle assessment: principles ans structure. Rio de Janeiro: ABNT.

[25] ABNT – Brazilian Association of Technical Standards (2014) NBR ISO 14044/2014 – Life cycle assessment: requirements and orientations. Rio de Janeiro: ABNT

[26] Préconsultants. Software SimaPro. (2018). Available at <http://www.pre.nl/simapro>. Access 26 june 2018.

[27] Ecoinvent. The ecoinvent data base 3.4. (2017). Available at <http://www.ecoinvent.org/>. Access 26 june 2018.

[28] IPCC. Revised supplementary methods and good practice guidance arising from the kyoto protocol. (2013). Available at <http://www.ipcc-nggip.iges.or.jp/public/kpsg/> Access 26 june 2018.

[29] Fellows, P.J. (2000) Food processing technology: Principles and practice, Cambridge: Woodhead Publishing.

[30] Lazzarin, R. M. (2012). Condensing boilers in buildings and plants refurbishment. Energy and Buildings, 47, 61-67.

[31] ABNT – Brazilian Association of Technical Standards (2008) NBR. 15569/2008: Direct system solar water heating system. Rio de Janeiro: ABNT.

[32] Brazilian National Agency of Sanitary Vigilance (ANVISA). (2003). Resolution RDC nº 267, of september 25, 2003. On the technical regulamentation of good manufacture practices for industrial facilities of frozen novelties and checklist of good manufacture practices for industrial facilities of frozen novelties. Brasília: ANVISA

[33] Brazilian Ministry of Environment. (2004). Countries and industries obtain carbon credits with CO2 reductions. Available at <http://www.brasil.gov.br/meio-ambiente/2014/05/paises-e-industrias-obtem-creditos-de-carbono-com-a-reducao-de-co2> Access 26 june 2018.

[34] BM&F Bovesta. (2012). Carbon credit auctions. São Paulo. Available at <http://www2.bmfbovespa.com.br/Consulta-Leiloes/leiloes-de-credito-de-carbono-login.aspx?idioma=pt-br>. Access 26 june 2018.

[35] El-Sharkawi, M. A. (2004). Electric energy: an introduction. CRC press.

[36] Kalogirou, S. (2001). The potential of solar energy in food-industry process heat applications. Proceedings of the 25 th National Renewable Energy Convection NREC'2001, Energy Security for India: Role for Renewables, 123-132.

Exergetic Pinch Evaluation of a Steam Power Plant Heat Exchanger Network

Howard O. Njoku[1], Linus C. Egbuhuzor[2] , Mkpamdi N. Eke[3], Samuel O. Enibe[4]

[1]Department of Mechanical Engineering, University of Nigeria, Nsukka, Nigeria, Howard.njoku@unn.edu.ng
[2]Egbin Power Plc, Ijede Lagos state, Nigeria, Chinwendu.egbuhuzor@egbin-power.com
[3]Department of Mechanical Engineering, University of Nigeria, Nsukka, Nigeria, mkpamdi.eke@unn.edu.ng
[4]Department of Mechanical Engineering, University of Nigeria, Nsukka, Nigeria, samuel.enibe@unn.edu.ng

Abstract — **In this paper, a steam power plant's heat exchanger network (HEN) is analyzed, using the pinch, exergy, and combined pinch and exergy methodologies, in order to evaluate its performance under design and operational conditions. The pinch analysis show that, under current operational conditions, the minimum hot utility requirement was 539,491kW at a temperature of 549°C, which is 30,618kW (6.02%) more than the design minimum hot utility requirement (508873.7kW), and the optimum minimum temperature difference between hot and cold streams (ΔT min) in the HEN is 12°C. Results from standard exergy analysis showed that heaters 5, 2 and deaerator performance improved while the other components experienced decrease in exergetic efficiencies. Though the boiler had the highest avoidable and inevitable exergy losses ($\dot{E}L_{AVO}$ and $\dot{E}x_{INE}$) respectively, Heater 3 showed the most potential for performance improvement with (158.04%). Followed by Heater 6 (54.7%), the deaerator (15.15%), the condenser (13.55%), and Heater 1 (12.62%) when we consider $\frac{\dot{E}L_{AVO}}{\dot{E}x_{INE}}$. A combined pinch and exergy analysis (CPEA) gave similar outcomes, and showed further that changes in cold stream properties majorly led to performance declines observed. For improved plant performance, the exergy losses identified in the HEN should be reduce beginning from the cold streams.**

Keywords - pinch analysis, heat exchanger network, exergy analysis, combined pinch-exergy analysis, steam power plant

I. INTRODUCTION

Energy and its exploitation, harnessing and uses are major factors determining the industrial development and economic growth of nations. The expansion of the electrical infrastructure, as well as the rapid growth of population has made electrical energy a major part of our life today. Steam Power Plants (SPPs) are popularly used, in particular, in countries where natural gas or coal is sufficiently available for electricity generation. Privatization and Deregulation are requiring power companies to operate their facilities and equipment more efficiently and cost-effectively. In addition, Power generation companies are looking for ways to do what was once perceived impossible which is complying with stricter environmental regulations while operating profitable, reliable, more productive plants. [1].

A lot of recoverable energy is lost in the form of heat in these heat exchanger networks and any effort to recover or minimize these heat losses will increase the overall plant efficiency. To further improve the thermal efficiency of the plant cycle, current SPPs have become more complex [2]. Previous researchers have investigated the impact of the efficiency of the Rankine cycle by varying cycle parameters such as the turbine inlet pressure, inlet temperature, reheat pressure and temperature, extraction pressure, and condenser pressure, in order to improve plant efficiency, [3].

ISBN: 978-86-80616-03-2

Assessment tools which have been used for evaluating SPPs include those based on the exergy and pinch methodologies. Pinch analysis is a powerful tool used in determining and minimizing the minimum heating and cooling requirements of heat exchanger networks whereas exergy analysis has proven to be effective in providing solution for improving the efficiencies of processes. In order to take advantage of the strength of both, Combining pinch and exergy analysis and applying it to HEN of the steam power plant has been proposed.

II. BACKGROUND

Pinch analysis is a method used for minimizing the energy consumption of process plants by calculating thermodynamically, the required minimum energy consumption and achieving them by optimizing heat recovery systems and process operating conditions. Linnhoff[4,5] developed the pinch analysis methodology and suggested that the most important steps to minimize energy requirements of a process is not (i) to transfer the heat across the pinch (ii) to cold utility above the pinch, and (iii) to use hot utility below the pinch. They state that any violation in these steps increases the actual energy consumption in a plant. The pinch point is the most constrained point in the design of a heat exchanger network. It refers to the location of closest temperature approach between hot and cold streams in the HEN, where a stream is any flow which requires heating or cooling but doesn't change in composition.

[6] presented a novel approach for increase in efficiency in power plant, using pinch analysis. After the analysis of the plant using this new method, the fuel consumption was reduced and the plant efficiency was improved by 2%. [7] at the University of Valladolid, Spain, developed The stand-alone software, HINT, that integrates the main features of the pinch methodology into a simple, intuitive and user-friendly tool. Though designed for educational use, the tool nevertheless has found research application in studies involving the pinch analysis of HENs [8, 9]. [10] developed a computer program which is related to pinch technology application in steam power plants, to obtain a higher efficiency. By the analysis performed, the cycle efficiency was increased and fuel consumption of the plant was reduced by closing pinch points. Although the method was simplified and good results were obtained, however computational load was increased in comparison to the earlier works.

The Primary purpose of an exergy analysis is generally to identify the location, sources and magnitudes of true thermodynamic inefficiencies in a system [11]. And to this end, numerous exergy studies of SPPs have been undertaken. [12] carried out an exergy analysis on the boiler of a cogeneration thermal power plant. Results obtained showed that in the boiler, the fraction of exergy destruction was 83.35% and as the load increased to the highest load capacity of the plant, the exergy destruction reduced. They concluded that as the load increased the first and second law efficiencies increase for the plant.

[13] analyzed the exergy performance of the different components of a 210MW thermal power plant. The results revealed that the exergy destructions were most in the intermediate pressure turbine. This revealed a potential for improving the efficiency of the plant but it was practically impossible because of the physical and economic constraints. [14] performed an exergy analysis of a 56MW thermal power plant Raipu, the result show that the ratio of the exergy destruction to total exergy destruction was found maximum at the boiler system (57%) followed by the turbine (33%) and the condenser(5.34%). The exergy efficiencies of the power plant was calculated to be 31.12% and they proposed that by introducing reheat the exergy destruction in the boiler can be reduced.

The lack of a formal procedure in using the result from an exergy analysis is simultaneously a weakness and strength of the method. It is strength because an exergy analysis can be conducted for every thermal system and an engineer can control the evaluation and optimization process by use of their intuition and creativity as opposed to a formal optimization method. On the other hand, with pinch analysis, complex system information can be represented using simple diagrams.

[15] combined PA and EA methods and represented it in graphical method called Exergy Composite Curves (ECCs) and Exergy Grand Composite Curves (EGCCs) based on Carnot factor. They further propose appropriate

placement of load, level and number of refrigeration cycles. [16] proposed the model for combining pinch and exergy analysis, which can represent a whole system, including individual units on one diagram which help to screen the promising modifications quickly for improving a base case design. To overcome limitation in both pinch and exergy analysis, they introduced a generic diagram called Ω-H diagram, where Ω indicates the energy level and H gives the amount of energy. They also introduce the concept of inevitable and avoidable exergy losses by using a combined-cycle power station to demonstrate the effectiveness of the new method.

[17] performed the combined pinch and exergy analysis corrected the temperature levels of an Olefin plant to minimize exergy loss in the network and to economically and efficiently reduce shaft work demand and energy consumption in the cycles. The results from the plant revealed that the power consumption could be reduced by 2553KW with a reasonable investment and payback period time.

The current study presents a cross-comparison of the methodologies of exergy analysis, pinch analysis, and the combined pinch and exergy analysis for evaluating HEN. The HEN of a 220 MW unit at the Egbin steam power plant, Lagos Nigeria was considered. The HEN components are separately analyzed as well as the heat transfer between the hot and cold streams in the HEN. The types of information derivable from the different methodologies are discussed, highlighting the usefulness of the exergy-based methodologies for fault diagnosis. The analysis presented is for processes involving only heat transfer, but not pressure and composition changes, because present CPEA graphical representations can only depict temperature-based processes.

III. ANALYSIS

A. Description of the plant Rankine cycle

The HEN of the Egbin thermal power plant is under consideration in this study. The plant is a self-contained dual fired (gas and oil) steam electric generating station. The plant comprises of six identical 220 MW steam turbine-generators giving a total installed capacity of 1320 MW. The process diagram of a typical unit is shown in Fig.1. Steam is generated in a boiler, which is the steam generator, and is directly sent to the high pressure (HP) turbine. At the exhaust of the HP turbine the steam is sent back to the steam generator for reheating. The reheated steam is sent to the intermediate pressure (IP) turbine. At the exhaust of the IP turbine, the steam is sent to the low pressure (LP) turbine. From the exhaust of the LP turbine the steam is sent to the condenser for condensation. Here cooling water is used to extract the thermal energy of the steam and cause its condensation. From the outlet of the condenser the condensate is pumped to the feedwater heaters as shown in Fig.1. Here the heat exchange will take place between the condensate and the steam extracted from the HP, IP and LP turbines, raising the temperature of the condensate. Finally the condensate at the exit of the last HP feedwater heater is sent to the steam generator for conversion to steam.

B. Pinch analysis

The first step in the pinch analysis is the extraction of data from the heat exchanger network flow sheet. Subsequent steps in the pinch methodology involve the creation of a problem table, the formation of a heat cascade from the problem table, the construction of composite curves (CC) and shifted composite curves (SCC) for the hot and cold steams, and

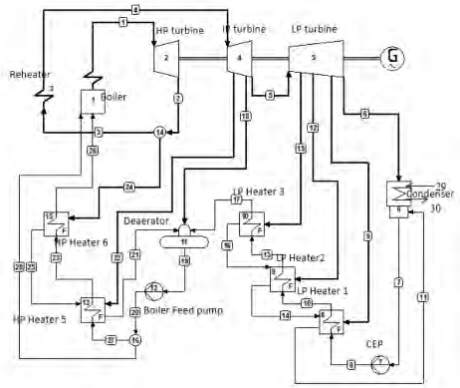

Figure 1. Schematic of case study plant showing hot and cold streams and their state numbers.

the construction of a grand composite curve (GCC). The CC, SCC and GCC are plots of the heat flow rates in streams against their temperatures. In the CC and SCC, the horizontal offset between cold stream and hot stream

curves, indicates the quantity of heat recovery that is possible between the streams at any given temperature. The point of closest approach (least horizontal offset) between the curves is known as the pinch point the GCC is obtained from the SCC by plotting the differences in the heat loads of hot and cold composite curves against their temperatures. Thus the GCC is a graphical depiction of the quantities of heating that can be provided by hot streams above the pinch point and the amount of cooling that can be achieved using cold streams below the point. At the pinch point, the cold curve touches the hot stream curve in the SCC, and hence the GCC touches the vertical (temperature) axis at the pinch point. Conceptually, this means that there can be no transfer of heat between hot and cold streams at the pinch point.

C. Exergy analysis

Exergy of a system at a certain thermodynamic state is the maximum amount of work that can be obtained when the system moves from that particular state to a state of equilibrium with the surrounding. A system is said to be at dead state when it is in equilibrium with its surrounding i.e. it has zero exergy. Disregarding kinetic and potential energy changes, the flow exergy of a fluid in a system at any cycle state is given by Eq. (2)

$$\dot{E}_x = \dot{m}\left[(h-h_0)-T_0(s-s_0)\right] \qquad (2)$$

Where $\dot{E}x$ is the flow exergy, $\dot{m}$ is the mass flowrate, h(kJ/kg) is the specific enthalpy, h_o is the specific enthalpy of the environment, T_o is the ambient temperature in Kelvin, s and s_o (kJ/kg˚K) are the entropies of the system and ambient condition. For a reversible system, the difference between the sum of exergies entering the component and the sum of exergies leaving the component is equal to the total exergy destruction within the system and exergy losses to surroundings. This exergy balance may be stated as

$$\sum \dot{E}x_{in} - \sum \dot{E}x_{out} = \dot{E}x_d + \dot{E}x_l \qquad (3)$$

Where $\sum \dot{E}x_{in}$ and $\sum \dot{E}x_{out}$ are the sum of exergies entering and leaving the system, $\dot{E}x_l$ the external losses is consider negligible. Exergy balances was done for the different HEN components shown in Fig.1. Each node was treated as a control volume and their respective properties corresponding to the state specified in Fig 1.

1) Feedwater heaters

The extracted steam from the HP, IP and LP turbines exchanges heat with the feedwater in the feedwater heaters (FWHs). The exergy balance for any FWH may be expressed as

$$\dot{E}x_{D,FWH} = \sum \dot{E}x_{in,FWH} - \sum \dot{E}x_{out,FWH} \qquad (4)$$

Where $\dot{E}x_{d,FWH}$ represents the rate of exergy destruction within the feedwater heater. $\sum \dot{E}x_{in,FWH}$ and $\sum \dot{E}x_{out,FWH}$ are the sum of the exergies entering and leaving the FWH respectively. The appropriate expressions for $\sum \dot{E}x_{in,FWH}$ and $\sum \dot{E}x_{out,FWH}$ for the FWHs are presented on second and third column in Table I, where the subscripts are the state points indicated in Fig 1.

TABLE I. APPROPRIATE EXPRESSIONS FOR OBTAINING THE TOTAL EXERGY INFLOWS AND OUTFLOWS, AND CHANGES IN COLD AND HOT STREAM EXERGIES OWING THROUGH THE FEEDWATER HEATERS

Feed water heater	$\dot{E}x_{in,FWH}$	$\dot{E}x_{out,FWH}$	$\Delta\dot{E}x_{,Cold}$	$\Delta\dot{E}x_{,Hot}$
Heater 1	$\dot{E}x_8 + \dot{E}x_9 + \dot{E}x_{14}$	$\dot{E}x_{10} + \dot{E}x_{11}$	$\dot{E}x_{10} - \dot{E}x_8$	$\dot{E}x_9 + \dot{E}x_{14} - \dot{E}x_{11}$
Heater 2	$\dot{E}x_{10} + \dot{E}x_{12} + \dot{E}x_{16}$	$\dot{E}x_{13} + \dot{E}x_{14}$	$\dot{E}x_{13} - \dot{E}x_{10}$	$\dot{E}x_{12} + \dot{E}x_{16} - \dot{E}x_{14}$
Heater 3	$\dot{E}x_{13} + \dot{E}x_{15}$	$\dot{E}x_{16} + \dot{E}x_{17}$	$\dot{E}x_{17} - \dot{E}x_{13}$	$\dot{E}x_{15} - \dot{E}x_{16}$
Heater 5	$\dot{E}x_{20} + \dot{E}x_{22} + \dot{E}x_{25}$	$\dot{E}x_{21} + \dot{E}x_{23}$	$\dot{E}x_{23} - \dot{E}x_{20}$	$\dot{E}x_{22} + \dot{E}x_{25} - \dot{E}x_{21}$
Heater 6	$\dot{E}x_{23} + \dot{E}x_{24}$	$\dot{E}x_{25} + \dot{E}x_{26}$	$\dot{E}x_{26} - \dot{E}x_{23}$	$\dot{E}x_{24} - \dot{E}x_{25}$

The exergetic efficiency, $\eta_{\varepsilon\mathrm{Hex}}$, of a heat exchanger is defined as the ratio of the exergy output to the exergy input in the heat exchanger given by Eq. (5).

$$\eta x_{Hex} = \frac{\Delta \dot{E}x_{l,Cold}}{\Delta \dot{E}x_{l,Hot}} = \frac{\left[\dot{E}x_{out} - \dot{E}x_{in}\right]_{Cold}}{\left[\dot{E}x_{in} - \dot{E}x_{out}\right]_{Hot}} \qquad (5)$$

The expression for $\Delta \dot{E}x_{,Cold}$ and $\Delta \dot{E}x_{,Hot}$ for the FWHs are presented in Table I.

2) Condenser

The surface condenser, which is a shell and tube heat exchanger, is used in the steam turbine plant, where the cooling water flows in the tube side and the steam for condensation on the shell side. The Exergy destruction in the condenser ($\dot{E}x_{l,Con}$) is expressed as

$$\dot{E}x_{l,con} = \sum \dot{E}x_{in,Con} - \sum \dot{E}x_{out,Con} \qquad (6)$$

Where the sum exergy into the condenser $\sum \dot{E}x_{in,Con} = \dot{E}x_{11} + \dot{E}x_{6} + \dot{E}x_{29}$ and the sum of stream exergies out of condenser $\sum \dot{E}x_{out,con} = \dot{E}x_{7} + \dot{E}x_{30}$. The exergetic efficiency of the condenser is given by Eq. (7)

$$\eta x_{Con} = \frac{\dot{E}x_{30} - \dot{E}x_{29}}{\dot{E}x_{11} + \dot{E}x_{6} - \dot{E}x_{7}} \qquad (7)$$

3) Deaerator

The deaerator is a contact type open heater for adiabatic mixing of hot streams and cold streams. The exergy destruction ($\dot{E}x_{l,\mathrm{Da}}$) in the deaerator can be calculated as follows;

$$\dot{E}x_{d,Da} = \sum \dot{E}x_{in,Da} - \sum \dot{E}x_{out,Da} \qquad (8)$$

Where the sum of stream exergies into and out of the condenser are $\sum \dot{E}x_{in,Da} = \dot{E}x_{17} + \dot{E}x_{18} + \dot{E}x_{21}$ and $\sum \dot{E}x_{out,Da} = \dot{E}x_{19}$ respectively. The exergetic efficiency of the deaerator is given by Eq. (9).

$$\eta x_{Da} = \frac{\dot{E}x_{19}}{\dot{E}x_{17} + \dot{E}x_{18} + \dot{E}x_{21}} \qquad (9)$$

4) Boiler

The boiler is a steam generator that converts the chemical energy of the fuel into heat energy and transfers it to the feedwater to generate steam. Assuming steady state conditions, the exergy destruction ($\dot{E}_{xl,B}$) in the boiler is expressed as

$$\dot{E}x_{d,B} = \sum \dot{E}x_{in,B} - \sum \dot{E}x_{in,B} + \dot{W}_{FDF} \qquad (10)$$

Where $\dot{W}_{FDF}$ is the shaft work of the Forced draft Fan (FDF), the sum of stream exergies into the boiler $\sum \dot{E}x_{in,B} = \dot{E}x_{in,Fuel} + \dot{E}x_{in,air} + \dot{E}x_{in,FW}$ is the sum of the exergy of the fuel and air supplied to the boiler and the exergy of the feedwater into the boiler, and $\sum \dot{E}x_{out,B} = \dot{E}x_{out,exhaust} + \dot{E}x_{out,FW}$ is the sum of the exergies of the boiler exhaust gases and outgoing feed water.

The exergy efficiency ηx_{Boiler} of the boiler is given by Eq. (11);

$$\eta x_{B} = \frac{\dot{E}x_{out,FW} - \dot{E}x_{in,FW}}{\dot{E}x_{in,Fuel} + \dot{E}x_{in,air} + \dot{W}_{FDF}} \qquad (11)$$

D. Inevitable and avoidable exergy losses

For a thermal process, there is no possibility to recover the full amount of a total exergy loss, since there is a minimum amount of exergy loss required to be the minimum driving force to operate the process at a desirable rate. Therefore, total exergy loss under operation conditions, ($\dot{E}x_{d,}$), maybe further divided into inevitable $\dot{E}x_{INE,}$) and avoidable exergy losses($\dot{E}x_{AVO,}$), [4]. Given by

$$\dot{E}L_{AVO} = \dot{E}x_{d} - \dot{E}x_{INE} \qquad (12)$$

Those exergy losses which cannot be avoided for a process to take place while considering both technical and economic constraints are defined as inevitable exergy losses [5]. These losses are determined by the minimum temperature difference between two streams exchanging heat. A process with smaller exergy losses than the inevitable losses will either not meet the requirement of a desirable production rate, or cannot be accomplished technically and economically. In this study, the exergy destruction under design conditions were used as inevitable losses. The avoidable Exergy loss ($\dot{E}\mathrm{L}_{\mathrm{AVO}}$) shows the practical improvements that can be affected in the processes and can be calculated by subtracting the inevitable exergy loss from the total operation exergy loss as

expressed by Eq. (12). Where T_o is the ambient temperature and T is the the hot or cold stream supply/target temperature. Then, η_c corresponds to the area between the CC and the enthalpy axis. Feng and Zhu [10].

E. Combined pinch and exergy analysis (CPEA)

The combine pinch and exergy analysis takes the advantages of the individual strength of pinch and exergy analysis and complex processes can be easily represented with diagrams which help to identifies promising modifications quickly. The Exergy composite curve (ECC) and the Exergy grand composite curve (EGCC) are the curves developed for (CPEA). The ECC and EGCC are produced by converting the temperature axis of Composite curves (CC) and Grand composite curves (GCC) to Carnot factor (η_c) which is expressed in Eq. (13)

$$\eta_c = 1 - \frac{T_0}{T} \tag{13}$$

IV. RESULT AND DISCUSSION

A. Data extraction

Table II and Table III shows the mass flow rates, ṁ, target temperature, T_{supply} and T_{target} and heat rate (ṁ ΔH) determined at MCR for the hot and cold streams respectively.

TABLE II. HOT STREAMS DATA AT MAXIMUM CONTINUOUS RATING FOR THE PLANT AT BASE (DESIGN) AND OPERATIONAL STATES

Stream No.	Description	ṁ (kg/h)	Design Conditions				Operational Conditions			
			T_{supply} (°C)	T_{target} (°C)	ΔH (kJ/kg)	ṁ ΔH (KW)	T_{supply} (°C)	T_{target} (°C)	ΔH (kJ/kg)	ṁ ΔH (KW)
9	Extraction steam into Heater 1	34739	105.7	51.7	2474	23873.41	110	56	2456.65	23705.99
11	Drain into Heater 1	79265	51.7	42.1	40.3	887.3276	56	43.3	53.09	1168.939
12	Extraction steam into heater 2	20953	180.1	94.7	2435.1	14172.96	210	95	2492.78	14508.67
14	Drain into heater 2	43285	94.7	51.7	180.1	2165.452	95	56	163.6	1967.063
15	Extraction steam into Heater 3	22332	257.1	118	2484.8	15414.04	269.5	118	2507.83	15556.91
16	Drain into Heater 3	22332	118	94.7	98.8	612.8893	118	95	97.27	603.3982
18	Extraction steam into Deaerator	22593	332.2	163	2438.8	15305.5	335.6	170	2411.44	15133.8
22	Extraction steam into heater 5	29942	437	171.5	2609	21699.63	456.6	190	2569.48	21370.94
21	Drain into Heater 5	80250	171.5	163	37.5	835.9375	190	170	88.35	1969.469
24	Extraction steam 6intoHeater	50308	352.2	202.6	2250.6	31450.88	350	205	2232.18	31193.48
25	Drain into Heate 6r	50308	202.6	171.5	138.7	1938.255	205	190	67.34	941.0391
40	Air through Exchanger	754900	350	145	247.24	51844.85	350	160	230.07	48244.4
6	LP Turbine Exhaust	459191	43.1	42.1	2221.6	283371.9	45.8	43.3	2210.75	281987.9
46	SSR to Condenser	1040	367.65	42.1	2982.2	861.5244	460	43.3	3018.36	871.9707
45	Gland Steam into condenser	950	367.65	42.1	2982.2	786.9694	460	43.3	3018.36	796.5117
47	SSR to HT 1 to condenser	1241	367.65	42.1	2982.2	1028.031	460	43.3	3018.36	1040.496
17	Ejector Steam into condenser	540	367.65	42.1	2982.2	447.33	460	43.3	3018.36	452.754

TABLE III. COLD STREAMS DATA AT MAXIMUM CONTINUOUS RATING FOR THE PLANT AT BASE (DESIGN) AND OPERATIONAL STATES

	Description	ṁ (kg/h)	Design Conditions				Operational Conditions			
			T supply (°C)	T target (°C)	Stream No.	Description	ṁ (kg/h)	T supply (°C)	T target (°C)	Stream No.
8	Feedwater through heater 1	540986	42.1	86.7	187	28101.22	43.3	90.5.00	187	14786.95
10	Feedwater through Heater 2	540986	86.7	110	98.4	14786.95	90.5	118	98.4	15433.13
13	Feedwater through Heater 3	540986	110	134.3	102.7	15433.13	118	140	102.7	21444.08
17	Feedwater through Deaerator	540986	134.3	165.5	142.7	21444.08	140	170	142.7	20362.11
27	Feedwater through Heater 5	627504	165.5	196.6	135.5	23618.55	170	210	135.5	31479.78
26	Feedwater through Heater 6	627504	196.6	236.6	180.6	31479.78	210	245	180.6	23177.56
28	Boiler Economiser	647504	236.6	264	132.97	23916.28	245	260	132.97	295439.9
32	Boiler Drum Water	647504	264	360	1642.59	295439.9	260	339	1642.59	86873.45
34	Boiler Primary Super Heater	647504	360	449	483	86873.45	339	430	483	46260.56
35	Boiler Reheater	579724	449	541	257.2	41418.06	358.7.00	538	257.2	70170.76
3	Boiler Secondary Superheater	647504	352.2	538	435.75	78374.96	430	543	435.75	44648.1
42	Air through Air Heater	776100	36	283	248.23	53514.25	40	260	248.235	6704.642

B. *Composite and grand composite curves*

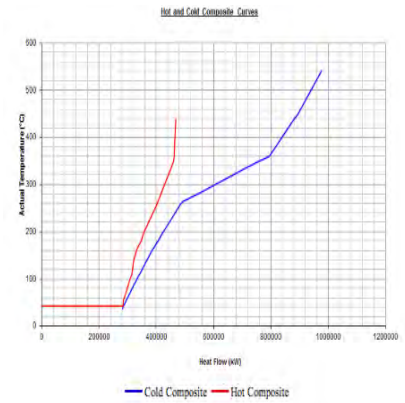

Figure 2. Composite curves for cold and hot streams in the HEN at conditions specified in plant design

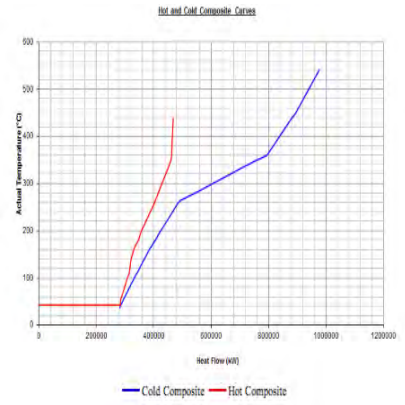

Figure 3. Composite curves for cold and hot streams in the HEN at conditions encountered in plant operation

Using the data shown in Table 2 and 3, the CC was constructed for the hot and cold streams and are shown in Fig. (2) and (3) respectively. Comparing the composite curves of the base and operation state Fig. (2) and (3), we see that the operational state have 539491KW minimum hot utility requirement which is 30618kW (6.02%) more than the design state. This is an indicating that a lot of energy is being lost in the heat exchange processes in the HEN under the

operational state while the minimum cold requirement for the operation state corresponds to that of the design state which is 282861kW. The Pinch point in the HEN occurred at 48.1˚C and 43.8˚C for the design and operational condition respectively.

The comparison of the GCCs of the plant under design and operational condition is shown in Fig 4; it is observed that the GCC under operation condition deviates from the design condition due to the energy losses occurring in the heat exchange processes. The figure also shows that a maximum heating utility of 538479kW is required at a temperature of 549°C for the operation condition while a maximum heating utility of 508873.7kW is required at temperature of 545°C for the design condition while the maximum cold utility of 282861kW at 37°C is required for both design and operation condition.

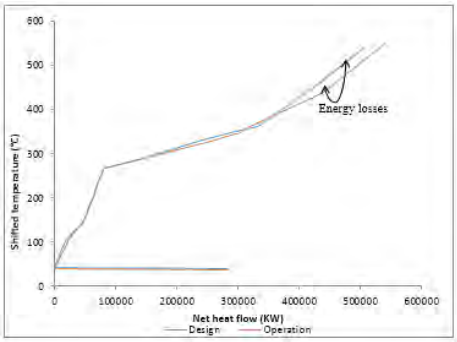

Figure 4. Grand composite curves for the HEN under plant design and operation condition

C. *Exergy performances*

All exergy computations were based on an ambient temperature of 30°C. By applying Eq.(3) – (11) and using data from the exergetic efficiencies for the feedwater heaters and other components of the HEN of the plant were determine for the design and operational conditions and compared as shown in Fig 5.

From the Fig. (5), it is observed that the exergetic efficiency of heaters 2 and 5 are improved while the rest recorded decline in their efficiencies when compared with the design conditions. The greatest exergetic efficiency reduction was observed from the heater 3 followed by the heater 6 and boiler. The results also show that the unavailability of either heaters

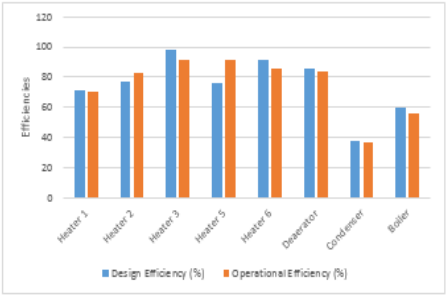

Figure 5. Exergy efficiencies of major HEN components under plant design and operation conditions

2 and 5 will greatly reduce the efficiency of the plant and also limit the load output from the generator.

Table IV and Fig. 5 breaks down the total exergy losses in HEN equipment into the unavoidable and avoidable exergy losses. The calculation of the avoidable exergy losses indicate that although the boiler incurs the biggest total exergy loss, which is 351500.29kW, the avoidable loss is only 49135.97kW (13.98%) of the total loss, while the heater 3 with a small total exergy loss of 230.82kW has a high proportion of avoidable exergy loss of 141.37kW. The heater 6 is the next equipment with the highest percentage of avoidable exergy loss of 634.48kW (35.58%). The potential for improvement in the condenser is very low because there is a limit to its vacuum pressure under operation.

TABLE IV. UNAVOIDABLE AND AVOIDABLE EQUIPMENT EXERGY LOSSES

Equipment	Unavoidable exergy loss	Avoidable exergy Loss	Total exergy Loss
Heater 1	1369.44	172.85	1542.29
Heater2	725.73	0	725.73
Heater 3	89.45	141.37	230.82
Heater 5	2214.7	0	2214.7
Heater 6	1159.01	634	1793.49
Deaerator	1288.94	195.32	1484.26
Condenser	12728.37	1724.98	14453.35
Boiler	302364.32	49135.97	351500.29

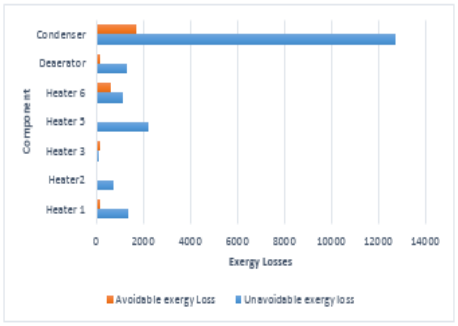

Figure 6. Inevitable and avoidable exergy losses of major HEN component

D. Exergy composite and grand composite curves

The area between the hot and cold exergy composite curves corresponds to the total exergy loss incurred during the processes of heat exchange. Calculating this area in Fig. 7 and 8, we obtained the total exergy loss in design as 496039kW and 572871.28kW for operation condition.

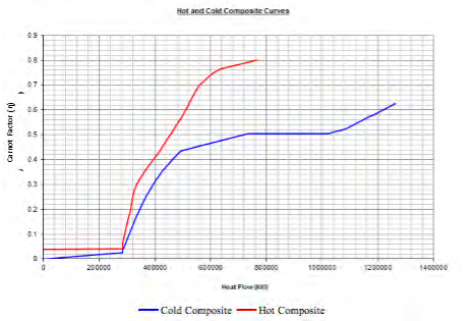

Figure 7. Exergy composite curves for cold and hot streams in the HEN at conditions specified in plant operation

Figure (9) and (10) shows the comparison of the exergy composite curves for cold and hot streams under design and operation conditions.

The curve for operation conditions is horizontally displaced to the right of the curve for design conditions for cold streams. This signifies increased heating requirements. The shift between the curves shows that in the operation of the plant, additional exergy destructions occur in the cold streams as the heat

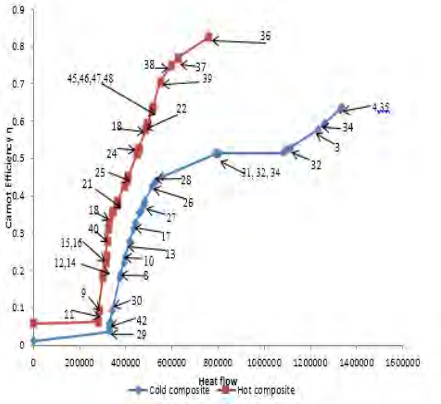

Figure 8. Exergy composite curves for cold and hot streams in the HEN at conditions encountered during plant operation

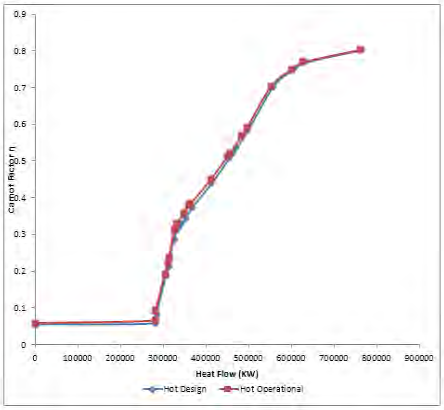

Figure 9. Inevitable and avoidable exergy losses of major HEN component

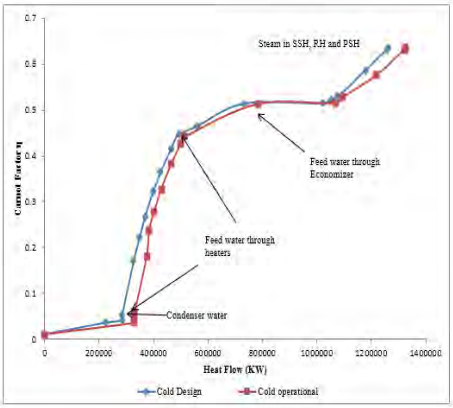

Figure 10. Exergy grand composite curves for the HEN under plant design and operation conditions

in the extraction steam is being transferred to the cold streams.

In addition, cold streams in the operating plant HEN are also at higher temperatures, shown by the slight upward shift in the operation curve relative to the design curve, especially in portions of the curves representing processes in the feedwater heaters. Consequently, less heat transfer will be achieved in the feedwater heaters due to the reduced temperature difference between the steam extractions and the feedwater. The temperature at the LP turbine exit will hence be higher, leading to greater energy losses as the steam condenses in the condenser.

V. CONCLUSIONS

Although with standard pinch analysis, global changes in utilities requirements of HEN can be determined, the actual HEN components responsible for the changes cannot be pinpointed. The standard exergy analysis provides this information, and in addition, provides a means of determining the magnitude of losses contributed by individual HEN components and the relative significance of the individual contributions to the overall changes in plant performance. The advantages of combining pinch and exergy analysis methodologies have been comparatively demonstrated in this study using a dual fired steam power plant and specific streams within which process deteriorations occur had further been identified.

REFERENCES

[1] Amir V., Sadegh V. (2011), Study of the thermal optimization in power plant. International Journal of Multidisplinary Science and Engineering, Vol 2, No 7, pp. 48-55.

[2] Ataei, A. (2009), Modification of Co-generation Plant in a Sugar Cane Factory for Reduction of Power Deficit. Res. J. Environ. Sci, Vol. 3, pp. 619- 630.

[3] Abtin Ataei, Changkyoo Yoo (2010), Combined pinch and exergy analysis for energy efficiency optimization in a steam power plant. Internal Journal of the Physical Sciences, Vol. 5 (7), pp. 1110 – 1123.

[4] Chao Z., Yan W. (2006). Exergy cost analysis of a coal-fired power plant based on structural theory of thermoeconomics. Energ. Convers Manage. Vol. 47, pp. 817-843.

[5] Hindmarch, Linnhoff (1998), Introduction to Pinch Technology. Targeting House Gadbrook Park, England.

[6] Sunasara S., Makadia J.J. (2014), Pinch analysis for plant: A novel approach for increase in efficiency. International Journal of Engineering Research and Technology, Vol 3. Issue 6, pp. 856-865.

[7] Angel Martin, F. A. Mato, Hint: An educational software for heat exchanger network design with the pinch method, Education for Chemical Engineers 3 (2008) e6{e14. doi:10.1016/j.ece.2007.08.001.

[8] Z. Mei-Ling, W. Wen, Seasonal energy utilization optimization in an enterprise, Energy 35 (9) (2010) 3932{3940.doi:https://doi.org/10.1016/j.energy.2010.06.019

[9] C. Oliveira, A. Cruz, C. Costa, Improving second generation bioethanol production in sugarcane biorefineries through energy integration, Applied Thermal Engineering 109 (2016) 819{827.doi:https://doi.org/10.1016/j.applthermaleng.2014.11.016.

[10] I. Dincer, M. A. Rosen, Exergy: energy, environment and sustainable development, Elsevier Science, Oxford, 2007

[11] Sarangj Gulhane, Amit Kumas (2013), Exergy analysis of boiler in cogeneration thermal power plant. American Journal of Engineering Research, Vol. 2, pp. 385-392.

[12] Nagan N, Satyanaranyana G. (2014), Exergy analysis of 210MW of Vijayawada thermal power station (V.T.P.S).International Journal of Latest Trends in Engineering and Technology, Vol 4, pp 84- 93.

[13] Sahil Suryvanshee, Alok Chaube, Sachin Kumar (2013), Exergy analysis of Raipur thermal power plant (India) A case study. International Journal of Engineering Sciences and Research Technology, Vol. 8, pp 2140-2147.

[14] Linnhoff B., Towsend D.W (1982), A User Guide on Process Integration for the Efficient Use of Energy. The Institution of Chemical Engineers, Rugby.

[15] Linnhoff B., Dhole V.R.(1992), Shaftwork targets for low-temperature process design, Chemical Engineering Science. Vol. 47, No 8, pp 2081-2091.

[16] Feng X. Zhu XX. (1997), Combining pinch and exergy analysis for process modifications. Appl. Therm. Eng., Vol. 17, pp. 250-260.

[17] Abtin Ataei (2011), Application of combined pinch and exergy analysis in Retrofit of an olefin plant for energy conservation. Scientific Research and Essays, Vol 6(12), pp 2437- 2446.

Water-Energy Nexus in Sustainable Development

Mara Tanasković[1], Ana Stanković[1], Ana Luković[1], Jelena Božilović[1]

[1]Research and Development Center "ALFATEC", Niš, Srbija, mara.tanaskovic@alfatec.rs, ana.stankovic@alfatec.rs, ana.lukovic@alfatec.rs, jelena.bozilovic@alfatec.rs

Abstract— **The paper explains the correlations and interdependencies between water and energy, consumption and production. The term of the nexus is introduced as an integrated approach in terms of sustainable resource management. The importance of the nexus is discussed in several locations that are facing safe water and/or energy deficiency.**

Keywords - water consumption, energy consumption, energy production, water energy nexus, sustainable development

I. INTRODUCTION

Humanity, with all attributes that it conveys affects the environment on many levels. Growing population on a global level is going to be demanding more food, energy and water in order to sustain its growth. To meet the growing demand for food, the farmers will need to increase production by 70-100%. Even today, there is a billion people suffering from hunger or malnutrition. According to the International Energy Agency (IEA) by 2030, world economy will demand a 40% increase in energy production. The need for energy production in developing countries is even higher, since it is estimated that 1.5 billion people lack access to electricity [2]. According to the Food and Agriculture Organization of the United Nations (UN FAO), water use has been growing globally at more than twice the rate of population increase in the last century, and an increasing number of regions are reaching the limit at which water services can be sustainably delivered. In order to fulfil those needs, humanity must address these issues accordingly.

The concept of nexus has been widely introduced at World Economic forum in 2008, when the economic development was perceived from the aspect of inter-linkages between water, energy, food and climate. There is no consensus on the definition of the nexus approach. UN FAO interprets the nexus as a way to systematically analyse the coupled human-nature system, as well as provide an integrated cross sectorial management of natural resources [1]. This paper will explore the correlation between water and energy as key nodes of the nexus.

II. ENERGY PRODUCTION

Electricity production is one of the drivers of modern economy. It is also one of the major water consumers in industry sector. In European Union (EU) as a whole, the energy sector accounts for 44 percent of total water consumption.

Water is crucial for many processes during the energy production; including removal of pollutants from power plants exhausts, generating the steam that turns the turbines, flushing away the residues of fossil fuels after the combustion is over, keeping the reactors cool. It is estimated that power plants withdrew nearly 550 km³ of water for cooling purposes in 2005, and out of that water 25 km³ is consumed by various processes. When the evaporation losses from the reservoirs used for hydropower generation are added, it is approximately a number of 75 km³ per year [4]. Electricity generation technologies have a wide range of water withdrawals and consumption rates, which are given in brief by Kyle et al. [3] in Table I, based on the data sources detailed by Davies et al. [4].

As it is shown in Table I, Enhanced Geothermal Systems (EGS) consume the biggest amount of water, 18.1 m³/ MWh. However, up to day deployment of EGS isn't very high; the amount it consumes is not considerable.

ISBN: 978-86-80616-03-2

TABLE I. ASSUMED WATER WITHDRAWAL AND CONSUMPTION INTENSITIES, BY ELECTRIC GENERATION TECHNOLOGY AND COOLING SYSTEM TYPE. 1-THRU: ONCE-THROUGH FLOW. EVP: EVAPORATIVE COOLING TOWER. POND: COOLING POND. HYBRID/DRY: HYBRID OR DRY. DATA SOURCES DETAILED IN DAVIES ET AL. [4]

Technology	Cooling system	Water withdrawals	Water consumption
Coal	1-thru	158	0.95
	Evp	3.8	2.6
	Pond	53.2	2.06
	1-thru w/CCS	241	1.25
	Evp w/CCS	4.83	3.57
Oil/Natural gas	1-thru	152	0.91
	Evp	4.55	3.13
	Pond	4.55	3.13
Other steam	1-thru	152	1.14
	Evp	3.32	2.09
	Pond	1.7	1.48
Nuclear	1-thru	193	1.02
	Evp	4.17	2.54
	Pond	30.7	2.31
Natural gas combined cycle	1-thru	49.5	0.38
	Evp	0.96	0.75
	Pond	25.9	0.91
	1-thru w/CCS	62.5	0.66
	Evp w/CCS	1.88	1.43
	Dry w/CCS	0.41	0.41
IGCC	1-thru	147	0.13
	Evp	1.48	1.41
	1-thru w/CCS	186	0.41
	Evp w/CCS	2.22	2.04
	Dry w/CCS	0.41	0.41
Geothermal (conventional)	Evp	6.82	6.82
	Hybrid/Dry	0.67	0.67
EGS	Evp	18.1	18.1
	Hybrid/Dry	3.2	3.2
CSP	Evp	3.35	3.35
	Hybrid/Dry	0.3	0.3
PV	n/a	0.02	0.02
Wind	n/a	0	0
Hydro	n/a	0	17

The second largest consumer of water is hydroelectric power generation, which amounts to 17 m³/ MWh used. Studies estimating water consumption by hydropower generation, account all evaporative water losses to the dam, even though most water reservoirs are for multipurpose use (water supply for irrigation, flooding control or recreation) [4].

A. Hydroelectric power and environment

Hydroelectric power or hydropower has been most widespread renewable electricity, producing around 17 % of world's electricity. In terms of carbon footprint, these types of installations have more than 4 times lower CO_2 or equivalent emissions considering non-renewable sources (coal power plant) [5]. Although hydropower generation is considered a highly valued alternative to fossil fuels, it has also other environmental impacts. The most frequently assessed are impacts to flora, fauna, landscape and remain [6]. The nature and severity of the impacts depends on many factors including the type of installation as well as the size of the installation and its location accordingly.

B. Types of hydropower installations

There are three types of hydropower facilities: impoundment, diversion, pumped storage and power plant in water distribution network.

Impoundment facilities or reservoir hydropower plants rely on stored water in the reservoir, and have low dependency on the variability of the inflows. Very large reservoirs can contain months or even years of average inflows. They also provide flood protection and irrigation services. Environmental impacts include methane production from decomposition of the flora and fauna in the water body. Currently there isn't a precise measuring methodology that is at the same time reliable and efficient. Also, it is a highly variable value to be measured, since the ecosystem components and quantities vary in the same water body. If properly maintained, other environmental impacts could be prevented or compensated.

Diversion or run-of-river hydropower plants, harness energy from the direct flow of the river. They could include short term water storage, that allows daily flexibility, but they have seasonal and yearly fluctuations. Environmental impact is mainly loss of fauna, when the water levels are low. However, flora should be very much considered, during the installation and construction of the infrastructure.

Pumped storage plants use water that is being pumped from a lower reservoir when the

demand for electricity is low or when cost is not high. When demand exceeds instantaneous electricity production, water is released from the upper reservoir through turbines in to the lower reservoir. Environmental impacts are similar to impoundment facilities.

Power plant in water distribution network is used to take advantage of the kinetic energy made available by pressurized water in the closed distribution network, depending on the system deployed and its characteristics. This type of hydropower generation has almost no impact on the environment, and as such is very favourable. It is installed in the existing water distribution infrastructure or with it.

According to the size and capacity of the hydropower plants definitions vary, but most common classification is as follow:

- Large – capacity above 10 MW
- Small – capacity below 10 MW
- Mini – capacity below 1000kW
- Micro – capacity below 100kW

III. WATER LIFE CYCLE AND ENERGY

Energy is needed for each stage of the water life cycle. The entire infrastructure employed to provide water for domestic use, sanitation and agricultural purposes requires a substantial amount of energy depending on the technologies applied; terrain conditions and regional climate, geological and biological preconditions. Varying factors include the end uses of water, water heating, showering, washing clothes and dishes, food preparation, water cooling and etc. Since energy requirements depend on so many factors, it not possible to give a global energy demand values in relation to water distribution, usage and disposal. Table II shows stages of water life within municipal sector with their respective energy consumption ranges for several specific locations aggregated. Energy consumption range is aggregated from three regions: Australian, Canadian and Californian [7].

Energy consumption for irrigation purposes is very hard to determine; it varies from the area irrigated, from the source of irrigation (weather it is ground water or surface water pumped), the amount of water needed for planted varieties of plants, the quality of the soil as well as the type of irrigation system.

TABLE II. ENERGY CONSUMPTION BY EACH STAGE OF THE WATER LIFE CYCLE. DATA SOURCES DETAILED IN PLAPPALLY AND LIENHARD [7]

Stage in the water life cycle	**Energy consumption range based on aggregated data in kWh/m^3**
Supply	0.035 – 3.59
Municipal Water Treatment	0.07– 8.5
Water Distribution	0.05 – 0.41
End Use	5.4 – 72.2
Waste water Collection	0.03 – 0.06
Waste Water Treatment	0.36 – 1.22
Recycled Water Treatment	0.33 – 3.8
Recycled Water Distribution	0.10 – 2.5
Waste Water Discharge	0.0 – 0.105

Energy recovery has become more frequent way to make the stage of Water Distribution more sustainable. Even though this is not the primary purpose of this installations, harnessing power dissipated by valves (in pressurized flow) or hydraulic jumps (in open canals), has been made possible by the development of the Fransis turbine for medium heads [5].

Waste water secondary treatment by anaerobic digestion of the sludge has a by-product of that process, methane that has approximate fuel value of 6.2kWh/m3. The amount of methane produced can in some cases be enough to supply energy equivalent needed to operate the waste water facility entirely [7]. The treated sludge can afterwards be used as a conditioner in agriculture. Some researchers show the importance of macrophytes (aquatic plants), in the process of nitrate and phosphorus removal in the biological treatment systems which reduces the overall energy consumption of the facility [8,9].

IV. THE IMPORTANCE OF WATER ENERGY NEXUS

A. Water and Energy in Sustainable Development

Sustainable development goals (SDGs) have been set in order to achieve sustainable development as it is most commonly defined: "*Sustainable development is development that meets the needs of the present, without compromising the ability of future generations to meet their own needs*". (by the Brundtland Commission in the 1987 report Our Common Future).

Studies show that accessible fresh water has a determinant role in the development (SDG6). Countries that had low incomes but also had access to safe water and sanitation 25 years ago grew their income on average 3.7% yearly. Comparable to that, countries that did not have safe water and sanitation grew only 0.1% on average [2]. By 2030, universal access to affordable, reliable and modern energy services needs to be ensured (SDG7). Water and energy are key drivers of economy, agricultural and industrial development. According to United Nations Development Programme (UNDP) [10], 663 million people lacked access to an improved water source. The planet's population is estimated to grow up to 9.7 billion in 2050, 85% of which are estimated to be living in developing countries [10].

B. Nexus versus sectorial approach in achieving sustainable development

The water energy nexus approach is of huge importance, since it differs from conventional sectorial decision making practices. Governments, for the sake of achieving sustainable development goals, have to adopt cross-sector coordination as a way to reduce unexpected sectorial trade-offs and promote the sustainable development of each sector [1].

National report of the government of Bangladesh states that about 82% of country's total electricity production is gas based, and that the reserves are diminishing significantly. It also states, that during the monsoon season large areas are prone to flooding, meanwhile in the summer due to high temperatures there are water and electricity shortages. However, studies show that Bangladesh has mini and micro hydropower potential present, with seasonal better efficiency. A positive example of the water energy nexus approach in Bangladesh is a first demonstration project of micro hydropower facility in Bamerchara. It was first implemented as an irrigation project, but the hydropower potential gave local farmers the ability to harness electricity for daytime irrigation and the remaining power is stored or used for training mills [11]. Impoundment facilities with air reserve, for flood mitigation, could be the solution for the above mentioned issues.

According to the national report of the government of Nepal, basic water supply coverage was 83.6 % in 2014, while sanitation had reached 70.3% of population. The proposed targets for 2030 include 95% of population having access to piped water supply and improved sanitation. Kathmandu, Nepal, has five wastewater treatment facilities, Guheshwori plant having the highest capacity and only one with activated sludge system [12]. The plant is only partially operative due to power shortages that last almost 14 hours per day. Modifications to the plant suggested by Regmi [13], including the instalment of a sequenced batch reactor could make it more efficient. Furthermore usage of anaerobic digestion could provide enough methane to sustain energy needs of the plant and make it energy wise less dependent on the power grid. That would produce better quality output water with irrigation as end use.

Irrigation as an important both water and energy end use consumer, can be affected by the misbalance in the nexus. Eren recognizes the influence of passing of The Electricity Market Law on the water energy nexus in Turkey, especially in the Ikizdere Valley. In pursuit of sustainable development, the state has made a series of legislative changes that allowed damming almost all rivers by 2023. In order to simplify the procedures for licensing, careful and detailed planning of the river basin were neglected as well as the water usage rights. After the erection of five diversion hydropower plants in the Ikizdere river basin (with their respective minimum water requirement releases), the river flow is completely regulated by the private companies that own the plants, with disregard of the downstream village needs. Aftermath of hasty sectorial planning in this case are also extinction of certain fish species, as well as drying up of native plant species that are more water demanding [15]. Water energy nexus approach would have been more inclusive of the water aspect in this case, in form of biodiversity losses, as well as downstream irrigation needs, as a water end use, which will consequently demand more energy.

While some countries have issues in cross-sectorial management, state of California has great amount of awareness of the existing interconnections. Plappally and Lienhard state that the most energy intensive stage of the water cycle is end use, while desalination processes (distillation and reverse osmosis) are most energy intensive in the water treatment stage. Southern California imports water from Northern California and surrounding states. The amount of energy needed for the transportation of that water is relatively larger than for desalting the water from Pacific Ocean and from

waste water recycling to potable [7]. This is happening due to technology advances in the last decades, in the field of reverse osmosis, which made the technology about 10 times less consuming, energy wise [16]. The California Energy Commission estimates that around 20% of energy consumption goes to some phase of the water life cycle [2]. To achieve better resource efficiency, California's Public Utilities Commission has developed a water energy cost effectiveness calculator in order to reduce energy consumption by water sector [14].

V. CONCLUSION

Water and energy are tightly linked, but understanding of this linkage is rarely put into policies. During the last century water and energy systems were constructed with the premise that water will be abundant and energy cheap. The concept of sustainable development of the 21st century brings a different perspective. To achieve the goals set by United Nations, governments must embrace cross-sector integrated approach that will enable overall and each sector's development. Further research should be done on the correlation between food and water and energy, as well as climate and water and energy.

ACKNOWLEDGMENT

This work has been funded by the Ministry of Education, Science and Technological Development of the Republic of Serbia (Project III 44006).

REFERENCES

[1] C.Zhang, X.Chen, Y.Li, W.Ding and G.Fu, "Water-energy-food nexus: Concepts, questions and methodologies", Journal of Cleaner Production, vol.195, 2018, pp.625-639

[2] The World Economic Forum Water Initiative, Water security: The-Water-Food-Energy-Climate Nexus, DOI 10.5822/978-1-61091-026-2_4, World Economic Forum 2011 ISBN 978-1-61091-026-2

[3] P. Kyle, E. G. R. Davies, J. J. Dooley, S. J. Smith, L. E. Clarke, J. A. Edmonds and M. Hejazi, "Influence of climate change mitigation technology on global demands of water for electricity generation," Int. J. Greenhouse Gas Control, vol. 13, 2013, pp. 112-123.

[4] E. G. R. Davies, P. Kyle and J. A. Edmonds, "An integrated assessment of global and regional water demands for electricity generation to 2095," Adv. Water Resour., vol. 52, 2013, pp. 296-313.

[5] M. Perez-Sanchez, F. J. Sanchez-Romero, H. M. Ramos and P. A. Lopez-Jimenez, "Energy Recovery in Existing Water Networks: Towards Greater Sustainability," Water, vol. 9, 2017, pp. 97-117.

[6] A. Botelho, P. Ferreira, F. Lima, L.M. Costa Pinto and S. Sousa, "Assessment of the environmental impacts associated with hydropower," Renewable Sustainable Energy Rev., vol. 70, 2017, pp. 896–904.

[7] A. K. Plappally and J. H. Lienhard V, "Energy requirements for water production, treatment, end use, reclamation, and disposal," Renewable Sustainable Energy Rev., vol. 16, 2012, pp. 4818–4848

[8] Y. S. Ng and D. J. Chieh Chan, "Wastewater phytoremediation by Salvinia molesta," J. Water Process Eng., vol. 15, 2017, pp. 107–115.

[9] S. Dhote and S. Dixit, "Role of Macrophytes in improving water quality of an aquatic eco-system," J. Appl. Sci. Environ. Manage., vol. 11, 2007, pp. 133 – 135

[10] "Human development report 2016", United Nations Development Programme, ISBN: 978-92-1-126413-5

[11] J. I, Razan, R. S. Islam, R. Hasan, S. Hasan, and F. Islam, "A Comprehensive Study of Micro-Hydropower Plant and Its Potential in Bangladesh," ISRN Renewable Energy, vol. 2012, Article ID 635396, 10 pages, 2012.

[12] H. Green, S. C. Poh and A. Richards,"Wastewater treatment in Kathmandu, Nepal" , Submitted to the Department of Civil and Environmental Engineering in Partial Fulfilment of the Requirements for the Degree of Master of Engineering in Civil and Environmental Engineering at the Massachusetts Institute of Technology June, 2003

[13] Shakil Regmi, Wastewater treatment in Kathmandu – Management, Treatment and Alternative", Bachelor's Thesis, Mikkeli University of applied Sciences April, 2013

[14] http://www.cpuc.ca.gov/nexus_calculator/

[15] Ayşen Eren „Transformation of the water –energy nexus in Turkey: Re-imagining hydroelectricity infrastructure", Energy Research & Social Science vol. 21, 2018, pp. 22-31

[16] M.Kumar, T.Culp and Y.Shen, "Water Desalination: History, Advances and Challenges", Frontiers of Engineering: Reports on Leading-Edge Engineering from the 2016 Symposium, 2017, pp. 55-68.

Improved Algorithm for FEM Analysis of MTL Problems

Ivica Jurić-Grgić[1], Rino Lucić[2], Ivan Krolo[3]

University of Split, Faculty of Electrical Engineering, Mechanical Engineering and Naval Architecture, R. Boskovica 32, HR-21000 Split, Croatia
[1]ijuricgr@fesb.hr; [2]rlucic@fesb.hr; [3]ikrolo@fesb.hr

Abstract— **This paper deals with improvement of time integration scheme for transient finite element method (FEM) analysis. FEM is applied to the system of hyperbolic differential equations i.e. system of multi-conductor transmission line (MTL) equations. Spatial integration of system of hyperbolic differential equations is usually done by the weighted residual method. Improvement of accuracy was obtained by using Heun's method. Numerical solutions obtained using Heun's method and using the generalized trapezoidal rule for different values of a time integration parameter ϑ are compared to analytical solution. It has been shown that Heun's method yields the results with much higher accuracy comparing to results obtained by generalized trapezoidal rule (ϑ-method) with the approximately equal computational time.**

Keywords - finite element method, multi-conductor transmission line, time domain, electromagnetic transients

I. INTRODUCTION

The finite element method (FEM) is the usual procedure for solving ordinary or partial differential equations (ODEs or PDEs) for boundary value problems of mathematical physics. The procedure is reduced to dividing the continuum into the finite elements, whereby for each finite element an appropriate algebraic system of equations approximates the original ODEs or PDEs [1]. Numerical model of the considered problem is achieved by assembling a local system of equations of all finite elements into a global system and incorporating appropriate boundary conditions. In the case of the non-stationary problems, assembling procedure and solution of the global system of equations is carried out for each time step.

In the case of a spatial-temporal problem defined by a PDE, it is necessary to get an algebraic equation system for each finite element. This system of algebraic equations is the result of approximate integration of spatial-temporal variables. Spatial integration of system of hyperbolic differential equations is usually done by the weighted residual method. There are several possibilities to do this depending on choice of weighting functions (point collocation method, subdomain collocation method, least square method, Galerkin method, etc.) whereas temporal integration can usually be done by the generalized trapezoidal rule (ϑ-method) as it is shown in [2]. This procedure has been successfully applied to solve multi-conductor transmission line (MTL) problems in the time-domain [3-4].

Although the generalized trapezoidal rule is A-stable method, in some cases it can produce numerical oscillations and numerical diffusion of results. This is because there is no universal value of time integration parameter ϑ that can achieve accurate results in all cases. When using the generalized trapezoidal rule, usual way to find an optimal value of time integration parameter for particular transmission line (TL) problem are numerical experiments.

The aim of this article is to improve the algorithm for electromagnetic transient analysis on MTL by improving the time integration scheme when forming a local system of equations for a finite element.

Instead of using the generalized trapezoidal rule when forming a finite element matrix, the accuracy of a numerical solution can be improved using one of the variant of the Runge-Kutta second-order method also known as Heun's method [5] for the time integration.

ISBN: 978-86-80616-03-2

Sometimes Heun's method is also referred as the improved Euler's method. Heun's method is suitable because, as a single-step method, it connects variables only at the beginning and at the end of the time interval and thus preserves the simplicity of numerical procedure. It is a single-step predictor-corrector method that improves the estimation of the slope for the time interval using an average value of slopes at the beginning and at the end of the time interval.

Desire for CPU speed must be balanced with the appropriate accuracy and stability required. We could get higher accuracy by multi-stage Runge-Kutta second-order method but it leads to time-consuming problem. Theoretically, one can develop infinite number of time schemes and their combinations, but the idea was to improve accuracy of FEM model computation for transient MTL analysis with one-step method that is not time-consuming.

II. FEM PROCEDURE

Fundamentals of FEM analysis of MTL problems have been described in [3] where the generalized trapezoidal rule (ϑ-method) is used for transient finite element method (FEM) analysis as time integration scheme. In the following text, it will be shown how to derive a local system of equations for a finite element by using Heun's method for time integration instead of the generalized trapezoidal rule.

A. MTL finite element – Heun's method

Propagation of traveling waves on MTL in the time-domain is governed by the Telegrapher Equations [3]. The weighted residual method [2] applied to the Telegrapher Equations [3] with unit test functions leads to the relations (1):

$$\int_{x_1}^{x_2}\left([L]\cdot\frac{\partial\{i\}}{\partial t}+[R]\cdot\{i\}+\frac{\partial\{u\}}{\partial x}\right)dx=\{0\}$$

$$\int_{x_1}^{x_2}\left([C]\cdot\frac{\partial\{u\}}{\partial t}+[G]\cdot\{u\}+\frac{\partial\{i\}}{\partial x}\right)dx=\{0\} \qquad (1)$$

where x_1 and x_2 are the coordinates of MTL finite element nodes shown in Figure 1.

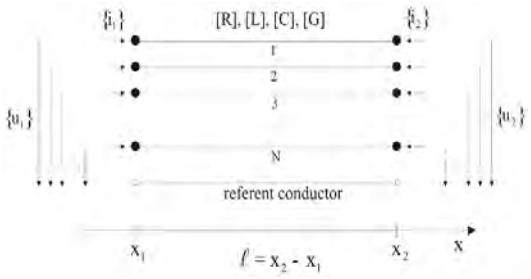

Figure 1. Multi-conductor transmission line finite element

Matrices [R], [L], [C] and [G] are frequency independent matrices of resistance, inductance, capacitance and conductance per-unit length, respectively. The voltage and current waves {u}, {i} over the MTL finite element are approximated by a linear combination of linear interpolation (shape) functions:

$$\{u^e\}=\frac{x_2-x}{x_2-x_1}\cdot\{u_1\}+\frac{x-x_1}{x_2-x_1}\cdot\{u_2\}$$

$$\{i^e\}=\frac{x_2-x}{x_2-x_1}\cdot\{i_1\}+\frac{x-x_1}{x_2-x_1}\cdot\{i_2\} \qquad (2)$$

The variables vectors $\{u^e\}$ and $\{i^e\}$ denote values of the voltage and the current wave vectors over the MTL finite element, $\{u_1\}$ and $\{i_1\}$ denote vectors of the voltage and the current wave associated to the nodes at the beginning of the MTL finite element, while $\{u_2\}$ and $\{i_2\}$ denote vectors of the voltage and the current wave associated to the nodes at the end of the MTL finite element.

After implementation of (2) into (1) and performing spatial integration, the coupled system of ODEs is obtained [3]:

$$\frac{\ell}{2}\sum_{k=1}^{2}\left[[L]\cdot\frac{d\{i_k\}}{dt}+[R]\cdot\{i_k\}\right]-\{u_1\}+\{u_2\}=\{0\}$$

$$\frac{\ell}{2}\sum_{k=1}^{2}\left[[C]\cdot\frac{d\{u_k\}}{dt}+[G]\cdot\{u_k\}\right]-\{i_1\}+\{i_2\}=\{0\} \qquad (3)$$

where $\ell=x_2-x_1$ is a finite element length.

The time integration of above equations using the generalized trapezoidal rule (ϑ-

method) can be found in [3]. When using the generalized trapezoidal rule, usual way to find an optimal value of time integration parameter for particular transmission line (TL) problem are numerical experiments.

Since numerical oscillations and/or numerical damping of results are the consequences of the choice of the numerical integration parameter (theta), the accuracy of a numerical solution can be improved using Heun's method for the time integration instead of using the generalized trapezoidal rule.

In order to perform the time integration according the Heun's method, it is necessary to put relations (3) into following form:

$$\frac{d}{dt}\left(\sum_{k=1}^{2}\{i_k\}\right)=f_1\left(\sum_{k=1}^{2}\{i_k\},\{u_1\},\{u_2\}\right)$$

$$\frac{d}{dt}\left(\sum_{k=1}^{2}\{u_k\}\right)=f_2\left(\sum_{k=1}^{2}\{u_k\},\{i_1\},\{i_2\}\right) \tag{4}$$

where:

$$f_1\left(\sum_{k=1}^{2}\{i_k\},\{u_1\},\{u_2\}\right)=-\frac{2}{\ell}\cdot[L]^{-1}\cdot[R]\cdot\sum_{k=1}^{2}\{i_k\}+\frac{2}{\ell}\cdot[L]^{-1}\cdot\{u_1\}-\frac{2}{\ell}\cdot[L]^{-1}\cdot\{u_2\}$$

$$f_2\left(\sum_{k=1}^{2}\{u_k\},\{i_1\},\{i_2\}\right)=-\frac{2}{\ell}\cdot[C]^{-1}\cdot[G]\cdot\sum_{k=1}^{2}\{u_k\}+\frac{2}{\ell}\cdot[C]^{-1}\cdot\{i_1\}-\frac{2}{\ell}\cdot[C]^{-1}\cdot\{i_2\} \tag{5}$$

According to Heun's method, the state of variables at the end of the time interval is defined by the following corrector equations:

$$\left(\sum_{k=1}^{2}\{i_k^+\}\right)=\left(\sum_{k=1}^{2}\{i_k\}\right)+\frac{\Delta t}{2}\cdot f_1\left(\sum_{k=1}^{2}\{i_k\},\{u_1\},\{u_2\}\right)+\frac{\Delta t}{2}\cdot f_1\left(\sum_{k=1}^{2}\{i_k^+\}^p,\{u_1^+\},\{u_2^+\}\right)$$

$$\left(\sum_{k=1}^{2}\{u_k^+\}\right)=\left(\sum_{k=1}^{2}\{u_k\}\right)+\frac{\Delta t}{2}\cdot f_2\left(\sum_{k=1}^{2}\{u_k\},\{i_1\},\{i_2\}\right)+\frac{\Delta t}{2}\cdot f_2\left(\sum_{k=1}^{2}\{u_k^+\}^p,\{i_1^+\},\{i_2^+\}\right) \tag{6}$$

The variables' vector, marked by "+", denote the variables' state at the end of the time interval, while variables' vectors without a mark denote the variables' state at the beginning of the time interval.

The predicted slopes f_1^+ and f_2^+ at the end of the time interval, according to (5), are:

$$f^+{}_1\left(\sum_{k=1}^{2}\{i_k^+\}^p,\{u_1^+\},\{u_2^+\}\right)=\frac{2}{\ell}\cdot[L]^{-1}\{u_1^+\}-\frac{2}{\ell}\cdot[L]^{-1}\{u_2^+\}-\frac{2}{\ell}\cdot[L]^{-1}[R]\cdot\left(\sum_{k=1}^{2}\{i_k^+\}^p\right)$$

$$f^+{}_2\left(\sum_{k=1}^{2}\{u_k^+\}^p,\{i_1^+\},\{i_2^+\}\right)=\frac{2}{\ell}\cdot[C]^{-1}\{i_1^+\}-\frac{2}{\ell}\cdot[C]^{-1}\{i_2^+\}-\frac{2}{\ell}\cdot[C]^{-1}[G]\cdot\left(\sum_{k=1}^{2}\{u_k^+\}^p\right) \tag{7}$$

where predicted voltage and current vector values at the end of the time interval are defined by the following predictor equations:

$$\left(\sum_{k=1}^{2}\{i_k^+\}^p\right)=\left(\sum_{k=1}^{2}\{i_k\}\right)+\Delta t\cdot f_1\left(\sum_{k=1}^{2}\{i_k\},\{u_1\},\{u_2\}\right)$$

$$\left(\sum_{k=1}^{2}\{u_k^+\}^p\right)=\left(\sum_{k=1}^{2}\{u_k\}\right)+\Delta t\cdot f_2\left(\sum_{k=1}^{2}\{u_k\},\{i_1\},\{i_2\}\right) \tag{8}$$

where f_1 and f_2 are defined by equation (5).

Combining (6) – (8) and separating the variables at the end of time interval to the left hand side and the variables at the beginning of time interval to the right hand side, the MTL finite element local system follows:

$$\begin{aligned}&\sum_{k=1}^{2}\{i_k^+\}-\frac{1}{\ell}\cdot\Delta t\cdot[L]^{-1}\{u_1^+\}+\frac{1}{\ell}\cdot\Delta t\cdot[L]^{-1}\{u_2^+\}=\\&=\sum_{k=1}^{2}\left([I]-\Delta t\cdot[L]^{-1}[R]+\frac{1}{2}\cdot\Delta t\cdot[L]^{-1}[R]\right)\{i_k\}\\&+\left(\frac{2}{\ell}\cdot\Delta t\cdot[L]^{-1}-\frac{1}{\ell}\cdot\Delta t\cdot[L]^{-1}-\frac{1}{\ell}\cdot\Delta t^2\cdot[L]^{-1}[R][L]^{-1}\right)\{u_1\}\\&+\left(-\frac{2}{\ell}\cdot\Delta t\cdot[L]^{-1}+\frac{1}{\ell}\cdot\Delta t\cdot[L]^{-1}+\frac{1}{\ell}\cdot\Delta t^2\cdot[L]^{-1}[R][L]^{-1}\right)\{u_2\}\end{aligned} \tag{9}$$

$$\begin{aligned}&\sum_{k=1}^{2}\{u_k^+\}-\frac{1}{\ell}\cdot\Delta t\cdot[C]^{-1}\{i_1^+\}+\frac{1}{\ell}\cdot\Delta t\cdot[C]^{-1}\{i_2^+\}=\\&=\sum_{k=1}^{2}\left([I]-\Delta t\cdot[C]^{-1}[G]+\frac{1}{2}\cdot\Delta t\cdot[C]^{-1}[G]\right)\{u_k\}\\&+\left(\frac{2}{\ell}\cdot\Delta t\cdot[C]^{-1}-\frac{1}{\ell}\cdot\Delta t\cdot[C]^{-1}-\frac{1}{\ell}\cdot\Delta t^2\cdot[C]^{-1}[G][C]^{-1}\right)\{i_1\}\\&+\left(-\frac{2}{\ell}\cdot\Delta t\cdot[C]^{-1}+\frac{1}{\ell}\cdot\Delta t\cdot[C]^{-1}+\frac{1}{\ell}\cdot\Delta t^2\cdot[C]^{-1}[G][C]^{-1}\right)\{i_2\}\end{aligned}$$

where [I] is the unity matrix.

Finally, the MTL finite element local system obtained by Heun's method can be clearly written in the matrix form:

$$\begin{aligned}\left[A_l\right]\cdot\begin{Bmatrix}\{i_1^+\}\\ \{i_2^+\}\end{Bmatrix}+\left[B_l\right]\cdot\begin{Bmatrix}\{u_1^+\}\\ \{u_2^+\}\end{Bmatrix}=\\ =\left[E_l\right]\cdot\begin{Bmatrix}\{i_1\}\\ \{i_2\}\end{Bmatrix}+\left[F_l\right]\cdot\begin{Bmatrix}\{u_1\}\\ \{u_2\}\end{Bmatrix}\end{aligned} \tag{10}$$

where:

$$\left[A_l\right]=\begin{bmatrix}[I] & [I]\\ -\frac{1}{\ell}\cdot\Delta t\cdot[C]^{-1} & -\frac{1}{\ell}\cdot\Delta t\cdot[C]^{-1}\end{bmatrix} \tag{11}$$

$$\left[B_l\right]=\begin{bmatrix}-\frac{1}{\ell}\cdot\Delta t\cdot[C]^{-1} & -\frac{1}{\ell}\cdot\Delta t\cdot[C]^{-1}\\ [I] & [I]\end{bmatrix} \tag{12}$$

$$\left[E_l\right]=\begin{bmatrix}\left([I]-\Delta t\cdot[L]^{-1}[R]+\frac{1}{2}\cdot\Delta t^2\cdot[L]^{-1}[R][L]^{-1}[R]\right) & \\ \left(\frac{2}{\ell}\cdot\Delta t\cdot[C]^{-1}-\frac{1}{\ell}\cdot\Delta t\cdot[C]^{-1}-\frac{1}{\ell}\cdot\Delta t^2\cdot[C]^{-1}[G][C]^{-1}\right) & \\ \left(-[I]+\Delta t\cdot[L]^{-1}[R]-\frac{1}{2}\cdot\Delta t^2\cdot[L]^{-1}[R][L]^{-1}[R]\right) & \\ \left(\frac{2}{\ell}\cdot\Delta t\cdot[C]^{-1}-\frac{1}{\ell}\cdot\Delta t\cdot[C]^{-1}-\frac{1}{\ell}\cdot\Delta t^2\cdot[C]^{-1}[G][C]^{-1}\right) & \end{bmatrix} \tag{13}$$

$$\left[F_l\right]=\begin{bmatrix}\left(\frac{2}{\ell}\cdot\Delta t\cdot[L]^{-1}-\frac{1}{\ell}\cdot\Delta t\cdot[L]^{-1}-\frac{1}{\ell}\cdot\Delta t^2\cdot[L]^{-1}[R][L]^{-1}\right) & \\ \left([I]-\Delta t\cdot[C]^{-1}[G]+\frac{1}{2}\cdot\Delta t^2\cdot[C]^{-1}[G][C]^{-1}[G]\right) & \\ \left(-\frac{2}{\ell}\cdot\Delta t\cdot[L]^{-1}+\frac{1}{\ell}\cdot\Delta t\cdot[L]^{-1}+\frac{1}{\ell}\cdot\Delta t^2\cdot[L]^{-1}[R][L]^{-1}\right) & \\ \left([I]-\Delta t\cdot[C]^{-1}[G]+\frac{1}{2}\cdot\Delta t^2\cdot[C]^{-1}[G][C]^{-1}[G]\right) & \end{bmatrix} \tag{14}$$

The variables' vectors in (10) marked by "+" denote vectors at the end of the time interval, while variables' vectors without mark denote vectors at the beginning of the time interval.

B. *Assembling Procedure*

The global system of equations is obtained by the standard assembling procedure which in a network analysis is equivalent to the satisfaction of Kirchhoff's law for current at every node of the finite element mesh.

In order to carry out assembling procedure, the local systems (10) of every FE have to be set in the form:

$$\begin{Bmatrix}\{i_1\}^+\\ \{i_2\}^+\end{Bmatrix}=[Q]\cdot\begin{Bmatrix}\{u_1\}^+\\ \{u_2\}^+\end{Bmatrix}+\begin{Bmatrix}F_1(\{u_1\},\{u_2\},\{i_1\},\{i_2\})\\ F_2(\{u_1\},\{u_2\},\{i_1\},\{i_2\})\end{Bmatrix} \tag{15}$$

The global matrix of the system (16) is banded and non-symmetric. The boundary conditions are the potentials or the currents at the boundary nodes.

$$\left[A_g\right]\cdot\left\{u_g^+\right\}=\left\{b_g\right\} \tag{16}$$

The computational procedure begins by imposing the initial and the boundary conditions. The global system has to be solved for each time step, evaluating unknown nodal potentials. The value of the current wave on each finite element is then computed using relation (15) for each time step.

III. ILLUSTRATIVE EXAMPLES

In order to verify a new numerical procedure, two illustrative examples are presented.

A. *Example 1 – Buried electrode*

The following numerical example presents propagation of an electromagnetic wave along a horizontal buried electrode. Per unit parameters of transmission line that represent buried electrode has been computed according to [6]. Burial depth of electrode is h = 0.3 m and radius of conductor is a = 0.5 cm. Buried conductor with length of 100 m has been modelled as a single transmission line with the following per-unit length parameters: $R=1.77\cdot10^{-4}$ Ω/m, $G=2.94\cdot10^{-3}$ S/m, $L=1.42\cdot10^{-6}$ H/m, $C=1.64\cdot10^{-10}$ F/m. The grounding electrode has been divided into 100 finite elements whose length is 1 m. The applied current waveform at the left end of the electrode is a step function with the amplitude of I = 100 kA and rise time of $T=15.2\cdot10^{-8}$ s. At the right end of the electrode the current is set to zero (Figure 2). A computational time interval is $\Delta t=1.52\cdot10^{-8}$ s.

Figure 2. The finite element mesh and boundary conditions of the grounding electrode.

Figure 3 shows spatial distribution of voltage wave along buried electrode at $50\cdot\Delta t$. Numerical solution obtained by Heun's method and the generalized trapezoidal rule (ϑ-method)

[3], for different values of a time integration parameter ϑ, are compared to the analytical solution obtained by the double Laplace transformation [7].

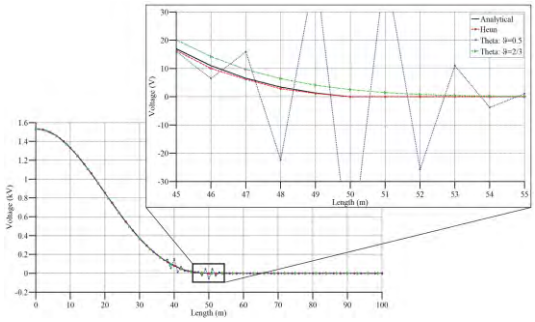

Figure 3. Spatial distribution of voltage wave along buried electrode at 50·Δt.

Since different values of ϑ yield different time-stepping schemes, all these schemes vary in accuracy. As it can be seen from Figures 3, numerical solution obtained by Heun's method yields highly accurate results while the generalized trapezoidal rule with $\vartheta = 0.66$ causes numerical damping of results. Furthermore, the generalized trapezoidal rule with $\vartheta = 0.5$ leads to numerical oscillations.

Absolute errors of numerical solutions related to the analytical solution at 50·Δt are shown in Figure 4.

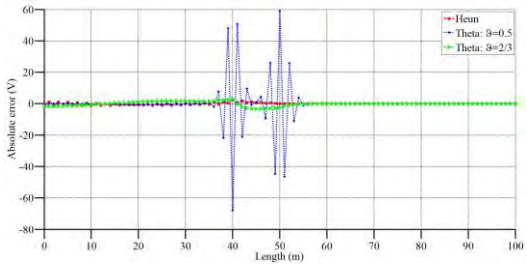

Figure 4. Absolute error of numerical solutions at 50·Δt.

Numerical experiments have shown that when using the generalized trapezoidal rule, in the case of a lossy line, optimal time integration parameter is $\vartheta = 0.66$ (Galerkin scheme).

B. Example 2 – Lossless MTL line

The following numerical example demonstrates the propagation of electromagnetic wave along simple 49.17-meter-long MTL, which is discretized into three MTL finite elements. Discretization into MTL finite elements, local nodes and global nodes are outlined in the (Figure 5).

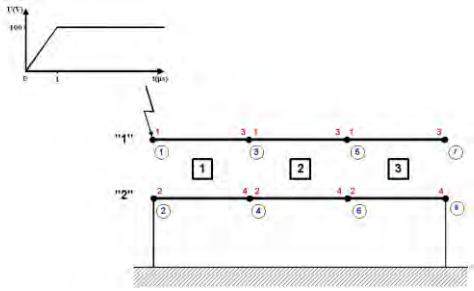

Figure 5. A two-conductor transmission line above reference plane.

In this example the conductor '2' of MTL has been grounded at the both sides (homogeneous Dirichlet boundary condition). The right end of the conductor '1' is open (the current at the boundary node is set to zero, homogeneous Neumann boundary condition) while on its left end the voltage wave is imposed (non-homogeneous Dirichlet boundary condition).

The applied voltage wave at the left end of conductor '1' is a step function with rise time of $T = 1 \cdot 10^{-6}$ s. The numerical values of per-unit length matrices are:

$$[L] = \begin{bmatrix} 1.532 & 0.766 \\ 0.766 & 1.532 \end{bmatrix} \mu H/m \quad ; \quad [R] = [0]$$

$$[C] = \begin{bmatrix} 3.12 & -1.56 \\ -1.56 & 3.12 \end{bmatrix} nF/m \quad ; \quad [G] = [0]$$

Numerical experiments have shown that when using the generalized trapezoidal rule, in the case of a lossless MTL, optimal time integration parameter is no longer $\vartheta = 0.66$, as it was in the previous case. In the case of a lossless MTL line, optimal time integration parameter is $\vartheta = 0.5$ (Crank-Nicolson scheme). This is because there is no universal value of time integration parameter ϑ that can achieve accurate results in all cases. When using the generalized trapezoidal rule, usual way to find an optimal value of time integration parameter ϑ for particular TL problem are numerical experiments.

Numerical solutions obtained by Heun's method and the generalized trapezoidal rule for $\vartheta = 0.5$ agrees with the analytical solution, while in a case of the generalized trapezoidal rule for $\vartheta = 0.66$, we have deviation of results (Figure 6-8).

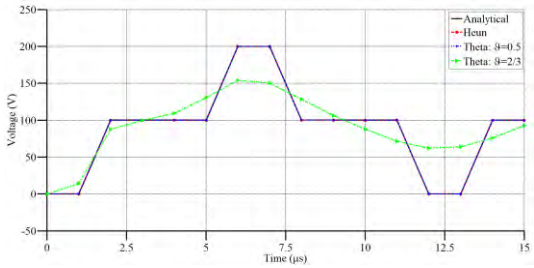

Figure 6. The voltage wave propagation at global node 3.

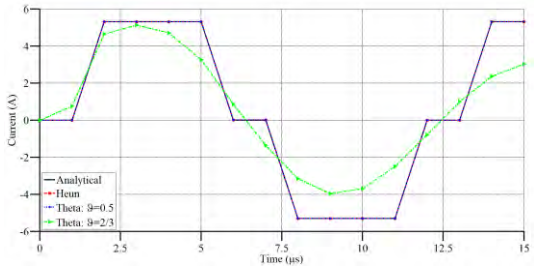

Figure 7. The current wave propagation at global node 3.

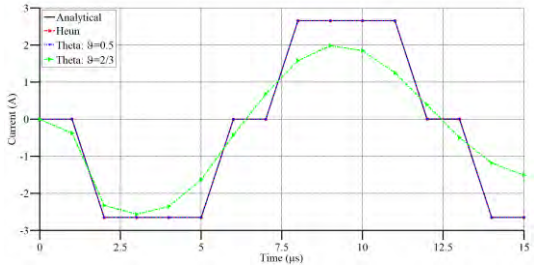

Figure 8. The current wave propagation at global node 4.

Above examples clearly shows that time integration obtained by Heun's method gives the higher accuracy of results.

IV. Conclusion

In this paper an improved time integration scheme for time dependent FEM analysis of MTL problems was presented. Improvement of accuracy was obtained by using Heun's method. Numerical solutions obtained using Heun's method and using the generalized trapezoidal rule for different values of a time integration parameter ϑ are compared to analytical solution. It has been shown that Heun's method yields the results with much higher accuracy comparing to results obtained by generalized trapezoidal rule (ϑ-method) with the approximately equal computational time. In some cases where the generalized trapezoidal rule is used, the choice of the numerical integration parameter (theta) generates numerical oscillations and/or numerical damping of results. Using the proposed approach, these unwanted consequences are avoided.

Appendix: Nomenclature

[R] – resistance per unit length matrix

[L] – inductance per unit length matrix

[C] – capacitance per unit length matrix

[G] – conductance per unit length matrix

$\{u\}$ – voltage waves over the MTL finite element

$\{i\}$ – current waves over the MTL finite element

$\{u^e\}$ – approximated values of the voltage wave vectors over the MTL finite element

$\{i^e\}$ – approximated values of the current wave vectors over the MTL finite element

$\{u_1\}$ – voltage wave vectors associated (joint) to the set '1' of local nodes

$\{i_1\}$ – current wave vectors associated (joint) to the set '1' of local nodes

$\{u_2\}$ – voltage wave vectors associated (joint) to the set '2' of local nodes

$\{i_2\}$ – current wave vectors associated (joint) to the set '2' of local nodes

[I] – unity matrix

ℓ – finite element length

Δt – time interval

References

[1] O. C. Zienkiewicz and R. L. Taylor, The Finite Element Method, vol. 1, McGraw-Hill: London, UK, 1989.

[2] O. C. Zienkiewicz and K. Morgan, Finite Element and Approximation, John Willey & Sons: New York, USA, 1983.

[3] R. Lucić, I. Jurić-Grgić and M. Kurtović, "Time domain finite element method analysis of multi-conductor transmission lines," Eur. Trans. Elect. Power, vol. 20, no. 6, 2010, pp. 822-832.

[4] I. Jurić-Grgić, R. Lucić and A. Bernardić, "Transient analysis of coupled non-uniform transmission line using finite element method," Int. J. Circ. Theor. Appl. vol. 43, no. 9, 2015, pp. 1167-1174.

[5] S. C. Chapra and R. C. Canale, Numerical Methods for Engineers (7th Edition), McGraw-Hill: New York, USA, 2015.

[6] E. D. Sunde, Earth Conduction Effects in Transmission Systems, D. Van Nostrand Company: New York, USA, 1949.

[7] R. Velazquez and D. Mukhedkar, "Analytical Modelling of grounding electrodes transient behavior," IEEE Trans. Power App. Syst., vol. PAS-103, no. 6, 1984, pp. 1314-1322.

Application of Pre-treatment for Enchancing Biogas Production from Plant-based Agricultural Waste

Marko Rakin[1], Karolj Damjanov[2], Goran Mitrović[3], Dragana Barjaktarević[1], Marica Rakin[1], Mirko Komatina[4], Branko Bugarski[1]

[1]University of Belgrade, Faculty of Technology and Metallurgy, Karnegijeva 4, 11000 Belgrade, Serbia, marko@tmf.bg.ac.rs, dbarjaktarevic@tmf.bg.ac.rs, marica@tmf.bg.ac.rs, branko@tmf.bg.ac.rs

[2]WV Biomass Operations Kida - 1 d.o.o., Svetosavska 43, 23300 Kikinda, Serbia, karolj.damjanov@gmail.com

[3]Biogas Power Solutions d.o.o., Sterije Popovića 2a, 23300 Kikinda, Serbia, gmitrovic@gmail.com

[4]University of Belgrade, Faculty of Mechanical Engineering, Kraljice Marije 16, 11000 Belgrade, Serbia, mkomatina@mas.bg.ac.rs

Abstract—**Agricultural waste is a suitable renewable source for the production of biogas, which can be converted into different forms of energy. Chemical pre-treatment can make anaerobic digestion faster and increase biogas yields. In this study, a mechanical and alkaline combination of pre-treatment is used. The aim of study is to compare the biogas yield with and without pre-treatment, as well as to develop a device which can be used as a system for chemical pre-treatment. Results show that a combination of the granulation of raw materials and alkaline treatment is an effective pre-treatment for increasing biogas yield.**

Keywords: agricultural waste, anaerobic digestion, biogas, chemical pre-treatment, mechanical pre-treatment

I. INTRODUCTION

The need for renewable energy has been increasing in recent decades. Among them, energy derived from biomass and biogas is becoming dominant. One of prediction is that in the next 15 years the needs for energy will increase by 50 %, as it was published in [1]. According to the European Biomass Industry Association, biogas production (till the year 2014) and predictions of production till 2030 - expressed in megatons of equivalent oil - is shown in figure 1 [2]. Suitable raw material for the production of biogas is agricultural waste.

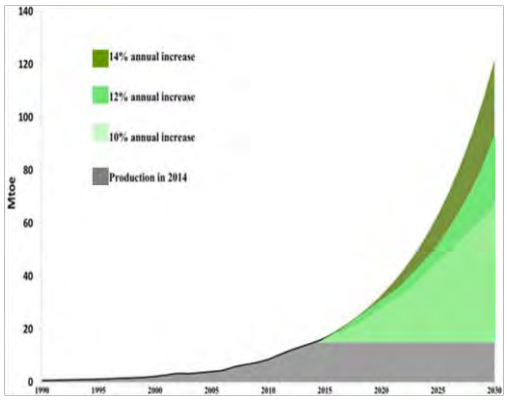

Figure 1.Prediction of biogas production in Europe [2]

The Republic of Serbia has relatively high potentials of biomass, which arises as a "surplus" in primary agricultural production. A large surplus in harvest residues is often solved in the most acceptable and ecologically problematic way, by burning on arable land. With the concept of industrial residue processing, in order to produce biogas, this problem can be significantly reduced.

ISBN: 978-86-80616-03-2

Agricultural waste are defined as the residues from farms, poultry houses and slaughter houses, harvest waste, fertilizer run off from fields, salt and dried sludge from fields.

The same definition is used by the United Nations (OECD), who also defines agricultural wastes as products of various agricultural operations [3]. Biogas is produced by the microbiological process in anaerobic conditions (without the presence of oxygen). Anaerobic digestion (AD) is the process whereat anaerobic bacteria break down organic matter, and as products obtained are heat, the rest of fermentation and biogas [4]. This process depends on several factors such as: the pH of the fermentable medium, the ratio of carbon to nitrogen in the fermentable substrate, the retention time, working pressure, temperature and the content of organic matter in the digester [5]. Only organic dry matter in added materials is important for the anaerobic digestion process. The amount of dry matter which can be added per day to the digester can be expressed as kg ODM /m^3 of digester. In a simple biogas plant the recommended amount of dry matter is 1.5 kg ODM /m^3 per day and in larger biogas plants with temperature control and mechanical agitation the amount of dry matter can be about 5 kg ODM /m^3 per day. The amount of dry matter has influence on the digestion process, larger amounts of dry matter decrease pH value in the digester and smaller loading of digester leads to longer retention time, see [6]. The methane bacteria have poor activity in pH value lower than 6, according to that the optimal pH value in anaerobic digestion is in range from 6.8 to 7.2 according to [2].

II. PRE-TREATMENT METHODS

The anaerobic digestion is not an efficient technology in treating plant-based agricultural waste because the lignin, cellulose and hemicellulose, which are the main agriculture plant components, are less available for anaerobic bacteria.

The pre-treatment is a method which breaks down the link between lignin, cellulose and hemicellulose, improving biodegradability and destroying cell walls in agricultural straw, in order to increase the enzymatic and sugar accessibility, which are used in biogas production, see [7]. Pre-treatments can be classified into four categories: physical methods, chemical methods, biological methods and combination of these methods.

The aim of pre-treatment technologies is:

- Make AD faster,
- Increase of biogas yields,
- Usage of new and locally available substrates (for details see [8]).

The application of pre-treatment could reduce the costs of raw material, make the production faster and make the biogas production more economical. Moreover, the application of pre-treatment increases the utilization of substrate, here residues of agricultural plants.

A. Phisical treatmants

Physical methods are classified in mechanical, thermal, ultrasonic and electrokinetic disintegration treatment. **The mechanical treatments** include various ways of physically disintegrating the substrate cells and partially dissolving their contents. The most commonly used appliances are different types of mills, such as mill with knifes or ball mills. Reducing the particle size increases the availability of the substrate, which increases the rate of anaerobic digestion [8, 9]. Recommended particle size for the efficient hydrolysis of lignocellulose is 1 to 2 mm according to [9]. Disadvantage of mechanical pre-treatment is using a large amount of electricity.

Thermal treatment has been used for many years in the treatment of waste active sludge. The heat leads to the breaking of chemical links between the cell wall and the membrane, and makes the dissolution of the cellular components easier. The use of thermal pre-treatment increases the price of the biogas because it requires a significant amount of energy. Therefore, thermal pre-treatment is often used in combination with some other kind of pre-treatment, for example hydrolysis or chemical pre-treatment. The maximum temperature for the thermal process depends on the substrate composition and the retention time, see [10].

On the other hand, **the ultrasonic and electrokinetic disintegration pre-treatments** are mainly used for the treatment of sludge from waste.

B. Chemical treatments

Chemical methods include alkaline, acid, and oxidation treatment. **The acid pre-treatment** leads to improvement of hemicellulose hydrolysis. Sulfuric, hydrochloric, phosphoric, nitric and carbonic acids are commonly used in this kind of pre-treatment as referred in [11]. Disadvantages of chemical pre-treatment are use of expensive acids and costly corrosion-resistance equipment [12]. **The oxidative pre-treatment** is performed with hydrogen peroxide or ozone, which can break lignin. Disadvantage of oxidative pre-treatment is high cost of chemicals. **The alkaline pre-treatment** leads to breaking of structural link between lignin and carbohydrates, reduction in degree of polymerization and destroying lignin structure. Also, alkaline pre-treatment removes acetate groups from hemicellulose, which makes hemicellulose available for hydrolytic enzymes. Generally, chemical pre-treatment is very convenient because it is very fast, inexpensive and has a good effect. Disadvantage of some chemicals commonly used for pre-treatment is possibility of pollution, see [13].

Alkaline pre-treatment can be carried out with a different concentration of ammonia, sodium hydroxide (NaOH), potassium hydroxide (KOH), calcium oxide (CaO). The most preferred reagent is NaOH, which has greater solubilization efficiency than other alkaline reagents, as given in [14]. Also, NaOH is cheap, fast as pre-treatment material and does not induce second-time pollution. B. Budiyono et al. [15] referred that the concentration of 4% NaOH solution is effective enough for increasing biogas yield. K. Michalska and S. Ledakowicz [16] investigated influence of NaOH solution on the degradation of lignocelluloses structure. They concluded that NaOH, which was used in chemical pre-treatment, removed almost all amount of lignin.

C. Biological methods

Biological methods include microbiological and enzyme treatment. The biological process is commonly performed in the presence of white fungi, enzyme from *Bacillus* sp. and *Aspergillus* sp. and alkaline endopeptidase, as referred in [9]. Biological pre-treatment, unlike chemical or thermal pre-treatment, can occur at lower temperatures without chemicals. The disadvantage of biological methods is these methods are most often slower than non-biological methods. The application of above mention pre-treatment technologies does not have the same effect for all types of substrates. The combination of pre-treatments usually leads to higher methane yields. In this study a combination of mechanical and alkaline pre-treatment is used. The aim of this study is to compare the methane yield after AD, with and without pre-treatment, and to develop a device for chemical pre-treatment. Experiments and development of the device for chemical pre-treatment is a part of the innovation project [17] that has been done by authors of this paper.

III. MATERIALS AND METHODS

A. Materials

Manure is used as a basic substrate in all experiments. The dry matter in manure is usually in the range 3-8% [18], therefore manure is suitable for mixing with other substrates which have a higher percentage of dry matter. The selection of the main substrate is made of two agriculture plant residues with high content of cellulose, lignocelluloses and hemicellulose: wheat straw and corn stover (all residues of corn). The selection is also made with regard to available materials in the environment. The retention time of materials with this content is 30 to 40 days in mesophilic conditions regardless whether treatment or pre-treatment has been done. The composition of wheat straw and corn stover are presented in table I and table II, respectively.

Based on the composition of wheat straw, ODM (Organic Dry Matter) is approximately 84%. The amount of dry matter is 2.35 $kg\ ODM/m^3$ per day and the total amount of material, according to the useful digester volume of 300 liters ($0.3m^3$), is approximately 0.7 kg of dry matter per day .More about the calculation see in [6]. Same procedure is applied for definition of required quantity of corn stover, as referred in [20].

TABLE I. COMPOSITION OF WHEAT STRAW [19]

Component	%
Hemicellulose	21- 26
Lignin	11-23
Cellulose	33.5 -40
Insoluble ash	7- 10

TABLE II.COMPOSITION OF CORN STOVER [20,21]

Component	%
Hemicellulose	≈30
Lignin	18- 20.7
Cellulose	37.4-38.1
Insoluble ash	5.2-8.8
Other	≈ 0.3

B. Pre-treatment process

The pre-treatment is performed as a combination of mechanical and alkaline treatment. Material granulation - mechanical treatment, achieves almost uniform size (≤ 1 cm) for treated plants. The milling is performed in the shredder of the Danish company "Cormall". The solution for the alkaline pre-treatment process is 6% NaOH. Treatment time is 30 days and the mixing period in the pre-treatment is 10 minutes, on a daily basis. The volume of the pre-treatment reactor is 100 liters. The device for chemical pre-treatment, designed by authors of this paper, is presented in figure 2.

C. Anaerobic Digestion

The capacity of the reactor is 400 liters. The volume of useful space for anaerobic digestion is 300 liters. Heating is important for this process, because the rate of anaerobic digestion and production of methane depends on temperature. Required temperature in the reactor is in the range 35 - 37 ^{0}C, as it is designed for mesophilic digestion. The reactor is a jacketed vessel, so designed temperature is provided in the jacket by circulating water..

TABLE III. PRE-TREATMENT AND ANAEROBIC DIGESTION DURING EXPERIMENTS

Materials	Chemical pre-treatment	Granulation	Retention time (day)	Manure	Period of pre-treatment
Wheat straw	no	≤ 1 cm	30	yes	0
Wheat straw	**yes**	≤ 1 cm	30	yes	30
Corn stover	no	≤ 1 cm	30	yes	0
Corn stover	**yes**	≤ 1 cm	30	yes	30

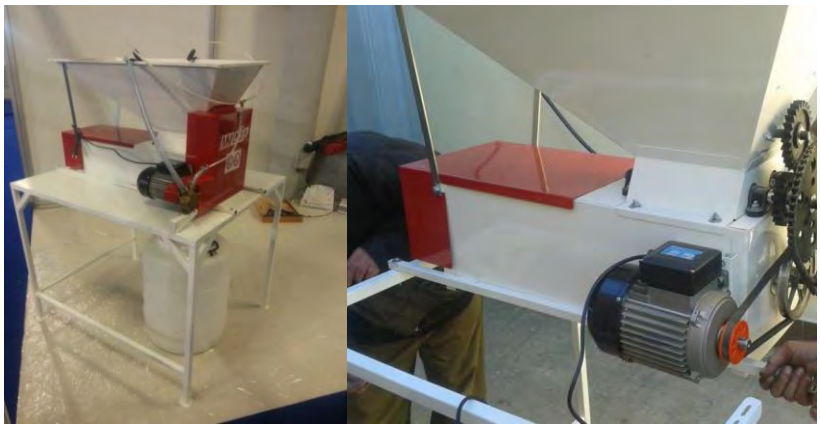

Figure 2. The device designed for chemical pre-treatment

During the process, the temperature is maintained in the range of ± 1 ^{0}C, because methanogenic bacteria are sensitive to temperature change. The water temperature in the jacketed vessel is provided through a solar collector with a defined surface, see [22], so it could be said that it is a hybrid system – we designated it: ASB – anaerobic solar bioreactor. More about the thermic part of the system and necessary computations are given in [23]. The agitation in the reactor is 2 times per day, and C/N ratio during the process is in the range 20-25. Table III presents the plan for pre-treatment and anaerobic digestion during experiments

IV. RESULTS

Table IV presents results and biogas yield with and without chemical pre-treatment. The obtained results show an increase in biogas yield for the treated substrate compared to untreated. The obtained results show that biogas yield from wheat straw is increased by 15% after a combination of mechanical and chemical pre-treatment, while biogas yield from corn is increased by 28% in the same pre-treatment conditions.

On the basis of the obtained results we can conclude that the pre-treatment was successfully performed and that the equipment shows the ability to perform mixing, wetting and dosing of the substrate.

The device for pre-treatment has a satisfactory size of the hopper. The dosing is done manually, but mixing, wetting, and transporting the material into the storage are semi-automatic.

The device parameters are:

- The motor, power 1KS 1400 rpm (mixer)
- The pump could achieve 1700 l/h (for alkaline solution dosing),
- The motor pump and the pulley system is in transmission 1:1
- The reactor capacity 100 l,
- The hopper volume 0.5 m^3

The device, together with the ASB system can be used as a small experimental pilot plant. For industrial application - it would be necessary to do a scale-up of the system. The construction of the device is universal, and there is the possibility of classifying materials at the exit of the device using a grid. The agitator and the pump operation are synchronous, which reduces loss of energy.

V. CONCLUSION

Bearing in mind the increasing need for energy production, energy obtained from biomass is becoming more and more in use, and among them, energy obtained from biogas becomes important. Considering that biogas is often obtained from agricultural waste, this work analyses pre-treatment of plant-based agricultural waste, as a process that is more and more in use prior to anaerobic digestion. An overview of the most commonly used methods

TABLE IV.BIOGAS YIELD BEFORE AND AFTER MECHANICAL AND CHEMICAL PRE-TREATMENT

Materials	**Pre-treatment**	**Retention time (day)**	**Substrate temperature (^{0}C)**	**Biogas yield (м^3)**	**Yield increase**
Wheat straw	no	30	28	4.25	
Wheat straw	**yes**	30	29	4.90	15%
Corn stover	no	30	28	4.50	
Corn stover	**yes**	30	32	5.75	28%

of pre-treatment is given, and advantages/ disadvantages of each of the methods are listed. The experimental part of the research included the development of a device for chemical pre-treatment of agricultural plant-based waste and its application to the alkaline pre-treatment of previously granulated wheat straw and corn stover. After anaerobic digestion in the pilot plant (also developed by the authors of this paper), the results showed that a combination of the granulation of raw materials and alkaline treatment is effective pre-treatment for increasing biogas yield (15% for wheat straw as a raw material and even 28% for corn stover).

REFERENCES

[1] J. Dodić, J. Grahovac, "Study over renewable energy souce", project - IPA Cross-border program, 2013.

[2] http://www.eubia.org/

[3] http://www.oecd.org/

[4] M. Martinov, K. Kovacs, Đ. Đatkov, "Biogas Technology" (in Serbian), Faculty of Technical Sciences, University of Novi Sad, 2012.

[5] P. Dobre, F. Nicole, F. Matei, "Main factors affecting biogas production - an overview", Romanian Biotechnological Letters, vol. 3, 2014, pp. 9283- 9296.

[6] B. T. Nijaguna, "Biogas Technology", JSS Academy of Technical Education, New Delhi, 2002.

[7] J. Zheng, L. Rehmann, "Extrusion Pre-treatment of Lignocellulosic Biomass: A Review", International Journal of Molecular Sciences, vol. 15, 2014, pp. 18967-18984.

[8] Z. Song, G. Yang, X. Liu, Z. Yan, Y. Yuan, Y. Liao, "Comparison of Seven Chemical Pre-treatments of Corn Straw for Improving Methane Yield by Anaerobic Digestion", online document, 2014

[9] L. Montgonery, G. Bochmann, "Pre-treatment of feedstock for enhanced biogas production", 2014, https://www.nachhaltigwirtschaften.at.

[10] G. Bochmann, L. Montgonery, "Storage and pre-treatment of substrates for biogas production", The Biogas Handbook - science, production and applications, 2013, pp. 85-103.

[11] R. Patinvoh, O. Osadolor, K. Chandolias, I. S. Horváth, M. Taherzadeh, "Innovative pretreatment strategies for biogas production", Bioresource Technology vol. 224, 2017, pp. 13–24.

[12] W. Xiao, W. Clarkson, "Acid solubilization of lignin and bioconversion of treated newsprint to methane", Biodegradation vol. 8, 1997, pp. 61–66.

[13] A. Ward, P. Hobbs, P. Holliman, D. Jones, "Optimisation of the anaerobic digestion of agricultural resources", Bioresource Technology vol. 99, 2008, pp. 7928–7940.

[14] W. Wonglertarak, B. Wichitsathian, "Alkaline Pre-treatment of Waste Activated Sludge in Anaerobic Digestion", Journal of Clean Energy Technologies, vol. 2, 2014, pp.118-121.

[15] B. Budiyono et al., "The effect of pre-treatment using sodium hydroxide and acetic acid to biogas production from rice straw waste", MATEC Web of Conferences, vol. 101, 2017, pp 1-6.

[16] K. Michalska, S. Ledakowicz, "Alkali pre-treatment of Moench for biogas production", Chemical Papers, vol. 67, 2013, pp. 1130–1137.

[17] M. Komatina et al., "Coupled solar-biogas plant for the needs of increasing the technical and technological performance of processing anaerobic manure" (in Serbian), innovation project (final report), 2013.

[18] M. Stanojević et al., „Biogas: preparation and application", Faculty for Mechanical Engineering, University of Belgrade, 2014.

[19] T. S. Khan, U. Mubeen, "Wheat Straw: A Pragmatic Overview", Current Research Journal of Biological Sciences vol. 4, 2012, pp. 673-675.

[20] V. Micky, A. Pometto, J. H. van Leeuwen, "Simultaneous Saccharification and Fermentation of Ground Corn Stover for the Production of Fuel Ethanol Using Phanerochaete chrysosporium Gloeophyllum trabeum, Saccharomyces cerevisiae, and Escherichia coli K011", Journal of Microbiological Biotechnology vol. 21, 2011, pp.703–710.

[21] H.-J. Huang, S. Ramaswamy, W. Al-Dajani, U. Tschirner, R. A. Cairncross, „Effect of biomass species and plant size on cellulosic ethanol: A comparative process and economic analysis", Biomass and Bioenergy vol. 33, 2009, pp. 234-246.

[22] M. Komatina et al., "New ecologically sustainable technology for obtaining biogas from agricultural waste" (in Serbian), innovation project (final report), 2015.

[23] D. Slavnić et al., "Modular system for biogas production from agricultural waste", XI International Symposium on Recycling Technologies and Sustainable Development, Proceedings, Bor, 2016, pp. 60-65.

Analysis of an Indirect Evaporative Air Cooler

Matjaž Prek[1], Gorazd Krese[2], Žiga Lampret[3]

[1]University of Ljubljana, Faculty of Mechanical Engineering, Ljubljana, Slovenia, matjaz.prek@fs.uni-lj.si
[2]Korona d.d., Ljubljana, Slovenia, gorazdkrese@gmail.com
[3]University of Ljubljana, Faculty of Mechanical Engineering, Ljubljana, Slovenia, ziga.lampret@fs.uni-lj.si

Abstract—**Performance of a counter-flow indirect evaporative air cooling device is analysed numerically. The device characteristic dimensions, inlet air temperature and humidity as well as inlet air velocity are investigated for the assessment of the thermal performance with the aim to determine the most influential design parameters. Additionally, design guidelines for central european climatic conditions are given.**

Keywords – evaporative cooling, indirect air cooling, counter-flow air cooler, renewable cooling, numerical analysis

I. INTRODUCTION

People spend in buildings between 80-90% of the time, which is why especially in recent decades, a lot of attention was paid to the comfort in the indoor environment. Air conditioning systems are becoming increasingly important in order to achieve the appropriate objectives of thermal comfort and air quality [1].

The building sector accounts for 40% of primary energy use, which makes the energy efficiency of air conditioning systems a key component in achieving the goals of reducing energy consumption [2]. Particular attention should be paid to the use of energy for cooling buildings, which is rapidly increasing as a result of global warming. Evaporative cooling represents an efficient and economically feasible method of air cooling as an alternative to a conventional compressor cooling system. The method is interesting because it uses air and water for cooling [3].

In hot and dry climates, the simplest method of cooling is spraying of water into the outdoor airflow, which is introduced into the occupied space. In this process of direct evaporative cooling, the temperature of the airflow decreases as energy is used to evaporate water, while the moisture content in the airflow increases. The increase in moisture in the airflow is often undesirable. In these cases, indirect cooling systems may be used. Here the energy of evaporative cooling from the direct evaporative cooler is used as a coolant in a heat exchanger and the moisture content does not increase [4]. The lowest temperature that can be achieved with such systems is the temperature of the wet-bulb thermometer, which is one of the disadvantages of such systems. The modification of the indirect volatile cooling system by the introduction of a counter flow regime allows the temperature to be reduced to the dew-point temperature of intake air. This paper presents a numerical analysis of such a system, analysing the influence of multiple parameters on the efficiency of the air cooler in order to identify the most critical design parameters.

II. EVAPORATIVE COOLING

Evaporative cooling is a process of conversion of liquid water into vapour using the thermal energy in the air, which results in a lower air temperature. Evaporation of water is done on the surface between the two media. The gas molecules near the surface of the liquid, due to the movement of the air, collide with the liquid molecules. Those water molecules that acquire sufficient energy to overcome the surface tension evaporate. The energy required for evaporation of water comes from the sensible heat affecting the temperature of the

ISBN: 978-86-80616-03-2

air. Sensible heat is converted into latent heat (water vapour component in the air), whilst air emperature decreases.

Evaporative cooling effect is used in various air cooling systems. Due to the simplicity and effectiveness of the process, devices using this effect achieve high cooling efficiency at low levels of primary energy consumption. There are two major types of evaporative cooling. Direct evaporative cooling where cooled air in in direct contact with the evaporating liquid which adds moisture to room air and indirect evaporative cooling, where the air is separated from the liquid and no moisture is added to the air.

A. Direct evaporative cooling systems

In this process the sensible heat of the air is used to evaporate the water, while lowering the air temperature. The heat and mass transfer between air and water reduces the air temperature and increases its humidity at a constant wet-bulb temperature. The process is adiabatic since only phase change occurs without external energy supplied into the system (Fig. 1).

Direct evaporative cooler can be represented as a series of wetted channels through which the air flows (Fig. 2). Inlet air (1) enters the wet channel in which heat and mass transfer occurs. In the process of evaporating the air sensible heat is converted into latent heat, which decreases air temperature and increases its moisture content [5].

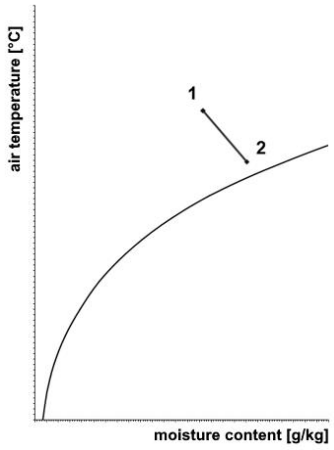

Figure 1: Direct evaporative cooling process in a psychrometric chart

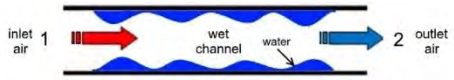

Figure 2: Working diagram of direct evaporative cooling

Air temperature is limited with the wet-bulb temperature of the inlet air as the air moisture content reaches saturation point and the process of evaporation is concluded. Important technical term for evaluating effectiveness of direct evaporative cooling systems is wet-bulb effectiveness, defined by the formula below:

$$\varepsilon_{DEC} = \frac{t_1 - t_2}{t_1 - t_{WB}} \qquad (1)$$

Wet-bulb effectiveness of direct evaporative cooling systems ranges between 70% to 95%, depending on the configuration. This type of systems are popular due to the simplicity of the structure and low operating costs.

B. Indirect evaporative cooling systems

In the case of indirect evaporative cooling systems airflows of the wet and dry channels are physically, so the inlet air is only cooled with no changes in moisture content. Product air flowing through the dry channel is in contact with the dry side of the wall, which is cooled by the working air flowing through the wet channel. In the wet channel evaporation of the water lowers the product air temperature and indirectly also the wall and product air as well (Fig. 3).

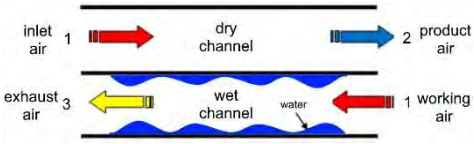

Figure 3: Working diagram of indirect evaporative cooling

Fig. 4 shows the indirect evaporative cooling process in the psychrometric chart. Inlet air at state 1 is cooled at the constant humid ratio toward the wet-bulb temperature of working air. Temperature of working air is lowered from state 1 to 3 along the isenthalpic line, as the thermal process of direct evaporative cooling.

Efficiency of indirect evaporative cooling is limited by the wet-bulb temperature of the working air.

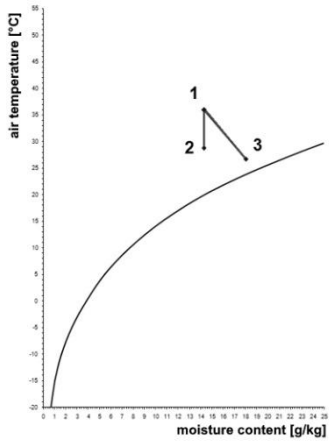

Figure 4: Indirect cooling process in a psychrometric chart

It is defined as a ratio of dry-bulb temperature decrease of the product air to the temperature difference of the state 1 dry-bulb temperature and the wet-bulb temperature of the working air (Eq. 2).

$$\varepsilon_{IEC} = \frac{t_1 - t_2}{t_1 - t_{WB,1}} \qquad (2)$$

Wet-bulb effectiveness of indirect evaporative cooling is typically lower than that of the direct evaporative cooling, typically in the range between 55% and 75% [6]. However, due to no moisture addition, indirect evaporative cooling systems are used, particularly in the tropic regions.

III. COUNTERFLOW INDIRECT EVAPORATIVE COOLING SYSTEM

Besides direct and indirect evaporative systems there are many different evaporative cooling systems, combining characteristics of the direct and indirect systems [1,3,4,7]. Due to some shortcomings of those systems this chapter will describe in more detail the conceptual design and operation of the counter-flow indirect evaporative cooling system which.

The device is composed of a series of parallel folded channels – wet and dry channels follow alternately. One set of a wet and dry channels are shown in Fig 5. Inlet air enters the channel from the right side. At the end of the channel a part of the inlet airflow is used to cool the ambient while the residual airflow is diverted into a wetted channel where it comes in contact with the wetted surface. This air flows through the wet channel countercurrently to the primary air and is discharged at the end of the channel as waste air.

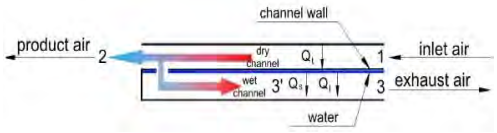

Figure 5: Wet and dry channel of the countercurrent indirect evaporative cooling device

During the process the inlet air can be cooled to the dew point temperature and not just the temperature of the wet-bulb temperature (as is the case with the conventional indirect evaporative cooling systems). This is because the secondary airflow is pre-cooled in a dry channel where dry-bulb and wet-bulb temperatures are reduced. Due to the preliminary cooling of the secondary air the device can achieve wet-bulb efficiency above 1 (Fig. 6) where moisture content of the product air does not change.

Since the wet-bulb temperature efficiency for these types of devices can exceed value 1, dew point effectiveness defined as the following formula (Eq. 3), can be used to rate the cooling systems.

$$\varepsilon_{DP} = \frac{t_{in} - t_{pr}}{t_{in} - t_{DP}} \qquad (3)$$

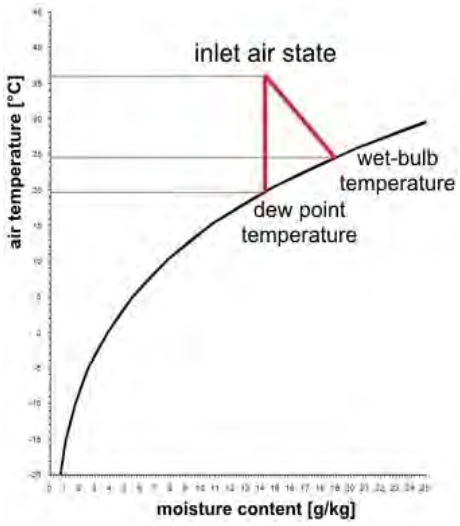

Figure 6: Wet-bulb and dew point temperatures of inlet air in psychrometric chart

Fig. 7 shows the primary and secondary air transformation of the countercurrent evaporative cooling device. Inlet airflow is cooled without adding moisture (1-2 state change). Lowest possible temperature is the dew point temperature of the inlet air. Part of the inlet air diverted to the wet channel is subjected to direct evaporative cooling. Lowest temperature that this diverted air can reach is the wet-bulb temperature (state 3'), where it reaches the saturation point. From this point on the evaporative cooling is stopped and the air is heated by the inlet air entering the dry channel.

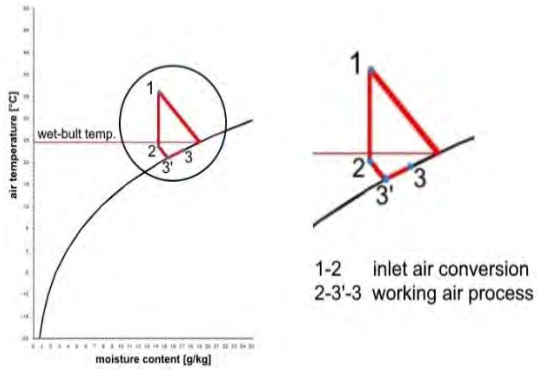

Figure 7: Primary and secondary air conversion in the countercurrent evaporative cooling device

Besides the latent heat of the secondary air, there is also sensible heat transfer of the primary air. For this reason, the transformation of the secondary airflow in a region where secondary air is not yet saturated does not follow the adiabatic line as shown Fig. 7. Secondary air conversion are separated into the process of evaporative cooling and air heating for the means of clearer representation.

IV. NUMERICAL ANALYSIS OF THE COOLING DEVICE

Purpose of the numerical analysis of the cooling device (shown schematically in Fig 5) to better understand the changing temperature of the airflows and the water film in the device, and to determine the optimum dimensions of the device, from the effectiveness standpoint. In order to obtain the desired results, it was necessary to define differential equations that describe the variation of temperatures along the airflow as a function of air velocity and dimensions of the device.

A. Heat and mass balances inside the control volume

Numerical analysis was based on the parametric analysis conducted for a cross-flow evaporative cooling device shown in [7]. Based on the assumptions from the paper heat and mass balance of the control volume. Fig. 8 shows the control volume of the cooling device (Fig. 5). Primary dry primary air flows through the upper channel, secondary air flows through the wet lower channel. Analysis of the cooling device is based on the following assumptions regarding the constant thermal properties of the water, negligible thermal resistance of the plate and the water film, changes in the temperature of the air flow only in the direction of motion and the locally identical temperature of the water film and the temperature of the plate [7].

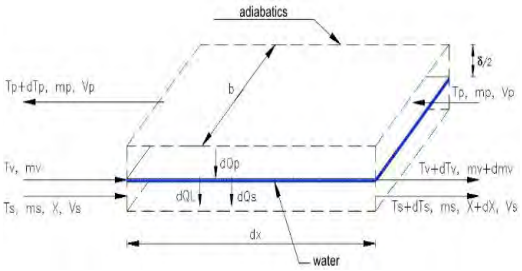

Figure 8: Control volume of the cooling device

For the control volume in the primary airflow (Fig. 8) energy conservation requires that:

$$-dQ_p = \dot{m}_p * c_p * dT_p \qquad (4)$$

Heat conversion can be also described as:

$$dQ_p = \alpha_p * b * dx * (T_p - T_v) \qquad (5)$$

Combining (4) and (5) we obtain an expression for describing the temperature changes for the primary air along the flow path:

$$\frac{dT_p}{dx} = -\frac{\alpha_p * b * (T_p - T_v)}{\dot{m}_p * cp} \qquad (6)$$

Similarly the conservation of energy at the air-water interface expression can be obtained:

$$\dot{m}_s \left[c_p * (T_s + dT_s) + (X + dX) * r(T_s + dT_s) \right] \qquad (7)$$

Latent and sensible heat changes in the secondary flow are given by:

$$dQ_L = d\dot{m}_v * r(T_v) \quad (8)$$

$$dQ_s = a_s * b * dx * (T_v - T_s) \quad (9)$$

The mass balance of the secondary air and the water falling film is given by:

$$\dot{m}_s * X * d\dot{m} = \dot{m}_s * (X + dX) \quad (10)$$

Equation (10) can be written as:

$$\frac{dX}{dx} = \frac{1}{m_s} * \frac{d\dot{m}_v}{dx} \quad (11)$$

Substituting equations 8, 9 and 11 into equation 7 and neglecting second-order differentials, we obtain:

$$\frac{dT_s}{dx} = \frac{\alpha_s * b * (T_v - T_s)}{\dot{m}_s * c_p} + \frac{dX}{dx} * \frac{r(T_v - T_s)}{c_p} \quad (12)$$

Energy balance in the water film can be written as:

$$\dot{m}_v * c_{p,v} * dT_v + d\dot{m}_v * r(T_v) = \dot{m}_p * c_p * dT_p + \dot{m}_s * c_p * dT_s \quad (13)$$

From (13) while considering (11) we obtain expression describing the changes of water film temperature along the water film flow:

$$\frac{dT_v}{dx} = \frac{\dot{m}_p * c_p * \frac{dT_p}{dx} + m_s * c_p * \frac{dT_s}{dx} - r(T_v) * \dot{m}_s * \frac{dX}{dx}}{\dot{m}_v * c_{p,v}} \quad (14)$$

B. Boundary conditions and the calculation procedure

Fig. 9 shows a dry and wet channel for the cooling device of length *L*, channel width *b* and channel height *δ*.

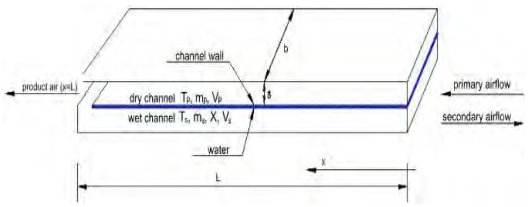

Figure 9: Scheme of the cooling device wet and dry channel

Differential equations calculations were carried out with the finite difference method. In order to calculate these differential equations, boundary conditions, the dimensions of the device and inlet airflow (primary airflow) and the ratio between primary and secondary airflow had to be determined. Ratio between airflows also determines the mass flow and velocity of the secondary airflow. Based on these velocities heat and mass transfer performance is evaluated. Necessary water flow rate for the needed moisture content in the wet channel also has to be determined.

Boundary conditions are as follows:

- temperature and absolute humidity of the inlet air are known: $T_p(x=0)$ and $X_p(x=0)$
- absolute humidity of the secondary airflow at the x=L point is equal to the absolute humidity of the primary airflow at this point, since the absolute humidity in the dry channel does not change $X_p(x=0) = X_s(x=L) = T_s(x=L)$
- airflow temperature in the wet and dry channel is equal at the x=L point; $T_p(x=L) = T_s(x=L)$

When all the aforementioned data is known, we assume the temperature of the dry and wet airflow at the x=L point; these temperatures are identical. After this assumption the relation between air temperature and water film temperature at the x=L point has to be known. By assumption water film temperature is equal to the channel wall temperature. To determine the water film temperature at the x=L energy balance condition is used.

V. NUMERICAL ANALYSIS RESULTS

A. Indirect cooling device length

Cooling device length is one of the crucial dimensions affecting the product air temperature and cooling effectiveness.

Fig. 10 shows a schematic description of the device on which the analysis was performed. At a constant velocity of primary and secondary airflow, which in our case is 1 m/s in dry and 0.5 m/s wet channel and constant air inlet conditions (35 °C, relative humidity 40%), we changed the length of the device while observing changing the temperature of the product air.

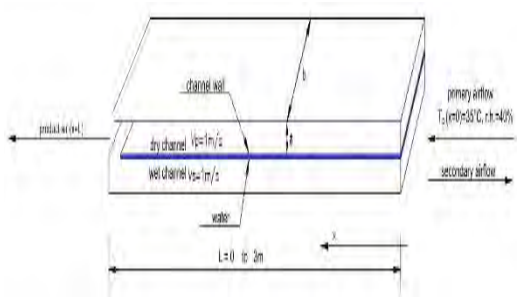

Figure 10: Indirect cooling device scheme – device length

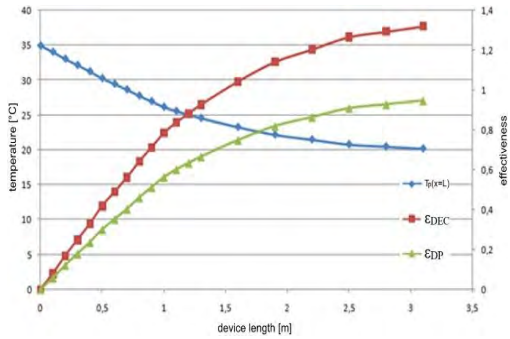

Figure 11: Product air temperature, wet-bulb and dew point temperature effectiveness' for different device lenghts

Theoretically the lowest temperature achievable for these input conditions is 19.4 °C, the temperature of the inlet air condensation. Depending on the product air temperatures, the wet-bulb and dew point temperature effectiveness' were calculated.

Fig. 11 shows the effect of different cooling device lengths on the product air temperature and cooling effectiveness. Trends are not linear. When selecting the length of the device, we must pay attention to the maximum temperature and humidity of the air that will enter the device during the summer.

B. *Primary (outside) air temperature and humidity*

Furthermore, a numerical calculation of the influence of the parameters of the ambient air on the temperature of the outgoing air was carried out. Constant parameters are the length of the device (L=1m), the width of the device, and the primary and secondary air velocity of 1m/s. The input temperature was changed in four steps, namely, 20°C, 25°C, 30°C and 40°C. For each of these temperatures, the air humidity content was changed; in the first case the absolute humidity was 7g/kg, in the second 10g/kg and in the third 13g/kg. The results of the numerical calculation are shown in the diagram below (Fig. 12).

Diagram in Fig. 12 shows that the temperature of the product air for the specific humidity of the inlet air is theoretically approximately linearly dependent on the temperature of the inlet air. Drier the air is, lower is the temperature to which it can be cooled. The diagram shows the potential of using the device under different operating conditions. In doing so, it should be emphasized that the slope of the lines can be changed by changing the parameters of the device.

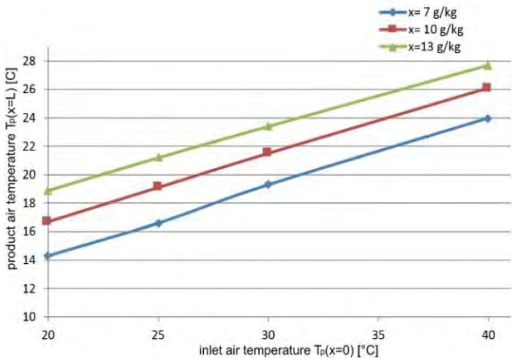

Figure 12: Product air temperature for different inlet air temperature and humidity conditions

C. *Wet and dry channel airflow velocity*

Primary and secondary airflow velocities have a key effect on the temperature of the product air, effectiveness of the device and its cooling capacity. A numerical calculation of the device under constant inlet air conditions and dimensions of the device at different primary and secondary airflow velocities was made.

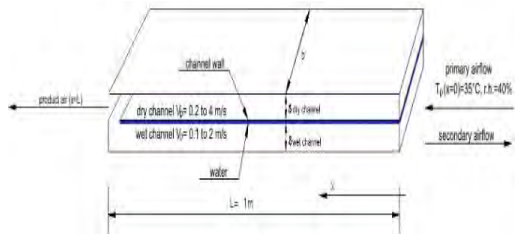

Figure 13: Indirect cooling device scheme – airflow velocity effect

Set ratio between the secondary and the primary airflow in the numerical calculation was 0.5. The device in question has the same

height of dry and wetted channels so the velocity ratio was 0.5 as well.

Fig. 14 shows the diagram of the project airflow temperature at the point of entering the indoor environment ($T_p(x=L)$). By lowering the speed, the project airflow temperature decreases exponentially.

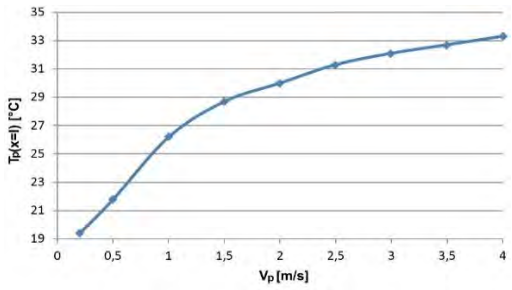

Figure 14: Primary airflow velocity effect on the product airflow temperature

In addition to the product airflow temperature, cooling load of the device is a crucial parameter as well. The device consists of a number of dry and wetter channels. Numerical calculation took into account the cooling load produced by the device with one wet and one dry channel. Cooling load was calculated with the following formula (15):

$$\dot{Q}_{cooling} = \left(\dot{m}_p - \dot{m}_s \right) * \left(h_p(x=0) - h_p(x=L) \right) \qquad (15)$$

Fig. 15 shows the relation between the device cooling load and the inlet airflow velocity.

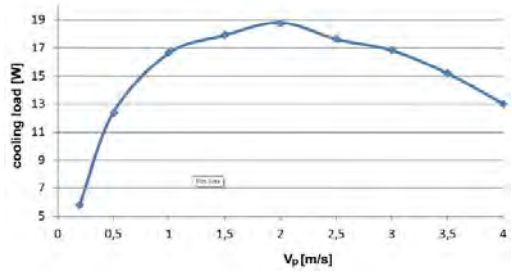

Figure 15: Primary airflow velocity effect on the device cooling load

At the lowest inlet airflow velocities, despite the lowest temperature (and consequently the maximum enthalpy difference), due to reduced air flow, the device produces minimum cooling load. Maximum cooling load achieved at airflow velocity of about 2 m/s with the product air temperature being 30 °C. This temperature level is too high for indoor environment air conditioning. Depending on the operational conditions in which the device operates, it is crucial to select a sufficient length of the device and airflow velocity. With the right choice, the maximum possible cooling power is obtained at a suitable product air temperature.

VI. CONCLUSION

A numerical analysis of a proposed counter-flow device for indirect air evaporation was performed. A number of parameters have been analysed to evaluate the effect on the device cooling effectiveness as well as on the cooling load.

The influence of the length of flow path has shown that increasing the length of the device results in higher device effectiveness. Temperature and humidity of the inlet (outer) air were analysed, showing that both parameters have a key influence on the parameters of the generated cool air stream. Velocity analysis showed the importance of choosing the optimal speed, since too low or too high air velocities in the channels can cause a decrease in the cooling power.

For local climatic conditions, where the maximum air temperature in the summer time is approximately 35°C at 40% relative humidity, a device must be at least 1.5m in length for an appropriately tempered inlet air into the space where the outlet air temperature is approximately 23.5 °C. By extending the flow path further, lower temperatures can be reached, with a theoretical minimum temperature of 19.4 ° C.

The obtained results will be taken into account when designing a prototype device for counter-flow indirect evaporation cooling.

REFERENCES

[1] H.Caliskan, A. Hepbasli, I. Dincer, and V. Maisotsenko, "Thermodinamic performance assessment of a novel air cooling cycle: Maisotsenko cycle," Int. Journal Refrig., vol. 34, 2011, pp. 980-990.

[2] G. Krese, J. Mandelj, M. Prek, and V. Butala, "Energy efficiency assessment of existing buildings based on measurements of HVAC Systems electric energy consumption: a case study," 11th REHVA World Congr., 8th Int. Conf. IAQVEC, 2013, pp. 8.

[3] A. Hasan "Indirect evaporative cooling of air to a sub-wet bulb temperature," Appl. Therm. Eng., vol. 30, 2010, pp. 2460–2468.

[4] S.T. Hsu, Z. Lavan, W.M. Worek, "Optimization of wet-surface heat exchangers," Energy vol. 14, 1989, pp. 757–70.

[5] D. Zhiyin, Investigation of a Novel Dew Point Indirect Evaporative Air Conditioning System for Buildings. University of Nottingham, 2011.

[6] ASHRAE, Handbook. Fundamentals. [SI ed.]. Atlanta, GA : American Society of Heating, Refrigerating, and Air-Conditioning Engineers, 1996.

[7] X.C. Guo, T.S. Zhao, "A parametric study of an indirect evaporative air cooler," Int. Commun. Heat. Mass. Transf., vol. 25, 1998, pp.217–26

District Heating Final Users Energy Efficiency Improvements – Goals And Challenges In Republic Of Serbia

Mirjana Laković Paunović[1], Ivan Pavlović[1]

[1]Faculty of Mechanical Engineering University of Niš, Niš, Serbia
[1]lmirjana@masfak.ni.ac.rs, [2]pivan@masfak.ni.ac.rs

Abstract— **Households in Serbia spend around 35% of the total final energy. This is the greatest potential for energy, economic and environment improvements. The apartment buildings, which cover 60% of total dwellings, are mostly in the lowest energy efficiency class. Transparent calculation of the heat energy price, based on the measured consumption, accompanied with founding a fund for energy efficiency improvement with significant human recourses and a budget is crucial for the energy efficiency improvement, heating costs reduction and increase in customers' satisfaction. Another possibility is application of an obligatory scheme of energy efficiency, according to Article 7 of the Directive 2012/27/EU, according to which distributors and retail energy sales companies are obliged to achieve end-users energy savings. It means the obligation of the heat suppliers to provide a financial and technical support for energy efficiency improvement in buildings.**

Keywords- thermal energy, energy efficiency, district heating

I. INTRODUCTION

The basic idea of district heating is to utilize local fuel resources or unused heat sources for meeting the needs of local buyers of thermal energy by using a distribution pipe network as a local market, [1]. Recently, more and more renewable energy sources are included into district heating, such as geothermal energy, biomass or solar energy, in order to reduce the share of fossil fuel in primary energy consumption [2,3]. In developed countries, district heating covers up to 50% of residential buildings, while other countries have only a small number of district heating systems is installed, either because of low awareness regarding the advantages of this system, or because of the lack of competition in the field of heating. According to [1], the total number of the installed systems in the world is 80000, with 6000 of them in Europe. Primary advantage of these systems are low expenses of thermal energy distribution in urban areas with concentrated demand for heat, while the basic disadvantages are low competitiveness in the cases of low princes of fuel at the international level and high expenses of distribution in suburban and rural areas with a less concentrated heat demand.

The basic categories of the district heating users are residential buildings and industry, as shown in Figure 1. During 2014, according to the International Energy Agency (IEA) [4], users bought 11.5 EJ of thermal energy from the district heating system, while Russia, China and the European Union made up to 85% of this amount. More than a half of this thermal energy, 51% was used for residential buildings, 45% by industry and 4% was used by other users.

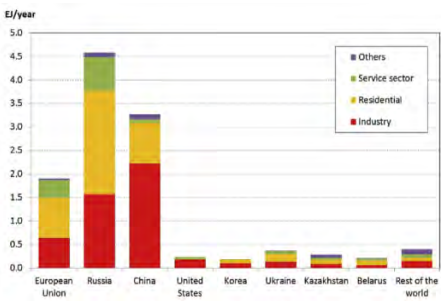

Figure 1 Basic characteristics of categories of district heating users [4]

ISBN: 978-86-80616-03-2

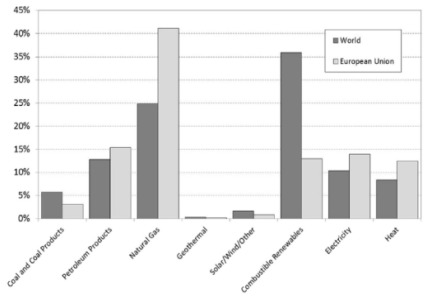

Figure 2 Shares of the primary energy for all types of heating in the world and the EU, according to [4]

Regarding the primary energy sources for all types of heating, natural gas is dominant in the European Union with 41%, since there is a well developed natural gas distribution network, and a large part of the population inhabits urban areas with high density. A direct use of fossil fuel amounts to 43% in the world, and even 60% in the European Union.

Concerning the district heating system, also according to the data from [4], the share of fossil fuel use is enormously high: 90% in the world and 70% in the European Union, as can be seen in Figure 3.

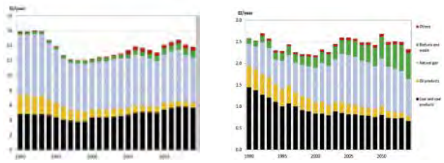

(a) (b)

Figure 3 Primary energy in system of district heating in the world (a) and in the EU (b) 1990-2010

In the study [5], published in 2017, district heating was assessed from several different aspects: commercial, technical, ecological and institutional. Based on the overview of the current situation in the world, the author concluded that it was necessary to put some effort in all these aspects, but district heating was an unavoidable perspective in the future.

District heating systems exist in 56 towns and cities in Serbia [6]. The installed heating capacities of these plants amounts to 6,600 MW, their distribution networks are approximately 2,100km, and the total number of substations is 23,042. Approximately 400,000 apartments are connected to the district heating network, which makes up to 17% of apartments in Serbia; this percentage is around 44% in Belgrade. In 2016,

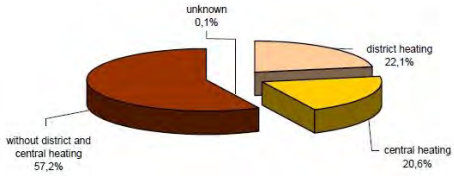

Figure 4 Occupied apartments by the type of heating in the RS [9].

the total consumption of plants was comprised of 74% of natural gas, 14% of oil derivates, 11% of coal and less than 1% of biomass. It is expected that the share of biomass increases to 12.5% by 2030 [7]. In the structure of final energy consumption, the industry makes 31% and households and other sectors 69%.

According to a study conducted by the Building Directorate of Serbia [8], 50% of the total energy consumption is spent in apartment buildings, and 60% of that goes to heating. According to the data of the Statistical Office of the Republic of Serbia [9], around 20% of occupied apartments use district heating, as can be seen in Figure 4.

Even if somewhat different statistical data is considered, according to which households spend approximately 40% of the total final energy consumption [10], this segment of spending is still a source of the enormous potential for an increase in energy efficiency, and therefore for achieving savings both on the part of producers and on the part of consumers of thermal energy.

II. Measures of Energy Efficiency of Buildings of District Heat Consumers

One of the characteristics of most residential and non-residential buildings in Serbia is irrationally large consumption of all types of energy, especially for heating, but recently also for cooling, due to an increase of mean temperatures during the summer months. Additionally, energy is used also for lighting and feeding electrical appliances in households. Energy used for heating in averagely thermally insolated buildings amounts to 60% of the total energy consumption. From that amount, 70% accounts for thermal energy consumption, which is influenced primarily by the duration of the heating season and demanded room temperature, influenced in turn by climate conditions and the quality standards of the used space. Furthermore, a significant impact has also the quality of a

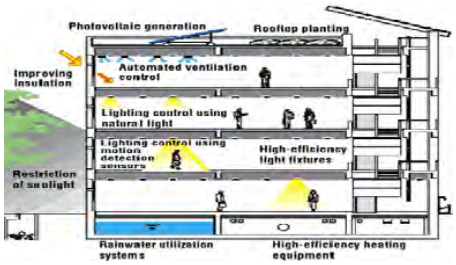

Figure 5 Heat balance and measures of improvement of energy efficiency of a building [11]

mechanical heating system, the total heating area, and thermal isolation of a building.

Measures that are applied to improve energy efficiency in buildings [11] can be divided into three basic groups:

- Measures to improve characteristics of the very building by reducing the needs for heating during the winter, and for cooling during the summer period (thermal isolation and sealing, protection against solar radiation in the summer);

- Measures to improve technical systems by using an adequate equipment and appliances with a high efficiency level, utilization of waste heat and renewable energy sources (better use of primary energy);

- Optimization measures for exploitation of technical systems through introduction of automatic control of installations for heating, cooling, vitalization and artificial lighting (thermal parameters of the space are maintained at the required level only when the space is used).

The Rulebook on Energy Efficiency of Buildings [12], regulates allowed limit energy consumption per a square meter for achieving energy efficiency. Thereby, the basic conditions of comfort cannot be disregarded. Additional demands set by this rulebook refer to: thermal isolation of buildings by limiting the maximal values of coefficient of heat transfer of elements contained in thermal covers of buildings; maximum allowed values of specific annual energy for heating; minimum technical demands for technical systems in buildings (heating, cooling, ventilation, sanitary hot water preparation, lighting).

III. Energy Class of Buildings

The energy class of buildings [13] is an indicator of energy properties of a building. It is expressed by a relative value of annual consumption of final heating energy [%] and represents a ratio of specific annual heat needed for heating QH,nd [kWh/(m2a)] and maximally allowed QH,nd,max [kWh/(m2a)] for a specific class of a building:

$$Q_{H},nd,rel = \frac{Q_{H,nd}}{Q_{H,nd},max} x100\%$$

Prescribed values are given in Table 1.

TABLE I. Maximum Allowed Annual Final Energy Consumption

Energy classes	$Q_{H,nd,rel}$	$Q_{H,nd}$	$Q_{H,nd}$	
	[%]	[kWh/(m^{2}a)]	[kWh/m^{2}a)]	[kWh/m^{2}a)]
		new	existing	existing
C	≤ 100	≤ 60	≤ 70	$35 \leq Q_{H,nd} \leq 70$
D	≤ 150	≤ 90	≤ 105	$70 \leq Q_{H,nd} \leq 105$
E	≤ 200	≤ 120	≤ 140	$105 \leq Q_{H,nd} \leq 140$
F	≤ 250	≤ 150	≤ 175	$140 \leq Q_{H,nd} \leq 175$
G	>250	>150	> 175	$Q_{H,nd} > 175$

According to the national typology of buildings, it can be seen that buildings covering over 60% of the area of the total available buildings fall into the lowest class of energy efficiency "G", Figure 6 [14]. These are mostly buildings dating before new laws and regulations on energy efficiency has been passed.

The energy class of a residential building, according to [13], is determined based on the maximum annual need for the final energy for heating [кWx/(м2a)], which is defined by the regulation on energy properties of buildings, especially for new and existing buildings. The maximum allowed annual demand for the final energy for heating QH, nd, max [kWh/(m2a)] corresponds to energy class "C", Table 2. This indicates a large potential and the need to

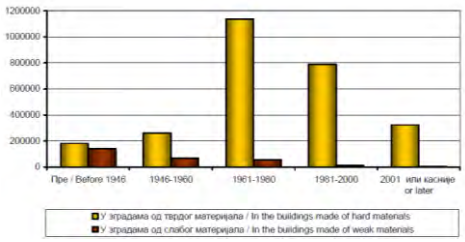

Figure 6. Buildings in the RS by the year of building and the material of external walls.

improve energy efficiency both of buildings connected to the district heating system and of those whose owners provide heating on their own and cover entire economic expenses.

TABLE II. MAXIMUM ALLOWED ANNUAL FINAL ENERGY CONSUMPTION

Buildings with multiple apartments		**New**	**Existing**
Energy classes	$Q_{H,nd,rel}$ [%]	$Q_{H,nd}$ [kWh/(m^{2}a)]	$Q_{H,nd}$ [kWh/m^{2}a)]
A+	≤ 15	≤ 9	≤ 10
A	≤ 25	≤ 15	≤ 18
B	≤ 50	≤ 30	≤ 35
C	≤ 100	≤ 60	≤ 70
D	≤ 150	≤ 90	≤ 105
E	≤ 200	≤ 120	≤ 140
F	≤ 250	≤ 150	≤ 175
G	>250	>150	> 175

A large number of different studies and projects have been conducted in order to prove and/or present an example of a good practice by comparing thermal energy consumption before and after the introduction of the energy efficiency measures and financial saving achieved by these measures. Figure 7 gives just one of the examples as to illustrate the significant potential of saving by applying just one of the methods for energy efficiency improvement [15]. The authors compared the existing condition with the one after the reconstruction, involving either or both an insulation of the cover of a building of

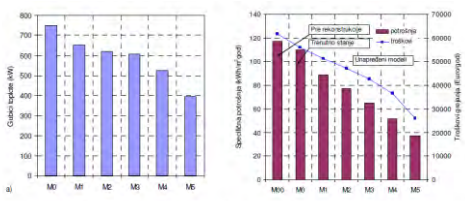

Figure 7 Influence of the EE measures on thermal losses and economic saving [15].

Figure 8 Model of "New Heating of Niš" losses and economic saving [15].

different thickness and/or material, or/and replacing old wooden doors and windows with new PVC ones.

It is entirely clear and obvious from numerous examples that putting thermal insulation is efficient both from the perspective of energetic and economic saving. The question raised here is – how to convince a buyer of thermal energy in the district heating system to invest into improvement of energy efficiency of their apartment?

IV. POSSIBILITIES OF APPLICATION OF THE MEASURES OF ENERGY EFFICIENCY IMPROVEMENT OF BUILDINGS OF DISTRICT HEATING USERS

Although even the introduction of legal regulation in the area of energetic and energy efficiency significantly raised the awareness of the importance of energy efficiency among population in the last decade, especially among the owners of buildings with individual heating, the level of the achieved results is still lower than expected. In the case of individual heating, it is much easier to promote the energy efficiency measures, since the financial investments in isolation, doors and windows replacement and/or replacement of the energy source pays itself in a certain period of time and the owner of such a building can relatively easy make a decision to invest into the energy efficiency improvement by making a relatively easy analysis of an investment return. On the other hand, the current state of financial capacities of the majority of citizens makes the introduction of this measured more difficult, so a financial and technical support is needed.

The problem with motivation is much more complex when it comes to the apartment owners who are buyers of thermal energy from the district heating system. Without the introduction of consumption billing, there is no other encouragement for these owners to undertake anything regarding the issue of energy efficiency improvement, but the introduction of consumption billing has been evidently made more difficult by the poor condition of building isolation covers.

Price calculation of the service of thermal energy providing based on transparency and measured consumption is crucial for energy efficiency, thermal energy cost reduction and consumers' satisfaction [16]. One of the priorities should be the elimination of non-

transparent and unsustainable billing for thermal energy by the unit of the heated area, which makes any initiatives for the energy efficiency improvement on the part of end users utterly pointless. Buyers need to be offered an opportunity to follow and influence their thermal energy consumption in their apartments, and thereby also the amount they need to pay. The introduction of this system is problematic, if not impossible, in older buildings where thermal energy is distributed vertically, i.e. not for every apartment separately. These apartments which are provided with thermal energy from a single substation get a common bill, which is then divided to apartment owners by the area of their apartments or by reading individual heat consumption dividers.

If the apartment owners want so, they should be given an opportunity to install dividers on their heating appliances and to pay their share of the bill according to the amount of heat emitted by radiators, and measured by dividers, or partly in this way, and partly according to the size of their apartment. Yet a better option, there where it is technically and financially possible, is to install thermal energy measuring devices, i.e. calorimeters in individual apartments, and the measured thermal energy can be a basis for dividing expenses or for a direct billing for thermal energy. Measuring of the thermal energy spent by every heating body individually by measuring devices in two-pipe systems may be irrational both for the number of heating bodies in apartments and for instruments every heating body should be equipped with (water meter, temperature sensors, computing unit). The thermal energy spent by a single heating body is determined, for the mentioned reason, "indirectly" by the use of dividers. What is determined by the dividers is the share of spending of a single heating body within the total thermal energy consumption in the building for the measuring period [17].

Either for individual or district heating, financial and technical support is needed, provided by programs for energy efficiency improvement of heated buildings. This can be accomplished in different ways. Certainly, one of them is founding a fund for energy efficiency improvement which would have significant human recourses and a budget that would allow systemic support for the conduction of energy efficiency improvements. A review of different financial possibilities for implementation of the energy efficiency measures in many different European countries is given in [18].

One of the models can be realization of investments through an institutionalized public-private partnership between the local authorities and a private partner – such a model is developed by Public Utility Company "Gradska Toplana" Niš.

In such a model, the private partner provides investments in façade, windows, pumps with frequency regulation and automatic regulation vent pipes, while the public partner provides goods, projects, necessary licenses and performs control over the quality of work. Users/buyers of thermal energy would obtain investments in energy efficiency of their buildings for a reduced price and with a repayment period of 12 years, and energy efficiency measures would provide savings of up to 50%. Table 3 (source: Public Utility Company "Gradska Toplana" Niš) illustrates thermal energy consumption and the current bill for distributed thermal energy for an apartment of 50m2, which currently belongs to energy class "E" and the comparison with the consumption and billing after performed intervention of energy efficiency improvement to energy class "C".

TABLE III. MAXIMUM ALLOWED ANNUAL FINAL ENERGY CONSUMPTION

	Before intervention	**After intervention**
Thermal energy consumption (kWh/m^2 per year)	120	70
Fixed part of the bill (RSD)	50x28,26=1413	50x28,26=1413
Variable part of the bill (RSD per year)	120x50x5,4=32 400	70x50x5,4= 18 900,00
Total (RSD per year)	12x1413,00+32400= 49 356	12x1413,00+32400= 35 856

Another possibility is application of a obligatory scheme of energy efficiency, according to Article 7 of the Directive 2012/27/EU on energy efficiency, which has been already introduced in some EU member countries, according to which distributors and retail energy sales companies are obliged to achieve certain energy saving by saving in the energy transport to the consumers.

The European Union adopted the Directive 2012/27/EU on energy efficiency on 25th October, 2012, and published it on 14th November in the Official Gazette of the European Union.

The Directive came into force on 4th December, 2012. The main measures regulated by the new Directive concerning transfer and distribution are:

• annual obligation of energy distributors and retail energy sales companies to reduce the energy sale to end users for 1.5% along with a possibility for member states to calculate energy savings realized in the sectors for energy distribution and transport, including efficient district heating and cooling infrastructure, in order to achieve this goal (Article 7.)

• obligation of a transport and distribution system operator to manage the system services in a transparent and non-discriminatory manner.

• obligation of distribution system operator to participate more actively in managing consumption and programs for a remote consumption reading.

In this sense, the introduction of consumption billing could be followed by the obligation on the part of plants to provide a certain degree of financial and technical support for energy efficiency improvement in buildings. According to the obligatory scheme, such an obligation can be issued both to distributors and providers of electric energy and natural gas, provided that no one should forget that help is possibly even more needed to those buildings that are not connected to the district heating system. Local self-government units should also be included in this process, but models of cooperation with commercial banks can be also considered.

V. Examples of Good Practice in the Surroundings

An example of neighboring Bulgaria can illustrate in the best way the necessity, but also the meaningfulness, of joined investments in the energy efficiency measures, to the mutual satisfaction and benefit of both buyers and producers/retailers of thermal energy [20]. Namely, a large number of users disconnected from the district heating system in the city of Pleven due to high prices and/or their inability to pay the heating. Heat consumption, due to the poor condition of buildings' insulation covers and internal thermal isolations, the lack of

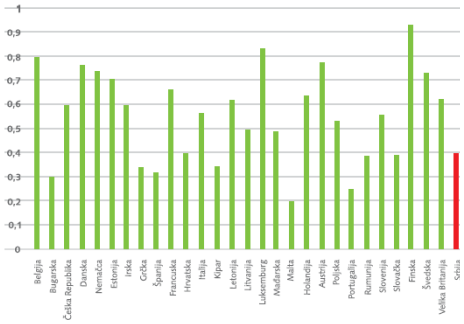

Figure 9 Final energy consumption in households per capita in the EU and Serbia, [18].

knowledge and motivation to apply the EE measures by the end users, inability and/or the lack of interest of the end users to measure spent heat, caused a dramatic increase in consumption, and consequently in bills, and this caused in turn inability to pay bills and, therefore, disconnection from the network. The implementation of the program of the energy efficiency measures in cooperation with the state, local self-government and foreign funds led to 94% of the disconnected users to reconnect to the district heating system, and by this were not only heating expenses reduced but also the comfort was increased.

The continuous realization of this and similar projects in Bulgaria led to billing of the distributed thermal energy almost entirely by consumption. Figure 9 shows the final energy consumption by a citizen, where it is obvious that consumption in Serbia, a geographically similar area, is higher in comparison to neighboring Bulgaria.

The necessity to implement the energy efficiency measures simultaneously with the introduction of the system of consumption billing is also illustrated by the example of Pančevo, where the project was founded by the European Agency for Reconstruction [21]. The goal of the project was to improve the sustainability of the district heating by implementing the EE measures in distribution and consumption. During the project implementation, households had an opportunity to choose whether they want to keep the old system of billing by the area, or to shift to the new one by consumption. It turned out that those households that had implemented the EE measures shifted to the billing by consumption, while energy inefficient households chose to keep the traditional billing type. After motivation and comprehensible

presentation of advantages of the energy efficiency measures implementation, especially in the economic sense, these households also chose the billing by consumption.

CONCULSION

The basic idea of district heating is the utilization of primarily energy in the most efficient way for providing consumers with thermal energy. District heating should, in its essence, provide high stability of distribution, cost-effectiveness, adequate comfort on the part of the users, on one hand, and to contribute to the stable and efficient utilization of primary energy sources and reduction of waste gases emission at the global level, on the other hand.

However, in the conditions of low energy efficiency of buildings of thermal energy end users, poor conditions of building covers, old and insufficient sealing of doors and windows, irrational consumption and the lack of ability to control the consumption by buyers, we come to the situation that district heating causes dissatisfaction of buyers, and significant expenses of producers and distributors of thermal energy.

In this paper, an overview of the current situation regarding energy efficiency of the district heating system users in Serbia is given, with a reference to other European countries. The basic conclusions are low utilization of district heating in apartment buildings, relatively low dedication to the idea of the implementation of district heating with the aim of waste gases reduction, and generally, poor recognition of benefits of district heating.

The all-encompassing solution implies investments in energy efficiency both in production and distribution, but also in consumption of thermal energy. Attention here is focused primarily on possibilities of motivation of thermal energy buyers to participate in the energy efficiency improvement of their heat consumption.

In order to motivate district heating system users to apply the energy efficiency measures in their buildings, it is necessary to introduce thermal energy consumption measuring and the transparent and comprehensible consumption billing. The next step is to provide an adequate model of financial support to citizens so that they realize necessary reconstructions of their buildings in order to improve the energy class of the building and consequently reduce thermal energy consumption and price for this service.

The experience of neighboring countries shows that systematic and all-encompassing approach to the implementation of the energy efficiency measures can produce significant results in a relatively short period of time to the satisfaction of both producers and buyers of thermal energy. Some of the possibilities are foundation of a fund for energy efficiency, conduction of the obligatory scheme of energy efficiency in accordance with Article 7 of the Directive 2012/27/EU on energy efficiency, according to which producers and distributors are obligated to achieve savings in final consumption, and the involvement of local self-government in the implementation of the energy efficiency measures. Furthermore, it is not to disregard the importance of continuous and comprehensible education of all citizens on the significance, advantages and possibilities of realization of energy efficiency improvement in all fields, especially in building design and construction.

REFERENCES

[1] Frederiksen S, Werner S. District heating and cooling. Lund Studentlitteratur;2013.K. Elissa, “Title of paper if known,” unpublished.

[2] Werner S. The position of district heating in the world and the corresponding use or renewables. Paper S2.1. GЄoteborg: Solar World Congress of International Solar Energy Society; 2003.

[3] Werner S. District heating and cooling. In: Cleveland CJ, editor. Encyclopediaof energy. New York: Elsevier; 2004.

[4] World energy balances until 2014. Paris: International Energy Agency; 2016.

[5] Werner, S. International review of district heating and cooling, Energy 137 (2017) 617-631.

[6] Министарство рударства и енергетике Републике Србије, Енергетски биланс РС, http://www.mre.gov.rs/

[7] Дејан Стојановић, Методологија за одређивање цене топлотне енергије и коришћење биомасе у системима даљинског грејања Републике Србије, http://www.coolheating.eu/images/downloads/4.pdf

[8] http://www.gds.rs/energetska-efikasnost/

[9] Република Србија, Републички завод за статистику, Попис становништва, домаћинстава и станова 2011. у Републици Србији, Станови Према Врсти Енергената За Грејање -Подаци по општинама/градовима, ISBN 978-86-6161-084-4

[10] Милетић М, Лукић Н, Коришћење финалне енергије у домаћинствима у Србији, 42. Конгрес о КГХ, Београд 2011

[11] Todorović Maja, Aleksandar Rajčić, Priručnik Za Energetsku Sertifikaciju Zgrada (Esz) – Vodič Za Investitore, Izvođače I Projektante, Deutsche

Gesellschaft Für Internationale Zusammenarbeit (Giz) Gmbh, Beograd, 2017

[12] Министарство рударства и енергетике РС, Правилник о енергетској ефикасности зграда, "Службени гласник РС", бр. 61/2011

[13] Правилник о условима, садржини и начину издавања сертификата о енергетским својствима зграда,"Службени гласник РС", бр. 69/2012

[14] Република Србија, Републички завод за статистику, Попис становништва, домаћинстава и станова 2011. у Републици Србији, СТАНОВИ ПРЕМА ВРСТИ ЗГРАДЕ -Подаци по општинама/градовима, ISBN 978-86-6161-084-4

[15] [15] Godišnja potrošnja energije za grejanje, http://enerese.np.ac.rs/documents/

[16] [16] Nuorkivi, A.: To the Rehabilitation Strategy of District Heating in Economies in Transition, Doctoral Dissertation, Helsinki University of Technology, Helsinki, Finland, 2005

[17] B. D. Blagojević et al, Heating cost allocation in Residential Buildings by Determining Actual Heat Consumption of Heating Bodies, IX Triennial International SAUM Conference, on Systems, Automatic Control and Measurements Niš, Serbia, November 22-23., 2007

[18] М. Ерић, М. Бабин, Компаративна анализа могућих финансијских модела за рехабилитацију постојећег стамбеног фонда у Србији и искуства других Европских земаља, ГИЗ, 2015

[19] DIRECTIVE 2012/27/EU OF THE EUROPEAN PARLIAMENT AND OF THE COUNCIL of 25 October 2012 on energy efficiency, amending Directives 2009/125/EC and 2010/30/EU and repealing Directives 2004/8/EC and 2006/32/EC

[20] The project ‘’Energy Efficiency for End-Users of District Heating City of Pleven Bulgaria’’, Municipal Network for Energy Efficiency “MUNEE”, dostupno na http://toolkits.reeep.org/file_upload/10302039_3.pdf

[21] Addressing Affordability of Utility Services in Urban Housing:Energy Efficiency Solutions, Alliance to Save Energy – Study on Residential Energy Efficiency and Affordability, 2007, dostupno na http://www.ase.org/sites/ase.org/files/residential_ee_study_final.pdf

Li-ion Battery-packs Modeling Based on Joint Time-frequency Analysis for Vehicle Applications

Sandra Castano-Solis[1], Daniel Serrano-Jimenez[2], Jesus Fraile-Ardanuy[3], David Jimenez-Bermejo[3], Javier Sanz[2]

[1]ETS Universidad Politécnica de Madrid, Madrid, Spain, sp.castano@upm.es
[2]Electrical Engeneering Department, Universidad Carlos III de Madrid, Madrid, Spain, danserra@ing.uc3m.es; jsanz@ing.uc3m.es
[3]ETSI Telecomunicación, Universidad Politécnica de Madrid, Madrid, Spain, jesus.fraile.ardanuy@upm.es; David.jimenezb@upm.es

Abstract — **In this paper a modeling procedure based on joint time-frequency analysis is presented. In this way, the parameters of the electrical circuit include the different time constants that affect the transient response of the battery-packs. The model has been experimentally validated by means of a hardware-in-the-loop (HIL) simulation. Simulations results show that the model presents consistent accuracy to reproduce the voltage response of the battery-pack at different driving cycles.**

Keywords – dynamic modeling, Li-ion battery-packs, time-frequency tests, electric vehicle applications.

I. INTRODUCTION

The automotive sector has been undergoing a definitive shift towards electrified transportation due to a specific set of social, environmental, and technical reasons [1], [2] since the late 90s. The improvement of energy and power of the batteries, first Ni based and later Li, drove the increase of commercially available electric vehicles [3]. Lithium based batteries are the choice for most vehicle manufacturers and forecasts are that they will continue to dominate the market in the medium term, with variations of the cathode material [4].

As the power supply of an electric vehicle the battery-pack is forced to operate at different acceleration-braking cycles, this produces that it works at different time constants. Batteries, whatever the technology, can operate under a wide interval of dynamic regimes due to their electrochemical nature [5], what affects their transient response. The relevance of each of these time constants is different depending on the application. For electrified transportation there are two issues of special interest. The first one relates with the electrical dynamic performance, which is dominated by the millisecond to second's dynamics, and is relevant for the real-time modeling and simulation. The second one is caused by working regime at different charge-discharge cycles. Because these processes affect the behavior of the battery-pack modeling procedure should taking into account these time constants to properly reproduce the dynamic response of the battery-pack.

Focusing on the dynamic performance, modeling techniques based on equivalent circuits can range from simple black box approaches to time or frequency domain based models. Black box models [6]-[8], even if simple to obtain, give no information on the battery internal phenomena. Time domain models [9]-[13], obtained from the analysis of the battery voltage evolution during tests, give more or less sophisticated models that can predict its dynamic behavior as a function of time. These models are relatively easy to obtain, but their validity is usually limited to a rather narrow bandwidth. Frequency domain based models are obtained after testing the battery with a superimposed frequency signal [14], and are called Electrochemical Impedance Spectroscopy Tests (EIS). These models can be time consuming to

ISBN: 978-86-80616-03-2

obtain, but can reveal information of the battery internal phenomena during highly dynamic to ageing processes. The most common approach when carrying out EIS tests is to test battery cells in a frequency interval ranging from mHz to kHz [15], [16]. This frequency range is based on the assumption that the most relevant dynamic phenomena take place in this range. However, previous literature has not made a frequency experimental analysis to determine which is the frequency' range of interest.

The common approach for all the previous modeling techniques is that the equivalent circuit models include a combination of passive elements, such as resistances and capacitors. Parallel combinations of resistances and capacitors (RC networks) are particularly used to represent the battery dynamic behavior [17], [18]. However, there is no agreement on which is the number of networks that should be used, which define the time constants represented. The root of this disagreement is the fact that there is no systematic study of the dynamic requirements for battery packs in electrified transportation.

This work presents a modeling procedure based on time and frequency tests that includes the different time constants associate with the internal processes that occur inside the battery-pack. From experimental results the parameters of an electrical circuit associated to different frequencies are calculated. The model is experimentally validated for an electric vehicle application by means of HIL (hardware-in-the-loop) simulation.

II. BATTERY-PACK MODELING

The Li-ion battery-pack tested in this work has four parallel-connected strings, each one composed by a series of seven groups of two cells in parallel (in total, 56 MP-176065 Saft cells), as shown in Fig. 1. There is a battery management system (BMS) that controls each of the four parallel strings and the whole pack. The main battery pack characteristics are: rated voltage 25.9 V, maximum voltage 29.4 V, capacity 50 Ah, and maximum current 50 A.

To obtain the electrical dynamic model of the Li-ion battery-pack time and frequency tests have been carried out. To reproduce the active behavior of the pack a voltage source is used. This voltage source simulates the relationship between the state of charge (SOC) and the open circuit voltage (OCV). The SOC-OCV characteristics is determined by current interruption tests (time domain). EIS tests have been carried out to calculate the complex impedance of the battery-pack (frequency domain).

A. Time domain tests

To determine the SOC-OCV characteristic the battery-pack has been discharged and charged at 10 A current-pulses. From fully charge (100% SOC), the battery-pack is discharged at 10 A current-pulses of 30 min and 90 min of relaxation time until the BMS

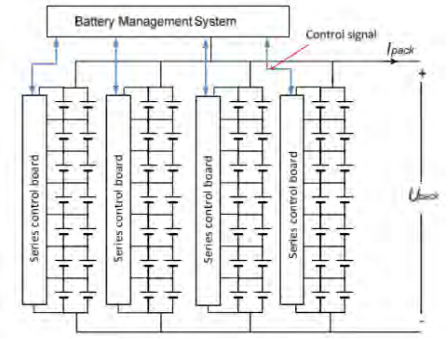

Figure 1. Battery-pack scheme.

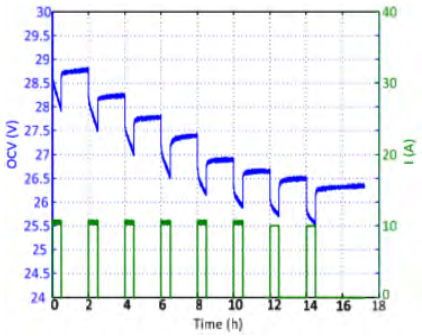

Figure 2. Discharge test.

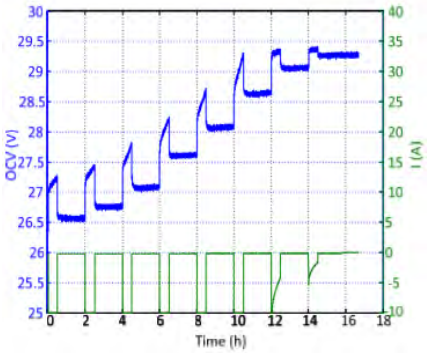

Figure 3. Charge test.

stops the discharge process. At the end of discharge test, the pack is charged at 10 A current-pulses (30 min and 90 min of relaxation) until the charge is finished by the BMS. The OCV is measured at packs terminals when the relaxation time ends in both discharge and charge tests. The results of time domain tests are shown in Figs. 2 and 3. The voltage source E_0 represents the relationship between OCV-SOC and it is defined by (1).

$$Eo = 26.05 - 0.15 \cdot SOC + 3.51 \cdot SOC^2 \quad (1)$$

B. EIS tests

To obtain the impedance of the Li-ion battery-pack, current-controlled EIS tests are carried out. Electrochemical impedance spectroscopy is a well proven and very precise method used to determine the complex impedance of electrochemical systems, such as fuel cells (FC) [19], ultracapacitors (UC) [20] or batteries [21]. The tests are carried out at 20%, 40%, 60%, 80% and 90% state-of-charge (SOC). The AC ripple amplitude was set to 5 A (10% of the maximum current), in order to test the battery pack under real operating conditions. To overcome the AC current limitation of the impedance analyzer, a power source and an electronic load are used to amplify the analyzer signal, using the experimental setup explained in [22]. Due to the symmetry of the positive and negative cycles, the net DC current is zero over a whole period, thus allowing a constant SOC value throughout the test. The frequency interval is variable from 1 mHz to 5 kHz.

EIS test results of the battery pack are shown in Nyquist plots (Fig. 4). This impedance spectra shows the characteristic behavior of lithium ion cells in a Nyquist plot [15], [16]. As it can be seen from 1 mHz to 4 Hz the complex impedance changes at different SOC values. From 1 mHz to 316 Hz the impedance presents a capacitive behavior (negative values of Z"). The equivalent serial resistance of the pack is 39 mΩ. Beyond 316 Hz the Nyquist plots show an inductive behavior (positive values of Z").

In Fig. 5 the Nyquist plot of the impedance of the battery-pack at 20% SOC is associated to an equivalent circuit [23]. To reproduce the capacitive behavior three elements are used: a Warburg impedance (W) that reproduces the 45º slope at frequency range of 1 mHz-23 mHz, and two constant phase elements (CPE) in parallel with resistances to simulate the semi-circles that appear from 53 mHz to 316 Hz. The internal resistance is represented by R_o. Finally, to represent the inductive behavior an inductance (L) is included.

C. Battery-pack model

Because CPE and Warburg elements correspond to frequency domain impedances, it is not possible to implement them directly in a general purpose simulation platform such as Matlab/Simulink®, or Labview®. For this reason these elements must be replaced using appropriate approximations. To maintain the capacitive behavior, the CPE is substituted by a capacitor, which is calculated by (2) [24].

The Warburg impedance can be replaced to a series of RC networks [25], but in this work

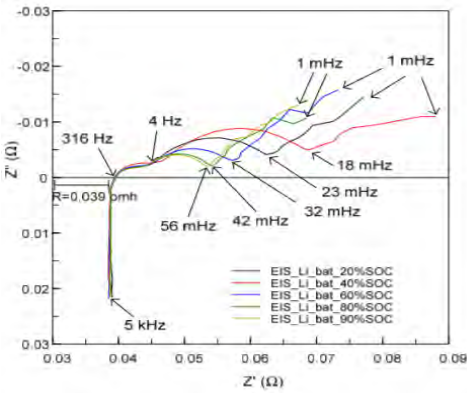

Figure 4. EIS test results.

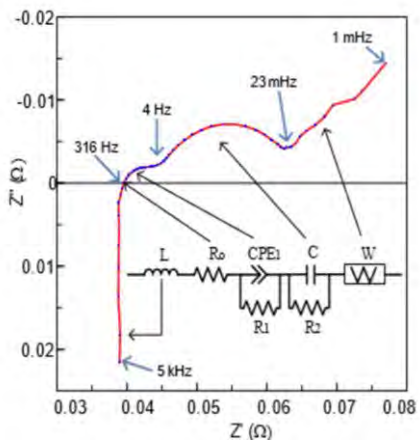

Figure 5. Equivalent impedance.

we have used just one single RC network. Table 2 shows the values for each parameter at different state-of-charge (SOC) values. Because Ro, R3 and C3 do not have a representative

statistical relationship with SOC, their average values are used.

$$C(F) = C_{CPE} \cdot (\omega_{\max})^{n-1} = \frac{(C_{CPE} \cdot R)^{\frac{1}{n}}}{R} \quad (2)$$

The model of the battery-pack based on time-frequency tests is presented in Fig. 6. *upack* represents the battery-pack voltage defined by eq (3), and *ipack* is the simulated current.

$$u_{pack} = E_0 - u_{Ro} - u_{C1} - u_{C2} - u_{C3} \quad (3)$$

III. HIL VALIDATION TESTS

The battery-pack model is experimentally validated for an electric vehicle application. For this purpose the electric vehicle is simulated using a hardware-in-the-loop simulation (HIL), in which a real device emulates the vehicle power demand [26], [27]. In this experimental test bench [22], the devices used to emulate the vehicle are an electronic load and a power source, which are controlled by means of a dSpace system in synchronization to simulate the vehicle power demand during acceleration and braking. The real battery-pack is tested under the power requirements of the electric vehicle simulated as HIL following the power profiles. Fig. 7 presents a picture of this setup in the laboratory.

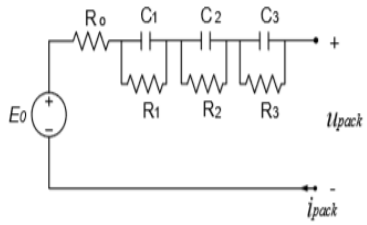

Figure 6. Battery-pack model.

TABLE I. IMPEDANCE PARAMETERS

Elem.	20% SOC	40% SOC	60% SOC	80% SOC	90% SOC
Ro (Ω)	0,0393	0,0393	0,0391	0,0391	0,0391
C1 (F)	0,4739	0,4684	0,4692	0,4652	0,4709
R1 (Ω)	0,0066	0,0066	0,0065	0,0063	0,0063
C2 (F)	40,920	39,574	33,044	28,266	30,235
R2 (Ω)	0,015	0,020	0,0088	0,0078	0,0069
C3 (F)	4550	3193	3854	4510	4836
R3 (Ω)	0,0224	0,0240	0,0268	0,0200	0,0218

To reproduce an electric vehicle application, different standard driving cycles have been used to analyze the power requirements imposed to the battery-pack. Standard driving cycles were initially used to evaluate pollutant emissions and calculate fuel efficiency for road transport studies [28], but due to the good results obtained, its use has spread to test EV's and PHEV's performance. This work analyze the urban and combined cycles for Europe, the urban cycle is NYCC, whilst the combined cycle (urban and highway) is NEDC [29].

Fig. 8 shows the urban cycle NYCC. For this cycle the maximum speed is less than 50 km/h. This cycle reproduces a driving route in New York City with during 598 s, with a total distance of 1902.8 m and average speed of 11.5 km/h. In Fig. 9 the combined cycle NEDC is presented. This cycle reproduces both urban and highway driving conditions. NEDC cycle has four ECE cycles followed by one EUDC cycle. The maximum speed is 120 km/h, the total time is 1180 s, the average speed is 42 km/h, and the total distance is approximately 11000 m.

During the HIL simulation the data of the current and voltage of the battery-pack at each driving cycle are recorded. The signals of the current profiles have been introduced as the input of the pack model (Fig. 6) which has been implemented in Matlab/Simulink®. To determine the model accuracy the voltage response of the battery-pack model has been compared with the real voltage measurements at battery-pack terminals.

The current profiles are shown in Figs. 10 and 11 and the comparison of the real pack voltage and the simulated voltage are presented in Figs. 12 and 13. As it can be seen, the model reproduce the voltage response of the battery- pack with high accuracy. The maximum error is less than 1% for the two cycles analyzed.

Figure 7. HIL test bench.

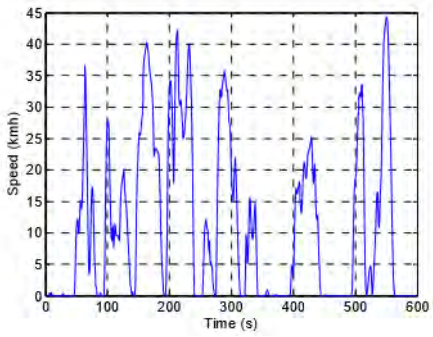

Figure 8. NYCC driving cycle.

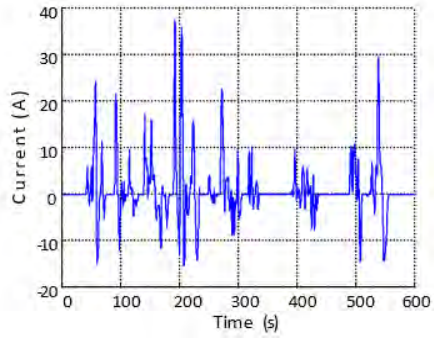

Figure 10. NYCC current profile.

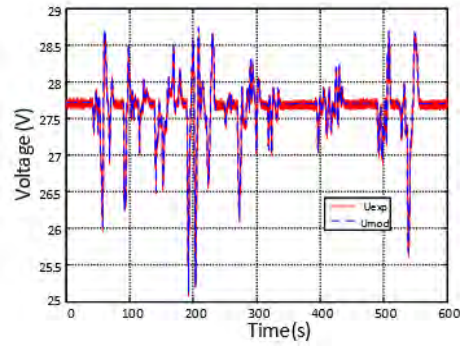

Figure 12. Simulated and real voltages at NYCC.

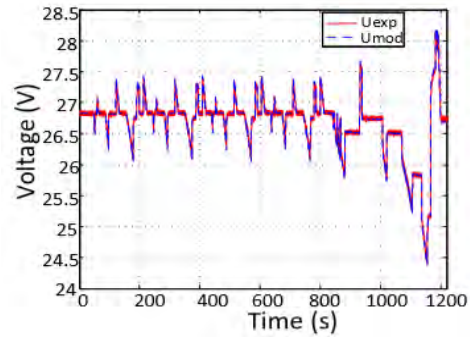

Figure 13. Simulated and real voltages at NEDC.

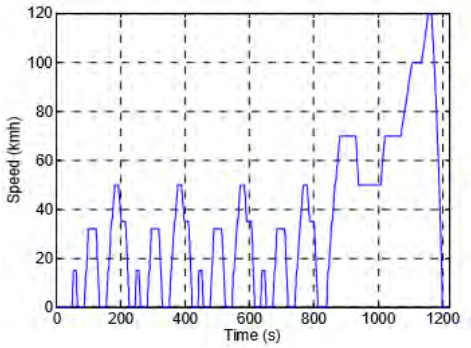

Figure 9. NEDC driving cycle.

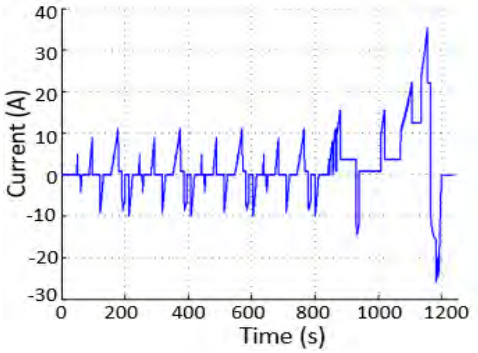

Figure 11. NEDC current profile.

IV. CONCLUSIONS

This work presents a battery-pack model based on joint time and frequency tests. From current interruption and EIS tests the parameters of the electrical model have been calculated. The model includes three RC networks which reproduce the dynamic behavior of the battery-pack. The model was validated for different driving cycles by means of a HIL experimental test bench. Validation tests show that the model is consistently accurate to reproduce the battery pack response under vehicle applications.

REFERENCES

[1] A. Emadi, L. Young Joo, K. Rajashekara, "Power Electronics and Motor Drives in Electric, Hybrid Electric, and Plug-In Hybrid Electric Vehicles," Industrial Electronics, IEEE Transactions on, vol. 55, no. 6, 2008, pp. 2237-2245.

[2] C. C. Chan, "The State of the Art of Electric, Hybrid, and Fuel Cell Vehicles," Proceedings of the IEEE, vol. 95, no. 4, 2007, pp. 704-718.

[3] S. M. Lukic, J. Cao, R. C. Bansal, F. Rodriguez, A. Emadi, "Energy storage systems for automotive applications," Industrial electronics, IEEE Transactions on, vol. 55, no. 6, 2008, pp. 2258-2267.

[4] A. Khaligh, Z. Li, “Battery, Ultracapacitor, Fuel Cell, and Hybrid Energy Storage Systems for Electric, Hybrid Electric, Fuel Cell, and Plug-In Hybrid Electric Vehicles: State of the Art,” Vehicular Technology, IEEE Transactions on, vol. 59, no. 6, 2010, pp. 2806-2814.

[5] A. Jossen, “Fundamentals of battery dynamics,” Journal of Power Sources, vol. 154, no. 2, 2006. pp. 530538.

[6] Y. Hu, S. Yurkovich, Y. Guezennec, B. J. Yurkovich, “A technique for dynamic battery model identification in automotive applications using linear parameter varying structures,” Control Engineering Practice, vol. 17, no. 10, 2009, pp. 1190-1201.

[7] A. Shafiei, A. Momeni, S. Williamson, “Battery Modeling Approaches and Management Techniques for Plug-in Hybrid Electric Vehicles,” Vehicle Power and Propulsion Conference, VPPC’11, 2011, pp. 1-5.

[8] G. Plett, “Extended Kalman filtering for battery management systems of LiPB-bases HEV battery packs. Part 2. Modeling and identification.” Journal of Power Sources, vol. 134, 2010, pp. 262-276.

[9] M. Einhorn, F.V. Conte, C. Kral, and J. Fleig. “Comparison, Selection, and Parameterization of Electrical Battery Models for Automotive Applications,” IEEE Trans. on Power Electronics, vol. 28, no. 3, 2013, pp.1429, 1437.

[10] L. Gao, S. Liu, R. A. Dougal, “Dynamic Lithium-Ion Battery Model for System Simulation,” Components, Packaging and Manufacturing Technology, IEEE Transactions on, vol. 25, no. 3, 2002, pp. 495-505.

[11] M. Dubarry, B. Y. Liaw, “Development of a universal modeling tool for rechargeable lithium batteries,” Journal of Power Sources, vol. 174, 2007, pp. 856-860.

[12] H. He, R. Xiong, X. Zhang, F. Sun, J. Fan, “State of-charge estimation of the lithium-ion battery using an adaptive extended Kalman filter based on an improved Thevenin model,” Vehicular Technology, IEEE Transactions on, vol. 60, no. 4, 2011, pp. 1461-1469.

[13] S. Abu-Sharkh, D. Doerffel, “Rapid test and nonlinear model characterization of solid-state lithiumion batteries,” Journal of Power Sources, vol. 130, no.1, 2004, pp. 266–274.

[14] E. Karden, S. Buller, R. W. De Doncker, “A frequency-domain approach to dynamical modeling of electrochemical power sources,” Electrochimica Acta, vol. 47, no. 13, 2002, pp. 2347-2356.

[15] Karden, E., Buller, S., De Doncker, R. W. “A frequency-domain approach to dynamical modeling of electrochemical power sources,” Electrochimica Acta, vol. 47, no. 13, 2002, pp. 2347-2356.

[16] S. Buller, M. Thele, R. W. A. A. De Doncker, E. Karden, “Impedance-based simulation models of supercapacitors and Li-ion batteries for power electronic applications,” Industrial Appications, IEEE Transactions on, vol. 41, no. 3, 2005, pp. 742-747.

[17] H. He, R. Xiong, H. Guo, S. Li, “Comparison study on the battery models used for the energy management of batteries in electric vehicles,” Energy Conversion and Management, vol. 64, 2012, pp. 113-121.

[18] S. Castano-Solis, D. Serrano-Jimenez, L. Gauchia, J. Sanz, “The Influence of BMSs on the Characterization and Modeling of Series and Parallel Li-Ion Packs,” Energies vol. 10, 2017, pp. 273.

[19] K. Cooper, M. Smith, “Electrical test methods for online fuel cell ohmic resistance measurement,” Journal of Power Sources, vol. 160, no. 1, 2006, pp. 1088-1095.

[20] S. Castano, L. Gauchia, J. Sanz, “Effect of packaging on Supercapacitors String Modeling: Proposal of a Functional Unit Defined Around the Balancing Circuit,” Components, Packaging and Manufacturing Technology, IEEE Transactions on, vol. 3, no. 8, 2013, pp. 1390-1398.

[21] D. Andre, M. Meiler, K. Steiner, H. Walz, T. SoczkaGuth, D. U. Sauer, “Characterization of highpower lithium-ion batteries by electrochemical impedance spectroscopy. I. Experimental investigation”. Journal of Power Sources, vol. 196, no. 12, 2011, pp. 5334-5341.

[22] S. Castano-Solis, L. Gauchia, D. Serrano Jimenez, and J. Sanz Feito, “Off-the-Shelf and Flexible Hybrid Frequency and Time Domain Experimental Architecture Setup for Electrochemical Energy Modules Testing under Realistic Operating Conditions,” IEEE Trans. on Energy Conversion , vol. 32, no. 2, 2017, pp. 620-627.

[23] D. Andre, M. Meiler, K. Steiner, C, Wimmer, T. Soczka-Guth, D. U. Sauer, “Characterization of high-power lithium-ion batteries by electrochemical impedance spectroscopy. II: Modelling,” Journal of Power Sources, vol. 196, no. 12, 2011, pp. 5349-5356.

[24] W. Zhu, R. Payne, R. Nelms, B. Tatarchuk, “Equivalent circuit elements for PSpice simulation of PEM stacks and pulse load,” Journal of Power Sources, vol. 178, no. 1, 2008, pp. 197-206.

[25] S. Buller, M. Thele, R. W. A. A. De Doncker, E. Karden, “Impedance-based simulation models of supercapacitors and Li-ion batteries for power electronic applications,” Industrial Appications, IEEE Transactions on, vol. 41, no. 3, 2005, pp. 742-747.

[26] A. Bouscayrol, “Different types of hardware-in-theloop simulation for electric drives", IEEE

International Symposium on Industrial Electronics, Cambridge, UK, June 2008.

[27] L. Gauchia, J. Sanz, “A per-unit hardware-in-theloop simulation of a fuel cell/battery hybrid energy system”, IEEE Transactions on Industrial Electronics, vol. 57, no. 4, 2010, pp. 1186-1194.

[28] T. J. Barlow, S. Latham, I. S. Mccrae, Boulter, P.G., “A reference book of driving cycles for use in the measurement of road vehicle emissions”, published Project Report PPR354.

[29] M. Andre, “The ARTEMIS European driving cycles for measuring car pollutant emissions”, Science of The Total Environment, Volumes 334–335, 1 December, Pages 73-84, 2004.

Range of Porosity in Typical Regenerators for an Appropriate Balance Between Heat Exchange and Pressure Drop

Paulo Cesar Mioralli[1], Marcelo Augusto Botan da Silva[1], Elson Avallone[1], Paulo Henrique Palota[1], Pablo Sampaio Gomes Natividade[1]

[1]Federal Institute of São Paulo - IFSP, Catanduva, Brazil
mioralli@ifsp.edu.br, marcelo.botan@aluno.ifsp.edu.br, elson.avallone@ifsp.edu.br, palota@ifsp.edu.br, pablo.sgn@ifsp.edu.br

Abstract — **Heat transfer analysis in a rotary regenerator is performed. The matrix porosity of the exchanger directly influences the amount of heat transfer between the circulating gases in the equipment and the matrix plates. From the pre-established flow rate values in the regenerator, the total heat transfer and the pressure drop are calculated for different matrix porosity values. The heat transfer coefficient in the equipment and the friction factor are obtained from correlations. The total heat transfer is obtained using the Effectiveness-NTU method specific to rotary regenerators. A computer program is developed for the simulation of typical rotary regenerators. The results show that there is a range of matrix porosity values in which there is a good relationship between the total heat transfer and the pressure drop in the equipment.**

Keywords - rotary regenerator, heat transfer, simulation.

NOMENCLATURE

A	free flow cross-sectional area, m^2
A_m	matrix cross-sectional area, m^2
A_T	total cross-sectional frontal area ($A+ A_m$), m^2
A_{tr}	heat exchange area, m^2
C	heat capacity rate of fluids, W/K
C_r	matrix heat capacity rate, W/K
C_r*	matrix heat capacity rate ratio on the cold or hot side
c_p	specific heat of gas under constant pressure, $J/kg\ K$
c_m	specific heat of matrix, $J/kg\ K$
D_h	hydraulic diameter, m
e	thickness of the plates that constitute the matrix channels, m
f	Darcy friction factor
h	convective heat transfer coefficient, $W/m^2\ K$
k	thermal conductivity, $W/m\ K$
L	length of matrix, m
$\dot{m}$	gas mass flow rate, kg/s
m_m	mass of matrix, kg
n	rotational speed, rpm
NTU	number of heat transfer units on the cold or hot side
Nu	Nusselt number
P	periphery of the channel, m
Pr	Prandtl number
Q	heat transfer rate, W
Re	Reynolds number
r_h	hydraulic radius $(D_h/4)$, m
T	temperature, K
V	fluid velocity in the channel, (m/s)

Greek Symbols

μ	dynamic viscosity, (Ns/m^2)
ε_0	effectiveness of counterflow heat exchanger
ε_r	regenerator effectiveness
φ_r	correction factor
ρ	fluid density, (kg/m^3)
σ	porosity
ΔP	distributed pressure drop, Pa

Subscripts

i	inlet
o	outlet
c	cold
h	hot
min	minimum
max	maximum

ISBN: 978-86-80616-03-2

I. INTRODUCTION

Rotary regenerator is used in several heat recovery systems. Among its varieties of applications stand out refrigeration systems, ventilation plants, thermal comfort, power plant boilers, recovery of waste thermal energy and a number of situations where the availability of the energy does not chronologically coincide with demand [1].

Over the years, researchers of the academic community and industry have focused efforts on improving the rotary regenerator due to some of its advantages such as compactness, efficiency, economy and high flexibility. The studies found in the literature incorporate various aspects of the equipment. The pioneer works about the rotary regenerator were essentially experimental with investigations that mainly included the effectiveness, the heat exchange and the pressure drop [2–5]. Later studies to the most recent ones include aspects of the rotary regenerator such as mathematical modeling and numerical analysis [6-9], mass transfer [10-13], leakage control [14-16], thermodynamic analysis [17-19], rotational speed of the matrix [20-22] and geometry of matrix ducts [23-26].

Analysis from the matrix porosity of the rotary regenerator are found in a small number of works [27-31]. The present study analyzes three typical rotary regenerators. The objective is to establish a range of matrix porosity values in which there is a good balance between the total heat transfer and the pressure drop in the equipment.

II. THEORETICAL ANALYSIS AND PROCEDURE

Description of the Regenerator

The schematic diagram of the rotary regenerator is show in Fig. 1. Two gas streams are introduced counterflow-wise through the parallel ducts of regenerator. Cold gas is injected inside one duct and hot gas inside the other. The porous matrix, that stores energy, continuously rotates through these parallel ducts. The matrix receives heat from the hot gas on one side and transfers this energy to the cold gas on the other side. The matrix channels were assumed smooth. The fluid velocity was considered constant inside each channel.

Some geometric parameters can be defined based on Fig. 1. The total frontal cross-sectional area A_T is determined by the sum of the free flow cross-sectional area A and the matrix cross-sectional area A_m of the regenerator

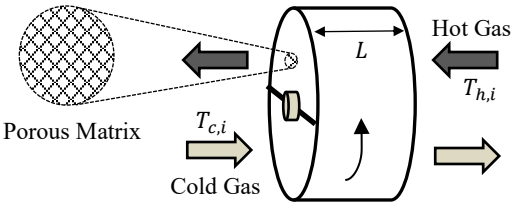

FIGURE 1. SCHEMATIC DIAGRAM OF THE ROTARY REGENERATOR.

$$A_T = A + A_m \,. \tag{1}$$

The matrix porosity σ is defined by the ratio between A and A_T

$$\sigma = \frac{A}{A_T} \,. \tag{2}$$

The hydraulic radius r_h is defined by the ratio between A and the perimeter P of the plates that compose the matrix. The matrix perimeter can be written as function of the matrix cross-sectional area A_m

$$r_h = \frac{D_h}{4} = \frac{A}{P} \,, \tag{3}$$

$$P = \frac{A_m}{(e/2)} \,, \tag{4}$$

where D_h and e are the matrix duct hydraulic diameter and the matrix duct wall thickness, respectively.

The porosity and the hydraulic radius are interdependent parameters and influence the thermal exchange in the regenerator. The hydraulic radius can be written as function of the porosity and the matrix duct wall thickness from the definitions above and algebraic manipulations

$$r_h = \frac{\sigma}{1-\sigma}\left(\frac{e}{2}\right) \,. \tag{5}$$

The hydraulic radius is an important parameter and its use is justified in the correlations for friction factor and Nusselt number.

Since the geometric characteristics of the regenerator are known, the heat transfer in the

equipment can be calculated using the Effectiveness-NTU method for rotary regenerators.

Effectiveness-NTU Method for Rotary Regenerators

The Effectiveness-NTU method for rotary regenerators [21] consists of calculating the effectiveness ε_0 of a conventional counterflow heat exchanger and correcting this effectiveness by a correction factor φ_r that takes into account the rotational speed and the matrix heat capacity rate of regenerator. Thus, the effectiveness of the regenerator ε_r is given by

$$\varepsilon_r = \varepsilon_0 \, \varphi_r \, . \tag{6}$$

The effectiveness ε_0 of a conventional counterflow heat exchanger is defined by

$$\varepsilon_0 = \frac{1 - exp\left[-NTU\left(1 - C^*\right)\right]}{1 - C^* exp\left[-NTU\left(1 - C^*\right)\right]} \tag{7}$$

where C^* is the ratio between the fluids heat capacity rates and NTU is the number of heat transfer units defined as follows

$$C^* = \frac{C_{mim}}{C_{max}} \tag{8}$$

$$NTU = \frac{1}{C_{min}} \left[\frac{1}{\left(1/hA_{tr}\right)_c + \left(1/hA_{tr}\right)_h} \right] \tag{9}$$

where h is the convective heat transfer coefficient and A_{tr} is the matrix thermal exchange area on the side of the hot or cold stream. The parameters C_{min} and C_{max} correspond to the minimum and maximum values of the fluids heat capacity rates.

The correction factor φ_r in Eq. (6) is given by

$$\varphi_r = \frac{1}{9 C_r^{*1.93}} \tag{10}$$

$$C_r^* = \frac{C_r}{C_{min}} \tag{11}$$

$$C_r = \frac{n}{60} m_m \, c_m \tag{12}$$

where C_r is the matrix heat capacity rate, n is the matrix rotational speed, m_m is the matrix mass and c_m is the specific heat of matrix.

Finally, the total heat transfer Q in the regenerator is obtained in the same way as the Effectiveness-NTU method for conventional heat exchangers

$$Q = \varepsilon_r \, Q_{max} \tag{13}$$

$$Q_{max} = C_{min} \left(T_{h,i} - T_{c,i}\right) \tag{14}$$

where Q_{max} is the maximum possible heat transfer and the term between parenthesis corresponds to the difference between the inlet temperature of the hot stream and the inlet temperature of the cold stream.

Hydrodinamic and Thermal Analysis

The hydrodynamic and thermal analysis are performed for each gas stream. The pressure drop ΔP in the matrix ducts and the convective heat transfer coefficient h are obtained from correlations for Darcy friction factor f and Nusselt number Nu. Correlations for smooth ducts with circular cross-sectional area were used based on the hydraulic diameter of matrix ducts for laminar flow regime. The correlations take into account hydrodynamically fully developed flow with thermal entrance length and constant wall temperature boundary condition.

$$f = \frac{64}{Re_{D_h}} \tag{15}$$

$$Nu = 3.66 + \frac{0.0668\left(\frac{D_h}{L}\right) Re_{D_h} Pr}{1 + 0.04\left[\left(\frac{D_h}{L}\right) Re_{D_h} Pr\right]^{\frac{2}{3}}} \tag{16}$$

where L is the length of matrix, Re_{Dh} is the Reynolds number and Pr is the Prandtl number.

The distributed pressure drop ΔP is given by equation of Darcy-Weisbach and the convective heat transfer coefficient h is expressed in terms of Nusselt number

$$\Delta P = f\ \rho \frac{L}{D_h}\frac{V^2}{2} \quad (17)$$

$$h = \frac{Nu\,k}{D_h} \quad (18)$$

where V, ρ and k are the fluid velocity, the fluid density and the fluid thermal conductivity, respectively.

Fluid and Matrix Properties

The fluid properties were obtained at the average temperature of each gas stream.

The fluid density for gases with moderate values of pressure and temperature is well represented by the equation of state of an ideal gas

$$\rho = \frac{p}{RT} \quad (19)$$

where p is the pressure of fluid, T is the average temperature of gas stream and R is the ideal gas constant. The values of air atmospheric pressure $p = 10^5 Pa$ and ideal gas constant for air $R = 287\ Nm/kgK$ were assumed.

The dynamic viscosity μ and the thermal conductivity k of fluids can be approximated by the Shuterland equations [32] as follows

$$\frac{\mu}{\mu_0} \approx \left(\frac{T}{T_0}\right)^{3/2} \frac{T_0 + S}{T + S} \quad (20)$$

$$\frac{k}{k_0} \approx \left(\frac{T}{T_0}\right)^{3/2} \frac{T_0 + S}{T + S} \quad (21)$$

where S is the Shuterland constant temperature, which is characteristic of each gas. Considering air, $S = 111K$ for dynamic viscosity and $S = 194K$ for thermal conductivity. The parameters T_0, μ_0 and k_0 are reference constants, whose values are $T_0 = 273K$, $\mu_0 = 1.716x10^{-5} Pa.s$ and $k_0 = 0.0241\ W/mK$ for air.

The specific heat of gas under constant pressure c_p is obtained by a polynomial equation [33] with application for several gases in the temperature range between *300* and *1,000 K*

$$\frac{c_p}{R} = \alpha_0 + \beta_0 T + \gamma_0 T^2 + \delta_0 T^3 + \varepsilon_0 T^4 \quad (22)$$

where $\alpha_0 = 3.653$, $\beta_0 = -1.337x10^{-3}$, $\gamma_0 = 3.294x10^{-6}$, $\delta_0 = -1.913x10^{-9}$ and $\varepsilon_0 = 0.2763x10^{-12}$ are the constants for air.

The Prandtl number Pr is obtained from the ratio between some fluid properties, as follow

$$Pr = \frac{\mu\, c_p}{k} \quad (23)$$

The matrix properties of the rotary regenerator were assumed constant. The AISI 1010 low alloy carbon steel and the 2024-T6 aluminum alloy materials were considered for the matrix in this work. The Table 1 shows the matrix properties used for the simulated regenerator cases, where c_m and ρ_m are the specific heat and the density of matrix, respectively.

TABLE 1. MATRIX PROPERTIES OF THE ROTARY REGENERATOR.

	c_m (J/kg K)	ρ_m (kg/m^3)
2024-T6 Aluminum	875	2,770
AISI 1010 Steel	434	7,832

Computational Program

A computer program written in *C* programming language was developed for the simulation of rotary regenerator. The *Dev-C++* software was used for compilation and recording results. Three typical sizes of regenerators were simulated: small, medium-sized and large.

The total heat transfer in the regenerator and the pressure drop of gas streams were calculated for each porosity level of the matrix from the prescribed mass flow rate for each gas stream. The other geometrical parameters of the equipment were fixed.

An iterative process was used to obtain the fluid flow and the heat transfer. An outlet temperature values of each stream was assumed at the beginning of this process. Then, the fluid properties were evaluated at the average temperature of each gas stream. Based on these properties, the fluid flow and the heat transfer were obtained from correlations and the Effectiveness-NTU method for rotary regenerators. The iterative process continued

until convergence of the outlet temperatures for both streams. The whole process was repeated for each matrix porosity value. Fig. 2 shows a schematic diagram of the calculation process for the regenerator analysis.

The subrelaxation factor of *0.5* was used to the convergence of the outlet temperature values. The tolerance for convergence iterative procedure was adjusted as 10^{-3} for the outlet temperatures.

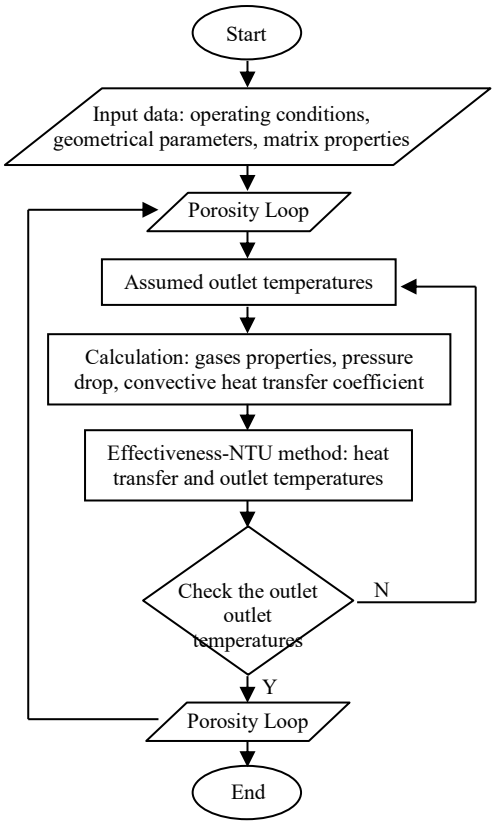

FIGURE 2. SCHEMATIC DIAGRAM OF THE CALCULATION PROCESS.

The calculations were performed considering the steady-periodic condition of the regenerator, indicating that the temperatures no longer changed in any angular or axial position of the matrix.

For the purpose of program validation, the outlet temperatures of gas streams were calculated at a medium-sized rotary regenerator with corrugated ducts. The results were compared with those obtained by Mioralli [34], who numerically simulated the equipment using the finite volume method and compared the numerical results with field data. The comparison between the results of presented study and those of Mioralli [34] are in good agreement with a larger discrepancy for the hot gas stream, as shown in Table 2.

TABLE 2. COMPARISON OF THE PRESENT DATA WITH THOSE OF MIORALLI [34].

Outlet Temperature (°C)	Present work	Mioralli [34]	Difference
$T_{c,o}$	441.26	428.92	0.028
$T_{h,o}$	160.51	142.43	0.113

III. RESULTS AND DISCUSSION

Three typical rotary regenerators of different sizes were simulated: a small, a medium-sized and a large regenerator. The operational conditions of the regenerators are based on information found in the literature and industry. The simulations were carried out from a variation of porosity values in the range of 0.2 to the last value that would guarantee both gas streams of the equipment in laminar regime. The input data of the computer program developed for the simulations are listed in Table 3.

TABLE 3. OPERATIONAL CONDITIONS: INPUT DATA FOR COMPUTER PROGRAM OF TYPICAL ROTARY REGENERATORS.

Regenerator	L (m)	e (m)	D (m)	n (rpm)	Inlet Temperature (°C)		Mass Flow Rate (kg/s)	
					$T_{h,i}$	$T_{c,i}$	$\dot{m}_{h,i}$	$\dot{m}_{c,i}$
Small	0.2	0.00035	0.7	8	50	20	0.68	0.76
Medium-sized	1.5	0.00050	6.0	3	450	80	39.00	62.00
Large	3.5	0.00060	15.0	2	600	150	292.50	411.30

Fig. 3 shows the total heat transfer in the small regenerator and the pressure drop of both gas streams as a function of the matrix porosity. It is observed that from the porosity value around *0.5*, the heat transfer in the equipment begins to decrease more significantly. The pressure drop for both gas streams behaves similarly. There is a decrease in the pressure drop values as the porosity increases. For $\sigma = 0.6$, the amount of heat transfer in the

equipment is significant. However, the pressure drop (around *600 Pa*) is still high for this typical regenerator size operating closer to optimal conditions [35]. For the porosities *0.70* and *0.76*, the percentages of the decrease in heat transfer are, respectively, 22% and 33% when compared to the highest value $Q \approx 20.5\ kW$ for $\sigma = 0.2$. The percentages of the decrease in the pressure drops values are greater than 99% for the same porosity range when compared to the highest values of ΔP for both streams with $\sigma = 0.2$. In this case, the pressure drops values are lower than *200 Pa*. The decrease of heat transfer is around 40% for $\sigma = 0.77$ when compared to the heat transfer obtained for $\sigma = 0.2$. So, the range $0.70 \leq \sigma \leq 0.76$ can be assumed for an appropriate balance between heat exchange and pressure drop for the typical small regenerator, considering the decrease of heat transfer less than 40%.

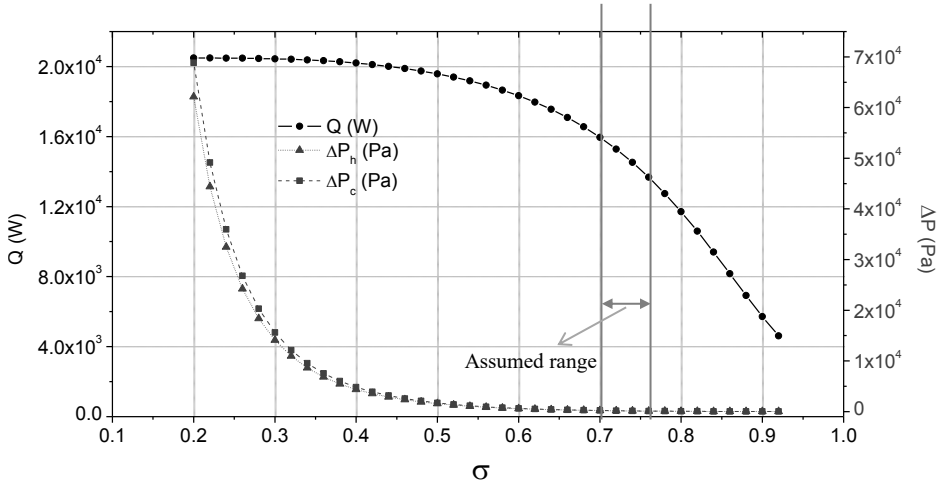

FIGURE 3. HEAT TRANSFER AND PRESSURE DROP VERSUS POROSITY FOR SMALL REGENERATOR.

Fig. 4 shows the total heat transfer in the medium-sized regenerator and the pressure drop of both gas streams as a function of the matrix porosity. For this regenerator, the pressure drop values are in the range of up to about *350 Pa* for operating conditions with satisfactory results [35]. Based on this information, the range $0.83 \leq \sigma \leq 0.90$ can be assumed for an appropriate balance between heat exchange and pressure drop for the typical medium-sized regenerator.

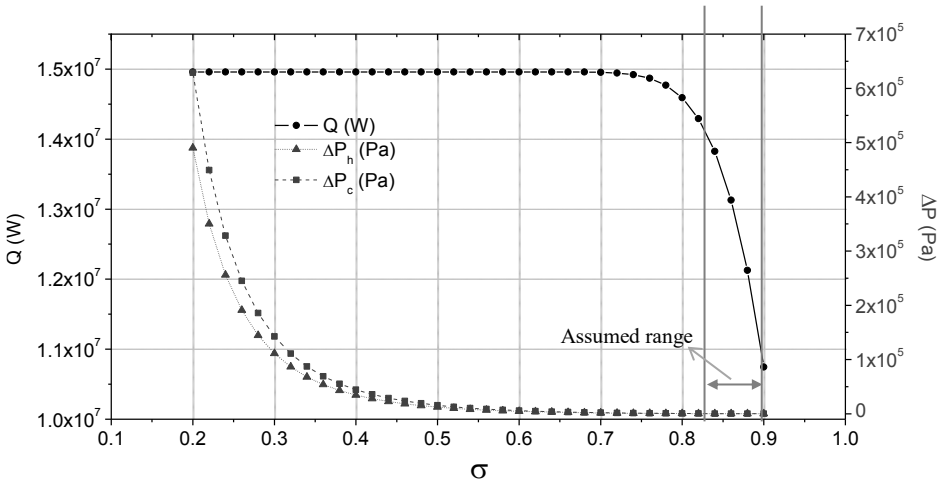

FIGURE 4. HEAT TRANSFER AND PRESSURE DROP VERSUS POROSITY FOR MEDIUM-SIZED REGENERATOR.

This range taking into account the decrease of heat transfer in the equipment less than 40% when compared to the heat transfer ($Q \approx 15\ MW$) obtained for $\sigma = 0.2$. The range also includes pressure drop values lower than *350 Pa*, which correspond to a decrease greater than 99% when compared to the highest values of ΔP for both streams with $\sigma = 0.2$. In this simulation, porosity values greater than *0.9* imply a turbulent flow regime for at least one of the gas streams, which is not the object of the presented study. Analogously to that observed in Figs. 3 and 4, Fig. 5 shows the total heat transfer in the large regenerator and the pressure drop of both gas streams as a function of the matrix porosity. The pressure drop values observed in the large regenerator for good operating conditions are in the range of up to about *600 Pa* [35]. Considering this aspect and the decrease of heat transfer less than 40% when compared to the heat transfer ($Q \approx 0.14\ GW$) obtained for $\sigma = 0.2$, the range $0.86 \leq \sigma \leq 0.90$ can be assumed for an appropriate balance between heat exchange and pressure drop for the typical large regenerator. In this case, porosity values greater than *0.9* imply a turbulent flow regime for at least one of the gas streams, as happened to the simulation of medium-sized regenerator.

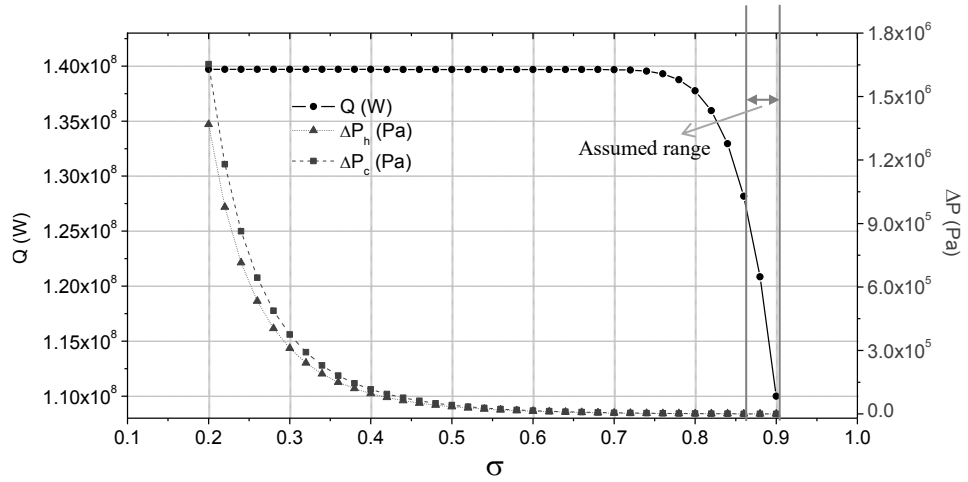

FIGURE 5. HEAT TRANSFER AND PRESSURE DROP VERSUS POROSITY FOR LARGE REGENERATOR.

A simultaneous analysis of Figs. 3, 4 and 5 shows that the assumed ranges of porosity values, for an appropriate balance between heat exchange and pressure drop, moves to the right on the abscissa axis as the dimensions and typical operational conditions of the rotary regenerators increase. It is also observed that the assumed porosity ranges for the three simulated cases of regenerator are relatively narrow.

A larger porosity range could be established if higher values for pressured drop in the regenerator were considered. However, this would imply higher pumping power and energy costs. On the other hand, for the considered pressure drop values, the assumed porosity range could be even lower if a decrease in heat transfer was desired to be less than 30% or 20% when compared to the heat transfer obtained for $\sigma = 0.2$.

IV. CONCLUSIONS

In this work, the heat transfer and the pressure drop in three typical rotary regenerators were computationally investigated from the pre-established mass flow rate for each gas stream of the equipment and different matrix porosity values. The influence of matrix porosity on the total heat transfer and the pressure drop of equipment was confirmed.

For each simulated typical regenerator, a range of porosity values for an appropriate balance between heat exchange and pressure drop was chosen. The results showed that the selected porosity ranges are narrow and moves to the right on the abscissa axis as the dimensions and typical operational conditions of the rotary regenerators increase. Nonetheless, the extent of porosity range may vary according to the desired limits for the heat transfer and the pressure drop of gas streams.

Additionally, the obtained results can contribute to the definition of operational conditions of rotary regenerators in search of better performance.

REFERENCES

[1] Y. L. Bae, "Performance of Rotary Regenerative Heat Exchanger - A Numerical Simulation", Doctoral Thesis, Oregon State University, 1986.

[2] H. Karlsson, S. Holm, "Heat Transfer and Fluid Resistances in Ljungstrom Regenerative-Type Air Preheaters", Transactions of the ASME, 1943, v. 65, pp. 61-72.

[3] A. L. London, W. M. Kays, "The Gas-Turbine Regenerator – the Use of Compact Heat-Transfer Surfaces", Transactions of the ASME, 1950, v. 72, pp. 611-621.

[4] D. B. Harper, W. M. Rohsenow, "Effect of Rotary Regenerator Performance on Gas-Turbine-Plant Performance", Transactions of the ASME, 1953, v. 75, pp. 759-765.

[5] T. J. Lambertson, "Performance Factors of a Periodic-Flow Heat Exchanger", Transactions of the ASME, 1958, v. 80, pp. 586-592.

[6] E. Van Den Bulck, J. Mitchell, S. A. Klein, "Design Theory for Rotary Heat and Mass Exchangers – I: Wavy Analysis of Rotary Heat and Mass Exchangers with Infinite Transfer Coefficients", International Journal of Heat and Mass Transfer, 1985, v. 28, pp. 1575-1586.

[7] N. Ghodsipour, M. Sadrameli, "Experimental and Sensitivy Analisys of a Rotary Air Preheater for the Flue Gas Heat Recovery", Applied Thermal Engineering, 2003, v. 23, pp. 571-580.

[8] Z. Wu, R. V. N. Melnik, F. Borup, "Model-Based Analysis and Simulation of Regenerative Heat Wheel", Energy and Buildings, 2006, v. 38, pp. 502-514.

[9] , C. E. L Nóbrega, N. C. L. Brum, "Local and Average Heat Transfer Coefficients for Rotary Heat Exchangers", Proceedings of COBEM, 2007, paper code 1119.

[10] W. Tanthapanichakoon, A. Prawarnpit, "New Simple Mathematical Model of a Honeycomb Rotary Absorption-Type Dehumidifier", Chemical Engineering Journal, 2002, v. 86, pp. 11-15.

[11] L. A.Sphaier, W. M. Worek, "Analysis of Heat and Mass Transfer in Porous Sorbents used in Rotary Regenerators", International Journal of Heat and Mass Transfer, 2004, v. 47, pp. 3415-3430.

[12] Y. M. Harshe, R. P. Utikar, V. V., Ranade, D. Pahwa, "Modeling of Rotary Desiccant Wheels", Chemical Engineering & Technology, 2005, v. 28, n. 12, pp. 1473-1479.

[13] L. A. Sphaier, "Unified Formulation for Heat and Mass Transfer in Rotary Regenerators", Proceedings of COBEM, 2007, paper code 1290.

[14] T. Skiepko, "Experimental Results Concerning Seal Clearances in Some Rotary Heat Exchangers", Heat Recovery Systems and CHP, 1988, v. 8, pp. 577-581.

[15] T. Skiepko, "Method of Monitoring and Measuring Seal Clearances in a Rotary Heat Exchanger", Heat Recovery Systems and CHP, 1988, v. 8, pp. 469-473.

[16] R. K. Shah, T. Skiepko, "Influence of Leakage Distribution on the Thermal Performance of a Rotary Regenerator", Applied Thermal Engineering, 1999, v. 19, pp. 685-705.

[17] T. Skiepko, "Irreversibilities Associated with a Rotary Regenerator and the Efficiency of a Steam Power Plant", Heat Recovery Systems and CHP, 1990, v. 10, pp. 187-211.

[18] R. K. Jassim, B. A. Habeebullah, A. S. Habeebullah, "Exergy Analysis of Carryover Leakage Irreversibilities of a Power Plant Regenerative Air Heater", Proceedings Institution of Mechanical Engineers, Part A: Journal of Power and Energy, 2004, v. 218, pp. 23-32.

[19] W. Shang, R. W. Besant, "Effects of Manufacturing Tolerances on Regenerative Exchanger Number of Transfer Units and Entropy Generation", Journal of Engineering for Gas Turbines and Power, 2006, v. 128, pp. 585-598.

[20] O. Büyükalaca, T. Yilmaz, "Influence of Rotational Speed on Effectiveness of Rotary-Type Heat Exchanger", International Journal of Heat and Mass Transfer, 2002, v. 38, pp. 441-447.

[21] W. M. Kays, A. L. London, "Compact Heat Exchangers", McGraw-Hill, 3rd, New York, U.S.A, 1964.

[22] P. Worsϕe-Schmidt, "Effect of Fresh Air Purging on the Efficiency of Energy Recovery from Exhaust Air in Rotary Regenerators", Rev. Int. Froid, 1991, v. 14, pp. 233-239.

[23] B. Sunden, I. Karlsson, "Enhancement of Heat Transfer in Rotary Heat Exchangers by Streamwise-Corrugated Flow Channels", Experimental Thermal and Fluid Science, 1991, v. 4, pp. 305-316.

[24] E. Utriainen, B. Sunden, "Numerical Analysis of a Primary Surface Trapezoidal Cross Wavy Duct", International Journal of Numerical Methods for Heat & Fluid Flow, 2000, v. 10, n. 6, pp. 634-648.

[25] G. Comini, C. Nonino, S. Savino, "Effect of Space Ratio and Corrugation Angle on Convection Enhancement in Wavy Channels", International Journal of Numerical Methods for Heat & Fluid Flow, 2003, v. 13, n. 4, pp. 500-519.

[26] L. Zhang, "Laminar Flow and Heat Transfer in Plate-Fin Triangular Ducts in Thermally Developing Entry Region", International Journal of Heat and Mass Transfer, 2007, v. 50, pp. 1637-1640.

[27] P. C. Mioralli, M. M. Ganzarolli, "Temperature Distribution in a Rotary Heat Exchanger", Proceedings of COBEM, 2005, paper code 0356.

[28] P. C. Mioralli, M. M. Ganzarolli, "Influence of Porosity in a Rotary Regenerator Performance", Proceedings of ENCIT, 2006, paper code CIT06-0549 (in Portuguese).

[29] P. C. Mioralli, M. M. Ganzarolli, "Optimal Porosity of a Rotary Regenerator with Fixed Pressure Drop", Proceedings of ECOS, 2007, pp. 1307-1314.

[30] P. C. Mioralli, M. M. Ganzarolli, "Thermal Optimization of a Rotary Regenerator with Fixed Pressure Drop", Proceedings of ENCIT, 2008, paper code 7-5302.

[31] P. C. Mioralli, M. M. Ganzarolli, "Thermal analysis of a rotary regenerator with fixed pressure drop or

fixed pumping power", Applied Thermal Engineering, vol. 52, 2013, pp. 187-197.

[32] F. M. White, "Viscous Fluid Flow", McGraw-Hill, New York, U.S.A, 1974.

[33] K. Wark, "Thermodynamics", McGraw-Hill, 4th, New York, U.S.A, 1983. Based in NASA SP-273, U. S. Government Printing Office, Washington, 1971.

[34] P. C. Mioralli, "Thermal Analysis of a Rotary Regenerator", Master dissertation, FEM/UNICAMP, Campinas-SP, Brazil, 2005 (in Portuguese).

[35] P. C. Mioralli, "Heat Transfer in a Rotary Regenerator with Fixed Pressure Drop", Doctoral thesis, FEM/UNICAMP, Campinas-SP, Brazil, 2009 (in Portuguese).

Online IFRA for Identification of Power Transformer Faults Based on Pulse Compression Method

Milan Ponjavic[1], Sasa Milic[2]

[1]Faculty of Electrical Engineering, Belgrade, Serbia, Milan@el.etf.rs
[2]Electrical Engineering Institute Nikola Tesla, Belgrade, Serbia, s-milic@ieent.org

Abstract—**The most accurate method, recommended for the energy transformers diagnostic, is the Frequency Response Analysis (FRA), in the form of two implementations, Impulse-Frequency Response Analysis (IFRA), and Sweep-Frequency Response Analysis (SFRA). Both implementations have their own advantages, as well as difficulties, when applied to a transformer without disconnecting them from the load. Till now, there is no clear consensus which of them is better. However, for the case of the IFRA method applied to distribution transformers, difficulties about signal injection on low voltage side can be easily overcome if the pulse compression method is used for generation of testing excitations. Using pulse compression method, other obstacles connected to high voltage application is avoided, and many signal processing advantages that exist in various system identification methods can be implemented. On that way on-line IFRA can be method of choice for preventive diagnostic of distribution transformers.**

Keywords - Power transformer, on-line diagnostic, winding deformation, frequency response analysis

I. INTRODUCTION

All transformers in power system are influenced to actions of different disturbances which can cause a several types of damage. On of the most important hazards in power transformers is mechanical defect in transformer windings. That defect can occur due to lack of appropriate transportation from the factory, explosions of combustible gas in transformer oil, earthquakes, electrodynamic forces caused by external electrical faults (such is short circuit fault), etc. Multiple stresses leads to accumulated deformations of transformation windings, insulation, or other vital parts, and finally to transformer failure, followed by withdrawal from exploitation and high follow-up costs.

In order to prevent and reduce negative consequences caused by power transformer failures, many diagnostic techniques are developed and standardized [1]-[5]. One of them, Frequency Response Analysis (FRA), is considered as a most powerful and accurate tool for sufficient winding deformation detection [1], [6]-[9]. Since the FRA considers a power transformer as a multi-input multi-output linear electric network, essence of the method is based on system identification theory [8], with specific details related only to hardware issues. Consequently, there are many particular FRA implementations, based on different hardware setups, different signal processing algorithms, with different performances under different conditions [1], [6]-[9].

In our paper, we suggest modification of IFRA method, directly applicable to distribution transformers. Particularly, we focus on excitation signal construction and some aspects of signal processing in analog and digital domain. We support some our claims by theoretical analysis and simulations, while experimental results are expected in near future.

II. FRA IN TRANSFORMER DIAGNOSTIC

Generally, any FRA implementation consists of 3 stages [9], [10], Fig 1. State 1 consists of a hardware that generates injection signal, and performs measurements of the response [9], [10]. Second and third stages deal with data storage, processing and interpretation.

ISBN: 978-86-80616-03-2

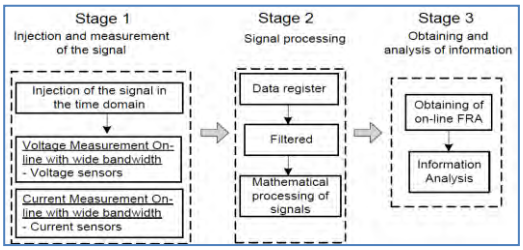

Figure 1. FRA test stages [10]

Despite great number of technical papers addressing third stage, it must be highlighted that not a single aspect of its implementation can be an issue. According to current state of information technology, A/D conversion hardware with sampling rates in order of tens mega samples per second are broadly available, high speed memories of GB capacity are at every step of life, and high throughput communication links, like 4G or 5G, makes cloud processing of practically any amount of data affordable to any Internet-connected edge device. Thus only critical part of FRA equipment is hardware from stage 1, responsible for:

- injection of appropriate excitation signal in order to ensure responses with decent signal to noise ratio, and,
- low noise acquisition with proper resolution and dynamic range.

When the response that contain sufficient information is acquired, it can be stored to virtually unlimited memory resources, and wirelessly transferred to the cloud where can be processed by endless processing power. Data can be analyzed with any of numerous system identification tools, commercial or customized, based on some high-tech algorithms such are neural nets, fuzzy logic systems, etc, or simple but effective brute-force algorithms [13]-[15].

Depending on whether the transformer being tested is in exploitation, implementations of the method are classified into on-line FRA and off-line FRA.

A. *Off-line FRA: Impulse-Frequency Response Analyses*

For the case of off-line FRA there are two main approaches for excitation signal generation. One of them is based on impulse type excitation, called Impulse-Frequency Response Analyses (IFRA) [4], [6], [7], [11]-[16]. In that case, detection of changes in the reactive resistance of the defective winding can be based on two principles:

- the analysis of transient response, arising after exposure of transformer to the excitation in the form of an electrical impulse;
- Periodic impulse train: if electrical impulses are periodic, response in time domain can be processed with some of discrete transforms, and further analysis is conducted in frequency domain.

If the excitation is in the form of low voltage impulses (1V–20V typically), then approach is also called Low-Voltage Impulse method (LVI).

B. *Off-line FRA: Sweep-Frequency Response Analysis*

Another approach is based on the analysis of the frequency transfer function of the windings, where result is obtained by successive supply of the sinusoidal test voltage, typically 1-20 V_{RMS}, with different frequencies. The result is the ratio of a steady sinusoidal output from a test object, subject to a steady sinusoidal input. However, testing excitation can be in the form of multi-sine, or sweep-sine signal with reach harmonic spectrum. In practice, the approach is called Sweep-Frequency Response Analysis (SFRA) [5]-[7], [12].

C. *Off-line SFRA and IFRA relation*

In essence, both approaches are very close, and differ only in the type of excitation. Detection of winding violations of in these methods is made by comparison of actual frequency or transient response on phases (defectogram), concerning each other, or concerning the basic responses registered on the transformer earlier (normogram) in a faultless state.

D. *On-line FRA*

Off-line FRA implementations yield very accurate results, but assume transformer disconnection from the power grid and loads, and leave consumers without electricity. On the other hand, on-line FRA implementation, with target transformer in service, is an attractive alternative, allowing transformer monitoring at any time, even continuously [6],[7],[9],[10], [17]-[19].

Since on-line FRA is only specific type of FRA it fits into same 3 stages from Fig 1. The main differences compared to off-line FRA are implementation of stage 1. There are several problems in the realization of the step 1 [6], [7], [9], [10], [17]-[19]; the main of them are following:

- The measurement is performed under high voltages present in the system, so the interface to measurement equipment must be properly isolated.
- The power grid and loads are part of the system, and the response to the excitation is response of the complete system, not only target transformer. Effects of external voltages and noise sources are also includded.
- Because of time varying power line voltage, and also time varying current amplitudes, hysteresis effects cause time wearying transformer reactance. This leads to different responses for the same healthy transformer.

There is extensive quantity of technical and scientific papers that suggest various solutions to mentioned problems. Most of them are based on IFRA implementation, where uncontrolled high voltage impulses, similar to lighting, are applied as excitation, and bushing tap couplers are used as an access point for measurement. There are also suggestions that commutation of power factor correction switches can be used as transformer excitation. In both cases, current transformers based on Rogowski coil can be used for current measurement.

There are also few reports that suggest application of SFRA method, but with serious drawbacks related to signal injection.

III. On-line IFRA for distribution transformers

For a 10kV/0.4kV distribution transformer, simplified grid connection with consumer loads, together with LV load Z_P, and grid MV generator V_g, is presented on Fig. 2.

Consequently, are two options about IFRA excitation: it can be applied on MV side (port A), or on LV side (port B).

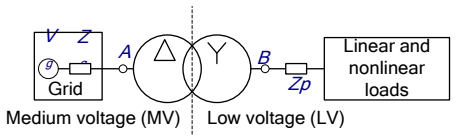

Figure 2. Simplified grid connection of 10kV/0.4kV distribution transformer

A. Excitation on primary side, port A

Since the grid impedance Z_g, is significantly lower than equivalent input impedance at the primary (MV) side of the transformer, it is questionable what portion of excitation current enters primary winding, and certainly a great part of excitation energy flows into the grid towards V_g. There is an option for signal injection, which is not mentioned in observed FRA literature, based on grid impedance measurement experiences, for example [20], but directly applicable only to small fraction of useful frequencies. Additionally, delta-connected primary windings requires differential excitation what further complicates implementation.

B. Excitation on secondary side, port B

Secondary (LV) side of the distribution transformer offers much more flexibility for connection of the excitation generator, due to lower voltage and more accessible terminals. Impedance seen in the secondary port of the transformer is much lower than impedance of the consumer loads, so the most of the excitation energy would enter transformer network. Connection is simpler, since wye configuration of the secondary windings allows single-ended excitation. On the other hand, excitation source requires much more current capacity, compared to source used for primary side. However, this approach has more advantages than disadvantages, and is used more frequently.

C. Measurement issues

Simplified principal diagram of measurement setup, used for measurement of equivalent impedance $Z_T(j\omega)$ presented on Fig 3. It should be noticed that $Z_T(j\omega)$ is not pure characteristic parameter of the transformer since it includes contribution of impedances connected to all other terminals.

Contribution of grid voltage and all voltages on other transformer terminals is represented as voltage generator V_{N1}, while contribution of consumer loads on LV side is represented as a current generator I_{N2}. Both

generators act as source of periodic noise with typically 50Hz fundamental frequency. Contribution of all other noise sources is represented with white noise current generator I_n. Voltage measured on point B consists of three parts:

$$V_B(j\omega) = \underbrace{I_T Z_T}_{V_T(j\omega)} + \underbrace{I_n Z_T}_{V_{Bn}(j\omega)} + \underbrace{V_{N1} + I_{N2} Z_T}_{V_{BN}(j\omega)} \quad (1)$$

First part, $V_T(j\omega)$ is response to the artificial excitation I_T. Second part, $V_n(j\omega)$ is the contribution of the white noise current generator I_n. It can be efficiently eliminated using well known noise mitigation techniques, based on extensive averaging, proper frequency bandwidth partitioning, and advanced filtration. Third part, $V_{BN}(j\omega)$ is contribution of periodic noise sources V_{N1} and I_{N2}. Theoretically, this part can be estimated by measurement with $I_T = 0$, together with random noise elimination techniques:

$$V_{BN}(j\omega) = V_B(j\omega, I_T = 0, I_n = 0). \quad (1)$$

Finally, the required response can be determined by formal equation:

$$V_T(j\omega) = V_B(j\omega) - V_{BN}(j\omega) + \underbrace{V_{Bn}(j\omega)}_{\to 0}. \quad (2)$$

The subtraction in the previous equation is not a mathematical operation, but rather a procedure for eliminating the contribution of $V_{BN}(j\omega)$. Usually, V_{BN} contribution to V_T is insertion of fundamental and several even harmonics, and usually its impact is present for frequencies below 1kHz. In that case, subtraction from the previous equation is performed by proper filtration in time domain. In rare, more complicated cases, additional countermeasures should be preformed.

IV. GENERATION OF EXCITATION SIGNAL

The best results for linear system identification in frequency domain is achieved by using sweep signal as excitation, and signal processing techniques developed for network analyzers. Such principle is applied in SFRA. But serious practical issue in all on-line FRA is interfacing of linear signal generator to power grid, and long lasting procedure. The alternative option is to design excitation signal in the form of narrow high amplitude impulse, which can mimic atmospheric lighting strokes, or to design

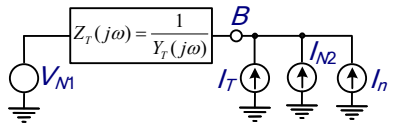

Figure 3. Simplified principal diagram of measurement setup

excitation signal which mimic normal operation of consumer load. In both cases, power system stays in normal operation condition.

A. Excitation signal in impulse form

Excitation signal in impulse form is basis of almost all IFRA methods. If signal is controllably generated by means of power electronic devices, it can be in rectangular form:

$$x(t) = A \cdot w \cdot \mathrm{rect}(w \cdot t). \quad (3)$$

$x(t)$ can be current or voltage, where w is width of the impulse, and Aw is impulse amplitude. If A=1 and $w \to \infty$, then $x(t)$ approaches Dirac Delta impulse, $x(t) \to \delta(t)$. In that case, response to $x(t)$ is impulse response, and Fourier transform of that response is required frequency response. In practice, such a case is far from true, since w and Aw are limited by safety and implementation reasons. For the practical $x(t)$, its frequency spectrum is in the form:

$$X(j\omega) = F_T\{x(t)\} = A \cdot \mathrm{sinc}(\omega / 2w). \quad (5)$$

First null of frequency spectrum is at $\omega_{01} / 2w = 1 \Rightarrow \omega_{01} = 2w$, giving useful range for transformer network identification of approximately ¾ of the (0, ω_{01}) interval, Fig. 4.

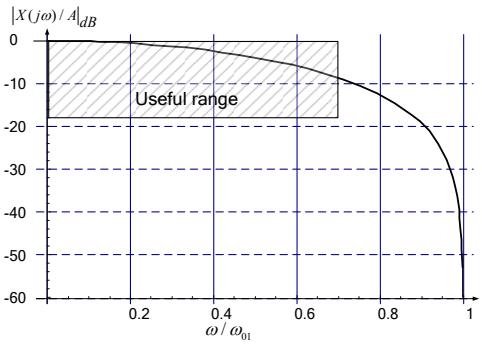

Figure 4. Amplitude spectrum of rectangular impulse

For the purpose of white noise elimination, extensive averaging should be implemented, and excitation signal should be periodic, and synchronized to line frequency (50Hz/60Hz). The train of excitation impulses should be accomplished by repetition period $T_0=2\pi/\omega_0$, giving discrete spectrum:

$$X[k]=\frac{1}{T}X(j\cdot(\omega=k\omega_0)),\ k\in\mathbf{Z} \qquad (4)$$

Applying such a signal as an excitation I_T from Fig. 3, and if noise sources are eliminated by proper signal processing techniques, discrete version of equivalent impedance (or admittance) can be estimated in the form:

$$Z_T[k]=1/Y_T[k]=V_T[k]/X[k]. \qquad (5)$$

B. *Excitation signal in compressed impulse form*

Narrow and high amplitude impulses are difficult to control. Reduction of the signal amplitude and expanding of the signal width is not a good option, since this approach leads to narrowing the excitation signal spectrum, decrease in signal power, and consequently to weak SNR. In order to overcome disadvantages of the impulse excitation in time domain, while keeping good characteristics in frequency domain, different pulse compression techniques can be applied [21], with a utilization of Maximum Length Binary Sequences (MLBS) as a most common [22]-[24].

Contrary to impulse shape, MLBS is the periodic sequence with two discrete amplitude levels, {0, X_0}, or { $-X_0/2$, $+X_0/2$}. Generation of the sequence is easily accomplished by means of circular shift register with proper feedback. The generated binary sequence is N periodic with repetition period T_0, giving the same amplitude spectra as rectangular impulse:

$$|X[k]|=\underbrace{\left(\frac{X_0\sqrt{N+1}}{2N}\right)}_{A}\mathrm{sinc}\left(\frac{k}{N}\right),\ k\neq 0, \quad (6)$$

where $N=2^n-1$ is the signal period, and n is a length of the shift register. The clock of the shift register $t_{clk}=2\pi/\omega_{clk}$ is related to the signal period in the form $T_0=2\pi/\omega_0=N\cdot t_{clk}$.

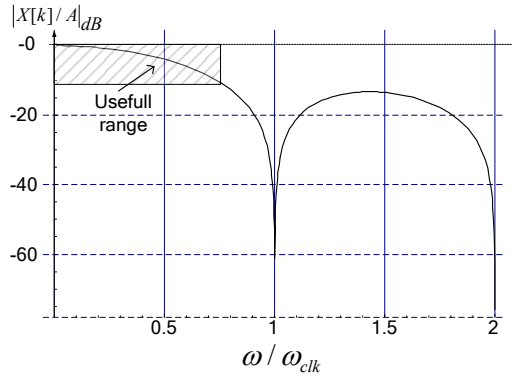

Figure 5. Amplitude spectrum of the MLBS excitation

Portion of the amplitude spectra (continual approximation) of the signal $X[k]$ is depicted on Fig. 5.

We defined useful part of the spectrum (~10dB reduction in harmonics amplitude) in the range ω < ~0.75 ω_{clk}, so the high-order low-pass filter with ~0.75 ω_{clk} cut-off frequency is applied later. However some other ranges can be used.

C. *Proposal of the injection of the excitation signal*

According to switching nature of the proposed excitation signal, and switching frequencies below 5MHz, signal injection can be accomplished using high-speed bilateral solid-state switch, Fig. 6, based on appropriate high-speed MOS transistor [25], for example APT6038BLL. Gate driver of the transistor M is driven by MLBS generator. When transistor is turned ON, voltage on *B*' port is ~0V. When transistor is turned off, voltage on *B*' port is equal to LV line voltage. On that way, voltage on port *B*' is modulated MLSB sequence:

$$v_{B'}(t)=x(t)\cdot 230\sqrt{2}\cos(\omega_L t),\ \omega_L=100\pi, \quad (7)$$

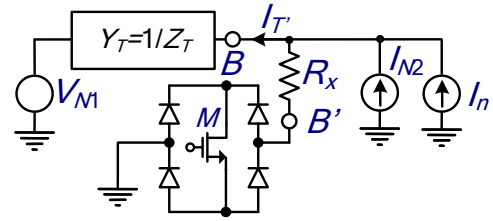

Figure 6. High speed bilateral solid-state switch.

where ω_L is power line frequency. Modulation of $x(t)$, with 50Hz cosine-wave, slightly changes original spectrum:

$$\left.\begin{aligned} V_{B'}(j\omega) &= \frac{X(j\omega+j\omega_L)+X(j\omega-j\omega_L)}{2} \\ V_{B'}(j\omega) &\approx X(j\omega) \end{aligned}\right\} \quad (10)$$

what have negligible influence if synchronization between ω_0 and ω_L is achieved.

Using injection circuit from Fig. 6, the resulting equivalent voltage generator at port *B*' have the same reach spectrum as displayed in Fig. 5.

V. MEASUREMENT PROPOSAL AND SIMULATION RESULTS

A. Transformer model

For the simulation purposes, simplified RLC equivalent circuit (single phase) of a distribution transformer is assumed (Fig. 7) [26], [27]. The meaning of the components in the model: $C_{S1,2}$ – serial capacitances, $R_{S1,2}$ – ohmic resistances $L_{S1,2}$ – leakage inductances, and $C_{g1,2}$ – parallel capacitances against copper/core in primary and secondary windings; L_m and R_m are magnetization inductance and magnetic core losses; C_{12} – mutual capacitive coupling between MV and LV windings. Primary of the transformer is terminated with grid impedance with typical value of 300Ω. Example of the theoretical equivalent LV admittance $Y_T = 1/Z_T$, of the assumed transformer is given in Fig 8. At low frequencies, below 1 kHz the magnetizing inductance is dominant. The first two parallel resonance frequency picks, at ~3kHz and ~10kHz originate from the anti-resonance between the magnetizing inductance L_m and parallel capacitances $C_{g1,2}$. The following resonance at ~20kHz is due to serial connection of leakage inductances and $C_{g1,2}$.

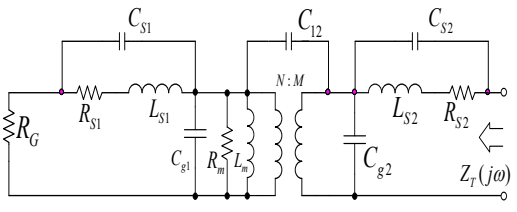

Figure 7. Transformer model, single phase, used for simulation

The third anti-resonance is caused by influence of parallel capacitances and leakage inductances. At higher frequencies, typically below 1MHz, the winding capacitances and inductances have dominant influence. Any mechanical change within the winding structure would affect this frequency range.

At frequencies of couple of MHz and beyond, several side effects have significant impact, and measurement results are unusable [26][27].

For the simulation purposes, measurement setup is made according to Fig. 6. Bilateral switch is implemented using universal Spice semiconductor models. Resistor R_x form Fig. 6. is set to 60Ω, what limits maximal injection current to ~5A, what is acceptable for transistor intended for the future real experiments. For the MLBS generator 12-bit shift register is used. Clock period T_{clk} is set to 0.6105μs, and together with $N = 4095$ provides $T_0 = 2.5$ms and synchronism to 50Hz. Current and voltage generators V_{N1} and I_{N2} are defined as a slightly clipped sine wave signals with net effect of 50Hz/230V$_{RMS}$ at port *B*. On that way even harmonic content is provided. White noise source I_n is not implemented, since in practice proper countermeasures efficiently suppress its influence [26].

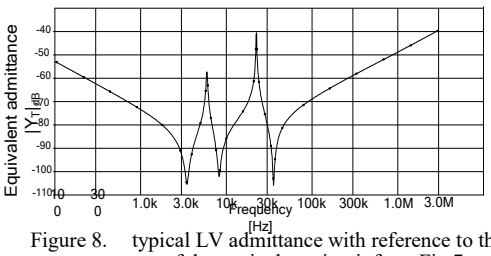

Figure 8. typical LV admittance with reference to the parameters of the equivalent circuit from Fig 7.

Current I_T (trough R_x) and voltage V_B are measured and processed with 50Hz notch filter in series with first order high-pass filter with 200Hz cut-off frequency, as well as anti-aliasing sixth order low-pass filter with 1MHz cut-off frequency. Acquisition of the response is started one T_0 period after start of excitation, on order to avoid transient regime. Response signals are acquired with 4MHz sampling rate, and FFT is performed over single T_0 period. Without any further processing, required admittance is calculated using (7), and result is depicted on Fig 9. The unsatisfactory result is achieved due to spectra leaking caused by V_{N1} and I_{N2} interference (higher harmonics).

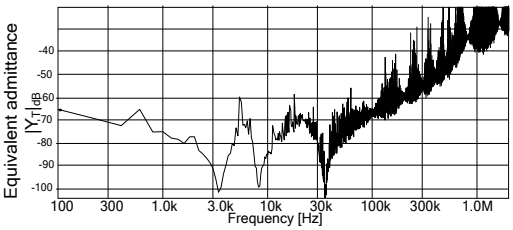

Figure 9. Calculated admittance by using (7), without post-processing.

By increasing high-pass filter to order of two, and by averaging 64 T_0 sampled intervals, significantly better result is achieved (Fig. 10). It can be seen that estimated admittance, in the 1kHz – 1MHz range is in good agreement with calculated admittance, even with simple data post processing.

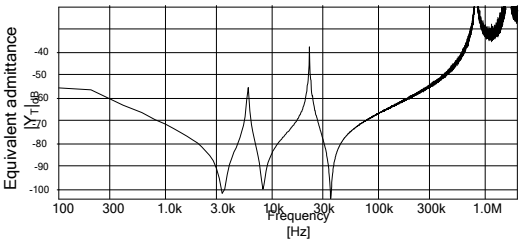

Figure 10. Calculated admittance by using (7), with post-processing

VI. CONCLUSION

According to simulations, proposed excitation signal in the form of MLBS, can be efficiently generated and injected in power lines on LV side of distribution transformer, without unnatural stress of the system. Since MLBS signal has identical spectral characteristics as high amplitude and narrow width rectangular impulse, it is suitable for identification of transformer frequency characteristics. As in all frequency domain system identification implementations, synchronization and averaging are mandatory. Even with simple post processing of the acquired response, results are promising.

Important aspect of the demonstrated measurement is a dynamic range of the response, in our example it is ~80dB, what can be covered by 16 bit AD conversion. However, required dynamic range in practice is 120dB [26], so the standard measures for greater dynamic range should be implemented in real implementation of the proposed method. Of course, final conclusion can be conducted after real hardware testing in real environment.

Proposed method, in the form described in our paper, is suitable for LV side of distribution transformers, due to breakdown voltages of semiconductor switches. With proper modifications, by using HF transformers for example, it is possible to adapt proposed method for MV side of transformer. However, principal obstacles related to excitation on MV side of transformer stays, no matter of excitation method.

REFERENCES

[1] X. M. Lopez-Fernandez, H. Bulent Ertan, and J. Turowski, Transformers Analysis, Design, and Measurement, CRC Press, Taylor & Francis Group, Boca Raton, FL 2013.

[2] Hydroelectric Research and Technical Services Group, Transformers: Basics, Maintenance, and Diagnostics, US Department of the Interior, Bureau of Reclamation, Government Printing Office, April 2005.

[3] ABB Business Area Power Transformers, Testing of Power Transformers and Shunt Reactors, 2nd Edition, ABB, Zurich, 2010.

[4] Breytenbach, R. “Winding frequency response analysis using the impulse frequency response analysis (IFRA) method” IEEE FRA Specification, Starlogic IFRA Submission Version 1.0; Starlogic Instrument Development:South Africa, 2003.

[5] Power Transformers—Part 18,Measurement of Frequency Response; IEC 60076-18 Ed.1; International Electrotechnical Commission (IEC): Geneva, Switzerland, 2012.

[6] G. U. Nnachi and D. V. Nicolae, "Diagnostic methods of frequency response analysis for power transformer winding a review," 2016 IEEE International Power Electronics and Motion Control Conference (PEMC), Varna, 2016, pp. 563-568

[7] Reza Khalili Senobari, Javad Sadeh, Hossein Borsi, "Frequency response analysis (FRA) of transformers as a tool for fault detection and location: A review", Electric Power Systems Research, vol. 155, 2018, pp. 172-180.

[8] Arun K. Tangirala, Principles of System Identification: Theory and Practice, CRC Press, Taylor & Francis Group, LLC, 2015.

[9] E. Gomez-Luna, G. Aponte Mayor, C. Gonzalez-Garcia and J. Pleite Guerra, "Current status and future trends in frequency-response analysis with a transformer in service," in IEEE Transactions on Power Delivery, vol. 28, no. 2, 2013,pp. 1024-1031.

[10] Gomez-Luna, Eduardo, Aponte Guillermo, Herrera, Wilder, Pleite, J. “Experimentally obtaining on-line FRA in transformers by injecting controlled pulses,” Ingeniería e investigación vol. 33 no. 1, 2013 pp. 43-45.

[11] Gomez-Luna, Eduardo, Aponte Guillermo, Herrera, Wilder, Pleite, J. “Non-invasive monitoring of transformers using the frequency response from

controlled transient signals," Electrical and Electronic Engineering, vol. 15 no. 2, 2013pp. 23-33.

[12] Yang Qing Su, Peiyu Chen Yong. "Comparison of impulse wave and sweep frequency response analysis methods for diagnosis of transformer winding faults". Energies, vol. 10, no. 4, 2017.

[13] H.Ch. Sun, Y.Ch. Huang, Ch.M. Huang,"Fault Diagnosis of Power Transformers Using Computational Intelligence - A Review", Energy Procedia, Vol. 14, 2012, pp. 1226-1231.

[14] Bhatt Palak, Nilesh Rabara, "Condition assessment of power transformer winding by FRA using different AI techniques", International Journal of Science Technology & Engineering, vol. 1, no. 12, |2015.

[15] Lekshmana Ramesh, Thangavelan, Prabavathi, "Review on power transformer internal fault diagnosis" Journal of Electrical Engineering, vol. 14, 2014, pp 70-79.

[16] C. Andrieu, D. Boss, "A wide frequency range model for a MV/LV core transformer", Proceedings of IPST'2001, pp. 81-86, June 24-28, Rio de Janeiro.

[17] Mehdi Bagheri, Mohammad Salay Naderi, Trevor Blackburn, "Advanced transformer winding deformation diagnosis: moving from off-line to on-line." IEEE Transactions on Dielectrics and Electrical Insulation, vol. 19, no. 4, 2012, pp. 1860-1870.

[18] E. Aburaghiega, M. E. Farrag, D. M. Hepburn and B. Garcia, "Power transformer health monitoring: A shift from off-line to on-line detection," 2015 50th International Universities Power Engineering Conference (UPEC), Stoke on Trent, 2015, pp. 1-6

[19] Zbigniew Staroszczyk, "Problems with in-service (on-line) power transformer parameters determination - case study", Harmonics and Quality of Power (ICHQP) 2016 17th International Conference on, pp. 962-967.

[20] A. Knop and F. W. Fuchs, "High frequency grid impedance analysis by current injection," 2009 35th Annual Conference of IEEE Industrial Electronics, Porto, 2009, pp. 536-541.

[21] Fulvio Gini, Antonio De Maio, and Lee Patton, eds. Waveform Design And Diversity For Advanced Radar Systems. Institution of engineering and technology, 2012.

[22] D. D. Rife & J. Vanderkooy, "Transfer-function measurement with maximum-length sequences," J. Audio Eng. Soc., vol. 37, 1989, pp. 419-444.

[23] Milan Ponjavic, Radivoje Djuric, "A Switching source of artifical electromagnetic field for geophysical prospecting", Electronics, vol. 6, no.1, Dec 2002.

[24] T. Roinila, M. Vilkko and J. Sun, "Online grid impedance measurement using discrete-interval binary sequence injection," in IEEE Journal of Emerging and Selected Topics in Power Electronics, vol. 2, no. 4, 2014, pp. 985-993.

[25] Microsemi Power Portfolio 2018, APT6838BLL, POWER MOS 7 MOSFET , available at: https://www.microsemi.com/document-portal/doc_download/14813-power-semiconductors-power-modules-and-rf-power-mosfets-catalog,

[26] "Electrical interferences - how to overcome undesirable effects," Transformers magazine, vol. 4. no. 2, april 2017, Merit Media Int. d.o.o, Croatia

[27] Florian Predl, "Interpretation of Sweep Frequency Response Analysis (SFRA) Measurement Results" OMICRON Australia, 2016.

Quality Management of Sugarcane focused on Efficient Bioelectricity, Ethanol and Sugar Production

Paulo Henrique Palota[1], Murilo Secchieri de Carvalho[1], Elson Avallone[1], Paulo César Mioralli[1], Manoel Fernando Martins[2]

[1]Federal Institute of Education, Science and Technology of São Paulo, Catanduva-SP, Brazil, palota@ifsp.edu.br
[2]Federal University of São Carlos, São Carlos, Brazil, manoelf@dep.ufscar.br

Abstract - **The main objective of this work is to present a proposal to manage sugarcane requirements in sugarcane growers' relations with their suppliers and customers, focusing on meeting the requirements of the product in order to produce ethanol efficiently as alternative energy source. To meet this objective, an empirical research of multiple cases was performed in the main agents of the sugarcane production chain in order to investigate the use of practices of the elements of supply chain quality management theory related to relationship with suppliers and clients. The field study showed that, in most cases, the relationship of both upstream and downstream growers is not of partnership, where there is a lack of actions that promote compliance with sugarcane quality requirements, such as actions to preserve product quality and incentives that promote quality as quality audits. The proposal is limited to a model that meets the requirements of sugarcane focusing on supplier-client integration. The proposal presents solutions to the existing gaps in sugarcane growers' relations with their suppliers and customers. This can corroborate towards the attendance and improvement of sugarcane quality, resulting in more efficiency in the production of the sugar, ethanol and electricity by milling plants.**

Keywords – Ethanol Production; Quality Management; Supplier/Costumer Relationship; Sugarcane Requirements.

I. INTRODUCTION

Sugar cane generates foreign exchange for Brazil through the production of sugar, ethanol and more recently the cogeneration of electric energy that has been gaining prominence as an alternative source in the Brazilian energy matrix.

With the advent of open markets, globalization and the prices of sugarcane main products are tied to commodity exchange and futures; the Brazilian sugarcane agribusiness needs to be competitive. The competitiveness and survival of the sugar-energy chain is subject to a management that add value to this chain through the improvement of the quality of its products and its processes for obtaining more competitive costs for the production chain. Since the quality of sugarcane, represented by Total Recoverable Sugar (TRS), which is the amount of sugar in kilograms per tons of sugarcane, was 141.85 in the 2008/2009 crop fell to 134 in the 2016/2017 harvest, a decrease of approximately 5,8%. Considering that the production of the 2016/2017 crop was 651.84 million tons of sugarcane [1], this represents a fall of approximately 37.81 million tons of sugar in a harvest. The indices of mineral and vegetable impurities from sugarcane are increased from 1% in 2008 to 1.3 in 2013 (up 18.8%) and 5.6% in 2008 to 8% in 2013 (increase of 42.86%), respectively [2]. The sugarcane production chain plays a very important role because it is the main raw material used in the milling and because it could result a higher efficiency in the production of sugar, and ethanol. The integration and coordination of activities between the links in the production chain should result in better quality, productivity and reduction of losses for the sugarcane production chain. To do this, the better the relationship

between sugarcane producers and their suppliers and their customers, the better the producers' ability to meet the requirements of the products demanded. In order to meet the requirements, it is necessary an integrated management that considers the agents of the production chain both downstream and upstream. This type of management should result in greater customer satisfaction and more competitiveness for the production chain with reduced losses and costs. To that end, the theory of Supply Chain Quality Management (SCQM) presents elements of Supplier Relationship Management (SRM) and Focus on Consumer and Market (FCM) as a basis to assist in the integration between the links of the agents that form a particular production chain. Companies of this chain must develop practices that are interconnected and based on collaboration, communication and participatory integration in quality improvement processes across Supply Chain (SC) to supply services and products with the quality that is required by the customer [3], and that the integration between partners in the CS positively affects the quality practices and the manufacturer's performance [3].

The main objective of this work is to present a proposal to manage sugarcane requirements based on growers' relations with their suppliers and customers.

Within this context, the research aims to answer the following question:

- How to manage the product requirements of the sugarcane production chain?

To achieve this work proposal, some specific objectives are considered:

- Identify the elements, related to the supplier and customer relationship of the GQCS in the literature;
- Find the main practices of these elements in the literature;
- Identify on the field research, the practices of these elements used by companies in the sugarcane production chain;
- Investigate in field research the product requirements demanded by the sugarcane production chain;
- Present a proposal based on what was identified in the previous steps.

II. SUPPLY CHAIN QUALITY MANAGEMENT

The GQCS concept is based on the common elements of Quality Management (QM) and Supply Chain Management (SCM) [4]. GQCS is an approach based on a systemic concept in order to improve the performance of a group of organizations in a SC. This approach uses supplies flows extending from the upstream toward the downstream suppliers towards the clients. GQCS helps to coordinate and integrate the business of the various processes in SC organizations with the purpose of adding value through the measurement, analysis and continuous improvement of products, services and processes for intermediate and final customers [4-5]. For the authors [6], supplier and customer relationships and product quality are the major concerns of the GQCS elements.

In the following topics, the FCM and SRM elements from the SCQM theory are discussed in order to identify their main practices.

A. Focus on Consumer and Market

The authors [7] argue that the greater is the sharing of information among SC members, the greater is the customer focus. Customer satisfaction can be achieved with common goals, which can lead to more stable purchases and lead to higher profitability with greater market share [8]. When customer needs and desires are determined, SC companies should focus their efforts on serving them [9]. The authors [4] emphasize the importance of strengthening relationships among SC members in order to share goals, coordinate activities, and improve performance. The authors [10] address the commitment organizations must have to integrate suppliers, manufacturers and customers to achieve both long-term growth and financial goals. The authors [11] define partnership as a business relationship based on mutual trust, with shared risks and benefits that result in greater business performance than would be found if firms worked without partnership. The author [12] highlights the importance of trust between the partners of a SC, where the higher the level of trust established between these partners, the less the action of opportunistic behavior in transactions. This leads to a greater benefit with strengthening of relationships with long-term contracts, greater intensity of personal

interactions and consequent accomplishment of agreements and promises. For the authors [8] it is important for all SC partners to have a clear understanding of the customer requirements. For the authors [13], there is a need for quality coordination through the responsible use of information sharing throughout CS, as well as the establishment of partnerships among the agents of this chain which is important for the future of the organization's business. Closer relationships with customers help identify their requirements and customer feedback [14]. For the authors [15], closer relationships with customers also result in the use of information related to quality in order to improve products from the viewpoint of customers.

Summarizing, it can be identified the following main practices related to the element "Focus on Consumer and Market" of SCQM theory:

- Actions towards guidelines for preserving the quality of the final product.
- Feedback information from customers regarding the demanded requirements, product quality and services offered.
- Elaboration of audits and action plans for improvement together with the clients.
- Measurement and analysis of quality performance indicators of the clients.
- Measurement and analysis of quality performance indicators of the clients.

B. Supplier Relationship Management

According to [16] more than 55% of an organization's costs are directed to the payment of its suppliers, which generates the need to economize in different ways: the traditional approach that is based on hard negotiations for price reductions and a recent approach that is towards the building relationships with suppliers in order to reduce the costs of the product or service in a joint way. In this approach, management is not only based on the selection of suppliers, but the objective is the development of long-term relationship and performance evaluation of suppliers [9]. A well-implemented supplier management can ensure that the materials comply with the standards and quality requirements, which facilitates the production of quality products [17]. Raw material quality characteristics within the specified help keeping costs related to quality [18]. Products supplied with quality, quantity and in right time required help the company in order to avoid downtime, reduce variability of production processes, scrap and rework rates [19]. Partnerships with suppliers are a source of competitive advantage over rivals [20]. The support of suppliers in the development of products and processes with better quality actually passes through partnerships established between the company and its main suppliers and customers. The development of joint solutions with suppliers through long-term partnerships and the establishment of trust between buyer and supplier encourage the establishment of more dedicated suppliers. Suppliers with a more stable relationship with the organization have a higher level of commitment to quality [21]. Measuring the performance of suppliers, giving them feedback, improves their performance [22].

Summarizing, it can be identified the following main practices related to the SRM element of the SCQM theory:

- Partnership relations between the company and its suppliers.
- Incentives and actions provided by the company to its suppliers in order to improve of the products' quality of the suppliers.
- Elaboration and implementation of improvement action plans together with suppliers.
- Measurement and analysis of quality performance indicators of the suppliers.

C. Ethanol, Bioeletricity and Sugar Chain

The configuration of the sugar and ethanol production chain can be seen in Fig. 1, where the main agents that make up the sugarcane production chain, are showed, as follow:

- Industries of agricultural inputs: the industries of correctives, fertilizers, agricultural defenses and irrigation systems for the farms of the sugarcane growers.
- Manufacturers of machinery and equipment: the harvesters, tractors, trucks, trailers, sprayers and various

implements used for the cultivation of land (subsoilers, plows, furrows, among others).

- Seedlings growers: the companies and/or institutions responsible for the development of new cultivars for sugarcane farms.
- Sugarcane growers: the growers that supply sugarcane to the millings, which can be both independent suppliers and integrated into the milling itself.
- Milling: the industry manufacturer of products, such as: ethanol, various types of sugar, electric power from cogeneration, yeast and additives.

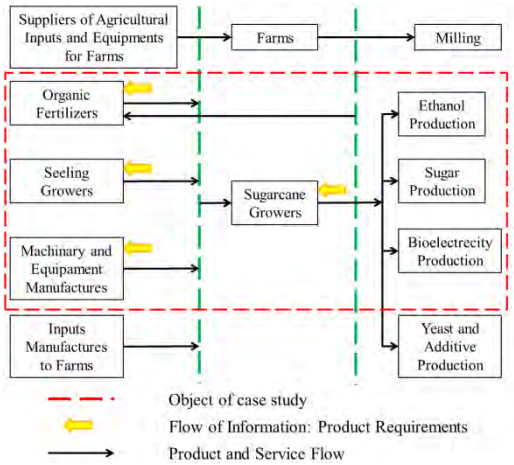

Figure 1. Production chain of sugar and ethanol

III. METHODOLOGY

The research method used in this work is the study of multiple cases, as it investigates deeply the phenomenon of the object of analysis.

The research is aimed at the elaboration of a proposal through the verification of the SRM and FCM elements from the SCQM for different approaches and with replication of it in the agents that holds part of the production chain of sugarcane as: seedlings growers, manufacturers of machines and equipment to growers, sugarcane growers and millings.

A. Overview Planning

The TABLE II shows a method of research planning for the conduction of the field research showing three phases and five steps. Each step is identified by the letter "S".

TABLE II. THE RESEARCH PLANNING METHOD.

Topics	Steps	Description	Results for the research
Literature Review	S1	Supply Chain Quality Management	Definition of the theory of SCQM, explanation of the elements FCM and SRM with their respective practices.
Field Research	S2	Establishment of criteria for case selection.	Identification and selection of companies for cases.
	S3	Elaboration and evaluation of the research protocol.	Better understanding of themes, validation and improvement of the questionnaire.
	S4	Conducting the interviews.	Field verification of the practices of the FCM and SRM elements of the SCQM theory for the cases.
Analysis of Results	S5	Case report, cases 'analysis and solution proposal.	Comparative analysis of the existing practices and the missing ones investigated in the cases. Proposal solution.

The elaborated research protocol aimed at, in overall way, to investigate the following questions:

- What are the main quality requirements for sugarcane production chain?
- What practices of the supplier-client relationship among the chain links: growers of seedlings - farms; manufacturers of machinery and equipment - farms; farms - milling are executed?

Two seedling growers (A and B), two sugarcane growers (A and B), two machine and equipment manufacturers (A and B) and two millings (A and B) were selected for the interviews. The purpose of these double cases was to allow data to be crossed by means of comparative analyzes in order to identify differences and similarities of the SRM and FCM practices from the SCQM theory.

IV. CASE STUDIES AND PROPOSAL FOR QUALITY MANAGEMENT IN THE CHAIN

In this topic, the analysis of the results from the cases of seedling growers (A and B), machine and equipment manufacturers (A and B), sugar cane growers (A and B) and millings (A and B) are presented. Besides of a proposal regarding the gaps found based on the practices of the elements FCM and SRM.

A. Seedlings Growers (A e B)

1) FCM

The seedlings growers A and B clients inform the development requirements of the sugarcane cultivars. There is no requirement of regulatory agencies for the development of new varieties of cultivars. Customers acquire these seedlings and multiply them on farms. There

are no actions jointly with sugarcane growers to improve the quality of seedlings.

2) SRM

The grower of seedlings B has a commercial partnership established with producer A, receiving seedlings certified and guaranteed. Grower B processes the genetically improved seedlings in the development of seedlings, such as pre-budded seedlings. Both grower A and B are secretive about the activities developed for seedling production. This is harmful to the use of practices aimed at shared actions of quality improvement with its suppliers.

B. Machine and Equipament Manufactures (A and B)

1) FCM

Equipment manufacturer B follows all practices of the FCM element, while manufacturer A makes use of practice only to preserve the quality of the final product through training, technical assistance and Performance Indicator (PI) to measure the customer satisfaction.

2) SRM

The manufacturer of equipment B complies with all practices of the SRM element, while manufacturer A makes use of the practice for conducting supplier audits and for measuring the satisfaction of the suppliers through PI.

C. Sugarcane Growers (A and B)

1) FCM

Grower B has a client-oriented relationship who involves him in actions to improve the quality of the sugarcane supplied to the milling, performs audits at the customer, and has a plan together with him in order to preserve the quality of sugarcane delivered to the milling. However it does not manage the PIs of the sugar quality requirements. Grower A does not share joint actions with the client to improve the quality of the cane produced in order to gain farm productivity. Grower A does not participate of customer audits to verify the performance of the quality of its product; it does not promote with the client the management of the PIs in order to improve the quality of the sugarcane supplied. The only incentive for the customer is the payment for quality related to the ATR quality requirement.

2) SRM

Grower B has not established a relationship with suppliers in ways to improve productivity and quality of sugarcane, due to lack of integration and cooperation in the upstream links of the farm. Grower A does not practice joint actions with his suppliers in order to improve the quality of the cane produced and to gain productivity of the farm.

D. Millings (A and B)

1) FCM

The practice of quality audits on suppliers is the differential of milling B with respect to A. Both milling A and B have PIs that measure suppliers' quality index and customer satisfaction. Milling B has the practice of managing these indicators with a plan of action to reach targets, while milling A does not management the PIs, it just has it.

2) SRM

Milling B has programs to manage its suppliers, one for cane suppliers and the other for suppliers of industrial and agricultural inputs, with the aim of moving shared actions in order to improve the quality, efficiency and productivity of products supplied to milling B. Milling B practices quality audits at suppliers. This differs milling B of A.

E. Proposal for Quality Management of Sugarcane Requirements

The TABLE I, the authors [23], highlight the key quality requirements of sugarcane.

The authors [23] define the quality requirements of sugars (soluble solids) present in sugarcane, such as:

- POL (Polymerization): apparent sucrose content in cane. For the sugarcane industry, the higher the sucrose content the better.
- TRS (Total Reducing Sugars): requirement representing the total sugar content of sugarcane (sucrose, glucose and fructose).
- Reducing sugars (RS): sugars, glucose and fructose present in sugarcane.
- Fiber content: water insoluble solid that reflects the efficiency of the extraction of the milling, that is, the higher the cane fiber, the lower the extraction efficiency.

TABLE I. THE MAIN QUALITY REQUIREMENTS FOR SUGARCANE

Sugarcane Requirements	Specifications	Measurement Units
Polymerization (POL)	>140	Kg/tonnes cane
Purity rates	>85	%
TRS	>150	Kg/ tonnes cane
Reducing Sugars (RS) Content	< 5	Kg/ tonnes cane
Fiber rates	11 – 13	%
Bacteriological Contamination	$< 5x10^5$	bacteria type rods/ml broth
Mineral Impurity rates	< 1,5	%
Vegetal Impurity rates	< 6	%
Shootborer rates	< 1	%
Dextran	< 500	ppm/Brix
Starch	<400	ppm/Brix
Total Acidity	< 0,8	-

- Purity rates: sugarcane requirement determined by ratio:

$$\frac{Pol}{Brix}100 \quad (1)$$

- Vegetable impurity: dry or green leaves, dry or withered stalks and sugarcane palm.
- Mineral impurity: the earth (clayey and sandy) or stones.
- Dextran: a glucose polymer, produced by the action of microorganisms on sucrose.
- Starch: reserve polysaccharide used bt the plant during its growth and appearance of roots and shoots.

Besides sugarcane requirements, the straw, by-product of the sugarcane harvest used to cogeneration of bioelectricity, has the following requirements: the moisture rate, which should be less than 15%, and mineral impurity less than 1,5 %, as well as the sugarcane requirements.

The product requirements demanded by farms from growers and developers of new varieties for cultivars are: sugar rate, fiber rate, resistance to pests and diseases, resistance to soil compaction (mechanized harvesting), suitability to soil types, tillering of the seedlings, productivity, attendance to the varietal management (super precocious, precocious, average and late varieties) and sanity for seedlings.

Product requirements demanded by farms to machinery and equipment manufacturers are related to the compliance function that each machine has.

The organic fertilizer (vinasse), by-product of the ethanol production process in the milling, and the "filter cake", solid organic fertilizer from the rotary filter broth decanting process at the milling plant, must be processed properly for fertilization as the need of the soil.

All of these products requirements of the sugarcane production chain must be accomplished by each one of its agents. Then, the quality of sugarcane needs of a management that enables the attainment of these requirements identified and also the gaps related to the practices of the FCM and SRM elements of the SCQM theory in the sugarcane production chain, as a lack of: partnership, quality preservation actions, incentives that foster quality, and quality. To perform these needs, a Quality Management (QM) proposal is presented, which seeks to fill these gaps in the supplier-customer relationship of the agents that forms the sugarcane production chain. This reveals the need for integration among the main agents of the chain through an information flow for the product quality requirements, having the FCM and SRM practices, as a basis for the implementation of the proposal. Fig. 2 shows an illustration of the proposal to manage the product requirements in the sugarcane production chain.

All product requirements of the main agents, represented by a red-yellow arrow on Fig.2, must be attained through the accomplishment of the FCM and SRM practices.

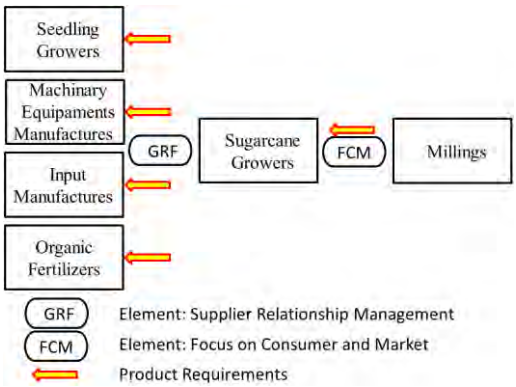

Figure 2. Illustration for managing the product requirements of the sugarcane production chain.

Follow in the specific subtopics how these practices can be managed.

1) Focus on Consumer and Market (FCM)

The sugarcane produced in the farms must meet the quality requirements of the millings. For this, the orientation of the quality for the client must evolve to a partnership with the milling in search of the best quality of the sugarcane. The agents that make up the sugarcane production chain must share ideas, action plans together with its partners in each links of the chain in order to realize an efficiently implementation of FCM practices.

2) Supplier Relationship Management (SRM)

The need to meet milling requirements leads farms to have a long-term, trusting relationship with their key suppliers in order to jointly deploy actions to effectively address SRM practices.

Fig. 3 shows a flowchart that guides how the information flow should be for joint actions, related to the practices of the SRM and FCM elements of the sugarcane growers, with their upstream suppliers and the downstream mills respectively.

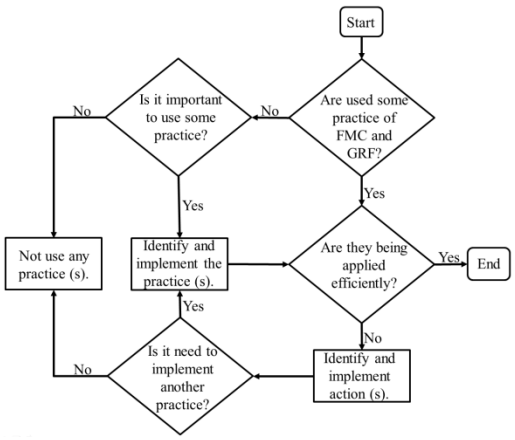

Figure 3. Flowchart of the information flow of the practices of the SRM and FCM elements.

V. CONCLUSION

The FCM and SRM elements and its main practices were identified in the literature of the SCQM theory. The empirical research of multiple cases investigated the use of the practices of these elements in the chain of production of sugarcane and also the product requirements demanded by the agents of this chain. Some shortcomings were identified regarding to relationship among sugarcane growers both upstream and downstream, such as the lack of: partnerships, quality preservation actions, incentives to promote quality in this chain and quality audits. To fill these gaps in order to meet the requirements on the chain, a proposal was presented to strengthen the relationship of the growers with their suppliers and customers, corroborating with the quality improvement of the sugarcane supplied to the milling. This proposal, once implemented, can maximize the efficiency in the sugar, ethanol and bioelectricity production at the milling plant.

The main objective of this work, which is to present a proposal to manage the requirements of sugarcane focused on the integration among sugarcane growers with their suppliers and customers, was performed. However, the proposal does not address aspects related to the internal activities of the sugar cane farms. This is a suggestion for a future work.

ACKNOWLEDGMENT

To the Federal Institute of Education, Science and Technology .of São Paulo, Catanduva-SP, Brazil for the support and incentive. To the University Federal of São Carlos for the support.

REFERENCES

[1] UNICA (2018). *Unicadata*. Available at: http://www.unicadata.com.br,

[2] J. Finguerut (2014). *Impurezas e Qualidade da Cana-de-Açúcar*. Available at: http://www.stab.org.br/palestra_ws_limpeza_da_cana/JAIME_FINGUERUT.pdf,

[3] H. Sun, and W. Ni, "The impact of upstream supply and downstream demand integration on quality management and quality performance," International Journal of Quality & Reliability Management. vol. 29, n. 8, 2012, pp. 872-890.

[4] C.J. Robinson, and M.K. Malhotra, "Defining the concept of supply chain quality management and its relevance to academic and industrial practice," International Journal of Production Economics, vol. 96, n. 3, 2005, pp. 315-337.

[5] M. benaissa, A. Benabdelhafid, and Z. Akkouri, "Quality management approach in supply chain logistics," Management Studies, 2010, pp.152-168.

[6] C. Lin, W.S. Chow, C.N. Madu, C.H. Kuei, and P.P. Yu, "A structural equation model of supply chain quality management and organizational performance," International Journal of Production Economics. vol. 96, n. 3, 2005, pp. 355-365.

[7] I. Sila, and M. Ebrahimpour, "Critical linkages among TQM factors and business results," International Journal of Operations & Production Management, vol. 25, n. 11, 2005, pp. 1123-1155.

[8] K. Rashid, and H. Aslan, “Business excellence through total supply chain quality management,” Asian Journal on Quality. vol. 13, 2012, pp. 309-324.

[9] H.T. Guang et al., “An extensive structural model of supply chain quality management and firm performance,” International Journal of Quality & Reliability Management, vol. 33, n.4, 2016, pp. 444-464.

[10] K.C. Tan, V.R. Kannan, and R.B. Handfield, “Supply chain management: An empirical study of its impact on performance,” International Journal of Operations & Production Management**,** vol.19, 1999, pp. 1034–1052.

[11] D.M. Lambert, A.M. Knemeyer, and J.T. Gardner, “Developing and Implementing Partnerships in the Supply Chain,” in D.M. Lambert, Supply chain management: Processes, Partnerships, Performance. Supply Management Institute, Sarasota, FL, 2008.

[12] H. L. Corrêa, Gestão de redes de suprimento: integrando cadeias de suprimento no mundo globalizado. São Paulo: Atlas, 2010, pp. 414.

[13] J.C. Toledo, M.A.A. Borrás, R.C. Mergulhão, and G.H.S. Mendes, Qualidade gestão e métodos. Rio de Janeiro: LTC, 2013.

[14] H. Kaynak, J.L. Hartley, “A replication and extension of quality management into the supply chain, ”Journal of Operations Management, vol. 26, n. 4, 2008, pp. 468-489.

[15] S.L. Ahire, and T. Ravichandran, “An innovation diffusion model of TQM implementation,” IEEE Transactions on Engineering Management**,** vol.48, 2001, pp. 445–464.

[16] R.M. Monczka, R.B. Handfield, L.C. Giunipero, and J.L. Petterson, Purchasing and Supply Chain Management. 4 Ed. Estados Unidos: South-Western Cengage Learning, 2009, pp.810.

[17] S. Li, S.S. Rao, and T.S. Ragu-Nathan, “Development and validation of a measurement instrument for studying supply chain management practices,” Journal of Operations Management, vol. 23, n. 6, 2005, pp. 618-641.

[18] A. Das, H. Paul, and F.W. Swierczek, “Developing and validating total quality management (TQM) constructs in the context of Thailand’s manufacturing industry,” Benchmarking: An International Journal, vol. 15, n. 1, 2008, pp. 52-72.

[19] C. Forza, and R. Filippini, “TQM impact on quality conformance and customer satisfaction: a causal model, ”International Journal of Production Economics, vol. 55, n. 1, 1998, pp. 1-20.

[20] P. Mangiameli, and C.J. Roethlein, “An examination of quality performance at different levels in a connected supply chain: A preliminary case study,” Integrated Manufacturing Systems, vol. 12, 2001, pp. 126–133.

[21] K. Lai, and T.C.E. Cheng, “Effects of quality management and marketing on organizational performance,” Journal of Business Research, vol. 58, 2005, pp. 446–456.

[22] D.R. Krause, “Supplier development: current practices and outcomes, ”International Journal of Purchasing and Materials Management, vol. 33, n.23, 1997, pp. 12–19.

[23] M.L.C. Ripoli, and T.C.C Ripoli, Biomassa de cana-de-açúcar: colheita, energia e ambiente. Piracicaba: Ed. dos Autores, 2004, pp.309.

Health Risk of Polycyclic Aromatic Hydrocarbons – PAHs in Primary School Environment in Serbia, Probabilistic Modeling Study

Rastko Jovanović[1], Marija Živković[1]

[1]University of Belgrade, "Vinča" Institute of nuclear sciences, Laboratory for Thermal Engineering and Energy, Belgrade, Serbia, virrast@vinca.rs, marijaz@vin.bg.ac.rs

Abstract—**Polycyclic aromatic hydrocarbons (PAHs) are a group of organic compounds and many of them are toxic and carcinogenic environmental contaminants. They typically result from the incomplete combustion processes of organic materials. Exposure to PAHs emissions can create a number of adverse health effects. Children represent one of the most susceptible population groups with regard to potentially harmful effects. The main objectives of this paper are: first, experimental evaluation of concentrations of 16 priority PAHs in indoor and outdoor air in Serbian school, where residential heating and traffic are the only major PAH sources. The second objective is calculation of cancer risk of PAHs for children from total suspended particles (TSP) using suggested incremental lifetime cancer risk (ILCR) model based on Monte Carlo simulations. The obtained measured values as well as calculated numerical results showed, that although PAHs concentration values are lower than suggested limits, additional care should be taken in order to further decrease children cancer health risk of PAHs' emissions.**

Keywords – Polycyclic aromatic hydrocarbons – PAHs, inhalation exposure, school, children, health risk assessment.

I. INTRODUCTION

Polycyclic aromatic hydrocarbons (PAHs) are a group of organic compounds and many of them are toxic and carcinogenic environmental contaminants. They typically result from the incomplete combustion processes of organic materials such as a wood, coal, petrol and diesel, and are primarily anthropogenic. Exposure to PAHs emissions can create a number of adverse health effects. The World Health Organization states that "On the basis of the experimental results, the most significant health effect to be expected from inhalation exposure to PAHs in an excess risk of lung cancer" [1]. The United States Environmental Protection Agency (US EPA) has identified 16 priority PAHs based on their abundance and toxicity.

Exposure to PAHs generally assumes exposure to a mixture of possibly toxic chemicals. However, the detailed effects of exposure to that mixture are still not fully understood. Benzo(a)pyrene (BaP) is by far the most intensively studied PAH and it is the only PAH for which a database is available, allowing a quantitative risk assessment. Because of this, in the most risk assessment studies, different individual PAHs are considered to be of equivalent toxicity as the BaP [2,3].

Air pollution is considered as a major cause for public health concern throughout the world. Children represent one of the most susceptible population groups with regard to potentially harmful effects induced by air pollution. In comparison with adults, children are more vulnerable to poor indoor air quality due to their still developing physiological and immunological systems, and greater inhaled breath per unit mass [4,5]. In recent years, more and more scientific papers have been done on PAHs in schools in Europe [6-10], but there is scarce information about cancer risks for children in Serbian schools [11]. Incremental lifetime cancer risk (ILCR) caused by long time humans' exposure to PAHs emissions is of special importance because of PAHs

ISBN: 978-86-80616-03-2

carcinogenic potential and because their large emissions, especially in urban areas. Generally, different mathematical approaches can be used to estimate PAHs ILCR. Monte Carlo method is well established technic for predicting stochastic behavior of different phenomena. This ability to describe stochastic nature of the modeled problem makes Monte Carlo simulation the most suitable method for ILCR estimation.

The main objectives of this paper are: first, experimental evaluation of concentrations of 16 priority PAHs in indoor and outdoor air in Serbian school, where residential heating and traffic are the only major PAH sources. The second objective is calculation of cancer risk of PAHs for children from total suspended particles (TSP) using suggested incremental lifetime cancer risk (ILCR) model based on Monte Carlo simulations.

II. Site Description

Zajecar is town located in the eastern part of Serbia (Fig.1.). The town was developed mainly as agricultural center with some food and metal processing industry. It is populated by around 44000 inhabitants, and the district heating is

Figure 1. Primary school (43.902695, 22.285223).

implemented only in small number of households (less than 20% of total number). Majority of households located in the town area are heated by the individual heating stoves burning wood and coal as a fuel. This significantly increases air pollution, and PAHs emissions, during the heating season.

The school building, in which measurement campaign was conducted, is located in residential area, the traffic has moderate intensity, and there is no industry in neighboring areas. The school is 40 years old and the total number of students attending the school is around 750. A detailed description and characteristics of the school are published in the paper Jovanovic et al. (2014).

III. Sampling Procedure and Chemical Analysis

The sampling campaign was conducted simultaneously in both indoor and outdoor environments during full ten working days in April of 2012. Samples were collected using the low volume reference sampler Sven/LACKEL LVS3 (LVS) with size-selective inlets for TSP fraction for 24 hours period. The sampling flow rate was 2.3 m3/h (38 L/min). The Whatman QMA (47 mm) quartz filters were used for sampling. After the sampling, the filters were extracted by mixture composed of acetone and hexane (1:1 ratio) for 8 h at 90 °C using microwave extraction. Known quantities of internal standard were added to estimate the method recovery. PAHs were collected, prepared and analyzed according to Compendium Method TO-13A [3]. Analysis was performed using GC-MS (gas chromatography coupled with mass spectrometry), with a DB-5 MS capillary column. The following sixteen US EPA priority PAHs were determined: naphthalene (Nap), acenaphthylene (Ace), acenaphthene (Ane), fluorene (Flu), phenanthrene (Phe), anthracene (Ant), fluoranthene (Fla), pyrene (Pyr), benz[a]anthracene (BaA), chrysene (Chy), benzo[b]fluoranthene (BbF), benzo[k]fluoranthene (BkF), benzo[a]pyrene (BaP), dibenz[a,h]anthracene (DbA), benzo[g,h,i]perylene (BgP), and indeno[1,2,3-cd]pyrene (InP).

IV. Mathematical Modeling

Monte Carlo simulation was used for probabilistic incremental lifetime cancer risk (ILCR) modeling. Developed model is based on MATLAB high-level programming language which offers greater efficiency in vector and matrix operations compared with commonly utilized packages based on spreadsheet software solutions. The main model feature is its ability to incorporate variability and uncertainty into risk assessment, thus providing more realistic view of long-time risk distribution.

Measured indoor and outdoor average PAHs concentrations were used to calculate BaP equivalent concentration (BaPeq). Then, the daily inhalation exposure dose, E, was calculated according to (1):

$$E = \sum_{i=1}^{2} C_i IR t_i \quad (1)$$

Where, it refers to different environments, indoors and outdoors. E is children daily exposure dose (mg·day^{-1}). C_i is BaPeq concentration in the i-th environment (mg·m^{-3}). IR is average children inhalation rate (m^3·h^{-1}). t_i is daily exposure time span in the i-th environment (h·day^{-1}).

ILCR is calculated in the next step, according to the following expression (2):

$$ILCR = \frac{CSF \cdot EF \cdot E \cdot ED}{AT \cdot BW} \quad (2)$$

Where $ILCR$ is incremental lifetime cancer risk of the PAHs exposure (dimensionless). CSF is inhalation cancer slope factor of BaP (kg·day·mg^{-1}). EF is exposure frequency (day·year^{-1}). AT is averaging time (equal to 70 years for carcinogens) (US EPA 1991). ED is exposure duration (years). BW is body weight (kg).

Each input variable was sampled independently from its appropriate distribution, as shown in Table 1.

TABLE I. INPUT PARAMETERS FOR ILCR CALCULATIONS USING MONTE CARLO METHOD.

Variable (measurement units)	Outdoor	Indoor	Distribution type
C_i [$ng \cdot m^{-3}$]	9.29± 8.07	16.29± 14.7	Log-Normal
IR [$m^3 \cdot day^{-1}$]	9.98±1.83		Log-Normal
t_i [$h \cdot day^{-1}$]	3	5	Constant
CSF [$kg \cdot day \cdot mg^{-1}$]	3.9		Constant
AT [$days$]	25500		Constant
ED [$years$]	3		Constant
BW [kg]	32.5±7.1		Log-Normal

Totally one million Monte Carlo iterations were performed in order to obtain stable results.

V. RESULTS AND DISCUSSION

The average indoor and outdoor concentrations of PAHs in TSP are presented in Table 1. The 2- and 3-ring PAHs were much lower than 5- and 6-ring PAHs. The 5- and 6-ring PAHs were the dominant compounds, which accounting for more of 90% of PAHs. These, high molecular weight components, are mostly bound with particulate phase. Thus, due to their limited influence, in this study, the gas phase samples were not collected. It is important to underline that the high molecular weight PAHs usually come from combustion of solid fuels.

The I/O ratios can be viewed as an indicator of the relative strengths of the indoor and versus outdoor sources. The I/O ratio was quite different for all PAHs, in contrast with previous studies in Serbian schools [Kovacevic et al. 2015, Zivkovic et al. 2015]. Especially for high molecular weight PAHs which are usually emitted from outdoor source, Table II. The higher indoor levels for some PAHs might result from the combination of various factors: characteristics of the building, different position and distance of the classrooms from the street and infiltration of outdoor particles to indoor air [5].

TABLE II. INDOOR AND OUTDOOR CONCENTRATIONS OF PAHS IN TSP (ng/m^3).

PAHs	Outdoor	Indoor	Outdoor/Indoor
Nap	0.21±0.34	0.07±0.08	2.05±3.39
Ace	0.56±1.20	0.20±0.14	2.41±2.69
Ane	0.16±0.10	0.19±0.12	1.23±0.49
Flu	0.34±0.38	0.28±0.13	1.28±0.54
Phe	0.26±0.17	0.37±0.21	1.58±0.64
Ant	0.16±0.13	0.12±0.07	1.00±0.54
Fla	3.71±4.37	2.69±2.39	1.39±1.10
Pyr	4.09±4.70	3.25±2.89	1.10±0.72
BaA	6.83±6.80	6.95±7.50	0.90±0.64
Chy	8.24±7.92	8.32±8.84	0.87±0.60
BbF	5.98±4.87	9.10±8.36	1.27±0.88
BkF	4.66±3.72	7.71±7.73	1.28±0.78
BaP	5.60±4.90	10.48±9.50	1.66±1.07
InP	4.07±3.03	7.62±6.37	1.54±0.81
DbA	1.41±1.21	2.50±2.04	1.70±1.22
BgP	4.17±2.94	7.99±6.56	1.57±0.71
SUM	46.78	67.83	

TABLE III. BaP EQUIVALENT CONCENTRATIONS OF INDIVIDUAL PAHs.

		Outdoor		Indoor	
PAHs	TEF	TSP	Stdev	TSP	Stdev
Nap	0.001	0.0002	0.0003	0.0001	0.0001
Ace	0.001	0.0006	0.0012	0.0002	0.0001
Ane	0.001	0.0002	0.0001	0.0002	0.0001
Flu	0.001	0.0003	0.0004	0.0003	0.0001
Phe	0.001	0.0003	0.0002	0.0004	0.0002
Ant	0.01	0.0016	0.0013	0.0012	0.0007
Fla	0.001	0.0037	0.0044	0.0027	0.0024
Pyr	0.001	0.0041	0.0047	0.0033	0.0029
BaA	0.1	0.6825	0.6803	0.6946	0.7500
Chy	0.01	0.0824	0.0792	0.0832	0.0884
BbF	0.1	0.5980	0.4865	0.9097	0.8361
BkF	0.1	0.4663	0.3722	0.7710	0.7734
BaP	1	5.5983	4.8993	10.4781	9.5028
InP	0.1	0.4070	0.3031	0.7622	0.6366
DbA	1	1.4069	1.2072	2.4981	2.0429
BgP	0.01	0.0417	0.0294	0.0799	0.0656
BaP-eq		9.2940	8.0699	16.2850	14.7024

Kinghham et al. [13] found that children activities may cause resuspension of coarse particles inside the buildings. All classrooms are on the ground floor, in the vicinity of heating boiler, which is placed in the school basement. Assumption can be made that increase of PAHs in TSP, must be due to inadequate elimination of flue gases from the boiler's furnace and poor ventilation in the basement [14].

The most widely used method for health risk assessment is the calculation of toxicity equivalency factors (TEF), which are based on the measured concentrations of BaP. The 16 priority PAHs are ranked according to their cancer potency relative to BaP [15]. The BaP equivalents (BaPeq) are calculated by multiplying each individual PAH concentration with its corresponding TEF to determine the concentration of total PAH expressed as BaP-eq (Table 2.) [3]. It can be seen that, in the indoor environment, the BaP-eq concentration is almost 2 times higher than in the outdoor environment, Table III.

Calculated ILCR probability histograms and fitted distributions presenting contribution from both indoor and outdoor PAHs' concentration for children population are shown in Figs. 1. and 2. It can be seen that both distributions give good with sampled data, although Gamma distribution produces somewhat better fit. It can be seen that ILCR in range of about 2·10-8 to 3.5 10-7 has high probability of occurrence. Mean value of ILCR distribution is 1.2 10-7 which is considered acceptable according to accepted standards. However, as ILCR of 1 10-6 is considered as minimum value for acceptable risk it is clear that efforts should be made to lower the current calculated ILCR values.

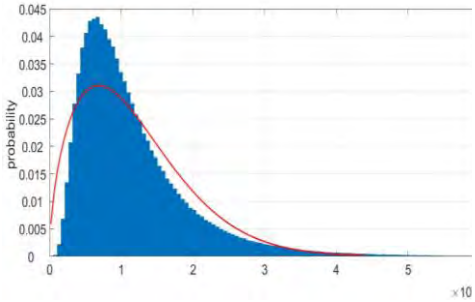

Figure 2. Children ILCR probability histogram fitted with Weibull distribution.

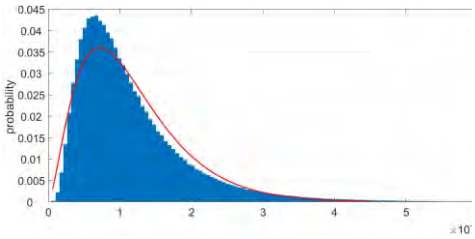

Figure 3. Children ILCR probability histogram fitted with Gamma distribution.

VI. CONCLUSIONS

The 16 priority PAHs in TSP were determined in indoor and outdoor environment in one primary school during heating season in the presented work. The levels of PAH were generally higher in indoor environment than in outdoor. The indoor PAH concentrations were higher than in the common European schools. This can be explained by poor ventilation, incomplete combustion in the boiler furnace, and poor condition of windows which allow PAHs penetration from outdoor environment.

The I/O ratios pointed out strong influence of indoor emission sources, especially for high molecular weight PAHs.

The average estimated lifetime lung cancer risk for this study was lower than the WHO and EPA recommended values. It is necessary to point out that the risk assessment was conducted using PAH concentrations only from TSP. Thus, it is expected that PAH concentrations in both gas and particle phases will be measured and taken into account in the model in the future work. It is also important to note that relatively low ILCR predicted values are caused only by PAHs which children inhaled during school time, and not during all 24 h, and thus should be taken carefully as an important factor for consideration for improving school heating and ventilation systems.

ACKNOWLEDGMENT

The authors would like to acknowledge high appreciation for the support and promotion of this work to the Public Enterprise Electric power industry of Serbia, Belgrade, Serbia, and Ministry of Education and Science of Republic of Serbia, Project No. III42010, TR33050, and III42008: Improving the energy performance and the indoor air quality of educational institution buildings in Serbia with the impact on health.

REFERENCES

[1] World Health Orgaizatio (WHO), 2000. Air Quality Guidelines for Europe, 2nd edition. WHO Regional Office for Europe, Copenhagen, Denmark.

[2] World Health Orgaizatio (WHO), 2010. WHO Guidelines for Indoor Air Quality: Selected Pollutants. Regional Office for Europe, Copenhagen, Denmark.

[3] U.S. Environmental Protection Agency (US EPA), 2005. Guidelines for Carcinogen Risk Assessment, EPA/630/P-03/001F. US Environmental Protection Agency, Washington, D.C.

[4] Mejia, J.F., Low Choy, S., Mengersen, K., Morawska, L., 2011. Methodology for assessing exposure and impacts of air pollutants in school children: Data collection, analysis and health effects – A literature review, Atmospheric Environment 45, 813-823.

[5] Oliveira, M., Slezakova, K., Madureira, J., de Oliveira Fernandes, E., Delerue-Matos, C., Morais, S., do Carmo Pereira, M., 2017. Polycyclic aromatic hydrocarbons in primary school environments: Levels and potential risks. Science of the Total Environment 575, 1156-1167.

[6] Alves, C.A., Urban, R.C., Pegas, P.N., Nunes, T., 2014. Indoor/outdoor relationships between PM10 and associated organic compounds in a primary school. Aerosol Air Quality Research 14, 86-98.

[7] Gatto, M.P., Gariazzo, C., Gordiani, A., L`Episcopo, N., Gherardi, M., 2013. Children and elders exposure assessment to particle-bound polycyclic aromatic hydrocarbons (PAHs) in the city of Rome, Italy. Environmental Science Pollution Research 21, 13152-13159.

[8] Krugly, E., Martuzevius, D., Sidaraviciute, R., Ciuzas, D., Prasauskas, T., Kauneliene, V., Stasiulaitiene, I., Kliucinikas, L., 2014. Characterization of particulate and vapor phase polycyclic aromatic hydrocarbons in indoor and outdoor air of primary schools. Atmospheric Environment 82, 298-306.

[9] Krugly, E., Martuzevius, D., Sidaraviciute, R., Ciuzas, D., Prasauskas, T., Kauneliene, V., Stasiulaitiene, I., Kliucinikas, L., 2014. Characterization of particulate and vapor phase polycyclic aromatic hydrocarbons in indoor and outdoor air of primary schools. Atmospheric Environment 82, 298-306.

[10] Krugly, E., Martuzevius, D., Sidaraviciute, R., Ciuzas, D., Prasauskas, T., Kauneliene, V., Stasiulaitiene, I., Kliucinikas, L., 2014. Characterization of particulate and vapor phase polycyclic aromatic hydrocarbons in indoor and outdoor air of primary schools. Atmospheric Environment 82, 298-306.

[11] Zivkovic, M., Jovasevic-Stojanovic, M., Cvetkovic, A., Lazovic, I., Tasic, V., Stevanovic, Z., Grzetic, I., 2015. PAHs levels in gas and particle-bound phase in schools at different locations in Serbia. Chemical Industry and Chemical Engineering Quarterly 21, 159-167.

[12] Kovacevic, R., Tasic, V., Zivkovic, M., Zivkovic, N., Djordjevic, A., Manojlovic, D., Jovasevic-Stojanovic, M., 2015. Mass concentrations and indoor-outdoor relationships of PM in selected educational buildings in Nis, Serbia. Chemical Industry and Chemical Engineering Quarterly 21, 149-157.

[13] Kingham, S., Durand, M., Harrison, J., Cavanagh, J., Epton, M., 2008. Temporal variations in particulate exposure to wood smoke in a residential school environment. Atmospheric Environment 42, 4619-4631.

[14] Jovanovic, M., Vucicevic, B., Turanjanin, V., Zivkovic, M., Spasojevic, V., 2014. Investigation of indoor and outdoor air quality of the classrooms at a school in Serbia. Energy 77, 42-48.

[15] Nisbet, I.C.T. and LaGoy, P.K., 1992. Toxic Equivalency factors (TEFs) for polycyclic aromatic hydrocarbons (PAHs). Regulatory Toxicology and Pharmacology 16, 290-300.

Energetic Potential of Microalgae from Swamps and Ponds of South Serbia

Jovan Ćirić[1], Nataša Vitošević[1], Ljubiša Stajić[1], Dušica Ilić[1]

[1]Research and Development Center "ALFATEC", 18000 Niš, Serbia

Abstract— **Algae offer solutions for many problems of our civilization. Biotechnological applications of algae have become a part of modern reality. As one of the many application possibilities, algae can be used as a renewable energy source. Algae can store energy in the form of oil which can be appropriate raw material for the biodiesel production. Microalgae are especially significant because of their high growth rate, high oil content and ability to grow in the unfavorable environment for agriculture. Also, the cultivation of microalgae can improve the reduction of carbon dioxide emissions. An overview of the existing studies of the possibility of using microalgae for the production of biodiesel and the results of experimental research with isolated microalgae strains from the South Serbia stagnant water are given in this paper.**

Keywords- energy, biodiesel, microalgae, oil

I. INTRODUCTION

One of the promising alternative oil sources that can be used as a raw material for the production of biodiesel are microalgae. These are single-cell or colonial photosynthetic organisms which have increasing industrial application in recent years [1]. The significance of algae in nature is to contribute to the restoration and maintenance of the amount of oxygen in the atmosphere thanks to the photosynthesis process. It is estimated that microalgae produce about half of the total atmospheric oxygen. So far, about 35.000 species of algae have been described, out of total 200.000 – 800.000 species that are presumed to exist in nature [2]. Potential industrial application of algae results from the fact that over 15.000 components (antioxidants, fatty acids, enzymes, peptides, toxins and sterols) are derived from algae. Novertheless, microalgae can grow very fast and can double their mass in 24 h or 3,5 h in the exponential growth phase [3]. The simple single-cell microalgae structure allows high speed photosynthesis, efficient carbon binding and rapid oil accumulation in biomass (up to 77 % of dry biomass or oil productivity of 122 mg/l/day [4]). A higher energy yield per unit area than in land crops can be achieved by cultivating algae [5]. Microalgae provide the ability to produce up to 100 times more biodiesel per unit of cultivation area compared to sunflower and rapeseed [6]. In addition, the advantages of using microalgae as a source for biofuel production are increased efficiency and reduced production costs. The cost of separation and transport of microalgae are lower than the costs of transporting other raw materials for the biodiesel production. Similarly, microalgae do not require lot of space for cultivation, whereby, unlike the use of cereals, oilseeds and other plant crops, the use of algae as a raw material for fuel does not have a negative impact on world food and water supplies [7]. Microalgae can be cultivated in different environments that are unsuitable for other plants, for example in fresh water, waste or salt water as well as on non-cultivated soil. They can also be grown on farms or in bioreactors.

After cultivation and collection of biomass, biodiesel from microalgae can be obtained in two ways. The first method involves the primarily oil extraction from the algal biomass with solvents, followed by the transesterification reaction and/or esterification with the corresponding alcohol in the presence of a catalyst (acid, base or enzyme) or in the absence of a catalyst under the naturally occurring methanol conditions. This method involves the consumption of solvents and energy for extraction and transesterification, which affects the increase in the price of raw biodiesel and contributes to environmental pollution. Another way is direct transesterification of algal biomass, (in situ procedure) which improves the process of

biodiesel producing from microalgae in terms of reducing production costs [8].

II. MICROALGAE FOR OIL PRODUCTION

Microalgae used for the production of biodiesel can be isolated from natural habitats or purchase from appropriate collections of cultures such as UTEX (USA), ANACC (Australia), CCAP (UK), NIES (Japan), SAG (Germany), CPCC (Canada) and so on. Although species from the collections of cultures are well studied, due to continuous migration, certain characteristics can be lost and isolation of microalgae from the environment is recommended [9]. The microalgae isolation process involves the selection of the appropriate natural habitat and cultivation and purification of the isolated culture. As a large number of habitats inhabit, different types of microalgae can be isolated from different water and soil samples. The published results of previous studies with microalgae are shown in TABLE I.

TABLE I. OIL CONTENT AND PRODUCTIVITY OF CERTAIN FRESHWATER MICROALGAE [10]

Microalgae	**Oil content,** %	**Oil productiviy,** mg/l/d
Chlorococcum sp.	19,3	53,7
Chlorococcum sp.	11	5,71
Chlorococcum macrostigmatum	25,1	-
Chlorella sp.	18,7	42,1
Chlorella sp.	20	-
Chlorella sp.	46	19,64
Chlorella sorokiniana	19,3	44,7
Chlorella vulgaris	18,4	36,9
Chlorella protothecoides	43-46	1400-1700
Scenedesmus sp.	21,1	53,9
Scenedesmus sp.	22-45	13,2-16,1
Scenedesmus quadricauda	18,4	35,1
Scenedesmus obliquus	17,7	15,9
Botryococcus sp.	5,7-25,8	3,5-46,9
Desmodesmus sp.	36-58	-
Desmodesmus sp.	34	5,7
Desmodesmus elegans	16,9	-
Chlamydomonas spp.	25,3	34
Chlamydomonas pitschmanii	51	25
Chlamydomonas mexicana	28	21
Neochloris oleabundans	29	26,1
Monodus subterraneus	16,1	30,4

III. ISOLATED FRESHWATER MICROALGAE FROM SOUTH SERBIA

Isolation of microalgae from the samples of South Serbian swamps and ponds was performed in the Laboratory for Microbiology and Food Technology of the Faculty of Technology in Leskovac, in order to study the possibility of cultivating microalgae for the production of oil as a raw material for the production of biodiesel. In addition to several isolated and identified strains, four strains of the genus *Chlorella*, *Chlorococcum*, *Scenedesmus* and *Desmodesmus* (Figure 1) were selected for further research. The purity of the strains and the reduced possibility of contamination during cultivation were decisive in selection.

Strains were grown on liquid Bolds Basal Medium (BBM) (pH at 22 o C under the constant light for 30 days at an orbital shaker (140 min-1). The concentration of dry biomass was measured at the end of the process [11]. The content of microbial oil was determined gravimetrically, after extraction by Bligh-Dayer method using chloroform and methanol (2:1 v/v) [12, 13].

In order to study the possibility of oil obtaining for the biodiesel production, four isolated microalgae strains were analyzed on biomass content, oil content and yield. Results are shown in TABLE II. The highest content of dry biomass have representatives of the genus *Chlorococcum* sp. and *Desmodesmus* sp. (1,5 i 1,5 g/l), less *Chlorella* sp. (1,2 g/l) and at least *Scenedesmus* sp. (1,0 g/l).

The highest oil yield of 0,4 g/l was achieved with strains *Chlorella* sp. and *Desmodesmus* sp., while the lowest productivity of oil (0,2 g/l) was observed with strain *Chlorococcum* sp.. Studies with similar cultivation conditions have shown that *C. vulgaris* reaches an oil yield of 0,4 g/l, S. obliqus 0,5 g/l [14], *Chlorococcum* sp. 0,1 g/l

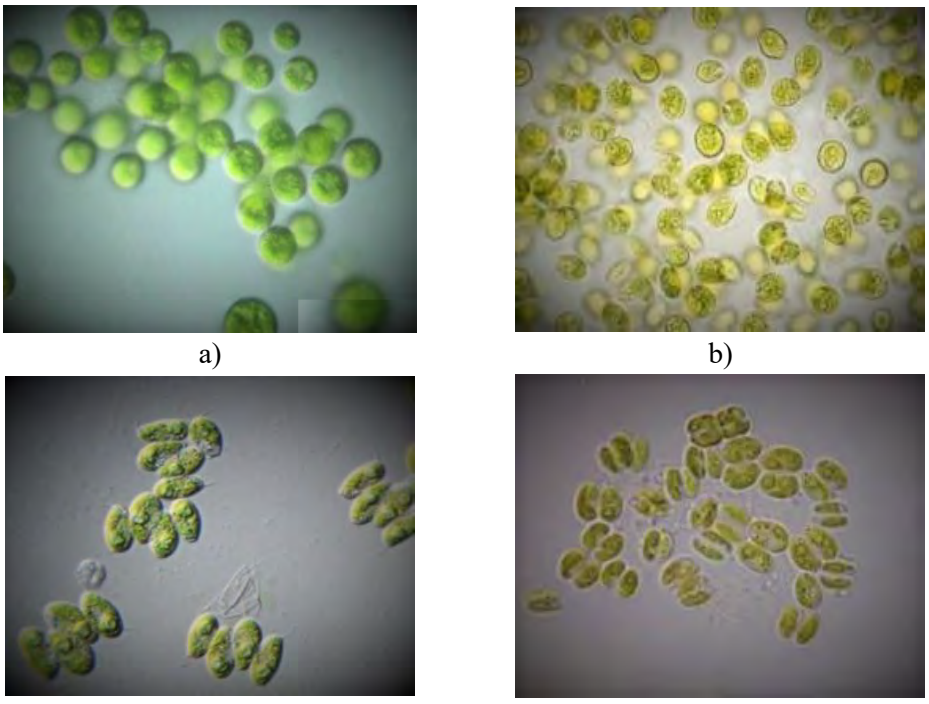

Figure 1 Microscopic appearance of isolated microalgae: a) *Chlorococcum sp.*, b) *Chlorella sp.*, c) *Desmodesmus sp.* and d) *Scenedesmus sp.* (photo Ćirić/Mikro-Lab TFL 2012., 60X)

[15], while the lowest production of 0,2 g/l is reached with *Desmodesmus* sp. [16]. These literature data for *Chlorella* sp., *Clorococcum* sp. and *Desmodesmus* sp. are in accordance with the results obtained in the mentioned study [10], while the values obtained with *Scenedesmus* sp. are lower.

The oil content of analyzed microalgae was ranged from 16 % to 33 %. The oil content of *Chlorella* strain was 33 % which is almost twice as high than *Chlorococcum* strain. Other studies have shown that the microalgae *Chlorococcum* sp., *C. vulgaris*, *S. obliqus* and *Desmodesmus* sp. cultivated under the same conditions have the following oil content: 19 % [17]; 26 %; 29 % and 28 % [14] and 20 % [16], respectively, which is in range with the results obtained for the strains tested in our research. It was also found that *Scenedesmus* sp. possesses the most suitable fatty acid composition for the production of biodiesel [15].

The highest content of dry biomass was found with *Chlorococcum* sp. and *Desmodesmus* sp. (1,5 g/l), while the oil content was ranged from 16 % (*Chlorococcum* sp.) to 33 % (*Chlorella* sp.). As the highest yield was found with microalgae *Chlorella* sp. and *Desmodesmus* sp., these two isolates are most suitable for further studies in order to improve the yield of oil and the possibilities of use in the biodiesel production process.

TABLE II. THE ACHIEVED MAXIMUM VALUES OF DRY BIOMASS (DBM), YIELD ($Y_{P/X}$) AND OIL CONTENT IN DRY BIOMASS, DURING THE AUTOTROPHIC CULTIVATION OF ISOLATED MICROALGAE STRAINS [10]

Isolated strain	DBM	Oil	
	g/l	$Y_{P/X}$ (g/l)	%
Chlorella sp.	1,2	0,4	33
Chlorococcum sp.	1,5	0,2	16
Desmodesmus sp.	1,5	0,4	23
Scenedesmus sp.	1,0	0,3	29

IV. CONCLUSIONS

Due to the increased demand for biofuel, the use of microalgae for the biodiesel production is an important step in replacing fossil fuels. For this purpose, continuous development of technologies and optimization of the process of cultivation and the production of biodiesel are necessary.

From various samples of standing water of South Serbia, four strains of microalgae were isolated and selected for the study. These selected strains were identified as a member of the genus *Chlorococcum*, *Chlorella*, *Desmodesmus* and *Scenedesmus*. Analyzing the content of biomass, the content and yield of oil, it has been found that the strains of *Chlorella* sp. and *Scenedesmus* sp. are most suitable for further studies in order to stimulate production of oil as well as possibility of its application in biodiesel production.

ACKNOWLEDGMENT

This work has been funded by the Ministry of Education, Science and Technological Development of the Republic of Serbia (Projects III 44006 and III 45001).

REFERENCES

[1] P. Chen, M. Min, Y. Chen, L. Wang, Y. Li, Q. Chen, Review of the biological and engineering aspects of algae to fuels approach, Int. J. Agricult. Biolo. Eng. 2 (2009) 1–28.

[2] K.H. Cardozo, T. Guaratini, M.P. Barros, V.R. Falcao, A.P. Tonon, N.P. Lopes, Metabolites from algae with economical impact, Com. Biochem. Physiol., C 146 (2007) 60–78.

[3] K. Vijayaraghavan, K. Hemanathan, Biodiesel production from freshwater algae, Energ. Fuels 23 (2009) 5448– 5453.

[4] J. Pruvost, G. Van Vooren, B. Le Gouic, A. Couzinet-Mossion, J. Legrand, Systematic investigation of biomass and lipid productivity by microalgae in photobioreactors for biodiesel application, Bioresource Technol. 102 (2011) 150–158.

[5] A.F. Clarens, E.P. Resurreccion, M.A. White, L.M. Colosi, Environmental life cycle comparisonof algae to other bioenergyfeedstocks, Environ. Sci. Technol. 44 (2010) 1813–1819.

[6] T. Mata, A. Martins, N. Caetano, Microalgae for biodiesel production and other applications: A review, Renew. Sustain. Energ. Rev. 14 (2010) 217–232.

[7] K. Hundt, B.V. Reddy, Algal biodiesel production from power plant exhaust and its potential to replace petrodiesel and reduce greenhouse gas emissions, Int. J. Low Carbon Technol. 6 (2011) 294–298.

[8] N. Mulumba, I.H. Farag, Tubular photobioreactor for microalgae biodiesel production, Int. J. Eng. Sci. Technol. 4 (2012) 703–709.

[9] I. Rawat, R. Ranjith Kumar, T. Mutanda, F. Bux, Biodiesel from microalgae: A critical evaluation from laboratory to large scale production, Appl. Energ. 103 (2013) 444–467.

[10] B. Danilović, J. Cvetković-Rakić, J. Ćirić, J. Simeunović, V. Veljković, D. Savić, The isolation and screening of microalgae for the production of oil, Chem. Ind. 71 (1) (2017) 69-74.

[11] Takagi M., Karseno S., Yoshida T., Effect of salt concentration on intracellular accumulation of lipids and triacylglyceride in marine microalgae *Dunaliella* cells, J. Biosci. Bioeng. 101 (2006) 223-226.

[12] Iverson S.J., Lang S.L.C., Cooper M.H., Comparison of the Bligh and Dyer and Folch methods for total lipid determination in a broad range of marine tissue, Lipids 36 (2001) 1283–1287.

[13] Kumari P., Reddy C.R.K., Jha B., Comparative evaluation and selection of a method for lipid and fatty acid extraction from macroalgae, Anal. Biochem. 415 (2) (2012) 134-144.

[14] R.A.I. Abou-Shanab, I.A. Matter, S.N. Kim, J. Oh, J. Choi, B.H. Jeon, Characterization and identification of lipidproducing microalgae species isolated from a freshwater lake, Biomass. Bioenergy 35 (2011) 3079–3085.

[15] J. Jena, M. Nayak, H.S. Pamda, N. Pradhan, C.H. Sarika, P.K. Panda,B.V.S.K. Rao, R.B.N. Prasad, L.N. Sukla, Microalgae of Odisha Coast as a potential source for biodiesel production, World Environ. 2 (2012) 11–16.

[16] L.F. Wu, P.C. Chen, A.P. Huang, C.M. Lee, The feasibility of biodiesel production by microalgae using industrial wastewater, Biores. Technol. 113 (2012) 14–18.

[17] T.M. Mata, A.A. Martins, N.S. Caetano, Microalgae for biodiesel production and other applications. A review, Renew. Sust. Energy Rev. 14 (2010) 217–232.

Benchmarking of Heat Energy Consumption in Public Buildings in the City of Kragujevac

Dušan Gordić[1], Nebojša Jurišević[1], Dubravka Živković[1], Vladimir Vukašinović[1], Dobrica Milovanović[1], Davor Končalović[1], Mladen Josijević[1]

[1]Faculty of Engineering, Kragujevac, Kragujevac, Serbia
gordic@kg.ac.rs jurisevic@kg.ac.rs, dubravka@kg.ac.rs, vladimir.vukasinovic@kg.ac.rs, dobrica@kg.ac.rs, davor.koncalovic@kg.ac.rs, mladenjosijevic@gmail.com

Abstract— **Final energy consumption in buildings has the highest share in final energy consumption on a global level. Heat has the highest share in final energy consumption in European buildings. Also, public buildings consume more final energy than residential buildings in general. Specific heat consumption is an important parameter that indicates the state of energy efficiency of the building sector. In this paper, specific heat consumption of public buildings in the city of Kragujevac is analyzed. Part of the data collected for the Energy Efficiency Program for the City of Kragujevac is presented and compared with similar results from other countries and cities. Authors conclude that specific heat consumption in municipal buildings of Kragujevac is relatively high compared to other countries and that its values also vary depending on building purpose and building built year.**

Keywords - energy consumption, energy efficiency, public buildings, specific heat consumption

I. INTRODUCTION

Lower values of specific heat consumptions are becoming imperative in a modern world as because of a decrease in costs of operational utilities in industry and buildings, as because of the necessity for gradual decrease of the energy dependence of local, regional and national, private and public services. According to energy balances for 2015, 39% of final energy consumption in EU went on buildings (residential and service sector), that is 13.5% higher than the share of final energy used in industry [1]. Shares of final energy consumption differ from country to country, for example, the share of final energy consumption in buildings, in total share of final energy consumption in Germany is around 41.4%, in Croatia 48%, Hungary 47% [1], while in Serbia the share is 45.5% [2]. Although final energy consumption in public buildings and service sector is lower than in residential, for 11.8% in total share [1], these sectors record constant growth in final energy consumption. Between 1990 and 2010 service sector (both public and private) in the EU recorded 41% of growth, while the growth between 2005 and 2010 was 12.2% [3].

Around 47% of final energy consumption on a global level went on heat (2009) [4]. In Serbia, 57.6% of heat energy consumption went on buildings [5]. Although consumption of heat, as well as final energy in general in public buildings, is lower than the consumption in residential buildings its share is not insignificant, 20.8% of total share of heat consumption in the EU [6] and 11.5% of total share in heat consumption in Serbia [2]. It is important to mention that specific heat consumption in public buildings in Serbia is for a half a value higher than in residential buildings [7].

According to all above mentioned it can be concluded that:

- Final energy consumption in buildings has the highest share in final energy consumption in total,
- Public buildings consume more final energy than residential buildings,

ISBN: 978-86-80616-03-2

• Public buildings record constant growth in its energy demands and

• Heating energy has the highest share in final energy consumption in buildings.

In order to achieve global goals dealing with the reduction of carbon dioxide emissions as well as lowering anthropogenic influence on climate change and environment, international agreements are adopted. Therefore, governments of countries and regions adopt regulative and limitations dealing with greenhouse gases emissions in accordance with their possibilities, so every party can contribute to global goals.

The government of the Republic of Serbia adopted a series of regulations and strategic documents in order to promote and improve the state of energy efficiency in public and residential buildings:

• Rulebook on the energy efficiency of buildings in 2011

• Rulebook on the conditions, content, and manner of issuance of certificates of energy performance of buildings in 2012

• Law on efficient energy use in 2013

• Energy sector development strategy in the Republic of Serbia by 2030

• Program for the implementation of energy strategy for the period from 2017 until 2023

In order to achieve the goals of national strategies, several energy efficiency action plans were adopted. 1st National action plan for energy efficiency (2010) predicted that public buildings can contribute in 9% of savings in total share of final energy consumption of public buildings up to 2018 [8]. Renovation conducted in a number of public buildings included in SEEP1 and SEEP2 (SEEP - Serbian Energy Efficiency Project) (2005 - 2012) resulted in 47% of savings in final energy consumption in the renovated buildings. 3rd National action plan for energy efficiency (2016) predicts annual energy savings of 1% in the public sector. This goal is related to all municipalities with more than 20000 residents. Complying with this, city assembly of Kragujevac adopted Energy efficiency program for the period of 2018 – 2020. The Energy efficiency program contains all the elements envisaged by article 10, Law on efficient energy use.

One of the results of the Energy efficiency program of the city of Kragujevac is benchmarking analysis of energy consumption in different public sectors. The results of benchmarking of heat energy consumption in public buildings are presented in this paper.

II. RESEARCH AREA

The city of Kragujevac is administrative, industrial, cultural, educational and health care center of central Serbia. It is located in Šumadija region that contains six more municipalities: Batočina, Lapovo, Knić, Rača, and Topola. City land area creates 35% of the land area of the region and 1% of the land area of the Republic of Serbia. According to the National census from 2011 Kragujevac has 179417 residents (2.49% of the population of the Republic of Serbia). Urban city area has 150835 residents (84% of total count). This makes Kragujevac the fourth largest city in Serbia and the first referring to the share of the city residents living in the urban area [9].

Public building in Kragujevac can be classified in 6 categories:

• Educational buildings – preschools and kindergartens (15 buildings), elementary and high schools (75),

• Buildings of cultural institutions – museums (2), libraries (6+), houses of culture (2+), theatres (2) and other (3)

• Administrative buildings (93)

• Community health centers' buildings (26),

• Sport and recreation buildings (3).

• Buildings of public utility services and companies (7)

A certain number of analyzed buildings has mixed purposes. Building purpose is determined according to the main activity of services conducted in its office space.

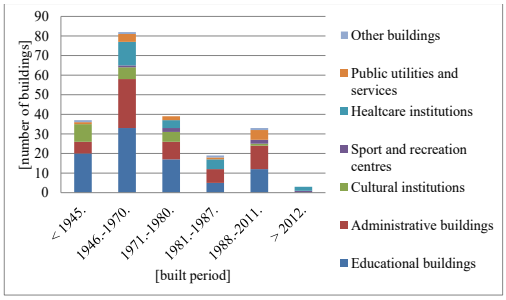

Figure 1. Overview of public buildings according to built year

According to a year of built, type of building construction and different legislation periods, public buildings in the city of Kragujevac can be classified into 6 categories:

- Buildings built before 1945,
- Buildings built between 1946 and 1970,
- Buildings built between 1971 and 1980,
- Buildings built between 1981 and 1987,
- Buildings built between 1988 and 2011,
- Buildings built after 2012.

The public building's structure according to the built period is presented in Figure 1.

Typical characteristics of the buildings in Serbia according to the period of construction are presented in table I [5].

TABLE I. CHARACTERISTICS OF BUILDINGS IN SERBIA ACCORDING TO THE PERIOD OF CONSTRUCTION

Period of construction	Basic characteristics
Before 1945	- construction without thermal regulations - traditional building techniques and full brick or stone materials - the thickness of external walls varies from 25 cm to 50 cm (U=1.33 – 1.05 W/m^{2}K). - ceilings are mostly wooden or massive (brick, stone or concrete elements) - floors often made on the layer of rammed earth - wooden doors and wooden double frame, double sash with single glazing windows (U=3.5 W/m^{2}K) - the buildings have lower thermal losses as newer lightweight concrete structures.
1946–1970	- period of intensive construction but without thermal regulations - lighter full brick or clay block structures without thermal insulation (U=1.61–1.74 W/m^{2}K) - wooden doors and wooden double frame, double sash with single glazing windows (U=3.5 W/m^{2}K)
1971–1980	- the first national regulation on thermal insulation of residential buildings - period of intensive construction – usage of light reinforced concrete structures without thermal insulation or with modest thermal insulation - wooden doors and wooden double frame, double sash with single glazing windows - no thermal regulations for windows and increase of glass surfaces on the facades
1981–1987	- standard JUS U.J5.600 – Thermal Engineering in Construction – Technical conditions for the design and construction of buildings (1980) - reinforced concrete walls are performed in minimal static thicknesses of 16 cm – 20 cm. Masonry structures are mainly made of a hollow block of bricks of 19 cm (or full bricks 25 cm) - roofs are often performed as flat roofs with a concrete slab and minimal isolation - large glass surfaces – windows with ISO glass, but very poor profiles, without an interrupted thermal bridge, and with bad sealing. - no thermal regulations for windows and increase of glass surfaces on the facades - almost no attention paid to solving the details of characteristic thermal bridges.
1987–2011	- standard JUS U.J5.600 – Thermal Engineering in Construction – Technical conditions for the design and construction of buildings (1987) - external walls with all available materials on the market and applied thermal insulation is such that it meets the existing regulations - most common insulation materials are rock wool and polystyrene, in the thickness of 4 cm, 6 cm and 8 cm for the external wall and 8 cm to 12 cm for a pitched roof.
2011	- according to Rulebook on the conditions, content, and manner of issuance of certificates of energy performance of buildings (“Official Gazette of RS”, No. 69/12)

The most of the analyzed buildings (more than 120) were built in between 1946 – 1980. Considering that measures for the increase of energy efficiency have been applied on just a few of them, it can be concluded that potential for energy savings in public buildings in the city of Kragujevac is significant.

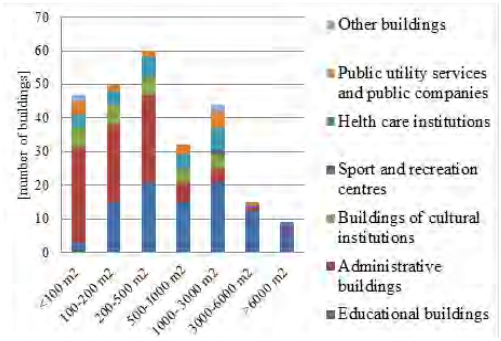

Figure 2. Overview of public buildings according to surface area

The highest share of public buildings in the city of Kragujevac has surfaces of 200 m^2 – 500 m^2. These groups contain the significant number of local community buildings and offices and the highest share of schools buildings in villages. Among the buildings with the useful surface higher than 1000 m^2 the highest share has educational buildings (Figure 2.).

III. METHODOLOGY

Specific heat consumptions per heated area of the buildings is the ratio of total heating consumption in observed period (period without changes of facility purpose, heating surface, thermal envelope and heating source) and heating surface area. In order to reduce the influence of difference of actual (measured in the observed period) and average number of HDD, considered as constant in energy classes labeling process according to Rulebook on the energy efficiency of buildings, specific heat consumption per heated area is determined according to (1):

$$SHC = \frac{1}{A} \cdot \left[\sum_{i=1}^{n} \frac{Q_i}{HDD_i} \right] \cdot \frac{1}{n} \cdot HDD_a \cdot 10^3 \quad (1)$$

Where:

SHC [kWh/m^{2}a] – annual specific heat consumption per heated floor area

A [m^2] – heated floor area

n [–] –number of heating seasons in analysis

Q_i [MWh] – consumption of heat during i– heating season

HDD_i [Kday] – the number of real (measured) HDD during i– heating season

HDD_a [Kday] – average number of HDD adopted by the (Rulebook on the energy efficiency of buildings, 2011).

The values of heating degree days (HDD) for the city of Kragujevac for the period 2014-2016 are shown in Table II. The values were calculated using data from the national hydro-meteorological service company (Republic Hydrometeorological Service of Serbia). The average value presents the value from the Rulebook on the conditions, content and manner of issuance of certificates of energy performance of buildings.

TABLE II. HEATING DEGREE DAYS FOR THE CITY OF KRAGUJEVAC

Average number of HDD	2014	2015	2016
2.610	2.133	2.510	2.349

Energy classes of building with different purposes were defined by the mentioned Rulebook on conditions, content and manner of issuing energy performance certificate of buildings. List of energy classes with its SHC thresholds for existing buildings is presented in Table III. In the case of reconstruction, modernization and revitalization, the renewed building has to improve its energy class for at least one level.

TABLE III. ENERGY CLASS THRESHOLDS FOR EXISTING BUILDINGS

En. class	Administr. and offices	Education. and cultural institutions	Health care institutions	Sport and recreation facilities
	[kWh/m^{2}a]	[kWh/m^{2}a]	[kWh/m^{2}a]	[kWh/m^{2}a]
A+	≤ 10	≤ 12	≤ 18	≤ 14
A	≤ 17	≤ 20	≤ 30	≤ 23
B	≤ 33	≤ 38	≤ 60	≤ 45
C	≤ 65	≤ 75	≤ 120	≤ 90
D	≤ 98	≤ 113	≤ 180	≤ 135
E	≤ 130	≤ 150	≤ 240	≤ 180
F	≤ 163	≤ 188	≤ 300	≤ 225
G	> 163	> 188	> 300	> 225

IV. RESULTS AND DISCUSSION

Specific heat consumption of public buildings in Kragujevac was calculated just for those buildings that are directly or indirectly financed by the city government. The share of heating energy consumed by each of the categories mentioned in chapter 2 is presented in figure 3.

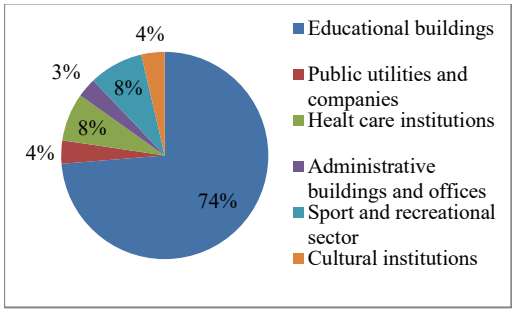

Figure 4. Heat consumption of different categories of public buildings in Kragujevac

A. *Educational buildings*

Because of their purpose, educational buildings have special social importance. They are responsible for the highest share in final energy consumption in the analyzed public buildings. There are 15 preschool and 75 elementary and high school buildings which energy costs are paid by local government. Among the analyzed public schools, there are also joint elementary and high schools, schools for the education of adults and schools for the students with special needs. Specific heat consumption of the schools classified according to built period, as well as average specific heat consumption of all the schools of the same built period is presented in figure 4.

Ten schools were excluded from the analysis because they went through full or partial thermal envelope renovation. Four village schools were also excluded, as they have local electric heating systems which prevent exact distinction of final energy consumption for heating and for other purposes. Average specific heat consumption of analyzed educational buildings in the city of Kragujevac is 175.6 kWh/m^{2}a. This value can be considered as relatively high having in mind that specific heat consumption in educational buildings in Austria is 117 kWh/m^{2}a [10], in Poland 123 kWh/m2a [11], Hungary 110 kWh/m2a [12], Slovakia 85 – 112 kWh/m^{2}a [13]. The reasons for relatively high values of specific heat consumption are nonexistence of legislation refereeing to energy savings in between 1946 – 1988 and existence of relatively week legislations and rulebooks dealing with thermal insulation of building envelope.

B. *Community health centers*

Results of specific heat consumption in tertiary healthcare institutions i.e. community health centers and ambulances are presented in this chapter. Generally, final energy consumption of a health care center depends on the specific type of laboratory and services it provides so final energy consumption cannot be a comparable indicator of building energy efficiency. Nevertheless, specific heat consumption definitely has more comparable value than final energy consumption. Results for community health centers are presented in figure 5.

Two ambulances were excluded from the analysis as their heating energy consumption was not able to be separated from total final energy consumption (heating on electricity). Average specific heat consumption of analyzed healthcare institutions is 149 kWh/m^{2}a, that can be considered as relatively moderate consumption comparing to educational buildings. However, according to research dealing with final energy consumption in health care centers in the city of Kragujevac [14], almost all analyzed healthcare buildings have

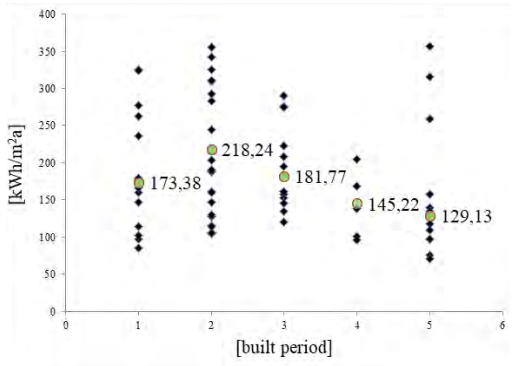

Figure 3. Specific heat consumption in educational buildings in Kragujevac classified according to built period

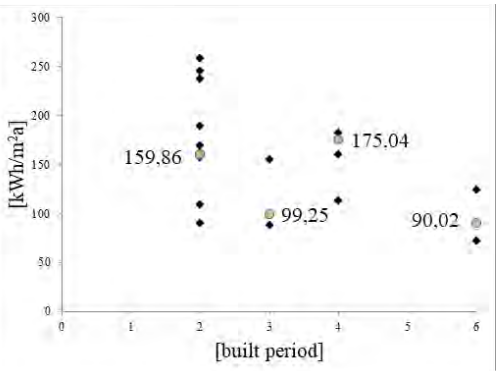

Figure 5. Specific heat consumption in health care institutions in Kragujevac classified according to built period

been reheated by some sort of individually installed electric heaters. Estimated share of electricity used for heating in total heating demand ranges from 6 – 60%, so average specific heat consumption in health care institutions calculated taking this into account is 195 kWh/m^{2}a. For comparison, specific heating consumption in health centers in Vojvodina (Northern Serbia) is 244 kWh/m^{2}a [15].

C. Administrative building

Many of 97 analyzed administrative buildings share building spaces with private entities through different types of private-public partnership. Majority of mentioned buildings have local heating systems that are used just occasionally during the heating season for infrequent meetings. For those local heating systems, electricity and fuelwood (provided from residents own funds) are used. Therefore, 89 municipal administrative buildings were excluded from the analysis and the results of the analysis are presented in figure 6.

Average specific heat consumption of analyzed administrative buildings in Kragujevac is 200 kWh/m^{2}a. Specific heat consumption in the buildings of the same type in AP Vojvodina is 254 kWh/m^{2}a [15], in Austria 251 kWh/m^{2}a, in the Czech Republic 294 kWh/m^{2}a, in Bulgaria 130 kWh/m^{2}a [16].

D. Buildings of cultural institutions

In this chapter, libraries, theatres, buildings of cultural and artistic societies, houses of culture and museums are considered as buildings of cultural institutions. Four buildings among all analyzed are not heated and for 5 other buildings it was not possible to separate heating from final energy consumption since the buildings use electricity for heating. Therefore, the analysis of specific heat consumption in

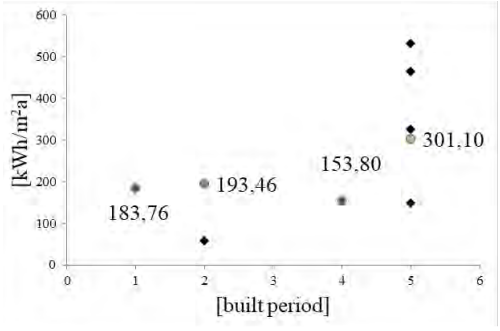

Figure 6. Specific heat consumption of administrative buildings in Kragujevac classified according to built period

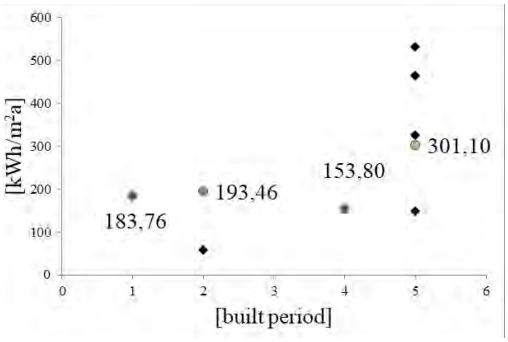

Figure 7. Specific heat consumption of cultural buildings in Kragujevac classified according to built period

buildings of cultural institutions was performed on the sample of 15 buildings (figure 7).

The lowest specific heat consumption has the building of cultural and artistic society "Abrašević" (58.7 kWh/m^{2}a) because its space is heated occasionally. Majority of the analyzed buildings have the status of cultural monuments and they are under direct jurisdiction and protection of the Ministry of Culture and Information of the Republic of Serbia. Preservation of cultural heritage is the primary goal to be achieved with these buildings; therefore their energy efficiency is not considered as a priority. In a case of potential reconstructions, the Ministry issues a special permit taking care that the visual identity of the building stays undisrupted.

E. Sport and recreation centers

Data for nine buildings for sport and recreation activities were collected and analyzed. Since four of the buildings do not have space heating and for two it was not possible to determine heat consumption, specific heat consumption for only two sport halls and indoor swimming pool were calculated. "G. Bogojevic" sport hall (89.7 kWh/m^{2}a) and indoor swimming pool (397.6 kWh/m^{2}a) are relatively new buildings, built in 2009 and 2011 respectively. "Jezero" Hall (267.8 kWh/m^{2}a) was built in 1978 and until now it has not been reconstructed while the building requires renovation. With 5320 seats "Jezero" is main city sports hall that hosts main sports events, while "G. Bogojevic" is used as concert and tournament hall. It has mounted seats and smaller useful space. Specific heat consumption of the sport halls in Stuttgart (Germany) is 140 kWh/m^{2}a [17].

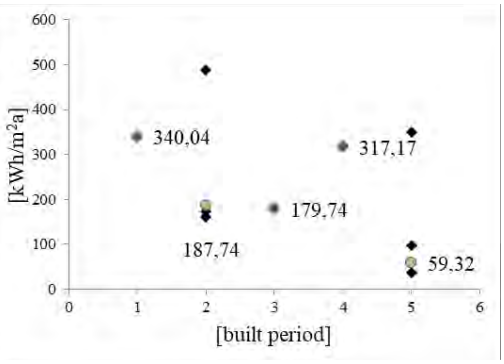

Figure 8. Specific heat consumption of the public services and companies in Kragujevac, classified according to the built period

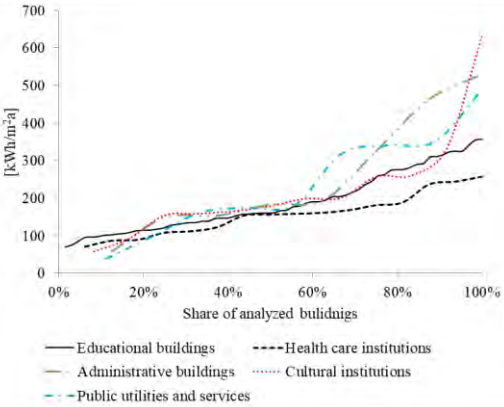

Figure 9. Share of the building of the same sector inside total heat energy consumption of the sector

F. Public services and companies

This group of buildings consists of city market halls, buildings of water supply and sewerage utility company, buildings of the waste management company, buildings of city greenery services, city sanitation and zoo-hygiene services and buildings of city cemetery services. Ten buildings do not have or have just occasional heat consumption (buildings of city cemeteries and inactive utility services) and the consumption of just nine buildings is presented in figure 8.

Average specific heat consumption in analyzed buildings is 130 kWh/m^{2}a, which is the lowest value of all types of public buildings in Kragujevac. City market halls have great influence on relatively low average specific heat consumption as they have useful space of 4828 m^2 and 1490 m^2 and consume in average 37.6 kWh/m^{2}a and 98.1 kWh/m^{2}a, respectively. Other buildings consume in average 227 kWh/m^{2}a of specific heat.

G. Overall analysis

The share of the building of the same sector inside total heating energy consumption of the sector is presented in picture 9. The sport facilities were excluded since the number of the buildings is small.

More than 90% of educational buildings consume more 100 kWh/m^{2}a. Around 40% of analyzed buildings have specific heat consumption in between 100 and 200 kWh/m^{2}a, while 35% of the analyzed buildings have consumption greater than 200 kWh/m^{2}a, and 20% of analyzed public utility services and administrative buildings have consumption greater than 300 kWh/m^{2}a as well as 10% of analyzed cultural institutions.

V. CONCLUSION

This paper analyzes specific heat consumption in public buildings calculated for the creation of the Energy Efficiency Program for the City of Kragujevac 2018 - 2020. All the buildings have been classified in groups according to their type and built period and the consumption of heat inside every group has been presented separately. Average specific heat consumption in public buildings in the city of Kragujevac is 216.6 kWh/m^{2}a. Sport and recreation facilities (influenced with high consumption of indoor swimming pool) and buildings of cultural institutions have bigger than this value. According to data from table III, higher than the calculated average value (149 kWh/m^{2}a) should be expected in health care institution. The lower than expected value is due to the fact that the clinical center is not included in the analyses (only municipal health centers were included). Although educational buildings do not have the highest average specific heat consumption, they consume the highest share of heating energy in public buildings 74%.

Comparing the calculated data of specific heat consumption of municipal public buildings in Kragujevac with data from table III it can be concluded that only 7,8 % of buildings have heat consumption that corresponds to “C” energy class, 19,1% to “E”, 33 % to “F” and 40 % to “G” energy class. The biggest number of energy inefficient buildings belongs to educational buildings, cultural institutions and

administrative buildings and offices and those buildings are the priority for defining energy efficiency measures. Energy efficiency measures in the buildings can be divided into two groups. The first group - technical measures are: improving building envelope thermal insulation, installation of new and more efficient doors and windows, improvement of heating system efficiency, automatic regulation of the heating system, fuel substitutions, etc. Another group of measures refers to introducing energy management system techniques of monitoring and targeting heat energy consumption in buildings.

ACKNOWLEDGMENT

This paper presents a result of research on III42013 project that has been financed by the Ministry of Education, Science and Technological Development of the Republic of Serbia.

REFERENCES

[1] Energy, EU Energie in Figures, Statistical Pocketbook. Luxembourg, Publications Office of the European Union, 2017

[2] Statistical Office of the Republic of Serbia, 2014. Total Energy Balance in 2014

[3] European Energy Agency, Final energy consumption by sector and fuel. Indicator Assessment | Data and maps. Available at: http://www.eea.europa.eu/data-and-maps/indicators/final-energy-consumption-by-sector-9/assessment

[4] D. Elzinga, Lew Fulton, Steve Heinen, Oscar Wasilik, Advantage energy – emerging economies, developing countries and the private-public sector interface, International Energy Agency, 2011.

[5] N. Jurišević, D. Gordić, N. Lukić, M. Josijević, Benchmarking heat consumption in educational buildings in the city of Kragujevac (Serbia), Energy Efficiency, vol. 4, 2018, pp. 1023–1039.

[6] Eurostat, Electricity and Heat Statistics 2016. Available at: https://ec.europa.eu/eurostat/statistics-explained/index.php/Electricity_and_heat_statistics

[7] S. Petrović Bećirović, M. Vasić, Methodology and results of Serbian Energy-Efficiency Refurbishment Project. Energy and Buildings, vol. 62, pp. 258-267

[8] M.S. Todorović, National energy efficiency action plan of buildings in Serbia – an approach to the large scale municipal energy refurbishment. REHVA Journal, vol. 6, 2010, pp. 22–26.

[9] Statistical Office of the Republic of Serbia, Census 2011. Available at: http://popis2011.stat.rs/?page id=2162&lang=en

[10] M. Santamouris, K. Sfakianaki, Predicted energy consumption of major types of buildings in European climates based on the application of EN 15251. Greece: National Kapodistrian University of Athens, 2009.

[11] L. Dias Pereira, D. Raimondo, S. P. Corgnati, M. Gameiro Da Silva, Energy consumption in schools—A review paper, Renewable and Sustainable Energy Reviews, vol. 40, 2014, pp.911–922.

[12] S. Schimschar, J. Grözinger, H. Korte, T. Boermans, V. Lilova, R. Bhar, Ecofys | Panorama of the European non-residential construction sector – Report Dec 2011, 2011.

[13] E. Maldonado, Implementing the Energy Performance of Buildings Directive (EPBD) – featuring country reports 2012, European U. Brussels, 2013, p. 372.

[14] N. Jurišević, D. Gordić, V. Vukašinović, A. Radojević, G. Stojanović, Analysis of specific energy consumption in health institutions in the city of Kragujevac, Energija, Vol.20, No.1-2, 2018, pp. 396-403. (Н. Јуришевић, Д. Гордић, В. Вукашиновић, А. Радојевић, Г. Стојановић, Анализа специфичних потрошњи енергије у здравственим установама у граду Крагујевцу, Енергија, Vol.20, No.1-2, 2018, pp. 396-403.

[15] J. Petrović, M. Medojević, I. Mujan, Energy indicators for public buildings in autonomous province of Vojvodina with focus on healthcare, educational, and administrative buildings, Thermal Science, vol. 20, 2016, pp.S331–S342.

[16] S. Birschall, I. Wallis, D. Churcher, S. Pezzutto, R. Fedrizzi, E. Causse, D2.1a: Survey on the energy needs and architectural features of the EU building stock, iNSPiRe Project (Development of Systemic Packages for Deep Energy Renovation of Residential and Tertiary Buildings including Envelope and Systems), 2014.

[17] E. Beusker, C. Stoy, S. Pollalis, Estimation model and benchmarks for heating energy consumption of schools and sport facilities in Germany. Building and Environment, vol.49, 2014, pp.324–335.

Local DC Power Network

Prahaladh Paniyil[1], Rajendra Singh[2], Vishwas Powar[3], John Kimsey[4]

[1]Holcombe Department of Electrical and Computer Engineering, Clemson University, Clemson, USA, ppaniyi@clemson.edu
[2]srajend@clemson.edu, [3]vpowar@clemson.edu, [4]jkimsey@clemson.edu

Abstract— **The energy sector is about to undergo a major transformation. In this paper, we discuss the best possible energy solution for a smart and green community. This paper focusses on the decentralized power generation, storage and distribution through photovoltaics and lithium batteries. It encompasses the need for local direct current (DC) power through the factors driving this change. The importance of local DC power in the surface transport sector is also established. Finally, we conclude with data bolstering our argument towards the paradigm shift in the power network.**

Keywords – Photovoltaics, Lithium-ion batteries, Electric Vehicles, Nano-grid, Internet-of-Things

I. INTRODUCTION

Alternating current (AC) has been dominating power networks in the world ever since it won the battle against direct current (DC) in the late 19th century. The invention of the transformer allowed AC power to transmit over long distances with minimal losses by stepping up/down voltages with ease. However, the scenario is very different today. Most of the loads used today, except for a few inductive ones, are DC powered. Owing to the prowess in photovoltaic (PV) and lithium-ion battery technologies today, we can generate and store DC power locally. Locally generated DC power encounters minimal losses and the use of DC appliances is much more energy efficient than the current AC network.

PVs coupled with batteries provides an ultra-low-cost, secure and self-sufficient power network. No other energy source currently can match the declining costs for PVs as they work on the principle of free fuel based solar energy. Batteries are also experiencing a similar trend in their cost owing to the increasing demand for Electric Vehicles across the world. Fig. 1 displays a slope for the cost reduction in PV and lithium-ion batteries. We will be discussing the current status of PVs and batteries in the subsequent section to establish its cost effectiveness.

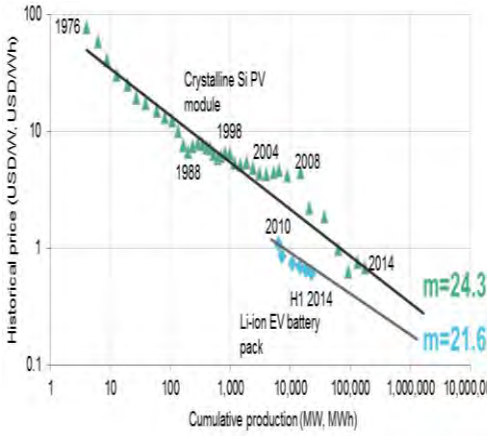

Figure 1. Cost reduction trends of photovoltaic modules and Lithium batteries [1].

II. CURRENT STATUS OF PHOTOVOLTAICS AND BATTERIES

The exponential growth of the PV and battery industries leading to a substantial reduction in their cost, can enforce the paradigm shift from AC to DC power. According to market analyst IHS Markit, the global PV installations for 2018 is forecasted to reach 108 GW by the end of the year [2]. This growing demand in PV can be majorly attributed to the immense increase in demand from China over the last year. The University of New South Wales in Sydney has signed an agreement for a period of 15 years to have all its energy demands met by Solar PV[3]. This agreement ensures the university to purchase 124,000 MW hours of electricity from a future solar farm called Sunraysia that is being constructed in the state [3]. The university aims

to achieve its goal of carbon neutrality of energy use by 2020 through this step [3].

A solar project in Saudi Arabia led by Masdar, Abu Dhabi's renewable energy company, and its French partner EDF have submitted the lowest bid in the world for solar power generation at 1.79 US cents per kilowatt-hour (kWh) [4]. Fig. 2 shows data analytics from last year in which there is a clear exponential decrease in cost for PV systems and an exponential increase in the installation volume across the globe.

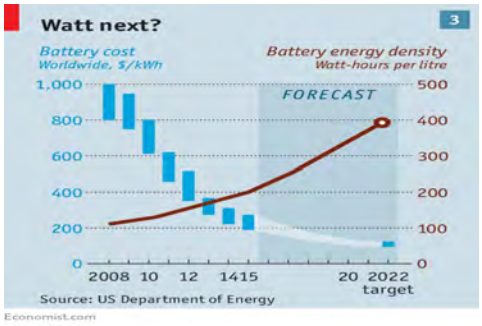

Figure 2. Lithium-ion battery vs Energy Density [7].

Due to demand for EVs, consumer products and storage for PV power, the battery industry is also experiencing a similar trend in the cost and manufacturing. Lithium batteries are an attractive option for these markets as they have the highest energy density per weight. Lithium batteries are already dominant in the consumer goods market such as mobile phones and laptops. They are also considered extremely viable for the EV industry owing to their weight benefits. To

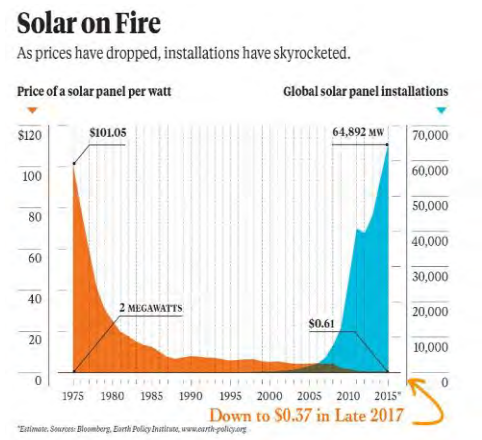

Figure 3. Cost vs Installation Volume for PV systems [5].

meet this increasing demand for lithium batteries, gigawatt factories like TESLA's $5 billion Giga-factory, are being built across the globe [6].

We have already concluded in our paper [8] in 2014 that if current trends of PV growth continue, we expect PV electricity cost with storage to reach $0.02 per kWh in the next 8-10 years (2022-2024). With the data that is available today, the goal of $0.02 per kWh can be seen to be achieved well ahead of the predicted time. According to Fig. 3, the average lithium battery cost is forecasted to fall below $100 per kWh by 2022.

III. Need for Local DC Power

The electricity industry is at the cusp of a dramatic transformation. The drivers for this paradigm shift are real-time grid monitoring, emergence of microgrid and nanogrid in place of centralized integrated electric grid, improved energy efficiency, cyber security in the grid, weather tolerant electricity infrastructure and intelligent loads [9]. We can discuss the importance of these factors and their fulfillment through a local DC power network.

A. Real-time grid monitoring

The concept of localized PV and battery-based DC power is further reinforced by the connectivity aspect of the Internet-of-Things (IoT). IoT is a boon in the domain of predictive analysis. The data collected over time can be utilized for predictive analysis to generate more efficient future outcomes. A solar energy company can install various IoT-based sensors on the solar panels and monitor their performance and provide real-time insight. Since these sensors can collect massive amounts of data, companies can utilize this to have a more granular oversight over their systems [10]. Various IoT based sensor techniques are available for monitoring solar energy grids for maximum power efficiency. We can see in [11], how an IoT-based network is created to monitor and control a smart farm utilizing solar panels as the power source.

Like PV systems, batteries can also be monitored through IoT based devices for enhanced performance in the grid. In [12], we can see the development of a battery monitoring system for the grid with the utilization of IoT. The combination of real time monitoring of the energy grid and utilization of intelligent DC loads can lead to immense power savings as opposed to the current power networks.

B. *Emergence of micro-grid and nano-grid in place of centralized energy grid*

In remote places, where the number of consumers is relatively small, it is quite challenging to draw transmission lines or to operate a generator that requires fuel delivery. On such instances, the PV and battery-based DC nano-grid system can provide optimum solution by eliminating the transmission challenges and by almost hassle-free operation. This holds the key to open the door of energy accessibility even to the people of underdeveloped economies where power for everyone is still a genuine issue [13]. Thus, such a decentralized power network empowers economic growth, creates a global middle-class and establishes social justice.

The local DC nano-grids can operate at a lower voltage (<1500V), and thus eliminate the environmental, health and safety issues associated with high voltage AC transmission and distribution. Local distribution will also get rid of expensive tree branch pruning and vegetation clearance activities that are associated with high voltage AC lines running through forests. There is no significant issue of safety for 48V DC applications. For the data center and other general-purpose higher voltage applications, several companies supply DC power distribution hardware operating at 380V including circuit breakers with rated currents ranging from 15A to 2,500A [14].

Local generation, storage and transmission of power do not require massive transmission network infrastructure and its associated investment. The operational cost is greatly reduced for a local network due to this exclusion of long-distance transmission networks.

C. *Improved energy efficiency*

Most of the loads that we use today (except for a few inductive ones) are all DC powered. There is a need for conversion of power for AC to DC at the device level with the existing centralized power network. Fig. 4 demonstrates the extra internal circuitry required for conversion of power from AC to DC in a 35W LED bulb. This conversion of power results in power losses at each stage of conversion. As reported in a study [15], 33% of electrical power can be saved by converting all appliances running currently on AC to high-efficiency and DC-internal technology. Implementation of local DC power through PV and battery can eliminate majority of the conversion losses leading to a much more efficient network.

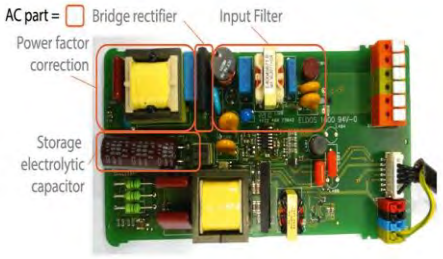

Figure 4. Conversion circuitry for AC to DC conversion for a 35W LED bulb [16]

A local DC network consists of DC power at generation and utilization. The elimination of conversion components leads to lesser capital cost for the network. Also, due to fewer components, the whole network has considerably lesser probability of component failures. Ultimately, it provides enhanced system reliability. Another important enabling prospect with fewer components in the system is the availability of less area for cyber-attacks. We would be discussing the overall aspect of cyber security in the following sub-section.

D. *Cyber security in the grid*

PV based DC microgrids are less vulnerable to cyber-attacks [17]. It is difficult for a remote attacker to access an isolated and self-contained PV based DC microgrid/nanogrid. Situational intelligence, real time monitoring, physical security and user control –all can be incorporated in PV based DC microgrid/nanogrid. Large grids and distributions require a lot of nodes where monitoring data are generated .and collected, and commands are sent to be executed. This transmission and reception of data creates opening for malicious intruders who might gain access to systems or data through sophisticated attacks [17].

In the age of internet of things (IoT) and remotely connected servers, a possible attack may come from any point, even from far ends of the internet. PV based DC microgrids/nanogrids will employ intelligent control systems that are local and can remain secured from cyber-attacks. A leading networking company, Cisco, reported that about 73% of IT professionals in (centralized) utility service experienced security breach whereas the other industry's average is 55% [18]. Hence, by decentralizing the energy grid through local DC power, the risks of cyber-attacks to the grid can also be minimized.

E. *Weather tolerant electricity infrastructure*

Recently, the nation has been witnessing nature's wrath through frequent hurricanes and hail storms causing power outages in many parts of the country. Recently, NERL's main campus in Golden, Colorado was hit by a hail storm. Only one broken panel was reported broken among the 3000 panels that were installed on the roof of a net-zero energy building [19]. To further reiterate the claim for resiliency of PV based solar systems in times of natural disasters, Hurricane Irma's path can be taken into consideration. A 650-kW rooftop solar array on San Juan's VA Hospital continued to operate at 100% post-storm even after being exposed to wind speeds of about 180 mph [20]. Resiliency to harsh weather conditions is not the only advantage to PV and battery-based power networks. A power failure of a plant in a centralized AC power network impacts a very large area that is incorporated under the same network. With the implementation of decentralized local DC power grids, the area impacted by such failures would be much smaller. PV and battery-based local DC power networks are also much more to geomagnetic storms caused by Coronal Mass Ejections (CMEs) [8].

F. *Intelligent loads*

The advent of IoT is a major revolution in the technological aspect of humanity. Every sector is working on incorporating smart devices that are embedded with sensors that relay information on the internet. From home appliances to automated robotics in manufacturing plants IoT-based products are being designed and implemented everywhere. The energy sector is also following the same path. As already discussed in this paper, IoT-based sensors enable real time monitoring of the grid for efficient energy output. However, IoT-based intelligent appliances can further enhance energy efficiency by demand-based utilization of power.

Such intelligent loads/appliances are already commercially available in the market. These loads can monitor electricity generated by solar and instruct ON/OFF times based on peak energy generation periods. For example, an automated washing machine can be instructed by the intelligent control hub to turn on only during periods of minimum load utilization and maximum free fuel based solar energy generation. Hence, a local DC power network has the incentive of easily coupling with the abundance of IoT-based intelligent loads that are making an entry into human lifestyle. To further bolster this idea of incentivization, we can refer to the recent article on the new range of EVs from BMW. According to the article [21], BMW i3 EV can be turned into cash cows by delaying their charging time to offset peak demand and align with maximization of renewable energy utilization [21].

IV. LOCAL DC POWER IN SURFACE TRANSPORT SECTOR

The recent data released by Environmental Protection Agency (EPA) signifies the growth of transport sector as a major contributor to US greenhouse gas (GHG) emissions [22] [23]. Transportation surpassed various economic sectors like electricity and industry to contribute for 28.5% of total US GHG emissions in 2016 (Fig. 5). This has raised several concerns about the petroleum-based transport sector and has called for transformation. There are four major drivers of change in the transport sector viz. – Electrification, Diverse Mobility, Autonomous Driving and Connectivity. The need for a cleaner, cheaper and cost efficient alternative technology for surface transport created the need for electrification. Increased carbon emissions and rising global temperatures have led to stricter laws and preventive measures by many EU countries [24]. Low cost and improved battery technology has also fueled electrification of surface transport sector which in-turn benefits the PV sector. Thereby establishing a triangular relationship between PV, EV and batteries. Furthermore, the cost of maintenance and operation aka Return on Investment (ROI) of electric DC vehicles is way cheaper than traditional IC engine-based automobiles [25] [26]. As the sharing economy expands and consumer preferences change, the standard one person-one car model will continue to evolve from outright purchase or lease to rentals and

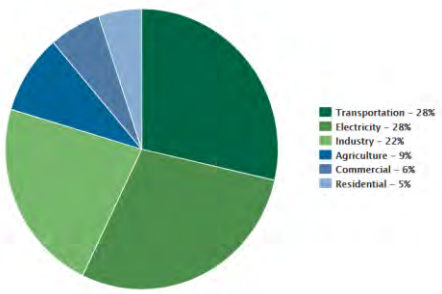

Figure 5. GHG emissions by sector, 2016, US [23]

carpooling, thus creating diverse mobility. The new era of IoT, wireless sensor networks, DC electric vehicles and improved battery technology have made it possible to envision autonomous driving and connected vehicle technology.

The rise in sales of EVs has accentuated the concept of localized DC charging using PV and battery-based systems. Localized charging for electric vehicles can be achieved in two ways; plug-in charging and onboard on-the-go charging.

A. Plug-in charging

Plug-in charging of electric vehicles is achieved by installing a charging station also known as electric vehicle supply equipment (EVSE) in your house or by accessing a public charge station in the neighborhood. The primary objective of local plug-in charging is to use current wall-outlet or some additional circuitry to charge the battery of electric cars. There are three types of electric charging stations available, Level 1, Level 2 and DC fast chargers.

A key observation is that both Level 1 and 2 chargers operate on AC input power (120 V and 240 V respectively). The Plug-in EVs internal battery charger converts it into DC power to charge up the car's traction battery [27]. This results in conversion losses and increases the charge time of the battery. The DC fast charging usually implements a direct link between a DC power source (either solar or battery) and the battery charging circuitry, thereby eliminating intermediate stages of conversion and rectifying [28].

This considerably reduces charge-time and has generated areas of smart control and PV based techniques for DC fast charging stations. Vehicle-to-Grid (V2G) and Grid-to-Vehicle (G2V) technologies that ensure smart control and flow of energy, to and fro form the grid are also be implemented. However, reducing conversion and step-up/ step down losses is the primary reason for utilizing direct localized DC systems instead of grid dependent AC [28].

B. Onboard PV charging

On-board DC charging of electric vehicles aims at continuously charging the batteries on-the-go. In this technique, energy is usually harvested from an on-board solar panel and smart control techniques for efficient charging of the traction battery are implemented. This method is challenging as it involves smart control algorithms to mitigate effects of variability of solar energy as the vehicle is moving from point A to point B. Effects of partial shading, tracking maximum power point, variability of irradiance and temperature have to be compensated by intelligent control techniques and algorithms [29] [30]. Another critical challenge lies in retrofitting the design of existing EV drivetrain to integrate PV modules and additional PV circuitry. Sometimes integrating the solar panel might be bulky and undermine speed and performance. But many lightweight, small distance and low speed prototypes have successfully integrated PVs in their design. The Ford C-Max Solar, Toyota Prius, Volkswagen ID Buzz and Lightyear one is some examples. According to [31], a light weight aerodynamically efficient, small distance, car can travel up to 60 kms using bulk Si-PV modules. As battery technologies improve and design principles are tweaked, there would be many more local DC generated and powered automobiles, primarily relying on PV modules for functional power.

The following section elaborates our work in studying benefits of localized DC power in field of transport.

V. PROOF OF CONCEPT

We have established the energy efficiency of local DC Power through our experiments.

A. Li-ion battery charging

Firstly, we will demonstrate the power savings of direct DC charging of Lithium battery through Solar Panels as compared to AC charging networks.

Fig. 6 demonstrates the experimental setup for direct DC charging. In the DC charging circuit, we connected the solar panel (320W) with an initial voltage of 41.7V to a Tristar MPPT charge controller at 1.19 pm when it was sunny. The charge controller is used to regulate

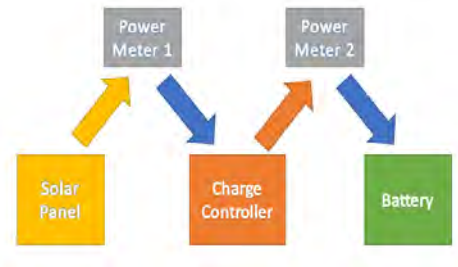

Figure 6. DC Charging Experimental Setup

the current and voltage for smooth charging process. The battery was previously discharged by connecting it to a DC powered refrigerator. The initial battery voltage was recorded as 15.7V. The charge controller equalizes the battery charging and hence, readings were taken every minute before and after the absorption state for 30 minutes.

Before reaching the absorption state, the panel delivered approximately 40W of power with voltage reading of 39.7V and current reading of 0.74A. The charging voltage and current delivered by the controller to the battery were 13.89V and 2.52A respectively. After reaching the absorption state, the power output from the solar panel stabilized at around 20W with a voltage and current reading of 39.5V and 0.5A respectively. The controller delivered constant power of approximately 18W with voltage and current readings of 13.93V and 1.3A respectively.

A charging network for the same battery was designed using an AC network as seen in Fig. 7. Such AC networks are prevalent today as the AC power network is dominant in the community. We constituted for all the elements in the AC network and took reading every minute for 30

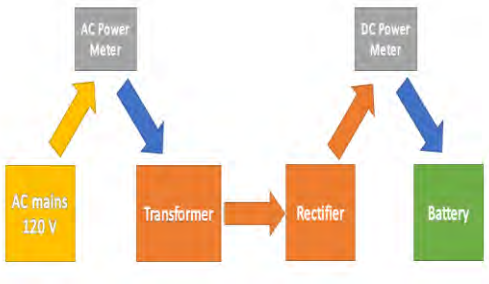

Figure 7. AC Charging Experimental Setup

minutes.

The initial voltage recorded for the AC mains was 119.1 V. The initially battery voltage recorded was 14.8V. While charging, the AC input power was approximately 60W and the DC charging power was approximately 35W. The charging voltage through the rectifier was recorded as approximately 11.8V and the current was recorded as approximately 3A.

We recorded the average power readings for both DC and AC mechanisms and calculated % power losses. Table I demonstrates the charging efficiency and power losses incurred in the DC vs AC charging mechanisms.

The DC charging incurs lesser losses due to fewer conversion components involved in its network. This experiment demonstrates the increased energy efficiency of DC charging as compared to the current AC technique.

B. On-board PV for battery operated golf cart

In this experiment, we designed and analyzed a simple on-board PV powered DC golf cart. Using localized DC charging we increased the run-time and distance traveled by the golf cart and got comparable results even on cloudy and rainy days.

TABLE I. DC VS AC CHARGING EFFICIENCY

Parameters	**Power Calculations**		
	Average input power (W)	***Average output power (W)***	***Power Loss (%)***
DC Power (W) (Before Absorption State)	43.2	39.375	8.85
DC Power (W) (After Absorption State)	20.31	17.44	2.87
AC Power (W)	59.05	31.45	46.74

In order to determine how the on-board solar panel would improve the electric golf cart performance, four types of trials were conducted in different weather conditions. For trial 1, the golf cart was driven on a set route on battery alone (without any solar panel). For trials 2, 3 and 4, the golf cart was driven on the same route as trial 1, but this time with battery and on-board PV solar panel. Trials 2, 3, and 4 were conducted on a hot sunny day, partly cloudy day and rainy day, respectively. Every 30 minutes, the golf cart was brought back to the initial start point to have battery voltage tested.

The distance traveled by the golf cart during each trial was measured using a GPS phone-based application. The circuit was retrofitted to include, a MPPT charge controller, a circuit breaker switch, an on-board solar panel rated (320W), along with the 6 batteries of 6.6 V each connected in series to produce a net 40 V golf cart battery. Fig. 8 shows the increased on-road distance travelled by the golf cart with on-board PV charging.

In Fig. 9 we can clearly see that with the help of on-board solar panel, the on-road run time has increased considerably. Table II summarizes the results of this experiment.

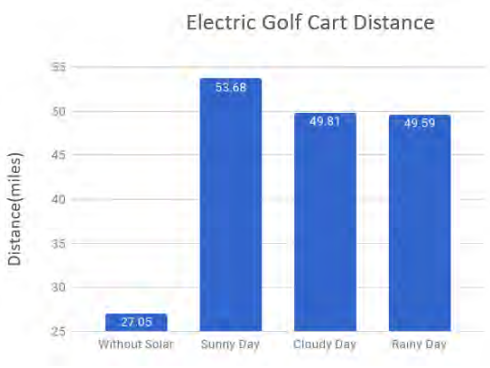

Figure 8. Enhanced Distance travelled by PV golf cart

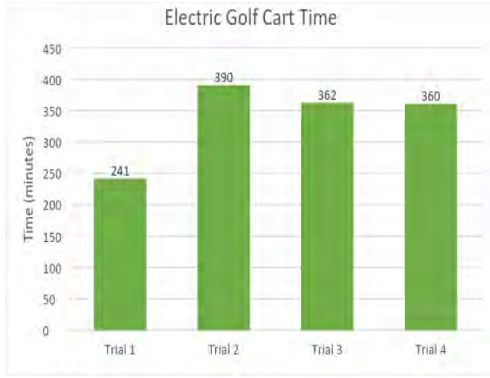

Figure 9. Enhanced time traveled by PV golf cart

TABLE II. IMPROVEMENT IN DC GOLF CART PARAMETERS USING ONBOARD PV

Parameters	Without Solar	With Solar		
	Sunny	*Sunny*	*Cloudy*	*Rainy*
Distance in miles	27.05	53.68	49.81	49.59
Time in minutes	241	390	362	360
Improvement in Distance over Without Solar	--	98.45%	84.14	83.33
Improvement in Time over Without Solar	--	61.83%	50.21%	49.38 %

VI. CONCLUSION

Based on the research conducted in this paper, we conclude that local DC power is shaping to be the energy network for the future. Our data indicates how local DC power is beneficial to the surface transport sector. It can cause an overhaul by introducing more efficiency and cost savings in the surface transport and ultimately the energy sector. With proper policy, PV and battery-based local DC power grids will be the main mode of the energy generation, storage and consumption.

ACKNOWLEDGMENT

Part of the work was supported by Clemson University Creative Enquiry Research Program.

REFERENCES

[1] R. Singh, Amir A. Asif, G. K. Venayagamoorthy "Transformative Role of Photovoltaics in Phasing out Alternating Current Based Grid by Local DC Power Networks for Sustainable Global Economic Growth", IEEE-PVS Conference, Portland 2016. IEEE , DOI: 10.1109/PVSC.2016.7750286

[2] M. Hutchins (2017). IHS Markit: Global solar installations to pass 100 GW in 2018. Available at: https://www.pv-magazine.com/2017/12/14/ihs-markit-global-solar-installations-to-pass-100-gw-in-2018/

[3] Websolutions (2018). Australian university to become 100% solar powered. Available at: http://www.climateactionprogramme.org/news/australian-university-to-become-100-solar-powered

[4] L. Graves (2017). World's cheapest prices submitted for Saudi Arabia's first solar project. Available at: https://www.thenational.ae/business/energy/world-s-cheapest-prices-submitted-for-saudi-arabia-s-first-solar-project-1.663842

[5] Z. Shahan (2018). Solar Panel Prices Continue Falling Quicker Than Expected. Available at: https://cleantechnica.com/2018/02/11/solar-panel-prices-continue-falling-quicker-expected-cleantechnica-exclusive/

[6] A. Moss (2017). 5 companies taking a share in the growing Lithium-ion batteries market. Available at: https://keepingstock.net/5-companies-taking-a-share-in-the-growing-lithium-ion-batteries-market-acc2828719f5

[7] San Diego and Sunderland (2017). After electric cars, what more will it take for batteries to change the face of energy. Available at: https://www.economist.com/news/briefing/21726069-no-need-subsidies-higher-volumes-and-better-chemistry-are-causing-costs-plummet-after\

[8] R. Singh, G. Alapatt and G. Bedi, "Why and How Photovoltaics Will Provide Cheapest Source of Electricity in the 21st Century," Facta Universitatis, Series: Electronics and Energetics, 2014, vol. 27, no. 2, pp. 275-298

[9] A. A. Asif, R. Singh and G. K. Venayagamoorthy, "Ultra-Low Cost and Solar Storm Secured Local DC Electricity to Address Climate Change Challenges for All Economies," in Clemson Power Systems Conference, Clemson, SC, 2016.

[10] M.D. Phung, M. Villefromoy, and Q. Ha, "Management of solar energy in microgrids using IoT-based dependable control," In Electrical Machines and

Systems (ICEMS), 2017 20th International Conference, pp. 1-6, IEEE, August 2017.

[11] O. Chieochan, A. Saokaew, E. Boonchieng, "Internet of things (IOT) for smart solar energy: A case study of the smart farm at Maejo University," InControl, Automation and Information Sciences (ICCAIS), 2017 International Conference, IEEE, Oct 2017, pp. 262-267

[12] K. Friansa, I. Haq, B. Santi, D. Kurniadi, E. Leksono, B. Yuliarto, "Development of Battery Monitoring System in Smart Microgrid Based on Internet of Things (IoT)," *Procedia engineering*, *170*, Jan 2017, pp.482-487

[13] World Economic Forum (2018). Global Risk Report. Available at: http://www3.weforum.org/docs/WEF_GRR18_Report.pdf

[14] ABB white paper. *Six stages of solar bankability.* Available at: https://library.e.abb.com/public/2fa374aa511be1558525792e005e47fb/ABB_%20solar_whitepaper_final.pdf

[15] S. Backhaus, G. W. Swift, S. Chatzivasileiadis, W. Tschudi, S. Glover, M. Starke, J. Wang, M. Yue and D. Hammerstrom (2015). DC Microgrids Scoping Study—Estimate of Technical and Economic Benefits. Available at: http://energy.gov/sites/prod/files/2015/03/f20/DC_Microgrid_Scoping_Study_LosAlamos-Mar2015.pdf. [Accessed 10 Dec 2016].

[16] LpR Article. Direct Current (DC) Supply Grids for LED Lighting. Available at: https://www.led-professional.com/resources-1/articles/direct-current-dc-supply-grids-for-led-lighting

[17] X. Zhong, L. Yu, R. Brooks and G. Venayagamoorthy, "Cyber security in smart DC microgrid operations," in IEEE 1st Intl. Conf. DC Microgrids, Atlanta, GA, 2015.

[18] Greentech Media white paper (2016). Utility Security: Exceeding Mandates to Mitigate Risk. Available at: http://www.cisco.com/c/dam/en_us/solutions/industries/energy/docs/greentech-white-paper.pdf

[19] Office of Energy and Renewable Energy (2017). Hail No! National Lab's Solar Panels Survive Severe Storm. Available at: https://www.energy.gov/eere/articles/hail-no-national-labs-solar-panels-survive-severe-storm

[20] J. Marsh (2017). Can solar panels withstand hail and survive hurricanes. Available at: https://news.energysage.com/solar-panels-hail-hurricanes/

[21] F. Lambert (2018). BMW says EV owners can turn i3 into 'cash cow', use more solar power with controllable load tech. Available at: https://electrek.co/2018/09/12/bmw-electric-car-owners-i3-into-cash-cow-controllable-load-technology/

[22] The United States Environmental Protection Agency (EPA). (2018). Inventory of U.S. Greenhouse Gas Emissions and Sinks: 1990–2016. Available at: https://www.epa.gov/sites/production/files/2018-01/documents/2018_complete_report.pdf

[23] Offce of Transportation and Air Quality EPA-420-F-18-013. (2018). U.S.Transportation Sector GHG Emissions - Fast Facts: 1990-2016. Available at: https://nepis.epa.gov/Exe/ZyPDF.cgi?Dockey=P100USI5.pdf

[24] Alex Gray. (2017). The best countries in Europe for using renewable energy. Available at: https://www.weforum.org/agenda/2017/04/who-s-the-best-in-europe-when-it-comes-to-renewable-energy/

[25] Fleetkarma. Everything you need to know about electric cars. Available at: https://www.fleetcarma.com/everything-need-know-electric-cars/

[26] M. Abdelhamid, I. Haque, S. Pilla, Z. Filipi, R. Singh, "Impacts of Adding Photovoltaic Solar System On-Board to Internal Combustion Engine Vehicles Towards Meeting 2025 Fuel Economy CAFE Standards," SAE Int. J. Alt. Power. 5(2):2016, doi:10.4271/2016- 01-1165.

[27] Doug Kettles, "Electric Vehicle Charging Technology Analysis And Standards," Florida Solar Energy Center, FSEC Report Number: FSEC-CR-1996-15, 2015, Available at: http://www.fsec.ucf.edu/en/publications/pdf/FSEC-CR-1996-15.pdf

[28] M. Abdelhamid, R. Singh, I. Haque, "Role of PV Generated DC Power in Transport Sector: Case Study of Plug-in EV," in First International Conference on DC Microgrids (ICDCM), IEEE, July 2015, pp. 299-304

[29] M. Abdelhamid, A. Qattawi, R. Singh, and I. Haque, " Comparison of an Analytical Hierarchy Process and Fuzzy Axiomatic Design for Selecting Appropriate Photovoltaic Modules for Onboard Vehicle Design," International Journal of Modern Engineering, 2014 vol. 15, no. 1, pp. 23-35

[30] Bhatti, A. R., Salam, Z., Aziz, M. J. B. A., and Yee, K. P, "A critical review of electric vehicle charging using solar photovoltaic" Int. J. Energy Res., 40: 439–461. doi: 10.1002/er.3472, 2016

[31] Abdelhamid, Mahmoud & Qattawi, Ala. (2014). "Evaluation of On-Board Photovoltaic Modules Options for Electric Vehicles. IEEE Journal of Photovoltaics", 4. pp. 1576 - 1584. 10.1109/JPHOTOV.2014.2347799.

Carbon Footprint Associated with a Cake Factory

Ana Lyvia Tabosa da Silva[1], Daniel de Paula Diniz[2], Alexandre Magno Vieira Gonçalves de Brito[1], Rommel de Santana Freire[3], Monica Carvalho[4]

[1]Center of Technology, Federal University of Paraíba, Brazil,
analyviatabosa@yahoo.com.br; alexandreh_magno@hotmail.com
[2,4]Center of Alternative and Renewable Energy, Federal University of Paraíba, Brazil,
danieldiniz@cear.ufpb.br, monica@cear.ufpb.br
[3]Center of Applied Social Sciences, Federal University of Paraíba, Brazil,
professorrommel@uol.com.br

Abstract — **Consumers are progressively more interested in purchasing products that are associated with environmental preservation and social development. In the food sector, the search for healthy food products is increasing, which is confirmed by the success of products that have different eco-labels or certifications. This demonstrates that consumers care about the source of the label and the quality of information it contains, especially regarding changes related to food production and processing. The food we eat also has different climatic impacts, and the food carbon footprint comprises the amount of greenhouse gases that are emitted in the stages of cultivation, processing, packaging and transportation of food products. Thus, choosing one nutrient, or another, affects not only our health but also the environment. In this context, eco-labels emerge to help the consumer in the decision-making process, thus contributing to a sustainable food production system. The objective of this study is to calculate the carbon footprint associated with two cake flavors, English pound cake and carrot cake, using SimaPro software. For the production of these cakes, the ingredients and consumption of energy (electricity and butane gas for cooking) were accounted for, along with water consumption and transportation to sale points. The carbon footprint for one English pound cake was 0.91 kg CO_2-eq ($0{,}81 \times 10^{-3}$ kg CO_2-eq/kcal) and for a carrot cake, 1.52 kg CO_2-eq ($1{,}42 \times 10^{-3}$ kg CO_2-eq/kcal). It was observed that the eggs were responsible for the highest share in the emissions.**

Keywords — Life Cycle Assessment, carbon footprint, food industry, cakes, sustainability

I. INTRODUCTION

According to the Brazilian Association of Cookie, Pasta, and Industrialized Bread & Cake Industries [1], in 2017 approximately 3.5 x 10^6 tonnes of cakes were sold in Brazil. In 2017, this sector grew by 3.2%, according to the Brazilian Association of the Bakery and Confectionery Industry [2] which represents a revenue of R$90.3 billion (US$23 billion, at the time of writing 1 US$ = 3.85 R$).

Healthy products, that also present social and environmental responsibility, attract the interest of consumers [3]. This means that the concern with environmental impacts has already gone beyond the consumption of water and energy associated with activities or services, and begins to include food products [4]. This is evidenced by the success of alternative initiatives such as seals and eco-labels, for example, of organic foods, which confirm the interest of consumers in changing the way food is produced, processed, and sold [5]. Thus, labels help in the decision-making process of the consumer, contributing to a food production system with greater ethical and political values and capable of generating sustainable production systems [5], with lower levels of carbon emissions. Brazil is well positioned to meet its emission mitigation targets by 2020; however, after 2020, there will be challenges to combine economic growth with low emissions associated with energy consumption [6].

This study calculates the carbon footprint associated with two cake flavors, which are produced in a small facility (overall monthly

production of 7580 cakes), in the city of João Pessoa, Paraíba (Northeast Brazil). The flavors analyzed herein are English pound cake and carrot cake. The carbon footprint is calculated using the Life Cycle Assessment (LCA) methodology with SimaPro software, and the final environmental impact is expressed in terms of kg CO_2-eq/kcal.

II. Materials and Methods

The quantification of the environmental impact generated in the production and distribution of the cakes was accomplished through the application of the Life Cycle Assessment (LCA) methodology. The European Commission recommends LCA as the most convenient method for the environmental assessment of products [7]. LCA is an internationally accepted and recognized tool, already widely used in Europe. LCA accounts for the impacts resulting from the extraction of raw materials, the manufacturing process, the transportation or distribution of the product, its use, and then its final destination, and thus, by means of a comparative analysis, the best system (from an environmental point of view) can be selected [8].

The use of LCA has proven to be successful for the control of the environmental impact of products and services. This is due to the variety of categories of impacts that can be accessed in an integrated manner and to the perspective of life cycle assessment, which considers the complete chain of inputs and outputs of a production system. This enables the quantification of the environmental impact in different dimensions (categories). LCA is therefore a very interesting tool for the demonstration of the sustainability of a product [7]. The process for conducting a LCA is regulated by the International Organization for Standardization (ISO), in its ISO 14040 and 14044 [9; 10], which establish four distinct phases: i) definition of purpose and scope; ii) inventory analysis; (iii) impact assessment; and iv) interpretation of results. More details on LCA can be found in [11].

The LCA was developed herein in the SimaPro software [12], which allows modeling and analysis of the most complex life cycles in a systematic and transparent way, following the recommendations of ISO 14040 and 14044 [9;10]. In this work, the software version 8.0.5.13 [12] and two databases for the inventory were used: Ecoinvent 3 [13] and Agri-footprint [14] which contain considerable processes of energy and materials necessary for the analysis and accounting of impacts.

Among the environmental impact assessment methods available, the IPCC 2013 GWP 100y method was selected due to concerns with global warming and climate change. This method uses the conversion factors published by the Intergovernmental Panel on Climate Change (IPCC) [15], which is an international committee dedicated to the study of climate change issues. The method was created due to the necessity of assessing the environmental impact caused by greenhouse gases. Therefore, the GWP (Global Warming Potential) expresses the environmental impact in terms of greenhouse gas emissions, generating a response in CO_2-eq [16]. The calculation is based on the relationship between the power to absorb radiation heat per 1 kg of a greenhouse gas and 1 kg of carbon dioxide (CO_2), integrated over time [15, 16]. The IPCC recommends a time horizon of 100 years as this allows verification of the cumulative effects of emissions.

A. Case Study

The analysis herein presented encompasses the environmental impact associated with the production of cakes in a small company, located in the city of João Pessoa, Northeast Brazil. There are 12 different flavors produced: banana, double-flavored (chocolate and vanilla), prune, vanilla with chocolate sprinkles, English pound cake, *baêta* (Brazilian milk cake), cassava (made from grated cassava/yucca/manioc), cream, carrot, lemon, chocolate and orange. These cakes are produced monthly in different quantities, totaling a monthly production of 7580 cakes. The English pound cake and carrot cake were the flavors selected to carry out the LCA.

Data necessary for calculating the environmental impact associated with the production and distribution of the cakes were collected through direct consultation with the company owner: ingredients, consumption of electricity, water, butane for cooking, packaging (Styrofoam dish and plastic film) and transportation fuel (distribution). All inputs and outputs of the system were identified and quantified, considering the energy and materials needed for the production and delivery of the cakes to the resellers. The monthly amount of cakes produced in each of

the two flavors was considered in the analysis: 468 English pound cakes and 196 carrot cakes. The functional unit considered herein was the emission of CO_2-eq per nutritional unit of cake (kcal).

The recipes of the cakes provided the ingredients per batch and the monthly quantity. For butane, the number of cylinders consumed monthly was reported, and once its calorific value was known it was possible to calculate the amount of MJ consumed per month. The monthly consumption of water and electricity was obtained from the corresponding invoices, in m^3 and kWh, respectively. In the case of transportation, for the distribution of cakes, the volume of gasoline consumed per week was reported, which enabled calculation of the average monthly mileage. Packaging included the Styrofoam plate and the plastic film (cling wrap). Electricity, water, butane and transportation figures were allocated equally to all cakes produced. These monthly values were introduced in SimaPro, and are depicted in Table 1.

TABLE I. INGREDIENTS AND PROCESSES ASSOCIATED WITH THE MONTHLY PRODUCTION OF CAKES

Monthly Ingredients	**English pound cakes (468 cakes)**	**Carrot cakes (196 cakes)**
Eggs	1040 eggs	196 eggs
Wheat flour	104 kg	29.4 kg
Sugar	78 kg	29.4 kg
Sunflower oil	-	15.72 kg
Margarine	78 kg	-
Carrot	-	31.36 kg
Milk	53.44 kg	-
Monthly processes		
Electricity	53.82 kWh	22.54 kWh
Butane	294.93 MJ	123.52 MJ
Packaging	0.936 kg Styrofoam, 0.585 kg plastic film	0.392 kg Styrofoam, 0.245 kg plastic film
Transportation	110.59 km	46.31 km
Water	1852.25 kg	775.73 kg
Nutritional value per cake (unit)	1121.4 kcal	1071.0 kcal

All processes utilized were available in the Ecoinvent [13] and Agri-footprint [14] databases, with the exception of margarine. The process for butter was adapted to result in a representative process equivalent to margarine, which included vegetable oil, sodium chloride and milk.

III. RESULTS AND DISCUSSION

With the inventory data described in Table 1, the environmental impact in terms of kg CO_2-eq was calculated. Table 2 presents data for the emissions involved in the productive and distributive processes associated with English pound cakes and carrot cakes.

Eggs are responsible for the greatest share of the carbon footprint, followed by the sugar. As aforementioned, the monthly consumptions of water, butane, electricity, packaging and transportation was allocated equally to the entire production of cakes. So the difference in the emissions associated with the different flavors was fundamentally due to the ingredients and their amounts.

TABLE II. CARBON FOOTPRINT ASSOCIATED WITH THE MANUFACTURE OF ENGLISH POUND CARROT CAKES

Carbon Footprint (kg CO_2-eq)		
Ingredients	***English Pound Cake***	***Carrot Cake***
Eggs	0.660	0.300
Wheat flour	0.080	0.060
Sugar	0.240	0.210
Sunflower Oil	-	0.120
Margarine	0.220	-
Carrot	-	0.070
Milk	0.180	-
Processes		
Eletricity	0.030	0.030
Butane	0.020	0.020
Packing	0.010	0.010
Transport	0.080	0.080
Water	0.003	0.003
TOTAL (kg CO_2-eq/unit)	1.523	0.903
TOTAL (kg CO_2-eq/kcal)	$1.42 \cdot 10^{-3}$	$0.81 \cdot 10^{-3}$

The overarching aim of this study is to encourage environmental labeling for food, but this has proved difficult since the definition of the functional unit is essential. In the specific case of cakes, two functions have been identified: nutrition and pleasure. For the latter, further research is required to identify the best way to express the environmental impact. For the nutritional case, the carbon footprint is provided in terms of nutritional value (kg CO_2-eq/kcal). Providing the environmental impact per unit of cake can provide the wrong impression that a carrot cake is directly comparable to an English pound cake (in which case labeling could influence the purchase option).

Herein the nutritional aspect of cakes was considered as the functional unit. The LCA of food products should include nutritional aspects in the analysis of products, as this can provide more details on the sustainability of food production and its use, for consumers and decision makers in general [17]. The nutritional dimension may be included in LCA in different functional unit types, *e.g.*, by combining protein content with amount, or even using Nutrient Density to Climate Impact (NDCI) [17]. The NDCI index is not the functional unit of the LCA but estimates the nutrient density of the component in relation to the climatic impact of a product. According to [17], there are several challenges along the way to try to include nutritional aspects in LCA, as nutritionists have already formulated several generic models to calculate and compare the nutritional composition of different food products for educational purposes. From a LCA point of view, all these functional unit definitions deserve more advanced studies.

After detailed and exhaustive bibliographical review, similar works for comparison were not found in the scientific literature. The keywords used were "life cycle assessment + cakes", then changing the product to muffins, cupcakes and cookies. Other initiatives, however, are already beginning to apply LCA in food products, such as potato chips [18], bread [19], muffins (for educational purposes only) [20], ice cream [21], chocolate [22], and sweets, snacks and soft drinks [23].

LCA has already helped several companies increase their knowledge of the production process [24]: The milk company Svensk Mjölk was able to concentrate its environmental research where it generated its greatest benefit; the Lantmännen Unibake Bakery now produces its hamburger bread in a much more environmentally friendly way; and the Swedish Potato Control Agency now has knowledge on the minimization of potato residues.

Finally, it is important to emphasize that the calculations presented herein are estimates, since a regional database is not available to develop LCA studies. The Ecoinvent database, however, already has several Brazilian processes, in an effort to internationalize its database and improve the accuracy of the developed LCAs. For this work, a detailed investigation of each process was performed, and processes were selected with a good representativeness of the technologies employed, to obtain coherent results for the cakes. The adaptation of databases is a resource that, if correctly applied with consistency, can help in obtaining representative results, as was the case with [25], which adapted the production process of lime (originally based on fossil fuels) for wood chip operation. One approach that can be explored in future work, based on the existence of Brazilian energy databases, is the estimation of the environmental impact associated with the energy processes involved in the production of cakes, and to develop sensitivity analyses for the incorporation of renewable energy in the supply of energy (following the suggestion of [26-29]). According to [30], the point at which the higher carbon footprint of some nutrient-dense foods is offset by their higher nutritional value is a priority area for additional research.

This work is part of a broader project aimed at establishing a relationship between the quantification-reduction-promotion (QRD) of the level of pollutants, emitted by companies, and society and governments [8], which can be translated as promoting sustainability by quantifying and reducing the carbon footprint, generating new practices for organizations [6]. The direction of Brazilian environmental policies seek to encourage sustainable development in several productive sectors, especially those with greater environmental impacts, such as agribusiness and electric power generation [8]. Therefore, companies with a greater focus on sustainable development, with practical application of the QRD relationship, in processes and products, generate greater competitive advantage within the market, providing better economic results for the organization [6].

IV. FINAL COMMENTS

In this work the Life Cycle Assessment methodology was used to estimate the carbon footprint associated with the production of two cake flavors: English pound cake and carrot cake.

The impact of the English pound cake was higher (1.42×10^{-3} kg CO_2-eq/kcal) than the carbon footprint of the carrot cake (0.81×10^{-3} kg CO_2-eq/kcal). In both flavors, eggs were responsible for the greater share of emissions.

Further research is suggested on the development of sensitivity analyses for the

substitution of ingredients: for example, eggs could be replaced by another product that is capable of performing the same nutritional or structural function. Considerations on the environmental impacts of food must be associated with nutrient density and health.

ACKNOWLEDGMENT

The authors are grateful for the support of the National Council for Scientific and Technological Development (Productivity Grant 303199/2015-6) and the UFPB Development Institute of Paraíba - IDEP / UFPB.

REFERENCES

[1] Brazilian Association of Cookie, Pasta, and Industrialized Bread & Cake Industries. (2018). Statistics on Bread and Cakes. Available at: http://www.abimapi.com.br/estatistica-paes-bolos.php

[2] Brazilian Association of the Bakery and Confectionery Industry. (2018). Indicators and market trends 2018. Available at: http://www.abip.org.br/site/wp-content/uploads/2018/03/INDICADORES-E-TENDENCIAS-DE-MERCADO.pdf.

[3] S. Rousseau, and L. Vranken, "Green Market expansion by reducing information asymmetries: Evidence for labeled organic food products," Food Policy, vol. 40, no. 1, 2013, pp. 31-43.

[4] C. Baldwin, N. Wilberforce, and K. Amit, "Restaurant and food service life cycle assessment and development of a sustainability standard," The International Journal of Life Cycle Assessment, vol. 16, no. 1, 2011, pp. 40-49.

[5] P. H. Howard, and P. Allen, "Beyond organic and fair trade?" Analysis of ecolabel preferences in the United States, Rural Sociology, vol. 75, no. 2, 2010, pp. 244-269.

[6] R. S. Freire, M. Carvalho, C. U. M. Carmona, A. M. V. G. Brito, "Perspectives on the Implementation of Climate Change Public Policies in Brazil in Energy," Transportation and Global Warming, Springer, Cham, 2016, pp. 13-20.

[7] R. Vázquez- Rowe, P. Villanueva- Rey, M. T. Moreira, G. Feijoo, "Opportunities and challenges of implementing life cycle assessment in seafood certification: a case study for Spain," The International Journal of Life Cycle Assessment, vol. 21, no. 4, 2016, pp. 451-464.

[8] R.S. Freire, M. Carvalho, A. M. V. G. Brito, "Promotion of sustainability by quantifying and reducing the carbon footprint: new practices for organizations," In: Grammelis, P. (Ed.). Energy, Transportation and Global Warming. Springer International Publishing, Switzerland, 2016.

[9] ISO 14040. Environmental management - Life cycle assessment - Principles and framework. International Organization for Standardization (ISO), Geneva, 2006.

[10] ISO 14044. Environmental management - Life cycle assessment - Requirements and guidelines. International Organization for Standardization (ISO), Geneva, 2006.

[11] J. B. Guinée, Handbook on life cycle assessment: operational guide to the ISO standards, Kluwer Academic Publishers, Boston, 2002.

[12] SimaPro software. PréConsultants. Available at: https://simapro.com/

[13] Ecoinvent Centre (2016). The Ecoinvent Database. Available at: http://www.ecoinvent.org/database/database.html

[14] Agri-Footprint. (2016). Products included in Agri-footprint. Available at: http://www.agri-footprint.com/assets/List%20of%20products%20in%20Agri-footprint%202.pdf.

[15] International Panel On Climate Change – Ipcc. (2014). Climate Changes 2014: Synthesis report – Summary for policy makers. Genebra: Secretariat of the WMO.

[16] IPCC. (2013). Revised supplementary methods and good practice guidance arising from the kyoto protocol. Available at: <http://www.ipcc-nggip.iges.or.jp/public/kpsg/>.

[17] M. Saarinen, S. Kurppa, Y. Virtanen, K. Usva, J. Mäkelä, and A. Nissinen, "Life cycle assessment approach to the impact of home-made, ready-to-eat school lunches on climate and eutrophication," Journal of Cleaner Production, vol. 28, 2012, pp. 177-186.

[18] M. Carvalho, M. M. D. S. Grilo, and R. Abrahao, "Comparison of greenhouse gas emissions relative to two frying processes for homemade potato chips," Environmental Progress & Sustainable Energy, vol. 37, no. 1, 2018, pp. 481-487.

[19] Espinoza-Orias, N., Stichnothe, A. A. "The carbon footprint of bread," The International Journal of Life Cycle Assessment, vol. 16, no. 4, 2011, pp. 351-365.

[20] College of Engineering and Applied Science. University of Colorado Boulder. Hands-on Activity: Mmm Cupcakes: What's Their Life Cycle Impact? Available at: https://www.teachengineering.org/activities/view/ucd-1371-cupcakes-product-life-cycle-assessment-impact

[21] Ben & Jerry's. (2016). A life cycle analysis study of some of our flavors. Available at: https://www.benjerry.com/values/issues-we-care-about/climate-justice/life-cycle-analysis

[22] N. Jungbluth, and A. König, Life Cycle Assessment of Swiss Chocolate. SETAC Europe 24th, 2014.

[23] K. Nilsson, V. Sund, B. Florén, "The environmental impact of the consumption of sweets, crisps and soft drinks," TemaNord 2011:509. © Nordic Council of Ministers, Copenhagen, ISBN 978-92-893-2197-6, 2011.

[24] SP Technical Research Institute Of Sweden. (2016). Life cycle assessment of food products. Available at https://www.sp.se/en/index/services/life-cycle/Sidor/default.aspx.

[25] T. I. Neves, C. A. Uyeda, M. Carvalho, and R. Abrahão, "Environmental evaluation of the life cycle of elephant grass fertilization—Cenchrus purpureus (Schumach.) Morrone—using chemical fertilization and biosolids," Environmental monitoring and assessment, vol. 190, no. 1, 2018, pp. 30.

[26] M. M. S. Grilo, A. F. C. Fortes, R. P. G. Souza, J. A. M. Silva, and M. Carvalho, “Carbon footprints for the supply of electricity to a heat pump: Solar energy vs. electric grid,” Journal of Renewable and Sustainable Energy, vol. 10, no. 2, 2018, 023701.

[27] Y. R. V. Araújo, M. L. Góis, L. M. Coelho Junior, and M. Carvalho, “Carbon footprint associated with four disposal scenarios for urban pruning waste,” Environmental Science and Pollution Research, vol. 25, no. 2, 2018, pp. 1863-1868.

[28] M. Carvalho, and R. Abrahao, “Environmental and Economic Perspectives in the Analysis of Two Options for Hand Drying At an University Campus,” International Journal of Emerging Research in Management and Technology, vol. 6, 2017, pp. 24-35.

[29] M. Carvalho, and D. Delgado, “Potential of photovoltaic solar energy to reduce the carbon footprint of the Brazilian electricity matrix,” LALCA-Revista Latino Americana em Avaliação do Ciclo de Vida, vol. 1, no. 1, 2017, pp. 64-85.

[30] A. Drewnowski, C. D. Rehm, A. Martin, E. O. Verger, M. Voinnesson, and P. Imbert, “Energy and nutrient density of foods in relation to their carbon footprint,“ The American journal of clinical nutrition, vol. 101, no. 1, 2014, 184-191.

Performance Improvement of AC Adjustable Speed Drives During Voltage Sag Events

Milutin Petronijević[1], Nebojša Mitrović[1], Filip Filipović[1], Bojan Banković[1],Vojkan Kostić[1]

[1]Faculty of Electronic Engineering, University of Niš, Serbia,
milutin.petronijevic@elfak.ni.ac.rs, nebojsa.mitrovic@elfak.ni.ac.rs,
filip.filipovic@elfak.ni.ac.rs, bojan.bankovic@elfak.ni.ac.rs, vojkan.kostic@elfak.ni.ac.rs

Abstract — **This paper analyses voltage sag effects on adjustable speed drives (ASDs) performance reduction with vector controlled induction motors (IMs). The ability of ASDs to maintain desired speed and/or torque responses during voltage reduction is of partial importance for some industrial ASDs. Improvement of motor control software is superior solution in relation to hardware modifications, primarily from the aspect of price, and also in terms of simple upgrade of existing electrical drives. Flux weakening with appropriate drive selection is efficient solution to overcome the most common voltage sag events. In this paper, theoretical explanation is supported with experimental tests of industrial and laboratory drives.**

Keywords - voltage sag, variable speed drives, vector control, direct torque control, flux weakening

I. INTRODUCTION

The use of sophisticated devices in industrial control applications with high accuracy requirements has been set as one of the priorities in the provision of reliable power supply within the prescribed limits. These devices are equipped with power electronic converters in very wide power range and employed as controlled power sources for actuators. Input power converters behave as highly non-linear consumers and contribute to deterioration of supply network power quality. New possibilities for correcting of non-linear equipment characteristics and reducing their sensitivity to power problems are available with hardware and software enhancements.

It is well-known [1] that voltage sags are the most common power quality event in networks interfaced to the end customers. The harmonized classification [1-4] introduce two basic parameters of the presumed rectangular shape voltage sag: the remaining root mean square (RMS) voltage h in range from 0.1 to 0.9 p.u. and the time duration Δt is assumed in the range of a half-period of the mains voltage up to 60 seconds. For now, there is no full agreement between researchers and professional associations regarding the classification problem of the voltage sag that respects the poly-phase nature of the event, residual RMS voltage shape, influence of the phase shift and the point on wave when the sag occurs, and other characteristics of the sag itself.

In the field of high-performance electric drives, especially in applications with tracking accuracy requirements for position, speed or torque regulation, numerous problems were detected [5], [6] caused by the deviation of the continuous, sinusoidal supply voltage. There is number of evidences [7], for these problems in different industrial users including: process industry, semiconductor plants, textile industry, petrochemical production, where the problems in these electric drives have led to high-cost downtime.

ISBN: 978-86-80616-03-2

Solutions based on additional devices for supply voltage conditioning or hardware modifications of industrial devices are unacceptable for most users due to price reasons. Consequently, there are particularly interesting improvements that use software modifications, which slightly increase the investment costs [6], and they are also suitable for upgrading existing ASDs. In this paper the possibilities for improving the response of ASDs with vector control algorithm in case of the temporary voltage degradation are firstly analysed theoretically. Then, experimental investigation of the proposed control algorithm enhancements is presented with comprehensive tests of modified industrial drives.

The rest of the paper is organized as follows. A brief description of the vector controlled IM ASDs voltage sags sensitivity, along with the illustrations of the expected problems are given in Section II. Section III explores the causes of the observed torque reduction and the drop in speed, while the Section IV describes new, software based solutions to overcome these problems in high performance vector controlled ASDs. Some experimental results that illustrate voltage performance degradation and proposed improvements are given in Section V. The paper ends with conclusions and the list of the used literature.

II. SENSITIVITY OF VECTOR CONTROLLED ASDS

Common classification of ASDs with alternate current (AC) motors implies two main groups according to the applied control algorithm. The first group, called scalar or V/Hz control suppose control of only output voltage frequency and magnitude The second group is named as vector control and it enables control of motor instantaneous voltage, current and flux vectors in different reference frames connected to appropriate motor variables vectors. This provides more precise control of motor speed or torque in steady state and especially in transient regimes. The two most significant groups of industrial vector controlled ASDs are field oriented control (FOC, with a featured group that uses orientation along the rotor field - RFO) and the second one - direct torque control (DTC). This division can be applied in drives with induction motors and with permanent magnet synchronous motors (PMSMs).

The IEC standards [2-3] and CIGRE/CIRED/UIE joint working group recommendation [4] for equipment immunity testing for three-phase devices proposes standardized voltages: unbalanced sags with phase shift (designated as type I and II) and balanced (type III) voltage sags. The vector diagrams of these typical test voltages are shown in Fig. 1, where it is important to note that these regulations consider the importance of testing the phase jump effect on the equipment under test (EUT).

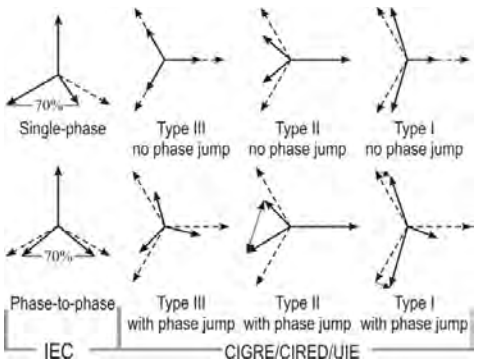

Figure 1. Basic sag types for three-phase EUT performance evaluation.

Disturbances caused by voltage sags in the case of a passive diode bridge lead to a reduction of the mean DC voltage and/or increase of DC voltage ripple [6]. They depend on the sag type and depth. It is clear that Type III sags certainly cause a decrease in DC voltage v_{dc}, while in the case of the other two types, combinations of voltage reduction and DC ripple are possible. Generally, this voltage can be expressed as:

$$V_{dc}(t) = V_{dc} + \sum_{h=1}^{\infty} V_h \sin(w_h t + \theta_h) \qquad (1)$$

where V_{dc} represents the mean value of DC voltage, V_h denotes amplitude of higher harmonic components (order h) with the angular frequency ω_h and the relevant phase displacement θ_h. Voltage sag disturbances in the case of a input diode bridge lead to the reduction of V_{dc} and/or the appearance of a voltage harmonic, where the 2nd and 4th orders are dominant in relation to the basic frequency ω_i. DC-link voltage is converted to the motor terminals three-phase voltages by means of Pulse Width Modulation (PWM). With the well-known transformation, these motor voltages can

be expressed in the two-phase, synchronous speed ω_e rotating reference frame through the corresponding quadrature voltages:

$$u_{ds}(t) = \frac{1}{2} m\left[V_{dc}\cos\varphi + V_{dc2}\cos(2w_i t + \theta_2)\cos\varphi\right]$$
$$u_{qs}(t) = \frac{1}{2} m\left[V_{dc}\sin\varphi + V_{dc2}\cos(2w_i t + \theta_2)\sin\varphi\right] \quad (2)$$

In the previous formula, the influence of the PWM control is valued through the modulation index m and the speed ω_e used for dq-coordinate system transformation with arbitrary chosen initial angle φ. For analysis simplicity, 4-th order harmonic is neglected in v_{dc}. The angle θ_2 represents the time instant (point on input voltage wave) of sag initiation and existence of phase jump in terminal voltages.

The results of the DC voltage deviation from the nominal one are the change of the stator currents waveform, reduction of the available motor torque, torque ripple, vibration and the speed deviation from the set point. Figs. 2-4 show experimentally recorded tolerance curves for type III voltage sag for RFO controlled industrial frequency converters applied in an identical ASD with an 1.5kW IM. In these experiments with ASDs, the reference speed is set to a nominal one, while the load is constant and rated. Based on catalogue data, the boundaries for warning and fault limits are drawn in these figures. It is noted that all tested devices are insensitive to voltage sags with residual voltages equal to or greater than 80% of the nominal one. Considering only these characteristics, it could be concluded that we should not expect any problems with the voltage sags above this limit. However, recorded speed diagrams during testing indicate that there are potential problems with ASDs speed reduction. The bottom diagrams in the above mentioned figures show that the drop in speed exists and has a different value during this supply disturbance. There are significant differences in speed reduction - the highest speed reduction is obtained in ASDs with RFOC2 ([14]) converter, while the least speed reduction is in case of RFOC1 ([13]) converter. In addition to the usually considered voltage sag immunity, drop in speed during these power quality events may be with crucial importance for the industrial users. In further consideration, this phenomenon will be analysed and explained with more details.

The experiments were repeated for the same IM, but now with an industrial frequency converter that uses DTC algorithm. The results obtained for sensitivity curve in case of voltage sag type III are shown in Fig. 5. In the same figure, the speed responses for two characteristics events, marked as b) and c), are shown. There is no drop in speed for sag marked with c) with $h = 0.8$, while the occurrence of temporary speed reduction for b) sag with $h = 0.76$ can be observed.

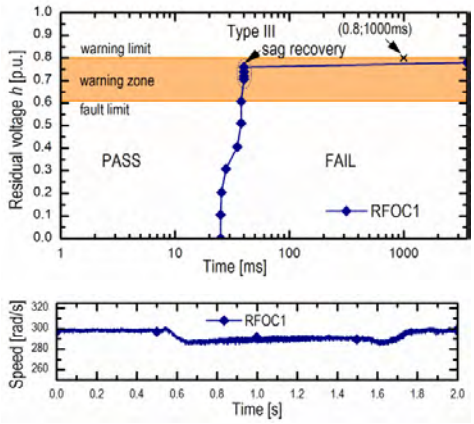

Figure 2. Voltage tolerance curves for industrial 1.5kW ASDs (marked as RFOC1 [13]) for voltage sag type III (top); Speed response under voltage sag with $h = 0.8$ and $\Delta t = 1000$ ms (bottom)

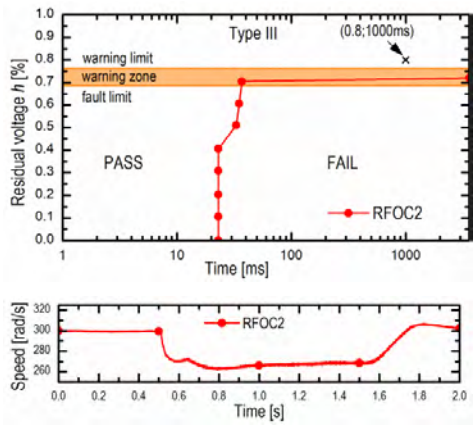

Figure 3. Voltage tolerance curves for industrial 1.5kW ASDs (marked as RFOC2 [14]) for voltage sag type III (top); Speed response under voltage sag with h=0.8 and Δt=1000 ms (bottom)

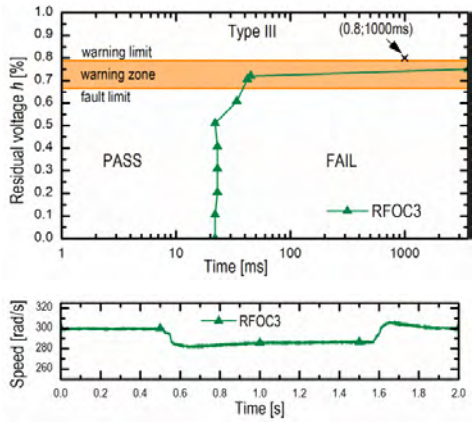

Figure 4. Voltage tolerance curves for industrial 1.5kW ASDs (marked as RFOC3 [15]) for voltage sag type III (top); Speed response under voltage sag with h=0.8 and Δt=1000 ms (bottom)

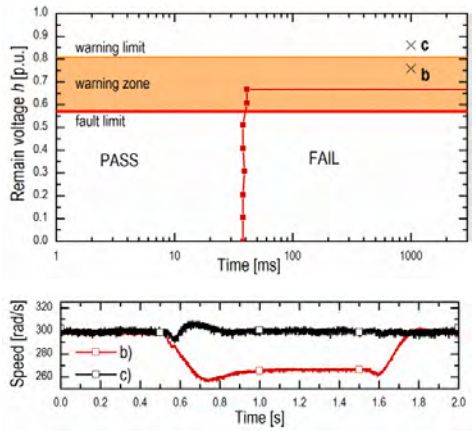

Figure 5. Voltage tolerance curves for industrial 1.5kW DTC drive ([16]) for voltage sag type III (top); Speed response under voltage sag with h=0.75 and h=0.86 and Δt=1000 ms (bottom)

III. ASDs Drop in Speed and Torque Reduction

The experimental results from the previous section illustrate the expected problems in ASDs malfunction and/or uncontrolled degradation of the performances. It has already been mentioned that an ideal solution would be to install a voltage corrector, but in most cases the price would be quite high. Research which propose software modifications on existing or newly installed devices are particularly interesting, as they can contribute to reducing voltage sag sensitivity with insignificant investment.

A well-known solution is the use of flywheel energy (energy of rotary masses) to preserve the DC link voltage, whereby a temporary speed reduction occurs depending on the type of load and its inertia. This method, known as kinetic buffering, is an integral part of the control software in most modern industrial inverters. It is also possible to improve the standard kinetic buffering algorithm by introducing enhancements for minimizing mechanical and electrical losses in drive, which further extends the time duration of the ride-trough by about 30% [17]. However, kinetic buffering also results in an uncontrolled speed reduction because the primary requirement is to maintain DC voltage, at the cost of the speed reduction.

It is well known [4] that the most common PQ events of significance for end users are just (exactly) single-phase voltage sags. In addition, a statistical analysis of numerous measured data shows that their duration is generally in the range of $\Delta t = 1\,\mathrm{s}$, with the residual voltage value $h \geq 0.7\,\mathrm{p.u.}$ Therefore, from the aspect of price optimization, it may be considered that the algorithms that compensate the previously mentioned effects of the most probable sags are of particular importance in applications with vector-controlled ASDs.

Figures 2-5 show the test results for commercially available devices that exhibit performance violation with symmetrical voltage sag events that do not initiate the ASDs trip. The analysis conducted in [6] and [10] shows that in this case, the main point of interest is to observe the influence of the voltage limitation on the maximum available motor torque. Due to the completeness of the paper, only the excerpts from the above analysis will be given here. For details, see [6] and [10] and the references therein.

Introducing the well-known principle of amplitudes equality between three-phase and transformed two-phase (dq) quantities, we can write the inequality for the voltage limit:

$$u_{qs}^2 + u_{ds}^2 \leq V_{\max}^2 \qquad (3)$$

where V_{max} is the amplitude of available stator voltage at the motor terminals. For a symmetrical squirrel cage IM, mathematical model describing voltage balance equations in dq coordinate system can be written in the form:

$$u_{ds} = R_s i_{ds} + \sigma L_s \frac{di_{ds}}{dt} + \frac{M}{L_r}\frac{d\psi_{dr}}{dt} - \omega_e(\sigma L_s i_{qs} + \frac{M}{L_r} d\psi_{qr})$$
$$u_{qs} = R_s i_{qs} + \sigma L_s \frac{di_{qs}}{dt} + \frac{M}{L_r}\frac{d\psi_{qr}}{dt} + \omega_e(\sigma L_s i_{ds} + \frac{M}{L_r}\psi_{dr}) \quad (4)$$

where the descriptions and numerical values of parameters are given in [6]. In order to simplify voltage sag influence analysis, the two-phase coordinate system is introduced with *d*- axis aligned with the rotor flux vector, i.e. $\psi_{dr} = \psi_r$, and respectively $\psi_{qr} = 0$. If RFO control method is applied, then the rotor flux is kept at constant value in base speed region. In steady-state regimes, derivative $d\psi_{dr}/dt = 0$, which additionally simplifies the voltage limit equation to the form:

$$(R_s^2 + \omega_e^2 L_s^2) i_{ds}^2 + (R_s^2 + \omega_e^2 \sigma L_s^2) i_{qs}^2 + 2R_s \omega_e \frac{L_m^2}{L_r} i_{ds} i_{qs} \le V_{\max'}^2 \quad (5)$$

Because of the introduced *dq* coordinate system orientation, the motor torque can be calculated in a simplified form:

$$T_e = \frac{3}{2} P_p \frac{M^2}{L_r} i_{ds} i_{qs}. \quad (6)$$

For the considered IM model in steady-state, the value of the maximum available electromagnetic torque at the voltage limit can be obtained from (5) and (6) as a function of the motor speed, for the given rotor flux.

A similar analysis is possible for IM drive if DTC algorithm is applied, where the flux controller keeps stator flux amplitude ψ_s at constant reference value designated as ψ_s^*. The previous equations can be used completely in unchanged form if we introduce the stator equivalent current for constant stator flux maintenance:

$$i_{ds} = \sqrt{\left(\psi_s^*\right)^2 - \sigma^2 \cdot L_s^2 \cdot i_{qs}^2} \,/\, L_s. \quad (7)$$

It should be noted that the presented analysis can be considered as general and equations (5) and (6) will be used for analysis of the vector-controlled drives operation in the case of limitations due to the voltage limit.

Beside the voltage limit, the IM current is limited with the maximum value of the inverter output current. This limitation is declared with respect to the nominal value as the temporarily available increase within the limits of 150% to 300%, for a few seconds to a few minutes (for details see [13] - [15]). Similar to (3), this current limit can be written in the form:

$$i_{qs}^2 + i_{ds}^2 \le I_{\max'}^2 \quad (8)$$

where $I_{\max}$ is the amplitude of the maximum allowed output current. Combining the equations (8) and (6) for RFO control and (6), (7) and (8) for DTC control, appropriate analytic expressions can be obtained for the maximum available torque in the case of a current limit. Therefore, it should be noted that the values of reference rotor and stator fluxes also affect the maximum available torque under current limit.

The previous analysis allows sketching the speed-torque curves that explain the effects of the current and voltage limit on the drive operation. For given load torque and with the torque T_e reduction under the influence of voltage and/or current limit, the drive speed will decrease until the stationary operating point is established. Figures 6 and 7 show the results of the previous analysis for the example of vector controlled ASDs with 1.5 kW (parameters are given in [6]). The appropriate static speed-torque curves are constructed for rated and reduced stator voltages (remaining voltage with $h = 0.8$). The reference value for rotor flux in RFO controlled IM drive, i.e. the *d*-axis current reference i_{ds}^* was selected to provide a maximum torque per ampere value. A similar principle for selecting the stator flux reference ψ_s^* was applied in ASD with DTC control. These values are denoted in Figs. 6 and 7 and used for numeric calculation of above mentioned speed-torque limits.

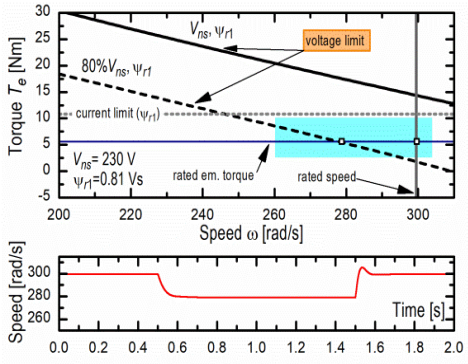

Figure 6. Voltage and current limits under rated and reduced (h=0.8) supply voltage in ASD drive with RFO control

In the same figures, the instantaneous speed traces are plotted for the 1-second voltage sag type III with $h = 0.8$ for RFO drive and with $h = 0.75$ for DTC drive. Values are recorded in the simulation of the complete system in Matlab/Simulink with implemented RFO and DTC algorithms.

IV. Flux Weakening Algorithm

In the previous sections, analytical relations explain the effects of symmetrical voltage sags on RFO and DTC ASDs motor drives. The purpose of the presented analysis is to show that the different control algorithms can change essentially the performance of the IM drive during the voltage limit. Another important aim of the presented research is to find the possibility to modify the observed limitations in order to preserve the declared control characteristics, possibly without hardware modifications of the devices.

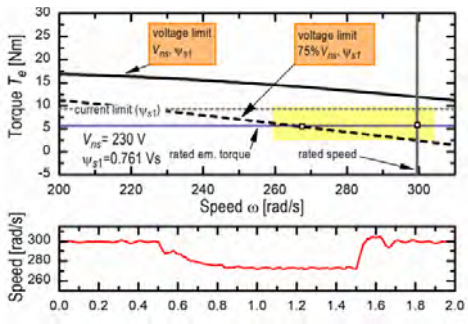

Figure 7. Voltage and current limits under rated and reduced (h=0.75) supply voltage in ASD drive with DTC

In the case of IM vector control, it is possible to adjust the flux values inside the appropriate limits, regardless of the motor load and speed. There is a question about choosing and adjusting the reference values of the rotor and stator fluxes during voltage reduction. Using the same principle for maximizing torque per ampere, for an illustrative example of the voltage sag type III with $h = 0.8$, the corresponding numeric values are calculated and the new speed-torque characteristics are shown in Figs. 8 and 9 for RFO and DTC drives respectively.

The proposed flux weakening algorithm is easy to implement because it only requires voltage measurement in a DC circuit using a voltage sensor that is often common in high performance frequency converters. The practical application of this algorithm is very simple. It is enough to calculate in advance a 2D-table with pairs of the DC-link mean value and the flux reference. Since the voltage sags are a fast phenomenon without previously known reduced-voltage values, it is necessary to

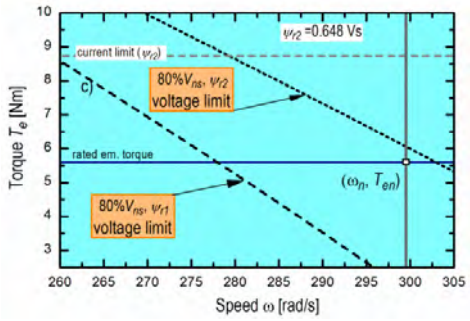

Figure 8. Torque-speed curves of RFO drive with different rotor reference fluxes and under reduced (h=0.8) supply voltage

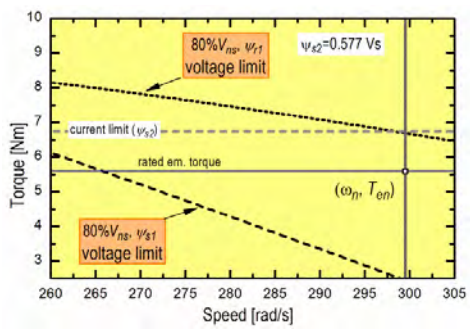

Figure 9. Torque-speed curves of DTC drive with different stator reference fluxes and under reduced (h=0.75) supply voltage

ensure that optimal flux values are reached very quickly. The latest requirement highlights the classical DTC drives (with hysteresis flux and torque controllers) as particularly suited because the response to the flux change command is almost instant (within a switching sequence).

In RFO vector-controlled drives the application of the flux-weakening algorithm is slightly more cumbersome, bearing in mind that the rotor flux changes with the time constant $T_r = L_r/R_r$, whose numerical values are in range from several hundred milliseconds up to several seconds. The limitation of the flux control loop response rate is mainly due to restriction in the converter maximum current, then because of the slave *d*-axis current control loop bandwidth, and finally due to the presence of the noise in the estimated signal of the rotor flux.

V. Experimental Results

The verification of the proposed software modifications was carried out on the ASD laboratory prototype with 1.5kW IM supplied with an industrial converter (RFOC2) used in the experiments described in Section II. Instead of the original factory control software, a custom-made interface card and a rapid prototyping system based on dSpace DS1103 developing board and Matlab/Simulink were used [10]. Constant motor load is emulated with the directly coupled IM operated in torque-control mode.

The first experiment examined the operation of RFO drive under type III voltage sag with $h = 0.8$ i $\Delta t = 1s$. The recorded results are shown in Fig. 10: instantaneous $v_{dc}(t)$ and mean V_{dc} DC voltage; the estimated ψ_r and reference ψ_r^* rotor fluxes; estimated torque T_e and calculated mean torque $T_{e,mean}$ and the reference ω^* and estimated ω motor axis speed. Notable speed reduction appears during sag as expected in accordance with Fig. 6, but it has been slightly increased due to voltage drops on real converter components. After sag ending, the regular control is established and drop in speed disappears. Next Fig. 11 shows the results recorded under the same conditions on RFO drive with flux weakening referring to dc-link voltage. Drop in speed problem is reduced, but the short speed deviation exists due to the slow response of the flux rotor. The last result shows that the drop in speed can be effectively reduced, but additional disturbance

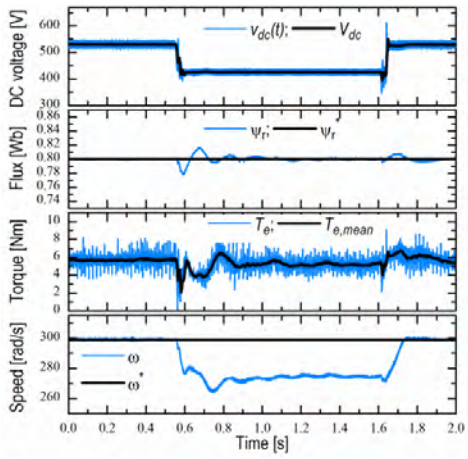

Figure 10. RFO drive response under voltage sag type III with h=0.8 and with constant rotor flux amplitude

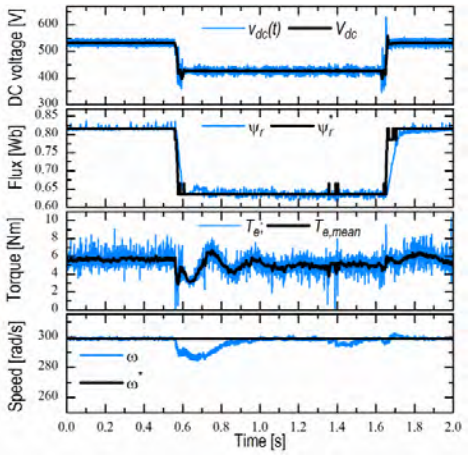

Figure 11. RFO drive response under voltage sag type III with h=0.8 and with rotor flux amplitude adjusted with mean DC voltage

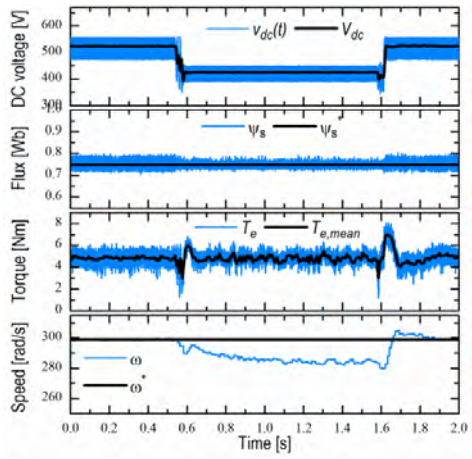

Figure 12. DTC drive response under voltage sag type III with h=0.75 and with constant stator flux amplitude

compensators must be applied in order to improve reduced rotor flux establishing.

Similar experiments are conducted in DTC vector controlled ASD under the same supply disturbance and loading conditions. In Fig. 12, the experimentally obtained results are shown for DC link voltage, estimated ψ_s and constant commanded ψ_s^* stator fluxes, instantaneous and mean torques and motor speed. The effectiveness of the flux weakening algorithm is documented in Fig. 13 for DTC drive with the stator flux adjusted with respect to the mean DC link voltage.

VI. Conclusion

The following conclusions can be made from this research:

1. Software improvements of the control algorithms that introduce flux weakening during voltage supply reduction have great potential in minimizing speed drop through increasing available torque;

2. The proposed modifications are relatively simple for implementation because they do not require intensive mathematical calculations and can be further accelerated by flux references pre-setting for the given motor, simultaneously with the control parameters identification;
3. This can be suitable for upgrade of the existing vector controlled drives because it does not require any hardware;
4. Field weakening is particularly effective in DTC drives and therefore the speed deviation is minimal. Additional improvements are necessary for RFO drives to reduce short-time speed deviation.

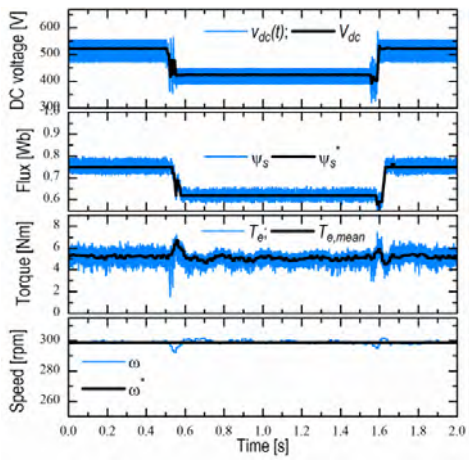

Figure 13. DTC drive response under voltage sag type III with h=0.75 and with proposed algorithm for field weakening

Acknowledgment

This research is partly supported by project grants III44006 and III44004 financed by the Ministry of education, science and technology development of the Republic of Serbia.

References

[1] M. H. Bollen, I. Gu, Signal Processing of Power Quality Disturbances, Wiley-IEEE Press, Hoboken, NJ, USA, 2006.

[2] Electromagnetic compatibility (EMC), Part 4: Testing and measurement techniques, Section 34: Voltage dips, short interruptions and voltage variations immunity tests for equipment with mains current more than 16 A per phase, IEC standard 61000-4-34:2005+A1:2009, International Electro-technical Commission, 2005, 2009.

[3] Electromagnetic compatibility (EMC), Part 4: Testing and measurement techniques, Section 11: Voltage dips, short interruptions and voltage variations immunity tests, IEC Standard 61000-4-11, International Electro-technical Commission, 2004.

[4] Bollen, M. et al., "Voltage dip immunity of equipment and installations," CIGRE/CIRED/UIE Joint Working Group C4.110, pp. 1–279, Apr. 2010.

[5] S. Z. Djokic, K. Stockman, J. V. Milanovic, J. J. M. Desmet, R. Belmans, "Sensitivity of AC adjustable speed drives to voltage sags and short interruptions," IEEE Transaction on Power Delivery, vol. 20, no. 1, 2005, pp. 494-505.

[6] M. Petronijevic, B. Veselic, N. Mitrovic, V. Kostic, B. Jeftenic, "Comparative study of unsymmetrical voltage sag effecs on adjustable speed induction motor drives," IET Electric Power Applications, vol. 5, no. 5, 2011, pp. 432-442.

[7] P. Heine, P. Pohjanheimo, M. Lehtonen and E. Lakervi, "A method for estimating the frequency and cost of voltage sags," IEEE Transactions on Power Systems, vol. 17, no. 2, May 2002, pp. 290-296.

[8] S. Arias-Guzman et all, "Analysis of Voltage Sag Severity Case Study in an Industrial Circuit," IEEE Transaction on Industry Applications, vol. 53, no. 1, 2017, pp. 15-21.

[9] O. Polat, M. S. Sezgin, K. Yumak, O. Gul and R. Unal, "Assessment of voltage sag events based on measurement studies in an industrial facility,"18th Int. Conf. on Harmonics and Quality of Power (ICHQP), Ljubljana, Slovenia, May 13-16, 2018, pp. 1-6.

[10] M. Petronijević, N. Mitrović, V. Kostić, B. Banković, "An Improved Scheme for Voltage Sag Override in Direct Torque Controlled Induction Motor Drives," Energies, vol. 10, no. 5, 2017, pp. 663.

[11] M. Petronijević, B. Veselić, N. Mitrović, V. Kostić, "Voltage sag sensitivity of industrial vector controlled induction motor drives – a comparative study," Facta Universitatis, Series: Automatic Control and Robotics, vol. 16, no. 2, 2017, pp. 167-183.

[12] T. Wymann, P. Jörg, "Power loss ride-through in a variable speed drive system," in *Proceedings of Petroleum and Chemical Industry Conference Europe PCIC 2014*, Amsterdam, Holland, 2014, pp. 1-9

[13] Siemens, "Sinamics S120 function manual drive functions," User`s manual, 07/2016. Available: https://support.industry.siemens.com

[14] Danfoss, "Programming Guide VLT AutomationDrive FC301/302," User`s manual, 2017. Available: http://drives.danfoss.com

[15] Schneider Electric, "Altivar 71 Variable speed drives for asynchronous motors," User`s manual, 2006. Available: http://www2.schneider-electric.com

[16] ABB, "ACS880 primary control program," Firmware manual, 2018. Available: https://new.abb.com/drives

[17] J. Titus, J. Teja, K. Hatua, K. Vasudevan, "An Improved Scheme for Extended Power Loss Ride-Through in a Voltage-Source-Inverter-Fed Vector-Controlled Induction Motor Drive Using a Loss Minimization Technique," IEEE Trans. Ind. Appl., vol. 52, no. 2, 2016, pp. 1500-1508.

[18] www.igrid.com/igrid (2018). i-Grid: Home. [online] Available at: https://www.igrid.com/igrid/ [Accessed 25 Sept. 2018].

The Influence of Nonlinear Background on the Quality of Electricity

Enver Agić[1], Damir Šljivac[2], Bakir Agić[3]

[1]Court expert electrical engineers, UI. A RBiH 19/IV/15, Tuzla, Bosnia and Hertzegovina, agabiem@bih.net.ba
[2]Electrical Faculty, The University J.J.Strossmayer of Osijek, Osijek, Croatia, damir.sljivac@etfos.hr
[3]Faculty of Electrical Engineering, The University of Tuzla, Tuzla, Bosnia and Hertzegovina, bakir.agicc@gmail.com

Abstract— **This paper discusses the load in the power distribution network, three-phase of the power supply where the transformer coupling via Y_gY_g powered nonlinear load for a set of personal computers. The load is balanced at each stage. The aim is partly to show through the analysis of higher harmonic loads of personal computers, coupling transformer Y_gY_g. The tool will be used software tool MATLAB.**

Keywords - higher harmonic, load, coupling transformer

I. INTRODUCTION

The interest in analyzing the quality of electricity has recently been steadily increasing because:

- Electrical and electronic equipment are becoming more susceptible to voltage disturbances,
- Electrical and electronic equipment are increasingly generating voltage disruptions,
- The quality of electricity is of particular importance in the conditions of the deregulated market and,
- With the development of modern measuring devices, today the quality of electricity can only be measured and memorized.

The two main categories of problems in the analysis of quality of electricity are [1]:

a) *Disorders:*
-Transits,
-Decay and increase voltage,
-Power supply interruptions,

b) *Stationary variations:*
-Voltage regulation,
-Harmonic distortion,
-Voltage flickers.

II. MODEL OF SOLVING PROBLEMS OF HIGHER HARMONICS

The paper is taken as an example in Fig. 1, where a three-phase part of the electrical network is presented, whereby the YgYg transformer connects the non-linear circuits of a set of personal computers (PCs) through the transformer. The load is balanced at each stage.

MATLAB software package is used for realization of the program. MATLAB/Simulink/Power System Blockset (PSB) is a software package for modeling, simulation and analysis of electrical energy systems within the known tool MATLAB. The package supports linear and nonlinear systems modeled in continuous time or discrete time moments, or in both ways. PSB contains a comprehensive block bibliotype of sources,

ISBN: 978-86-80616-03-2

linear and non-linear elements, connectors and accompanying block subsystems.

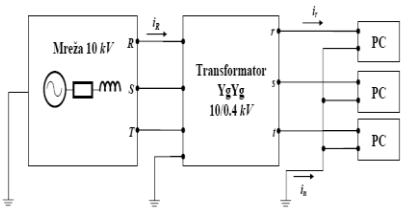

Figure 1. The analyzed part of the network

In Fig. 2, the equivalent nonlinear load model for each phase is reset.

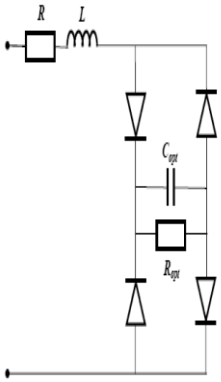

Figure 2. An equivalent non-linear load model (PC)

The model parameters are:

Network:

Voltage level: U_n = 10 kV (line voltage)

Phase angle of the first phase: = 0

Network parameters: R_s = 2.5Ohm; L_s = 0.05H

Transformer (linear model):

Nominal power: S_n = 50kVA

Transformer Transformer Ratio: 10/0.4kV

Working resistance and primary and secondary winding reactance:

$R_p = R_s = 0.0025\ p.u$;

$X_p = X_s = 0.06\ p.u.$

Magnetization branch parameters are:

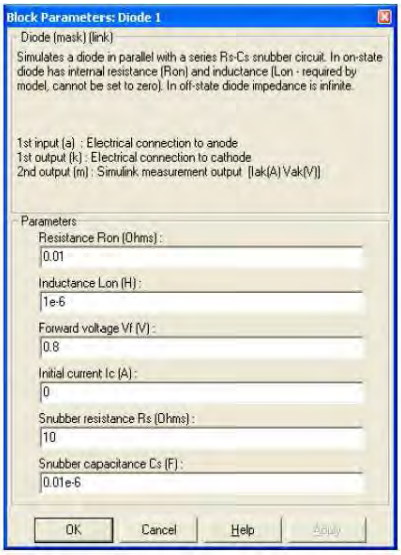

Figure 3. Internal diodes parameters

$R_m = 500\ p.u.$; $X_m = 500\ p.u.$

Nonlinear Load Parameters (PC):

R = 0.5Ohm; L = 0.004H

The work is:

1. Theoretically briefly explains the cause of the formation of higher harmonic components in the electric power network, their consequences on consumers and the ways of their elimination. The role of the transformer in the DY_g compound is explained. A concrete example is given.

2. For the part of the electrical network from Fig. 1, a waveform of phase R at 10kV voltage level will be determined, the current of the neutral conductor phase at 0.4kV voltage level, as shown in Fig. 1. The harmonic content will be determined up to 15 accordion and the effective value of all these currents (phases R and r). The % THD for current R and r will be calculated.

3. The three-phase filter set to eliminate the maximum harmonic component current phase R at the 10kV side of the transformer will be dimensioned. The waveform and the corresponding harmonic content of phase R phase will be determined. In this case, the THD% will be calculated for the phase R phase.

4. Additional measures will be proposed to reduce the THD% of current phase *R*. It will be realized another parallel filter for elimination of the second by size of the harmonic component of phase *R* phase. Comparison of THD% for the phase *R* phase will be made in cases under 3 and 4.

5. For the total duration of the simulation, the time taken $T_{stop} = 0.1s$.

6. The mentioned simulations will be realized with the MATLAB / PSB type program package. The corresponding simulation models will be displayed.

III. The Causes of the Formation of Higher Harmonics

More harmonics in the network are caused by the generation of non-linear consumers in the electric power network, which inject the more harmonic components of the current into the system, which through the impedance of the system result in distortion of the supply voltage, which affects the reduced reliability and shortening of the life of electrical equipment [2]. Praxis are interesting to the higher ranks of the order from 0 to 100.

The causes of higher harmonics are:

- transformers, due to non-linear Φ - and characteristics of the iron core,
- semiconductor electronic converters that due to their switching nature represent non-linear consumers for the network and cause distortion of the waveform of the current and voltage,
- electric furnace furnaces,
- Inverters,
- discharge lamps,
- saturated electrical machines.

Components of the power system and consumers are designed for sinusoidal forms of voltage and current, and any appearance of higher harmonics brings negative effects. Some of the side effects are:

- the occurrence of serial and parallel resonance in the network resulting in increased voltage and current,
- Impact on condenser batteries - causes an increase in losses,
- the influence on the protection elements, which leads to unwanted protection of the protective devices (protection) or fuse overheating,
- Impact on the accuracy of indications of standard measuring instruments,
- additional losses in electrical machines (eg. overheating, heating of cables, and the like),
- interference with *tt* signals (higher harmonics from power lines are transmitted by electromagnetic interference to *tt* cables, thus creating noise and disturbances in telecommunications,
- influence on transformers.

A. Reduction of negative impacts

In order to minimize the negative effects of higher harmonics, the following measures are necessary:

1) Reduce the intensity of harmonic currents:

- by installing chokes in series with non-linear consumers
- transformers in the Y_d or D_d connection, since the compound in *D* retains odd harmonics compatible with three,
- transformers in connection Y_d dimensioning of neutral conductors 2: 1 in relation to phase or installation of two with old dimensions,
- installation of 12 pulse converters.

2) Installation of filters

Passive filters that are split into:

a) Ordinary

- First order
- Second order
- Third row

b) Active filters

- active filters have the ability generating and managing non-linear currents

3) Resonant frequency change system

When there are condensing batteries in the system or with consumers, compensation resonance can occur to compensate for the reactive energy. Since the resonant frequency

of the system, including capacitor batteries, is often close to the frequency of characteristic harmonics of non-linear consumers, there are undesirable effects.

The change in the resonance frequency of the system is realized:

- by changing the size of the capacitor,
- by adding a serial choke,
- moving the capacitor to another location, or
- disconnecting the capacitor.

B. The role of the transformer in the Dyg compound

When we look at the magnetization component $i_\mu(t)$ in Fig. 1 we see that it is not a sinusoid but a recited periodic function with nulls having maximal values at the same moments as the induction function $B(t)$.

Fourier's analysis of one such function gives data for the amplitude of higher harmonics:

- First harmonic 100%
- Third harmonic 24.5%
- Fifth harmonic 3.43%

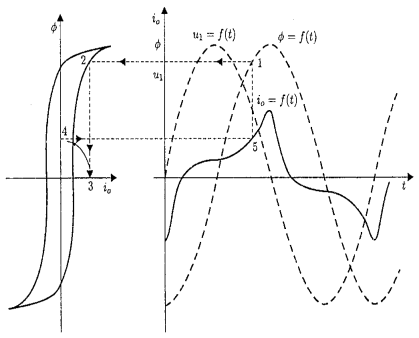

Figure 4. Hysteresis transformer curve

Fig. 5 shows the first, third and fifth harmonics. There is an important influence of the third harmonic (which is a negative sinusoid).

In the first third of the semiperduct, negative values $i_{\mu 3}$ decrease the positive values $i_{\mu 1}$. In the second third of the semiperduct, the positive values $i_{\mu 3}$ are summed up with positive values $i_{\mu 1}$, and in this way a sharpening form occurs $i_\mu(t)$.

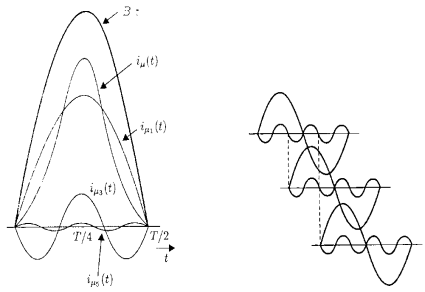

Figure 5. First, third and fifth harmonics

With zero water, each single-phase transformer pulls along the basic accordion $i_{\mu 1}$ and more harmonics.

The magnetization current of the first harmonic is (1):

$$i_{\mu 1A} = I_{\mu 1A_m} \sin(\omega t)$$
$$i_{\mu 1B} = I_{\mu 1B_m} \sin(\omega t - 120^\circ) \qquad (1)$$
$$i_{\mu 1C} = I_{\mu 1C_m} \sin(\omega t - 240^\circ)$$

Where m is the mark for the maximum value of the current.

Without zero water, the magnetization current is sinusoidal, since there is no 0-conductor, so the third harmonics of the current can not be closed.

Flux will have the first and third harmonics Φ_3, so it will be non-linear.

Because the air has a high magnetic resistance, between the upper and lower yoke, the amplitude of the third harmonic of the flux will be considerably lower.

In the case when the transformer is connected to the *DYg* compound, the third harmonic component and all others that are its multiplicity are closed in the triangle, but as a result, we have additional heating of the winding.

IV. USE OF MATLAB/PSB IN THE SOLUTION PROBLEMS

A simulation was performed for the part of the electrical network from Fig. 1 with the help of the MATLAB/PSB computer program [3]. The observation time was $T_{stop} = 0.1s$ and the harmonic currents were counted up to the fifth period [4].

In Fig. 6 the wave form of phase R current is shown on the 10kV side and here it is clearly seen that due to the influence of higher harmonics, the current does not have a sinusoidal shape. The rectifiers are the most commonly used single-energy electronic converters and one of the main sources of higher harmonics [5].

The switching mode has the effect of continuously changing the configuration of the active diode of the rectifier, resulting in the waveform of the rectifier current composed of segments and it is insufficiently shaped.

The flow of the insoluble current causes a decrease in the perpendicular to the impedance of the net, which leads to the distortion of the basic sinusoid voltage, while on the consumer side, the waveform of the voltage consists of parts of the sinusoid, that is, in addition to the one-way component, there are also alternating components-higher (steam) harmonics [6].

Most personal computers use mono-outs in the power supply section and have the role of generating stable single-voltage voltages with simple designs and reliability. For these reasons, most commonly are diode rectifiers with a filter capacitor on a one-way side or, more recently, one-way switching power supplies, which also have a capacitor at the output.

In case of need for another voltage level or more stable voltage, a linear or switching power supply is connected behind the capacitor. However, in both cases, this rectifier distorts the network current, and partly the voltage. Due to the filling of condensation in periods when the mains voltage is higher than one-way, there is a distortion of the current, that is, the voltage at the condenser. The paper deals with the detail and analyzes the distortion of the wave shape of the current, as a quality factor, when sup-plying consumers that generate more harmonic components of the current. It is possible to filter the source harmonics by using filters and analyze all relevant design parameters [7].

In our case, we have a low voltage installation that is connected via the transformer 10/0.4kV to the conventional electricity distribution network 3x10kV. The load we have is a non-linear set of personal computers and is balanced at each stage. The non-linear load for each phase generates more harmonics, the composition of which is approximately defined as $I_n = I_1/n$ where I_1 is the current of the basic and I_n-n harmonic.

The wave forms of the phase R and r phases are given in the figures as follows:

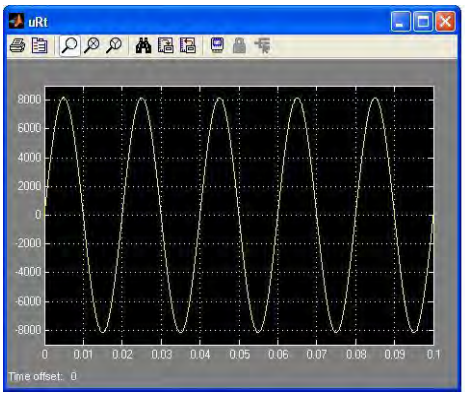

Figure 6. Wave phase voltage waveform on the 10kV side

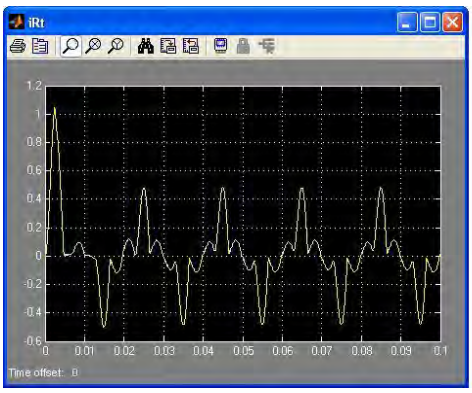

Figure 7. The wave form of the iRt phase on the 10 kV side

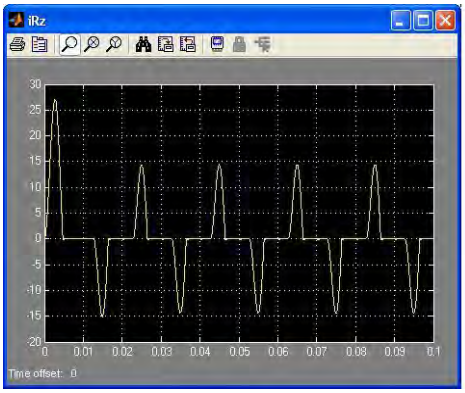

Figure 8. Wave phase current iRz at 0.4 kV side

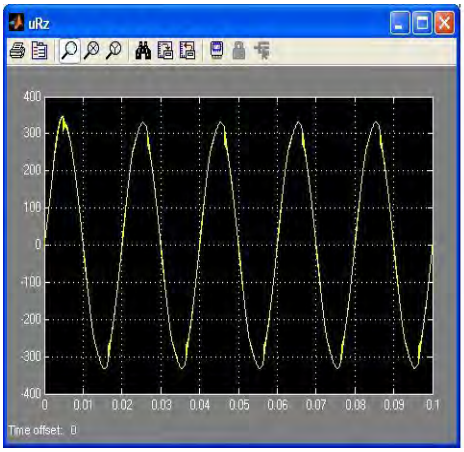

Figure 9. Wave waveform of phase uRz at 0.4 kV voltage level

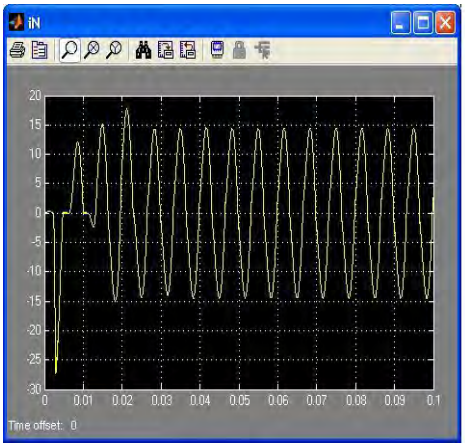

Figure 10. The current shape of the iN-neutral conductor at 0.4 kV voltage

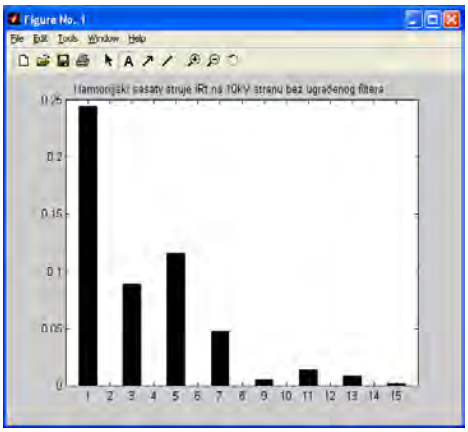

Figure 11. Harmonic current content iRt on 10 kV side without filter / not installed //

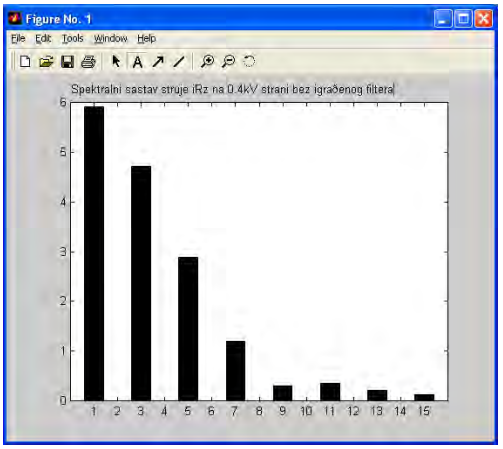

Figure 12. Harmonic current content iRz on 0.4 kV side without filter / not installed //

In the power spectrum iR_t dominants are non-harmonic harmonics, there are no steam. Measurements of the current of the computer have shown that the shape of the current is very distorted due to such non-linear consumer, which generates more odd harmonics (electronic equipment) [8]. THDI is calculated according to the formula below:

$$THDI\% = \sqrt{\sum_{n=2}^{10} \frac{I_n^2}{I_1^2}} * 100\% \qquad (2)$$

For phase current R (on the 10-kV side):

$$THDI\% = 268\%$$

For the current phase r (at 0.4-kV side):

$$THDI\% = 279\%$$

V. Results and Solutions to the Problem

This section shows the possibility of filtering source higher harmonics using filters as well as analyzing all relevant design parameters.

In our case, we have a low voltage installation that is connected via the 10/0.4kV transformer to the 3x10 kV classical electricity distribution network. The load we have is a non-linear set of personal computers and is balanced at each stage. Non-linear load for each phase generates more harmonics, the composition of which is approximately defined as $I_n = I_1/n$, where I_1 is the current of the basic and I_n, n harmonic.

The dimensioned three-phase filter is set to eliminate the maximum harmonic component of

phase *R* current on the 10kV side of the transformer [9]. Also, in this part of the paper, the wave-form and corresponding harmonic content of phase R phase are shown. In this case, THDI% is calculated for phase *R* phase (10kV side).

With the help of the MATLAB/PSB computer program, a simulation was performed. The observation time was $T_{stop} = 0.1s$.

The value of THDI% for phase *R* current is (3):

$$THDI\% = \sqrt{\sum_{n=2}^{10} \frac{I_n^2}{I_1^2}} * 100\% = 0.239\% \quad (3)$$

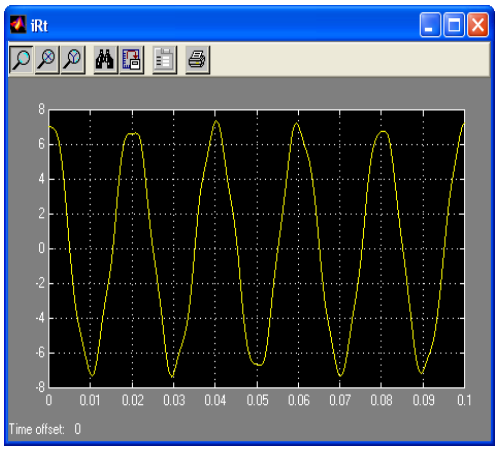

Figure 13. Phase R current waveform on a 10-kV side (build-in filter)

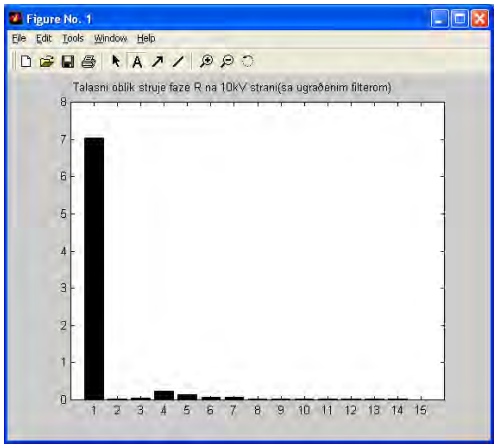

Figure 14. Frequency spectrum of phase R current on 10 kv side (with built-in filter)

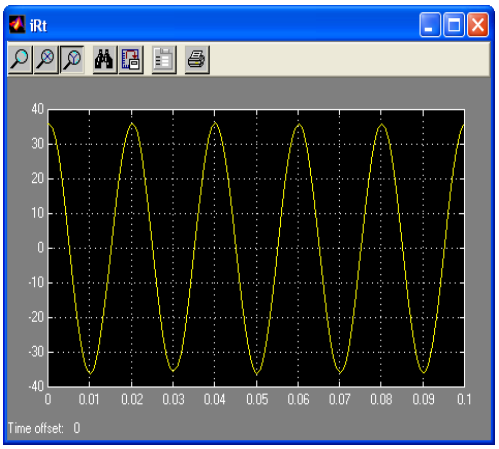

Figure 15. The phase wave R wave on the 10 kV side (two filters)

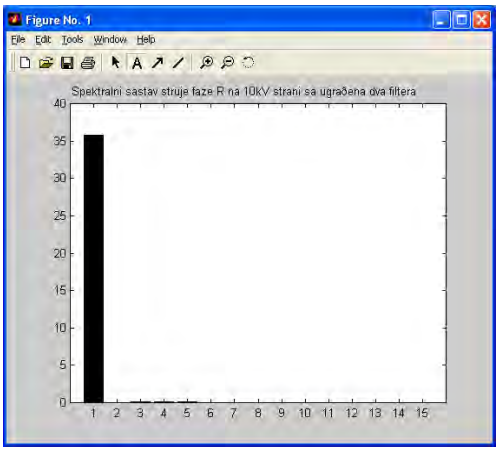

Figure 16. The phase wave R wave on the 10 kV side (two filters)

The pictures show the oscillogram of the phase wave *R* waveform and the spectral composition of the same current.

It turned out that this filter has done a good job of eliminating the third and all other odd and odd harmonics, so that the total THDI % of the phase current *R* is about 0.239 %, which is quite satisfactory, given the regulations in this field and the transformators' in practice often does not meet.

VI. CONCLUSION

In order to further reduce the THDI% of the current phase *R*, another parallel three-phase filter is set up to eliminate the maxi-mum harmonic component of the *R* phase current on the 10kV side of the transformer.

Also, in this part of the paper, the waveform and the corresponding harmonic content of the phase R phase are shown. In this case, the THDI% for the current phase *R* (10kV side) is calculated.

With the help of the MATLAB/PSB computer program, a simulation was performed. The observation time was $T_{stop} = 0.1s$.

With this filter we completely reduce the second and third harmonic components [11]. The second filter is installed in parallel with the first one that we installed earlier. The capacity of the second filter is that its capacity is 2.25 times smaller than the first because of the frequency of the second amount, 150 Hz. The parameters of both filters are:

First: $R = 0.1$Ohm-a, $L = 0.156$ H, $C = 20$e-06F

Second: $R = 0.1$Ohm-a, $L = 0.156$H, $C = 8.94$e-06F

The value of THDI% for phase *R* current is:

$$THDI\% = \sqrt{\sum_{n=2}^{10} \frac{I_n^2}{I_1^2}} * 100\% = 0.0023\% \quad (4)$$

Comparison of THDI in either case:

From the analysis, we can see that THDI% is the smallest when both filters are eliminated for the elimination of the 2 and 3 current harmonics, but then the current in the *R* phase has the highest value, i.e. 36A.

The THDI current of the phase *R* is distinguished on the 10kV voltage because it is higher THDI% in the case of installing one in relation to the two filters (in parallel).

REFERENCES

[1] V.Katić, "The quality of electrical energy [Kvalitet električne energije]", CEFES, November, 2005.

[2] A. Tokić, "The quality of electrical energy [Kvalitet električne energije]", CEFES, November, 2005.

[3] Matlab Simulink Power System Blockset 7, Available at: https://www.mathworks.com/products/matlab.html

[4] E.Agić, "Power Quality", CEFES, 2006.

[5] M.R. Iravani et al., "Modeling and analysis guidelines for slow transietns. III. The study of fl\erroresonance," IEEE Transactions on Power Delivery, vol. 15, no. 1, January 2000, pp.255-265

[6] K. Miličević, "Ferroresonance: Systems, Analysis and Modeling," Wiley Encyclopedia of Electrical and Electronics Engineering, 2014, pp.1-8.

[7] A.Vinkovic, and R.Mihalic, "A curent-based model of the static synchronous series compensator (SSSC) for Newton-Raphson power flow," Electr. Power Syst. Res., vol. 78, no.10, October 2008, pp.1806-1813.

[8] Mathworks, "SimPowerSystems user's guide", 2013.

[9] W. Piasecki, M. Florkowski, M. Fulczyk, P. Mahonen, and W. Nowak, "Mitigating Ferroresonance in Voltage Transformers in Ungrounded MV Networks," IEEE Trans. on

[10] Power Delivery, vol. 22, no.4, 2007, pp. 2362-2396.

[11] D.A. Tziouvaras et al., "Mathematical models for current, voltage, and coupling capacitor voltage transformers," IEEE Transactions on Power Delivery, vol. 15, no. 1, January 2000, pp. 62-72.

[12] N. Janssens, T. Van Craenenbroeck, D. Van Dommelen, and F. Van de Meulebroeke, "Direct calculation of the stability domains of three-phase ferroresonance in isolated neutral networks with grounded neutral voltage transformers," IEEE Transactions on Power Delivery, vol. 11, no. 3, July 1996, pp. 1546-1553.

PV based Automated Irrigation Management in Remote Onshore Area in India

Subhajit Das[1], Soumik Nath[1], Shreyasi Majumder[1], Sagnik Ghosh[1], Subhasis Sarkar[1] Arunava Chatterjee[1]*

[1]Electrical Engineering Deptt., Meghnad Saha Institute of Technology, Kolkata-700150, India, *arunava7.ju@gmail.com

Abstract—**Photovoltaic (PV) based irrigation is one of the most promising application of renewable energy for agronomy. This paper presents an PV based automated irrigation management system and its implementation for a remote onshore area in India. In this work, the effects of parameters such as solar irradiation, soil moisture, selection of pump, etc. has been studied. The plant is also capable of storing excess generated PV as a backup for retrieval during lean periods. An economic analysis is also performed using *HOMER* software. Suitable simulations and experimental implementation on a laboratory prototype validates the proposed study.**

Keywords – Photovoltaic (PV) system, automated irrigation, PV pumping.

I. INTRODUCTION

Solar energy is the most common and abundantly used source of renewable energy in the world. Also it is a clean source with minimal cost of installation and maintenance. Use of photovoltaic (PV) energy for domestic applications has always been a wide and expanding area of research [1]. In recent times, use of PV panels for driving small water pumps for irrigation has been found promising [2]. Although PV based irrigation is practiced widely in Europe and the middle east [3], it has not been successfully tested on larger scale in Indian conditions. In Indian conditions, existing technologies give importance mostly to conservation of water for irrigation purpose using moisture sensors [4], or microcontroller based sensors are used [5]. Although PV based pumping and irrigation is studied by some researchers [2], [6]-[8], the economic consideration is missed out in such papers. Although PV based irrigation is an emerging area of research, the use of PV panels incurs some installation cost and an economic analysis is important in all such studies.

This paper presents a technical and economic analysis of a PV based automated irrigation system which is implemented in a remote isolated onshore area in eastern India. *The study mainly concentrates on optimal design of the system with an economic study which is also non-existent in available literatures.* Although [8] discusses the economic considerations, however the location is not set. The location plays an important part in economic analysis of a solar system and it is considered in this paper. Also for the proposed system, the solar energy that will be surplus will be stored for later retrieval during lean irradiation periods. The proposed study is validated by suitable simulations backed by experimental findings on a laboratory based prototype.

II. DESCRIPTION OF THE SYSTEM

The proposed system uses PV panels for powering a DC motor based pumping system. The main components of the system include a PV panel, a storage battery and associated charge controller, a DC motor based pump, water tank, soil moisture sensor and water storage unit. The unit also has a controller for automated operation. The operation of the unit will depend on the solar irradiation and the soil moisture content. If solar irradiation is high, generation will also be high and need for watering will also increase.

ISBN: 978-86-80616-03-2

The block diagram of the proposed system is shown in Fig.1. The control unit used for the laboratory setup is a Atmega based Arduino Uno controller. The laboratory setup can be scaled up for higher ratings also.

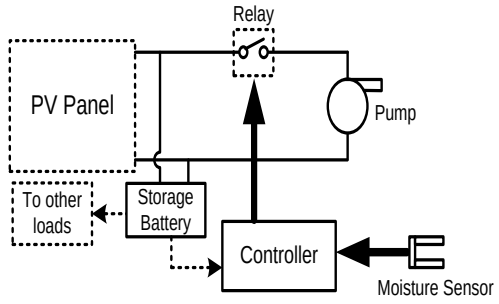

Figure 1. Block diagram of the proposed system.

III. PV Based System Design

The PV panel generates power with incident solar irradiation which helps in operation of the pump. The pump will operate only when command pulses are received from the controller. The controller will send a pulse to the relay circuit when the moisture sensor sends an input based on the moisture content of the soil. If the soil is dry, the controller gets a signal as positive and the relay gets a pulse signal from the controller and the circuit gets completed which switches the pump on. The pump is supplied from a PV panel. The PV panel output when surplus is stored in the storage battery. It can be retrieved during night time or cloudy conditions. The storage battery can supply the controller power as well as some other loads when energy is surplus.

The system is to be installed in a remote onshore area in West Bengal state in eastern India. The place is chosen to have good solar irradiance throughout the year. The geographical location is provided in Fig.2.

Figure 2. Location of the proposed system setup installation.

IV. Results and Discussion

Studies are performed for the proposed system at first using a laboratory prototype. The prototype uses an Arduino based system with a 15W, 12V DC motor based pump. The system uses a PV panel with rating of 42W. The size of the system will change according to the area of the land under irrigation. The system also uses a two terminal moisture sensor for sensing the moisture level of the soil and to decide if the soil needs watering.

The designed system yielded good results. The simulated PV panel power versus voltage curve is shown in Fig.3.

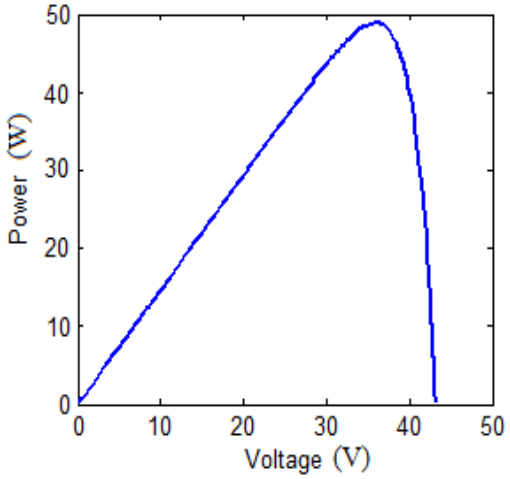

Figure 3. PV panel power versus voltage curve.

The system also uses a rechargeable battery for storage purpose. A charge controller is also used for proper charging of the battery from the PV panel.

The system is chosen to be used in the proposed area as shown in Fig.2. The system is also simulated in *HOMER* (Hybrid Optimization Model for Electric Renewables) software [9] for techno-economic analysis of the proposed system. The designed system is scaled up for the proposed techno-economic study. In the simulation, a system is considered where the electric load of the plant is taken as 1.00kWh/day with a peak load of 0.21kW. A suitable battery of 48V is considered with the PV panel rated at 800 Watts.

The solar daily radiation data as obtained from *HOMER* software is shown in Fig.4. The data is directly procured in the software from the

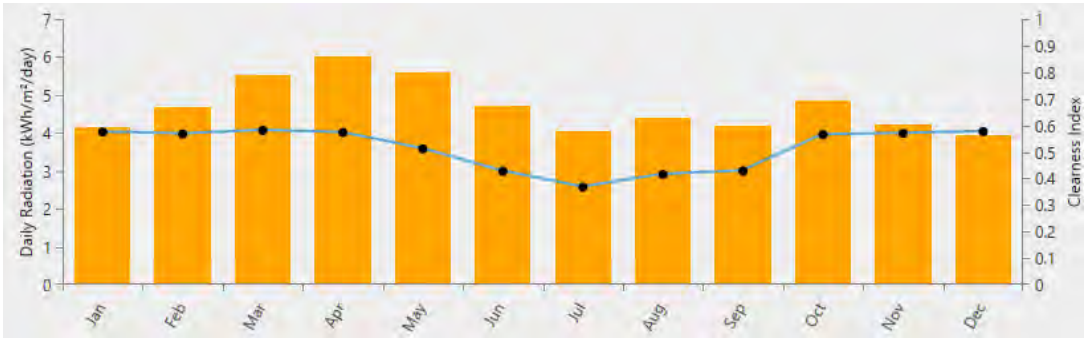

Figure 4. Solar daily radiation data of the location.

surface metrological data as obtained from NASA, USA. The data shows that the area is well supported by solar radiation throughout the year and the plant can be setup in the said area. April and May are summer months in the area. The *HOMER* based system model is shown in Fig.5 below.

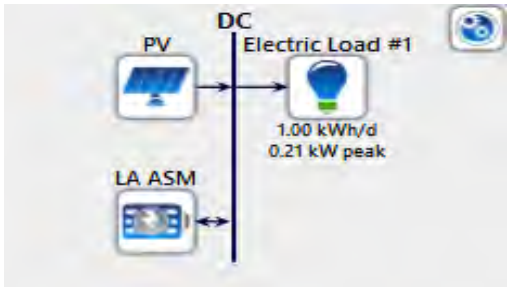

Figure 5. Simulated system in *HOMER* for techno-economic analysis.

The system is simulated for a total period of 25years. The initial capital cost of the system is found to be around $1044 with net present cost of $1143. The system operating cost was found to be $42.84. The seasonal load profile is shown for the irrigation plant in Fig.6.

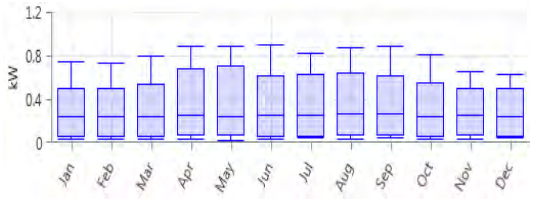

Figure 6. Seasonal variation of pump load for proposed plant system.

As observed, the load is higher during the summer months of April and May when the soil moisture content is also low.

The increased system cost of installation is primarily due to the high initial cost of the PV panel rated at $1000/kW-pk. The battery and charge controller also adds up to the higher system cost. It is expected that with time of operation chosen as high, the cost of the system will decrease. The system runs with 100% renewable fraction of energy with good feasibility.

The system is found sensitive to the cost of the battery and the PV panel. The operation and maintenance cost of the system is also nominal at $2.00 per year.

The experimental system is shown in Fig.7. The flowchart of the automated system is shown in Fig.8.

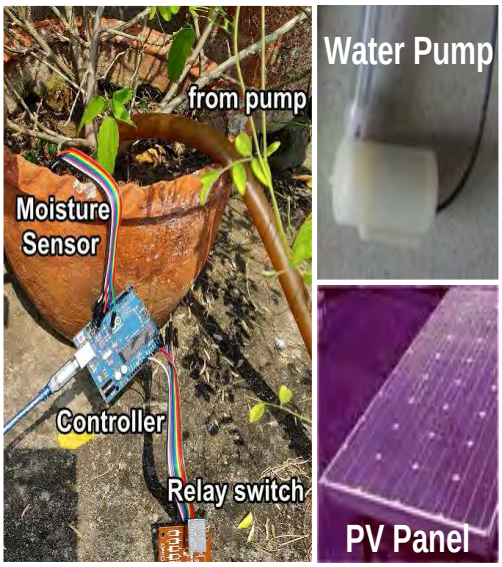

Figure 7. Laboratory experimental setup..

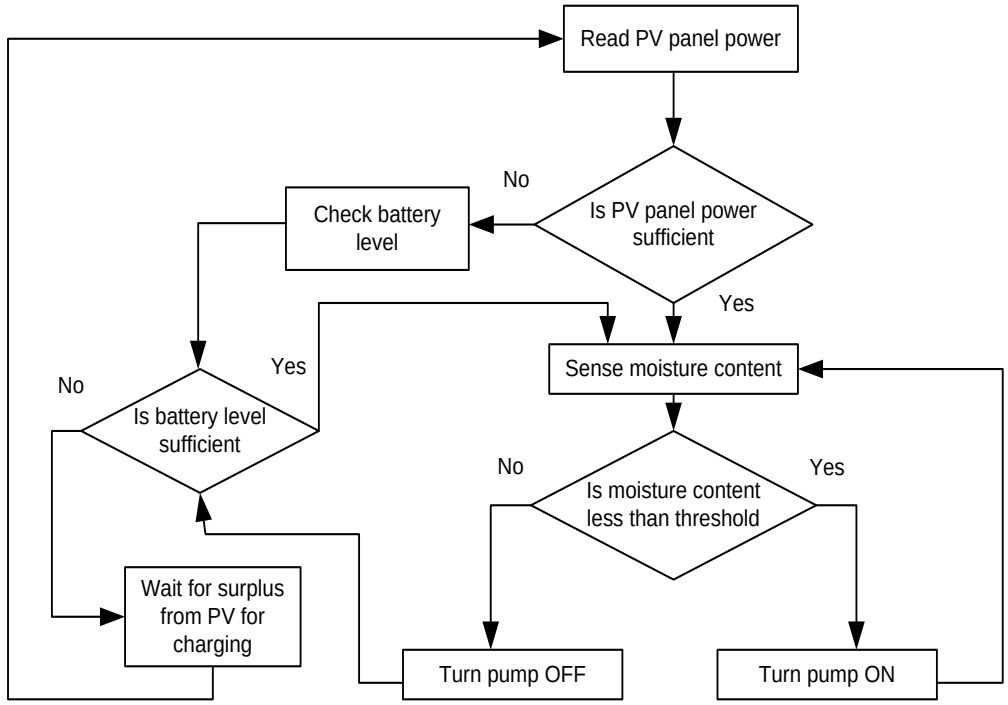

Figure 8. Flowchart of the proposed automated system.

V. CONCLUSION

The paper presented a study on an automated irrigation system with a PV panel as power source. The proposed study focuses on two major aspects: technical and economic analysis

If such an irrigation project is setup, the cost implication is also within affordable limit. It was found that the system is a good prospect for installation in an onshore area in eastern Indian conditions. The simulations with suitable laboratory based prototype validates the proposed study.

REFERENCES

[1] M.R. Patel, Wind and solar power systems: Design, analysis and operation. 2nd ed. Boca Raton, USA: CRC Press; 2006.

[2] A. Senpinar, Using Photovoltaic Panels for Irrigation, Acta Physica Polonica A, vol. 132, no.3, 2017, pp. 625-628.

[3] A.A. Zekry, M.A. Elgendy, Estimated performance of photovoltaic irrigation systems under different operating conditions, 2lSt National Radio Science Conference (NRSC2004) (NTI) March 16-18,2004.

[4] M. Karthikeswari, P. Mithradevi, “International Journal of Advanced Research in Electrical, Electronics and Instrumentation Engineering, vol. 3, no. 12, Dec. 2014.

[5] J. Gutiérrez, J.F. Villa- Medina, A. Nieto Garibay, M. Ángel Porta- Gándara , Automated irrigation system using a wireless sensor network and gprs module, IEEE Transactions on Instrumentation and Measurement, vol. 63, no. 1, Jan. 2014, pp. 166-176.

[6] G. Alex, M. Janakiranimathi, Solar based plant irrigation system, international conference on advances in electrical, electronics, Information, Communication and Bio-Informatics (AEEICB16), 2016, pp.1-4.

[7] S. Harishankar, R.S. Kumar, Sudarshan K.P, U. Vignesh, T. Viveknath, Solar powered smart irrigation system, Advance in Electronic and Electric Engineering, vol. 4, no. 4, 2014, pp. 341-346.

[8] P. Persad, N. Sangster, E. Cumberbatch, A. Ramkhalawan, A. Maharajh, "investigating the feasibility of solar powered irrigation for food crop production: a caroni case," The Journal of the Association of Professional Engineers of Trinidad and Tobago, vol. 40, no.2, pp. 61-65, October/November 2011.

[9] NREL. HOMER User Manual. Golden, CO, USA: National Renewable Energy Laboratory, 2002.

Comparing Multilayer Perceptron and Multiple Regression models for Predicting Energy Use in the Balkans

Radmila Janković[1], Alessia Amelio[2]

[1]Mathematical Institute of the S.A.S.A, Belgrade, Serbia, rjankovic@mi.sanu.ac.rs
[2]DIMES, University of Calabria, Rende, Italy, aamelio@dimes.unical.it

Abstract— **Global demographic and economic changes have a critical impact on the total energy consumption, which is why demographic and economic parameters have to be taken into account when making predictions about the energy consumption. This research is based on the application of a multiple linear regression model and a neural network model, in particular multilayer perceptron, for predicting the energy consumption. Data from five Balkan countries has been considered in the analysis for the period 1995-2014. Gross domestic product, total number of population, and CO_2 emission were taken as predictor variables, while the energy consumption was used as the dependent variable. The analyses showed that CO_2 emissions have the highest impact on the energy consumption, followed by the gross domestic product, while the population number has the lowest impact. The results from both analyses are then used for making predictions on the same data, after which the obtained values were compared with the real values. It was observed that the multilayer perceptron model predicts better the energy consumption than the regression model.**

Keywords – energy use, regression, neural network

I. INTRODUCTION

The energy consumption worldwide is rising as the population numbers grow. It is estimated that the world population growth was 1.2% in 2016 [1]. Higher population numbers indicate a fast expansion of residential and industrial buildings, which further increases the energy consumption. The industrial processes also impact on the energy use, since the countries try to stay within positive economic growth rates. As the society becomes more demanding, the need to successfully manage the energy consumption rises.

Usually, the modeling of the energy use is based on time series data that is often incomplete and complex. Creating a model that would be able to accurately predict the energy use is still challenging, as these models can be very complex and hard to manage [2]. But, even when complex, these models are necessary for future planning and production of energy.

A report by the Balkan green foundation [3] indicated that in 2015, Serbia had the highest final consumption of electricity (28,551 GWh), compared to Bosnia and Herzegovina (11,183 GWh) and Macedonia (6,600 GWh). The consumption structure of these three countries indicates that more than 50% of energy was used in the industrial sector, transport, services and agriculture, with the rest of the energy being used in households. Slovenia has obligated to improve its energy efficiency until 2020 by 20% [4], while projections for Serbia state that the final energy consumption will increase of 10.1% by 2020, compared to the energy consumption in 2010 [5]. In the action plan it was reported that Serbia managed to accomplish savings of 4.4% in the period from 2010 to 2015, with the goal of achieving 9% savings in 2018 [6]. Croatia projected that the final energy consumption will increase of 5.85% in 2020, compared to 2015, but it will decrease of 3.19% compared to 2010 [7].

ISBN: 978-86-80616-03-2

Bosnia and Herzegovina set a reduction of 9% in final energy consumption as a goal by the end of 2018 [8]. All this clearly emphasizes the need for accurate and simple to use prediction models and techniques, as energy efficiency goals are hard to maintain if the energy forecast is not reliable.

The aim of this paper is to investigate and model the energy consumption in West Balkan using two techniques: (i) multiple linear regression, and (ii) artificial neural network (ANN), in particular multilayer perceptron. The relationship between the energy use as a dependent variable and gross domestic product (GDP), population, and CO_2 emissions as independent variables was investigated. The purpose is to determine which variable has the biggest impact on the energy use, and to see which technique best predicts the values of energy consumption. Moreover, based on the regression analysis, the energy consumption elasticity was also calculated.

II. LITERATURE REVIEW

Kankal et al. [9] modeled the energy consumption based on GDP, population, import, export, and employment as variables. They have developed different models based on a multiple linear regression analysis, power regression analysis, and ANN. It was concluded that the ANN model predicts the energy use better than the regression models. Borozan [10] investigated the relationship between energy consumption (in particular liquid fuel, natural gas, hydropower, electricity and coal) and GDP in Croatia using the bivariate vector autoregression and Granger causality tests. It was concluded that savings in energy consumption can negatively affect the economic growth. Moreover, a causal relationship was not found between GDP and coal, but a relationship exists for other investigated forms of energy. In [11], the authors have compared regression models, neural networks and least squares support vector machine models for forecasting the electricity consumption. As predictors in their study, gross electricity generation, installed capacity, total subscribership and population were used. The results indicate that the least squares support vector machine was the most effective for predicting electricity consumption. In [12], the authors applied an ANN model to monthly build electric energy consumption data. Their results indicated that the ANN model relatively accurately predicted the energy consumption, but the accuracy slightly varies depending on the prediction period. In [13], the authors developed a weighted multi Support Vector Regression (SVR) model with a differential evolution optimization algorithm for predicting the buildings' energy consumption. It was concluded that the model which used the optimization algorithm achieved higher accuracy and could be used for predicting daily and half-hourly energy consumption of a building. A decision tree model, in particular the Random Forest, and the ANN model were compared in [14] in terms of predicting the energy consumption of a building. Based on the analysis, the authors concluded that ANN performed better than the Random Forest algorithm, with higher accuracy on the testing set of data.

Differently from the previous literature, this paper introduces a comparison between a regression model and an ANN model developed on a dataset from Balkan countries. We try to answer the following questions: (1) Can the energy use be predicted based on the values of CO_2 emissions, population, and GDP from five Balkan countries, and (2) What model better predicts the energy use in this situation.

The paper is organized as follows. Section III describes the data and methodology used in the research. Section IV shows the results and makes a discussion. Finally, Section V draws conclusions from this research.

III. DATA AND METHODOLOGY

The purpose of this research was to investigate if the energy use can be successfully modeled by two techniques: (1) multiple linear regression, and (2) multilayer perceptron neural network. Multiple linear regression is a method used when there is one outcome and more than one predictor variable. It creates a statistical relation between the predictor variables and the outcome, and can be represented by the following equation [15]:

$$Yi = \beta_0 + \beta_1 x_{i1} + \beta_2 x_{i2} + ... + \beta_{p-1} x_{i,p-1} + \varepsilon_i \quad (1)$$

where Yi is the dependent variable, β_0 is the intercept, β_1 is the coefficient of the independent variable, x_i is the predictor variable, and ε_i is the random error.

The multilayer perceptron, on the other hand, is a type of ANN and consists of one or more input layers, hidden layers that are formed by nodes, and output layers [16]. A linear activation function is contained in the neurons of the output layer, while in the hidden layer this function is nonlinear. The nodes in the network are interconnected and actually represent units for information processing that are arranged in layers [16]. The task of each type of layer differs, so the input layer receives the information, the hidden layer processes it, while the output layer performs predictions. Before passing information to the hidden layer, the values from the input layer are multiplied by weights, with results being added in order to get only one number. This number represents an argument to the activation function [17].

The data used in this research has been downloaded from World Bank [1]. The created dataset consists of six variables: (1) Country, (2) Year, (3) CO_2 emissions in metric tons per capita, (4) GDP per capita in constant 2010 US$, (5) Energy use in kilograms of oil equivalent per capita, and (6) Total population. The research involved annual data from five Balkan countries: Bosnia and Herzegovina, Croatia, Former Yugoslav Republic of Macedonia, Serbia, and Slovenia, and included the period from 1995 to 2014. All analyses were performed using the software SPSS v.23 and Microsoft Excel 2010.

The trend of CO_2 emissions in the observed period represented in metric tons per capita is shown in Fig. 1. The highest CO_2 emissions are observed for Slovenia, with a peak in 2008, while the lowest values are observed for Croatia and Macedonia.

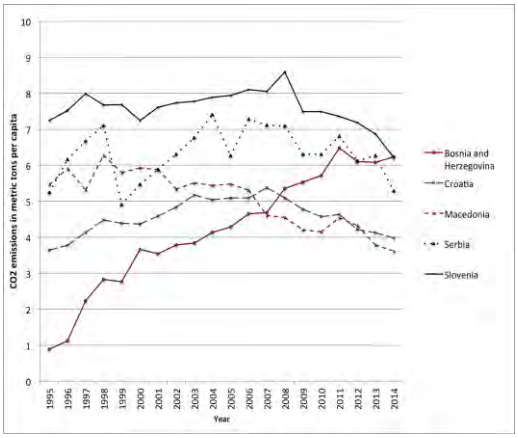

Figure 1 CO_2 emissions in the observed period

Fig. 2 shows the trend of GDP per capita for the period from 1994 to 2014. The highest GDP per capita is observed for Slovenia, while the lowest GDP per capita is found for Macedonia and Bosnia and Herzegovina.

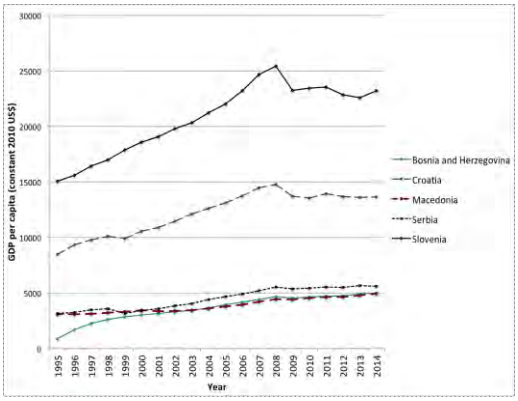

Figure 2 GDP per capita for the observed period

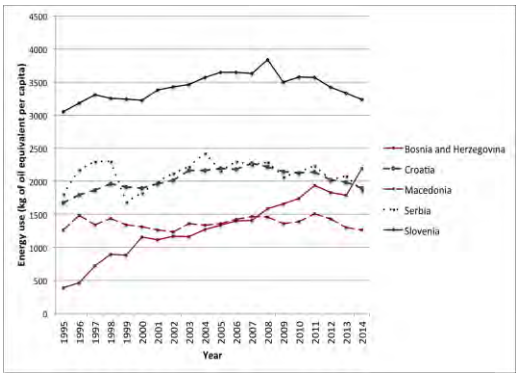

Figure 3 Energy use in the observed period

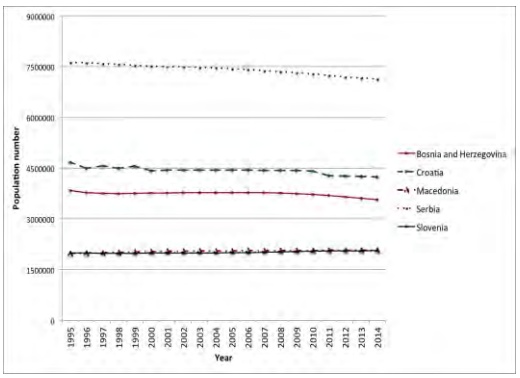

Figure 4 Population of the tested countries

The energy use in the observed period for the five Balkan countries is shown in Fig.3. Based on the chart, the highest energy use is observed for Slovenia, while the lowest energy use is found for Macedonia.

Considering the population of the tested countries, it is worth noting that the highest number of population is in Serbia, while Macedonia and Slovenia have the lowest number of population. These trends can be clearly observed from Fig. 4.

In Table I, descriptive statistics of the dataset – mean, standard deviation, minimum and maximum values, can be observed for the five countries in terms of the following variables: (a) CO_2 emissions, (b) GDP, and (c) Energy use. As observed, the highest mean value of CO_2 emissions in metric tons per capita in the period from 1995 to 2014 can be found for Slovenia (M=7.58, SD=0.502), while the lowest is observed for Bosnia and Herzegovina (M=4.195, SD=1.647). Considering the GDP per capita, the highest mean can be found for Slovenia (M=20761.686, SD=3153.642), and the lowest one is found for Bosnia and Herzegovina (M=3617.605, SD=1157.083). The highest energy use can be observed for Slovenia (M=3424.976, SD=198.278), while the lowest energy consumers in this period are Bosnia and Herzegovina (M=1304.608, SD=484.574), followed by Macedonia (M=1365.916, SD=81.077).

TABLE I. DESCRIPTIVE STATISTICS FOR THE TESTED COUNTRIES

Country		CO_2 emissions (metric tons per capita)	GDP per capita (constant 2010 US$)	Energy use (kg of oil equivalent per capita)
Bosnia and Herzegovina	Mean	4.195	3617.605	1304.608
	Std. Deviation	1.647	1157.083	484.574
	Minimum	.892	866.941	388.736
	Maximum	6.475	4992.949	2194.056
Croatia	Mean	4.568	12172.629	2029.330
	Std. Deviation	.493	1934.668	159.545
	Minimum	3.638	8475.140	1674.411
	Maximum	5.372	14777.350	2272.141
Macedonia	Mean	5.069	3856.556	1365.916
	Std. Deviation	.781	640.549	81.077
	Minimum	3.615	3057.004	1233.482
	Maximum	6.275	4920.216	1506.138
Serbia	Mean	6.336	4457.660	2113.553
	Std. Deviation	.7145	966.004	196.501
	Minimum	4.910	3150.464	1686.929
	Maximum	7.400	5670.712	2424.404
Slovenia	Mean	7.580	20761.686	3424.976
	Std. Deviation	.502	3153.642	198.278
	Minimum	6.214	15062.818	3049.387
	Maximum	8.586	25447.426	3836.622

IV. ANALYSIS AND DISCUSSION

The analysis included the development of a multiple regression model and also a neural network model. These two models were then compared in terms of their root mean square error (RMSE) and mean absolute percentage error (MAPE).

A. Multiple linear regression model

The multiple regression model includes one dependent variable (Energy use) and three independent variables: (1) CO_2 emissions (metric tons per capita), (2) GDP per capita (constant 2010 US$), and (3) Population. All variables were logarithmically transformed, and a log-log model was developed. A Stepwise regression method was used for developing a regression model, with the following criteria: probability of F to enter <=.050; probability of F to remove >=.100. The F-statistic is used for testing the significance of the regression coefficients of the independent variables that will be included or excluded from the model. The regression equation for log-transformed models can be expressed as in (2):

$$\ln(Y) = \beta_0 + \beta_1 \ln(X_1) + \beta_2 \ln(X_2) + \varepsilon_1 \quad (2)$$

By applying the general equation to the data, the following regression equation can be generated:

$$\ln(EU) = \beta_0 + \beta_1 \ln(GDP) + \beta_2 \ln(P) + \beta_3 \ln(CO_2) \quad (3)$$

where EU represents the energy use, GDP is the gross domestic product, P is the population, and CO_2 are the emissions.

TABLE II. RESULTS OF MULTIPLE LINEAR REGRESSION

	B	Std. Error	t	Sig.
Intercept (constant)	1.481	0.286	5.169	.000
ln(CO2)	0.665	0.025	26.252	.000
ln((GDP)	0.334	0.012	27.026	.000
ln(P)	0.134	0.016	8.248	.000

R^2=0.969, F-statistics = 1000.933, p=0.000

Based on the results from the regression analysis (Table II), it is visible that the energy use can be explained by GDP, CO_2 emissions and total population number with high fit (R^2=0.969), with a significant F-statistics value (p=0.000).

By incorporating the regression results into (3), the following regression equation can be generated:

$$\ln(EU) = -1.481 + 0.665 \ln(CO_2) + 0.334 \ln(GDP) + 0.134 \ln(Population) \quad (4)$$

As observed (4), a 1% change in CO_2 emissions results in 0.67% increase in energy use. Moreover, a 1% change in GDP per capita results in 0.33% increase in energy use, while 1% increase in population results in 0.13% increase in energy use. All predictors in the model are statistically significant and impact on the energy use by increasing it.

The regression equation was then applied to present and past values in order to compare the correctness of the regression model. Fig. 5 shows the actual and predicted energy use. As observed, the predicted values are very similar to the actual values, with some deviations.

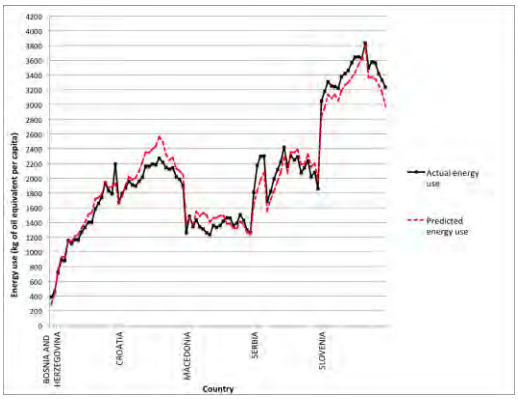

Figure 5 Actual and predicted values of energy use (multiple linear regression method)

B. Multilayer perceptron model

Before employing a neural network model, the number of samples belonging to the training, testing and holdout sets was specified to be 70% for training, 18% for testing and 12% for holdout. The scaled conjugate gradient was used as an optimization algorithm.

There were two units in the hidden layer, and the schematic representation of the neural network model is represented in Fig. 6. The diagram shows 3 input nodes, 2 hidden nodes and one output node representing the energy use.

Table III presents the results after applying the multilayer perceptron network to the sample. As the output layer consists of a scale dependent variable, a sum of squares error is presented here. The sum of squares error is the error that the neural network tries to minimize during the training phase.

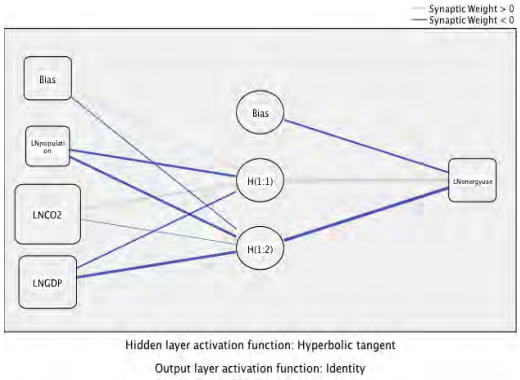

Figure 6 Schematic representation of the multilayer perceptron model

The used stopping rule is one consecutive step with no decrease in the error. The relative errors for training, testing and holdout are very similar (0.013, 0.026 and 0.020, respectively), hence it can be assumed that the model is not overtrained. The computation of the errors was based on the testing set.

TABLE III. ERRORS OF THE MULTILAYER PERCEPTRON MODEL

Training	Sum of squares error	.444
	Relative error	.013
Testing	Sum of squares error	.475
	Relative error	.026
Holdout	Relative error	.020

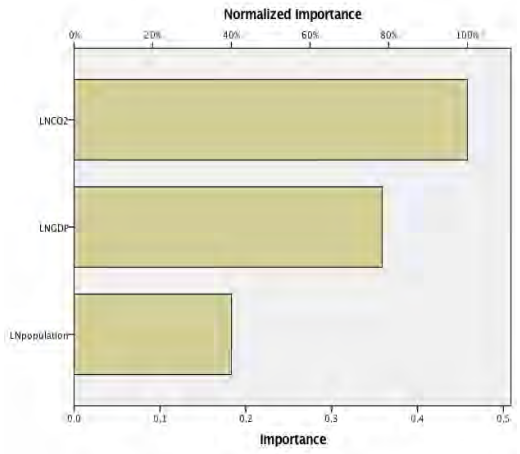

Figure 7 Sensitivity analysis

It can be observed that the importance of the independent variable, i.e. how much the model predicted the value, changes for different values of the independent variables. A sensitivity analysis that calculates the importance of each predictor variable has been computed (see Fig. 7), and shows that the most important factors are the CO_2 emissions (in logarithmic format), followed by the GDP and Population.

A comparison between actual values and values predicted by the multilayer perceptron model was performed. It can be observed that the deviations from the actual values were relatively small, and that in general this model predicts the energy consumption better than the regression model. This is presented in Fig. 8:

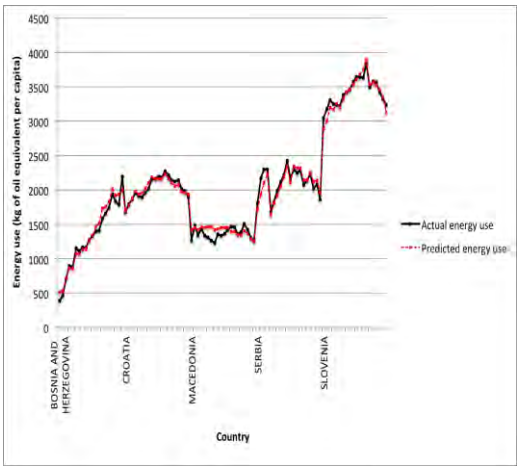

Figure 8 Actual and predicted values of energy use (multilayer perceptron model)

Lastly, the RMSE and MAPE for both models were calculated. The RMSE is calculated as follows:

$$RMSE = \sqrt{\frac{\sum_{i=1}^{n}(O_i - P_i)^2}{n}} \qquad (5)$$

where *Oi* is the i-th observed value, *Pi* is the i-th predicted value, and *n* is the number of samples in the dataset.

MAPE is calculated as follows:

$$MAPE = \frac{\sum_{i=1}^{n}\left|\frac{O_i - P_i}{O_i}\right|}{n} * 100 \qquad (6)$$

Both of these measures were compared in Table IV. Based on the calculations, it can be

concluded that the multilayer perceptron model generally performs much better than the regression model, with lower values of both RMSE and MAPE.

TABLE IV. COMPARISON OF RMSE AND MAPE FOR BOTH MODELS

Errors	Multiple linear regression	Multilayer perceptron
RMSE	144.7187899	8.09430595
MAPE	6.377091484	3.972917354

V. CONCLUSION

The multiple regression model and the multilayer perceptron neural network model were developed to predict the energy use, using population, GDP and CO_2 emissions indicators. Both models performed relatively well, with the multi-layer perceptron model performing the best, with very small deviations from the actual values and lower values of RMSE and MAPE.

The results indicate that the CO_2 emissions mostly influence the energy use, followed by the GDP indicator, while the population number influences the energy use relatively less. The neural network model performed much better compared to the multiple linear regression model. As observed, both models predicted the energy use more accurately for Bosnia and Herzegovina, while the neural network model performed with minimal deviations for all countries, except for Macedonia, where the deviations from the actual values were slightly bigger. Moreover, the CO_2 emissions are generally the best fitted predictors of energy use in the Balkan countries. The future research will involve developing a forecasting model based on different demographic and quality-of-life factors, with a focus on Serbia.

ACKNOWLEDGMENT

This work was supported by the Mathematical Institute of the Serbian Academy of Sciences and Arts (Project III44006).

REFERENCES

[1] The World Bank (2018). World Bank Open Data. Available at: https://data.worldbank.org/indicator/EN.ATM.CO2E.PC

[2] V. Bianco, O. Manca, and S. Nardini, "Electricity consumption forecasting in Italy using linear regression models," Energy, vol. 34 , 2009, pp. 1413-1421.

[3] Balkans Energy Prospect, "Balkan Energy Overview," Balkan green foundation, June, 2017.

[4] Republic of Slovenia, Ministry of Infrastructure, "National Energy Efficiency Action Plan 2014-2020," 2015.

[5] Department for strategic planning in energy sector, Energy sector development strategy of the Republic of Serbia for the period by 2025 with projections by 2030. Belgrade, Republic of Serbia, Ministry of Mining and Energy, 2016.

[6] Energy Community, Annual implementation report. Energy Community Secretariat , 2017.

[7] Ministry for protection of the environment and energy. "Fourth National Energy Efficiency Action Plan of the Republic of Croatia for the Period from 2017 to 2019." Ministry for protection of the environment and energy, 2017.

[8] Energy Community. Energy Efficiency Action Plan in Bosnia and Herzegovina 2016 - 2018. Energy Community Secretariat, 2017.

[9] M. Kankal, A. Akpınar, M. İ. Kömürcü, and T. Ş. Özşahin, "Modeling and forecasting of Turkey's energy consumption using socio-economic and demographic variables," Applied Energy, vol. 88, no.5, 2011, pp. 1927-1939.

[10] Dj. Borozan, "Exploring the relationship between energy consumption and GDP: Evidence from Croatia," Energy Policy, vol. 59 , 2013, pp. 373-381.

[11] F. Kaytez, M.C. Taplamacioglu, E. Cam, and F. Hardalac, "Forecasting electricity consumption: A comparison of regression analysis, neural networks and least squares support vector machines," Electrical Power and Energy Systems, 2015, pp.431-438.

[12] S.Ferlito, M.Atrigna, G.Graditi, S.De Vito, M.Salvato, A.Buonanno, and G. Di Francia, "Predictive models for building's energy consumption: An Artificial Neural Network (ANN) approach", AISEM Annual Conference. IEEE, 2015, pp. 1-4.

[13] F. Zhang, C. Deb, S.E. Lee, J. Yang, and K.W. Shah, "Time series forecasting for building energy consumption using weighted Support Vector Regression with differential evolution optimization technique," Energy and Buildings, vol. 126, 2016, pp. 94-103.

[14] M.W. Ahmad, M. Mourshed, and Y. Rezgui, "Trees vs Neurons: Comparison between random forest and ANN for high-resolution prediction of building energy consumption," Energy and Buildings, July 2017:, pp. 77-89.

[15] L.E. Eberly, "Multiple linear regression," Topics in Biostatistics, Humana Press, 2007, pp. 165-187.

[16] S.S. Haykin, Neural networks and learning machines. Vol. 3. Upper Saddle River, NJ: Pearson, 2009.

[17] N.Z. Zacharis, "Predicting student academic performance in blended learning using Artificial Neural Networks," International Journal of Artificial Intelligence and Applications, vol. 7, no. 5, 2016, pp.17-29

Reducing Smart Microgrid Dependency on the Main Grid using Electric Vehicles and Decentralized Control Systems

R. Jalilzadeh Hamidi[1], T. Ashuri[1], R. H. Kiany[1]

[1]Arkansas Tech University, Russellville, USA, reza.j.hamidi@gmail.com, tashuri@atu.edu, rheidarykiany@atu.edu

Abstract —**This paper proposes a new control system to reduce the power flow at the integration point of DC smart microgrids (SMGs) equipped with non-dispatchable renewable energy resources. The control system is fully decentralized, and it is based on the cooperative control, which requires the minimal communication infrastructure. In the proposed method, plug-in electric vehicles are utilized as distributed energy storage systems to mitigate the power-flow fluctuation. The PEVs start charging in excess of generation, and discharge in generation shortage. The proposed method decreases the dependency of SMGs on the main grid. It also improves the overall power quality in the bulk power systems by minimizing the integration point power-flow fluctuations. The proposed control system is evaluated using Matlab/Simulink. According to the simulation results, the performance of the proposed method is assessed, and its pros and cons are discussed.**

Keywords – Auxiliary Services, cooperative control, electric vehicle, smart microgrid.

I. INTRODUCTION

It has been a while that the use of Distributed Generations (DGs) for supplying Microgrids (MGs) has been practically and theoretically addressed. Renewable-based DGs seem to be more interesting to the community as they are economically and environmentally more beneficial in comparison to non-renewable-based DGs. Renewable energy resources (RESs) are broadly divided into two groups: 1) dispatchable RESs, such as biomass and hydroelectricity. 2) non-dispatchable RESs, also referred to as Variable Renewable Energies (VREs), such as wind and solar.

MGs must be able to supply the loads during both grid-connected and islanding modes [1]. Therefore, the MGs depending on only VREs should be equipped with energy storage systems (ESSs). ESSs are able to store the over-generation, and supply the loads during generation shortage. ESSs are also categorized into lump and distributed ESSs.

As the distributed ESSs (DESSs) are able to improve the power system performance more efficiently compared to ESSs, DESSs seem to be more interesting [2]-[4].

Integration of large shares of VREs leads to the following concerns [5] and [6]: 1) the power grids require to extend for exchanging power in the system. 2) Unpredicted widespread power flows in the grid increases the power loss. 3) An increase in overall ESS capacity is required to suppress the power fluctuations. 4) Degradation of power quality if the power-flow fluctuations are not addressed. In order to mitigate the mentioned issues with VREs, the researchers suggested several methods as follows:

In [7], the application of ESSs for power-flow fluctuation suppression resulted by wind farms is addressed. In that, ESSs are connected to wind farms to reduce the power fluctuation, and a central controller controls ESSs. In [8], an optimal method for DC smart-houses is proposed that decreases the interconnection power-flow fluctuation utilizing a central

control. The central controller governs the charging and discharging of the batteries installed at each house, considering the interconnection power flow as well as the electricity price.

Plug-in electric vehicles (PEVs) are equipped with chargeable batteries. Bidirectional PEV chargers enable the PEVs to provide ancillary services (also referred to as auxiliary services). Thus, a large number of PEVs are able to serve as DESSs. The charging and discharging rates of PEVs can be controlled by central or decentral controllers. As the decentral control systems are cost-effective and require minimal communications [9] and [10], they seem to be a practical choice for SMGs. Moreover, decentral control methods provide integrate-ability and scalability for the systems in a plug-and-play way [11].

Accordingly, in this paper, a distributed control system is proposed to decrease the SMG's dependency on the main grid through reduction of interconnection power-flow fluctuations. The control system is designed for DC SMGs as they seem to be the next generation of SMGs. The proposed control system utilizes the PEVs as DESS as well, considering the proliferation of the PEVs.

The rest of this manuscript is organized as follows: in Section 2, the objectives and design of the proposed control system are described. In Section 3, the test case and simulation results are presented and discussed. Finally, in Section 4, the conclusion is presented.

II. CONTROLLER DESIGN

In this section, the control system objectives are explained. Then, the control system design is elaborated.

A. Control System Objectives

Fig. 1 shows the schematic of a typical DC SMG with PEVs and VERs. For the PEVs to reduce the power-flow fluctuation at the integration point (the main converter in Fig. 1), the following objectives should be pursued.

A. Minimization of Power-flow between the DC SMG and the Main Grid

For a reduction in the dependency of the SMG on the main grid as well as power-flow fluctuations, the power at the power integration should be ideally zero as $P_{\text{int}} \to 0$, where P_{int} [W] is the power flow at the integration point

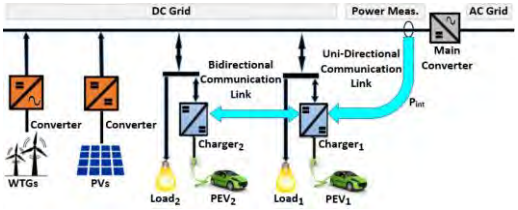

Figure 1. A typical DC SMG with PEVs and VERs.

and '$\to$' denotes that the left side approaches the right side.

B. Fair Discharging Rates

The power rates of PEV chargers are different. Level-1 and Level-2 charger types can charge or discharge at a rate up to 1.4 kW and 6.6 kW, respectively [11]. When the power flows out or into the DC SMG, PEVs start Charging or discharging at different rates proportional to their capacities. We call this concept "Fair Charger Rates" based on [11], in that the ratios of the preferred inputs or outputs of the chargers to their capacities are identical after the system becomes steady [11]. This concept can be shown mathematically as,

$$\frac{P_1}{P_{Ch_1}} = \frac{P_2}{P_{Ch_2}} = \ldots = \frac{Pi}{P_{Ch_i}}, \forall i = 1,2,\ldots,\text{m} \qquad (1)$$

where Pi is the desired charging or discharging rate of the i-th charger in watts. P_{Ch_i} [W] is the i-th charger capacity with respect to its type, and m indicates the number of the chargers in the power grid.

C. Minimum State of Charge

PEV owners will be reluctant to provide ancillary services if that restricts them from using their PEVs. Therefore, care must be taken that no PEV discharges to less than the minimum required charge by providing ancillary services. The proposed control system secures the states of charges (SoC) of PEVs not to become less than a minimum SoC ($SoC^{\min}$) by contributing in ancillary services. PEV owners select the $SoC^{\min}$ of their PEVs according to the distance they expect to drive. This objective is mathematically expressed as,

$$P_{o_i} = -P_c \; if \quad SoC_i < SoC_i^{\min}, \forall i = 1,2,\ldots,\text{m} \quad (2)$$

where P_{oi} [W] is the i-th charger's actual output power and $SoC_i^{\min}$ [%] is the minimum acceptable SoC for the i-th PEV. With respect to (2), any PEV whose $SoC < SoC^{\min}$ continues charging at its charger capacity and does not provide ancillary services.

B. Control System Design

1) Control System Requirements

As the first objective of the system is to minimize the power flow through the main converter, a directional power measuring device is necessary to be installed at the integration point as shown in Fig. 1

2) Local Controllers

A local controller should be installed on each charger to control its charging and discharging rates based on the PEVs parameters, neighbor charger's rates, and the possibly the power measured at the integration point (P_{int}), as depicted in Fig. 2. It is enough that at least one of the local controllers receives P_{int} . The state-space representation of the proposed control method is

$$\begin{cases} \dot{x} = -Lx + Bu & \text{(3.a)} \\ P_o = h\left(x, S_oC, S_oC^{\min}, P_{ch}\right) & \text{(3.b)} \end{cases}$$

where (3.a) is the state equation [11], $X = [x_1, x_2, \ldots, x_i]$ is the state vector, and the states are defined as $x_i = \frac{Pi}{P_{Ch_i}}, \forall i$ as described in (1). $B = [b_1, b_2, \ldots, b_i]$ is the input vector, with reference to Fig. 1, $b_i = 1$ if the i-th charger receives the control signal, otherwise $b_i = 0$. $u = P_{\text{int}}$ [W]. In (3.b), which is the output equation, $SoC = [SoC_1, SoC_2, \ldots, SoC_i]$ is the vector of SoCs, $SoC^{\min} = \left[SoC_1^{\min}, SoC_2^{\min}, \ldots, SoC_i^{\min}\right]$ is the vector of the minimum SoCs that PEV owners determine, $P_{ch} = [P_{ch1}, P_{ch2}, \ldots, P_{chi}]$ is the charger capacities vector, $P_o = [P_{o1}, P_{o2}, \ldots, P_{oi}]^T$ is the actual charger output vector. The output function, $h(.)$, determines the actual charger outputs, considering the SoC and $SoC^{\min}$ of the PEVs. The output function is described in Table I. $L = [l_{ij}]$ is the Laplacian matrix, which is defined as **Error! Reference source not found.** [11],

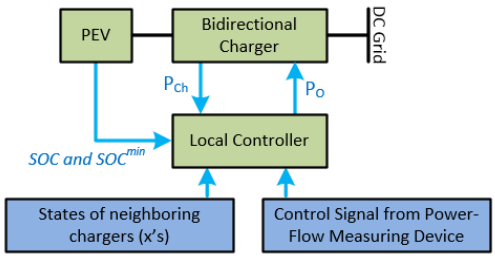

Figure 2. Diagram of the local controllers.

TABLE I. THE DEFINITION OF THE OUTPUT FUNCTION

if ($SoC_i < SoC_i^{\min}$)
  $P_{o_i} = -P_C$; (Charging)
elseif ($SoC_i > SoC_i^{\min}$)
  $P_{o_i} = P_{Ch_i} \times x_i$; (Providing ancillary services)
else $P_{o_i} = 0$; (Charger is Idle)
endif

$$l_{ij} = \begin{cases} -1, j \in N_i \\ |N_i|, j = i \\ 0, else \end{cases} \quad (5)$$

where N_i is the set of the chargers neighbor to the i-th charger. $|N_i|$ is the in-degree of the i-th charger. The states (x) are updated through an integrator (PI) in the local controllers as,

$$x_i = G_i \int \dot{x}_i \, dt, \forall i = 1,2,\ldots,m \quad (6)$$

where G_i is the i-th integrator gain.

III. TEST CASE

Fig. 3 depicts the test-system one-line diagram. Two PEVs along with bidirectional chargers are connected to the system. Two loads continuously consume 8 kW in total. The parameters of the test case are provided in Table II based on [13]. Chargers 1 and 2 are assumed to be Level-2 and Level-1, respectively. The system is equipped with VERs as follows: two Wind Turbines (WTGs) and one Photovoltaic (PVs). Their generation patterns are based on [14] and [15] and shown in Fig. 4. The communication system frequency is 10 Hz meaning that the chargers exchange the data 10

times per second. The system is normally functions and both PEVs are charging. In all the scenarios, it is assumed that the WTGs and PVs disconnect at t = 1 and t = 3 s as Fig. 4 shows.

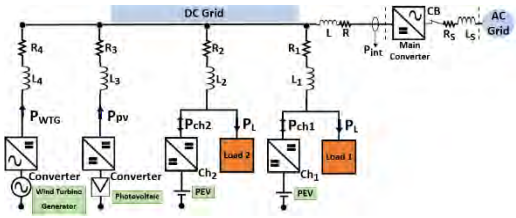

Figure 3. One-line diagram of the test case.

TABLE II. THE PARAMETERS OF THE TEST CASE

Symbol	Description	Value
L_s	Main Grid Inductance	86 μH
R_s	Main Grid Resistance	2.38 $m\Omega$
R,R_1,R_2	200-m Cable Segment	19.8 $m\Omega$
L,L_1,L_2	200-m Cable Segment	109.5 μH
V_{DC}	DC Grid Voltage	400 V
P_{ch1}	Charger Capacity (Level 2)	6.6 kW
P_{ch2}	Charger Capacity (Level 1)	1.4 kW
P_{L1}	Load 1	4 kW
P_{L2}	Load 2	4 kW
SoC_1	Minimum Required SoC	50%
SoC_2	Minimum Required SoC	50%

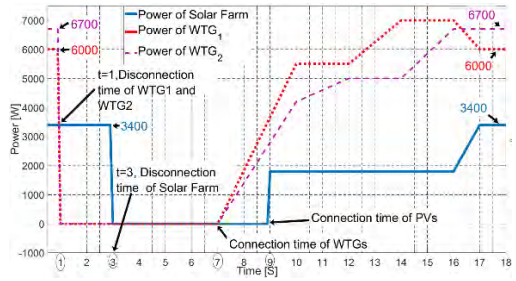

Figure 4. The output powers of VERs.

However, different $SoC^{\min}$ for the PEVs are considered in the scenarios. Two scenarios using Matlab/Simulink are provided as follows:

• Scenario 1: in this scenario, the $SoC^{\min}$ of both the PEVs are 25% ($SoC_1^{\min}=25\%$ and $SoC_2^{\min}=25\%$). Therefore, SoC_1 and SoC_2 are both larger than $SoC^{\min}$ as given in Table II. As Fig. 4 shows, for $t<1$ s total renewable generation is 16.1 kW (WTG-based, 12.7 kW; PV-based, 3.4 kW). As the total consumption is 16 kW, therefore, 56 W passes the main converter from the DC SMG to the main grid (-56 in Fig. 5(a) indicates that the direction of power is to the main grid) and the loss is 44 W. The loss is relatively high, and it is caused by the grid, charger losses, and the power-electronic

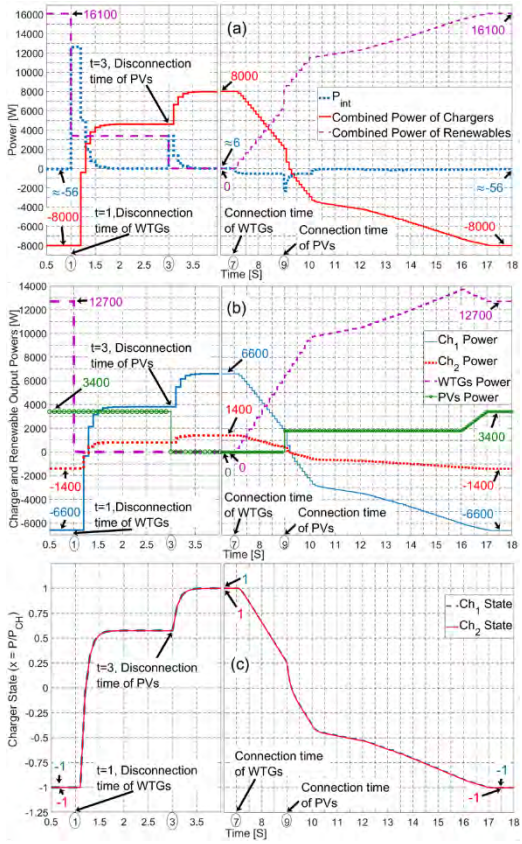

Figure 5. (a) Power transfer between the main grid and DC SMG, PEV and VER outputs. (b) The output powers of PEVs, VERs, and the power at the integration point. (c) The charger states.

interfaces of the PVs and WTGs. As Fig. 4(a) depicts, for $1<t<3$ s, WTG-based generation is zero, and therefore, the missing 12.7 kW is compensated by the main grid (+12.7 kW in Fig. 5(a)). However, the PEVs start discharging to reduce P_{int} as Fig. 4(c) depicts. At $t=3$ s, the PVs become disconnected. Then, again P_{int} becomes 3.4 kW and the discharging rates of the PEVs increases, as Fig. 5(c) shows, after a short time, the PEVs supply the loads as shown in Figs. 4(a) and 4(b). For $t>7$ s WTG-based generation increases as Figs. 4(a) and 4(b) show. Thus, the discharging rates of PEVs decreases as depicted in Fig. 4(c). At $t=9$ s the PVs are reconnected to the DC SMG, and the total VER

generation again becomes 16.1 kW, and finally, both PEVs charge at their nominal capacities as shown inn Figs. 4(a) and 4(b). Fig. 4(c) shows the states of the chargers that vary with the same pattern between -1 to 1 in line with "Fair Charger Rates".

• Scenario 2: all the assumptions for Scenario 1 and this scenario are identical except for $SoC_2^{\min}$, which is 75%. Therefore, it is expected that Charger 2 continues charging PEV_2 during the simulation regardless of the outage of the WTGs and PVs. The sequence of the events are the same as Scenario 1. Fig. 6(a) shows the disconnection of the WTGs at $t=1$ s, however, only as Figs. 6(b) and 6(c) show, only the first PEV reduces its charging rate and starts discharging for partially compensation of the generation shortage. The combined charger powers becomes 5.2 kW ($-1.4+6.6=5.2$ kW). As shown in Fig. 6(b) P_{int} becomes negligibly larger than 2809 W, covering the loads and charger's demand as well as the system losses. Although Charger 1 power rate varies between -1 and 1 during the simulation, charger 1 power rate is consistently -1 (Fig. 6(c)) showing that it continues charging PEV_2 regardless of power-flow at the integration point. Accordingly, Charger 2 does not provide ancillary services as its SoC is less than the minimum desired SoC.

IV. Conclusion

A new decentral control system based on the cooperative control to reduce the fluctuations of power flow at the integration point of DC smart microgrids (SMGs) is proposed. The method utilizes Plug-in Electric Vehicles (PEVs) as Distributed Energy Storage Systems (DESSs). As the output power of non-dispatchable distributed generation units unpredictably change, the proposed method tunes the power outputs of the bidirectional chargers connected to PEVs to minimize the power-flow passing the integration point.

Matlab/Simulink is utilized for performance of the simulations. According to the simulation results, the proposed method is able to decrease the power fluctuations at the integration point of a DC SMG and the main grid or reduces the dependency of the DC SMG to the main grid. However, as the minimal communication frequency and the links are considered for the simulation results, the long-term power fluctuations are mitigated (dependency reduction) and immediate changes generation are compensated with a delay that, however, to some extent decreases the efficiency of the method in improving power quality in the main grid.

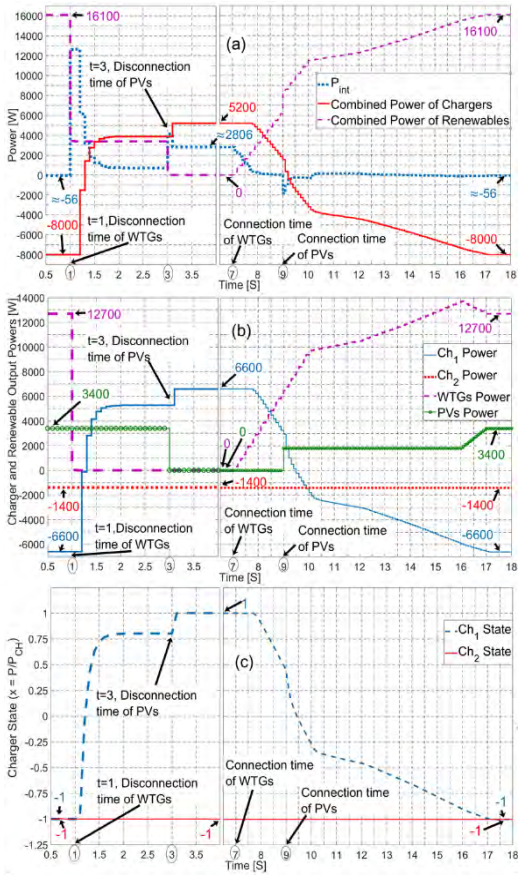

Figure 6. (a) Power transfer between the main grid and DC SMG, PEV and VER outputs. (b) The output powers of PEVs, VERs, and the power at the integration point. (c) The charger states.

References

[1] Microgrid Institute. (2015). *Microgrid Definition*. Available at: http://www.microgridinstitute.org

[2] I. Atzeni, L. G. Ordóñez, G. Scutari, D. P. Palomar, and J. R. Fonollosa, "Demand-side management via distributed energy generation and storage optimization," IEEE Trans. Smart Grid, vol. 4, no. 2, 2013, pp. 866-876.

[3] A. Mohd, E, Ortjohann, A, Schmelter, N, Hamsic, and D. Morton, "Challenges in integrating distributed energy storage systems into future smart grid," ISIE, Cambridge, UK, 2008.

[4] L. Wang, S. Sharkh, A. Chipperfield, and A. Cruden, "Dispatch of vehicle-to-grid battery storage using an

analytic hierarchy process," IEEE Trans. Vehicular Technology, vol. 11, no. 1, 2016, pp. 1-13.

[5] M. A. Delucchi and M. Z. Jacobson, "Providing all global energy with wind, water, and solar power, Part II: reliability, system and transmission costs, and policies," Energy Policy, vol. 39, no. 3, 2011, pp. 1170-1190.

[6] J. Arai, K. Iba, T. Funabashi, Y. Nakanishi, K. Koyanagi, and R. Yokoyama, "Power electronics and its applications to renewable energy in Japan," IEEE Circuits and Systems Magazine, vol. 8, no. 3, 2008, pp. 52-66.

[7] K. S Kook, K. J. McKenzie, Y. Liu, S. Atcitty, "A Study on applications of Energy Storage for the wind Power Operation in Power Systems," IEEE PES-GM, Montreal, Canada, 2006, pp. 1-5.

[8] K. Tanaka, K. Uchida, K. Ogimi, T. Goya, A. Yona, T. Senjyu, T. Funabashi, and C. Kim, "Optimal Operation by Controllable Loads Based on Smart Grid Topology Considering Insolation Forecasted Error," IEEE Trans. Smart Grid, vol. 2, no. 3, 2011, pp. 438-444.

[9] R. Jalilzadeh Hamidi, H. Livani, S. H. Hosseinian, and G. B. Gharehpetian, "Distributed cooperative control system for smart microgrids," EPSR, vol. 130, 2016, pp. 241-250.

[10] C. Wu, H. Mohsenian-Rad, and J. Huang, "Smart grid communications and networking," Cambridge University Press, 2012.

[11] R. Jalilzadeh Hamidi and H. Livani, "Myopic real-time decentralized charging management of plug-in hybrid electric vehicles," Electric Power Systems Research, vol. 143, 2017, pp. 522-532.

[12] R. Jalilzadeh Hamidi, R. Heidarykiany, and T. Ashuri, "Decentralized control system for electric vehicles in islanded DC smart grids," IEEE ISGT, Washington DC, VA, Feb. 2019, in press.

[13] M. Tabari and A. Yazdani, "Stability of a dc distribution system for power system integration of plug-in hybrid electric vehicles," IEEE Trans. Smart Grid, vol. 5, no. 5, 2014, pp. 2564- 2573.

[14] V. A. Kleftakis, D. T. Lagos, C. N. Papadimitriou, and N. D. Hatziargyriou, "Seamless transition between interconnected and islanded operation of DC Microgrids," IEEE Trans. Smart Grid, vol. PP, no. 99, 2017, pp. 1-1.

[15] P. Kou, D. Liang, and L. Gao, "Distributed coordination of multiple PMSGs in an islanded DC microgrid for load sharing," IEEE Trans. Energy Convers., vol. 32, no. 2, 2017, pp. 471-485.

The Effect of Solar Radiation on the Ampacity of an Underground Cable with XLPE Insulation

Dardan Klimenta[1], Miroljub Jevtić[1], Jelena Klimenta[2], Bojan Perović[1]

[1]University of Priština in Kosovska Mitrovica, Kosovska Mitrovica, Serbia,
dardan.klimenta@pr.ac.rs, miroljub.jevtic@pr.ac.rs, bojan.perovic@pr.ac.rs
[2]Independent Consultant in the Field of Urban and Spatial Planning, Niš, Serbia,
klimenta.jelena@gmail.com

Abstract— **The main purpose of this paper is to quantify the thermal effect of solar radiation on the ampacity of a low voltage underground cable with cross-linked polyethylene (XLPE) insulation. The quantification was performed for different laying depths of the cable, different colors of the upper surface of the pavement above the cable, different dimensions of the cable bedding, various load currents, various solar irradiances and different periods of the year. Simulation results were obtained using the finite element method in COMSOL and were compared with the corresponding experimental data. It was found that the ampacity of the XLPE-cable installed at a standard depth of 0.7 m can be increased up to 25.6 % in summer and up to 10.2 % in winter compared to the corresponding base cases.**

Keywords— ampacity, finite element method (FEM), heat transfer, power cable, solar radiation

I. INTRODUCTION

The thermal effect of the Sun on underground power cables is becoming more important with the overall average rise in temperature of the Earth's surface (and atmosphere) due to climate change. During the summer months, the electricity consumption for air conditioning of residential and business premises is growing with the increase in ambient temperature. Accordingly, solar heating of soils reduces the ampacity of underground cable lines, and the increase of electricity consumption reduces their power availability. In addition, the thermal effect of the Sun on underground power cables is more pronounced at lower laying depths.

The relevant standards [1-3] do not take into account the thermal effect of the Sun on the ampacity of underground power cables. The number of research papers dealing with this effect is small. All of these papers were written by Klimenta et al. [4-6]. In addition to this, there are researchers who found that solar radiation only affects the cables laid at law depths [7], and researchers who concluded that the effect of the Sun can not be ignored in the case of cables under dynamic loading [8-10].

In this paper, it is shown how the solar heating affects the ampacity of an underground XP-00 4×16 mm^2 0.6/1 kV cable through five different cool pavements at laying depths of 0.4, 0.7 and 1 m where this effect is significant. It is assumed that the three-phase system is balanced, that the heat flux vanishes at a reference distance, and that the 0.5-m-wide cable trench is covered with a cool pavement [4]. The following two cases are considered herein. The first is that the cable is installed in the bedding of standard size. The second is that the cable is installed in the trench completely filled with bedding material. Some simulation results are obtained for known laboratory conditions, for the most unfavourable summer conditions and for the most common winter conditions. The results are generated so that they can be easily compared with the results from [4]. A solid experimental background is provided as well. The XP-00 4×16 mm^2 0.6/1 kV cable considered herein corresponds to the N2XY type in accordance with the DIN VDE standards.

ISBN: 978-86-80616-03-2

II. EXPERIMENTAL BACKGROUND

The apparatus, procedure, materials and measurement results that were used as an experimental background for this paper are described in detail in [4-6]. In [4-6], the following experiments were conducted: (i) with pavement made of concrete blocks, (ii) with concrete-pavement coated with acrylic white paint, and (iii) with concrete-pavement coated with acrylic black paint. The reference [4] gives experimental data obtained for the cases where the specified control temperature was fixed at 51, 56 and 61 °C, while the references [5,6] provide data obtained for the cases where this temperature was 66 and 71 °C.

Within the experimental apparatus described in [4-6], the temperature was measured at several points. In this paper, for the purposes of comparing the simulation results with the experimental data from [4-6], the following three points are singled out: A – on the outer surface of the physical model of the cable, B – on the lower surface of the pavement above the physical model of the cable, and C – on the upper surface of the pavement above the physical model of the cable. The temperature at point A was obtained by averaging the measured values at three different points along the physical model of the cable, while the temperatures at points B and C were measured directly. Points A, B, and C are marked within the small-size computational domain, which will be used for numerical simulations in COMSOL. This domain is shown in Fig. 1.

III. 2D FEM-BASED HEAT CONDUCTION MODEL

A two-dimensional (2D) FEM-based heat conduction model is created based on the following equation [4]:

$$\frac{\partial}{\partial x}\left(k\frac{\partial T}{\partial x}\right)+\frac{\partial}{\partial y}\left(k\frac{\partial T}{\partial y}\right)+Q_v=0\,, \qquad (1)$$

where k is the thermal conductivity in W/(m·K); T is the temperature in K; x, y are Cartesian spatial coordinates in m; and Q_v is the volume power of heat sources in W/m^3.

The XP-00 4×16 mm^2 0.6/1 kV cable is modelled by an equivalent construction composed of the four round copper conductors, 0.7-mm-thick core insulations of XLPE, 1.7-mm-thick layer of unvulcanised rubber under the outer sheath and 1.8-mm-thick outer polyvinyl-chloride (PVC) sheath with outer diameters 4.8, 6.2, 18.4 and 22 mm, respectively. In addition, it is assumed that the core insulations and some filling (of unvulcanised rubber) between and around these core insulations represent one object (i.e. block) having the same thermal conductivity as XLPE. Moreover, it is assumed that the 1.7-mm-thick cylindrical layer of unvulcanised rubber has the same thermal conductivity as PVC. The cross-section of this equivalent cable construction is shown in Fig. 1. Fig. 2 presents the large-size computational domain for the case when the cable is laid in the bedding of a standard size 0.5 m × 0.4 m.

In order to increase the mesh density within and around the blocks with heat sources, in both domains, the surface layers of all conductors were modelled by hollow cylinders having thicknesses of 0.4 mm. In addition, in order to ensure the mesh independence, the temperatures of the phase conductors and the load current were tracked. The numbers of nodes and elements were varied from the numbers of nodes and elements corresponding to automatic mesh generation to the numbers of nodes and elements corresponding to mesh refinement, respectively. The differences between the temperatures obtained using different meshes were lower than 0.002 °C for the small-size computational domain and lower than 0.03 °C for the largre-size computational domain. Accordingly, meshes with the number of nodes corresponding to automatic mesh generation were used. Table I deals with the details relating to meshes generated in the considered computational domains, as well as mesh independence tests performed on them.

The volume power of heat sources in the phase conductors with a diameter of d_1=0.0048 m and with a geometric cross-section area of $S'_c = 18.096\cdot10^{-6}$ m^2 is

$$Q_v = \frac{R_{ac}(T_{cp})}{S'_c}\cdot I^2\,. \qquad (2)$$

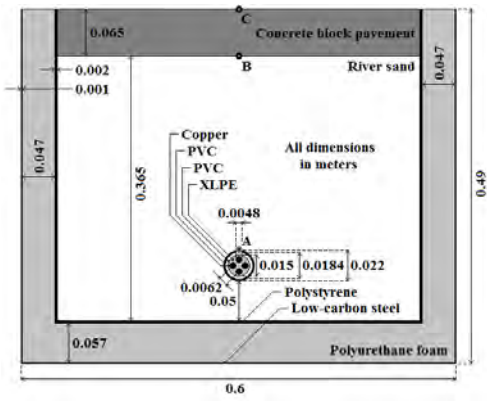

Figure 2. Presentation of the small-size computational domain corresponding to the experimental apparatus.

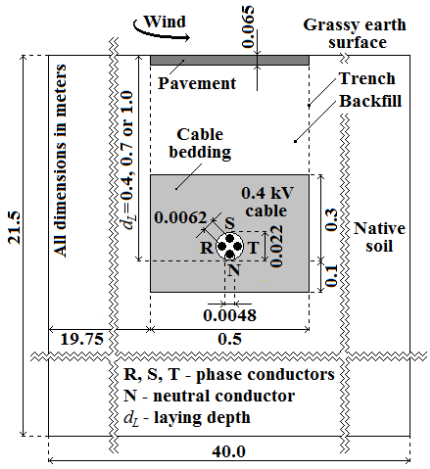

Figure 1. Presentation of the large-size computational domain.

TABLE I. DETAILS ON FINITE ELEMENT MESHES AND MESH INDEPENDENCE TESTS

Domain	Finite element mesh				Temp. differences
	Automatically generated		After refinement		
	No. of nodes	*No. of elements*	*No. of nodes*	*No. of elements*	°C
Small	15146	29101	59392	116404	<0.002
Large, with d_L=0.4 m	1776	3459	7010	13836	<0.03
Large, with d_L=0.7 m	1739	3399	6876	13596	<0.01
Large, with d_L=1 m	1758	3438	6953	13752	<0.02

where $R_{ac}(T_{cp})=R_{20}\cdot(234.5+T_{cp})/254.5=1479.057\cdot10^{-6}$ Ω/m is the a.c. resistance per unit length of a single copper conductor at temperature T_{cp}=90 °C, $R_{20}=1.16\cdot10^{-3}$ Ω/m is the a.c. resistance per unit length of a single copper conductor measured at 20 °C, T_{cp} is the continuously permissible temperature of the XLPE-cable in °C, and I is the cable load current (or cable ampacity when $I=I_{cp}$) in A. In addition, there are no heat sources in the neutral conductor and XLPE insulation [1,4].

From an engineering point of view, it is customary to consider the ampacity I_{cp} for known laboratory conditions, the most unfavourable summer conditions and the most common winter conditions. All these conditions, thermal conductivities of all used materials, boundary conditions and assumptions are the same as in [4]. Therefore, in order to leave more space for the results and discussion, as well as to avoid a repetition of the data, all these details will not be listed here.

IV. RESULTS AND DISCUSSION

A. Validation of the Model

Results obtained by simulating the temperature distribution over the small-size computational domain in Fig. 1 for the known laboratory conditions [4] are listed in Table II. For the small-size domain, a sequence of simulations is carried out with white, grey and black pavement surfaces.

When the simulation results from Table II are compared with the corresponding measurement data from [4-6], observations indicating a satisfactory level of accuracy on account of the model used in this paper can be made. The observations are similar to the ones from [4]. The only differences are that the continuously permissible temperature of the considered XLPE-cable is T_{cp}=90 °C and that the results from Table II corresponds to this temperature.

B. Numerical Results

In order to generalise the results presented in the previous subsection, the large-size domain in Fig. 2 was created. Temperature distributions over this domain are calculated for the following two cases: I – the cable is installed in the bedding of standard size, and II – the cable is installed in the trench completely filled with bedding. For each of these cases, a sequence of simulations is performed with the laying depth d_L=0.4 m and with cool white coating, acrylic white paint, uncoated concrete blocks, uncoated asphalt and acrylic black paint.

TABLE II. SIMULATION RESULTS OBTAINED FOR THE LABORATORY CONDITIONS

Pavement surface			Temperature							Q_v	I
Color	*Absorptivity,* α	*Emissivity,* ε	Phase conductors	Cable's outer surface		Pavement					
						Lower surface		Upper surface			
	–	–		*Sim* *	*Diff* *	*Sim* *	*Diff* *	*Sim* *	*Diff* *	W/m^3	A
			°C	°C	°C	°C	°C	°C	°C		
White	0.26	0.9	56.2	50	-1.4	25.12	-0.28	24.29	-0.11	242410	54.46
Grey	0.56	0.94	56.21	50	-1.3	25.11	+0.31	24.27	+0.57	242540	54.47
Black	0.97	0.91	56.2	50	-1.7	25.12	-1.38	24.28	-1.42	242440	54.46
White	0.26	0.9	62.35	55	-1.3	25.52	-0.38	24.52	-0.78	287310	59.29
Grey	0.56	0.94	62.36	55	-0.7	25.49	+1.39	24.5	+1.0	287450	59.3
Black	0.97	0.91	62.35	55	-1.4	25.51	-1.39	24.52	-1.48	287360	59.29
White	0.26	0.9	68.5	60	-1.1	25.91	+1.01	24.76	+1.26	332200	63.75
Grey	0.56	0.94	68.51	60	-0.6	25.88	+1.68	24.73	+1.23	332390	63.77
Black	0.97	0.91	68.5	60	-1.0	25.9	-0.9	24.75	-1.15	332250	63.76
White	0.26	0.9	74.65	65	-0.9	26.3	-0.6	25.0	-1.2	377100	67.92
Grey	0.56	0.94	74.66	65	-0.2	26.27	+1.47	24.97	+1.17	377310	67.94
Black	0.97	0.91	74.65	65	-0.8	26.29	-1.01	24.99	-1.31	377150	67.93
White	0.26	0.9	80.79	70	-0.9	26.69	-0.21	25.24	-0.66	421960	71.85
Grey	0.56	0.94	80.8	70	-0.3	26.66	+2.06	25.2	+1.6	422200	71.87
Black	0.97	0.91	80.8	70	-0.7	26.69	-0.41	25.23	-0.67	422070	71.86

* "Sim" denotes the simulated value, while "Diff" denotes the difference between the simulated and experimental values.

The thermal conductivities of all used materials are given in [4-6], while the radiation properties of pavement surfaces are outlined in Table III.

For the two cases relating to the large-size domain (Fig. 2), values for Q_v and I_{cp} are selected in such a manner so that they correspond to radiation properties of the acrylic black paint α=0.97 and ε=0.91, thermal conductivity of the concrete blocks k=1.3 W/(m·K) and continuously permissible temperature of the cable T_{cp}=90 °C, as follows: Q_v=448340 W/m^3 and I_{cp}=74.1 A – for the case I; and Q_v=445940 W/m^3 and I_{cp}=73.9 A – for the case II. The remaining input parameters are constant and can be found in [4]. The temperatures of the pavement, cable's outer surface and S-phase conductor which are obtained by simulations of the temperature distribution over the large-size domain are given in Table III.

Based on the results presented in Table III, it can be seen that the temperatures of the pavement, cable's outer surface and S-phase conductor decrease with decreasing the absorptivity-to-emissivity ratio α/ε. The same applies in both cases related to Fig. 2. This means it is possible to increase the ampacity by selecting a coating, paint or material with a lower value of the ratio α/ε. The phenomenon will be quantified later in this section. From Table III it can, also, be seen that the thermal effect of solar radiation increases by increasing the size of the cable bedding.

Fig. 3 presents the effect of the ratio α/ε on the temperature distribution over the part of the domain from Fig. 2 that represents the cable trench. It can be seen from these temperature distributions that, when the cool pavement with low α/ε ratio (according to [4-6], lower than 0.6) is applied, the temperature gradients within the cable, bedding and native soil are lower. This agrees with the observation derived from Table III. Hence, the heat is conducted in a more efficient manner from the cable to the cool pavement surface.

TABLE III. EFFECT OF PAVEMENT SURFACE RADIATION PROPERTIES ON TEMPERATURES OF PAVEMENT, CABLE'S OUTER SURFACE AND S-PHASE CONDUCTOR FOR THE CASES I AND II RELATING TO THE LARGE-SIZE DOMAIN IN FIG. 2

Material, coating or paint	Surface radiation property		Case I			Case II		
			Temperature			Temperature		
	Absorptivity, α	*Emissivity,* ε	*Pavement surface*	*Cable's outer surface*	*S-phase conductor*	*Pavement surface*	*Cable's outer surface*	*S-phase conductor*
	–	–	°C	°C	°C	°C	°C	°C
Cool white coating	0.15	0.9	20.5	52.5	64.1	21	50.8	62.3
Acrylic white paint	0.26	0.9	27.7	56.3	67.9	28.1	54.9	66.4
Concrete blocks	0.56	0.94	45	65.5	77	45.2	64.7	76.1
Asphalt	0.87	0.93	63.3	75.3	86.6	63.2	75.1	86.4
Acrylic black paint	0.97	0.91	69.7	78.7	90	69.5	78.8	90

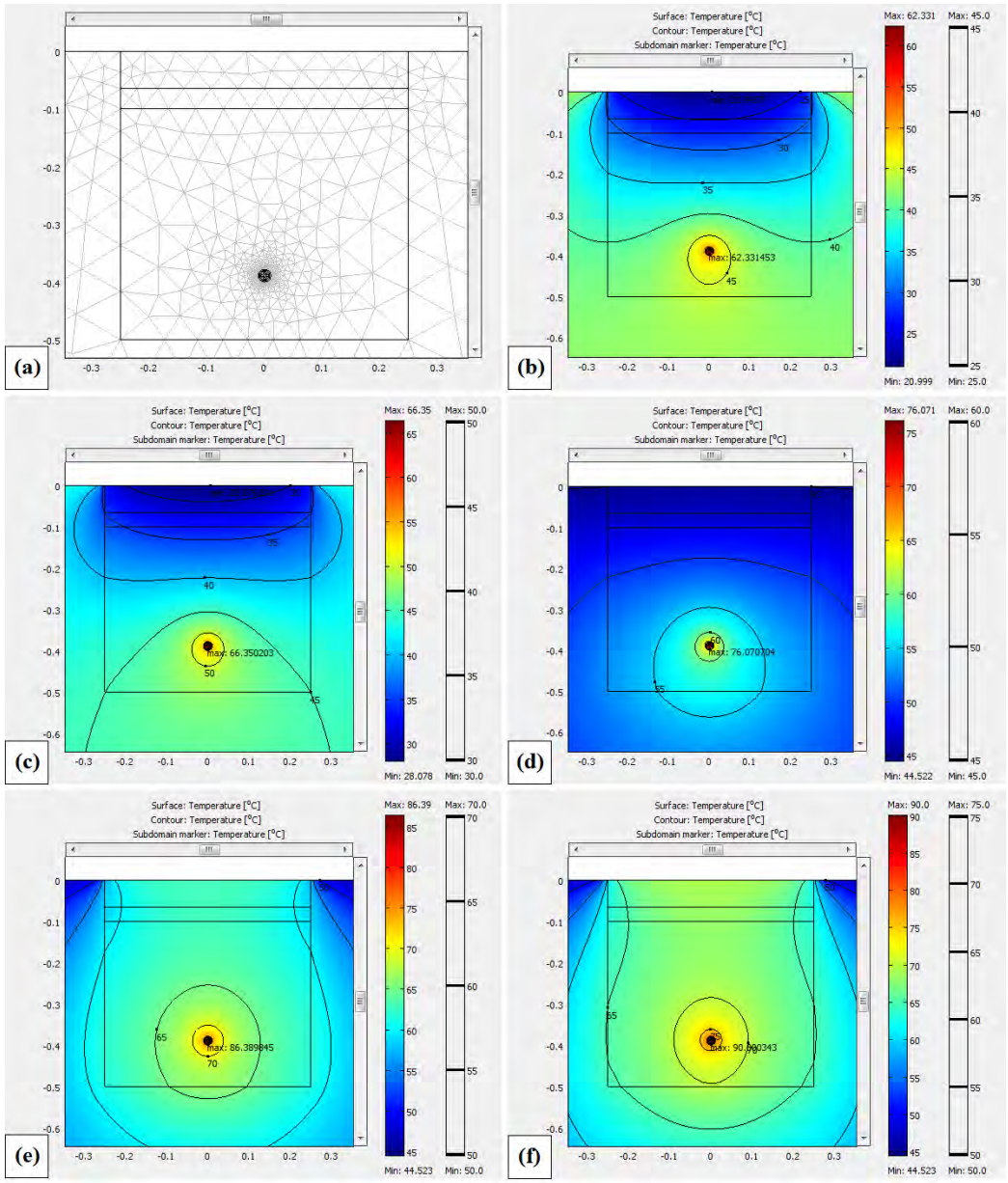

Figure 3. Temperature distribution over (a) the part of the computational domain from Fig. 2 that represents the cable trench, obtained for the case II when the upper surface of the trench is covered with (b) cool white coating, (c) acrylic white paint, (d) uncoated concrete blocks, (e) uncoated asphalt, and (f) acrylic black paint.

For the XP-00 4×16 mm^2 0.6/1 kV cable at reference operating conditions (laying depth 0.7 m, soil temperature at laying depth 20 °C and thermal conductivity of the soil 1 W/(m·K)), the ampacity making the temperature of the cable construction elements 90 °C equals 111 A [11]. The same ampacity can also be obtained numerically using the large-size model associated with Fig. 2 and a complete set of reference operating conditions. The complete set of reference operating conditions consisted of the following: laying depth 0.7 m, reference soil temperature 20 °C (at the boundaries positioned on the left-hand, right-hand and bottom side of the large-size domain), thermal conductivity of the native soil, cable bedding, backfill and pavement 1 W/(m·K), temperature of the air contacting the earth surface T_a=293.7 K, heat transfer coefficient due to convection

h=7.382 W/(m^2·K) obtained using the empirical correlation $h = 7.382 + 1.925 \cdot v_a^{0.75}$ for a wind velocity of v_a=0 m/s [4], thermal emissivity of the earth surface ε=0 and solar absorptivity of the earth surface α=0. Based on this FEM-based simulation, it is evident that the IEC-based procedure from [1] completely ignores the earth surface radiation properties and that the ampacity (I_{cp}=111 A) obtained for the standard reference operating conditions is about 1.5 times larger than the ampacities (I_{cp}=74.1 A and I_{cp}=73.9 A) obtained for the most unfavourable summer conditions.

Fig. 4 shows the temperatures of the S-phase conductor depending on the load current for laying depths of 0.4 m, 0.7 m and 1 m and for white, grey and black pavement surfaces. Fig. 4a corresponds to the case when the cable is laid in the bedding of size 0.5 m × 0.4 m, while Fig. 4b corresponds to the case when the trench is completely filled with bedding material.

Figs. 4a and 4b show that the installation of the cable closer to the earth surface increases the load current for the white and grey pavement surfaces and decreases the load current for the black pavement surface. This applies to a temperature range up to about 81 °C. In the range from about 81 °C up to T_{cp}=90 °C, the installation of the cable closer to the earth surface increases the load current and ampacity for all three considered colors. For the temperatures up to about 81 °C, the results obtained for all three considered surfaces are in agreement with those reported in [4].

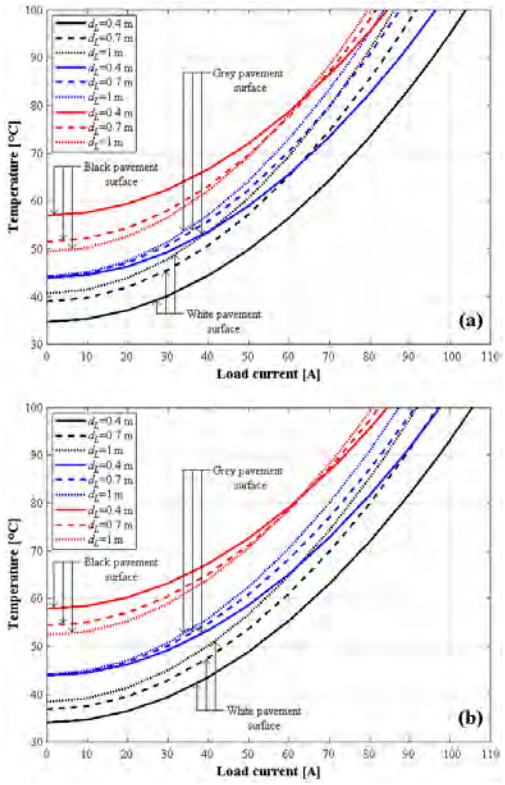

Figure 4. Temperature of the S-phase conductor versus load current for different laying depths and pavement surfaces: (a) bedding having dimensions 0.5 m × 0.4 m, and (b) trench completely filled with bedding material.

The ampacity values relating to a laying depth of 0.4 m and the white, grey and black pavement surfaces are, respectively, 95.7 A, 87.5 A and 74.1 A – according to Fig. 4a, and 97.2 A, 88.4 A and 73.9 A – according to Fig. 4b. When the cable is laid at a depth of 0.7 m, the ampacity values corresponding to the white, grey and black pavement surfaces are, respectively, 83.7 A, 79.4 A and 72.8 A – according to Fig. 4a, and 88.9 A, 82.7 A and 72.9 A – according to Fig. 4b. The ampacity values relating to the cable installed in the bedding of standard size at a depth of 1 m are 78.7 A, 75.8 A and 71.4 A for the white, grey and black pavement surfaces, respectively. When the cable is laid in the trench completely filled with bedding at a depth of 1 m, the ampacities corresponding to the white, grey and black pavement surfaces are 84 A, 79.2 A and 71.8 A, respectively. In addition, it can be observed that a completely filled trench does not contribute to the increase of cable ampacity only for the black pavement surface, because in this case the bedding material provides a better conductive path for the solar heat from the earth surface to the cable.

Standard procedures for calculation of the ampacity of underground cable lines do not take into consideration the effects of solar irradiance and earth surface radiation properties [1-3]. The effect of variation in solar irradiance on temperatures of underground cable conductors will be discussed in this and the next paragraph. Temperatures of the S-phase conductor are calculated for the different solar irradiances and white, grey and black pavement surfaces, at each of laying depths, by considering the load current values that make the temperature of the S-phase conductor 90 °C as constant value. As shown in Fig. 5, the decreasing solar irradiance contributes to the cooling of the S-phase conductor of the cable. In this case, the

temperature of the S-phase conductor will reduce and there will be a significant increase in the ampacity. This applies to the other two phase conductors as well.

A value of 500 W/m^2 is taken as typical of the average solar irradiance on a clear day. By taking into account this solar irradiance and Fig. 5a, the temperature of the S-phase conductor of the cable installed in the bedding of standard size at depths of 0.4 m, 0.7 m and 1 m will decrease respectively by 13 °C, 14.3 °C and 14.7 °C – for the white pavement surface, 17.5 °C, 16.8 °C and 16.5 °C – for the grey pavement surface, and 23.3 °C, 20 °C and 18.7 °C – for the black pavement surface. These decreases for the cable installed in the bedding of standard size at depths of 0.4 m, 0.7 m and 1 m mean that the cable can respectively be loaded by 10.7 A, 11 A and 11 A – for the white pavement surface, 15.3 A, 13.4 A and 12.6 A – for the grey pavement surface, and 22.6 A, 16.9 A and 14.9 A – for the black pavement surface.

According to Fig. 5b, similar results are

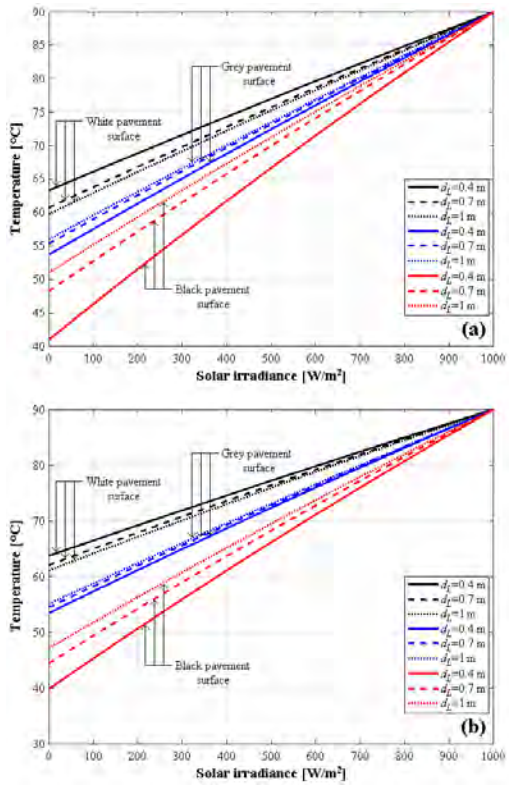

Figure 5. Temperature of the S-phase conductor versus solar irradiance for different laying depths and pavement surfaces: (a) bedding having dimensions 0.5 m × 0.4 m, and (b) trench completely filled with bedding material.

obtained when the cable trench is completely filled with bedding material. Therefore, it is clear that the installation of the cable closer to the earth surface increases the ampacity for the grey and black pavement surfaces. For the white pavement surface, the cable ampacity remains almost constant at 11 A.

In order to determine the cable ampacity I_{cp}, simulations of temperature distribution in the cases I and II at a depth of 0.7 m were performed with the most unfavourable summer conditions and the most common winter conditions, as well as with the radiation and thermal properties (α, ε and k) of the previously selected pavement surfaces and materials (Table III). The values for Q_v are gradually increased or decreased from arbitrary prescribed initial values to their values corresponding to T_{cp}=90 °C. Then, these values for Q_v and (2) are used to calculate the values of I_{cp}. The values of Q_v and I_{cp} are listed in Table IV.

Based on the quantification of the effects of the ratio α/ε and bedding size on the ampacity of the considered cable, the following can be observed: (i) In comparison with the black concrete-pavement, the other coated or uncoated surfaces can increase the ampacity up to 12.6 A – for the most unfavourable summer conditions and up to 5.2 A – for the most common winter conditions. (ii) The bedding having a size of 0.5 m × 0.735 m can additionally increase the ampacity up to 6 A – for the most unfavourable summer conditions and up to 5.6 A – for the most common winter conditions. Therefore, the ampacity can be increased by 18.6 A in summer and by 10.8 A in winter if the pavement is coated with cool white coating and if the trench is completely filled with the bedding material.

V. CONCLUSIONS

The conclusions that can be drawn from the presented results and discussion of them are:

- The simulated and experimental results are in good agreement.
- Compared to the corresponding cases with the black pavement, the ampacity of the considered cable laid at 0.7 m can be raised up to 25.6 % (or 18.6 A) in summer and up to 10.2 % (or 10.8 A) in winter. These results are obtained by taking into account the effects of the pavement surface radiation properties and bedding size.

TABLE IV. VOLUME POWERS OF HEAT SOURCES AND CABLE AMPACITIES CALCULATED FOR THE LAYING DEPTH OF 0.7 METERS AND DIFFERENT THERMAL ENVIRONMENTS IN SUMMER AND WINTER

Material, coating or paint	Surface radiation property	Results obtained for the most unfavourable summer conditions				Results obtained for the most common winter conditions			
		Case I		*Case II*		*Case I*		*Case II*	
	α/ε	Q_v	I_{cp}	Q_v	I_{cp}	Q_v	I_{cp}	Q_v	I_{cp}
	–	W/m^3	A	W/m^3	A	W/m^3	A	W/m^3	A
Cool white coating	0.167	596590	85.4	682240	91.4	1018540	111.6	1122160	117.2
Acrylic white paint	0.289	572850	83.7	646280	88.9	1005330	110.9	1102250	116.1
Concrete blocks	0.596	515480	79.4	559140	82.7	973160	109.1	1053800	113.5
Asphalt	0.935	454920	74.6	466640	75.6	937180	107.1	999100	110.6
Acrylic black paint	1.066	433540	72.8	433950	72.9	924500	106.4	980110	109.5

- The ampacity of the considered cable was found to increase with decreasing the absorptivity-to-emissivity ratio of the pavement surface, as well as with decreasing the laying depth of the cable (excluding the case of black pavement surface for the range up to about 81 °C).
- All the ampacity values obtained for the laying depth of 0.7 m and the most unfavourable summer conditions are lower than the reference value of 111 A. In addition, for the most common winter conditions, the ampacity values are lower or greater, by 4.6-6.2 amperes, than the reference value of 111 A.
- From the point of view of the solar irradiance, the ampacity of the considered cable increases with decreasing the laying depth in the case of grey or black pavement surface, and stays almost constant with decreasing the laying depth in the case of white pavement surface.
- The results obtained for the XLPE-cable changes according to a law similar to that observed in [4] for a PVC-cable. This should be further investigated in one of the next studies.

ACKNOWLEDGMENT

This paper was based on research conducted within the project TR33046 funded by the Ministry of Education, Science, and Technological Development of the Republic of Serbia.

REFERENCES

[1] International Electrotechnical Commission, IEC 60287-1-1:2006+AMD1:2014 CSV, Electric Cables – Calculation of the Current Rating – Part 1-1: Current Rating Equations (100% Load Factor) and Calculation of Losses – General, 2.1 edition, Geneva, Switzerland, 2014.

[2] International Electrotechnical Commission, IEC TR 62095:2003, Electric cables – Calculations for current ratings – Finite element method, 1st edition, Geneva, Switzerland, 2003.

[3] National Fire Protection Association, NFPA 70, National Electrical Code, 2017 Edition, Quincy, MA, USA, 2016.

[4] D. Klimenta, B. Perović, J. Klimenta, M. Jevtić, M. Milovanović, I. Krstić, "Modelling the thermal effect of solar radiation on the ampacity of a low voltage underground cable," International Journal of Thermal Sciences, Vol. 134, 2018, pp. 507–516.

[5] D. Klimenta, B. Perović, J. Klimenta, M. Jevtić, M. Milovanović, I. Krstić, "Controlling the thermal environment of underground cable lines using the pavement surface radiation properties," IET Generation, Transmission & Distribution, Vol. 12, Issue 12, 2018, pp. 2968–2976.

[6] D. O. Klimenta, B. D. Perović, J. Lj. Klimenta, M. M. Jevtić, M. J. Milovanović, I. D. Krstić, "Controlling the thermal environment of underground power cables adjacent to heating pipeline using the pavement surface radiation properties," Thermal Science, Vol. 22, No. 6A, 2018, pp. 1–16.

[7] L. Lindström, "Evaluating impact on ampacity according to IEC-60287 regarding thermally unfavourable placement of power cables," Masters' Degree Project, Royal Institute of Technology (KTH), Stockholm, Sweden, November 2011, XR-EE-ETK 2011:009.

[8] J. Nahman, M. Tanaskovic, "Calculation of the ampacity of high voltage cables by accounting for radiation and solar heating effects using FEM," International Transactions on Electrical Energy Systems, Vol. 23, Issue 3, 2013, pp. 301–314.

[9] J. Nahman, M. Tanaskovic, "Evaluation of the loading capacity of a pair of three-phase high voltage cable systems using the finite-element method," Electric Power Systems Research, Vol. 81, Issue 7, 2011, pp. 1550–1555.

[10] J. Nahman, M. Tanaskovic, "Calculation of the loading capacity of high voltage cables laid in close proximity to heat pipelines using iterative finite-element method," International Journal of Electrical Power and Energy Systems, Vol. 103, 2018, pp. 310–316.

[11] L. Heinhold, Power Cables and their Application – Part 1, third revised ed., Siemens Aktiengesellschaft, Berlin and Munich, Germany, 1990.

Comparative Analysis of Operating Parameters of Medium-Speed Diesel, Gas Diesel and Gas Engines

Mikhail G. Shatrov[1], Vladimir V. Sinyavski[2], Ivan G. Shishlov[3], Andrey V. Vakulenko[4]

Moscow Automobile and Road Construction State Technical University (MADI), Moscow, Russia
[1]dvs@madi.ru;[2]sinvlad@mail.ru;[3]astra510@yandex.ru;[4]ingener-avto@yandex.ru

Abstract–**Conversion of medium-speed engines to operate on natural gas is a pressing issue because gas is cheaper than oil and combustion of gas in the cylinders of IC engines decreases emissions of pollutants and CO_2. Using gas as fuel for medium-speed engines is especially reasonable because they consume a lot of fuel during their life cycle. Two main methods of conversion of diesel engines were examined: gas engines operating on a lean mixture and gas diesel engines. Comparative analysis of parameters of diesel, gas diesel and gas versions of a medium-speed locomotive engine was carried out using a simulation model developed in MADI calibrated by the results of experimental research of a high-speed diesel and gas diesel engines and medium-speed diesel engine, as well as calculations using a multi-zone model. Transfer from diesel cycle to gas and gas diesel cycles resulted in considerable decrease of fuel consumption and emissions of particles, NO_x and CO_2. Medium-speed gas engine was found to be most suitable for electric energy generation and gas diesel engine – for transport application such as locomotive engine.**

Keywords- diesel engine, gas engine, gas diesel engine, medium-speed engine, engine simulation

I. INTRODUCTION

Conversion of middle-speed engines to operate on natural gas is a pressing issue because gas is cheaper than oil. Today, the price of natural gas in Russia is almost twice lower than of diesel fuel, and the price difference will grow as more oil is produced from hard-to-extract reserves. Using gas as fuel for medium-speed engines is especially reasonable because, in contrast to passenger cars which are used few hours a day, locomotives, large dump-trucks, generator sets and ships often operate 24 hours a day. Therefore medium-speed engines consume a lot of fuel during their life cycle. Combustion of natural gas in the cylinders of IC engines decreases emissions of the main diesel pollutants: soot and nitrogen oxides NO_x. Conversion to natural gas also decreases emissions of carbon dioxide CO_2 and hence the greenhouse effect due to lower content of carbon in methane which composes more than 98% of the Russian natural gas and also due to lower mass consumption of natural gas because the lower caloric value of methane is higher than that of diesel fuel.

Two basic methods of conversion of medium-speed diesel engines to operate on natural gas exist: spark ignition gas engines using a lean gas-air mixture and gas diesel or dual fuel engines.

The main problem of using the gas cycle on medium-speed engines is knock. Its probability grows as the cylinder size and power augmentation ratio increase and when the gas-air mixture is lean. The chance of knock origination also grows at low engine speeds and transient modes. Lean gas-air mixture is required for improvement of fuel efficiency and considerable decrease of NO_x emissions. If air-fuel ratio λ is 1.6-1.7 or higher, the engine may comply with NO_x ecological standards without using ammonia catalyst which lowers its price considerably.

Jenbacher 6th series gas engines for electric power plants using a lean gas-air mixture have the brake mean effective pressure p_e=2.4-2.6 MPa and operate at a high rated speed 1500

ISBN: 978-86-80616-03-2

rpm [1, 2]. For operation on a lean mixture with λ close to 2.0, a prechamber with enriched mixture is used in which the gas fuel is initially ignited by a spark-plug and then the sprays of burning gas inflame the lean mixture in the main combustion chamber. To prevent knock, the Miller cycle is used which additionally improves the effective efficiency η_e up to 49% and decreases emissions of NO_x. A two-stage turbocharging system is mounted to compensate for the loss of filling efficiency caused by early closure of the intake valves in the Miller cycle. This method of conversion is excellent for engines operating at a constant high speed because it prevents knock. Gas engines have less fuel efficiency than gas diesel engines, but in case of stationary application, they may be supplied by gas directly from the pipe lines which, in Russia, is up to four times cheaper than the same gas bought at the gas filling station [3]. But for high boosted transport medium-speed engines working in a wide range of speeds and loads, as well as at transient modes, implementation of this method results in the origination of knock which is very difficult to eliminate.

The first gas diesel engines used traditional fuel feed system with mechanical control. These engines had a relatively low substitution of diesel fuel by gas: the percentage of diesel fuel is 20-30% at full loads, grows at low loads and becomes 100% at idle [4]. The portion of diesel fuel can be decreased in case of using a special fuel supply system designed for small injection rates of diesel fuel [5].

The analyses performed in [6] showed that the need to increase the igniting portion of diesel fuel at low loads is caused by the growth of fuel drops size due to reduction of injection pressure and counterpressure of the working medium in the cylinder. The counterpressure lowers because the boost pressure decreases at low loads. As the size of the fuel drop grows, its ability to ignite the air-gas mixture degrades and one has to inject more diesel fuel at low loads. Situation may be improved if the injection pressure is considerably increased.

This is realized in gas diesel engines with a minimized portion of diesel fuel injected by a high pressure fuel feed system with electronic control (Common Rail, unit-injector, etc.). A high injection pressure, multiple injections and optimal injection timing guarantee good ignition of natural gas by fine atomized diesel fuel sprays which makes it possible to decrease the percentage of diesel fuel to 3-5% at full load and keep it small at low loads and idle [7, 8]. This method ensures a high substitution of diesel fuel by gas and improves significantly engine fuel efficiency and ecological parameters. Though when using the fuel supply system of the base diesel engine, its injectors may overheat because only 3-5% of diesel fuel portion is injected and cooling of the injector nozzles by diesel fuel is poor.

On the basis of the analysis performed, a gas diesel working cycle with minimized portion of diesel fuel injected by a high pressure CR system was selected for the medium-speed locomotive engine as it ensures the best fuel efficiency and low emissions, high percentage of diesel fuel substitution, allows to have a large cylinder size, the engine can be high boosted and operate in a wide range of speeds and loads without limitations related to knock. Medium-speed gas engine with a lean gas-air mixture is the best solution for power generation.

II. Calculation of Parameters of the Diesel/Gas Diesel/Gas Engine

As conversion of diesel engines for operation on natural gas requires expenses including systems of on-board gas transportation, as well as building infrastructure for refueling engines with gas, it is important to estimate how will the fuel efficiency and ecological parameters of the base diesel engine change if it is converted for operation on natural gas by gas cycle and gas diesel cycle. The estimation was made using simulation by the known multi-zone FIRE model of the AVL company and a one-zone model of diesel/gas diesel/gas engine calculation developed in MADI [9].

A. Research object

Calculated comparison of diesel/gas diesel/gas engine parameters was carried out for the medium speed locomotive 6-cylinder in-line D200 engine developed by the Penzadieselmash OAO. For calibration of the one-zone MADI model, engine test results of diesel and gas diesel versions of the 6-cylinder in-line Cummins KAMA high-speed engine with gas feed and electronic control systems developed in MADI were used. Basic parameters of both the engines are given in Table 1: cylinder stroke S, cylinder diameter D,

compression ratio ε, rated break mean effective pressure p_e, rated engine speed n_{rat}.

TABLE 1. PARAMETERS OF TWO ENGINES USED IN THE RESEARCH

Engine	S (mm)	D (mm)	ε	p_e (MPa)	n_{rat} (rpm)
D200	280	200	15.0:1	2.0	1000
Cummins Kama	124	107	17.3:1	1.73	2300

B. Modelling method

The multi-zone FIRE model requires much processor time, it calculates only compression-combustion-expansion processes and needs parameters of the air at the inlet to the cylinder and of the exhaust gases at the outlet from the cylinder as input data. The one-zone model developed in MADI is simple and fast. It gives pretty accurate results if it is properly calibrated by the results of engine tests. The one-zone MADI model calculates the combustion process using the I.Viebe empirical formula for heat release rate which, in its turn, may be calculated by the multi-zone FIRE model. Therefore the following simulation method was used.

1. Calculations of the 4-stroke cycle of diesel/gas diesel/gas versions of the D200 engine by the one-zone MADI model to get parameters of the fresh charge at the inlet to the cylinder and parameters of the exhaust gases at the outlet of the cylinder using the approximate values of heat release rate parameters φ_z and m for the I.Viebe formula

2. Calculations of compression-combustion-expansion processes of diesel/gas diesel/gas versions of the D200 engine by the multi-zone FIRE model to get more precise values of heat release rate parameters φ_z and m for the I.Viebe formula.

3. Calculations of the 4-stroke cycle of diesel/gas diesel/ gas versions of the D200 engine by the one-zone model using more precise values of heat release rate parameters φ_z and m for the I.Viebe formula.

Calculations of diesel, gas diesel and gas versions of the D200 engine were made for the rated mode n=1000 rpm, p_e=2.0 MPa at optimal by fuel efficiency ignition advance angle. Compressor and turbine maps of the turbocharger mounted on the D200 diesel engine were used.

C. Model calibration using experimental results

The one-zone MADI model was calibrated by results of engine tests. Modular gas fuel feed system and electronic engine control system were developed in the engine laboratory of MADI which can be used both on high- and medium-speed gas and gas diesel engines [7, 8]. Both the systems were perfected on a Cummins Kama gas diesel engine.

The gas fuel system has several modules connected with each other. Every module reduces pressure and supplies gas to the cylinders. This enables to select the right number of modules for every engine. One module is used for the high-speed Cummins Kama gas diesel engine and three modules – for the medium-speed D200 gas diesel engine. The CR fuel supply system of the base Cummins Kama diesel engine was used for injection of igniting portion of diesel fuel.

An electronic engine control system was developed that controls supply of diesel and gas fuel. The electronic engine control system for the L6 gas diesel engines produces control impulses for actuators and carries out synchronization and distribution of impulses across the cylinders depending on the engine operating conditions based on the data supplied from many sensors.

After perfection of the two systems on the high-speed Cummins Kama gas diesel engine, pretty high engine parameters were obtained. At full load and various engine speeds, on the average, the brake specific fuel consumption decreased by 11%, NO_x emissions – by 30% and CO_2 emissions – by 13% compared with the base diesel engine. A good percentage of diesel fuel substitution by gas was attained: correspondingly, at full load and approximately 40% load, on the average, the percentage of diesel fuel was 5.2% and 8.8%.

To see if the results obtained for a high-speed gas diesel engine may be used for forecasting of parameters of a medium-speed gas diesel engine in case of similar organization of their working processes (the same modular gas feed system and electronic engine control system), calculations were performed for the

D200 and Cummins Kama gas diesel engines for certain equal conditions: mean piston speed, brake mean effective pressure and air access coefficient [10]. The results showed very close indicated parameters and close thermal strength for two engines, though thermal strength of the high-speed engine was by 10-20% higher.

For additional calibration of the MADI model in respect to the medium-speed engine, an experimental locomotive characteristic of the L6 diesel engine having D/S=200/280 mm was used [11].

III. Results and Discussions

Parameters of air at the inlet to the cylinder and exhaust gases at the outlet of the cylinder were calculated by the one-zone MADI model using approximate values of coefficients required for the I.Vibe formula. Calculations were made for the rated mode: engine speed 1000 rpm, brake mean affective pressure 2.0 MPa, optimal by fuel efficiency ignition advance angle.

A. Selection of combustion chamber for the gas engine

Combustion chamber of the base diesel engine D200 and its gas diesel version is shown in Fig. 1. It can't be used for the gas engine because of knock, therefore the compression ratio was decreased from 15 to 10. The value of the overpiston clearance of the base diesel engine (15 mm) was not changed and compression ratio was reduced by increasing the volume of the combustion chamber in the piston.

The shape of combustion chamber should be optimized to ensure as much as possible complete combustion of the gas and minimal toxic emissions. Three different shapes of combustion chamber were investigated which are presented in Fig. 2: hemispheric, cylindrical and ω-shaped.

As the result of calculations by the FIRE model, emissions of NO_x and soot for diesel, gas diesel and gas versions (with three combustion chambers) of the D200 engine are presented in Table 2 and for gas engine with three versions of combustion chambers – in the histogram shown in Fig. 3.

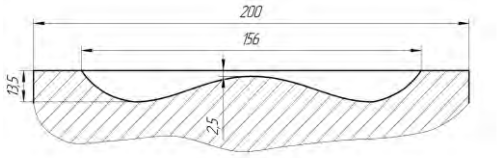

Fig. 1. Schematic of the combustion chamber of the D200 diesel and gas diesel engine (compression ratio = 15, overpiston clearance = 15 mm)

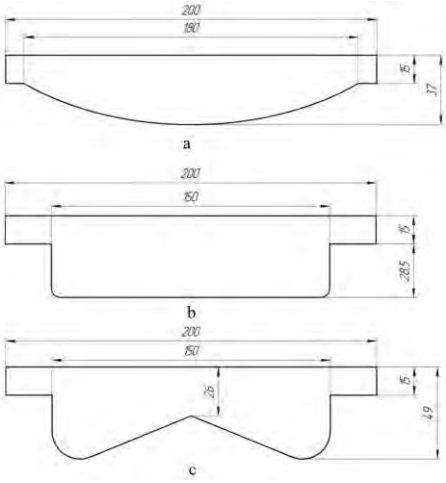

Fig. 2. Schematics of combustion chambers of the D200 gas engine: a) hemispheric; b) cylindrical; c) ω-shaped

As seen from Table 2 and Fig. 3, the semispherical combustion chamber produces the minimal amount of NO_x and in cylindrical combustion chamber – the minimal amount of soot. As emissions of soot in all the three combustion chambers are negligible low compared with those of the diesel engine, semispherical combustion chamber was selected for further calculations because it has the lowest NO_x emission.

Table 2. Emissions of NO_x and soot by diesel, gas diesel and gas versions of the D200 engine

	NOx (g/(kW·h))	**Soot (g/(kW·h))**
Diesel engine	17.742	0.0089
Gas diesel engine	5.743	5.3492·10-5
Gas engine with combustion chamber		
Semispherical	1.2945	3.0173·10-5
Cylindrical	1.5146	1.3243·10-5
ω-shaped	1.7481	7.7823·10-7

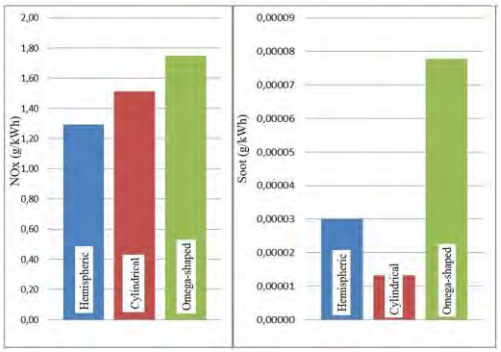

Fig. 3. Emissions of NO_x and soot for hemispheric, cylindrical and ω-shaped versions of combustion chamber of the D200 gas engine

B. *Determining of the I.Viebe formula coefficients for heat release rate*

One should know heat release rate for diesel, gas diesel and gas versions of the medium-speed engine to obtain the heat release duration φ_z and heat release law parameter *m* used in the I.Viebe formula. These parameters are required for calculation of operation parameters of all the three versions of the D200 engine by the one-zone model of MADI.

Heat release rate diagrams for diesel, gas diesel and gas versions of the D200 engine calculated by the multi-zone model are shown in Fig. 4, 5, and 6. In the same figures, the heat release rate diagrams calculated by the I.Viebe formula are presented. The heat release duration φ_z was determined as an interval between the start and end of the heat release process. The heat release law parameter *m* was determined by alignment of the diagrams calculated by the multi-zone model with the heat release rate lows calculated by the I.Viebe formula using already known φ_z values for each of three engines and several values of *m* taken with a step of 0.5.

Analysis of the values of φ_z and *m* shows that the heat release duration decreases by about 20ºCA when passing from diesel to gas diesel and gas cycle (correspondingly, 70, 36 and 40ºCA) which seems quite logical because in diesel engine, after combustion has already started, fuel injection continues and its preparation for combustion takes some time (needed for fuel drops flight, braking, evaporation, mixing with air, heating, etc.). In gas diesel and gas engines, the gas-air mixture is already prepared for combustion and it just needs inflammation by a spark plug or igniting portion of diesel fuel. When passing from diesel to gas diesel and gas cycles, the heat release law parameter *m* increased correspondingly from 0.5 to 1.0 and 2.0, ensuring a more "soft" combustion which results in less noise level and loads on the engine parts. This may be explained by the fact that the portion of diesel fuel injected during the ignition delay period ignites in an "explosion" manner. This amount of fuel is the largest in diesel engine, much smaller in gas diesel engine and is not present in gas engine.

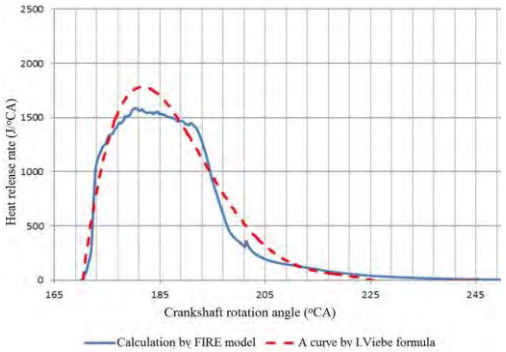

Fig.4. Heat release rate for D200 diesel engine: φ_z =70ºCA, *m*=0.5

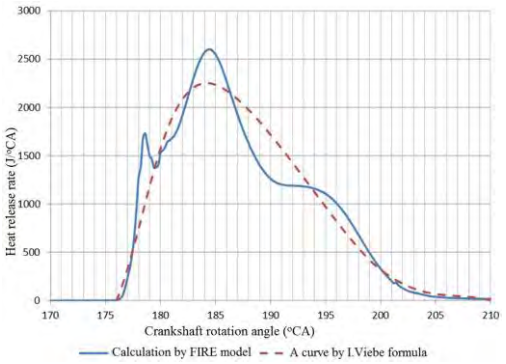

Fig. 5. Heat release rate for D200 gas diesel engine: φ_z =36ºCA, *m*=1

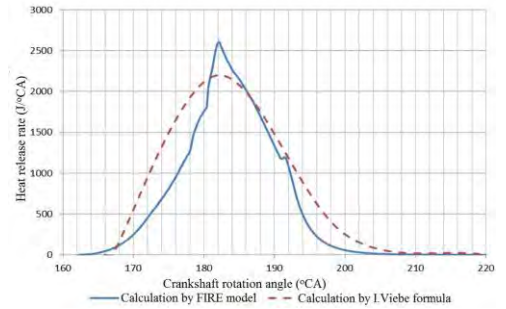

Fig. 6. Heat release rate for D200 gas engine: φ_z =40ºCA, *m*=2

C. *Comparison of parameters of the 4-stroke cycle of diesel/gas diesel and gas engine*

For determining parameters of the D200 engine when passing from diesel to gas diesel and gas cycle, calculations of three version of the engine were carried out at a rated mode using the MADI one-zone model and parameters of the I.Viebe formula for heat release rate obtained earlier by the multi-zone model. Calculation results for the three engines are presented in Table 3. Injection rate of diesel fuel for the diesel engine was 920 mg/cycle, of gas for the gas engine - 840 mg/cycle and of gas and diesel fuel for the gas diesel engine, correspondingly, 755 and 38 mg/cycle.

As seen from Table 3, most of parameters of the 4-stroke cycle of diesel and gas diesel engines have close values: indicated efficiency η_i, air access coefficient λ, peak combustion pressure p_z, resulting by heat exchange temperature T_{res}, average by the 4-stroke cycle heat transfer coefficient α_{av}, heat supplied in the cycle $Q_в$, heat lost into the walls Q_w, boost air pressure p_c. Compared with diesel engine, the brake specific fuel consumption g_e of the gas diesel engine is by 27.7 g/(kW·h) or by 14.2% lower and of the gas engine – by 17.2 g/(kW·h) or by 9.1% lower. This is mainly due to higher specific heat of methane compared to diesel fuel and also due to shorter duration of heat release of the gas diesel engine and gas engine. Reduction of compression ratio of the gas engine compared to the diesel engine from 15.0 to 10.0 resulted in less benefit in fuel efficiency and decrease of the peak combustion pressure p_z by 4.3 MPa, lowering the indicated efficiency η_i by 5.9% and as a consequence – one had to increase the quantity of heat supplied in the cycle $Q_в$ by 6.4% to obtain the same brake mean effective pressure p_e=2.0 MPa as the base diesel engine. Decrease of relative heat losses into walls $Q_w/Q_в$ of the gas engine by 26% compared with the diesel engine is caused by reduction of the cycle average heat transfer coefficient α_{av}, which is the result of decreasing of the peak combustion pressure p_z and maximal temperature of the cycle due to lower compression ratio. The lower compression ratio and hence expansion ratio resulted in the increase of the exhaust gases temperature T_m of the gas engine by 21° higher than that of the diesel engine. This resulted in the increase of the work output of gases at the turbine inlet and hence the growth of almost all parameters of turbocharging system: turbocharger rotor speed, boost pressure p_c. Thermal factor which is characterized in our model as a product of the cycle average heat exchange coefficient α_{av} by the resulting by heat exchange temperature $\alpha_{av} \cdot T_{res}$ is lower by 15% in the gas engine than in the diesel engine which may be explained by a lower compression ratio.

TABLE 3. PARAMETERS OF THE D200 DIESEL/GAS DIESEL/GAS ENGINE AT RATED MODE

Engine	g_e	η_i	λ	p_z	T_{res}	α_{av}	$T_{res} \cdot \alpha_{av}$	Q_b	Q_w	Q_w/Q_b	T_t	p_c
	g/kW·h	-	-	MPa	K	W/m²·K	kW/m²	kJ	kJ	-	K	MPa
Diesel	188.9	0.503	2.10	20.6	1110	759	842.5	390	46.50	0.119	757	0.317
Gas diesl	162.1	0.507	2.04	20.7	1100	752	834.7	390	47.10	0.121	755	0.315
Gas	171.7	0.475	2.15	16.3	1040	705	733.2	415	39.00	0.094	778	0.355

IV. CONCLUSIONS

1. Analysis performed demonstrates that medium-speed gas engines are most suitable for energy generation because operation at a constant high speed minimizes the risk of knock. Gas diesel engines can be successfully used for transport because they do not have problems with knock.

2. Calculation of compression-combustion-expansion processes by a multi-zone model enabled to obtain parameters of the I.Viebe heat release rate formula for diesel/gas diesel/gas engines which were required for calculation of the 4-stroke cycle parameters of these engines by a one-zone model.

3. Calculated comparison of operation parameters of diesel/gas diesel/gas engine showed that compared to the diesel engine, the gas diesel and gas engines have, correspondingly, by 14.2% and 9.1% lower brake specific fuel consumption, as well as 3.09 times and 13.7 times lower NO_x emissions. Soot emissions of the gas diesel and gas engines are negligibly low. Thermal strength of the gas engine is by 26% lower than that of diesel and gas diesel engines.

REFERENCES

[1] J. Klausner, J. Lang, C. Trapp, "J624 – Der weltweit erste Gasmotor mit zweistufiger Aufladung", MTZ – Motortechnische Zeitschrift Ausgabe, 04, 2011

[2] M. Grotz, R. Böwing, J. Lang, J. Thalhauser, P. Christiner, A. Wimmer, "Efficiency increase of a high performance gas engine for distributed power generation", 6th CIMAC Cascades, Dual Fuel and Gas Engines – Their Impact on Application, Design and Components, February 27, 2015.

[3] V.A. Luksho. "A complex method of increasing energy efficiency of gas engines with high compression ratio and shortened intake and exhaust strokes", Ph.D. thesis, NAMI, Moscow, 2015, 365 p.

[4] B. P. Zagorskih, Yu. A. Kozar, Ye. B. Babenich. (2012). "Perfection of gas supply for diesel engine operation by gas diesel cycle". Avtozapravochni complex + Alternativnoye toplivo, no 5, pp. 3-6.

[5] A.A. Kapustin. "Fuel feed and control system for gas diesel engine operating on natural gas". Transport na alternativnom toplive, no. 4, 2008, pp. 46-49.

[6] L. V. Grehov, N. A. Ivsachenko, V. A. Markov, "On ways to improve the gas-diesel cycle", AvtoGasoZapravochniy komplex + Alternatvnoye toplivo 7(100), 2010, pp. 10-14.

[7] M. G. Shatrov, V. V. Sinyavski, A. Yu. Dunin, I. G. Shishlov, A. V. Vakulenko, "Method of conversion of high- and middle-speed diesel engines into gas diesel engines". Facta universitatis. Series: Mechanical Engineering. Vol. 15, no 3, 2017, pp. 383-395.

[8] M. G. Shatrov, V. V. Sinyavski, A. Yu. Dunin, I. G. Shishlov, A. V. Vakulenko, A. L. Yakovenko. "Using simulation for development of the systems of automobile gas diesel engine and its operation control". International Journal of Engineering & Technology, 7 (2.28), 2018, pp. 288-295.

[9] A. S. Khatchijan, V. V. Sinyavskiy, I. G. Shishlov, D. M. Karpov, "Modeling of parameters and characteristics of engines fed with natural gas", Transport na Alternativnom Toplive", 3 (15), 2010, pp.14-19.

[10] V. V. Sinyavski, I. V. Alekseev, I. Ye. Ivanov, S. N. Bogdanov, Yu. V. Trofimenko. "Physical simulation of high- and medium-speed engines powered by natural gas", Pollution Research, Vol. 36 (3), 2017, pp. 684-690.

[11] M. G. Shatrov, V. V. Sinyavski, I. G. Shishlov, A. V. Vakulenko. "Forecasting of parameters of boosted locomotive diesel engine fed by natural gas". Naukograd Nauka Proizvodstvo Obschestvo, No2 (4), 2015, pp. 26-31.

AHP Application for Vehicle Type Selection

Nikola Stevanović[1], Marko Živković[2], Đorđe Lazarević[3]

[1]Research and Development Center "ALFATEC", Niš, Serbia,
nikola.stevanovic@alfatec.rs, marko.zivkovic@alfatec.rs, djordje.lazarevic@alfatec.rs

Abstract—**In this paper an Analytic Hierarchy Process (AHP) is applied as multi-criteria decision-making tool to determine which type of vehicle is best to buy nowadays. Four types of vehicles were analyzed: conventional vehicle, hybrid electrical vehicle (HEV), plug-in hybrid electrical vehicle (PHEV) and battery electrical vehicle (BEV). Analysis is provided at four different random chosen car models (one model from every vehicle type).**

Keywords–AHP, decision-making, conventional vehicle, HEV, PHEV, BEV.

I. INTRODUCTION

The issues of climate change or global warming have been rigorously discussed by many governments since the early 21st century. The great number of relevant reports has revealed the negative impact of climate changes dominantly driven by human activities [1]. The significant growth of today's cities has led to an increased used of transportations. The city pollution is very important issue which affects on daily life and people's health. Commercial vehicles which run on internal combustion engine on gasoline or diesel are responsible for most of the pollution in our cities. Emissions from vehicles used in commercial transportation are part of the human impact on global warming and the greenhouse effect. One method for cutting the greenhouse gases from the vehicles is by decreasing the fuel consumption. With the new intelligent hybrid and plug-in hybrid technology fuel consumption can be reduced by more than a half [1-3].

Nowadays, the most used vehicles are conventional vehicles that run on gasoline or diesel. These vehicles, because of incomplete fuel combustion in engine, are emitting exhaust gases. Exhaust gases are CO2, CO and NOx and they have impact on global warming and the greenhouse effect. Additional problem that refers to conventional vehicles is limited fuel reserve. Alternatives for conventional vehicles are hybrid electrical vehicles, plug-in hybrid electrical vehicles and battery electrical vehicles whose operation principle and structure will be explained in following sections of the paper.

In this paper the emphasis is placed on application of an Analytic Hierarchy Process (AHP) as multi-criteria decision-making tool to determine which type of vehicle is best to buy based on assigned desired criterions. All vehicle types can be classified in groups: conventional vehicle, hybrid electrical vehicle (HEV), plug-in hybrid electrical vehicle (PHEV) and battery electrical vehicle (BEV). The analysis was provided at four different car models – one car model belongs to one vehicle group.

II. THEORETICAL BACKGROUND

A. Conventional Vehicles

Conventional vehicle uses gasoline or diesel to power an internal combustion engine. The gasoline or diesel powered internal combustion engine takes air from the atmosphere and gasoline or diesel from the fuel tank and through the process of combustion makes energy for vehicle work. Combustion, also known as burning, is the basic chemical process of releasing mechanical energy from the fuel and air mixture. In an internal combustion engine, the ignition and combustion of the fuel occurs within the engine itself. The engine then partially converts the energy from the combustion to the mechanical work.

Internal combustion engine is not "perfect": one part of the fuel is completely combusted

ISBN: 978-86-80616-03-2

and converted to the energy while another part creates carbon monoxide that goes into the atmosphere and has a contribution to the air pollution. The structure of gasoline conventional vehicle is shown in Fig. 1.

B. Hybrid Electrical Vehicles

Hybrid Electrical Vehicles (HEVs) are powered by an internal combustion engine that runs on conventional fuel and an electromotor that uses energy stored in a battery. HEVs do not require a plug to charge the battery; instead, they are charged using regenerative braking and the internal combustion engine. Electromotor was used as a traction motor and it drives the wheels of the vehicle. Unlike a traditional vehicle, where the engine must "ramp up" before full torque can be provided, an electromotor provides full torque at low speeds. The motor also has low noise and high efficiency. HEVs combine the benefits of high fuel economy and low emissions with the power and range of conventional vehicles.

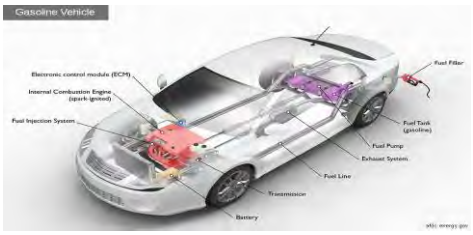

Figure 1. Gasoline conevtional vehicle structure [4]

Depending on the drive train structure (the method in which motor and engine are connected), the structure of the HEVs can be parallel, series or combined. All of these structures are represented in [5]. The structure of parallel HEV is shown in Fig. 2.

C. Plug-in Hybrid Electrical Vehicles

Plug-in Hybrid Electrical Vehicles (PHEVs) are powered by conventional fuels and by electrical energy stored in batteries. PHEV is in close resemblance to HEV and it has all advantages as HEV. PHEV has larger battery pack than HEV. This large battery pack can be charged by an outside electric power source, by the internal combustion engine, or through regenerative braking. Electrical grid represents outside electric power source and it charges battery pack using electrical vehicle charger. Electrical vehicle charger can be placed in charging stations on the road or in the homes. Using electricity from the electrical grid to charge the battery costs less and reduces petroleum consumption compared to conventional vehicles. The structure of PHEV is shown in Fig. 3.

D. Battery Electrical Vehicles

Battery Electrical Vehicles (BEVs) are vehicles powered only by electromotors. Electromotors run using the power stored in batteries. BEVs do not use internal combustion engine like another types of vehicles. BEVs

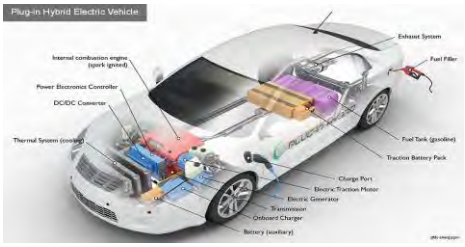

Figure 3. PHEV structure [7]

have larger battery pack and similar charging principle like PHEVs.

BEVs have many advantages: they are highly efficient, have zero emissions what is benefit for local air quality, they have good acceleration; can be charged overnight during low cost electricity. However, despite these advantages, electricity storage is still expensive, and the charging of the battery is

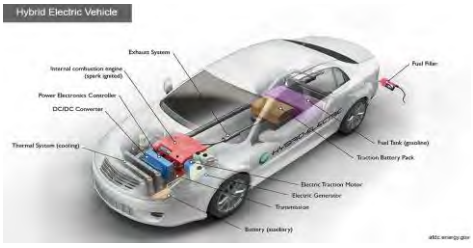

Figure 2. Parallel structure of HEV [6]

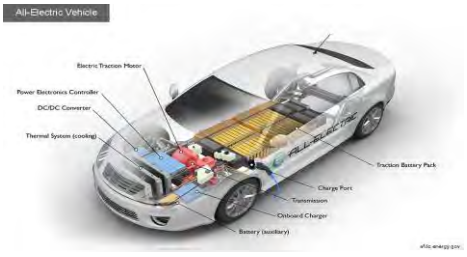

Figure 4. BEV structure [8]

time consuming process, therefore the driving range of these vehicles is limited. The structure of the BEV is shown in Fig 4.

E. Analytic Hierachy Process

The Analytic Hierarchy Process (AHP), introduced by Thomas Saaty (1980), is an effective tool for dealing with complex decision making, and may aid the decision maker to set priorities and make the best decision. AHP is especially suitable for complex decisions that involve the comparison of decision elements which are difficult to quantify. AHP is simple because there is no need of building a complex expert system with the decision maker's knowledge embedded in it. It is popular and widely used in many applications of the public and private sectors. The mathematics of the AHP and the calculation techniques are briefly explained in [9].

III. PRACTICAL APPLICATION OF AHP

One of very important questions that all vehicle buyers ask is which type of vehicle is currently best to buy. The answer to this question can be obtained by characteristics comparing of desired car models from each group of vehicle types using AHP analysis. In this paper following car models will be considered: Volkswagen Golf GTI 2.0 TSI as conventional vehicle, Toyota Prius Prime Hybrid as HEV, Toyota Prius Prime Plug-in Hybrid as PHEV and Volkswagen e- Golf as BEV. Characteristics of these models are represented in following:

B1 – Volkswagen Golf GTI 2.0 TSI [10,11]:

- price: 22773 € (26415 $);
- fuel tank's volume: 50 l;
- fuel consumption: 6.4 l/100 km;
- CO_2 emission: 148 g/km.

B2 – Toyota Prius Prime Hybrid [12-14]:

- price: 29000 €;
- fuel tank's volume: 43 l;
- fuel consumption: 4.4 l/100 km;
- CO_2 emission: 78 g/km.

B3 – Toyota Prius Prime Plug-in Hybrid [15-17]:

- price: 39200 €;
- fuel tank's volume: 43l
- fuel consumption: 1.8 l/100 km;
- driving range: 1035 km;
- battery capacity: 7.2 kWh;
- CO_2 emission: 22 g/km.

B4 – Volkswagen e-Golf [18,19]:

- price: 26290 e (30495 $);
- driving range: 200 km;
- battery capacity: 35.8 kWh;
- CO_2 emission: 0 g/km.

Each of these car models represents one of alternatives in AHP model.

The next step is definition of criterions that will be used for car models comparison. These criterions are:

A1 – price,

A2 – driving range,

A3 – fuel and/or electricity price,

A4 – CO_2 emission.

The fuel that will be used in internal combustion engine is Euro Premium BMB 94 Plus and its price is 1.37 €/l (161.7 RSD/l) [20].

PHEV and BEV use electrical vehicle charger to charge their batteries. Electrical vehicle charger can be placed in electrical charger stations on the roads and in homes. The map of electrical charging vehicle stations on the roads in Serbia is presented in Fig. 5. From represented map it can be conclude that there are only few electrical charging vehicle stations in Serbia. The small number of electrical charging stations may constitute an obstacle to use PHEV and BEV vehicles. Therefore, it will be necessary to have electrical vehicle charger

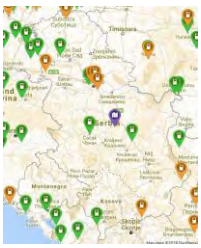

Figure 5. The map of charging car stations [21]

in home. The electrical vehicle charger for domestic application that will be used in consideration is Smart Wallbox EVB1A22P2RI which price is 3065 € (362304 RSD) [22].

It is assumed that the PHEV and BEV will be charged overnight when the price of electricity is lower. Price of electrical energy that should be used for battery charging is calculated by official *Calculator of electrical energy* made by Serbian electrical utility company "EPS Snabdevanje" [23]. Calculation is made by battery capacitance inputting to a point for electricity lower price with neglecting of the other consumption during the month. The obtained value represents the approximative price of electrical energy P_A that should be payed for one battery charging.

The calculation of total price of vehicle P_{TV} is shown in (1).

$$P_{TV} = P_M + P_C \tag{1}$$

where P_M is model price and P_C is price of the electrical vehicle charger for homes.

The calculation of driving range DR is shown in (2).

$$DR = \frac{T_V}{F_C} \tag{2}$$

where T_V is fuel tank volume and F_C is fuel consumption.

The calculation of fuel and electricity price P_{FE} is shown in (3).

$$P_{FE} = T_V P_F + P_A \tag{3}$$

where P_{FE} is fuel price.

For the easier comparison of selected models, a table of vehicles characteristics has been formed and shown in Table I. AHP starts with comparison of criterions based on Saaty Rating Scale and with the creation of matrix of the criterions shown in Table II. The weights of criterions are given by subjective feeling and therefore, model price has the greatest significance. Using calculations described in [9], the priority vector of criterions is obtained and presented in (4).

According to calculated weights presented in the priority vector of criterions, it can be concluded that criteria A1 has the highest importance.

TABLE I. VEHICLES CHARACTERISTICS

Models	P_{TV}(€)	*DR(km)*	P_{FE}(€)	CO_2(g/km)
B1	22773	780	65.15	148
B2	29000	980	58.91	78
B3	42265	1035	67.046	22
B4	29355	200	7	0

TABLE II. MATRIX OF CRITERIONS

	A1	***A2***	***A3***	***A4***
A1	1	4	3	5
A2	0.25	1	0.5	3
A3	0.33	2	1	4
A4	0.2	0.33	0.25	1

$$[y] = \begin{bmatrix} 0.5378 \\ 0.1495 \\ 0,2427 \\ 0.0699 \end{bmatrix} \tag{4}$$

Thereafter, it is necessary to compare alternatives based on criterions and create matrices of alternatives for each criterion, presented in Tables III - VI.

TABLE III. MATRIX OF ALTERNATIVES BASED ON CRITERION A1

	B1	***B2***	***B3***	***B4***	***Weight***
B1	1	3	7	4	0.5476
B2	0.33	1	5	2	0.2403
B3	0.14	0.2	1	0.2	0.6502
B4	0.25	0.5	5	1	0.1619

TABLE IV. MATRIX OF ALTERNATIVES BASED ON CRITERION A2

	B1	***B2***	***B3***	***B4***	***Weight***
B1	1	0.33	0.33	5	0.1639
B2	3	1	0.5	6	0.3252
B3	3	2	1	6	0.4585
B4	0.2	0.17	0.17	1	0.0524

TABLE V. MATRIX OF ALTERNATIVES BASED ON CRITERION A3

	B1	*B2*	*B3*	*B4*	*Weight*
B1	1	0.25	0.5	0.17	0.0661
B2	4	1	3	0.2	0.2217
B3	2	0.33	1	0.25	0.1105
B4	6	5	4	1	0.6017

TABLE VI. MATRIX OF ALTERNATIVES BASED ON CRITERION A4

	B1	*B2*	*B3*	*B4*	*Weight*
B1	1	0.33	0.14	0.11	0.0491
B2	3	1	0.25	0.17	0.0922
B3	7	4	1	0.25	0.2550
B4	9	6	4	1	0.6109

The following obtained result is priority matrix of alternatives shown in (5).

$$[P] = \begin{bmatrix} 0.5476 & 0.1639 & 0.0661 & 0.0491 \\ 0.2403 & 0.3252 & 0.2217 & 0.0922 \\ 0.0502 & 0.4585 & 0.1105 & 0.2550 \\ 0.1619 & 0.0524 & 0.6017 & 0.6109 \end{bmatrix} \quad (5)$$

Finally, vector of optimal alterative (A_{opt}) shown in (6) is calculated by multiplication of priority matrix of alternative by priority vector of criteria and the highest value is chosen as the best solution.

$$A_{opt} = \begin{bmatrix} 0.7091 \\ 0.5904 \\ 0.3210 \\ 0.8473 \end{bmatrix} \quad (6)$$

The highest value from the vector of optimal alternatives is 0.8473 and it refers to BEV. Therefore, it can be concluded that currently it is best to buy car model from the BEV group.

IV. CONCLUSION

In this paper application of Analytic Hierarchy Process (AHP) at example from practice was presented. At this example AHP methodology helped to make a good decision to select the best type of vehicle. For selected models the best type of vehicle is BEV. However, using of vehicles form this group in Serbia requires building of more charging stations because of the limited driving range of 200 km/per charging.

In future researches this methodology can be applied to more car models from all vehicle types what would lead to more precise and comprehensive results.

ACKNOWLEDGMENT

This paper is a part of the research done within the project III 44006, supported by the Ministry of Education, Science and Technological Development of the Republic of Serbia.

REFERENCES

[1] N. Ding, K. Prasad, T. T. Lie, "The electrical vehicle: a review", International Journal of Electrical and Hybrid Vehicles, Vol. 9, No. 1, pp:49-66, January 2017.

[2] D. Janulevičius, A. Valinevicius, D. Andriukaitis, "Intelligent plug-in hybrid electrical vehicle", Institutional Repository of Kaunas University of Technology (2015).

[3] M. A. Hannan, F. A. Azidin, A. Mohamed, "Hybrid electrical vehicles and their challenges: a review", Renewable and Sustainable Energy Reviews, January 2014.

[4] How do gasoline cars work. Avaliable at: https://www.afdc.energy.gov/vehicles/how-do-gasoline-cars-work.

[5] D. Lanzarotto, M. Marchesoni, M. Passalacqua, A. P. Prato, M. Repetto, "Overview of different hybrid vehicle architectures", IFAC PaparsOnLine 51-9 (2018), pp: 218-222.

[6] How do hybrid electric cars work. Available at: https://www.afdc.energy.gov/vehicles/how-do-hybrid-electric-cars-work

[7] How do plug-in hybrid electric cars work. Available at: https://www.afdc.energy.gov/vehicles/how-do-plug-in-hybrid-electric-cars-work

[8] How do all-electric cars work. Available at: https://www.afdc.energy.gov/vehicles/how-do-all-electric-cars-work

[9] N. Stevanovic, A. Janjic, M. Rasic, "AHP application on circuit breakers", 3rd Virtual International Conference on Science, Technology and Management in Enegy, ISBN: 978-86-80616-02-5, Serbia, Nis, October 2017, pp: 33-39.

[10] Wolkswagen Golf GTI. Available at: http://www.vw.com/models/golf-gti/section/colors/.

[11] Wolkswagen Golf GTI 2.0 TSI: Available at: https://www.auto-data.net/en/volkswagen-golf-vii-facelift-2016-gti-2.0-tsi-230hp-bmt-27832.

[12] Toyota Prius Hybrid. Available at: https://www.toyota.rs/new-cars/prius/index.json

[13] Toyota Prius Prime Hybrid. Available at: https://www.auto-data.net/en/toyota-prius-prime-1.8-122hp-hybrid-automatic-32436.

[14] Toyota Prius the pioneer.Available at: https://www.toyota-europe.com/new-cars/prius/index/specs

[15] Toyota Prius Plug-in hibrid. Available at: https://www.toyota.rs/new-cars/prius-plugin/index.json

[16] Toyota Prius Prime. Available at: https://www.toyota.ca/toyota/en/vehicles/prius-prime

[17] Toyota Prius Prime Plug-in Hybrid. Available at: https://www.auto-data.net/en/toyota-prius-prime-1.8-122hp-plug-in-hybrid-automatic-32552

[18] Wolkswagen e-Golf. Available at: http://www.vw.com/models/e-golf/section/masthead/

[19] Technical specification: Wolkswagen e-Golf: https://www.auto-data.net/en/volkswagen-e-golf-35.8-kwh-136hp-cvt-32179

[20] Fuel price in Serbia. Available at: https://www.retailserbia.com/info/cene-goriva-srbija

[21] Map of electrical vehicle charger stations. Available at: https://www.plugshare.com/

[22] Electrical vehicle charger Smart Wallbox EVB1A22P2RI. Available at: https://www.elektropunjaci.com/product/komplet-punjac-smart-wallboxkabl-t2set-zastitne-opreme/

[23] Electricity price calculator in Serbia. Available at: http://kalkulator.eps-snabdevanje.rs/kalkulator

CFD Study of a Stirling Engine Regenerator as a Porous Medium

Emmanouil Rogdakis[1], Panagiotis Bitsikas[1 *], George Dogkas[1]

[1]NTUA, Zografou, Greece
[1]rogdemma@central.ntua.gr, [2]pbitsikas@hotmail.com, [3]geodogas@hotmail.com

Abstract—**In the present study, a small compact regenerator is simulated by three-dimensional (3D) Computational Fluid Dynamics (CFD) analysis. The regenerator is studied as a part of a Stirling Engine. After the basic outcomes related to gas flow, pressure drop and heat transfer are discussed, the values of friction factor and Nusselt number in the regenerator are obtained and correlated with Reynolds number. Then, the engine is simulated with the regenerator being modeled as a porous medium. The correlation equations that were derived for the metal regenerator friction factor are transformed into two resistance coeffients and are used as input data for the porous medium. The engine is successfully simulated with the use of porous media feature, as it is shown by the good agreement of Reynolds number and temperature. However, the drop of pressure through the porous media is lower to the pressure drop through the metal regenerator. The simulation is repeated after the resistance coefficients are modified and the values of pressure drop in both cases are close to each other. The outcomes of this work can be applied to more complex Stirling Engine Regenerators.**

Keywords – Regenerator, Stirling Engine, CFD, Computational

I. INTRODUCTION

The ideal Stirling cycle is a closed cycle during which gas undergoes cyclic compression and expansion at different temperature levels. Stirling engines are capable of utilizing different types of heat source, such as solar energy or biomass. Moreover, they can achieve high thermal efficiency, they produce low noise and require little maintenance. [1] Stirling Engines are mainly used for co-generation applications

All Stirling engines incorporate an expansion space (expander) and a compression space (compressor). The expander is kept under high temperature by absorbing heat by a heat source (heater), while compressor is kept at low temperature due to heat rejection to a heat sink (cooler). The two parts of the engine are connected via the regenerator. The regenerator is an internal heat exchanger that incorporates plenty of layers of metal wire. While gas is flowing towards the compressor, heat is transferred from the hot gas to the regenerator matrix. On the other, during gas flow towards the engine's hot part, the previously heated metal matrix provides heat to the working gas. [2] The ability of the regenerator matrix to store heat increases the efficiency of the engine. On the other hand, the matrix acts as an obstacle to gas flow and results to pressure drop and reduced power output.

The regenerator is considered to be the key component in order to improve the efficiency of Stirling Engines. The aim of the research work is the increase of heat transfer capacity and the reduction of pressure losses. [3] For the estimation of the regenerator performance, the knowledge of friction factor and heat transfer coefficient is necessary.

Experiments have been the prevailing method of the estimation of both properties. Several proposed correlations related to friction factor are presented by Thomas and Pittman. [4] The heat transfer phenomena can be described by equations correlating Nusselt number with Reynolds. [5] However, the derivation of an analytical formula for heat transfer is difficult due to the oscillating flow in the regenerator and the varying temperature.

Due to the advancing computer technology, Computational Fluid Dynamis (CFD) can be successfully utilized for the simulation of complex thermodynamic systems. Costa et al [6] applied CFD to investigate pressure drop in stacked matrix. Their method was

experimentally validated and then was applied to a wound matrix. In a similar way, Costa et al [7] studied the phenomena of heat transfer in both stacked and wound woven wire matrix. Moreover, the same group of researchers studied both experimentally and numerically the pressure drop phenomena in a Stirling engine regenerator under oscillating flow. The derivation of a friction factor vs Reynolds number correlation is among the main findings of the specific work [3].

Due to the small wire diameter of the metal matrix, the geometry of the regenerator is too complex to be imported in a CFD simulation, given the available computational power. For example, the regenerator of GPU-3 Stirling Engine incorporates about $2 \cdot 10^5$ metal wires of 40 μm diameter. [8] If the regenerator is studied separately, this problem can be overcome by designing and studying a small descriptive part of the regenerator, as it was done in [6] and [7]. However, if the regenerator is studied as a part of a Stirling Engine it can be modelled as a porous medium. Except of geometrical data of the regenerator, data related to friction factor and heat transfer are required as input for the porous media feature. [9]

In the present work, a metal regenerator is designed and simulated as part of Stirling engine. For the simulation, the ANSYS software is used. [10] After the results are obtained, the correlations of friction factor and Nusselt number versus Reynolds number are derived. Then, an identical engine is again simulated, but the regenerator is modeled as a porous medium. The data required as input for the porous media model are obtained from the correlations derived in the metal regenerator simulation. The comparison of the results coming from the two approaches will indicate whether the designed regenerator can be studied as porous medium in a CFD simulation. If the proposed method can be applied to the designed regenerators, it can also be applied in more complex regenerators that are used in Stirling Engines.

II. DESIGN AND SETUP

A. Design of the regenerator matrix

Due to the difficulty in simulating a real regenerator as part of Stirling Engine, a compact regenerator of simple design was studied. The regenerator is a slice of a cylinder and can be patterned in both radial and circumferential direction. The regenerator geometry is illustrated in Figure 1. The geometric data of the regenerator are listed in Table I.

In the present work, the regenerator is modelled as a part of a complete Stirling Engine. This leads to more accurate results than a simulation under steady flow, as the conditions at the boundaries between the components change every time step in a way dictated by the conditions occurring in every space of the engine. [11]

The integrated assembly consists of the expansion space, the heater, the regenerator, the cooler and the compression space. Gas is oscillating towards a single direction. With the exception of the regenerator, the cross sectional areas of the engine spaces are equal to each other. The domain of the engine is illustrated in Figure 2. The selection of the length of the heat exchangers, as well as the motion of the pistons are based on a previous work. [12] The data related to the geometry of the heat exchangers are presented in Table II, while the variation of volume is illustrated in Figure 3.

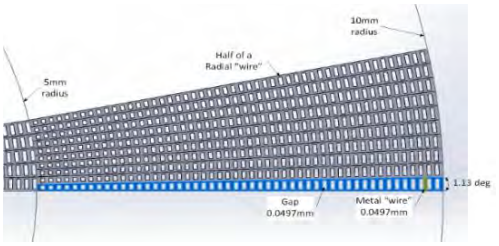

Figure 1: Geometry of the designed regenerator module.

Figure 2: Schematic view of the engine domain

TABLE I: REGENERATOR GEOMETRIC DATA

Magnitude	***Value***
Length	33 mm
Fluid Volume	8.07 mm^3
Metal matrix Volume	16.54 mm^3
Porosity	32.77 %
Wire diameter	49.7 μm
Hydraulic diameter	65.85 μm
Area of heat transfer	4.899 cm^2

TABLE II: GEOMETRY DATA OF THE ENGINE

Magnitude	***Value***
Cooler Volume	4.48 mm^3
Heater Volume	23.86 mm^3
Cooler Length	6 mm
Heater Length	32 mm
Cross-sectional area	0.746 mm^2
Heat transfer area - Cooler	0.618 cm^2
Heat transfer area - Heater	3.295 cm^2

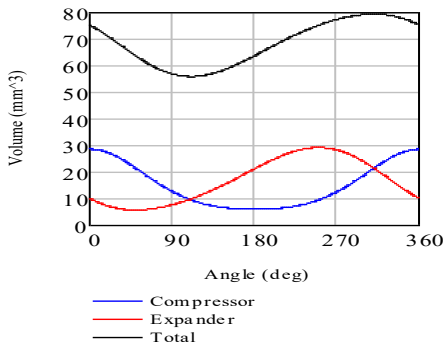

Figure 3: Volume variation

B. *Setup of the CFD simulation*

The computational grid consists of approximately 305000 nodes and 620000 elements. The grid is denser in the area of the regenerator. That grid was the best that could be utilized in this simulation, given the available computational power and the existing time limitations. Due to these limitations, a grid independence analysis could not be performed and will be a subject for investigation in the future. However, it is believed that the utilized grid can provide acceptable results.

The thickness of all the outer walls of the engine is set equal to zero and heat is transferred to and rejected by the engine by convection. The temperature of the heating and the cooling free-stream are equal to 977 K and 288 K respectively. The heat transfer coefficients were set equal to 10^{10} W/(m^2·K). These high values imply that the heat source and the heat sink attached to the heater and the cooler respectively, can provide and absorb the heat required so that the temperature of the walls of the two heat exchangers remain constant and equal to those of the respective free-streams. Furthermore, the piston walls, as well as the walls of the compression and expansion spaces were set as adiabatic. The engine operates with helium as working gas, which is assumed to be ideal, while the walls and the metal regenerator are made of steel. Finally, the rotational speed of the engine was set equal to 2500 rpm.

For the elaboration of the simulation, the Realizable k-e model was selected. Previous analysis has showed that there are areas inside the engine where eddies are formed, even in the case that gas velocity is low. Finally, the cycle was divided into 720 time steps.

III. RESULTS OF METAL MATRIX SIMULATION

A. *Mass flow-rate and velocity*

The time variation of mass flow-rate and gas velocity in the regenerator are shown in Figure 4. The values of both magnitudes were calculated in the middle of the regenerator, as it is the best descriptive point of the regenerator.

When the mass flow rate is positive, gas under low temperature is moving from the cooler towards the heater. The described flow can also be defined as “cold blow” hereafter. Negative mass-flow rate implies that hot gas is flowing towards the cold part of the engine. This flow may also be defined as “hot blow”. At the studied point, cold blow starts at 15^o of crank angle and ends at 209^o. It must be noticed that flow reversal occurred earlier in the area adjacent to the cooler, while the opposite was seen for the areas close to the heater. The difference between the time instances of flow reversal at the two ends of regenerator did not exceed 10^o of crank angle.

The maximum value of gas velocity during cold blow occurs at 76^o of crank angle, while during hot blow velocity peaks at 308^o. At a given time instance, velocity is higher at points close to the heater. However, the trend of velocity variation and the points of maximum velocity at different levels of the regenerator are the same for all levels.

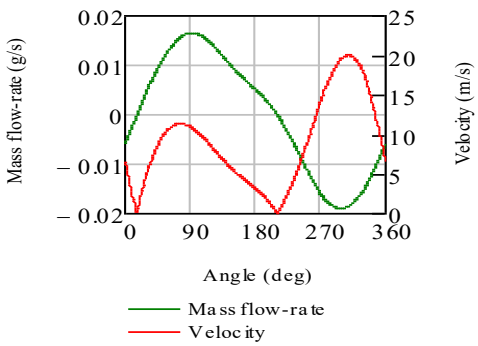

Figure 4: Mass flow-rate and velocity in the regenerator

Based on the direction of gas flow and the trend of velocity change, the engine cycle can be divided in four parts:

- Positive flow – accelerating: $15^o < \theta \leq 76^o$
- Positive flow – decelerating: $76^o < \theta \leq 209^o$
- Negative flow – accelerating: $209^o < \theta \leq 308^o$
- Negative flow – decelerating: $308^o < \theta \leq 360^o$ and $0^o < \theta \leq 15^o$:

B. Friction factor

Reynolds number (Re) is defined by (1). For the calculation of Reynolds number at each time instance, the values of density (ρ), gas velocity magnitude (u), hydraulic diameter (d_h) and dynamic viscosity (μ) must be known.

$$\mathrm{Re} = \frac{\rho \cdot u \cdot d_h}{\mu} . \qquad (1)$$

The variation of Reynolds number is plotted along with pressure drop in Figure 5. Positive pressure drop indicates that pressure at the cold end of the regenerator is higher to that the hot end. This implies that gas is flowing towards the heater. Opposite to that, negative pressure drop is associated with gas flow towards the cooler. Moreover, flow is laminar, as Reynolds number does not exceed the value of 175, which is regarded to be a point under which flow in the regenerator is laminar. [6]

The friction coefficient (Cf) is calculated by (2). Apart from pressure drop (dp), the mass of working gas in the regenerator (m), mass flow-rate (gA) and dynamic viscosity (μ) must be know.

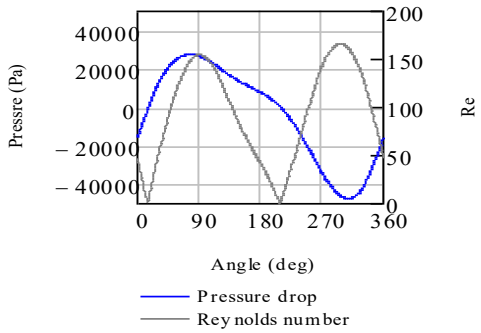

Figure 5: Pressure drop and Reynolds number

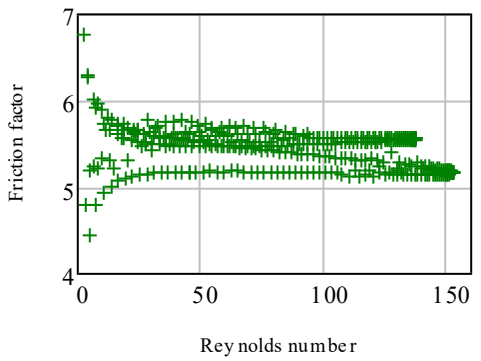

Figure 6: Friction factor vs Reynolds number

Moreover, friction factor is dependent on the regenerator's length and hydraulic diameter. The calculated values of friction factor are plotted against the calculated values of Reynolds number in Figure 6.

$$Cf = \frac{dp \cdot m \cdot d_h^{\,2}}{2 \cdot \mu \cdot L^2 \cdot gA} . \qquad (2)$$

The correlations of Cf and Re must be in the form of a two-coefficient Ergun equation, so their transformation into the coefficients of the porous medium is enabled [9]. It is clear that there is no equation that can fit well the data shown in Figure 6 for the total cycle. The effort to derive two correlating equations based on flow direction led to very low regression coefficients between the data and the derived equations. The proposed solution was the division of the cycle into four parts, depending on the direction of gas flow and gas acceleration or deceleration.

Some points of low Reynolds numbers that worsened the fit between the correlation equations and the data were eliminated. Those points were found to be near the instances of flow reversal, where the mass flow-rate at the middle of regenerator is almost equal to zero but there is a considerable drop of pressure between the regenerator ends. This is associated to the existence of multiple instances of flow reversal in the volume of the regenerator, as it has been mentioned in III.A. Four correlating equations were derived. The type of the equations is indicated by (3) while the coefficients for each time interval are presentd in Table III.

$$Cf(\mathrm{Re}) = a + b \cdot \mathrm{Re} . \qquad (3)$$

The derived equations along with the simulation data are illustrated in Figure 7. The top graphs correspond to positive flow and the graphs below describe negative flow. Moreover, the graphs on the left describe the instances while gas is accelerating, while the graphs on the right correspond to decelerating flow. It is seen that the two derived correlations for negative flow fit the respective data better than the correlations for positive flow.

TABLE III: COEFFICIENTS FOR CF VS RE CORRELATIONS – METAL REGENERATOR

Type of flow	***a***	***b***
Positive - accelerating	5.426	$8.338 \cdot 10^{-4}$
Positive - decelerating	5.68	$-9.215 \cdot 10^{-4}$
Negative - accelerating	5.731	$-3.647 \cdot 10^{-3}$
Negative - decelerating	5.205	$-3.747 \cdot 10^{-4}$

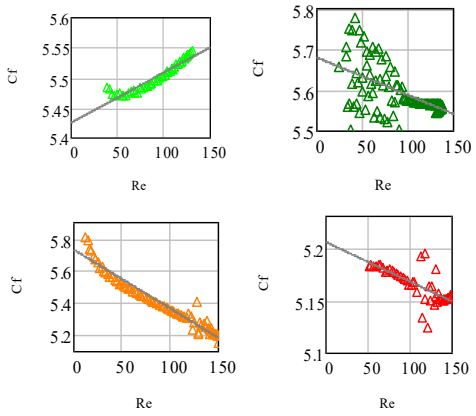

Figure 7: Corellations for friction factor

The regression coefficient of positive-decelerating flow is the lowest among the four ones, while most of the eliminated points that were mentioned before corresponded to positive-accelerating flow.

C. Heat transfer coefficient

The variation of gas and fluid temperature in the regenerator is presented in Figure 8. The mean values of fluid and solid temperature are equal to each other, but the deviation of fluid temperature is considerably higher to that of metal. The range of fluid and solid temperature variation equal to 27 K and 3 K respectively.

In Figure 9, the variation of heat and temperature difference versus time is illustrated. Positive temperature difference implies that gas is hotter than the regenerator metal. The opposite is valid for negative temperature difference. The heat transferred is positive while gas gets heat from the metal. Positive values of heat correspond to negative values of temperature difference, as the colder gas subtracts heat from the hotter metal.

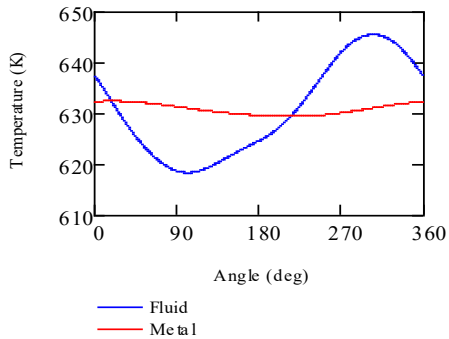

Figure 8: Fluid and metal temperature variation

Moreover, if Figure 9 is compared to Figure 4, it can be noticed that when gas is moving towards the heater (*positive flow*) it is colder than the metal matrix (*negative temperature difference*) and gets heat from that (*positive heat*). The opposite is valid for flow towards the cooler.

The coefficient of heat transfer between gas and metal in the regenerator is calculated by (4). For the calculation of the coefficient, the heat (Q) and temperature difference (ΔT) illustrated in Figure 9 are necessary. Heat (J) is multiplied by 360 times the frequency (f) in order to be expressed as power (W). The area indicated by A is the wetted area of the regenerator matrix. Given the heat transfer coefficient, Nusselt number (Nu) can be calculated by (5). Because of the low variation of solid temperature, the thermal conductivity of metal (k) can be regarded as constant.

$$h = \frac{Q \cdot 360 \cdot f}{A \cdot \Delta T}, \qquad (4)$$

$$Nu = \frac{h \cdot d_h}{k}. \qquad (5)$$

From the simulation results and by using (4) and (5), one value for Nusselt number can be calculated for each time instance of the cycle. If the values of Reynolds number are used (Figure 5), one pair of Reynolds and Nusselt numbers for each time instance is obtained. For the derivation of the Nu vs Re correlations, the same procedure as in the case of friction factor was followed. The difference in the case of Nusselt number is that the derived correlations do not have to be linear equations. Because of that, the correlations fit the simulation data better than in the case of friction factor. Indeed, the regression coefficients for the four correlations exceeded 97%, while the regression coefficient for the Cf vs Re correlations for positive flow were lower to 75 %. The cycle was again derived in four parts, as it was presented in III.B. Each correlation was in the form of (6). The values of the coefficients for each interval are listed in Table IV.

$$Nu(\mathrm{Re}) = a' + b' \cdot \mathrm{Re} + c' \cdot \mathrm{Re}^2 + d' \cdot \mathrm{Re}^3 \qquad (6)$$

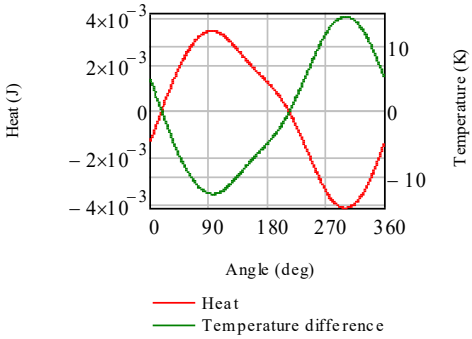

Figure 9: Heat transferred and temperature difference

TABLE IV: COEFFICIENTS FOR NU VS RE CORRELATIONS

Type of flow	***a'***	***b'***	***c'***	***d'***
Positive - accelerating	2.35	$-7.63\cdot10^{-3}$	$8.85\cdot10^{-5}$	$-3.25\cdot10^{-7}$
Positive - decelerating	1.77	$6.55\cdot10^{-3}$	$-5.75\cdot10^{-5}$	$2.15\cdot10^{-7}$
Negative - accelerating	2.58	-0.011	$9.57\cdot10^{-5}$	$-2.87\cdot10^{-7}$
Negative - decelerating	2.01	$3.26\cdot10^{-3}$	$-2.84\cdot10^{-5}$	$9.62\cdot10^{-8}$

After the correlations have been derived and as the variation of Reynolds versus crank angle is known, the variation of Nusselt number versus crank angle can be obtained. By (5) the variation of heat transfer coefficient versus crank angle can be extracted. The final outcome of this procedure is a function in the form $h=f(\theta)$.

IV. MODELING OF REGENERATOR AS POROUS MEDIUM

After the derivation of the correlations, the regenerator is modeled as porous medium. The engine design, the volume variation and the operational parameters remain unchanged. However, due to the elimination of the metal matrix the computational grid has changed. The new grid consists of 153000 nodes and 98000 elements and is considerably ligher than the grid generated in the case of the metal regenerator.

The flow of working gas was set as laminar (Figure 5). For the definition of porous medium, regenerator porosity, along with viscous resistance coefficient and intertial resistance coefficient are required. Porosity (ψ) is equal to 32.77%. Given the nomenclature of the correlation defined by (3), the viscous ($1/\alpha$) and the inertial (C_2) resistance coefficients are calculated by (7) and (8) respectively. These equations are based on the method proposed by Costa et al. [9]

Table V: Viscous and inertial resistance coefficients

Type of flow	***1/α (m^{-2})***	***C_2 (m^{-1})***
Positive - accelerating	$1.909\cdot10^{9}$	117.89
Positive - decelerating	$1.998\cdot10^{9}$	130.29
Negative - accelerating	$2.016\cdot10^{9}$	515.68
Negative - decelerating	$1.831\cdot10^{9}$	52.972

$$\frac{1}{\alpha} = \frac{a}{2\cdot\psi\cdot d_h^2}, \tag{7}$$

$$C_2 = \frac{b}{\psi^2\cdot d_h}. \tag{8}$$

If (7) and (8) are applied to the data listed in Table III, the viscous resistance and inertial resistance coefficients for the four time intervals are derived. For negative coefficients, their absolute values are used. The viscous and resistance coefficients to be imported in the porous media feature are listed in Table V.

Afterwards, the existence of *thermal equilibrium* or *non-thermal equilibrium* between the solid and the fluid zone of the regenerator is selected. In an actual engine there is no thermal equilibrium betwen gas and regenerator matrix. However, the derived heat transfer coefficient lead to a simulation associated with high residuals and low convergence. Because of that, the *thermal equilibrium* feature was finally selected. Under this, no heat transfer coefficient is required. In a porous medium with thermal equilibrium between the fluid and the solid zone, the temperature of the regenerator metal is constant. Because of the very low deviation of solid temperature (Figure 8), this assumption was considered to be relatively correct.

V. RESULTS AND DISCUSSION

A. Initial modeling

The agreement of the two approaches will be checked by the comparison of properties that are regarded as descriptive of the gas flow. Hereafter, the label *Metal regenerator* will describe the result coming from the simulations where the metal regenerator was used (II and III). The term *Porous media* corresponds to the simulation at which the regenerator was modeled as porous medium (IV).

The variation of Reynolds number is illustrated in Figure 10. The results are almost identical to each other. The agreement in the values of Reynolds number indicates an agreement of the two approaches in terms of gas mass flow rate and velocity.

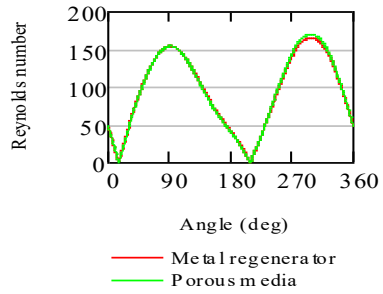

Figure 10: Variation of Reynolds number

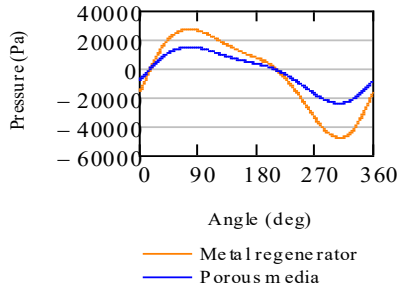

Figure 11: Pressure drop

The comparison of pressure drop is illustrated in Figure 11. Contrary to what was noticed in the case of Reynolds number, there is a clear difference in pressure drop according to the two simulations. The drop resulted from porous media modelling is roughly half of the pressure drop that came out from the simulation of the metal regenerator. As a result, the resistance coefficients that define pressure drop and were inserted to ANSYS Fluent (Table V) have to be modified.

B. Modification of resistance coefficients

At first, the Cf vs Re correlations for the porous medium modeling were derived. The respective coefficients are presented in Table VI. It is clear that these correlations are quite different than those obtained from the metal regenerator simulation (Table III). This difference can explain the deviation illustrated in Figure 11. For each one of the four time intervals, the ratio of the coeffients listed in Table III to the coefficients listed in Table VI was calculated. For negative ratios, their absolute value was used. Moreover, the ratio of the values of the resulting pressure drop was calculated for each time instance and a mean ratio was calculated for each time interval. The ratios of the coefficients and the pressure drop are presented in Table VII. From the ratio of pressure drop, it can be seen the metal regenerator simulation resulted in rougly double pressure drop than the porous medium approach. It can be noticed that the values of the ratio of a are close to those of pressure drop for each time interval. On the other hand, the ratio of b coefficient cannot be related to the respective ratio of pressure drop.

Based on (7) and (8), the correction of the viscous resistance coefficient should be based on the ratio of *a* coefficient, while the inertial resistance coeffient modification has to be based on the ratio of *b* coefficient. However, only the ratio of *a* coefficient fits well with that of pressure drop. As a result, it is expected that an increase in both resistances according to the ratio of *a* coefficient will lead to a similar increase of pressure drop. So, the viscous and inertial resistance coefficients were modified by being multiplied with the ratio of *a* coefficient for each time interval. The modified coefficients are listed in Table VIII.

TABLE VI: COEFFICIENTS FOR CF VS RE CORRELATIONS – POROUS MEDIUM

Type of flow	***a***	***b***
Positive – accelerating	2.902	$5.826 \cdot 10^{-4}$
Positive – decelerating	2.75	$1.83 \cdot 10^{-3}$
Negative – accelerating	3.251	$-3.374 \cdot 10^{-3}$
Negative – decelerating	2.449	$1.795 \cdot 10^{-3}$

TABLE VII: RATIOS OF FRICTION FACTOR CORRELATION COEFFICIENTS AND PRESSURE DROP

	Ratio		
Type of flow	***a***	***b***	***dp***
Positive – accelerating	1.87	1.431	1.83
Positive – decelerating	2.065	0.504	1.95
Negative – accelerating	1.763	1.081	1.92
Negative – decelerating	2.125	0.209	2.12

TABLE VIII: CORRECTED VISCOUS AND INERTIAL RESISTANCE COEFFICIENTS.

Type of flow	***1/α (m^{-2})***	***C_2 (m^{-1})***
Positive – accelerating	$3.57 \cdot 10^{9}$	220.5
Positive – decelerating	$4.126 \cdot 10^{9}$	269.1
Negative – accelerating	$3.553 \cdot 10^{9}$	909
Negative – decelerating	$3.891 \cdot 10^{9}$	112.6

The pressure drop resulted from the simulation with the modified coefficients is presented and compared with the pressure drop resulted from the metal regenerator simulation in Figure 12. It is clear that the two plots are closer to each other, compared to Figure 11. This shows that the corrected coefficients better represented the metal regenerator. However, the pressure drop resulting from the porous medium is still lower that that of the metal regenerator case. So, the process described in V.B may be repeated. Finally, it must be noticed that the modification of the resistance coefficients did not cause any

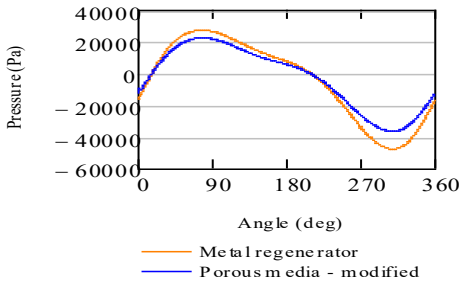

Figure 12: Pressure drop – corrected coefficients.

change is the other properties of working gas in the regenerator, such as mass flow-rate, velocity, Reynolds number and temperature.

VI. CONCLUSIONS

In the present work, a small compact regenerator is designed and simulated as a part of a Stirling Engine. Properties including Reynold number, mass flow-rate, velocity and pressure drop are presented and discussed. Due to the oscillating flow and the existence of different instances of flow reversal at different levels of the regenerator, no single equation can be used to correlate friction factor (Cf) with Reynolds number (Re) for the total duration of the cycle. The cycle must be divided in four parts, with the division being based on the flow direction and the acceleration or deceleration of gas flow. Four correlating equations are derived. The same procedure is followed for the derivation of correlations between Nusselt number (Nu) and Reynolds number, in order that the heat transfer coefficient can be expressed. Along with that, the variation of temperature and heat transfer in the regenerator is discussed.

The engine is again simulated with the regenerator modelled as porous medium. From the Cf vs Re correlations, two resistance coefficients are derived for each time interval and are inserted as input for the porous media modeling. Due to simplicity reasons, the thermal equilibrium feature was selected and no heat transfer coefficient was imported. The results of the two simulations are in good agreement in terms of flow-rate and velocity. However, the pressure drop resulting from the porous medium was lower than that caused by the metal regenerator. The Cf vs Re equations were derived for the porous media simulation. Their difference with the coefficients coming from the metal regenerator simulation can explain the respective difference in pressure drop. The viscous and inertial resistance coefficients of the porous medium were corrected based on the ratio of the Cf vs Re correlation coefficients coming from the two approaches. After the modification of the resistance coefficients, the values of pressure drop resulting from the porous medium approach is relatively close to that resulting from the metal regenerator. The porous media resistance coefficients may be again modified according to the described method, so the two approaches result to equal pressure drops.

REFERENCES

[1] Xiao G., Peng H., Fan H., Sultan U., Ni M., "Characteristics of steady and oscillating flow through regenerator". s.l. : International Journal of Heat and Mass Transfer, 2017, Vols. 108, pp 309-321.

[2] Rogdakis E., Dogkas G., Bitsikas P., "Study of gas flow through a Stirling engine regenerator", Tampa, Florida, USA : ASME 2017 IMECE, 2017.

[3] Costa, C et al., "Experimental and numerical flow investigation of Stirling engine regenerator", Energy, 2014, Vols. 72, pp. 800-812.

[4] Thomas B., Pittman D., "Update on the evaluation of different correlations for the flow friction factor and heat transfer of Stirling Engine regenerators", 35th Intersociety of Energy Conversion Engineering Conderence and Exhibition, 2000. Vols. 1, pp. 76-84.

[5] Gedeon D., Wood J.G. *Oscillating-Flow Regenerator Test Rig: Hardware and Theory with Derived Correlations for Screens and Felts.* Cleveland, Ohio : NASA Le.R.C., 1996.

[6] Costa C., Barrutia H., Esnaola J., Tutar M., "Numerical study of the pressure drop phenomena in a wound woven wire matrix of a Stirling regenerator" Energy conversion and management, 2013, Vols. 67, pp. 57-65.

[7] Costa C., Barrutia H., Esnaola J., Tutar M., "Numerical study of the heat transfer in wound woven wire matrix of a Stirling regenerator", Energy Conversion and Management, 2014, Vols. 79, pp. 255-264.

[8] Urieli I., Berchowitz D. Stirling cycle engine analysis. Bristol : Adam Hilger, 1983.

[9] Costa C., Barreno I., Tutar M., Esnaola J., Barrutia H., " The thermal non-equilibrium porous media modelling for CFD study of woven wire matrix of a Stirling regenerator.", Energy Conversion and Management, 2015, Vols. 89, pp 473-483.

[10] ANSYS FLUENT 12.0, User's Guide. 2009.

[11] Dyson R., Wilson, S., Tew, R., Demko, R., "Fast whole-engine Stirling analysis" San Francisco, USA : 3rd IECEC, 2005.

[12] Rogdakis E., Bitsikas P., Dogkas G. "Numerical Simulation of Prime Mover Stirling Engine by Finite Volume Method" Newcastle, UK : Inernational Stirling Engine Conference, 2016.

Review of GIS application in energy research

Petar Vranić[1], Milan Milovanović[2]

[1]Mathematical Institute SASA, Belgrade, Serbia, petarvvv@gmail.com
[2]Department of Geography, Faculty of sciences and mathematics, University of Niš, Serbia, milovanovic.milan89@gmail.com

Abstract— **Research in energy industry involves various types of tools and methods. The objective of this paper is to review the application of GIS in this field. The analysis includes 123 articles for the period 2014-2018. The articles were analysed according to following criteria: 1) research objective, 2) type of energy according to source, 3) methodological priority, 4) the tool/method applied, 5) methodological approach, 6) purpose of use, 7) innovation, 8) spatial level, 9) software used, 10) geographical distribution. Results shows an increase in the use of GIS in energy research from 2014 onwards, mostly in feasibility studies with a prominent focus on solar energy. In most cases, GIS is employed as a primary tool usually combined with multi-criteria decision making methods. In the term of purpose and innovation, analysis and application of existing tools dominate. The most used software is ArcGIS while a considerable number of articles comes from Italy.**

Keywords – GIS, energy research, spatial analysis, review

I. INTRODUCTION

Studies show that energy consumption will grow in the future, partly due to the continuous energy access oriented policies, especially in the developing countries [1]. As estimated by World Bank, considering only electrical energy, 2.6 billion people will get access to electricity by 2030, while 4.4 billion will be served with modern cooking services [2]. Therefore, as pointed in [1] the need for sustainable and appropriate approaches in energy planning is obvious.

In order to address challenges like supply-demand side, life cycle analysis, government support, policy, land-use changes, spatial and temporal dynamics, a climate dependence of renewable energy sources (RES), etc. energy planning field relies on diverse decision-making methods. In the past four decades, many aspects of energy planning within a wider umbrella of sustainability concept has increasingly gain research interests [3]. The significant increase is prominent in RES

In reference [4] authors identified what are potentially the most popular evaluation and selection approaches for the sustainable energy and highlighted commonly used criteria in assessing and selecting best green energy sources worldwide. As they found out, there is various techniques and individual or hybrid approaches applied in RES planning and scheduling. Also, they pointed out that field of strategic energy planning decision-making research increased last decade, largely influenced by a global transition towards RES.

Research and planning in the energy domain often call for spatially explicit methods. Some examples cover energy demand in built environment [4], feasibility studies or energy potential assessments [5] [6], analysis for energy power-plants [7], or infrastructure planning [8]. In these terms, Geographical Information Systems (GIS) has proved as valuable tool for supporting spatial decision-making process [9] [10]. Although GIS offer numerous possibilities to enhance the energy systems modeling process it is still underutilized.

Resch et al., in their study review some of the main shortcomings of previous approaches in using GIS in RES modeling highlighting twelve aspects for future research avenues [11]. They critically reflect on the lack of generic methods for trans-domain integration of energy (system) models and geospatial analysis processes and still dominant application of GIS for singular cases. Among other improvements, they suggest

ISBN: 978-86-80616-03-2

1) integration of spatial and temporal dynamics into energy system modeling processes for improving understanding of real-time energy demand, capacity and load patterns of energy infrastructures and 2) the potential return of investments and economic profitability. Also, they point out the potential of open data (or crowdsourcing data) due to its increasing importance worldwide, as a means of overcoming the lack of relevant geodata or deficient data quality.

Taking into account aforementioned, the objective of this research is to review the application of GIS in energy research shading a light on some of the recent research in the field.

II. METHODOLOGY

This paper applies 'the use of GIS technology in energy research' as the search topic. For that, we conducted a literature search using EBSCO Discovery Service. In order to reach a larger number of articles, we used rather broadly defined keywords "energy" and "GIS" instead of focusing on specific types of energy and narrow the results. The period is from 2014-2018, and types of literature include review and proceeding papers. We did not limit reference databases to any particular citation index (e.g. SCI Expanded or SSCI). Articles that include the marginal use of GIS in applied methodology were not considered in further analysis. Finally, 123 articles are selected for the analysis. After the search process, we explored the articles based on twelve criteria as shown in Table 1. Due to inconsistency in used keywords for some of the phrases we performed manual consolidation. For instance, in case of GIS tool, the keyword 'interpolation' has different forms, respectively, ordinary Kriging, inverse weighted distance, spatial interpolation, Kriging interpolation, etc. We merged those variations into interpolation. Similarly, other synonyms were grouped into word or relevant phrases.

TABLE I. CRITERIA FOR ANALYSIS

1. **PUBLICATION TREND**
2. **LEADING ACADEMIC JOURNAL**
3. **TYPE OF ENERGY ACCORDING TO SOURCE**
   Solar
   Wind
   Hydro
   Geothermal
   Biogas
   Combined
4. **RESEARCH OBJECTIVE**
   Feasibility - research focuses on potential for use of particular energy source
   Allocation - research focuses on the selection of sites for exploitation of particular energy source
   Optimization - research focuses on the optimization of use of particular energy source
5. **METHODOLOGICAL PRIORITY**
   Primary - spatial analysis through GIS is used as primary method in research
   Secondary - spatial analysis through GIS is used as secondary method in research
6. **METHODOLOGICAL APPROACH**
   Individual - spatial analysis through GIS is used as the only method in research
   Hybrid - spatial analysis through GIS is used in combination with other methods in research
7. **TOOL / METHOD APPLIED** - refers to type of GIS tool applied in research
8. **PURPOSE OF USE**
   Analysis - GIS tool is applied primarily for analysis
   Synthesis - GIS tool is applied primarily for synthesis
   Data integration and visualization - GIS tool is primarily for data integration or visualization
9. **INNOVATION**
   Application - research applied existing GIS tools
   Development - research developed new GIS tools
10. **SPATIAL LEVEL** - indicates the spatial level at which the research is applied
    Regional
    National
    County
    City /Municipality
    Local
11. **SOFTWARE USED**
    Not defined
    Open Source
    Commercial
12. **GEOGRAPHICAL DISTRIBUTION** - study area

III. FINDINGS

Publication trend and leading academic journals. One significant indicator for measuring research trends is a number of published academic papers for the observed period. This paper takes into account only four years, thus, any thorough conclusion regarding research trend is highly arbitrary. However, some indication can be drawn from the analysis. It is apparent that the application of GIS tools in energy research is gaining a peace starting from 2014. According to the results 10 articles were published in 2014 (8.13%), 19 (15.5%) in 2015, 26 (21.4%) in 2016 and 47 (38.2) in 2017. We assume that trend will continue since 21 articles

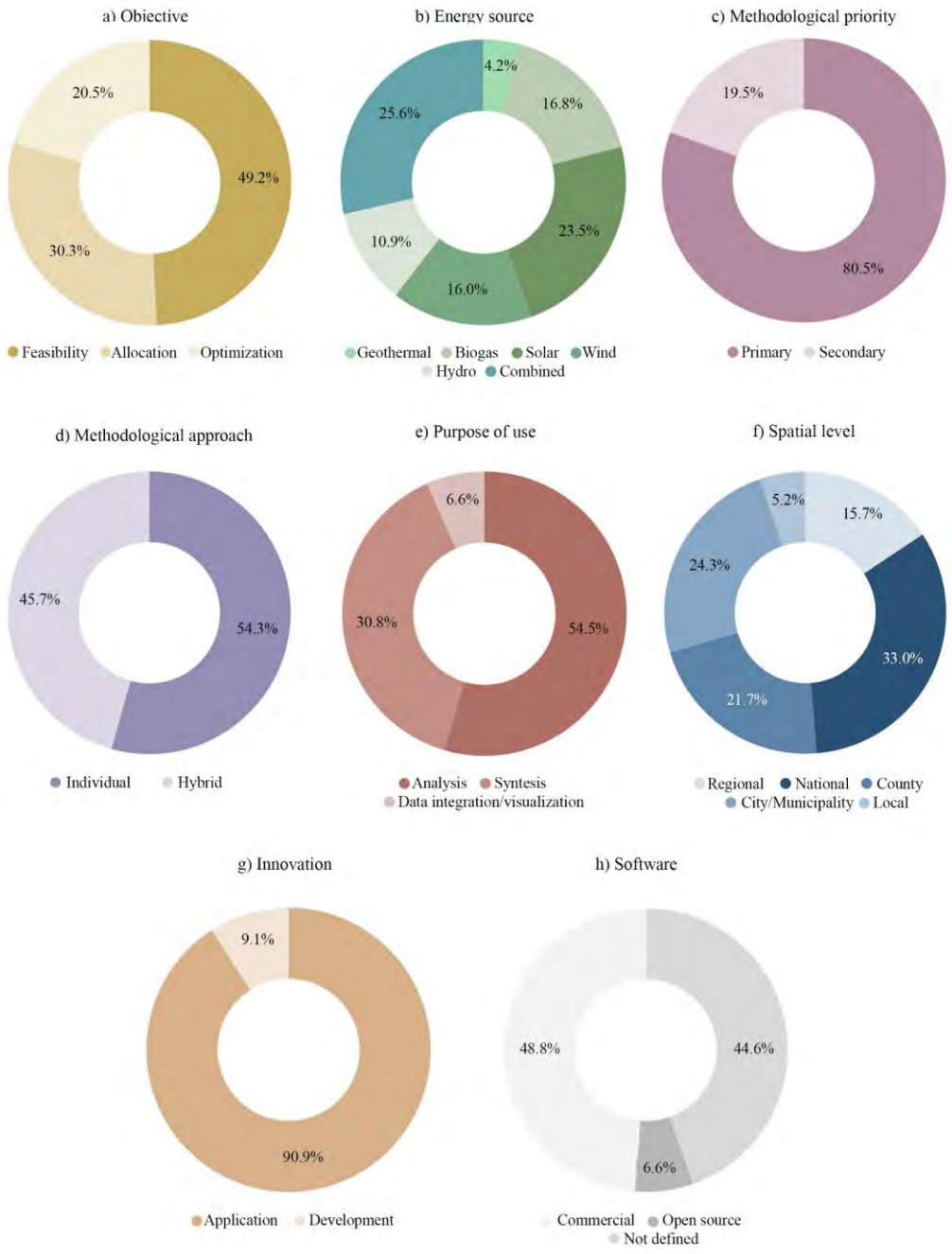

Figure 1. Distribution of articles based on defined criterria

(17%) are published in the first half of 2018 (that was almost equal as a number of published articles in 2016).

There are more than 50 journals that cover the subject matter. However, as is shown in Table II. 11 journal counts for 54.7% of all analyzed articles. The rest of the journals (42) have a cumulative share of 45.3%. When it comes to journals with the considerable number of published papers the following are leading: *Renewable and Sustainable Energy Reviews* 17 (13.8%), *Renewable Energy* 8 (6.5%), *Applied*

Energy 7 (5.7%), *Sustainability* 7 (5.7%), and *Energy Proceedia* 6 (4.9%). Considering the impact factor, most of the leading journals have an impact factor greater than 1 (10 out of 11), indicating their academic influence.

Research objective. The analysis shows that the GIS was mostly used in feasibility studies (49.2%). Some examples include the assessment of offshore wind energy potential, feasibility analysis in large and small PV plants, confirmation of the financial feasibility of rooftop wind turbines in urban areas, etc. Its application for analysis of issues related to allocation has a share of 30.3% (Figure 1a). Allocation is mostly related to the selection of the best site for use of particular energy source and often includes multi-criteria decision techniques as a supportive method, e.g. GIS-AHP combination for the site's assessment of large-scale concentrated solar power plants [12], assessment of the opportunities for small-scale pumped hydro energy storage in middle-mountain areas [13] etc. Optimization (with share of 20.5%) principally relates to various studies on energy use and the increasing of energy efficiency in built environment; for instance assessing energy performances toward energy efficiency at the municipal level [14], estimation of the building energy use intensity at urban scale by integrating GIS and big data technology [15], smart energy utilities based on real-time GIS web services and the internet of things [16], optimization and GIS-based combined approach for the determination of the most cost-effective investments in biomass sector [17].

Type of energy according to the source. Results show that GIS, as a research tool, is widely used in the field of energy research in recent years despite the source of energy being analyzed. However, considering the energy source, GIS was dominantly employed in research of solar energy (23.5%), followed by biogas energy (16.8%), wind energy (16 %), and hydro energy (10.9%). In the domain of geothermal energy, it was used to a lesser degree (4.2%). So considerable number of articles are dedicated to RES. The highest share of analyzed articles (28.6%) applied GIS tools for research of combined energy sources e.g. development of a geospatial database for the wind and solar energy application using multi-criteria GIS model [18]. These criteria also include researches that focus on energy consumptions, despite the source of energy (e.g. built environment energy use at urban scale).

Methodological priority and methodological approach. Due to the scope of research and applied approach, as assumed, in 80.5% of a total number of the articles GIS was used as a primary research tool/method (Figure 1c). In cases where it was used as a primary method, GIS typically perform an integrative role. It serves as a platform for the integration of diverse data derived from secondary methods (e.g. statistical analysis, cost-benefit analysis, multi-criteria analysis, etc.) and their further processing applying different geospatial tools; for instance using GIS analytics and social preference data to evaluate utility-scale solar power site suitability [19], integrating GIS databases and ICT applications for the design of energy [20]. In a case where GIS is used as a secondary method, it typically served as a tool for partial analysis or visualization of research results.

TABLE II. METHODS COMBINED WITH GIS TOOS IN HYBRID APPROACHES

BIM	PRAMETRIC MODELING	AHP (FUZZY)
NEURAL NETWORKS	LEVELISED COST ENERGY	SYSTEM ADVISORY MODEL
LCA	NUMERICAL WAVE MODEL	MULTIPLE LINEAR REGRESSION
CBA	STAT. ANALYSIS	ELASTIC NET ALGORITHM
ORDERED WEIGHTED AVERAGING	ECONOMETRIC ANALYSIS	ENTROPY-WEIGHT METHOD
SACS	WEIGHTED LINEAR COMBINATION	MONTE CARLO SIMULATION
WASP	NETWORK PROGRAMMING	DATABASE MANAGEMENT

Looking at the methodological approach, analysis point to the relatively equal use of GIS as a single method or combined with other methods (Figure 1d). Results point to a variety of GIS tools applied in both cases. In cases when research employs a hybrid approach, GIS tools were combined with a substantial number of various methods (Table II). However, some of them are used more frequently such as AHP and statistical analysis. Application of hybrid approaches includes diverse research aspects e.g. BIM-GIS integrated pre-retrofit model for building data mapping [21], optimizing the

location of a biomass plant with a fuzzy-decision-making trial and evaluation laboratory (F-DEMATEL) and multi-criteria spatial decision assessment for renewable energy management [22], the Levelized Cost of Energy (LCOE) of wave energy using GIS based analysis [23].

Tool/method applied. In terms of tools/methods, despite the software used, GIS offers the large number of options for advanced spatial analysis. However, four tools are more exploited than others, contributing with 57.7% of all analyzed tools (Table III). These tools/methods represent *spatial mapping* (17.1%), cluster of tools related to manipulation with *Digital Elevation Models - DEM* (15.4%), *interpolation* (14.6%) and *overlaying* (10.6%). *Spatial mapping* is typically used for the representation of data generated through application of other methods (e.g. statistical analysis). Some examples include for instance mapping of urban heat demand [24], or using participatory GIS to examine social perception towards proposed wind energy landscapes [25]. Toolset for manipulation with *Digital Elevation Models* (e.g. analysis of aspect, slope, view-shade, etc.) is mostly used in allocation studies and primary in solar energy research, often combining other spatial data, through the multi-criteria evaluation model to extract the most suitable location for power plant implementation. For instance, Charabi et al., use it to identify the optimal location for installation of sitting PV power plants on inclined terrains [26]. While Massimo et al., use it to determine spatial variations of solar radiation for development of a GIS for the Integration of solar energy in the energy planning processes [27]. *Interpolation* is the procedure of using points with known values or sample points to predict the values at other unknown points. It is based on principles of spatial autocorrelation (spatial dependences) that allows a user to measure dependence between near and distant objects In their research, for instance, Bosch et al., use bilinear interpolation to estimate average capacity factor for onshore wind turbine installation in China [28]. In other example Noorollahi et al., applied spatial interpolation through Kriging method using neighboring known values for spatial analysis of a ground source heat pump systems for regional shallow geothermal mapping [29]. *Overlaying* is operation that superimposes multiple data sets together in order to identify relationships between them. Analysis shows that this tool is mostly used in allocation and feasibility studies. For instance, Vasileiou et al., employed this tool for selection of hybrid offshore wind and wave energy systems superimposing thematic maps related to utilization, technical, economic and social constraints [30].

TABLE III. GIS TOOLS

Tool	**%**
SPATIAL MAPPING DEM INTERPOLATION OVERLAYING	57.7
MULTI-CRITERIA ANALYSIS IMAGE CLASSIFICATION AND REMOTE SENSING TECHNOLOGY PYTHON SCRIPTING DATABASE CREATION BOOLEAN OPERATION MODEL BUILDER BUFFER GEOSPATIAL MULTILINEAR REGRESSION FIELD CALCULATOR PROXIMITY ANALYSIS RASTER CALCULATOR MULTIPLE LINEAR REGRESSION CALCULATE METRICS GEOSTATISTICS HYDROLOGY TOOLSET FOCAL STATISTICS ZONAL STATISTICS AREA SOLAR RADIATION TOOL WATER BALANCE ANALYSIS SOLAR ANALYST MODEL GDAL EXTRAPOLATION EUCLIDEAN DISTANCE GEOCODING GPS MAPPING REAL-TIME WEB GIS R.SUN AGGREGATION FUZZY LOGIC (STATISTICS) SPATIO-TEMPORAL ANALYSIS	42.3

Purpose of use. In line with aforementioned discussion, research in energy mostly apply tools for analysis of either location, according to

multiple criteria, or spatial distribution of energy sources (54.5%). Some examples include the estimation of energy savings for the residential building stock, planning land use for biogas energy crop production or the end-use electric energy consumption in urban areas. In 38.8% of the analysed articles GIS tools are used for synthesis (Figure 1e). For instance application of GIS in researches like an assessment of sustainable grassland biomass potentials for energy supply [31], multiregional potential evaluation, and strategies selection framework for various renewable energy sources, targeting and modeling urban energy retrofits using a city-scale energy mapping approach [32], etc.

Spatial level. As is shown in Figure 1f, when it comes to spatially explicit research in energy planning, analysis on the national level is dominant (33%). They primarily employ GIS tools for assessment/feasibility study of energy sources, e.g. solar power potential of Tanzania [33], spatial assessment of the potential of renewable energy in Ecuador [34], the levelized cost of energy of wave energy in Portugal [23]. On the other hand, secondly most researched spatial level represent the city/municipality level (24.3%). At this level, GIS tools are often applied for studying energy consumption and optimization, e.g. estimation of the building energy use intensity in the urban scale [35], analysis of e-mobility in urban areas - evaluation of the impact on the electric energy grid [36], targeting and modeling urban energy retrofits using a city-scale energy mapping approach). County level is third most researched level (21.7%), followed by regional (15.7%) and local level (5.2%). The local level typically considers block or building level focusing on energy efficiency, e.g. integrating BIM and GIS in design process for high energy efficiency hospital buildings [37].

Innovation. In spite of potential for development of new tools that most of GIS softwares offer, through various means (python programming, model builder, etc.) 87% of analyzed articles applied already existing tools for research (Figure 1g). The marginal share of research is based on newly developed methods or tools (13%). For instance in article *Smart Energy Utilities based on Real-time GIS Web Services and Internet of Things* [38], the authors developed a web-based system capable of real-time web mapping services (WMS). The introduced system consists of the autonomous computer program, spatial database, GIS server, cloud computing platform, a WMS and web-feature service. Another example includes the development of bottom-up urban energy computing based on reductive procedure using generated python plug-in [39]. In their research, Cevallos-Sierra and Ramos-Martin developed the script for layer values normalization in order to perform a spatial assessment of the potential of renewable energy using open-source programming language Python which was afterward introduced in a GIS environment [34].

TABLE IV. GEOGRAPHICAL DISTRIBUTION OF ARTICLES

Country	%	Country	%
Italy	8.9	Gran Canarias	0.8
USA	5.7	Hong Kong	0.8
China	4.9	Hungary	0.8
India	4.1	Kurdistan	0.8
Iran	4.1	Malaysia	0.8
Japan	4.1	Mauritius	0.8
Spain	4.1	Sweden	0.8
Turkey	4.1	Netherlands	0.8
Germany	3.3	Oman	0.8
Portugal	3.3	Pakistan	0.8
UK	2.4	Russia	0.8
Austria	1.6	Serbia	0.8
Greece	1.6	South Africa	0.8
Mexico	1.6	South Korea	0.8
Poland	1.6	Switzerland.	0.8
Chile	0.8	Taiwan	0.8
Korea	0.8	Tanzania	0.8
Egypt	0.8	Tibet	0.8
Romania	0.8	Thailand	0.8
Finland	0.8	UAE	0.8
France	0.8	Africa	4.1
Bangladesh	0.8	Europe	1.6
Canada	0.8	Middle East	0.8
Cyprus	0.8	Northwest Europe	0.8
Ecuador	0.8	Not defined	12.5
Total			**100**

Software used. GIS software market is expanding. There is growing share of Open Source GIS softwares like *QGIS, GRASS, SPRING, gVGIS, uDig GIS* and *Open Source Web Mapping like GeoMajas, GeoServer, MapFish, OpenWebGIS* etc. Nevertheless, commercial software ArcGIS dominates in analyzed articles (48.8%). Even though the tools presented in analyzed researches are “common”

for most of the software, Open Source software retains a marginal share of (6.6%), with QGIS as the leading one. Finally, a sheer number of cases, as much as 44.6%, did not specify software used in research.

Geography distribution of articles. In terms of geographical distribution analyzed articles come from 46 countries, while 9 are related to regional research (e.g. Africa, Northwest Europe, Middle East, etc.). However, several countries contribute with a large share of articles (49%), among which Italy, USA, and China counts for nearly 20% (Figure 1h). The remaining countries mostly contribute with 1 article.

IV. Concluding remarks

This paper analyzed the application of GIS in energy research according to 12 criteria. The results point to the diverse application of GIS tools both in the case of energy sources and spatial levels, as well as, geographical distribution. In terms of tools applied, limited options are explored, thus, further exploration of development aspects can contribute to energy research in the future. Presented results confirmed the capacity of GIS to enhance the energy researches. Considering many pieces of research that employ combined methods, it is apparent that GIS is suitable for the development of hybrid methodologies and thus can, as an integrative tool, contribute to cohesive research in this field that requires the simultaneous application of several methods in a decision-making process. However, in line with discussion presented in research [11], results confirm that GIS is still largely applied in individual cases, thus, trans-domain integration of energy (system) models are yet to be explored. We can expect a further increase in the use of GIS in this domain, since the Open Source market is expanding, and thus, the affordability and accessibility of tools for spatially explicit analysis of energy systems.

Acknowledgment

Petar Vranić acknowledge the support by the Ministry of Education, Science and Technological Development of the Republic of Serbia through Mathematical Institute of Serbian Academy of Sciences and Arts (Project III 044006). Milan Milovanović acknowledge the support from research project “Development programs of revitalization of Serbia Villages” no. 176008, funded by Ministry of education, sciences and technological development of the Republic of Serbia.

References

[1] F. Riva, A. Tognollo, F. Gardumi and E. Colombo, "Long-term energy planning and demand forecast in remote areas of developing countries: Classification of case studies and insights from a modelling perspective" *Energy Strategy Reviews,* vol. 20, pp. 71-89, 2018.

[2] IEA, World Bank, "Sustainable Energy for All 2015-Progress toward Sustainable" World Bank, Washington, DC, 2015.

[3] A. Aravossis, and E. Strantzali, "Decision making in renewable energy investments: a review" *Renew Sustain Energy Rev,* pp. 858-898, 2016.

[4] V. Howard, et al., "Spatial distribution of urban building energy consumption by end use" *Energy Build,* vol. 45, pp. 141-151, 2012.

[5] M. Mirhosseini, F. Sharifi, and A. Sedaghat ,"Assessing the wind energy potential locations in province of Semnan in Iran" *Renew. Sustain. Energy Rev.,* vol. 15, pp. 449-459, 2011.

[6] I. Schardinger, F. Botzenhart, M. Biberacher, T. Hamcher and T. Blachke, "Integrating spatial models into regional energy system optimisation: Focusing on biomass" *Int. J. Energy Sector Manag.,* vol. 6, pp. 5-32, 2012.

[7] V. Fthenakis and R. Van Haaren, "GIS-based wind farm site selection using spatial multi-criteria snalysis (SMCA): Evaluating the case for New York State" *Renew. Sustain. Energy Rev.,* vol. 15, pp. 3332-3340, 2011.

[8] J. Vogt and B. Sliz-Szkliniarz, "GIS-based approach for the evaluation of wind energy potential: A case study for the Kujawsko–Pomorskie Voivodeship" *Renew. Sustain. Energy Rev.,* vol. 15, pp. 1696-1707, 2011.

[9] M. Blesl, S. Kempe, H. Huther, "Capture of spatial high-resolution building heating energy demand" *Euroheat Power,* vol. 39, pp. 28-33, 2010.

[10] M. Schoof, B. Resch and D. Ludwig "A GIS-based concept for solar energetic examination of new building projects" *gis.SCIENCE,* vol. 3, pp. 97-103, 2013.

[11] B. Resch, "GIS-Based Planning and Modeling for Renewable Energy: Challenges and Future Research Avenues" *ISPRS Int. J. Geo-Inf.* , vol. 3, pp. 662-692, 2014.

[12] A. Yushchenko, A. Bono, B. Chatenoux, M. K. Patel and N. Ray, "GIS-based assessment of photovoltaic (PV) and concentrated solar power (CSP) generation potential in West Africa" *Renewable and Sustainable Energy Reviews,* vol. 81, pp. 2088-2103, 2018.

[13] A. Rogeau, R. Girard and G. Kariniotakis, "A generic GIS-based method for small Pumped Hydro Energy Storage (PHES) potential evaluation at large scale" *Applied Energy,* vol. 197, pp. 214-253, 2017.

[14] F. Poggi, A. Firmino and M. Amado, "Assessing energy performances: A step toward energy

efficiency at the municipal level" *Sustainable Cities and Society,* vol. 33, pp. 57-69, 2017.

[15] J. MaJack and C. Cheng, "Estimation of the building energy use intensity in the urban scale by integrating GIS and big data technology" *Applied Energy,* vol. 183, pp. 182-192, 2016.

[16] R. Nourjoua and M. Hashemipour, "Smart Energy Utilities based on Real-Time GIS Web Services and Internet of Things" *Procedia Computer Science,* vol. 110, pp. 8-15, 2017.

[17] V. Vukašinović and D. Gordić, "Optimization and GIS-based combined approach for the determination of the most cost-effective investments in biomass sector" *Applied Energy,* vol. 178, pp. 250-259, 2016.

[18] K. Al-Joburi and N. Dahman, "A Geospatial Database for Wind and Solar Energy Applications: The Kingdom of Bahrain Study Case" in *E3S Web Conf.-World Renewable Energy Congress-17*, 2017.

[19] J. Brewer, D. P. Ames, D. Solan, R. Lee and J. Carlisle, "Using GIS analytics and social preference data to evaluate utility-scale solar power site suitability" *Renewable Energy,* vol. 81, pp. 825-836, 2015.

[20] T. Togawa, T. Fujita, L. Dong, S. Ohnishi and M. Fujii, "Integrating GIS databases and ICT applications for the design of energy circulation systems" *Journal of Cleaner Production,* vol. 114, pp. 224-232, 2016.

[21] Ö. Göçer, Y. Hua and K. Göçer, "A BIM-GIS integrated pre-retrofit model for building data mapping" *Building Simulation,* vol. 9, pp. 513-527, 2016.

[22] J. SuJeong and Á. Ramírez-Gómez, "Optimizing the location of a biomass plant with a fuzzy-DEcision-MAking Trial and Evaluation Laboratory (F-DEMATEL) and multi-criteria spatial decision assessment for renewable energy management and long-term sustainability" *Journal of Cleaner Production,* vol. 182, pp. 509-520, 2018.

[23] L. Castro-Santos, G. P. Garcia, A. Estanqueiro and P. A. Justino, "The Levelized Cost of Energy (LCOE) of wave energy using GIS based analysis: The case study of Portugal" *International Journal of Electrical Power & Energy Systems,* vol. 65, pp. 21-25, 2015.

[24] A. Wyrwa and Y.-k. Chen, "Mapping Urban Heat Demand with the Use of GIS-Based Tools" *Energy,* vol. 10, no. 5, 2017.

[25] A. Lombard, "Using participatory GIS to examine social perception towards proposed wind energy landscapes" *Journal of Energy in Southern Africa,* vol. 26, no. 2, 2015.

[26] A. Georgiou and D. Skarlatos, "Optimal site selection for sitting a solar park using multi-criteria decision analysis and geographical information systems" *Geosci. Instrum. Method. Data Syst.,* vol. 5, pp. 321-332, 2016.

[27] A. Massimo, M. Dell'Isola, A. Frattolillo and G. Ficco, "Development of a Geographical Information System (GIS) for the Integration of Solar Energy in the Energy Planning of a Wide Area" *Sustainability,* vol. 2104, no. 6, pp. 5730-5744, 2014.

[28] J. Bosch, I. Staffell and A. D. Hawkes, "Temporally-explicit and spatially-resolved global onshore wind energy potentials" *Energy,* vol. 131, pp. 207-217, 2017.

[29] Y. Noorollahi, H. G. Arjenaki and R. Ghasempour, "Thermo-economic modeling and GIS-based spatial data analysis of ground source heat pump systems for regional shallow geothermal mapping" *Renewable and Sustainable Energy Reviews,* vol. 72, pp. 648-660, 2017.

[30] M. Vasileiou, E. Loukogeorgaki and D. G. Vagiona, "GIS-based multi-criteria decision analysis for site selection of hybrid offshore wind and wave energy systems in Greece" *Renewable and Sustainable Energy Reviews,* vol. 73, pp. 745-757, 2017.

[31] D. Ketzer, C. Rösch and M. Haase, "Assessment of sustainable Grassland biomass potentials for energy supply in Northwest Europe" *Biomass and Bioenergy,* vol. 100, pp. 39-51, 2017.

[32] Y. Sun, R. Wang, J. Li and . J. Liu, "GIS- based multiregional potential evaluation and strategies selection framework for various renewable energy sources: a case study of eastern coastal regions of China" *Energy science & engineering,* 2017.

[33] A. Aly, S. S. Jensen and A. B. Pedersen, "Solar power potential of Tanzania: Identifying CSP and PV hot spots through a GIS multicriteria decision making analysis" *Renewable Energy,* vol. 113, pp. 159-175, 2017.

[34] J. Cevallos-Sierra and J. Ramos-Martin, "Spatial assessment of the potential of renewable energy: The case of Ecuador" *Renewable and Sustainable Energy Reviews,* vol. 81, pp. 1154-1165, 2018.

[35] J. Ma and J. C. Cheng, "Estimation of the building energy use intensity in the urban scale by integrating GIS and big data technology" *Applied Energy,* vol. 183, pp. 182-192, 2016.

[36] M. De Gennaro, E. Paffumi, H. Scholz and G. Martini, "GIS-driven analysis of e-mobility in urban areas: An evaluation of the impact on the electric energy grid" *Applied Energy,* vol. 124, pp. 94-116, 2014.

[37] R. Di Giulio, B. Turillazzi, L. Marzi and S. Pitzianti, "Integrated BIM-GIS based design for high energy efficiency hospital buildings" *TECHNE,* vol. 13, 2017.

[38] R. Nourjou and M. Hashemipour, "Smart Energy Utilities based on Real-Time GIS Web Services and Internet of Things" *Procedia Computer Science,* vol. 110, pp. 8-15, 2017.

[39] N. Ghiassi and A. Mahdavi, "Reductive bottom-up urban energy computing supported bymultivariate cluster analysis" *Energy and Buildings,* vol. 144, pp. 372-386, 2017.

[40] C. Bhowmika, B. Sumit, A. Rayb and K. M. Pandeya, "Optimal green energy planning for sustainable development: A review" *Renewable and Sustainable Energy Reviews,* vol. 71, pp. 796-813, 20117.

Circuit Breaker Replacement Strategy Based on the Substation Risk Assessment

[1]Dragan Stevanović, [2]Aleksandar Janjić

[1]Electric Power Industry of Serbia, Zaječar, Serbia, dragan.stevanovic1@epsdistribucija.rs
[2]Faculty of Electronic Engineering, Niš, Serbia, aleksandar.janjic@elfak.ni.ac.rs

Abstract— **Using statistical data of 427 circuit breakers gathered in past 10 years, Weibull probability distribution of contact resistance for breakers on both overhead and underground feeders is determined. Substations reliability is calculated using minimal path and minimal cuts method. With this methodology influence of CB's condition on substations reliability can be observed by using real field data. In this paper influence of CB removal on substations reliability is presented, together with cost justification of such investment. Example of calculation will be shown on 35/10kV substation.**

Keywords – circuit breaker, substation, Weibull, cost evaluation, reliability.

I. INTRODUCTION

Circuit breaker is a device used for switching feeder power supply in any working mode (normal load, no load, short circuit current…), and therefore represents the vital element of power system stability. CB failure threatens work of other equipment, which directly affects reliability of whole substation. This makes good reason of finding correlation between CB condition and substations reliability.

To determine economic effects of maintenance, overhaul or CB removal [1], [2], assessment of circuit breakers RUL must be done [3], [4]. Remaining useful life is the lifetime from current time to the time that the device fails [1]. It is random variable which depends on various factors (device age, working conditions, and level of maintenance) [5]. CB's reliability analysis depends of type of available data, which can be: contact resistance, commutation noise, erosion resistance [6], ultrasound detectors, transient earth voltage, infrared thermo scanning [7], CB control circuit data [8] and collected data of CB faults [9]. Depending of collected data type, RUL can be assessed with: knowledge based models (fuzzy method [10]); life expectancy models (statistical method [5], [11] – [15]); artificial neural networks and physical models [4].

Utilities, grid operators and industrial power consumers are facing unprecedented challenges. With increasingly aging infrastructure combined with cost-cutting pressures to operate into today's competitive environment, prioritizing investment has never been so important. [16]

In [17] reliability of different substation configurations is evaluated using the minimal cut-set method based on the criterion of continuity of service.

In [18] reliability indices of each failure events and entire reliability indices in the ring bus substation and double bus double breaker substation were calculated and quantitatively compared.

Method that combines the modeling of failures and repairs as stochastic point processes and a procedure of sequential Monte Carlo simulation for computing the reliability indexes is presented in [19].

In [20] comparison between the reliability of different substation constructions is shown.

A number of methods have been used in determining the final substation indices, such as Markov model, minimal cut-set method based on the criterion of continuity of service. [21] have developed a Monte Carlo approach to solving a system with non Markovian models.

ISBN: 978-86-80616-03-2

The mostly used methods are fault tree analysis, event tree analysis, Monte Carlo simulation and State enumeration. [20]

Because of importance of reliability, some companies [16] are started to use software, algorithms and analysis techniques for reliability management services to provide substation owners with the right insights to make optimal investments to improve system performance.

II. CB AGEING PROCESS

The main causes of CB deterioration are the age, the number of operations under normal and fault conditions and the operational conditions like the temperature and contaminants content.

Measuring the contact resistance is usually done by using the principles of Ohm's law. Since the interrupting chamber is a closed container, we have only access to the entry and exit conductors; the measured *R* between these two points would be the sum of all the contact resistances found in series, (fixed, make-break and sliding contacts). According to the IEC 60694 [22], article 6.4.1, the current value to use should be the closest to the nominal current the interrupting chamber is designed for. If it is impossible to do so, lower currents can be used but not less than 50 A to eliminate the galvanic effect that might affect the readings.

A. Data collecting

Analysis covers 42 35/10 kV substations and 427 circuit breakers, mounted on 10kV and 35kV feeders. Measurement of static contact resistance presented by the voltage drop on contacts is collected in past 10 years, where voltage drop was measured on every two years.

Other data regarding to circuit breakers that are collected are: voltage level, feeder type, manufacturing year, number of fault trips, number of short circuit current trips, number of customers, and annual consumption.

B. Data analyzing

In first step, state of every CB is determined, according to its voltage drop value. CB's with voltage drop value beyond permissible are set in "failed" state (F), and those which still have voltage drop value below allowed are in "suspension" state (S). For failed CB's precise year of reaching that condition is defined.

Weibull distribution is most commonly used method for equipment failure, ageing and reliability analysis [23]. It can describe three types of equipment states (infant mortality, normal work, wear out), through bathtub curve [24].

Weibull cumulative distribution function represents probability of failure in given period of time (1). It is two-parametric distribution, with slop parameter η and shape parameter β.

$$F(t) = 1 - e^{\left(\frac{t}{\eta}\right)^{\beta}} \quad (1)$$

Slop parameter shows time at which 63.2% of analyzed units are failed. Shape parameter represents failure rate behavior. Its value tells whether failures are decreasing or increasing. $\beta<1$ indicates infant mortality, while $\beta>1$ shows wear out failures. Higher value of beta indicates greater rate of failure. In Table I Weibull parameters for different criteria are shown.

TABLE I. WEIBULL PARAMETERS

CB feeder type	**η**	**β**	**Fail \ Suspens**
Overhead +25%	39.1	5.2	100 \ 87
Overhead	37.1	4.8	131 \ 56
Underground +25%	41.5	6.1	63 \ 169
Underground	38.1	6.1	97 \ 135
10 kV feeders +25%	43.4	5.6	87 \ 224
10 kV feeders	40.4	5.1	135 \ 176
35 kV feeders +25%	35.2	5.6	79 \ 31
35 kV feeders	33.8	5.6	96 \ 14
all feeders +25%	40.4	5.6	166 \ 255
all feeders	38.0	5.3	231 \ 190

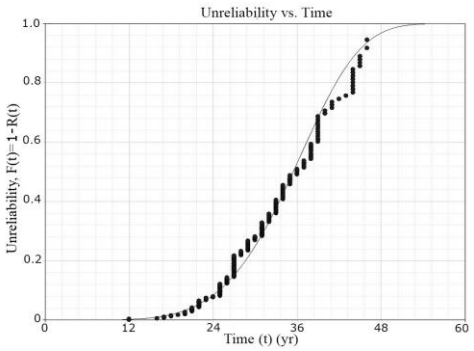

Figure 1. Weibull unreliability for distribution of different criterions: all feeders

Manufacturer's recommendation is also taken in consideration that CB's voltage drop can be reached by 25%. Both β and η parameters are calculated for the whole CB population from the statistical data using the least square method [25]. Weibull distribution function with right censored data (case when some devices didn't failed during period of analysis) unreliability is calculated for all CB's categories. On Fig. 1 unreliability distribution of all CB's is shown.

TABLE II. CB'S RELIABILITY INDICES FROM WEIBULL ANALYSIS

Feeder type	Age	Unreliability	Failure rate
Transformer 35kV	32	0.532	0.226
Transformer 10kV	41	0.278	0.11
Supply 35kV	32	0.532	0.226
Load 10kV	41	0.612	0.11

III. SUBSTATION RELIABILITY ANALYSIS

In this example 35/10kV substation will be used, which has two 8MVA power transformers, two 35kV supply feeders and ten 10kV feeders. Functional blocks are defined and shown in Fig. 2.

Functional block consists of elements which would be out of supply if only one of them fails. Active failure is an event that causes the protection system to operate and isolate a failed component. [17]

Active failure events refer to all failures that induce the actions of protective breakers adjacent to the component where failure occurred and affect normally operating components where no failure occurred. [18]

A minimal cut-set is a set of components that when all fail, the continuity of service is lost, but if any one of the components doesn't fail, the continuity remains. [17]

Using functional blocks from Fig. 2, functional graph can be created. In this case it is considered that 10kV feeders can supply the same load (ring connection).

Substations reliability is calculated with minimal path and minimal cuts method [26].

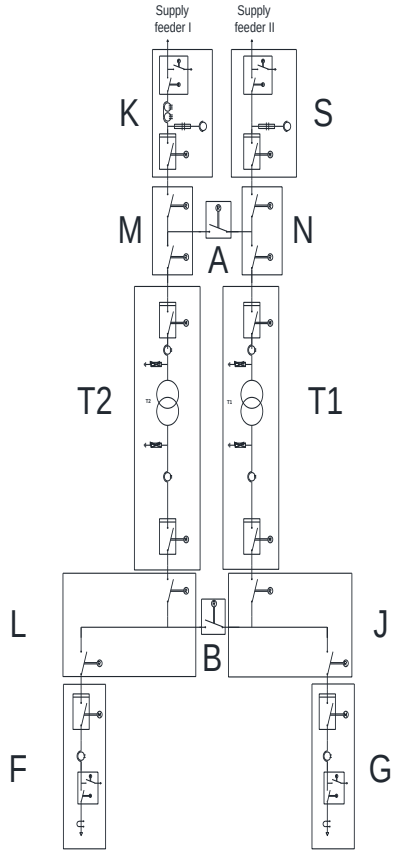

Figure 2. Functional blocks of substation

A. Minimal path method

Path is serial connection of graph branches which connects input and output nod. Minimal path doesn't cross the same nod more than once. For this substation connection matrix C (2) can be made using Fig. 3, where the element E_{ij} is branch which connects nods „*i*" and „*j*".

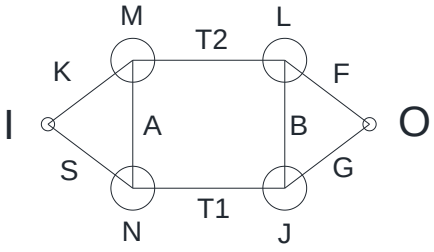

Figure 3. Functional graph

$$C = \begin{bmatrix} 0 & K & S & 0 & 0 & 0 \\ K & 0 & A & T2 & 0 & 0 \\ S & A & 0 & 0 & T1 & 0 \\ 0 & T2 & 0 & 0 & B & F \\ 0 & 0 & T1 & B & 0 & G \\ 0 & 0 & 0 & F & G & 0 \end{bmatrix} \quad (2)$$

Minimal paths of first order doesn't exist here, because there is no just one branch which connects input and output nod.

Minimal paths of second order are obtained by multiplying (from right side) first row of matrix *C* with whole matrix *C*.

Minimal paths of third order are obtained by multiplying former result with whole matrix *C*. Identical process is carried for minimal paths of next orders.

After calculations, minimal paths are:

III: FKT_2, SGT_1

IV: $KAT_1G, KT_2BG, SAT_2F, ST_1BF$

V: KAT_1BF, SAT_2BG

B. Minimal cuts method

Cut of a graph consists of group of branches by which removal connection between input and output nod is broken. Minimal cut is unique and doesn't include other cuts.

Matrix of minimal paths *P* (4), with size *mxn*, where is *m*- number of minimal paths and *n* – number of branches, has elements E_{ij} which are equal to 1 if branch „*j*" is part of the minimal path „*i*", otherwise it is equal to 0.

If minimal paths are given in next order:

FKT_2; SGT_1; KAT_1G; KT_2BG; SAT_2F; ST_1BF; KAT_1BF; SAT_2BG

$$P = \begin{bmatrix} 1 & 0 & 0 & 0 & 1 & 0 & 1 & 0 \\ 0 & 1 & 0 & 1 & 0 & 0 & 0 & 1 \\ 1 & 0 & 1 & 1 & 0 & 0 & 0 & 1 \\ 1 & 0 & 0 & 0 & 1 & 1 & 0 & 1 \\ 0 & 1 & 1 & 0 & 1 & 0 & 1 & 0 \\ 0 & 1 & 0 & 1 & 0 & 1 & 1 & 0 \\ 1 & 0 & 1 & 1 & 0 & 1 & 1 & 0 \\ 0 & 1 & 1 & 0 & 1 & 1 & 0 & 1 \end{bmatrix} \quad (3)$$

And branches are defined in next order:

K, S, A, T1, T2, B, F, G.

For the graph from Fig. 3 matrix of minimal paths is:

If all elements of one column are all equal to (1), than that branch is minimal cut of first order. Minimal cuts of second order are obtained by adding columns of matrix P (every column is added to next columns). Adding is done by law of Bool algebra (1+1=1, 1+0=1, 0+1=1, 0+0=0).

As the result, minimal cuts of second and third order are:

II: K-S, T1-T2, F-G

III: K-A-T1, S-A-T2, T1-B-F, T2-B-G

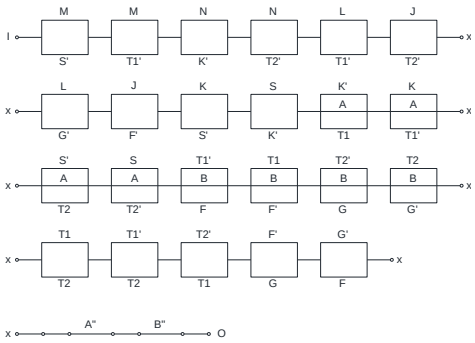

Figure 4. Equivalent minimal paths graph

With all results that are obtained so far, equivalent minimal paths graph of substation can be made (Fig. 4).

IV. DIFFERENT SCENARIOS OF CB REPLACEMENT

Analysis of CB replacement profitability and its influence on substations unreliability will be shown through 4 different scenarios.

New CB unavailability would be equal to *U=0.00000822* [20] (with assumption that failure frequency and probability of failure are remaining unchanged).

List of actions:

- I – No CB replacement
- II – Replacement of CB's on supplying feeders
- III – Replacement of CB's on power transformers
- IV – Replacement of all CB's on 10kv feeders
- V – Replacement of all CB's

Results of different actions are shown in Table III.

TABLE III. UNAVAILABILITY RESULTS IN DIFFERENT SCENARIOS

	Results of different actions (%)			
Parameter	***Action II***	***Action III***	***Action IV***	***Action V***
Unavailability reduction (%)	5.07	91.57	3.36	99,99
Failure frequency	6.59	80.26	8.73	95.59

V. COST ESTIMATION OF ACTIONS

Considering price of CB replacement of 5 000 € for 35kV CB and 2 000 € for 10kV feeder (including labor cost) with average time of replacement of 6h (from decision making, transporting and mounting), cost of different actions are presented in Table IV.

TABLE IV. COST OF CB REPLACEMENT

	Results of different actions (%)			
Parameter	***Action II***	***Action III***	***Action IV***	***Action V***
Unavailability reduction (%)	5.07	91.57	3.36	99,99
Number of CB's	2x35 kV	2x35, 2x10	2x10	4x35, 4x10
Costs (€)	10 000	14 000	4 000	28 000

VI. CONCLUSION

Substations reliability analysis can be used for determining size of new investments and their financial justifications.

Used methodology is easy to utilize because all data are already available and there is no need for extra investments or labor cost in order calculation to be carried out.

CB's removal can be assessed by risk assessment and substation's reliability improvement calculation. Substations reliability is better from investment point of view, because in that way, best case scenario in which CB's have biggest influence on substations reliability considering invested money, can be observed.

In the example which was analyzed in this paper best scenario for substations reliability is replacement of CB's on both power transformers.

REFERENCES

[1] Y. Hu, S. Liu, H. Lu, H. Zhang, "Remaining useful life assessment and its application in the decision for remanufacturing", Procedia CIRP, vol. 15, pp. 212–217, 2014.

[2] H. Picard, J. Verstraten, M. Hakkens, R. Vervaet, "Decision model for End of Life management of switchgears", El. and Instr. Appl. in the Petroleum & Chem. Ind., PCIC Europe 4th European Conference, Jun. 2007.

[3] C. Okoh, R. Roy, J. Mehnen, L. Redding, "Overview of Remaining Useful Life Prediction Techniques in Through-Life Engineering Services", ScienceDirect, Procedia CIRP, vol. 16, pp. 158 – 163, 2014.

[4] J. Z. Sikorska, M. Hodkiewicz, L. Ma, "Prognostic modelling options for remaining useful life estimation by industry", Mech. Syst. and sign. Process., vol. 25, no. 5, pp. 1803-1836, Jul. 2011.

[5] X. S. Si, W. Wang, C. H. Hu, D. H. Zhou, "Remaining useful life estimation – A review on the statistical data driven approaches", European Journal of Operational Research , vol. 2013, no. 1, pp. 1-14, Aug. 2011.

[6] M. Braunović, V. V. Konchits, N. K. Myshkin, *Fundamentals of Electrical Contacts*, CRC Press, 2006.

[7] A. H. A. Bakar, H. A. Illias, M. K. Othman, H. Mokhils, "Identification of failure root causes using condition based monitoring data on a 33 kV switchgear", *El. Power and Energy Systems*, vol. 47, pp. 305-312, May, 2013.

[8] S. Natti, M. Kezunovic, "Assessing circuit breaker performance using condition-based data and Bayesian approach", El. Power Systems Research, vol. 81, no. 9, pp. 1796-1804, Sep. 2011

[9] A. Janssen, D. Makareinis, C. E. Sölver, "International Survey on Circuit-Breaker Reliability Data for Substation and System Studies", IEEE Trans. Power Delivery. vol. 29, pp. 808-814, Apr. 2014.

[10] P. Sun, H. Jiang, H. Yu, X. Huang, Y. Sun, X. Wang, "Reliability evaluation of high voltage circuit breaker based on IFAHP and GA", ICAEES, Nov. 2015.

[11] J. F. Boudreau, S. Poirier, "End-of-life assessment of electric power equipment allowing for non-constant hazard rate – Application to circuit breakers", *El. Power and Energy Systems*, vol. 62, pp. 556-561, Nov. 2014.

[12] X. Zhang, E. Gockenbach, Z. Liu, H. Chen, L. Yang, "Reliability estimation of high voltage SF6 circuit breakers by statistical analysis on the basis of the field data", *El. Power System Research*, vol. 103, pp. 105-113, Oct. 2013

[13] L. Jian, T. Tianyuan, "LS-SVM based substation circuit breaker maintenance scheduling optimization", *El. Power and Energy System*, vol. 64, pp. 1251-1258, Jan. 2015.

[14] G. Balzer, F. Heil, P. Kirchesch, R. Meister, C. Neumann, "Evaluation of failure data of HV circuit-breakers for condition based maintenance", CIGRE, Paris, report A3-305, 2004.

[15] T. M. Lindquist, L. Bertling, R. Eriksson, “Circuit breaker failure data and reliability modelling”, *IET Gen., Transm. & Distrib.* vol. 2, no. 6, pp. 813-820, Nov. 2008.

[16] ABB Switzerland Ltd, Substation Reliability Management Services, 2016, www.abb.com/substationservice

[17] D. Nack, Reliability of Substation Configurations, Iowa State University, 2005.

[18] S.H. Kim, D. J. Lee, Substation Reliability Evaluation Considering the Failure Events, IOP Conf. Ser.: Earth Environ. Sci. 159, 2018.

[19] C. J. Zapata, A. Alzate, M. A. Ríos, “Reliability Assessment of Substations using Stochastic Point Processes and Monte Carlo Simulation”, IEEE PES General Meeting, July 2010

[20] F.Wang, “Reliability Evaluation of Substations Subject to Protection Failures”, Delft University of Technology, Netherlands, July 2012.

[21] R. Billington and G. Lian, “Monte Carlo Approach to Substation Reliability Evaluation,” IEE Proceedings-C, Vol. 1 40, No. 2, March 1 993.

[22] Common specifications for high-voltage switchgear and controlgear standards, International standard IEC 60694, Edition 2.2, 2002-01

[23] (T. Suwanasri, M. T. Hlaing, C. Suwanasri, „Failure Rate Analysis of Power Circuit Breaker in High Voltage Substation“,GMSARN International Journal 8 (2014) 1 – 6.

[24] J. Z. Sikorska, M. Hodkiewicz, L. Ma, “Prognostic modelling options for remaining useful life estimation by industry”, Mech. Syst. and sign. Process, vol. 25, no. 5, pp. 1803-1836, Jul. 2011.

[25] W. Li, J. Zhou, J. Lu, W. Yan "A Probabilistic Analysis Approach to Making Decision on Retirement of Aged Equipment in Transmission Systems" *IEEE trans. on power delivery*, vol. 22, pp. 1891–1896, no. 3, July 2007.

[26] J. Nahman, V. Mijailović, “Razvodna postrojenja”, Beograd, 2005

Fuzzy Measurement Algorithm for Fault Detection in the Hydrogenerator

Saša D. Milić[1], Blagoje M. Babić[2,1], Aleksandar Ž. Rakić[2]

[1]University of Belgrade, Electrical Engineering Institute 'Nikola Tesla', Belgrade, Serbia,
s_milic@yahoo.com, blagojebabic@gmail.com
[2]University of Belgrade, School of Electrical Engineering, Belgrade, Serbia,
rakic@etf.rs

Abstract—**Fault detection involves the detection, location, and identification of faults. Three types of unbalances (mechanical, hydraulic and magnetic) can occur in hydrogenerators. There are two main reasons for the existence of magnetic unbalance: shorted turns in the windings of the rotor poles and geometric asymmetry of the air gap. In this study, the authors propose a novel fuzzy measurement algorithm for fault detection in the hydrogenerator. The proposed algorithm has been developed with aim to detect the presence and cause of the magnetic unbalance and vibrations of the hydrogenerator. The study is based on fuzzy theory and three measurement methods for measuring inner and outer magnetic fluxes and measuring mechanical vibrations. The fuzzy algorithm has to ensure, in situ and real time, magnetic and vibration monitoring and fault detection and as such it is suitable for implementation in on-line and real time monitoring systems. The main benefit of the proposed solution lies in the support for the optimal decision making regarding the predictive maintenance.**

Keywords - hydrogenerator, fuzzy measurement algorithm, fault detection, magnetic flux

I. INTRODUCTION

Hydrogenerators are exposed to severe stresses and loads of electrical, mechanical, hydraulic and thermal nature, resulting in a large number of potential failures [1].

The proposed fuzzy measurement algorithm (FMA) belongs to the type of fault detection algorithms and is based on measurement of the main radial magnetic flux in the air gap, leakage radial magnetic flux on the stator housing and mechanical vibrations on the upper guide bearing of hydrogenerators. These three concepts are combined and used to complement each other.

FMA has been developed with the aim to detect the presence of the magnetic unbalance of the hydrogenerator. Magnetic unbalance will at least reduce operating efficiency and in more severe cases can lead to heavy damage [2].

There are two main reasons for the existence of magnetic unbalance: shorted turns in the windings of the rotor poles and geometric asymmetry of the air gap. The magnetic flux in the air gap, corresponding to the pole with the shorted turns, is smaller in comparison with the magnetic flux of other poles [3, 4]. Oscillations of the magnetic flux in the air gap can also be caused by the air gap asymmetry, which is most often the consequence either of the eccentricity of the rotor or irregularly shaped rotor/stator. Due to changes in the length of air gap, the magnetic flux in hydrogenerator also changes. The change in the magnetic flux density in the air gap (with generators which have a different degree of rotor eccentricity) was discussed in [5].

Generally speaking, the mechanical vibrations recorded on the housings of guide generator bearings are indicator of the presence of mechanical and magnetic rotor unbalance. Magnetic unbalance changes the vibration levels in the regimes of no-load unexcited/excited operations. The levels of the vibrations that are belong to the range of the normal operation are given in [6].

II. FUZZY MEASUREMENT ALGORITHM (FMA)

With the aim of a comprehensive analysis, FMA takes into account the value of mechanical

ISBN: 978-86-80616-03-2

vibrations of the upper guide bearing and magnetic flux (Fig.1).

The algorithm consists of two separate parts. The first one takes into accunt magnetic and vibration measurements and the second one is useful for fuzzy approaching in the making decision.

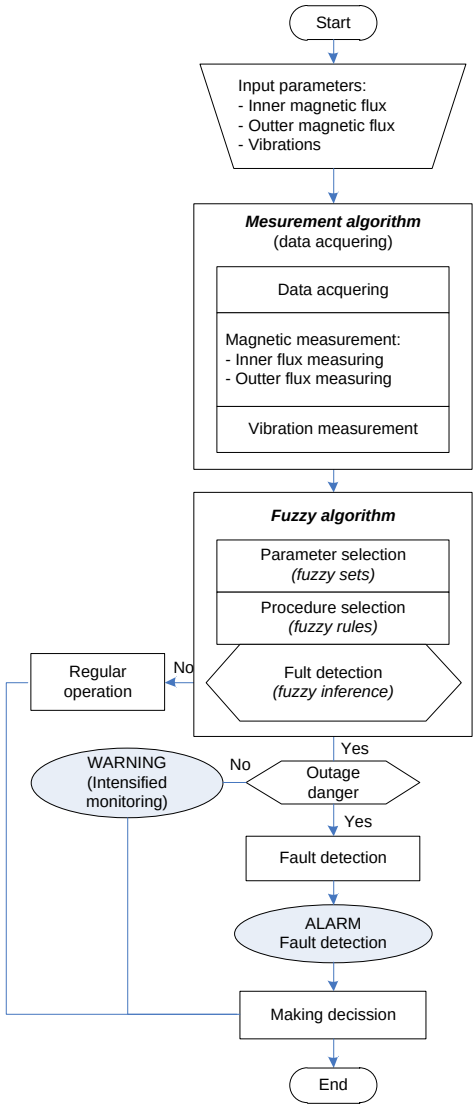

Fig. 1 Fuzzy measurement algorithm (FMA)

III. Fuzzy Logic and Making Decision

Conventional system theory relies on crisp mathematical models of systems. However, for a large number of practical problems, which are described by linguistic forms, fuzzy logic theory is more suitable. According to the above mentioned, modeling the decision-making process often relies on a fuzzy-based decision model applications.

The pioneer and founder of the fuzzy logic theory is Lotfi A. Zadeh [1, 2]. He introduced fuzzy sets for describing ambiguity and fuzziness of the linguistic representation of certain physical phenomena and technological processes. This study presents a fuzzy-measurement algorithm (FMA) which is based on fuzzy logic theory and fault detection methodology related to generators in hydro power plants.

A. Fuzzy Logic System (FLS)

Let X be the universe of discourse and its elements be denoted as x. Fuzzy set A of universe X is defined by function $\mu_A(x)$ called the membership function of set A:

$$f_A(x): X \rightarrow \{0, 1\}, \quad f_A(x) = \begin{cases} 1, \text{if } x \in A \\ 0, \text{if } x \notin A \end{cases} \qquad (1)$$

Fuzzy set A of universe X is defined by function $\mu_A(x)$ called the membership function of set A:

$$\mu_A(x):X\rightarrow[0,1], \quad \begin{aligned} \mu_A(x) &= 1 \text{ if } x \text{ is totally in } A \\ \mu_A(x) &= 0 \text{ if } x \text{ is not in } A \\ 0 < \mu_A(x) &< 1 \text{ if } x \text{ is partly in } A \end{aligned} \qquad (2)$$

This presentation of set allows a continuum of possible choices. For any element x of universe X, membership function $\mu_A(x)$ equals the degree to which x is an element of set A. This degree, a value between 0 and 1, represents the degree of membership, also called membership value, of element x in set A (*Fuzzy Logic lecture* – A.Rakić).

The fuzzy logic system (FLS) was first proposed by Mamdani [3,4] and then has been widely applied in many practical applications in which there are many uncertainties. In addition to the Mamdani FLS, today the most commonly used system is Takagi-Sugeno FLS (TS-FLS) [5,6]. These systems differ in the structure, but have the same rules (if-then).

For a Mamdani FLS with MISO structure (multiple input, single output) the nth rule can be expressed as:

$$\begin{aligned} Rule^n &: \text{IF } x_1 \text{ is } F_1^n \text{ and } \ldots \text{ and } x_m \text{ is } F_m^n \\ &\text{THEN } y \text{ is } Q^n, \; n = 1, \ldots, N \end{aligned} \qquad (3)$$

where:

n - nth rule

m - number of inputs
F_m^n - antecedent fuzzy set
Q^n - consequent fuzzy set

For a TS-FLS with MISO structure (multiple input, single output) which uses function of input variables as rule consequents, the nth rule can be expressed as:

$$\begin{aligned} &Rule^n : \text{IF } x_1 \text{ is } F_1^n \text{ and ... and } x_m \text{ is } F_m^n \\ &\text{THEN } y = y^n(\mathrm{x}) \equiv y^n(x_1,...,x_m)\ ,\ n = 1,...,N \end{aligned} \tag{4}$$

where $y^n(\mathrm{x})$ is a function (linear or nonlinear) of the inputs variables.

For a TS-FLS with MISO structure (multiple input, single output) which uses linear function of input variables as rule consequents, the nth rule can be expressed as:

$$\begin{aligned} &Rule^n : \text{IF } x_1 \text{ is } F_1^n \text{ and ... and } x_m \text{ is } F_m^n \\ &\text{THEN } y = y^n(\mathrm{x}) = c_0^n + c_1^n \cdot x_1 + ... + c_m^n \cdot x_m\ ,\ n = 1,...,N \end{aligned} \tag{5}$$

where $c_0^{\mathrm{n}},..., c_{\mathrm{m}}^{\mathrm{n}}$ are the consequent parameters.

The main shortcomings of A and B is that they do not take into account the connection between inputs and consequents. Therefore, care should be taken in the selection of parameters for the fuzzy rules.

FLS is composed of four main components (Fig.2): fuzzifier, fuzzy rules, inference engine, and defuzzifier [20].

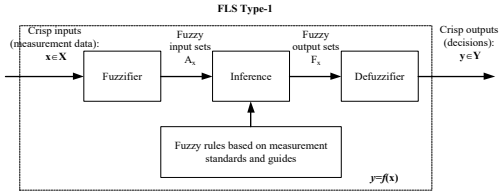

Fig. 2. FLS Type-1

B. Fuzzy Modeling

In this study, for the needs of fuzzy modeling, the following membership functions are used:

1. Triangular-shaped membership function:

$$f(x;a,b,c) = \begin{cases} 0, & x \le a \\ \dfrac{x-a}{b-a}, & a \le x \le b \\ \dfrac{c-x}{c-b}, & b \le x \le c \\ 0, & c \le x \end{cases} \tag{6}$$

2. Trapezoidal-shaped membership function

$$f(x;a,b,c,d) = \begin{cases} 0, & x \le a \\ \dfrac{x-a}{b-a}, & a \le x \le b \\ 1, & b \le x \le c \\ \dfrac{d-x}{d-c}, & c \le x \le d \\ 0, & d \le x \end{cases} \tag{7}$$

3. Gaussian curve membership function:

$$f(x;\sigma,c) = e^{\frac{-(x-c)^2}{2\cdot\sigma^2}} \tag{8}$$

4. Π-shaped membership function

$$f(x;a,b,c,d) = \begin{cases} 0, & x \le a \\ 2\cdot\left(\dfrac{x-a}{b-a}\right)^2, & a \le x \le \dfrac{a+b}{2} \\ 1-2\cdot\left(\dfrac{x-b}{b-a}\right)^2, & \dfrac{a+b}{2} \le x \le b \\ 1, & b \le x \le c \\ 1-2\cdot\left(\dfrac{x-c}{d-c}\right)^2, & c \le x \le \dfrac{c+d}{2} \\ 2\cdot\left(\dfrac{x-d}{d-c}\right)^2, & \dfrac{c+d}{2} \le x \le d \\ 0, & x \ge d \end{cases} \tag{9}$$

5. Z-shaped membership function:

$$f(x;a,b) = \begin{cases} 1, & x \le a \\ 1-2\cdot(\dfrac{x-a}{b-a})^2, & a \le x \le \dfrac{a+b}{2} \\ 2\cdot(\dfrac{x-b}{b-a})^2, & \dfrac{a+b}{2} \le x \le b \\ 0, & x \ge b \end{cases} \tag{10}$$

6. S-shaped membership function:

$$f(x;a,b) = \begin{cases} 0, & x \le a \\ 2\cdot(\dfrac{x-a}{b-a})^2, & a \le x \le \dfrac{a+b}{2} \\ 1-2\cdot(\dfrac{x-b}{b-a})^2, & \dfrac{a+b}{2} \le x \le b \\ 1, & x \ge b \end{cases} \tag{11}$$

7. Generalized bell-shaped membership function:

$$f(x;a,b,c) = \frac{1}{1+\left|\dfrac{x-c}{a}\right|^{2\cdot b}} \tag{12}$$

IV. FMA VALIDATION

Measuring part of FMA conducts analysis of magnetic flux. The algorithm also takes into account the parameters of vibration recorded on bearing of hydrogenerator.

Figs. 3 and 4 show the change in magnetic flux in the air gap of the generator and change of leakage magnetic flux of stator in real exploitation [2].

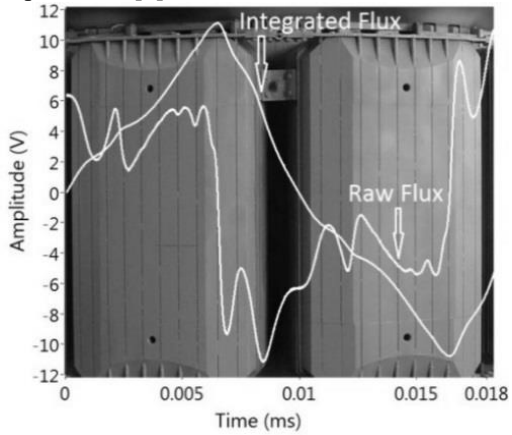

Fig. 3 Change in magnetic flux in the air gap of the full load generator.

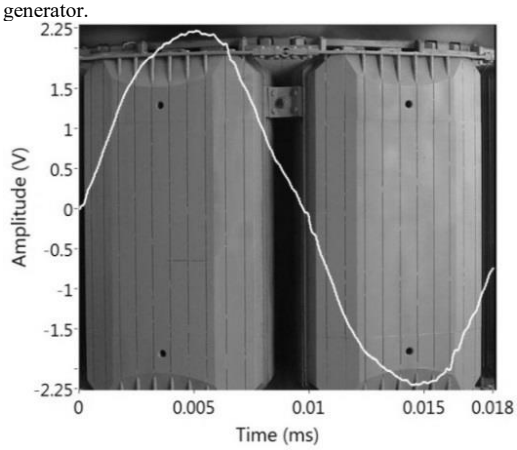

Fig. 4 Change of leakage magnetic flux of stator (raw flux). of the full load generator.

Due to shorted turns, there has been a reduction in the value of the magnetic flux of given pole (integrated flux, see Fig. 3) in relation to the magnetic flux of the other poles for approximately 2.7%.

The FFT analysis of leakage magnetic flux of stators of generator was performed. Increase of value (of 21.41db) of harmonic with frequency 16.66Hz (where rotor mechanical rotating frequency is: 8.33Hz) in the spectrum of leakage flux, was the consequence of existence of shorted turns. Amplitude of mechanical vibrations (the peak value of amplitude of basic components per number of rotations ($A_{0\text{-peak}}$)) reached approximately 5/12μm (no-load unexcited/excited operation) on upper generator bearing. It can be concluded that magnetic unbalance exists. In the regime of maximum load (40MW) measured value is approximately 15μm.

The fuzzy model (Figs. 5-7) was made in MatLab and verified the previously presented measured results of vibration and magnetic fluxes (inner and outer).

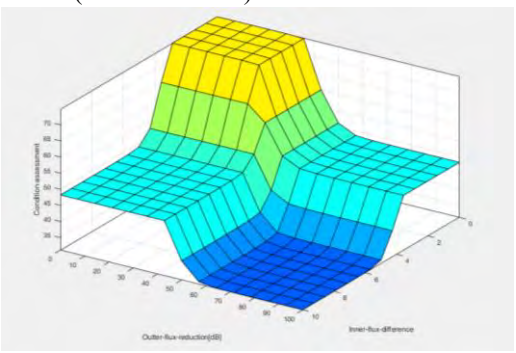

Fig. 5 Condition assessment is a function of outer and inner flux.

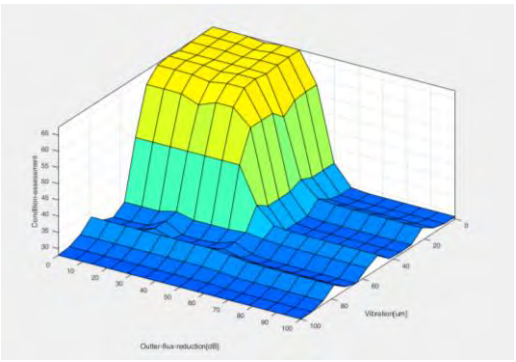

Fig. 6 Condition assessment is a function of outer flux and vibration.

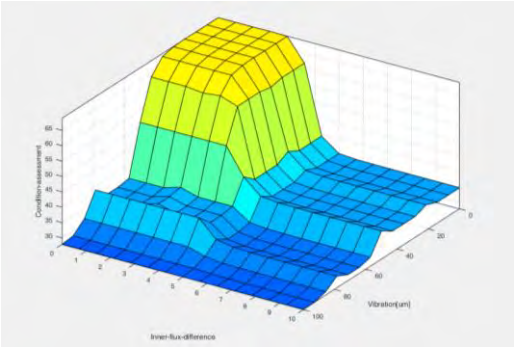

Fig. 7 Condition assessment is a function of inner flux and vibration.

Despite the detected failure, it can be concluded that there is no significant increase in vibrations.

V. CONCLUSION

This study presents a novel fuzzy measurement algorithm for fault detection in the hydrogenerator with the aim to combine the advantages of fuzzy logic with the advantages of improved measurement methods for measuring vibrations and inner and outer magnetic fluxes in the hydrogenerator.

Two types of fuzzy logic systems were considered (Mamdani and Takagi-Sugeno) and then applied.

The last part of the study discusses the validation of the proposed fuzzy-measurement algorithm that was carried out using appropriate software (MATLAB) and results obtained in real exploitation (in situ).

ACKNOWLEDGMENT

This research was funded by grant (Project No. TR 33024) from the Ministry of Education, Science and Technological Development of Serbia.

REFERENCES

[1] P. Tavner, L. Ran, J. Penman, H. Sedding, *Condition Monitoring of Rotating Electrical Machines*, The Institution of Engineering and Technology, London, United Kingdom, 2nd ed., 2008, pp. 35-40.

[2] Blagoje M. Babić, Saša D. Milić, Aleksandar Ž. Rakić: "Fault Detection Algorithm Used in a Magnetic Monitoring System of the Hydrogenerator", in IET Electric Power Aplications, doi: 10.1049/iet-epa.2016.0232, vol. 11, Issue 1, 26 January 2017, pp. 63 – 71

[3] G. C. Stone, E. A. Boulter, I. Culbert, *Electrical Insulation for Rotating Machines: Design, Evaluation, Aging, Testing, and Repair*, John Wiley & Sons, New Jersey, 2nd ed., 2014, pp. 420-427

[4] R. Fiser, D. Makuc, H. Lavric, D. Miljavec, M. Bugeza, "Modeling, analysis and detection of rotor field winding faults in synchronous generators", Proc. XIX Int. Conf. on Electrical Machines (ICEM), Rome, Italy, Sept. 2010, pp. 1-6

[5] R. Chin, P. Kanninen, "The Phenomenon of magnetic force: Estimating its Effects on Wind Turbine Generators", IEEE Industry Applications Magazine, vol. 19, no. 4, 2013, pp. 39-46

[6] *Mechanical vibration - Evaluation of machine vibration by measurements on non-rotating parts - Part 5: Machine sets in hydraulic power generating and pumping plants*, ISO 10816-5:2000, 2000.

[7] L. A. Zadeh, Fuzzy Sets, Information and Control, 8, pp. 338-353, 1965.

[8] C. Kahraman, U. Kaymak, A Yazici, *Fuzzy Logic in Its 50th Year,*

[9] E. H. Mamdani, "Application of fuzzy logic to approximate reasoning using linguistic synthesis", Computers IEEE Transactions on, vol. 100, no. 12, 1977, pp. 1182-1191

[10] P. J. King, E. H. Mamdani, "The application of fuzzy control systems to industrial processes", Automatica, vol. 13, no. 3, 1977, pp. 235-242

[11] T. Takagi, M. Sugeno, "Fuzzy identification of systems and its application to modeling and control", IEEE Trans. Sys. Man and Cyber., vol. 15, no. 1, 1985, pp. 116-132

[12] M. Sugeno, T. Yasukawa, "A fuzzy-logic-based approach to qualitative modeling", IEEE Trans. Fuzzy Systems, vol. 1, no. 1, 1993, pp. 7-31

[13] T. Takagi, M. Sugeno, "Fuzzy identification of systems and its applications to modeling and control", IEEE Trans. Syst., Man, Cybern., vol.15, 1985, pp. 116–132

Thermal Energy Recovery in Critical Areas of Hospitals

Gonzalo Sánchez-Barroso[1], Justo García Sanz-Calcedo[1]

[1]University of Extremadura, Badajoz, Spain, gsanchezbmoreno@gmail.com, jgsanz@unex.es

Abstract—**Hospitals are very energy-intensive due to their uninterrupted activity. High performance is required from heating, ventilation, and air conditioning (HVAC) systems to meet the cleaning requirements needed in critical areas of hospitals. This paper analyses available information about energy-saving and heat recovery techniques and equipment applied in high-performance HVAC systems in operating theatres. Discussion on the applicability of this equipment in critical areas of hospitals is presented. The heat recovery systems allow to reduce the energy consumption of the hospital, the value of the investment in equipment and the costs of exploitation maintaining the environmental conditions that favor the safety of the patient.**

Keywords – Energy-saving, Heat recovery, Operating theatre, Hospital Engineering, Healthcare building project.

I. INTRODUCTION

The average energy consumption of Spanish hospitals amounts to 6.9% of the total consumption of the tertiary sector [1]. It is estimated that 40% of consumption is demanded by heating, ventilating and air-conditioning (HVAC) systems, 35% for lighting, 20% for domestic hot water production (DHW) and the rest for other uses [2]. A Spanish hospital working under standard conditions has an average consumption of 0.27 MWh/m2, 9.99 MWh/worker and 34.61 MWh/bed [3].

In Spain the annual increase in energy consumption is 4.2% while the average for European countries is 1.5% [4]. Near zero energy building (nZEB) must be publicly owned buildings newly constructed by 2019 [5]. This justifies carrying out an energy audit to learn about consumption and, through optimization, reduce operating and maintenance costs and collaborate in environmental conservation [6]. Pérez-Lombard et al (2008) [4] analyzed energy consumption in buildings, especially focused on HVAC systems. They concluded that it is necessary to have information regarding the energy consumption of buildings in order to develop energy and use policies in the future.

The critical areas of hospitals are mainly operating theatres, intensive care units, post-surgical resuscitation units and isolation rooms. The thermal loads to be considered in the design of the HVAC system are: ventilation loads and transmission loads through walls. The latter is often overlooked since critical areas are interior rooms and adjoining rooms are also air-conditioned (such heat transfer will be minimal). In critical areas, HVAC systems are necessary to achieve levels of surgical field cleanliness required for aseptic processes. More than 20 air change per hour (ACH) with 100% oudoor air is necessary. Therefore, an awful lot of energy is required to achieve the required performance.

Critical rooms require large flow rates of supply and exhaust. In addition, large lighting requirements are required, which means a significant thermal load to overcome. The devices employed also generate significant thermal loads. A study of simultaneity is important since the energy demand is much higher than that demanded by a standard building [7]. Waste heat recovery systems can reduce the energy demand for powering HVAC systems. The heat recovery systems can be integrated in air conditioning installations powered by renewable energy: photovoltaic, cogeneration, aerothermal, etc.

Thermal conditions in critical areas in hospitals should be strictly designed due to their involvement in people's health. Khodakarami and Nasrollahi (2012) [8] presented a literature review on thermal comfort in hospitals due to the

lack of studies on the influence of thermal comfort on people's health. They concluded that it is important to study the relationship between the level of productivity of the medical staff and the thermal conditions of the room.

García-Sanz-Calcedo (2016) [9] analyzed the energy efficiency of 55 health care centers in Extremadura (Spain). The potential energy savings in HVAC systems were calculated. Annually it is possible to save 0.75 €/m2 by implementing optimization measures previously analyzed was concluded. García-Sanz-Calcedo et al. (2018) [10] analysed the potential for savings in the use of the HVAC system in health centres (< 5,000 m2) and hospitals (> 5,000 m2). An average annual savings of 1.50 kWh/m2 and 1.80 kWh/m2, respectively, were calculated. This author and others (2014) [11] conducted a quantitative analysis of the relationship between the energy efficiency of healthcare centers and their size. They concluded that, if the size of the building is not optimised, energy consumption can increase by 15%.

Noie-Baghban et al. (2000) [12] studied the applicability of heat pipes as a sensible heat recovery in an HVAC system in a hospital operating theatre. The results were obtained by computer simulation and corroborated after laboratory tests on a built model. The results of their studies pioneered further research. Balaras et al. (2007) [13] reviewed published standards and guidelines on HVAC systems in hospitals operating theatres. In their studies they detected different problems (insufficient air exchange, poor control on indoor thermal conditions, bad spaces ergonomics). They concluded that there are opportunities to save energy without compromising the patient's health.

The aim of this work is to analyse the applicability of residual energy recovery systems in high-performance HVAC systems used in critical areas of hospitals.

II. METHODOLOGY

Different heat recovery systems were studied to reduce energy consumption. Techniques and equipment that allow the exploitation of residual energy and increase energy efficiency in HVAC systems of critical areas in hospitals were studied.

III. ENERGY RECOVERY SYSTEMS

In the high-performance air-conditioning process applied to operating theatres, isolation rooms and other critical areas it is possible to recover residual energy. This residual energy can be used to reduce the energy demand of HVAC systems. This is achieved by recovering energy from the air extracted from the room. In Spain it is obligatory to recover energy when there is an extraction volume through mechanical means greater than 1,800 m3/h [14].

Energy recovery systems consist of air-to-air or air-to-water heat exchangers. The air stream extracted from the room has thermo-hygrometric conditions close to those of the room air. It is made to pass through the exchanger on its way to the exterior. At the same time, an outside air stream is forced to circulate through another cavity of the equipment on its way in. The conditions of the supply air stream are approximate to the point of the room, decreasing the work required by air handle unit (AHU). In the exchange of mass and energy between both airstreams an intermediate liquid fluid may intervene, like water or glycol. An exchange air-to-water and after water-to-air take place.

The heat recovery rate or efficiency of the equipment depends on its design and the operating conditions (temperature and relative humidity of the fluids). The minimum recovery rate is defined in Directive 2009/125/EC. This parameter, ε, is calculated in a simplified way according to the Equation (1):

$$\varepsilon = \frac{t_{ext,2} - t_{ext,1}}{t_{int,1} - t_{ext,1}} \quad (1)$$

where the first suffix (int/ext) means interior and exterior air and the second suffix (1/2) means the inlet and outlet of the exchanger, respectively.

Depending on how heat transmission is carried out, these systems are divided into two categories: sensible heat recovery and enthalpic (or total energy) recovery. There are other techniques for the recovery of residual energy.

A. Sensible recovery systems

Energy due to the dry bulb temperature difference between the exhaust and supply air stream is recovered in sensible heat recovery units. The air stream with the highest dry bulb temperature gives off heat. It will condense if its temperature reaches dew-point. Due to the thermal jump, the hotter air stream lowers its temperature below dew-point. Both the latent heat of condensation and the sensible heat are

received as sensible heat by the lower temperature air stream. Energy is required to decrease moisture from the supply air and adapt it to the design value.

The equipment that carries out this work are: pipe heat (Fig. 1), run-around (Fig. 2), exterior coil, water coil loop (Fig. 3), and recovery with refrigerating circuit (Fig. 4).

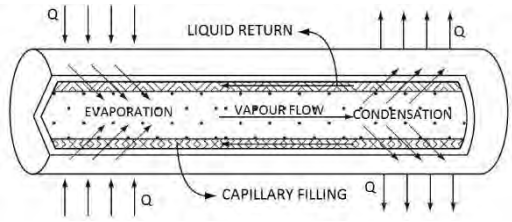

Figure 1. Heat pipe (air-to-air). Source: [15].

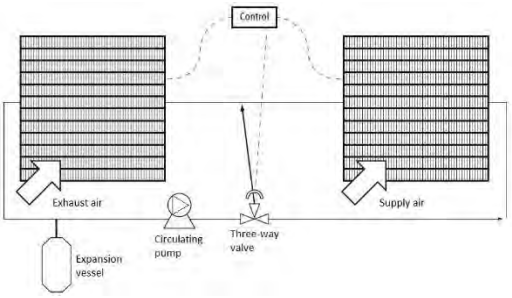

Figure 2. Run-around (air-to-water). Source: [15].

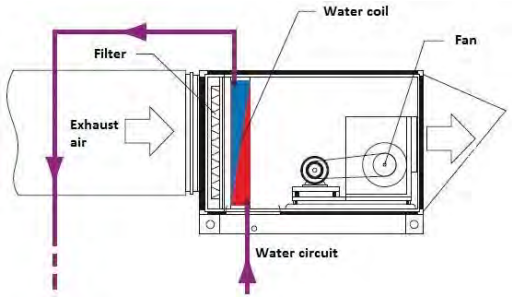

Figure 2. Water coil loop (air-to-water). Source: [15].

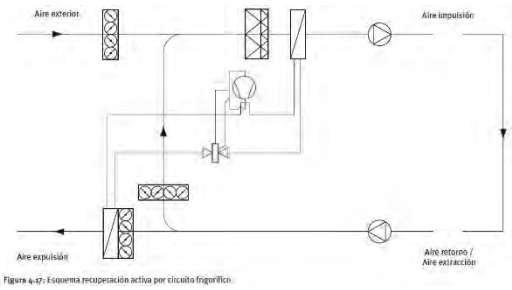

Figure 3. Recovery from refrigerating circuit (air-to-water). Source: [15].

The thermal power of sensible heat that can be taken advantage of a system with these equipment is estimated with the Equation (2):

$$q = \varepsilon Q \rho c_p \left(t_{in} - t_{out} \right) \quad (2)$$

where: ε is efficiency, Q is air flow rate, ρ is air density, c_p is specific heat, t_{in} and t_{out} is inlet and outlet dry-bulb temperature.

B. Enthalpy recovery systems

Energy due to the thermal jump between air streams and the vapour pressure gradient of both streams is exchanged in enthalpic heat recuperators. They allow the temperature and relative humidity of the supply air to be varied. Under equal conditions, energy recovery rate is greater than sensible recovery units.

They are two equipment: 1) rotating energy wheel regenerator (Fig. 5) and 2) permeable walled flat-plate recuperator (Fig. 6). The latter can be: cross flow or countercurrent parallel flow. Both are air-to-air exchangers. Hygroscopic material covering exchange surface is necessary to favour mass transfer. Desiccant film covers the surface of the wheel. This surface absorbs moisture from the supply air stream. Moisture is transferred to the less humid supply airstream, balancing the system. The surfaces of the static recuperator are porous, therefore, it favors the equilibrium of the system by transferring humidity to the less humid fluid.

The energy that can be exploited from a system with these equipments is estimated with the Equation (3):

$$q = \varepsilon Q \rho \left(h_{in} - h_{out} \right) \quad (3)$$

where: ε is efficiency, Q is air flow rate, ρ is air density, c_p is specific heat, h_{in} and h_{out} is supply and exhaust air enthalpy.

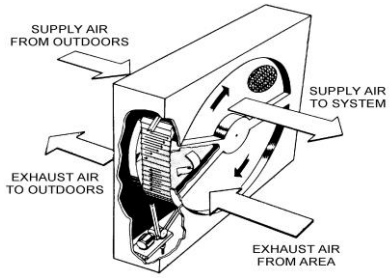

Fig. 4. Rotating energy wheel regenerator. Source: [16].

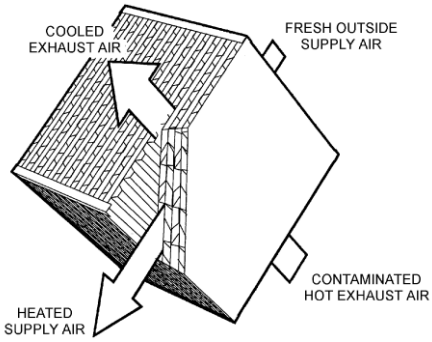

Fig. 5. Fixed-plate cross-flow heat exchanger. Source: [16].

IV. CASE STUDY

Let us suppose a surgical block with four operating theatres suitably air-conditioned. Each requires 2,400 m^3/h of all outdoor air. We have 9,600 m3/h of supply air with 24 air change per hour. Winter conditions are assumed. The operating theatres are at t_{in} = 22ºC and the outside air at t_{out} = 8ºC.

A sensitive energy recovery unit is installed. A total energy recovery unit is not installed to avoid problems arising from an inadequate maintenance plan. According to Directive 2009/125/EC the minimum recovery factor of the energy recovery unit must be ε = 68%.

The used thermal power derived from the installation of a sensitive energy recovery unit in the system at full-load is calculated using Equation (2). The result is shown in the Equation (4).

$$q = 31.10\ kW \tag{3}$$

The recovered thermal energy is calculated by multiplying this power by the number of operating hours of the installation under these conditions. The coefficient of performance (COP) and energy efficiency ratio (EER) are then calculated, in the case of summer mode, with the system at full load.

V. DISCUSSION

The heat recovery rate is related to the design of the equipment (parallel flow, countercurrent or cross flow, number of passes and presence of fins) and to the working conditions of the fluids circulating through it. These systems increase their recovery rate when there is a greater transmission of mass and energy (as the thermal jump and, if applicable, the vapour pressure gradient increases). Effectiveness must be distinguished in the transfer of sensible heat, in the transfer of latent heat and in the transfer of energy [16]. The installation of this equipment involves a load loss that will increase the electrical consumption of the fans. They also represent an investment to adapt existing ducts.

The use of enthalpic heat recovery systems is not recommended for this type of HVAC systems in critical areas. Exchange of energy between air streams through water vapor will be required. Water vapour is a means of transport for viruses and bacteria. However, they can be used attended by an adequate maintenance plan [17] and hygienic verification of particle transmission. In critical areas of hospitals, enthalpic heat recovery units are used for production of DWH or hot-water to laundry.

Thermal by-pass is achieved through three options: physical circuit, stop recirculation pumps or stop wheel motor. Thermal by-pass is complementary to free-cooling. Due to the specific conditions of humidity, temperature and microbiological load that critical areas require, free-cooling is of limited application here.

The simulation of the annual energy consumption of the system is used to study the economic viability of the installation. The required outdoor and indoor conditions are taken into account for one year. Taking into account the value of the investment (replacement of equipment, adaptation of air circuits, etc.) and the operating costs (energy production, transport and maintenance of the installation) is necessary.

COP and EER variables are calculated to evaluate the performance of air conditioning systems at full load. These variables are calculated for certain static conditions, such as the case study. By means of simulation, seasonal coefficient of performance (SCOP) and seasonal energy efficiency ratio (SEER) can be calculated. These take into account the variability of the equipment's annual workload due to outdoor and indoor conditions.

VI. CONCLUSSIONS

Heat recovery systems allow the energy demand to be reduced and, consequently, the power of the cooling equipment to be reduced. System operating costs and investment costs are reduced respectively.

Sensitive heat recovery systems do not compromise the quality of the air supplied to the room, and are therefore suitable for use in HVAC

systems in critical areas of hospitals. It is not feasible to use enthalpic heat recovery units in these critical areas of hospitals. Due to the mass transfer, these systems compromise the indoor environmental quality that will be achieved in the room.

The sensible heat recovery unit maximizes its performance at the greater temperature difference between exhaust air and supply air. The ideal conditions to maximize the performance of the enthalpic recuperator are both hot and humid climates to dissecant supply airstream and cold and dry climates to moisturize supply airstream.

ACKNOWLEDGMENT

The authors wish to acknowledge to the Junta de Extremadura and the European Social Found (FEDER) for the support of this research work. This study has been carried out through the Research Project GR-18029 linked to the VI Regional Plan for Research, Technological Development and Innovation from the General Government of Extremadura 2017–2020.

REFERENCES

[1] Instituto para la Diversificación y el Ahorro Energético (IDAE), Informe anual de consumos energéticos (2017).

[2] Informe Grupo de Trabajo sobre Rehabilitación 2014, Estrategia para la rehabilitación. Claves para transformar el sector de la edificación en España.

[3] A. González González, J. García-Sanz-Calcedo, and D. Rodríguez Salgado, "A quantitative analysis of final energy consumption in hospitals in Spain", Sustainable Cities and Society, 2018, vol. 36, pp. 169–175.

[4] L. Pérez-Lombard, J. Ortiz, and C. Pout, "A review on buildings energy consumption information, Energy and Buildings, 2008, vol. 40, pp. 394-398.

[5] Real Decreto 564/2017 por el que se aprueba el Procedimiento básico para la certificación de la eficiencia energética de los edificios.

[6] J. García Sanz-Calcedo, F. Cuadros, and F. López Rodriguez, "La auditoría energética: una herramienta de gestión en atención primaria", Gaceta Sanitaria, 2011, vol. 25, issue 6, pp. 549–551.

[7] Singer, Brett C. Hospital Energy Benchmarking Guidance-Version 1.0. 2009.

[8] J. Khodakarami and N. Nasrollahi, "Thermal comfort in hospitals–A literature review", Renewable and Sustainable Energy Reviews, 2012, vol. 16, issue 6, pp. 4071-4077.

[9] J. García Sanz-Calcedo, "Analysis on energy efficiency in healthcare buildings", Journal of Healthcare Engineering, 2016, vol. 5, issue 3, pp. 361-373.

[10] J. García Sanz-Calcedo, A. Al-Kassir, and T. Yusaf, "Economic and environmental impact of energy sving in healthcare buildings", Applied Science, 2018, vol. 8, issue 3, pp. 440-452.

[11] J. García Sanz-Calcedo, F. López Rodríguez, and F. Cuadros, "Quantitative analysis on energy efficiency of health centers according to their size", Energy and Buildings, 2014, vol. 73, pp. 7-12.

[12] S. H. Noie-Baghban and G. R. Majideian, "Waste heat recovery using heat pipe heat exchanger (HPHE) for surgery rooms in hospitals", Applied thermal engineering, 2000, vol. 20, issue 14, pp. 1271-1282.

[13] C. A. Balaras, E. Dascalaki, and A. Gaglia, "HVAC and indoor thermal conditions in hospital operating rooms", Energy and Buildings, 2007, vol. 39, issue 4, pp. 454-470.

[14] Real Decreto 1027/2007, de 20 de julio, por el que se aprueba el Reglamento de las Instalaciones Térmicas en los Edificios.

[15] Instituto para la Diversificación y Ahorro Energético (IDAE), Guía técnica: Ahorro y recuperación de energía en instalaciones de climatización, 2012.

[16] American Society of Heating, Refrigerating and Air-conditioning Engineers (ASHRAE), Systems and Equipment Handbook, 2000.

[17] J. García-Sanz-Calcedo and M. Gómez-Chaparro, "Quantitative analysis of the impact of maintenance management on the energy consumption of a hospital in Extremadura (Spain)", Sustainable Cities and Society, 2017, vol. 30, pp. 217–222.

Cloud-based SCADA Systems: Cyber Security Considerations and Future Challenges

Mirjana D. Stojanović[1], Slavica V. Boštjančič Rakas[2], Jasna D. Marković-Petrović[3]

[1]University of Belgrade, Faculty of Transport and Traffic Engineering, Belgrade, Serbia, m.stojanovic@sf.bg.ac.rs
[2]University of Belgrade, Mihailo Pupin Institute, Belgrade, Serbia, slavica.bostjancic@pupin.rs
[3]CE Djerdap Hydroelectric Power Plants Ltd., HPP Djerdap 2, Negotin, Serbia, Jasna.Markovic@djerdap.rs

Abstract— **In this paper, we first describe basic operation principles of SCADA system, and analyze migration strategies of such systems to public, private or hybrid cloud infrastructure. Further, special attention is dedicated to the cloud service selection as well as to the analysis of benefits and risks of cloud-based SCADA applications. Finally, we address security threats in cloud environment and present challenges in security provisioning regarding security solutions, risk management and test environment.**

Keywords – Cloud computing, cyber security, quality of service, SCADA

I. INTRODUCTION

Supervisory Control And Data Acquisition (SCADA) systems are class of industrial control systems that control and monitor geographically dispersed process equipment in a centralized manner. They are widely used in the industrial sectors like electric power systems, oil refineries and natural gas distribution, water and wastewater treatment, and transportation systems. Failures and malfunctions of such systems may have serious consequences due to their strategic importance for national critical infrastructures. Modern SCADA systems are based on open communication standards, such as Ethernet, Transmission Control Protocol/ Internet Protocol (TCP/IP) suite and a variety of wireless standards. The growing trend of internetworking continues toward smart grids and cloud computing.

In the past few years, the focus of cloud computing has progressively shifted from consumer applications towards corporate control systems. The migration of applications, such as SCADA, into the cloud environment is interesting for business users due to potential reduction of costs, scalability, efficient system configuration and maintenance. Access and lease of resources are on-demand, with costs that are much lower than buying, installing and maintaining the hardware and software, and with decreasing the number of technical staff.

The main objectives of this paper are: (1) to discuss security issues of cloud-based SCADA systems, regarding different migration strategies and types of cloud services and (2) to consider security solutions and challenges in security provisioning in the cloud environment.

The rest of the paper is organized as follows. In Section II, a basic operation principle of SCADA system is described, as well as migration strategies of SCADA systems to different cloud infrastructures. Section III discusses selection of cloud service regarding SCADA-specific requirements. In Section IV, benefits and risks of cloud-based SCADA systems are identified. Section V deals with security threats regarding cloud computing and cloud-based SCADA systems. Challenges in security provisioning are presented in Section VI. Section VII concludes the paper.

ISBN: 978-86-80616-03-2

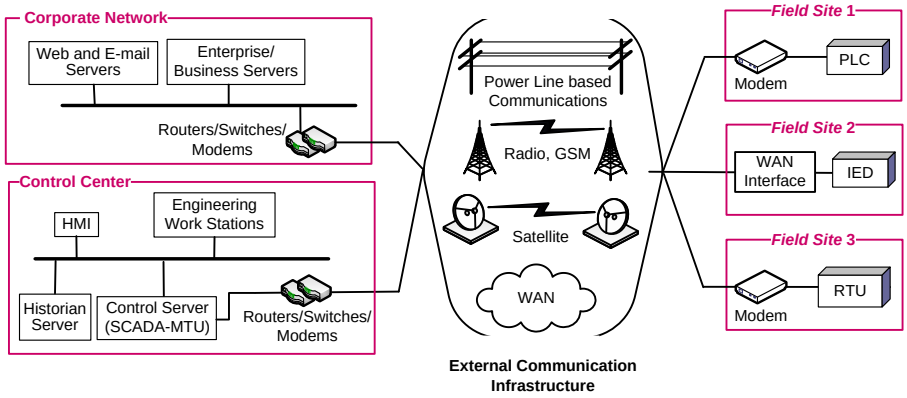

Figure 1. General layout of a SCADA system.

II. Migration of SCADA Systems to Cloud

Fig. 1 presents general layout of a SCADA system, with common components and configuration. Local area network in the control center connects control server (Master Terminal Unit, MTU), historian server, engineering work stations, human machine interface (HMI) server and consoles, as well as communication devices, such as routers, switches or modems. Control center collects and analyzes information obtained from field sites, presents them on the HMI consoles, and generates actions based on detected events. Control center is also responsible for general alarms, analysis of trends and generating the reports. Field sites encompass remote terminal units (RTUs), programmable logic controllers (PLCs) and intelligent electronic devices (IEDs) that perform local control of actuators and sensor monitoring. Communication subsystem connects control center with field sites and allows operators remote access to field sites for diagnostic and failures repairing purposes.

A set of standard or proprietary protocols are used for communications, over point-to-point links or a broadband IP-based wide area network. There are several standard and vendor-specific SCADA communication protocols, and the most widespread are Modbus, DNP3 (Distributed Network Protocol), IEC 60870-5 series and IEC 61850 series used for electrical substation automation systems. Most of these protocols are designed or extended to operate over TCP/IP networks. Besides, most of the existing fieldbus protocols are based on Ethernet technology. A comprehensive review of SCADA protocols can be found in [1], [2].

Layered hierarchy of SCADA system is defined according to interconnection of its components and their connectivity with external networks, as depicted in Fig. 2 [1], [3]. The lowest layer represents physical devices that are in direct interaction with industrial hardware, interconnected via fieldbus. Controllers at layer 1 process signals from field devices and generate appropriate commands for these devices. Processing results are forwarded to layer 2 for further analysis and response control. Layer 3 typically represents demilitarized zone (DMZ), where application servers, historian servers and domain controllers are located. The upper layers correspond to the enterprise IT network, which is connected to the Internet.

In the case of migration of SCADA systems to cloud environment, it should be taken into account that the cloud infrastructure can be public, private and hybrid.

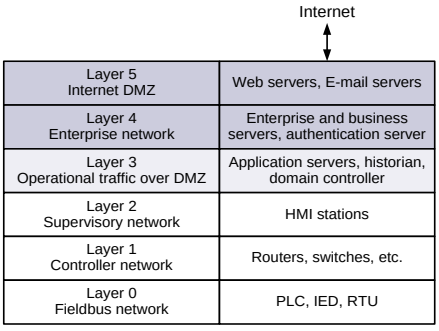

Figure 2. The layered structure of SCADA system.

Public cloud infrastructure is owned by a provider and sold as a service to business and residential users. Private cloud refers to an infrastructure that is owned or leased by a business user (single organization). Such an infrastructure can be managed by this organization or by a third party and it can be located on or off premises. Hybrid cloud infrastructure is a combination of private and public cloud infrastructures, which remain mutually independent and connected by standard or proprietary technology that enables portability of data and applications.

Cloud computing provides support for SCADA applications in two ways [4]:

1. SCADA application is executed on premises (company, organization, etc.). It is directly connected with control center and transfers data to the cloud where they can be stored and distributed.
2. SCADA application is completely executed in the cloud environment, and is remotely connected to the control center.

The first method, presented in Fig. 3, is more widely used. Control functions of SCADA application are isolated in the controller network, while SCADA application is connected to cloud services that allow visualization of processes, reports and remote access. Such applications are usually implemented on a public cloud infrastructure.

Implementation illustrated in Fig. 4 is suitable for distributed SCADA applications. Controllers are connected via WAN link to SCADA application that is executed in cloud environment. Such applications are usually implemented on private and hybrid cloud infrastructures.

III. SERVICE SELECTION

Layered service architecture of a cloud computing system is presented in Fig. 5 [5]. The lowest, hardware layer at the data center actually consists of the physical hardware devices including the CPU, memory, storage and bandwidth.

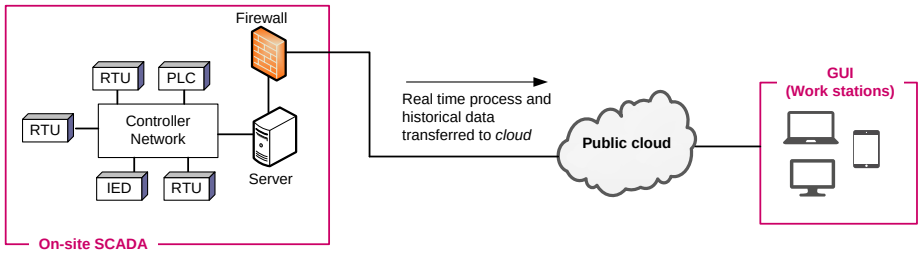

Figure 3. Public cloud infrastructure, with SCADA system operating on-premises and sending data thorugh cloud.

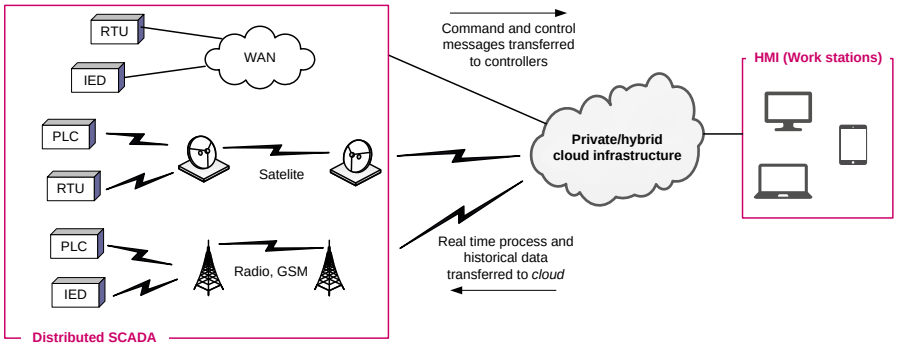

Figure 4. Private or hybrid cloud infrastructure where controllers are connected viah WAN links to SCADA application that is executed in the cloud.

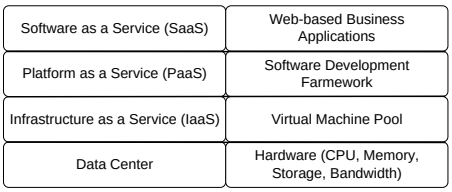

Figure 5. Cloud computing service architecture.

The infrastructure layer assumes the virtualization to provide the **Infrastructure as a Service (IaaS)**, which usually consists of a pool of virtual machines (VMs) that can be provisioned on demand to the IT consumers.

Further, the platform layer enables creation and development of software, which can be later delivered over the Web. Hence, this layer provides the **Platform as a Service (PaaS)** by utilizing the components and services of the infrastructure layer.

Finally, the software layer provides the ready-to-use software and applications for the business needs of the cloud service customers. Hence, this layer facilitates and provides the **Software as a Service (SaaS)** by utilizing the components and services of the platform layer.

Regarding SCADA systems, IaaS is the most developed and most widely used service model that allows customers to install and execute an off-the-shelf SCADA software product, like they would do on their own IT infrastructure. IaaS provides on-demand services of virtual servers, memory capacities and other fundamental computer resources. Customers pay for using such resources and can, if needed, purchase additional resources. Even though, the cloud infrastructure is not under the customer control, they keep the control of the operating systems, memory resources, installed applications and they can choose network components such as firewall.

PaaS represents a set of tools, available in the cloud infrastructure, for customers to develop applications that are executed over the Internet. Customers don't control the underlying cloud infrastructure, but they have control over the installed applications as well as environment configuration. PaaS is suitable for customers that want to develop their own SCADA applications with off-the-shelf development and runtime platforms.

SaaS allows customers to use provider's applications that are executed on a cloud infrastructure, from different client devices to client interfaces, such as Web browsers. Users do not have the control over the underlying cloud infrastructure; they only pay for the use of particular applications. Vendors are relatively slow with the adoption of this service model for core SCADA applications. They rather release specific SCADA components and functions, such as visualization and historical reports. Distribution of customer and provider responsibilities in different cloud services is depicted in Fig. 6.

Regarding service selection, there are three possible migration scenarios of SCADA system to the cloud environment.

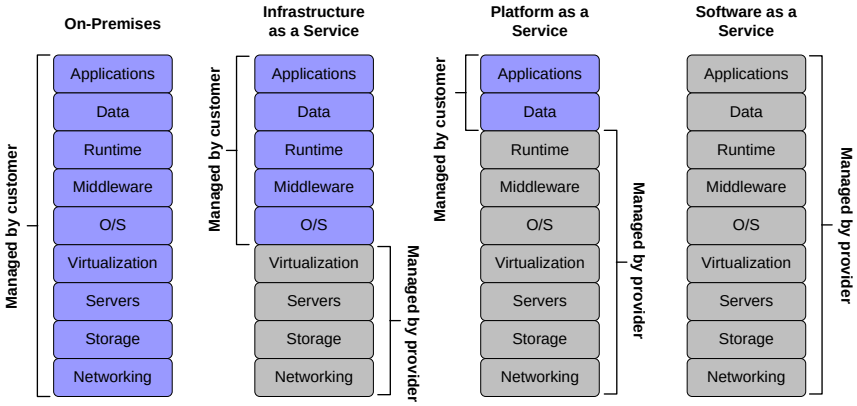

Figure 6. Customer and provider responsibilities in different cloud services.

The first scenario (re-hosting) is the fastest and the simplest, and represents installing the existing SCADA applications to cloud environment, based on IaaS. This is the first step of the gradual migration, that allows analysis and, if needed, extension of the applications, through several iterations.

The second and the third scenarios assume re-engineering to better benefit from the characteristics of cloud computing, primarily in terms of scalability and reliability. This can be a simple modification of particular features (refactoring). An example is implementation of resource control capabilities that allows adding additional resources when the application is intensively used and releasing resources when they are not needed. Larger modifications at the application core are also possible (revising). An example is the use of PaaS database for modification of application in such a way that multi-tenancy SaaS offering is possible. The increase of the number of SaaS offers requires the replacement of the existing SCADA applications with cloud-based SaaS solutions.

IV. Cloud-based SCADA Systems: Benefits and Risks

The basic advantages of cloud computing that motivate users to migrate to cloud-based SCADA system are as follows [6]:

- Access and lease of resources are on-demand, at a much lower price than purchasing, installing and maintaining their own software and hardware.
- Scalability is enhanced, since there is no need for purchasing and installing server farm, databases, Web servers, when more resources are needed. Users can easily purchase additional resources on a virtual cloud server, with no need of installing and maintaining the additional hardware.
- The number of technical staff, needed for IT resource maintaining, decreases.
- Information located on a cloud server can be accessed from anywhere.
- Since the access to information is easy, the collaboration on projects is more efficient.
- Upgrade of existing and implementation of new applications is simplified.

The main risk factors for cloud-based SCADA systems are **cyber security** and **quality of service (QoS)**.

Unlike public and corporate information systems, where information and network infrastructure security has reached a certain level of maturity, industrial systems cannot use the same solutions. In most cases there is a need for new security solutions that are extended to operate in the control environment. The security issue of the hard real-time system requires overall analysis and holistic understanding of network protection, management theory and physical systems. This problem is getting even more complex in the case of migration to the cloud environment, and it will be discussed in more details in Section V.

QoS refers to system's performance, as well as reliability and availability.

Most of the industrial applications pose stringent performance requirements regarding delay, packet loss and bandwidth. The most stringent requirements for delay are in the fieldbus and controller networks. Response times are in the range of 250 microseconds to 1 millisecond, while for less demanding processes they are in the range of 1 to 10 milliseconds [1]. Upper layers have progressively less stringent delays, typically up to 1 second. The use of public cloud services increases the risk that these requirements will not be met, because the user cannot control the network performance. Increased and unpredictable delay is particularly challenging, since it can block the real-time operation of the SCADA system.

The problems of availability and reliability exist in every system in the cloud network. The servers are placed in unknown locations that users cannot access. The data of SCADA systems encompass results of the industrial process control in real time; therefore, the loss of functionality, even for a few seconds, can cause serious consequences to the industrial process. For example, according to CIGRÉ (Conseil International des Grands Réseaux Électriques) recommendation, availability of SCADA systems in power utilities needs to be higher than 99.98% [7].

V. Security Threats

Besides security threats that are present in the existing computing platforms and networks, cloud computing faces a number of additional

vulnerabilities [8]. They include: (1) attacks by other customers; (2) shared technology issues; (3) failures in provider or customer security systems; (4) issues concerning integration of provider and customer security systems; (5) insecure application programming interfaces; (6) data loss or leakage and (7) account or service hijacking. In particular, susceptibilities depend on the type of cloud service.

In general, IaaS is susceptible to all of the threats that are well known from the traditional information and communication environment [9]. All of the client applications running on the virtual machines are like "black boxes" for the provider. In other words, the customer is responsible for securing these applications.

PaaS is particularly susceptible to shared technology issues, because security settings may differ for various kinds of resources. Another problem caused by shared resources refers to data leakage. Finally, protection of user objects is one of the most serious issues of PaaS [10].

Since SaaS requires only a Web browser and the internet connection, its security aspects are similar to the Web service [11]. SaaS is susceptible to data security, and particularly to their confidentiality. The other common problems with data security include data backup, data access, storage locations, availability, authentication, etc.

Table I summarizes the attacks types and their impacts, regarding layered cloud service architecture and emphasizes responsibilities of cloud service provider (CSP).

Cyber attacks on SCADA systems can be categorized into: hardware attacks, software attacks and communication stack attacks [12]. SCADA control center performs its actions based on the data received from RTUs. Attacks that jeopardize process control focus on modifying control data or blocking the data transfer. Primary threats to SCADA systems are response injection, command injection, various forms of denial of service (DoS) attacks and man-in-the-middle (MITM) attack [13], [14].

Cloud-based SCADA systems suffer from the same cyber security risks as the other systems integrated into cloud. Still, there are a number of threats in cloud environments that might make SCADA systems more vulnerable:

- Cloud-based SCADA systems are more exposed to cyber threats such as command/response injection, various forms DoS attacks, including distributed DoS (DDoS), and MITM attack.
- Network connections between SCADA systems and the cloud potentially increase the risk of jeopardizing the whole industrial control systems by outside attackers.
- Some of SCADA-specific application layer protocols lack protection.
- The use of commercial off-the-shelf solutions (instead of proprietary ones) potentially increases the cyber security risk.

VI. Challenges in Security Provisioning

In general, continual real-time system such as control environment requires new security solutions that may differ from security products in public and enterprise IT networks.

A. Security Solutions

Security solutions for cloud-based SCADA systems strongly depend on the type of the cloud infrastructure, i.e., public, private or hybrid clouds.

It is essentially important not to expose the critical, control infrastructure to the Internet. For that reason, when using public cloud

TABLE I. Types of Attacks on the Cloud and their Impacts

Security issues	Attack Types	Impacts	CSP Responsibility		
			SaaS	*PaaS*	*IaaS*
Software layer	SQL injection attacks, cross site scripting	Modification of data, confidentiality, session hijacking	✓		
Platform layer	DNS attacks, sniffer attacks, reuse of IP address	Traffic flow analysis, exposure in network security	✓	✓	
Infrastructure layer	DoS and DDoS, VM escape, hypervisor rootkit	Software interruption and modification, programming flaws	✓	✓	✓
Hardware layer	Phishing attacks, malware injection attack	Limited access to data centers, hardware modification and theft	✓	✓	✓

infrastructure, push technology should be utilized to move data to the cloud rather than pull technology. Thus, there are no open network ports on the control infrastructure, while SCADA applications remain isolated in the controller network.

Another issue concerns selection of CSP. When assessing maturity of the offered cloud service, the following criteria should be taken into account [15]:

- Ensuring secure user access.
- Mutual isolation of information originating from different applications.
- Determining the level of users control regarding changes of the CSP infrastructure.
- Data encryption.
- Automated distribution of software patches.
- Provisioning scheduled and unscheduled reports that satisfy business needs.
- Continuous monitoring, which includes assessment of security mechanisms efficiency in near real-time.
- Continuous analysis of events, incidents, suspicious activities and anomalies.
- Capabilities to create and analyze log files, to detect intrusions in real-time, to generate responses to detected attacks.
- Readiness to take immediate corrective actions of all vulnerabilities identified.
- Consistent and reliable customer service.

The most efficient way to protect SCADA system connected to the public cloud is to establish well-defined service level agreement (SLA) that fulfills the aforementioned criteria. Similar research, regarding enterprise resource planning (ERP), pointed out the importance of introducing SLAs in the context of using SaaS and free and open source software [16].

SCADA protection is much simpler in private cloud, since security solutions are responsibility of the network owner. It is recommended to apply a strategy known as "defense-in-depth", i.e., a multilayer security architecture that minimizes the impact of a failure in any one layer mechanism [17]. This strategy assumes corresponding security policies, employing DMZ network architecture to prevent direct traffic between the corporate and SCADA networks, as well as security mechanisms such as smart access control, firewalls, intrusion detection and prevention systems, antivirus software, deploying security patches on a regular basis, etc.

In hybrid cloud, using virtual private network (VPN) connection to the control infrastructure is strongly recommended.

B. Risk Management

Security risk management is a cyclic process that encompasses several phases: risk analysis through identification of vulnerabilities and threats, risk assessment, making decisions on acceptable risk level, selection and implementation of measures to mitigate the risk.

Risk assessment is the most important phase in the risk management process, but also most susceptible to errors. According to [17], risk assessment is "the process of identifying risks to operations, assets, or individuals by determining the probability of occurrence, the resulting impact, and additional security controls that would mitigate this impact".

Different approaches, methods and tools for risk assessment in industrial control environment can be found in the literature. A comprehensive review of 24 risk assessment methods for SCADA systems is presented in [18], but none of them considers cloud-based SCADA systems. Hence, additional research efforts are needed to address this issue.

C. Test environments

Due to need to support the operational continuity, it is often unfeasible to perform security experiments on a real SCADA system. Hence, proper test environments should be developed, consisting of testbeds, datasets and simulated attacks. While test environments for SCADA in traditional IP-based networks have gained certain level of maturity, research work is still needed regarding cloud-based SCADA systems.

SCADA security testbed can be implemented as: (1) a single software simulation package; (2) laboratory testbed, which may have several interacting simulations and (3) emulation or implementation-based, which uses emulator or real hardware [19]. In the context of cloud-based SCADA, probably the most prevalent will be laboratory testbeds that are typically

built on the top of some of the general-purpose cloud simulators, which interact with domain specific models or real world field devices. Some examples of such simulators are CloudSim, GreenCloud, CloudAnalyst. iCanCloud, EMUSIM, etc. [20]

Besides synthetic datasets, there is a strong need to use datasets from real SCADA networks or to reuse publicly available ones.

Finally, proper attack models and scenarios, in which the attackers try to exploit vulnerabilities in cloud-based SCADA systems, should be developed.

ACKNOWLEDGMENT

This work was partially funded by grants (No. TR 32025 and TR 36002) from the Ministry of Education, Science and Technological Development of Serbia.

VII. CONCLUSION

Cloud-based SCADA systems represent relatively new business strategy that requires deep analysis and careful assessment of benefits and risks. Even though cloud computing decreases costs and improves business efficiency, there is a need for gradual migration of SCADA applications to the cloud environment, due to stringent security and QoS requirements.

Since SCADA systems are a part of critical infrastructure, they are very susceptible to additional security threats and vulnerabilities, introduced by cloud. Hence, additional work is needed to address security challenges, particularly in terms of new security mechanisms, risk assessment methods and realistic test environments. Taking into account the assessed risk, the cost increase is justified to provide secure cloud services.

REFERENCES

[1] B. Galloway and G. P. Hancke, "Introduction to industrial control networks", IEEE Commun. Surv. Tut., vol. 15, no. 2, 2013, pp. 860–880.

[2] J. Gao et al., "SCADA communication and security issues", Secur. Commun. Netw., vol. 7, no. 1, 2014, pp. 175–194.

[3] I. Ahmed et al., "SCADA systems: Challenges for forensic investigators", Computer, vol. 45, no. 12, 2012, pp. 44–51.

[4] L. Combs. (2011). *Cloud Computing for SCADA. InduSoft, White Paper*. Available at: http://www.indusoft.com/Documentation/White-Papers/ArtMID/1198/ ArticleID/430/Cloud-Computing-for-SCADA.

[5] A. Bashar, "Modeling and Simulation Frameworks for Cloud Computing Environment: A Critical Evaluation", Int. Conf. on Cloud Computing and Services Science (ICCCSS 2014), Los Angeles, USA, September 29-30, 2014, pp. 1–6.

[6] *Cloud-Based SCADA Systems: The Benefits & Risks*. (2011). *Inductive Automation White Paper*. Available at: https://www.controlglobal.com/assets/ 11WPpdf/ 111202-inductiveautomation-cloud.pdf.

[7] Integrated Service Networks for Utilities. CIGRÉ Technical Brochure TB 249, WGD2.07, 2004.

[8] B. Hari Krishna, Dr. S. Kiran, G. Murali, and R. Pradeep Kumar Reddy, "Security issues in service model of cloud computing environment", Procedia Comput. Sci., vol. 87, 2016, pp. 246-251.

[9] C. Wueest, M. Ballano Barcena, and L. O'Brien. (2015). *Mistakes in the IaaS cloud could put your data at risk. Symantec White Paper*. Available at: http://www.symantec.com/content/en/us/enterprise/media/security_response/whitepapers/mistakes-in-the-iaas-cloud-could-put-your-data-at-risk.pdf .

[10] M. T. Sandikkaya and A. E. Harmanci, "Security Problems of Platform-as-a-Service (PaaS) Clouds and Practical Solutions to the Problems", 31st Int. Symp. on Reliable Distributed Systems, 2012, pp. 463-468.

[11] S. Soufiane and B. Halima, "SAAS Cloud security: attacks and proposed solutions", Trans. on Machine Learning and Artificial Intelligence, vol. 5, no. 4, 2017, pp. 291–301.

[12] B. Zhu, A. Joseph, and A. Sastry, "A Taxonomy of Cyber Attacks on SCADA Systems", Int. Conf. on the Internet of Things and the 4th Int. Conf. on Cyber, Physical, and Social Computing, 2011, pp. 380–388.

[13] Z. El Mrabet, N. Kaabouch, H. El Ghazi, and H. El Ghazi, "Cyber-security in smart grid: Survey and challenges", Comput. Electr. Eng., vol. 67, 2018, pp. 469–482.

[14] W. Gao, T. Morris, B. Reaves, and D. Richey, "On SCADA Control System Command and Response Injection and Intrusion Detection", eCrime Researchers Summit, 2010.

[15] P. D. Howard. (2015). *A Security Checklist for SCADA Systems in the Cloud.* Available at: https://gcn.com/articles/2015/06/29/scada-cloud.aspx.

[16] M. Stojanović, V. Aćimović-Raspopović, and S. Boštjančič Rakas, "Security management issues for open source ERP in the NGN environment", in Enterprise Resource Planning: Concepts, Methodologies, Tools, and Applications, vol. II, M. Khosrow-Pour, Ed. New York: IGI Global, 2013, pp. 789–804.

[17] K. Stouffer, J. Falco, and K. Scarfone, Guide to Industrial Control Systems (ICS) Security. NIST Special Publication 800-82 Rev. 2, 2015.

[18] Y. Cherdantseva et al., "A review of cyber security risk assessment methods for SCADA systems", Comput. Secur., vol. 56, 2016, pp. 1–27.

[19] S. Nazir, S. Patel, and D. Patel, "Assessing and augmenting SCADA cyber security: A survey of techniques", Comput. Secur., vol. 70, 2017, pp. 436–454.

[20] A. Ahmed and A.S. Sabyasachi, "Cloud Computing Simulators: A Detailed Survey and Future Direction" *Int. Advance Computing Conf*, 2014, pp. 866–872.

Reduction of True Power Loss by Improved Teaching Learning Based Optimization Algorithm

Dr.K.Lenin[1]

[1]Professor, Department of EEE Prasad V.Potluri Siddhartha Institute of Technology, Kanuru, Vijayawada, Andhra Pradesh -520007, gklenin@gmail.com

Abstract—**This paper presents an Improved Teaching-Learning-Based Optimization (ITLBO) algorithm for solving reactive power flow problem. Basic Teaching-Learning-Based Optimization (TLBO) is reliable, accurate and vigorous for solving the optimization problems. Also it has been found that TLBO algorithm slow in convergence due to its high concentration in the accuracy. This paper presents an, improved version of TLBO algorithm, called as Improved Teaching-Learning-Based Optimization (ITLBO). A parameter called as "weight" has been included in the fundamental TLBO equations & subsequently it increases the rate of convergence. In order to evaluate the proposed algorithm, it has been tested in Standard IEEE 30 bus system and compared to other standard reported algorithms. Simulation results reveal about the better performance of the proposed algorithm in reducing the real power loss & voltage profiles are within the limits.**

Keywords- optimal reactive power, Transmission loss, Improved Teaching Learning

I. INTRODUCTION

Optimal reactive power dispatch problem is one of the difficult optimization problems in power systems & various mathematical techniques [1-7] have been utilized to solve the problem. Recently many types of Evolutionary algorithms [8-9] have been used to solve the reactive power problem. This paper presents an Improved Teaching-Learning-Based Optimization (ITLBO) algorithm for solving reactive power flow problem. Basic Teaching-Learning-Based Optimization (TLBO) [10-16] is reliable, accurate and vigorous for solving the optimization problems. Also it has been found that TLBO algorithm slow in convergence due to its high concentration in the accuracy. This paper presents an, improved version of TLBO algorithm, called as Improved Teaching-Learning-Based Optimization (ITLBO). A parameter called as "weight" has been included in the fundamental TLBO equations & subsequently it increases the rate of convergence. In order to evaluate the proposed algorithm, it has been tested in Standard IEEE 30 bus system and compared to other standard reported algorithms. Simulation results reveal about the better performance of the proposed algorithm in reducing the real power loss & voltage profiles are within the limits.

II. OBJECTIVE FUNCTION

Active power loss

The objective of the reactive power dispatch is to minimize the active power loss in the transmission network, which can be described as follows:

$$F = PL = \sum_{k \in Nbr} g_k (V_i^2 + V_j^2 - 2V_i V_j \cos\theta_{ij}) \quad (1)$$

where F- objective function, P_L – power loss, g_k- conductance of branch,V_i and V_j are voltages at buses i,j,Nbr- total number of transmission lines in power systems.

Voltage profile improvement

For minimizing the voltage deviation in PQ buses, the objective function becomes:

$$F = PL + \omega_v \times VD \quad (2)$$

Where VD - voltage deviation,ω_v- is a

weighting factor of voltage deviation.

Voltage deviation given by:

$$VD = \sum_{i=1}^{N_{pq}} |V_i - 1| \quad (3)$$

Where Npq- number of load buses

Equality Constraint

The equality constraint of the problem is represented by the power balance equation, where the total power generation must cover the total power demand and the power losses:

$$P_G = P_D + P_L \quad (4)$$

Where P_G- total power generation, P_D - total power demand.

Inequality Constraints

The inequality constraints in the power system as well as the limits created to ensure system security. Upper and lower bounds on the active power of slack bus (Pg), and reactive power of generators (Q_g) are written in mathematically as follows:

$$P_{gslack}^{\min} \le P_{gslack} \le P_{gslack}^{\max} \quad (5)$$

$$Q_{gi}^{\min} \le Q_{gi} \le Q_{gi}^{\max}, i \in N_g \quad (6)$$

Upper and lower bounds on the bus voltage magnitudes (V_i):

$$V_i^{\min} \le V_i \le V_i^{\max}, i \in N \quad (7)$$

Upper and lower bounds on the transformers tap ratios (T_i):

$$T_i^{\min} \le T_i \le T_i^{\max}, i \in N_T \quad (8)$$

Upper and lower bounds on the compensators reactive powers (Q_c):

$$Q_c^{\min} \le Q_c \le Q_C^{\max}, i \in N_C \quad (9)$$

Where N is the total number of buses, N_T is the total number of Transformers; N_c is the total number of shunt reactive compensators.

III. Basic Teaching-Learning-Based Optimization

Based on the consequence of the influence of a teacher on the output of students in a class, Teaching-Learning-Based Optimization (TLBO) optimization algorithm has been framed. It is a population based method & there are numbers of different design variables. Different subjects offered to learners and the learners' result is analogous to the "fitness" & it act as different design variables in TLBO. The most excellent solution is analogous to Teacher in TLBO. The algorithm consist of first part "Teacher Phase" and the second "Learner Phase". Learning from the teacher is the "Teacher Phase" means and learning through the interaction between learners is the "Learner Phase". The execution of TLBO as follows,

A. Initialization

Following are the notations used for describing the TLBO:

L: "class size "of the learners;

C: list of the courses offered to the learners to learn;

MAX IT; number of maximum iterations.

In search space bounded the population *Y* is arbitrarily initialized by a by matrix of *L* rows and *C* columns. In *ith* learner . the *jth* parameter is assigned values arbitrarily by equation

$$y_{(i,j)}^0 = y_j^{\min} + rand \times (y_j^{\max} - y_j^{\min}) \quad (10)$$

Within the range (0,1) "*rand"* represents a uniformly distributed arbitrary variable, minimum and maximum value for *jth* parameter is represented by y_j^{max} and y_j^{min}. For the generation *g* parameters of the *ith* learner are given by,

$$y_{(i)}^{g} = \left[y_{(i,1)}^{g}, y_{(i,2)}^{g}, y_{(i,3)}^{g}, .., y_{(i,j)}^{g}, .., y_{(i,D)}^{g} \right] \quad (11)$$

B. Teacher Phase

At generation g the mean parameter E_g of each subject learners in the class is given as,

$$E^{g} = \left[e_1^{g}, e_2^{g}, .., e_j^{g}, .., e_D^{g} \right] \quad (12)$$

The teacher $X_{Teacher}^{g}$ with the minimum objective function value of the learner is considered as for respective iteration. Shifting the mean of the learners towards its teacher is done by Teacher phase. An arbitrary weighted differential vector is formed to obtain a new-fangled set of improved learners from the current mean, desired mean parameters and is added to the existing population of learners.

$$Y_{new(i)}^{g} = Y_{(i)}^{g} + rand \times (Y_{Teacher}^{g} - Te_F E^{g}) \quad (13)$$

The value of mean to be changed is decided by "Te_F" - teaching factor. Value of T_F can be either 1 or 2. With equal probability the value of Te_F is decided arbitrarily as,

$$Te_F = round\left[1 + rand(0.1)\{2-1\} \right] \quad (14)$$

The value of T_F value is arbitrarily decided by the algorithm using Equation (14). In generation g if $Ynew_{(i)}^{g}$ is superior learner than $Y_{(i)}^{g}$, than it swap the inferior learner $Y_{(i)}^{g}$ in the matrix.

C. Learner Phase

In this phase the mutual interaction tends to augment the knowledge of the learner. The arbitrary inter- action among learners improves the knowledge. For a given learner $Y_{(i)}^{g}$ another learner $Y_{(r)}^{g}$ is arbitrarily selected($i \neq r$). In the learner phase the i^{th} parameter of the matrix Y_{new} is given as,

$$Y_{(i)}^{g} = \begin{cases} Y_{(i)}^{g} + rand \times (Y_{(i)}^{g} - Y_{(r)}^{g}) \\ if \quad f(Y_{(i)}^{g}) < f(Y_{(r)}^{g}) \\ Y_{(i)}^{g} + rand \times (Y_{(i)}^{g} - Y_{(r)}^{g}) otherwise \end{cases} \quad (15)$$

D. Algorithm Termination

After *MAXIT* conditions satisfied the algorithm is terminated.

IV. Improved Teaching-Learning-Based Optimization (ITLBO) Algorithm

The principles of teaching-learning approach, is imitated in Teaching-Learning-Based Optimization (TLBO) & draw analogy with the real class room. Teaching-learning process is an iterative process where in the continuous interaction takes place for the transfer of knowledge. A parameter known as "weight" is added in the Equations (13) and (15) of original TLBO algorithm. In contrast to the original TLBO, while computing the new learner values the part of its previous value is considered and decided by a weight factor "*wf*" in our Improved Teaching-Learning-Based Optimization (ITLBO) algorithm. During the early stages of the search Individuals are encouraged to sample diverse zones of the exploration space. It is important to adjust the movements of trial solutions finely & they can explore the interior of a relatively small space in the later stages. Value of the weight factor reduced linearly with time from a maximum to a minimum value by,

$$wf = wf_{\max} - \left(\frac{wf_{\max} - wf_{\min}}{\max iteration}\right) * i \quad (16)$$

The maximum and minimum values of weight factor *w* are wf_{max} and wf_{min} , "*I*" - iteration is the current iteration number and max iteration is the maximum number of iterations. wf_{max} & wf_{min} are selected between 0.9 -0.1, respectively. New set of improved learners in the teacher phase can be,

$$Y_{new(i)}^{g} = wf * Y_{(i)}^{g} + rand * (Y_{Teacher}^{g} - Te_F E^{g}) \quad (17)$$

And in learner phase a set of improved learners are,

$$Y_{(i)}^{g}=\begin{cases} wf * X_{(i)}^{g}+rand\times(Y_{(i)}^{g}-Y_{(r)}^{g}) \\ if \quad f(Y_{(i)}^{g})<f(Y_{(r)}^{g}) \\ wf * Y_{(i)}^{g}+rand\times(Y_{(i)}^{g}-Y_{(r)}^{g}) otherwise \end{cases} \quad (18)$$

V. Simulation Results

Validity of proposed Improved Teaching-Learning-Based Optimization (**I**TLBO) algorithm has been verified by testing it in standard IEEE 30-bus, which has 41 branches, 6 generator-buses, 4 transformer-tap settings, 2shunt reactive compensators.

TABLE I. Key Variable Limits (Pu)

List of Variables	Min	Max	Type
Generator Bus	0.950	1.10	Continuous
Load Bus	0.950	1.050	Continuous
Transformer-Tap	0.90	1.10	Discrete
Shunt Reactive Compensator	-0.110	0.310	Discrete

In Table II Generators power limits are listed. Bus 1 is considered as slack bus. 2, 5, 8, 11 and 13 are taken as PV buses & remaining as PQ buses. Control variables limits are given in Table I.

Table III gives the control variables obtained after optimization.Table IV presents the performance of the proposed ITBLO. Table V list out the overall comparison of real power loss.

TABLE III. Control variables values after optimization

List of Control Variables	ITLBO
V1	1.04182
V2	1.04173
V5	1.02014
V8	1.03122
V11	1.07031
V13	1.05121
T4,12	0.0000
T6,9	0.0000
T6,10	0.9000
T28,27	0.9000
Q10	0.1000
Q24	0.1000
Real power loss (MW)	4.2212
Voltage deviation	0.9096

TABLE IV. Narration of projected ITBLO algorithm

No. of Iterations	32
Time taken (sec)	9.36
Real power loss (MW)	4.2212

TABLE II. Generators Power Limits

Bus	Pg	Pgminimum	Pgmaximum	Qgminimum	Qgmaximum
1	96.000	49.000	200.000	0.000	10.000
2	79.000	18.000	79.000	-40.000	50.000
5	49.000	14.000	49.000	-40.000	40.000
8	21.000	11.000	31.000	-10.000	40.000
11	21.000	11.000	28.000	-6.000	24.000
13	21.000	11.000	39.000	-6.000	24.000

TABLE V. EVALUATION OF OUTCOME

List of Techniques	Real power loss (MW)
SGA [22]	4.98
PSO [23]	4.9262
LP [24]	5.988
EP [24]	4.963
CGA [24]	4.980
AGA [24]	4.926
CLPSO [24]	4.7208
HSA [25]	4.7624
BB-BC [26]	4.690
MCS [27]	4.87231
Proposed ITBLO	4.2212

VI. CONCLUSION

In this paper a novel approach Improved Teaching-Learning-Based Optimization (ITLBO) algorithm used to solve reactive power problem, considering various generator constraints, has been successfully applied. Also it has been found that TLBO algorithm slow in convergence due to its high concentration in the accuracy.The performance of the proposed Improved Teaching-Learning-Based Optimization (ITLBO) algorithm has been has been tested in standard IEEE 30 bus system and simuation results expose about the decrease of real power loss when compared with other standard algorithms and mostly volatge profiles are within the limits.

REFERENCES

[1] O.Alsac,and B. Scott, "Optimal load flow with steady state security",IEEE Transaction. PAS -1973, pp. 745-751.

[2] Lee K Y ,Paru Y M , Oritz J L –A united approach to optimal real and reactive power dispatch , IEEE Transactions on power Apparatus and systems 1985: PAS-104 : 1147-1153

[3] A.Monticelli , M .V.F Pereira ,and S. Granville , "Security constrained optimal power flow with post contingency corrective rescheduling" , IEEE Transactions on Power Systems :PWRS-2, No. 1, pp.175-182.,1987.

[4] Deeb N ,Shahidehpur S.M ,Linear reactive power optimization in a large power network using the decomposition approach. IEEE Transactions on power system 1990: 5(2) : 428-435

[5] E. Hobson ,'Network consrained reactive power control using linear programming, ' IEEE Transactions on power systems PAS -99 (4) ,pp 868=877, 1980

[6] K.Y Lee ,Y.M Park , and J.L Oritz, "Fuel –cost optimization for both real and reactive power dispatches" , IEE Proc; 131C,(3), pp.85-93.

[7] M.K. Mangoli, and K.Y. Lee, "Optimal real and reactive power control using linear programming" , Electr.Power Syst.Res, Vol.26, pp.1-10,1993.

[8] K.Anburaja, "Optimal power flow using refined genetic algorithm", Electr.Power Compon.Syst , Vol. 30, 1055-1063,2002.

[9] D. Devaraj, and B. Yeganarayana, "Genetic algorithm based optimal power flow for security enhancement", IEE proc-Generation.Transmission and. Distribution; 152, 6 November 2005.

[10] R. V. Rao, V. J. Savsani and D. P. Vakharia, "Teaching- Learning-Based Optimization: A Novel Method for Con- strained Mechanical Design Optimization Problems," Computer-Aided Design, Vol. 43, No. 1, 2011, pp. 303- 315. doi:10.1016/j.cad.2010.12.015 .

[11] R. V. Rao, V. J. Savsani and D. P. Vakharia, "Teaching-Learning-Based Optimization: An Optimization Me- thod for Continuous Non-Linear Large Scale Problems," INS 9211 No. of Pages 15, Model 3G 26 August 2011.

[12] R. V. Rao, V. J. Savsani and J. Balic, "Teaching Learning Based Optimization Algorithm for Constrained and Un- constrained Real Parameter Optimization Problems," En- gineering Optimization, Vol. 44, No. 12, 2012, pp. 1447- 1462. doi:10.1080/0305215X.2011.652103.

[13] R. V. Rao and V. J. Savsani, "Mechanical Design Optimization Using Advanced Optimization Techniques," Springer-Verlag, London, 2012. doi:10.1007/978-1-4471-2748-2

[14] V. Toğan, "Design of Planar Steel Frames Using Teach- ing-Learning Based Optimization," Engineering Struc- tures, Vol. 34, 2012, pp. 225-232. doi:10.1016/j.engstruct.2011.08.035

[15] R. V. Rao and V. D. Kalyankar, "Parameter Optimization of Machining Processes Using a New Optimization Algo- rithm," Materials and Manufacturing Processes, Vol. 27, No. 9, 2011, pp. 978-985. doi:10.1080/10426914.2011.602792.

[16] S. C. Satapathy and A. Naik, "Data Clustering Based on Teaching-Learning-Based Optimization. Swarm, Evolu- tionary, and Memetic Computing," Lecture Notes in Com- puter Science, Vol. 7077, 2011, pp. 148-156, doi:10.1007/978-3-642-27242-4_18 .

[17] Chaohua Dai, Weirong Chen, Yunfang Zhu, and Xuexia Zhang, "Seeker optimization algorithm for optimal reactive power dispatch," IEEE Trans. Power Systems, Vol. 24, No. 3, August 2009, pp. 1218-1231.

[18] J. R. Gomes and 0. R. Saavedra, "Optimal reactive power dispatch using evolutionary computation: Extended algorithms," IEE Proc.-Gener. Transm. Distrib.. Vol. 146, No. 6. Nov. 1999.

[19] IEEE, "The IEEE 30-bus test system and the IEEE 118-test system", (1993), http://www.ee.washington.edu/trsearch/pstca/.

[20] Jiangtao Cao, Fuli Wang and Ping Li, "An Improved Biogeography-based Optimization Algorithm for Optimal Reactive Power Flow" International Journal of Control and Automation Vol.7, No.3 (2014), pp.161-176

Electrical Equipment's Condition and Remaining Useful Life Assessment - a Review

Sanja Stanković[1], Milica Rašić[2], Zoran Stajić[3], Miomir Stanković[4]

[1]Research and Development Center "ALFATEC", 18000 Niš, Serbia,
sanja.stankovic@alfatec.rs, milica.rasic@alfatec.rs, zoran.stajic@alfatec.rs,
miomir.stankovic@gmail.com

Abstract— **Condition-based maintenance (CBM) is a preferable type of maintenance nowadays in power utilities. Assessment of equipment's health condition and remaining useful life (RUL) is the main goal of CBM in order to allocate resources correctly and optimally, to make system more reliable and to reduce overall costs for the maintenance. There are a lot of methods and techniques used for condition and RUL assessment. This paper presents general approach for CBM and through the review of references presents three common techniques – ranking and scoring health index method, artificial neural network method and fuzzy logic method for evaluating electrical equipment's condition. In the end, comparison of mentioned methods is briefly presented.**

Keywords - condition-based maintenance, remaining useful life, fuzzy logic, health index, artificial neural network

I. INTRODUCTION

Maintenance of electrical power plants and electrical equipment is one of prioritized activities of distribution system operators. Electrical equipment, whose lifespan can be more than 40 years, requires a timely and proper response in the form of condition-based maintenance actions in order to achieve the maximum of its lifespan. Maintenance actions at certain time intervals, i.e. time-based maintenance, which is mostly applied in electrical systems today, and in Serbia's as well, is not the most optimal type of maintenance, so it is essential to move on to maintenance based on condition of the equipment or reliability of the system (the latter one in the form of reliability - centered maintenance (RCM)). Assessment of the equipment's condition is very important due to the increased requirements for its reliable and safe operation, minimized cost of maintenance and its maximized RUL [1-2].

This paper presents the overview of trending and mostly used methods for evaluating the health condition and, as a result, RUL of the equipment or probability of failure. The emphasis is put on main parts of power equipment installed in substations, transformers and circuit breakers, but reviewed methods can be generalized and adjusted for any type of electrical equipment. The aim of the paper is to clarify the concept of condition and RUL assessment for the purpose of CBM.

Section 2 presents general definitions and explanation of CBM and RUL. Section 3 introduces and classifies methodologies for equipment's health condition and RUL evaluation, reviews and compares three mostly used methods for their application on electrical equipment, while Section 4 presents conclusion on the topic.

II. CONDITION-BASED MAINTENANCE (CBM)

A. General Definition and Practices

Condition-based maintenance is practice that requires appropriate condition assessment by different sensors and on-line monitoring systems, in order to obtain actual health state and condition of equipment and its parts; to plan and perform appropriate and timely maintenance actions, just when they are needed according to the condition of the equipment and based on technical and economic aspects. In this term, maintenance can be optimized and

ISBN: 978-86-80616-03-2

unnecessary costs that are often related to time-based maintenance can be drastically reduced. With condition parameters properly monitored and data obtained, variety of methods can be applied for determining the overall health and RUL of electrical equipment.

However, current practice in Serbia's electrical energy system (EES), because of the lack of on-line monitoring systems for collecting data about equipment's condition, includes mostly equipment's condition evaluation during substations' inspections and overhauls. Relevant tests and examination activities for substation's equipment that are usually conducted to collect information on equipment's condition during inspections are listed in [1-2] and upon that, subjective assessment is done by maintainers and real condition of the equipment is obtained. These tests can deprive an excessive amount of time and financial resources, what is certainly not optimal for electrical utilities. This is one of the main reasons for utilizing on-line condition monitoring systems, forming decision-support systems for maintenance optimization and applying different techniques and methodologies for extracting useful knowledge about equipment's condition from relevant condition monitoring systems and databases [3].

B. Remaining Useful Life of Equipment (RUL)

Condition and RUL assessment are results of diagnostics and prognostics, respectively. However, the difference between RUL and prognostics of failure can be made, in the sense that the first one represents the total lifetime of the equipment remained to its end from the moment of observation, notwithstanding failures and repairs. On the other hand, the prognostics of failure determines the time that remains to the first failure or the moment just before the failure so that maintenance actions can be done correctly, and it is one of the issues of RCM [5-7]. However, some other references emphasize the fact that because of the correlation between condition of the equipment, probability of failure and RUL, they cannot be defined and considered separately, no matter what type of maintenance is performed [3, 8, 13]. Fig. 1 shows the "bathtub" curve, which presents the dependency between the number of failures or failure rate and the lifespan of the equipment. The relationship between the health condition of the equipment and its remaining useful life is more important for the research done in this paper. This curve is also called "deterioration" or "degradation" curve and it is shown in Fig. 2 [9].

The following section presents the most often used methods and techniques for condition and remaining useful life of equipment assessment found in the literature, with specific emphasis on three methods that are mostly used for power transformers and circuit breakers.

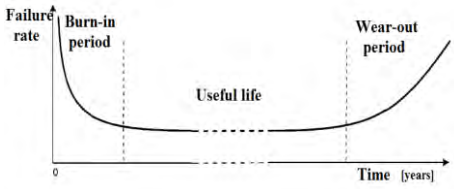

Figure 1. Bathtub curve [7]

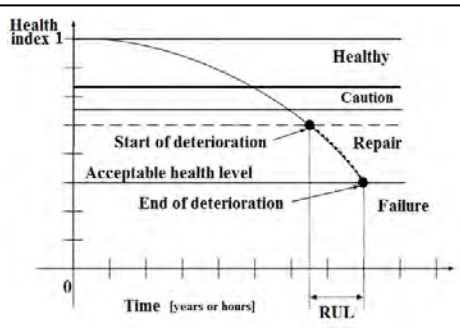

Figure 2. Deterioration curve [9]

III. METHODOLOGIES FOR EQUIPMENT'S CONDITION AND RUL ASSESSMENT

A. Classification of Methodologies

Current practices and researches emphasize the importance of multi-parametric condition assessment due to the impossibility to obtain enough information just from one single parameter analysis. Regardless of that, there are many proposed methods for this kind of analysis in the literature. Reference [10] can be denoted as an example of comparative study for evaluation of RUL of transformer by analyzing single parameters of insulation, such as degree of polymerization, hotspot temperature, dissipation factor, etc. In [11], comparison between different machine learning methods for calculating RUL of transformer's insulation based on hotspot temperature of windings was shown. However, this paper deals with

methodologies based on two or more parameters that are being researched and used for CBM in recent years.

Firstly, in order to classify methodologies for condition and RUL assessment, available and necessary datasets and basic principles should be designated and defined. One wider classification of techniques for RUL predictions is presented in [9]. Methodologies are more often roughly divided into two classes, one using combination of historical and statistical information about equipment's condition, so-called data-driven methodologies, and another one is a model-based class of methodologies, so-called physics-of-failure methodologies [3, 5, 12]. First one uses data obtained through monitoring of the equipment and extracts knowledge through process called data mining, and the second one uses physical parameters of equipment and the damage analysis in order to analytically predict future failures. The latter one is strongly connected to the reliability and probability of failure theory, and these methods are more suitable for RCM. When data-driven methods for equipment's health assessment are considered, there is a variety found in the literature, from empirical and mathematical techniques, which include health index (HI) ranking method reviewed in this paper, pattern recognition and machine learning algorithms, to advanced computational methods such as methods based on artificial intelligence (AI), like swarm optimization methods, fuzzy logic and artificial neural networks (ANN)[3].

B. Ranking Health Index Method

The Health Index calculation is conventional, but practical and useful method for determining the overall condition of the equipment, by means of condition monitoring, overhaul inspections and other available data obtained during equipment's life, thus enabling maintainers to better evaluate and decide which part of the equipment needs to be replaced or repaired first. This methodology is usually based on ranking or scoring methods and mathematical formulations developed empirically by electrical utilities and working groups in the domain of electrical engineering like CIRED, CIGRE, IEC, IEEE or others [14]. General CBM based on health index methodology is shown in Fig. 3. For the output of final health index various ranges amongst researchers have been used, e.g. ranges of 0-100, 1-10, 1-5, 1-4, with exact definitions of values in the range that designate the state of asset's condition or health [15].

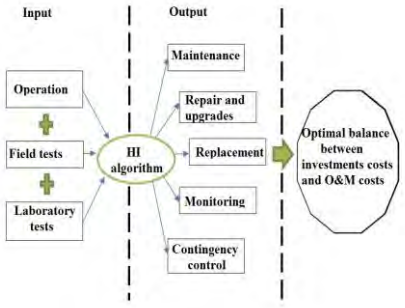

Figure 3. Health index methodology [15]

For data-driven health index calculation, it is important to choose suitable parameters and assign to them appropriate weights and scores. Some of the most important parameters used for HI method for power transformer are listed in [14-16], and for circuit breakers in [17]. One detailed overview of the health index methodologies can be found in [15]. Comparative review of HI methods used in a large number of papers is presented, with listed parameters and their weights for ranking, and listed mathematical formulations for HI calculation as well. Transformer HI concept from [15] can be generalized for another type of equipment.

Calculation of HI is often accompanied with calculation of probability of failure and RUL [14-15, 18]. Health index approach for asset's future health condition based on current condition was explained in [18-19]. The key point of the methodology was presented as understanding of equipment's functionality. It is defined how different components of system or equipment affect it and how condition ratings of different components can create one overall rate of the equipment as unity. The application of the method for distribution voltage regulators was also presented in [18], with listed parameters and their weights and scores for composing HI.

Another approach that combines HI calculation and Markov Chain Model to determine equipment's future health is presented in [20]. Health index scores had firstly been used to obtain the information about transformers' overall health condition in the moment of observation, and then Markov Chain Model was used to determine transformers' future condition. The results were expressed in

the form of deterioration curve and it was observed that prediction accuracy with this method could be more than 95%.

It should be pointed out that these techniques have more subjective impact than others because they include engineers' and maintainers' personal imprint in giving weights to parameters, so this methodology is suitable when there are no advanced on-line monitoring systems.

C. *Artificial Neural Networks*

Artificial Neural Networks are one of the most common techniques because of their ability to "learn" about complex systems, without any previous assumptions or knowledge about it. The concept of ANN dates from the mid-20th century, and their name indicates that they are similar to biological neural network. The framework of such networks is shown in Fig. 4.

In the simplest words, ANN uses initialized input values and desired or known output values as training vectors with associated random weights to calculate actual output, and then to adjust weights to reduce the total error to acceptable threshold level. For the case of electrical equipment, input values are usually measurements obtained during the lifetime of the equipment, and output values can be health indices, age of the equipment or probability of failure [22, 24].

Application of artificial neural networks for equipment's failure detection dates from the last century. In [22], ANN was used to detect faults and malfunctions of oil-filled transformers based on dissolved gas analysis. General approach for ANN in the domain of CBM is explained in [23], with application example for pump bearings, where input layer consists of age values, current and previous condition monitoring measurements. The output is prediction of RUL or time to failure. Another application of ANN is presented in [21], where different failure history and condition data of power transformer, such as dissolved gasses and furan analyses results, power factor, transformer's age, operation and maintenance history data, degree of polymerization, etc. were used to train neural network, and the result is their overall health condition.

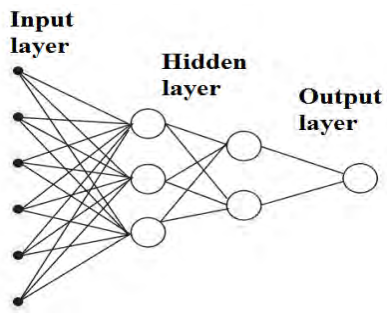

Figure 4. Multi-layer ANN

Reference [25] proposed another application of specific type of neural networks and ensemble method based on relationship between degree of polymerization and furfural content in transformer's oil, combined with other historical, specification and ambient data like age, temperature, load factor, etc. Experimental research implemented in [27] shows practical application of ANN for monitoring and diagnostics of circuit breakers, where system was designed to give an alarm for the malfunction of breakers based on the following parameters: temperature, humidity, travel and vibration of contacts of the breaker. In [26], a feed forward artificial network was used for 88 different oil transformers' parameters, with 2 hidden layers and health condition index as output value. Training set from this neural network consists of data for 59 transformers, and testing set consists of data for 29 transformers. The output set has values from 0 to 1, where 0 means totally new transformer and 1 means transformer in the last stage of deterioration that requires replacement. The method was concluded to be 96.55 % accurate.

In order to be more accurate, this method requires a large amount of data, because ANN learns directly from training samples. In addition, it is totally freed from subjective impact, which is significant benefit for CBM.

D. *Fuzzy Logic*

Fuzzy logic is a type of logic where values of variables can be any number in the range of 0-1. This concept was introduced by Lotfi Zadeh in 1965, and it has been the most popular method with various applications in different systems, especially in electrical systems for condition monitoring and diagnostics. The method can use the same condition and historical data as input data like ANN, but the main difference is that fuzzy logic uses defined linguistic rule base with standard "if-then" rules instead of assigned weights to train the system and give an output. In other words, fuzzy logic

represents an approximation of reasoning used in expert systems for decision-making based on the rules derived from experience. Fuzzy output of such system is in form of a fuzzy number. Fuzzy logic method is especially suitable for electrical equipment's condition and RUL evaluation because it can help with decision-making process for CBM. Fuzzy logic expert system, for equipment's condition assessment, is comprised of equipment's knowledge database, fuzzification process, inference mechanism and defuzzification process. This is shown in Fig. 5 [28].

References [29-30] proposed and explained in detail fuzzy expert systems for transformer's failure prognostics, whose inputs are thermography, dissolved gas analyses and frequency response analyses results, transformer's age, temperature of insulation, dielectric losses and degree of polarization. The rule database for the system was designed of measurements from real case power system in Serbia with different high voltage transformer stations, and two different cases of fuzzy systems have been presented and explained in detail. Outputs of these systems are numbers from the interval 0-1 and they present the probability of failure, which indicates necessity for maintenance actions. The results were also compared with HI scoring results that had been obtained for the same transformers and they had matched.

Another application was presented in [31] for diagnostics of high voltage circuit breakers, where main indicators for the health of circuit breaker are parameters of breaker's contacts, arc chamber and medium, and operating mechanism. The results clearly showed the most critical parts and priorities for the maintenance actions for observed circuit breakers and they were compared with another method's results, unsupervised machine learning method.

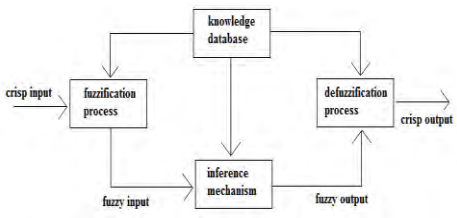

Figure 5. Fuzzy logic expert system

Fuzzy systems are also often used as advanced method for obtaining health index of the equipment, like presented in [32-34] for the case of power transformers. Ref. [32] proposed evaluating six different oil parameters: dielectric breakdown voltage, dissipation factor, water content, acidity, dissolved gas analysis and degree of polymerization, and forming fuzzy logic systems for each parameter. The output values represented five different states of transformer's condition, which are actually health indices, meaning from "very good" to "very bad" and they indicate necessity for maintenance action.

In [33], three indicators were evaluated - current, voltage and oil quality, and results were compared with HI given from the utility, whereby 80% of the results matched. In [34] transformer's parameters have been denoted as "attributes" and scores used as inputs for fuzzy logic system have been assigned to them. As a result and output of the system, overall health index of transformer was obtained.

It is also worth mentioning that fuzzy logic is sometimes combined with neural networks in order to reduce fuzziness from the output. This concept is called neuro-fuzzy system, where either neural networks are used to "learn" from rule database (input and output of neural network are fuzzy sets) or fuzzy system is embedded into hidden layers of neural network [35-38].

E. Comparisson of Three Presented Methods

- The main difference between proposed methods is that health index ranking method uses recommendations and subjective evaluation for weighting and empirical mathematical formulations for calculation of health index value, while fuzzy logic and especially artificial neural networks use principles of computational algorithms without subjective perspective.
- The difference between two proposed AI-based methods is that ANN method learns about systems only from training examples without any previously specified rule or any knowledge about the system, while fuzzy logic method uses strictly defined rules from rule database that are formed based on previous experience.
- One big advantage of HI over fuzzy logic and ANN is that it can be used with smaller amount of condition data with maintainers'

subjective observations, without complex monitoring systems, while two proposed AI-based methods require "big data" in order to be more accurate, which can only be accomplished by installing previously mentioned on-line condition monitoring systems.

- The advantage of HI and ANN over fuzzy logic is reflected through the output; they can give strict values that mean unambiguous condition states of the equipment. This is not the case with fuzzy logic method, where the certainty of the output depends exclusively on specified rules. This is due to the purpose of fuzzy logic to quantify the ambiguity of linguistic terms that are used to describe the condition of the equipment.
- One great advantage of these three methods is that they can be used either for the whole system, or for each part or component. In this way, critical points can be determined and maintenance actions can be carried out on them.

IV. CONCLUSION

Evaluation of electrical equipment's condition and remaining useful life is the main task of condition-based maintenance. It is the future of maintenance practices, and it is very important to enable condition monitoring and collecting data, so this type of maintenance could be performed. This paper reviews some of the methods used nowadays and indicates their main characteristics, advantages and disadvantages. Proposed and mentioned techniques for condition and RUL assessment have great significance because they can be embedded into decision-support systems that are likely to be formed and used in the upcoming years. This could be a part of the future research.

ACKNOWLEDGMENT

This paper is a part of the research done within the project III 44006, supported by the Ministry of Education, Science and Technological Development of the Republic of Serbia within the framework of technological development.

REFERENCES

[1] R&D Center "Alfatec", "Racionalizacija rezervne opreme i poboljšanje pouzdanosti elektrodistributivnih objekata 110 kV i 35 kV", Niš, December 2017. (in Serbian)

[2] R. M. Ćirić, S. N. Mandić, Održavanje elektroenergetske opreme, AGM knjiga, Belgrade, 2015. (in Serbian)

[3] Z. Zhang, "Data Mining Approaches for Intelligent Condition-based Maintenance," Doctoral Thesis, Norwegian University of Science and Technology, Trondheim, 2014.

[4] E. L. Kokorin, A. I. Khalyasmaa, "Electrical Equipment Condition Based Maintenance Strategy," Proceedings of International Conference and Exposition on Electrical and Power Engineering (EPE 2016), 20-22 October, 2016, Iasi, Romania, pp. 748-753.

[5] X. Si, Z. Zhang, C. Hu, Data-Driven Remaining Useful Life Prognosis Techniques: Stochastic Models, Methods and Applications, National Industry Press, China, and Springer-Verlag GmbH, Germany, 2017.

[6] X. Zhang, E. Gockenbach, V. Wasserberg, H. Borsi, "Estimation of the lifetime of the electrical components in distribution networks", IEEE Transactions on Power Delivery, Vol. 22, No. 1, January 2007, pp. 515-522.

[7] M. Rausand, A. Høyland, System Reliability Theory: Models, Statistical Methods and Applications, 2nd Edition, John Wiley and Sons, Inc., Hoboken, New Jersey, 2004.

[8] Y. Guan, M. Kezunovic, P. Dehghanian, G. Gurrala, "Assessing circuit breaker life cycle using condition-based data", IEEE Power & Energy Society General Meeting, Vancouver, Canada, July 21-25, 2013, pp. 1-5.

[9] C. Okoh, R. Roy, J. Mehnen, L. Redding, "Overview of Remaining Useful Life Prediction Techniques in Through-Life Engineering Services", Proceedings of 6th CIRP Conference on Industrial Product-Service Systems, Vindsor, Canada, May 1-2, 2014, pp. 158-163.

[10] A. Kumari, H.C. Verma, A. Baral, S.Chakravorti "Comparison of Different Methods Available for Evaluating Remaining Life of OIP Insulation Used in Power Transformers", Proceedings of 6th International Conference on Computer Applications In Electrical Engineering-Recent Advances (CERA), Roorkee, India, October 5-7, 2017, pp. 209-214.

[11] J. I. Aizpurua, S. D. J. McArthur, B. G. Stewart, B. Lambert, J. G. Cross, V. M. Catterson, "Adaptive power transformer lifetime prediction through machine learning & uncertainty modelling in nuclear power plants", IEEE Transactions on Industrial Electronics, in press.

[12] M. Mishra, "Model-based Prognostics for Prediction of Remaining Useful Life", Licentiate Thesis, Lulea University of Technology, 2015.

[13] M. Wang, A. J. Vandermaar, "Review of condition assessment of power transformers in service", IEEE Electrical Insulation Magazine, Vol. 18, 2002, pp. 12-25.

[14] A. N. Jahromi, R. Piercy, S. Cress, J. R. R. Service, W. Fan, "An approach to power transformer asset management using health index", IEEE Electrical Insulation Magazine, vol. 25, Issue: 2, March-April 2009, pp. 20-34.

[15] A. Azmi, J. Jasni, N. Azis, M. Z. A. A. Kadir "Evolution of transformer health index in the form of mathematical equation", Renewable and Sustainable Energy Reviews Vol. 76, 2017, pp. 687-700.

[16] J. H. Jürgensen, A. S. Godin, P. Hilber, "Health Index as Condition Estimator for Power System Equipment: a Critical Discussion and Case Study", Proceedings of 24th International Conference & Exhibition on Electricity Distribution (CIRED), Glasgow, Scotland, June 12-15, 2017, pp. 202-205.

[17] P. Dehghanian, T. Popovic, Mladen Kezunovic, "Circuit Breaker Operational Health Assessment via Condition Monitoring Data", North American Power Symposium (NAPS), Pullman, WA, USA, September 7-9, 2014, pp. 1-6.

[18] T. Hjartarson, S. Otal, "Predicting Future Asset Condition Based on Current Health Index and Maintenance Level", 11th International Conference on Transmission & Distribution Construction, Operation and Live-Line Maintenance, Albuquerque, NM, USA, October 15-19, 2006, pp. 1-8.

[19] T. Hjartarson, B. Jesus, D.T. Hughes, R.M. Godfrey "Development of Health Indices for Asset Condition Assessment", Proceedings of IEEE PES Transmission and Distribution Conference and Exposition, Dallas, TX, USA, September 7-12, 2003, pp. 541-_544.

[20] M. S. Yahaya, N. Azis, M.Z.A. Ab Kadir, J. Jasni, M. H. Hairi, M. A. Talib, "Estimation of transformers health index based on the Markov chain", Energies, Vol. 10, 2017, 1824.

[21] P. H. Mukti, F. A. Pamuji, B. S. Munir, "Implementation of Artificial Neural Networks for Determining Power Transfomer Condition", Proceedings of 5th International Symposium on Advanced Control of Industrial Processes, Hiroshima, Japan, May 28-30, 2014, pp. 473-477.

[22] Y. Zhang, X. Ding, Y. Liu, P. J. Griffin, "An artificial neural network approach to transformer fault diagnosis", IEEE Transactions on Power Delivery, Vol. 11, No. 4, October 1996, pp. 1836-1841.

[23] B. Wu, Z. Tian, M. Chen, "Condition-based maintenance optimization using neural network-based health condition prediction", Quality and Reliability Engineering International, Vol. 29, December 2013, pp. 1151-1163.

[24] Z. Tian, "An Artificial Neural Network Approach for Remaining Useful Life Prediction of Equipments Subject to Condition Monitoring", Proceedings of 8th International Conference on Reliability, Maintainability and Safety, Chengdu, China, July 20-24, 2009, pp. 143-148.

[25] T. Matsui, Y. Nakahara, K. Nishiyama, N. Urabe, M. Itoh, "Development of Remaining Life Assessment for Oil-immersed Transformer Using Structured Neural Networks", Proceedings of CROS-SICE International Joint Conference, Fukuoka, Japan, August 18-21, 2009, pp. 1855-1858.

[26] A. E. B. Abu-Elanien, M. M. A. Salama, M. Ibrahim, "Determination of Transformer Health Condition Using Artificial Neural Networks", International Symposium on Innovations in Intelligent Systems and Applications, Istanbul, Turkey, June 15-18, 2011, pp. 1-5.

[27] Y. Hou, T. Liu, X. Lun, J. Lan, Y. Cui, "Research on Monitoring System of Circuit Breakers Based on Neural Networks", Proceedings of International Conference on Machine Vision and Human-machine Interface, Kaifeng, China, April 24-25, 2010, pp. 436-439.

[28] G. Peng, S. Tang, Z. Lin, Y. Zhang, "Applications of Fuzzy Multilayer Support Vector Machines in Fault Diagnosis and Forecast of Electric Power Equipment", Proceedings of 2nd Advanced Information Technology, Electronic and Automation Control Conference (IAEAC), Chongqing,China, March 25-26, 2017, pp. 457-461.

[29] M. Žarković, Z. Stojković, "Analysis of artificial intelligence expert systems for power transformer condition monitoring and diagnostics", Electric Power System Research 149, 2017, pp. 125-136.

[30] M. Žarković, "Monitoring and Diagnostics of Substation Based on Fuzzy Model of High Voltage Equipment Condition", Doctoral Thesis, University of Belgrade, 2017.

[31] M. Žarković, Z. Stojković, J. Mikulović, "Application of Artificial Inteligence in the Monitoring and Diagnostic of High Voltage Circuit Breaker", Proceedings of 17th International Symposium INFOTEH, Jahorina, RS, BiH, March 21-23, 2018, pp. 82-87.

[32] R. D. Medina, J. P. Lata, D. P. Chacón, "Health Index Assessment for Power Transformers with Thermal Upgraded Paper up to 230kV Using Fuzzy Inference Systems", International Caribbean Conference on Devices, Circuits and Systems (ICCDCS), Cozumel, Mexico, June 5-7, 2017, pp. 1-6.

[33] G. C. Jaiswal, M. S. Ballal, D.R. Tutakne, "Health Index Based Condition Monitoring of Distribution Transformer", International Conference on Power Electronics, Drives and Energy Systems (PEDES), Trivandrum, India, December 14-17, 2016, pp. 1-5.

[34] C. Ranga, A. K. Chandel, R. Chandel, "Fuzzy logic expert system for optimum maintenance of power transformers", International Journal on Electrical Engineering and Informatics, Vol. 8, No 4, December 2016, pp. 836-850.

[35] M. Samhouri, A. Al-Ghandoor, S. Alhaj Ali, I. Hinti, W. Massad, "An intelligent machine condition monitoring system using time-based analysis: neuro-fuzzy versus neural network", Jordan Journal of Mechanical and Industrial Engineering, Vol. 3, No 4, December 2009, pp. 294-305.

[36] A. K. Kori, A.K. Sharma, A.K.S. Bhadoriya, "Neuro fuzzy system based condition monitoring of power transformer", International Journal of Computer Science Issues, Vol. 9, Issue 2, No 1, March 2012, pp. 495-499.

[37] S. Forouhari, A. Abu-Siada, "Application of adaptive neuro fuzzy inference system to support power transformer life estimation and asset management decision", IEEE Transactions on Dielectrics and Electrical Insulation, Vol. 25, Issue 3, June 2018, pp. 845-852.

[38] E. J. Kadim, N. Azis, J. Jasni, M. A. Talib, "Transformers health index assessment based on neural-fuzzy network", Energies, Vol. 11, 2018, 710.

Research & Development Centre
ALFATEC

Bul. Nikole Tesle 63/5, 18000 Niš
Tel. 018 293 920; Fax: 018 293 921
e-mail: office@alfatec.rs; http://www.alfatec.rs
PIB: 104099234; m.b. 20090219; š.d. 73102
t.r.: 165-4863-06; 275-0010220587184-85

R&DC "ALFATEC" was founded in November 2005, with the purpose of enabling placement of innovative products and services developed by a group of researchers, who have worked as a part of the Section of Electric Machinery, at the Department of Energetics of the Faculty of Electronics in Nis.

R&DC "ALFATEC", upon being founded, worked in the field of measurement and control systems, where it has developed a substantial number of innovative products for the needs of various users.

In February 2008, R&DC "ALFATEC" became registered as a research and development centre by the Ministry of Science and Technological Development of the Republic of Serbia.

R&DC "ALFATEC" is currently the leader in:

- the number of realised innovative products and services which are successfully administered on the market of Serbia;
- the diversity of realised projects;
- the projecting and realisation of complex measurement and information systems, as well as measurement and control systems;
- savings of electric energy achieved by various users;
- innovative investment models for electric energy consumption reduction in small and medium-sized enterprises;
- software for decision support in emergency situations;
- design of electrical installations according to international standards.

www.energetics.cosrec.org